

## ABSTRACT

HEMPERLY, JOSHUA J. The Application and Evaluation of the Global Weather Research and Forecasting (GWRf) Model. (Under the direction of Dr. Yang Zhang.)

Global WRF (GWRf) is an extension of previous versions of the atmospheric mesoscale Weather Research and Forecasting (WRF) model in WRF version 3.0. GWRf enables the modeling of global climate of the Earth system and the coupling between weather systems on global and regional scales. The main objective of this study is to evaluate the capability of GWRf for an accurate representation of the global atmosphere by exploring the most accurate configuration of runtime and physics options. The objectives of the proposed thesis research are: to quantify the accuracy of GWRf model output in reproducing observational data for the year 2001, conduct a sensitivity study and identify the most appropriate physical parameterizations in GWRf that produce the highest accuracy for global scale modeling for 2001, and assess the capability of GWRf to predict future-year climate using benchmark results from an established future climate model.

The baseline GWRf simulation will be conducted at a horizontal grid resolution of  $1^\circ \times 1^\circ$  with a baseline physics configuration. The modular nature of physics in the WRF system allows users to investigate the impact that various parameterizations of microphysics, cumulus formation, land surface models, radiation, as well as horizontal grid resolution have on simulation accuracy. These microphysics schemes include a simple-ice scheme (WSM3) and two complex-ice microphysics schemes (WSM6 and Purdue Lin). The influence of the cumulus parameterization on model performance is evaluated by conducting a sensitivity simulation using the Kain-Fritsch and Grell-Devenyi ensemble schemes. The sensitivity of land surface parameterization is conducted using the Noah and Slab LSMs. Three sets of radiation scheme combinations will be evaluated including Goddard, Dudhia, and CAM shortwave parameterizations, as well as the RRTM and CAM longwave radiation schemes. The future GWRf simulation (2050) is initialized using output from the IPCC Special Report on Emission Scenario (SRES) B1 550 ppm stabilization experiment from the NCAR Community Climate System Model 3.0 (CCSM3).

The model evaluation focuses on major boundary layer meteorological variables including accumulated precipitation, 2-meter temperature and specific humidity, and the zonal and meridional components of 10-meter wind velocities, as well as downward shortwave and longwave fluxes at the surface. The overall performance of GWRP is evaluated in terms of spatial distribution, seasonal variations, and statistics over the global domain, Northern and Southern Hemispheres, the six populated continents, and the six circulations cells (Northern and Southern Polar Cells, Northern and Southern Ferrel Cells, and the Northern and Southern Hadley Cells). GWRP model output is evaluated using observational datasets from a variety of sources including surface based observations (NCDC and BSRN), model reanalyses (NCEP/ NCAR Reanalysis and GPCP), and remotely-sensed data (TRMM) to evaluate the ability of GWRP to simulate atmospheric variables at the surface as well as aloft in 2001.

The results from a baseline simulation of 2001 show that GWRP is able to reproduce meteorological fields with comparable or improved accuracy to the majority of current, mature GCMs. The fine resolution simulation was able to produce point observations with a higher level of accuracy than the coarse resolution simulation. Based on the results from this study, the most accurate physics configuration is WSM6 microphysics, CAM shortwave, RRTM longwave, SLAB Land Surface Module, and the Grell-Devenyi cumulus parameterization because each of these parameterizations produced the most accurate simulations when compared with observations. Results from the 2050 simulation indicate that GWRP does not replicate the large magnitude of near surface warming reported in the IPCC AR4 during the mid-21<sup>st</sup> century relative to the late 20<sup>th</sup> century, mainly because of the absence of forcings in the GWRP 2050 simulation (e.g., increased CO<sub>2</sub> concentrations, aerosols, and future SST). Geographically, annual and seasonal GWRP-CCSM comparisons consistently show the largest temperature changes at high latitudes, which is consistent with the IPCC report.

The Application and Evaluation of the Global Weather Research and Forecasting Model

by  
Joshua John Hemperly

A Thesis submitted to the Graduate Faculty of  
North Carolina State University  
in partial fulfillment of the  
requirements for the degree of  
Master of Science

Atmospheric Sciences

Raleigh, NC

2009

Approved By:

---

Dr. Nicholas Meskhidze  
Co-chair of Advisory Committee

---

Dr. Anantha Aiyyer

---

Dr. Yang Zhang  
Co-chair of Advisory Committee

## **BIOGRAPHY**

Joshua Hemperly was raised in Apex, North Carolina where he developed a respect and interest for the complexity of natural processes. He graduated from Apex High School in 2003 and moved to Raleigh in the fall of that year to attend the Meteorology program at North Carolina State University. His first research experience was working with Dr. John Fountain tracking wells with high arsenic concentrations in Gaston County, N.C. Later in his undergraduate career he worked at the State Climate Office of North Carolina, developing an interest in observational techniques in the atmospheric sciences, atmospheric modeling, micrometeorology, and climatology. In May 2007 he graduated with a B.S. in Meteorology with a concentration in Marine Science. He worked as a meteorologist at the State Climate Office of North Carolina and a student intern at the NWS Raleigh office during the summer of 2007. That fall he entered the M.S. Atmospheric Sciences program at NC State with a focus on Atmospheric Modeling under the tutelage of Drs. Yang Zhang and Nicholas Meskhidze.

## ACKNOWLEDGEMENTS

First, I would like to thank my committee members, Drs. Yang Zhang, Nicholas Meskhidze, and Anantha Aiyyer. I am very grateful to Drs. Zhang and Meskhidze for giving me the opportunity to work on this project, attend graduate school at North Carolina State University, and providing numerous academic and professional opportunities. I also greatly appreciate the scientific knowledge and guidance provided by the staff and faculty of the Marine, Earth, and Atmospheric Sciences department at NCSU. Finally, I wish to thank Drs. John Fountain, Sethu Raman and Ryan Boyles for providing undergraduate research opportunities which inspired the interest for my graduate school endeavors.

Thanks are also due to the following people for their scientific contributions and past comments on this research. Special thanks go to Drs. William Skamarock and Jimy Dudhia from the National Center for Atmospheric Research, for helpful discussions. I would also like to thank Eric Sills and Gary Howell from High Performance Computing at NCSU. I also wish to thank those that funding my research: EPA STAR grant #R8337601 and the U.S. Department of Energy Grant #DE-FG02-08ER64508. Finally, I wish to extend special thanks to all the members of the Air Quality Forecasting Lab, as well as students from Dr. Meskhidze's group. Thank you for your insight, advice, and companionship.

## TABLE OF CONTENTS

LIST OF TABLES.....	viii
LIST OF FIGURES.....	xiv
ACRONYMS.....	xxiv
1 INTRODUCTION.....	1
1.1 Background and Motivation.....	1
1.2 Objectives.....	3
1.3 Overall Technical Approach.....	4
2 LITERATURE REVIEW.....	6
2.1 A brief history of GCMs.....	6
2.2 Current state of GCMs.....	11
2.2.1 Coupled Model Intercomparison Project (CMIP).....	11
2.2.2 Atmospheric Model Intercomparison Project (AMIP).....	12
2.2.3 IPCC AR4.....	13
2.2.4 Geophysical Fluid Dynamics Laboratory Model (GFDL).....	16
2.2.5 Community Atmospheric Model version 3 (CAM3).....	17
2.3 Horizontal Grid Resolutions.....	18
2.4 Sensitivity to Initial Conditions (IC) and Boundary Conditions (BC).....	19
2.4.1 Sensitivity on a Regional Scale.....	19
2.4.2 Sensitivity on a Global Scale.....	21
2.5 Radiation schemes.....	23
2.5.1 RRTM Longwave.....	24
2.5.2 CAM3 Longwave.....	24
2.5.3 Dudhia Shortwave.....	25
2.5.4 CAM Shortwave.....	25

2.5.5	Goddard Shortwave.....	25
2.5.6	Radiation scheme sensitivity studies.....	26
2.6	Cloud microphysics schemes.....	29
2.6.1	WRF Single Moment 3-Class (WSM3).....	31
2.6.2	WRF Single Moment 6-Class (WSM6).....	31
2.6.3	Purdue-Lin.....	32
2.6.4	Microphysics scheme sensitivity studies.....	32
2.7	Land Surface Modules (LSMs).....	34
2.7.1	Noah LSM.....	35
2.7.2	Five Layer Thermal Diffusion (Slab).....	36
2.7.3	LSM sensitivity studies.....	36
2.8	Cumulus Parameterizations.....	37
2.8.1	Kain-Fritsch cumulus parameterization.....	38
2.8.2	Grell-Devenyi ensemble cumulus parameterization.....	38
2.8.3	Cumulus parameterization sensitivity studies.....	39
3	<b>SIMULATION DESIGN AND METHODOLOGY</b>	41
3.1	Current-year initialization.....	41
3.2	Current-year simulation.....	41
3.2.1	Baseline simulation.....	41
3.2.2	Sensitivity simulations.....	42
3.3	Future-year initialization and simulation.....	44
3.4	Surface Observational Networks.....	45
3.4.1	Baseline Surface Radiation Network (BSRN).....	46
3.4.2	National Climactic Data Center (NCDC).....	47
3.5	Remote Sensing.....	48

3.5.1	Tropical Rainfall Measuring Mission (TRMM).....	48
3.6	Reanalysis Datasets.....	48
3.6.1	NCEP/NCAR Reanalysis.....	48
3.6.2	Global Precipitation Climatology Project (GPCP).....	49
3.7	Current-year simulation evaluation protocol.....	49
3.7.1	Spatial Distribution.....	50
3.7.2	Temporal Variation.....	50
3.7.3	Performance Statistics Distribution.....	51
3.7.4	Vertical Profile and Zonal Mean Distribution.....	52
3.8	Future-year simulation evaluation protocol.....	52
4	SENSITIVITY TO MODEL CONFIGURATIONS.....	54
4.1	Baseline configuration evaluation.....	54
4.1.1	2001 Annual Mean Evaluation.....	54
4.1.2	2001 Evaluation of summer (JJA) Simulation.....	68
4.1.3	2001 Evaluation of winter (DJF) Simulation.....	88
4.2	Sensitivity to Horizontal Grid Resolution.....	106
4.2.1	2001 Annual Simulations ( $4^{\circ} \times 5^{\circ}$ ).....	106
4.2.2	$4^{\circ} \times 5^{\circ}$ Summer Simulation.....	121
4.2.3	$4^{\circ} \times 5^{\circ}$ Winter Simulation.....	140
4.3	Sensitivity to Radiation Schemes.....	158
4.3.1	Summer (JJA) mean RAD1 evaluation.....	159

4.3.2	Summer (JJA) mean RAD2 evaluation.....	171
4.3.3	Summer (JJA) mean RAD3 evaluation.....	184
4.4	Sensitivity to cloud microphysics schemes.....	200
4.4.1	Summer (JJA) mean WSM6 evaluation.....	200
4.4.2	Summer (JJA) mean PL evaluation.....	213
4.5	Sensitivity to Land Surface Module.....	228
4.6	Sensitivity to Cumulus Parameterizations.....	241
5	FUTURE-YEAR SIMULATION RESULTS.....	257
5.1	2050 January Mean Evaluation.....	257
5.2	2050 July Mean Evaluation.....	267
5.3	2050 Evaluation of winter (DJF) Simulation.....	276
5.4	2050 Summary.....	289
6	SUMMARY AND RECOMMENDATIONS.....	287
6.0	Summary and Recommendations.....	287
6.1	Summary of Baseline Simulation Results.....	288
6.2	Summary of Sensitivity Simulations.....	291
6.2.1	Sensitivity to Horizontal Grid Resolution.....	291
6.2.2	Sensitivity to Microphysics.....	293
6.2.3	Sensitivity to Radiation Configuration.....	293
6.2.4	Sensitivity to Land Surface Module.....	295
6.2.5	Sensitivity to Cumulus Parameterization.....	296
6.3	Summary of Future year (2050) Results.....	297

6.4 Recommendations..... 297

REFERENCES..... 299

## LIST OF TABLES

Table 2.1 Brief Summary of GCM history.....	10
Table 2.2 Current State of GCMs.....	11
Table 3.1 GWRf baseline and sensitivity simulations.....	43
Table 3.2 Summary of datasets used to evaluate GWRf.....	46
<b>BASELINE EVALUATION</b>	
Table 4.1 Performance Statistics of GWRf 2001 Annual Mean temperature at 2-meter as compared with NCEP/NCAR Reanalysis.....	55
Table 4.2 Performance Statistics of GWRf 2001 Annual Mean Water Vapor Mixing Ratio at 2-meter as compared with NCEP/NCAR Reanalysis.....	60
Table 4.3 Performance Statistics of GWRf 2001 Annual Mean downward shortwave flux at the surface as compared with NCEP/NCAR Reanalysis.....	62
Table 4.4 Performance Statistics of GWRf 2001 Annual Mean downward longwave flux at the surface as compared with NCEP/NCAR Reanalysis.....	63
Table 4.5 Performance Statistics of GWRf 2001 Annual Mean zonal wind at 10-meter as compared with NCEP/NCAR Reanalysis.....	65
Table 4.6 Performance Statistics of GWRf 2001 annual mean meridional wind at 10-meter as compared with NCEP/NCAR Reanalysis.....	66
Table 4.7 Performance Statistics of GWRf 2001 annual mean daily precipitation rate as compared with Global Precipitation Climatology Project.....	68
Table 4.8 Performance Statistics of GWRf 2001 summer mean temperature at 2-meter compared with NCEP/NCAR Reanalysis and NCDC data.....	70
Table 4.9 Performance Statistics of GWRf 2001 summer mean water vapor mixing ratio at 2-meter compared with NCEP/NCAR Reanalysis.....	75
Table 4.10 Performance Statistics of GWRf 2001 summer mean downward shortwave flux at the surface compared with NCEP/NCAR Reanalysis and BSRN data....	78
Table 4.11 Performance Statistics of GWRf 2001 summer mean downward longwave flux at the surface compared with NCEP/NCAR Reanalysis and BSRN data....	81
Table 4.12 Performance Statistics of GWRf 2001 summer mean Zonal Wind at 10-meter as compared with NCEP/NCAR Reanalysis.....	83
Table 4.13 Performance Statistics of GWRf 2001 summer mean Meridional Wind at 10-meter as compared with NCEP/NCAR Reanalysis.....	84
Table 4.14 Performance Statistics of GWRf 2001 summer mean daily rainfall rate for compared with GPCP (mm day <sup>-1</sup> ) and NCDC (mm month <sup>-1</sup> ).....	87

Table 4.15 Performance Statistics of GWRf 2001 winter mean temperature at 2-meter as compared with NCEP/NCAR Reanalysis and NCDC data. ....	90
Table 4.16 Performance Statistics of GWRf 2001 winter mean water vapor mixing ratio at 2-meter compared with NCEP/NCAR Reanalysis.....	94
Table 4.17 Performance Statistics of GWRf 2001 winter mean downward shortwave flux at the surface as compared with NCEP/NCAR Reanalysis. ....	97
Table 4.18 Performance Statistics of GWRf 2001 winter mean downward longwave flux at the surface as compared with NCEP/NCAR Reanalysis and BSRN data.....	100
Table 4.19 Performance Statistics of GWRf winter mean zonal wind at 10-meter as compared with NCEP/NCAR Reanalysis.....	102
Table 4.20 Performance Statistics of GWRf 2001 winter mean meridional wind at 10-meter as compared with NCEP/NCAR Reanalysis.....	103
Table 4.21 Performance Statistics of GWRf 2001 winter mean daily precipitation rate as compared with GPCP (mm day <sup>-1</sup> ) and NCDC (mm month <sup>-1</sup> ).....	105
<b>SENSITIVITY TO HORIZONTAL GRID RESOLUTION</b>	
Table 4.22 Performance Statistics of GWRf 2001 Annual Mean temperature at 2-meter as compared with NCEP/NCAR Reanalysis.....	107
Table 4.23 Performance Statistics of GWRf 2001 Annual Mean Water Vapor Mixing Ratio at 2-meter as compared with NCEP/NCAR Reanalysis.....	111
Table 4.24 Performance Statistics of GWRf 2001 Annual Mean downward shortwave flux at the surface as compared with NCEP/NCAR Reanalysis.....	113
Table 4.25 Performance Statistics of GWRf 2001 Annual Mean downward longwave flux at the surface as compared with NCEP/NCAR Reanalysis.....	115
Table 4.26 Performance Statistics of GWRf 2001 Annual Mean zonal wind at 10-meter as compared with NCEP/NCAR Reanalysis.....	117
Table 4.27 Performance Statistics of GWRf 2001 annual mean meridional wind at 10-meter as compared with NCEP/NCAR Reanalysis.....	119
Table 4.28 Performance Statistics of GWRf 2001 annual mean daily precipitation rate as compared with Global Precipitation Climatology Project.....	121
Table 4.29 Performance Statistics of GWRf 2001 summer mean temperature at 2-meter compared with NCEP/NCAR Reanalysis and NCDC data.....	123
Table 4.30 Performance Statistics of GWRf 2001 summer mean water vapor mixing ratio at 2-meter compared with NCEP/NCAR Reanalysis.....	128
Table 4.31 Performance Statistics of GWRf 2001 summer mean downward shortwave flux at the surface compared with NCEP/NCAR Reanalysis and BSRN data	131
Table 4.32 Performance Statistics of GWRf 2001 summer mean downward longwave flux at the surface compared with NCEP/NCAR Reanalysis and BSRN data	133
Table 4.33 Performance Statistics of GWRf 2001 summer mean Zonal Wind at 10-meter as compared with NCEP/NCAR Reanalysis.....	135

Table 4.34 Performance Statistics of GWRf 2001 summer mean Meridional Wind at 10-meter as compared with NCEP/NCAR Reanalysis.....	137
Table 4.35 Performance Statistics of GWRf 2001 summer mean daily rainfall rate for compared with GPCP ( $\text{mm day}^{-1}$ ) and NCDC ( $\text{mm month}^{-1}$ ).....	139
Table 4.36 Performance Statistics of GWRf 2001 winter mean temperature at 2-meter as compared with NCEP/NCAR Reanalysis and NCDC data.....	141
Table 4.37 Performance Statistics of GWRf 2001 winter mean water vapor mixing ratio at 2-meter compared with NCEP/NCAR Reanalysis.....	146
Table 4.38 Performance Statistics of GWRf 2001 winter mean downward shortwave flux at the surface as compared with NCEP/NCAR Reanalysis.....	149
Table 4.39 Performance Statistics of GWRf 2001 winter mean downward longwave flux at the surface as compared with NCEP/NCAR Reanalysis and BSRN data.....	151
Table 4.40 Performance Statistics of GWRf winter mean zonal wind at 10-meter as compared with NCEP/NCAR Reanalysis.....	153
Table 4.41 Performance Statistics of GWRf 2001 winter mean meridional wind at 10-meter as compared with NCEP/NCAR Reanalysis.....	155
Table 4.42 Performance Statistics of GWRf 2001 winter mean daily precipitation rate as compared with GPCP ( $\text{mm day}^{-1}$ ) and NCDC ( $\text{mm month}^{-1}$ ).....	157
SENSITIVITY TO RADIATION SCHEME (RAD1)	
Table 4.43 Performance Statistics of GWRf 2001 summer mean temperature at 2-meter compared with NCEP/NCAR Reanalysis and NCDC data.....	160
Table 4.44 Performance Statistics of GWRf 2001 summer mean water vapor mixing ratio at 2-meter compared with NCEP/NCAR Reanalysis.....	164
Table 4.45 Performance Statistics of GWRf 2001 summer mean downward shortwave flux at the surface compared with NCEP/NCAR Reanalysis and BSRN data.....	166
Table 4.46 Performance Statistics of GWRf 2001 summer mean downward longwave flux at the surface compared with NCEP/NCAR Reanalysis and BSRN data.....	168
Table 4.47 Performance Statistics of GWRf 2001 summer mean daily precipitation rate as compared with GPCP ( $\text{mm day}^{-1}$ ) and NCDC ( $\text{mm month}^{-1}$ ).....	171
SENSITIVITY TO RADIATION SCHEME (RAD2)	
Table 4.48 Performance Statistics of GWRf 2001 summer mean temperature at 2-meter compared with NCEP/NCAR Reanalysis and NCDC data.....	173
Table 4.49 Performance Statistics of GWRf 2001 summer mean water vapor mixing ratio at 2-meter compared with NCEP/NCAR Reanalysis.....	177

Table 4.50 Performance Statistics of GWRf 2001 summer mean downward shortwave flux at the surface compared with NCEP/NCAR Reanalysis and BSRN data.....	180
Table 4.51 Performance Statistics of GWRf 2001 summer mean downward longwave flux at the surface compared with NCEP/NCAR Reanalysis and BSRN data.....	182
Table 4.52 Performance Statistics of GWRf 2001 summer mean daily precipitation rate as compared with GPCP (mm day <sup>-1</sup> ) and NCDC (mm month <sup>-1</sup> ).....	184
<b>SENSITIVITY TO RADIATION SCHEME (RAD3)</b>	
Table 4.53 Performance Statistics of GWRf 2001 summer mean temperature at 2-meter compared with NCEP/NCAR Reanalysis and NCDC data.....	186
Table 4.54 Performance Statistics of GWRf 2001 summer mean water vapor mixing ratio at 2-meter compared with NCEP/NCAR Reanalysis.....	190
Table 4.55 Performance Statistics of GWRf 2001 summer mean downward shortwave flux at the surface compared with NCEP/NCAR Reanalysis and BSRN data.....	193
Table 4.56 Performance Statistics of GWRf 2001 summer mean downward longwave flux at the surface compared with NCEP/NCAR Reanalysis and BSRN data.....	195
Table 4.57 Performance Statistics of GWRf 2001 summer mean daily precipitation rate as compared with GPCP (mm day <sup>-1</sup> ) and NCDC (mm month <sup>-1</sup> ).....	197
Table 4.58 Intercomparison of GWRf GLW over circulation cell domains for summer 2001 compared with NCEP/NCAR Reanalysis.....	198
Table 4.59 Intercomparison of GWRf GLW over continental domains for summer 2001 compared with NCEP/NCAR Reanalysis.....	198
Table 4.60 Intercomparison of GWRf SWDOWN over circulation cell domains for summer 2001 compared with NCEP/NCAR Reanalysis.....	199
Table 4.61 Intercomparison of GWRf SWDOWN over continental domains for summer 2001 compared with NCEP/NCAR Reanalysis.....	199
<b>SENSITIVITY TO CLOUD MICROPHYSICS SCHEMES (WSM6)</b>	
Table 4.62 Performance Statistics of GWRf 2001 summer mean temperature at 2-meter compared with NCEP/NCAR Reanalysis and NCDC data.....	202
Table 4.63 Performance Statistics of GWRf 2001 summer mean water vapor mixing ratio at 2-meter compared with NCEP/NCAR Reanalysis.....	205
Table 4.64 Performance Statistics of GWRf 2001 summer mean downward shortwave flux at the surface compared with NCEP/NCAR Reanalysis and BSRN data.....	208

Table 4.65 Performance Statistics of GWRf 2001 summer mean downward longwave flux at the surface compared with NCEP/NCAR Reanalysis and BSRN data.....	211
Table 4.66 Performance Statistics of GWRf 2001 summer mean daily precipitation rate as compared with GPCP (mm day <sup>-1</sup> ) and NCDC (mm month <sup>-1</sup> ).....	213
SENSITIVITY TO CLOUD MICROPHYSICS SCHEMES (Purdue-Lin)	
Table 4.67 Performance Statistics of GWRf 2001 summer mean temperature at 2-meter compared with NCEP/NCAR Reanalysis and NCDC data.....	215
Table 4.68 Performance Statistics of GWRf 2001 summer mean water vapor mixing ratio at 2-meter compared with NCEP/NCAR Reanalysis.....	219
Table 4.69 Performance Statistics of GWRf 2001 summer mean downward shortwave flux at the surface compared with NCEP/NCAR Reanalysis and BSRN data.....	222
Table 4.70 Performance Statistics of GWRf 2001 summer mean downward longwave flux at the surface compared with NCEP/NCAR Reanalysis and BSRN data.....	225
Table 4.71 Performance Statistics of GWRf 2001 summer mean daily precipitation rate as compared with GPCP (mm day <sup>-1</sup> ) and NCDC (mm month <sup>-1</sup> ).....	227
SENSITIVITY TO LAND SURFACE MODULE	
Table 4.72 Performance Statistics of GWRf 2001 summer mean temperature at 2-meter compared with NCEP/NCAR Reanalysis and NCDC data.....	230
Table 4.73 Performance Statistics of GWRf 2001 summer mean water vapor mixing ratio at 2-meter compared with NCEP/NCAR Reanalysis.....	233
Table 4.74 Performance Statistics of GWRf 2001 summer mean downward shortwave flux at the surface compared with NCEP/NCAR Reanalysis and BSRN data.....	236
Table 4.75 Performance Statistics of GWRf 2001 summer mean downward longwave flux at the surface compared with NCEP/NCAR Reanalysis and BSRN data.....	238
Table 4.76 Performance Statistics of GWRf 2001 summer mean daily precipitation rate as compared with GPCP (mm day <sup>-1</sup> ) and NCDC (mm month <sup>-1</sup> ).....	241
SENSITIVITY TO CUMULUS PARAMETERIZATION	
Table 4.77 Performance Statistics of GWRf 2001 summer mean temperature at 2-meter compared with NCEP/NCAR Reanalysis and NCDC data.....	244
Table 4.78 Performance Statistics of GWRf 2001 summer mean water vapor mixing ratio at 2-meter compared with NCEP/NCAR Reanalysis.....	248

Table 4.79 Performance Statistics of GWRF 2001 summer mean downward shortwave flux at the surface compared with NCEP/NCAR Reanalysis and BSRN data.....	251
Table 4.80 Performance Statistics of GWRF 2001 summer mean downward longwave flux at the surface compared with NCEP/NCAR Reanalysis and BSRN data.....	253
Table 4.81 Performance Statistics of GWRF 2001 summer mean daily precipitation rate as compared with GPCP (mm day <sup>-1</sup> ) and NCDC (mm month <sup>-1</sup> ).....	256
<b>2050 SIMULATION</b>	
Table 5.1 Performance Statistics of GWRF 2001 and 2050 January Mean temperature at 2-meter.....	260
Table 5.2 Performance Statistics of GWRF 2001 and 2050 January Mean water vapor mixing ratio at 2-meter.....	262
Table 5.3 Performance Statistics of GWRF 2001 and 2050 January Mean downward shortwave flux at the surface.....	263
Table 5.4 Performance Statistics of GWRF 2001 and 2050 January Mean downward longwave flux at the surface.....	265
Table 5.5 Performance Statistics of GWRF 2001 and 2050 January Mean daily precipitation rate.....	267
Table 5.6 Performance Statistics of GWRF 2001 and 2050 July Mean temperature at 2-meter.....	269
Table 5.7 Performance Statistics of GWRF 2001 and 2050 July Mean water vapor mixing ratio at 2-meter.....	271
Table 5.8 Performance Statistics of GWRF 2001 and 2050 July Mean downward shortwave flux at the surface.....	273
Table 5.9 Performance Statistics of GWRF 2001 and 2050 July Mean downward longwave flux at the surface.....	274
Table 5.10 Performance Statistics of GWRF 2001 and 2050 July Mean daily precipitation rate.....	276

## LIST OF FIGURES

Figure 1.1	A graphical representation of transport around the polar regions of GWRP. The symbol “ $\mu$ ” represents a mass point in the model, “u” represents the zonal component of wind velocity, and “v” represents the zonal component of wind velocity.....	2
Figure 3.1	Spatial distribution of BSRN sites as of February 2009.....	47
<b>BASELINE EVALUATION</b>		
Figure 4.1	2001 Annual mean bias of temperature at 2-meters.....	54
Figure 4.2	2001 Annual Mean normalized mean bias (%) of major meteorological variables for (a) the six continental domains and (b) the six circulation cell domains.....	57
Figure 4.3	Vertical profiles of annual mean temperature mean bias over the six populated continents.....	58
Figure 4.4	2001 Annual mean zonal mean bias of temperature.....	59
Figure 4.5	2001 Annual mean bias of water vapor mixing ratio at 2-meter.....	60
Figure 4.6	2001 Annual mean bias of downward shortwave flux at the surface.....	61
Figure 4.7	2001 Annual mean bias of downward longwave flux at the surface.....	63
Figure 4.8	2001 Annual mean bias of zonal wind at 10-meter.....	64
Figure 4.9	2001 Annual mean bias of meridional wind at 10-meter.....	66
Figure 4.10	2001 Annual mean bias of daily precipitation rate.....	67
Figure 4.11	2001 Summer mean bias of temperature at 2-meters compared with NCEP/NCAR Reanalysis.....	69
Figure 4.12	2001 Summer mean bias of temperature at 2-meter compared with NCDC...	70
Figure 4.13	2001 Summer Mean normalized mean bias (%) of major meteorological variables for (a) the six continental domains and (b) the six circulation cell domains.....	72
Figure 4.14	Vertical profiles of Summer mean temperature mean bias over the six populated continents.....	73
Figure 4.15	2001 Summer mean zonal mean bias of temperature. ....	74
Figure 4.16	2001 Summer mean bias of water vapor mixing ratio at 2-meter compared with NCEP/NCAR Reanalysis.....	75

Figure 4.17 2001 Summer mean bias of downward shortwave flux at the surface compared with NCEP/NCAR Reanalysis.....	77
Figure 4.18 2001 summer mean bias of downward shortwave flux at the surface compared with BSRN.....	77
Figure 4.19 2001 Summer mean bias of downward longwave flux at the surface compared with NCEP/NCAR Reanalysis.....	79
Figure 4.20 2001 Summer mean bias of downward longwave flux at the surface compared with BSRN.....	80
Figure 4.21 2001 Summer mean bias of zonal wind at 10-meter.....	82
Figure 4.22 2001 Summer mean bias of meridional wind at 10-meter.....	84
Figure 4.23 2001 Summer mean bias of daily precipitation rate compared with NCEP/NCAR Reanalysis.....	85
Figure 4.24 2001 Summer mean bias of monthly mean accumulated precipitation compared with NCDC.....	86
Figure 4.25 2001 Winter mean bias of temperature at 2-meters compared with NCEP/NCAR Reanalysis.....	88
Figure 4.26 2001 Winter mean bias of temperature at 2-meter compared with NCDC.....	89
Figure 4.27 2001 Winter Mean normalized mean bias (%) of major meteorological variables for (a) the six continental domains and (b) the six circulation cell domains.....	91
Figure 4.28 Vertical profiles of Winter mean temperature mean bias over the six populated continents.....	92
Figure 4.29 2001 Winter mean zonal mean bias of temperature.....	93
Figure 4.30 2001 Winter mean bias of water vapor mixing ratio at 2-meter compared with NCEP/NCAR Reanalysis.....	94
Figure 4.31 2001 Winter mean bias of downward shortwave flux at the surface compared with NCEP/NCAR Reanalysis.....	96
Figure 4.32 2001 Winter mean bias of downward shortwave flux at the surface compared with BSRN.....	96
Figure 4.33 2001 Winter mean bias of downward longwave flux at the surface compared with NCEP/NCAR Reanalysis.....	98
Figure 4.34 2001 Winter mean bias of downward longwave flux at the surface compared with BSRN.....	99
Figure 4.35 2001 Winter mean bias of zonal wind at 10-meter.....	101
Figure 4.36 2001 Winter mean bias of meridional wind at 10-meter.....	103

Figure 4.37 2001 Winter mean bias of daily precipitation rate compared with NCEP/NCAR Reanalysis.....	104
Figure 4.38 2001 Winter mean bias of monthly mean accumulated precipitation compared with NCDC.....	105
<b>SENSITIVITY TO HORIZONTAL GRID RESOLUTION</b>	
Figure 4.39 2001 Annual mean bias of temperature at 2-meters.....	106
Figure 4.40 2001 Annual Mean normalized mean bias (%) of major meteorological variables for (a) the six continental domains and (b) the six circulation cell domains.....	108
Figure 4.41 Vertical profiles of annual mean temperature mean bias over the six populated continents.....	109
Figure 4.42 2001 Annual mean zonal mean bias of temperature.....	110
Figure 4.43 2001 Annual mean bias of water vapor mixing ratio at 2-meter.....	111
Figure 4.44 2001 Annual mean bias of downward shortwave flux at the surface.....	113
Figure 4.45 2001 Annual mean bias of downward longwave flux at the surface.....	114
Figure 4.46 2001 Annual mean bias of zonal wind at 10-meter.....	116
Figure 4.47 2001 Annual mean bias of meridional wind at 10-meter.....	118
Figure 4.48 2001 Annual mean bias of daily precipitation rate.....	120
Figure 4.49 2001 Summer mean bias of temperature at 2-meters compared with NCEP/NCAR Reanalysis.....	122
Figure 4.50 2001 Summer mean bias of temperature at 2-meter compared with NCDC....	123
Figure 4.51 2001 Summer Mean normalized mean bias (%) of major meteorological variables for (a) the six continental domains and (b) the six circulation cell domains.....	125
Figure 4.52 Vertical profiles of Summer mean temperature mean bias over the six populated continents.....	126
Figure 4.53 2001 Summer mean zonal mean bias of temperature.....	127
Figure 4.54 2001 Summer mean bias of water vapor mixing ratio at 2-meter compared with NCEP/NCAR Reanalysis. ....	128
Figure 4.55 2001 Summer mean bias of downward shortwave flux at the surface compared with NCEP/NCAR Reanalysis.....	130
Figure 4.56 2001 Summer mean bias of downward shortwave flux at the surface compared with BSRN.....	130

Figure 4.57 2001 Summer mean bias of downward longwave flux at the surface .compared with NCEP/NCAR Reanalysis.....	132
Figure 4.58 2001 Summer mean bias of downward longwave flux at the surface compared with BSRN.....	132
Figure 4.59 2001 Summer mean bias of zonal wind at 10-meter.....	134
Figure 4.60 2001 Summer mean bias of meridional wind at 10-meter.....	136
Figure 4.61 2001 Summer mean bias of daily precipitation rate compared with NCEP/NCAR Reanalysis.....	138
Figure 4.62 2001 Summer mean bias of monthly mean accumulated precipitation compared with NCDC.....	139
Figure 4.63 2001 Winter mean bias of temperature at 2-meters compared with NCEP/NCAR Reanalysis.....	140
Figure 4.64 2001 Winter mean bias of temperature at 2-meter compared with NCDC.....	141
Figure 4.65 2001 Winter Mean normalized mean bias (%) of major meteorological variables for (a) the six continental domains and (b) the six circulation cell domains.....	143
Figure 4.66 Vertical profiles of Winter mean temperature mean bias over the six populated continents.....	144
Figure 4.67 2001 Winter mean zonal mean bias of temperature.....	145
Figure 4.68 2001 Winter mean bias of water vapor mixing ratio at 2-meter compared with NCEP/NCAR Reanalysis.....	146
Figure 4.69 2001 Winter mean bias of downward shortwave flux at the surface compared with NCEP/NCAR Reanalysis.....	148
Figure 4.70 2001 Winter mean bias of downward shortwave flux at the surface compared with BSRN.....	148
Figure 4.71 2001 Winter mean bias of downward longwave flux at the surface compared with NCEP/NCAR Reanalysis.....	150
Figure 4.72 2001 Winter mean bias of downward longwave flux at the surface compared with BSRN.....	150
Figure 4.73 2001 Winter mean bias of zonal wind at 10-meter.....	152
Figure 4.74 2001 Winter mean bias of meridional wind at 10-meter.....	154
Figure 4.75 2001 Winter mean bias of daily precipitation rate compared with NCEP/NCAR Reanalysis.....	156
Figure 4.76 2001 Winter mean bias of monthly accumulated precipitation as compared with NCDC	156

SENSITIVITY TO RADIATION SCHEME (RAD1)

Figure 4.77 2001 Summer mean bias of temperature at 2-meters compared with NCEP/NCAR Reanalysis..... 159

Figure 4.78 2001 Summer mean bias of temperature at 2-meter compared with NCDC..... 159

Figure 4.79 2001 Summer Mean normalized mean bias (%) of major meteorological variables for (a) the six continental domains and (b) the six circulation cell domains..... 161

Figure 4.80 2001 Summer mean zonal mean bias of temperature..... 162

Figure 4.81 2001 Summer mean bias of water vapor mixing ratio at 2-meter compared with NCEP/NCAR Reanalysis..... 163

Figure 4.82 2001 Summer mean bias of downward shortwave flux at the surface compared with NCEP/NCAR Reanalysis..... 165

Figure 4.83 2001 Summer mean bias of downward shortwave flux at the surface compared with BSRN..... 165

Figure 4.84 2001 Summer mean bias of downward longwave flux at the surface compared with NCEP/NCAR Reanalysis..... 167

Figure 4.85 2001 Summer mean bias of downward longwave flux at the surface compared with BSRN..... 167

Figure 4.86 2001 Summer mean bias of daily precipitation rate compared with NCEP/NCAR Reanalysis..... 169

Figure 4.87 2001 Summer mean bias of monthly accumulated precipitation as compared with NCDC..... 170

SENSITIVITY TO RADIATION SCHEME (RAD2)

Figure 4.88 2001 Summer mean bias of temperature at 2-meters compared with NCEP/NCAR Reanalysis..... 172

Figure 4.89 2001 Summer mean bias of temperature at 2-meter compared with NCDC..... 173

Figure 4.90 2001 Summer Mean normalized mean bias (%) of major meteorological variables for (a) the six continental domains and (b) the six circulation cell domains..... 175

Figure 4.91 2001 Summer mean zonal mean bias of temperature..... 175

Figure 4.92 2001 Summer mean bias of water vapor mixing ratio at 2-meter compared with NCEP/NCAR Reanalysis..... 176

Figure 4.93 2001 Summer mean bias of downward shortwave flux at the surface compared with NCEP/NCAR Reanalysis..... 178

Figure 4.94 2001 Summer mean bias of downward shortwave flux at the surface compared with BSRN.....	179
Figure 4.95 2001 Summer mean bias of downward longwave flux at the surface compared with NCEP/NCAR Reanalysis.....	181
Figure 4.96 2001 Summer mean bias of downward longwave flux at the surface compared with BSRN.....	181
Figure 4.97 2001 Summer mean bias of daily precipitation rate compared with NCEP/NCAR Reanalysis.....	183
Figure 4.98 2001 Summer mean bias of monthly accumulated precipitation as compared with NCDC.....	183
<b>SENSITIVITY TO RADIATION SCHEME (RAD3)</b>	
Figure 4.99 2001 Summer mean bias of temperature at 2-meters compared with NCEP/NCAR Reanalysis.....	185
Figure 4.100 2001 Summer mean bias of temperature at 2-meter compared with NCDC.....	186
Figure 4.101 2001 Summer Mean normalized mean bias (%) of major meteorological variables for (a) the six continental domains and (b) the six circulation cell domains.....	188
Figure 4.102 2001 Summer mean zonal mean bias of temperature.....	188
Figure 4.103 2001 Summer mean bias of water vapor mixing ratio at 2-meter compared with NCEP/NCAR Reanalysis.....	189
Figure 4.104 2001 Summer mean bias of downward shortwave flux at the surface compared with NCEP/NCAR Reanalysis.....	191
Figure 4.105 2001 Summer mean bias of downward shortwave flux at the surface compared with BSRN.....	192
Figure 4.106 2001 Summer mean bias of downward longwave flux at the surface compared with NCEP/NCAR Reanalysis.....	194
Figure 4.107 2001 Summer mean bias of downward longwave flux at the surface compared with BSRN.....	194
Figure 4.108 2001 Summer mean bias of daily precipitation rate compared with NCEP/NCAR Reanalysis.....	196
Figure 4.109 2001 Summer mean bias of monthly accumulated precipitation as compared with NCDC.....	196
<b>SENSITIVITY TO CLOUD MICROPHYSICS SCHEME (WSM6)</b>	
Figure 4.110 2001 Summer mean bias of temperature at 2-meters compared with NCEP/NCAR Reanalysis.....	201
Figure 4.111 2001 Summer mean bias of temperature at 2-meter compared with NCDC.....	201

Figure 4.112	2001 Summer Mean normalized mean bias (%) of major meteorological variables for (a) the six continental domains and (b) the six circulation cell domains.....	203
Figure 4.113	2001 Summer mean zonal mean bias of temperature.....	204
Figure 4.114	2001 Summer mean bias of water vapor mixing ratio at 2-meter compared with NCEP/NCAR Reanalysis.....	205
Figure 4.115	2001 Summer mean bias of downward shortwave flux at the surface compared with NCEP/NCAR Reanalysis.....	207
Figure 4.116	2001 Summer mean bias of downward shortwave flux at the surface compared with BSRN.....	207
Figure 4.117	2001 Summer mean bias of downward longwave flux at the surface compared with NCEP/NCAR Reanalysis.....	209
Figure 4.118	2001 Summer mean bias of downward longwave flux at the surface compared with BSRN.....	210
Figure 4.119	2001 Summer mean bias of daily precipitation rate compared with NCEP/NCAR Reanalysis.....	212
Figure 4.120	2001 Summer mean bias of monthly accumulated precipitation as compared with NCDC.....	212
<b>SENSITIVITY TO CLOUD MICROPHYSICS SCHEME (Purdue-Lin)</b>		
Figure 4.121	2001 Summer mean bias of temperature at 2-meters compared with NCEP/NCAR Reanalysis.....	214
Figure 4.122	2001 Summer mean bias of temperature at 2-meter compared with NCDC.....	215
Figure 4.123	2001 Summer Mean normalized mean bias (%) of major meteorological variables for (a) the six continental domains and (b) the six circulation cell domains.....	217
Figure 4.124	2001 Summer mean zonal mean bias of temperature.....	217
Figure 4.125	2001 Summer mean bias of water vapor mixing ratio at 2-meter compared with NCEP/NCAR Reanalysis.....	218
Figure 4.126	2001 Summer mean bias of downward shortwave flux at the surface compared with NCEP/NCAR Reanalysis.....	220
Figure 4.127	2001 Summer mean bias of downward shortwave flux at the surface compared with BSRN.....	221
Figure 4.128	2001 Summer mean bias of downward longwave flux at the surface compared with NCEP/NCAR Reanalysis.....	223
Figure 4.129	2001 Summer mean bias of downward longwave flux at the surface compared with BSRN.....	224

Figure 4.130	2001 Summer mean bias of daily precipitation rate compared with NCEP/NCAR Reanalysis.....	226
Figure 4.131	2001 Summer mean bias of monthly accumulated precipitation as compared with NCDC.....	227
<b>SENSITIVITY TO LAND SURFACE MODULES</b>		
Figure 4.132	2001 Summer mean bias of temperature at 2-meters compared with NCEP/NCAR Reanalysis.....	229
Figure 4.133	2001 Summer mean bias of temperature at 2-meter compared with NCDC.....	229
Figure 4.134	2001 Summer Mean normalized mean bias (%) of major meteorological variables for (a) the six continental domains and (b) the six circulation cell domains.....	231
Figure 4.135	2001 Summer mean zonal mean bias of temperature.....	232
Figure 4.136	2001 Summer mean bias of water vapor mixing ratio at 2-meter compared with NCEP/NCAR Reanalysis.....	233
Figure 4.137	2001 Summer mean bias of downward shortwave flux at the surface compared with NCEP/NCAR Reanalysis.....	235
Figure 4.138	2001 Summer mean bias of downward shortwave flux at the surface compared with BSRN.....	235
Figure 4.139	2001 Summer mean bias of downward longwave flux at the surface compared with NCEP/NCAR Reanalysis.....	237
Figure 4.140	2001 Summer mean bias of downward longwave flux at the surface compared with BSRN.....	237
Figure 4.141	2001 Summer mean bias of daily precipitation rate compared with NCEP/NCAR Reanalysis.....	239
Figure 4.142	2001 Summer mean bias of monthly accumulated precipitation as compared with NCDC.....	240
<b>SENSITIVITY TO CUMULUS PARAMETERIZATION</b>		
Figure 4.143	2001 Summer mean bias of temperature at 2-meters compared with NCEP/NCAR Reanalysis.....	242
Figure 4.144	2001 Summer mean bias of temperature at 2-meter compared with NCDC.....	243
Figure 4.145	2001 Summer Mean normalized mean bias (%) of major meteorological variables for (a) the six continental domains and (b) the six circulation cell domains.....	245
Figure 4.146	2001 Summer mean zonal mean bias of temperature.....	246

Figure 4.147	2001 Summer mean bias of water vapor mixing ratio at 2-meter compared with NCEP/NCAR Reanalysis.....	247
Figure 4.148	2001 Summer mean bias of downward shortwave flux at the surface compared with NCEP/NCAR Reanalysis.....	249
Figure 4.149	2001 Summer mean bias of downward shortwave flux at the surface compared with BSRN.....	250
Figure 4.150	2001 Summer mean bias of downward longwave flux at the surface compared with NCEP/NCAR Reanalysis.....	252
Figure 4.151	2001 Summer mean bias of downward longwave flux at the surface compared with BSRN.....	253
Figure 4.152	2001 Summer mean bias of daily precipitation rate compared with NCEP/NCAR Reanalysis.....	255
Figure 4.153	2001 Summer mean bias of monthly accumulated precipitation as compared with NCDC.....	255
<b>2050 SIMULATION</b>		
Figure 5.1	Spatial distribution of January mean temperatures at 2-m simulated by GWRF 2001 and 2050 simulations.....	259
Figure 5.2	Spatial distribution of January mean water vapor mixing ratio at 2-m simulated by GWRF 2001 and 2050 simulations.....	261
Figure 5.3	Spatial distribution of January mean downward shortwave flux at the surface simulated by GWRF 2001 and 2050 simulations.....	263
Figure 5.4	Spatial distribution of January mean downward longwave flux at the surface simulated by GWRF 2001 and 2050 simulations.....	264
Figure 5.5	Spatial distribution of January mean daily precipitation rate simulated by GWRF 2001 and 2050 simulations.....	266
Figure 5.6	Spatial distribution of July mean temperature at 2-meter simulated by GWRF 2001 and 2050 simulations.....	269
Figure 5.7	Spatial distribution of July mean water vapor mixing ratio at 2-meter simulated by GWRF 2001 and 2050 simulations.....	270
Figure 5.8	Spatial distribution of July mean downward shortwave flux at the surface simulated by GWRF 2001 and 2050 simulations.....	272
Figure 5.9	Spatial distribution of July mean downward longwave flux at the surface simulated by GWRF 2001 and 2050 simulations.....	274
Figure 5.10	Spatial distribution of July mean daily precipitation rate by GWRF 2001 and 2050 simulations.....	275

## ACRONYMS

<u>Acronym</u>	<u>Definition</u>
AGCM	Atmospheric General Circulation Model
AMIP	Atmospheric Model Intercomparison Project
AOD	Aerosol Optical Depth
AR4	IPCC 4 <sup>th</sup> Assessment Report
ARW	Advanced Research WRF core
BC	Boundary Conditions
BSRN	Baseline Surface Radiation Network
CalTech	California Institute of Technology
CAM3	NCAR Community Atmospheric Model Version 3
CAPE	Convective Available Potential Energy
CCM	Community Climate Model
CCOS	2000 Central California Ozone Study
CCSM	Community Climate System Model
CFL	Courant-Friedrich-Levy
CMAP	CPC Merged Analysis of Precipitation
CMIP	Coupled Model Intercomparison Project
CPC	Climate Prediction Center
CRM	Cloud Resolving Model
DJF	December, January, February

ECHAM4	ECMWF Hamburg Model Version 4 (Max Planck Institute)
ECMWF	European Centre for Medium-Range Weather Forecasts
ENIAC	Electronic Numerical Integrator And Computer
ENSO	El Nino Southern Oscillation
ERA	ECMWF Re-Analysis
ERBE	Earth Radiation Budget Experiment
FEWS	African Famine Early Warning System
GCM	General Circulation Model
GEBA	Global Energy Balance Archive
GEWEX	Global Energy and Water Cycle Experiment
GFDL	Geophysical Fluid Dynamics Laboratory
GFS	Global Forecasting System
GISS	Goddard Institute for Space Studies
GLW	Downward Longwave Flux at the Surface
GPCP	Global Precipitation Climatology Project
GWRF	Global WRF
IC	Initial Conditions
IPCC	Intergovernmental Panel on Climate Change
ITCZ	Inter-Tropical Convergence Zone
JJA	June, July, August
LBC	Lateral Boundary Conditions

LSM	Land Surface Module
MCS	Mesoscale Convective System
MM5	PSU/NCAR model Mesoscale Model Version 5
NCAR	National Center for Atmospheric Research
NCDC	National Climatic Data Center
NCEP	National Center for Environmental Prediction
NCL	NCAR Command Language
NEAQS	2002 New England Air Quality Study
NMB	Normalized Mean Bias
NME	Normalized Mean Error
NOAA	National Oceanic and Atmospheric Administration
NWP	Numerical Weather Prediction
OLR	Outgoing Longwave Radiation
PBL	Planetary Boundary Layer
PSU	Pennsylvania State University
Q2	Water Vapor Mixing Ratio at 2-meters
QPF	Quantitative Precipitation Forecasts
RAINNC	Convective Precipitation
RAINNC	Non-convective Precipitation
RCM	Regional Climate Model
RMSE	Root Mean Square Error

RRTM	Rapid Radiative Transfer Model
SREF	Short-Range Ensemble Forecast
SRES	Special Report on Emission Scenarios
SST	Sea Surface Temperature
SWAbs	Net shortwave absorbed
SWDOWN	Downward Shortwave Flux at the Surface
T2	Temperature at 2-meters
TexAQS	Texas Air Quality Experiment
TIROS	Television and Infrared Observation Satellite
TOVS	TIROS Operational Vertical Sounder
TRMM	Tropical Rainfall Measuring Mission
U10	Zonal wind at 10-meters
UCLA	University of California at Los Angeles
U.K.	United Kingdom
V10	Meridional wind at 10-meters
WCRP	World Climate Research Program
WPS	WRF Preprocessing System
WRF	Weather Research and Forecasting model
WSM3	WRF Single Moment 3-Class
WSM6	WRF Single Moment 6-Class

## CHAPTER 1. INTRODUCTION

### 1.1 Background and Motivation

The Weather Research and Forecasting (WRF) model was originally developed as a multi-agency initiative at the National Center for Atmospheric Research (NCAR) to develop a model for both atmospheric research and operational forecasting (Skamarock, 2007). The goal of the NCAR WRF development team was to improve some of the weaknesses of the Pennsylvania State University/NCAR model, known as the Mesoscale Meteorological Model, Version 5 (MM5) in the modeling community. Goals were to develop a new model that is flexible, portable across a number of common High Performance Computing environments, and to utilize parallel computing environments to improve the speed and efficiency of the code (Skamarock, 2007). The development of WRF is unique in that it is maintained as a “community” model, in which the code developers allow the code to be downloaded and run by anyone, and rely on researchers to recommend improvements for functionality. The WRF system also allows users to interchange the various cores and physics packages, which is useful for inter-model evaluations and module sensitivity studies (Rao et al., 2007). By 2008, WRF had over 6,000 users around the world, being utilized in many different areas of atmospheric research (Skamarock et al., 2008).

The Global WRF (GWRF) in the latest WRF Version 3.0 (WRFV3) released in 2008, is an extension of previous versions of mesoscale WRF. Mesoscale WRF was originally modified by Mark Richardson’s group at the California Institute of Technology (CalTech) beginning in 2004 for application to the Earth’s global atmosphere through three key modifications: modification of projection from conformal to non-conformal grid, addition of a filter for polar boundary conditions, and adaptation of planetary constants and timing parameters for Earth (Richardson et al., 2005). The original version of mesoscale WRF was on a conformal grid, meaning that the map scale factors that relate model space to actual space were independent of direction. The global version of the model requires a non-conformal grid because it uses a

spherical coordinate, e.g., the model's  $x$  and  $y$  directional components for each grid cell are not equal. Thus the model's map scale factors had to be altered to allow for a latitude-longitude projection. The second major modification to mesoscale WRF is that GWRP uses polar Fourier filters to handle polar boundary conditions (BCs) and to reduce model instabilities near the poles. A visualization of mass transport around the poles in GWRP is presented in Figure 1.1.

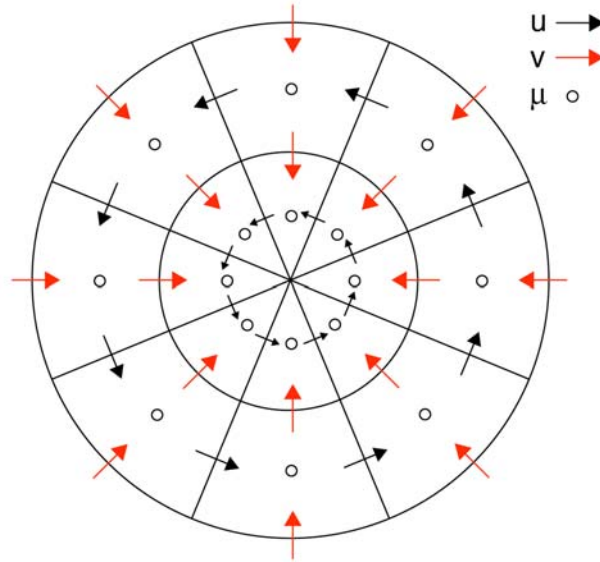


**Figure 1.1** A graphical representation of transport around the polar regions of GWRP. The symbol “ $\mu$ ” represents a mass point in the model, “ $u$ ” represents the zonal component of wind velocity, and “ $v$ ” represents the meridional component of wind velocity. Taken from Skamarock (2008).

These polar filters are necessary because with a constant time-step, the large difference in grid cell size between cells at the equator and cells at high latitudes would cause the model to violate the Courant-Friedrich-Levy (CFL) condition. To adapt the planetary model to the Earth, as opposed to other planets, certain Earth-specific planetary constants and timing conventions have also been incorporated into GWRP. These planetary constants include parameters distinct to the Earth such as correct acceleration due to gravity, reference pressure, and ideal gas constants. The necessary timing conventions include orbital parameters specific to Earth and the relationship between actual time and simulation time. This latter relationship is necessary

because the GWRF core calculates timing parameters based on Earth seconds (i.e., 24 hours per day, 60 minutes per hour, 60 seconds per minute). Therefore, the relationship derived for other planets will not be accurate when used for the Earth, and the model must convert from that planet's timing convention to Earth's before integration so that there are always an integer number of time-steps per day. At the WRF/MM5 User's Workshop in June 2005, Mark Richardson and faculty at the California Institute of Technology (CalTech) and Kobe University presented their WRF code modifications for application to planetary atmospheres such as Titan and Mars (Richardson, 2005). The first journal article about the performance of planetary WRF for the atmospheres of Titan and Mars was published by Richardson et al. (2007) which demonstrated that the code is applicable to a variety of planets and physical scales. On April 4<sup>th</sup>, 2008 NCAR released version 3.0 of the WRF package (WRFV3) which contains the latest version of the GWRF code. GWRF, initially designed to study the atmospheres and climate systems of other planets such as Titan and Mars, enables modeling of global climate of the Earth system and the coupling between weather systems on global and regional scales (Richardson et al., 2007). One of the main advantages of using GWRF is to provide initial and boundary conditions for the mesoscale version of WRF thus avoiding inaccuracies arising from the use of different models with inconsistent model physics. The global domain in GWRF also enables a unified framework for the modeling of atmospheric processes from global to local scales.

## **1.2 Objectives**

The main objective of this study is to evaluate the capability of GWRF for an accurate representation of the global atmosphere by exploring the most accurate configuration of runtime and physics options for current-year and future-year scenarios. Such an evaluation is a critical step toward the extension of GWRF to include emissions and chemistry needed to simulate the global transport of air pollutants, the impact of emissions on global air quality and radiative forcing, as well as forecasting the future climate and air quality. To evaluate GWRF's ability to simulate the atmosphere, model simulations using a variety of physics configurations will be conducted to examine the influence of physical parameterizations on model performance. The

accuracy of physics schemes in atmospheric models is a research topic that is fundamental to the use of models to study atmospheric processes, as well as make accurate predictions of future atmospheric states. In particular, this study examines the use of various physics schemes in the Weather Research and Forecasting model to establish the most accurate physics suited for atmospheric predictions. As climate change comes to the forefront of the environmental sciences, the nesting capability of GWRP presents an opportunity to explore the regional impacts that may occur from a changing climate. The ability of GWRP to simulate future atmospheric states is also evaluated through a simulation for a future year (i.e., 2050). The specific objectives of the proposed thesis research are

- (1) to quantify the accuracy of GWRP model output in reproducing observational and reanalysis data for the year 2001;
- (2) to conduct a number of sensitivity simulations and identify the most appropriate physical parameterizations in GWRP that produce the highest accuracy for global scale modeling for 2001;
- (3) to assess the capability of GWRP to predict future-year climate using benchmark results from an established future climate model.

### **1.3 Overall Technical Approach**

The ability to accurately model the atmosphere is paramount when facing two of the major areas of research in atmospheric sciences: global transport of pollutants and global climate dynamics. Using a global, single-domain atmospheric model represents an improvement in the practical use of the model, because it represents an improvement in computational efficiency. It also represents an improvement in the scientific capability of the simulation over the use of multiple different models (e.g., mesoscale WRF and the Global Forecasting System (GFS)) at multiple different scales (e.g., a continental United States domain and a global domain) because GWRP is a flexible system for global to microscale interactions, which presents a new capability for the scientific exploration of atmospheric dynamics (Richardson et al., 2005). As computer

models are utilized more in atmospheric predictions, the validation of these large scale models is a very important part of evaluating the ability of the model to accurately perform. The rise in the use of computer models is paralleled by an abundance of satellite and ground-based observations. Thus a review of datasets, both remote and ground-based, will be conducted in this research to validate various parameters in global computer models. After a review of the advantages and disadvantages for each dataset used to validate past global models, a comparison will be made between applicable datasets and the recently-developed Global Weather Research and Forecasting (GWRF) system. To accurately predict global transport of pollutants and future climates, the meteorological fields from the global model must first be validated by a representative dataset.

## CHAPTER 2. LITERATURE REVIEW

### 2.1 A brief history of GCMs

In 1922, Lewis Fry Richardson attempted the first forecasts using numerical weather prediction (NWP) and helped make meteorology an exact science with his famous book *Weather Prediction by Numerical Process* published in the same year (Platzman, 1979). This first attempt at NWP exhibited the base characteristics for the first General Circulation Models (GCMs). The most important aspect of this approach was using the finite difference solutions of differential equations in a space divided into grid cells. This approach proved to be impractical at the time due to the large calculation requirements (Randall, 2000). Numerical Weather prediction would not be feasibly utilized until automatic calculations or computational power was developed. This was realized by John Von Neumann in 1946, who envisioned the application of numerical simulation to meteorology for regional forecasting, which could then lead to climate modeling (Randall, 2000). The inspiration for this conclusion was the recently-developed Electronic Numerical Integrator And Computer (ENIAC). Charney et al. (1950) used ENIAC to complete the first computerized weather forecast. This model used a two-dimensional grid for North America with a time step of three hours, and 270 grid points of 700 km spacing (Charney et al., 1950). It is of great importance that at this point in time, models used simplifying assumptions (i.e., barotropic and baroclinic models) and were not based on Bjerknes/Richardson primitive equations until the 1960s, which was a direct consequence of increased computational power. The first modeling experiment utilizing the primitive equations was conducted by Hinkelman in 1959 (Randall, 2000). ENIAC continued to be a milestone in NWP when Phillips (1956) conducted the first GCM experiment as it is known today by using a model with two layers that used the quasi-geostrophic approximation. What made this model different was that it was a hemispheric representation, where as previous models were regional or continental (Randall, 2000).

Joseph Smagorinsky and Syukro Manabe at the General Circulation Research Laboratory (now known as the Geophysical Fluid Dynamics Laboratory) made valuable contributions to the

growing field of GCM experimentation and laid the ground work for later GCM development (Randall, 2000). In the mid 1950s, Smagorinsky working with Phillips, Von Neumann, and Charney developed a two-level, zonal hemispheric model based on the primitive equations (Smagorinsky, 1958). In the early 1960's, Smagorinsky and Manabe published a paper reporting the results from their hemispheric, nine layer GCM based on the primitive equations (Smagorinsky et al., 1965). Later Manabe was the first to publish papers using NWP experiments to gauge the effects of carbon dioxide doubling (Manabe, 1970, 1971) as well as the first ocean-atmosphere coupled model (Manabe and Bryan, 1969). These issues are still a topic of GCM research and improvement today.

The development of GCMs in the 1960s and 1970s were greatly influenced by the group at the University of California at Los Angeles (UCLA), including such scientists as Mintz and Arakawa. This was due to technical innovation, as well as a willingness to share information in the pursuit of the overall scientific objective (Randall, 2000). The most revolutionary of the models produced during this time was the UCLA II which began production in 1965 (Randall, 2000). The UCLA II was a two-level model which exhibited thus far the smallest horizontal resolution of any GCM at  $4^\circ$  latitude  $\times$   $5^\circ$  longitude. Another important aspect of this GCM was that it pioneered a new horizontal, finite difference grid structure named the Arakawa-Lamb B Grid (Arakawa and Lamb, 1977). This grid was altered for UCLA III and is still in use at UCLA for some current GCMs (Randall, 2000). This is also the horizontal grid used in the current WRF-ARW (WRFV3) core used in this study. During this time there was also important development occurring at the National Center for Atmospheric Research (NCAR). NCAR's most lasting contribution during this time was the Community Climate Model (CCM) series, which was utilized on a large scale by researchers and thus placed a large emphasis on model documentation (Randall, 2000). NCAR's continued development of this model has evolved to the present CCSM3, which was used in the IPCC 4<sup>th</sup> assessment report (Randall, 2007). The late 1960s and early 1970s introduced a number of innovative ideas into the GCM community. Manabe et al. (1975) continued his work on coupled ocean and atmospheric GCMs, and

improved the continent-ocean representation from his previous work (Manabe, 1969). This time period was characterized by an increase in computational power, which allowed for the idea of spectral transforms to be realized about 1970. Spectral transforms are a way to simplify the solutions of the nonlinear partial differential equations used in the models for the primitive equations. They use orthogonal spherical harmonics to express the horizontal variation of model fields (Randall, 2000). Another one of Manabe's experiments, the effect of global temperature in response to an increase of carbon dioxide (CO<sub>2</sub>) gained scientific notice at this time. In 1975 Manabe and Wetherald completed the first GCM experiment to study the effect on temperature by CO<sub>2</sub> doubling (Randall, 2000). This was in response to the observations of increasing CO<sub>2</sub> from the Mauna Loa observatory. The use of GCMs to predict future climates based on increases of CO<sub>2</sub> caused GCM development to come to the forefront in politics, and a frequently conducted experiment. A possible increase in global temperature or global warming became a topic of scientific debate that continues today (Randall, 2000). Due to Keeling's observations, the National Academy of Sciences asked a panel of scientists to investigate this possible correlation between anthropogenic rise in CO<sub>2</sub> and an increase in temperature in future climates. Jule Charney was the head of this group and the report provided an overview of the problems and uncertainties in this type of climate modeling to policy makers, as well as scientists (Randall, 2000).

Important work in this type of GCM experimentation continued through the mid-1980s, as James Hansen at the Goddard Institute for Space Studies (GISS) produced a number of important experiments concerning the effect of humans on the atmosphere. The report "Climate sensitivity to increasing greenhouse gases" explored the causes and calculation of climate sensitivity, as well as the prediction of future temperature trends (Hansen, 1984). Hansen also published a similar paper that year using GCMs to investigate the possible feedbacks associated with climate change (Hansen, 1984). After an intense period of development, the focus of the GCM community became which problems to focus on and how to build reliable datasets. It was clear that this was the direction of future research involving GCMs; however the models still

contained many assumptions and parameterizations which called for further improvement. The improvements that would be explored in the following years dealt with improving the coupled atmospheric and oceanic GCMs, modeling the Antarctic ozone hole, capturing inter-annual trends, modeling ENSO events, and the inclusion of aerosols. In 1990, the Intergovernmental Panel on Climate Change (IPCC) released its first report, which utilized GCMs to simulate future climates (IPCC, 1990).

The eruption of Mount Pinatubo in the Philippines provided a data set to test GCMs against large scale atmospheric aerosol releases. This research was spurred by James Hansen publishing an initial report on the potential for the Pinatubo eruption to affect climate (Hansen, 1992). In the early 1990s, the first Atmospheric Model Intercomparison Project (AMIP I) began as an attempt to evaluate the performance of 29 different GCMs on inter-annual time scales based on their simulated variables from realistic conditions. These realistic conditions are a reanalysis of the period from 1979 to 1988, which contains the well documented 1982-1983 ENSO event. This represents a large scale inter-comparison of the performance of coupled GCMs by the international atmospheric modeling community. The comparison would be repeated in the following years forming the projects named AMIP II and III. Inter-comparisons of GCMs through the AMIP programs and the IPCC reports would continue to influence GCM use through the present day. Although little actual GCM code development occurred in the recent past, GCMs are still used in many important experiments throughout the scientific community, and their evaluation is still very important.

**Table 2.1 Brief Summary of GCM history compiled from Wen 2007 and Randall 2000.**

<b>Year</b>	<b>Name</b>	<b>Dimensions</b>	<b>Domain</b>	<b>Grid Spacing</b>	<b>Vertical Resolution</b>
1950	Charney ENIAC	2	North America	700 km	none
1956	Phillips	3	Hemispheric	375 × 625 km	2
1959	Smagorinsky	3	Hemispheric	5° × 5°	9
1965	Livermore Atmospheric Model	3	Hemispheric	5° × 5°	5
1973	NCAR 3	3	global	5° × 5°	6
1977	UCLA II	3	global	4° × 5°	2
1990	IPCC First Report	3	global	5.6° × 5.6°	varies
1994	ECHAM4	3	global	2.8° × 2.8°	19
1995	IPCC Second Report	3	global	2.8° × 2.8°	varies
2001	IPCC Third Report	3	global	1.8° × 1.8°	varies
2007	IPCC Fourth Report	3	global	1° × 1°	varies
Current	NCAR	3	global	1.4° × 1.4°	26
Current	GFDL	3	global	2.0° × 2.5°	24
Current	U.K MetOffice	3	global	2.5° × 3.75°	19
2007	GWRF	3	global	125 km	27

## 2.2 Current state of GCMs

To interpret the results from GWRP and understand how it compares with other climate and forecasting models, it is important to review the current abilities and shortcomings of GCMs used in the atmospheric sciences.

**Table 2.2 Summary of current state of GCMs.**

Model	Temperature bias (°C)	Temperature Corr	Precipitation bias (mm day <sup>-1</sup> )	Precipitation Corr	SLP Corr	Specific Humidity bias
AMIP	< ± 2	0.97	-	0.7-0.9	0.7-0.9	-
CMIP	< ± 2	0.93	1.0	0.4-0.7	0.7-0.9	-1 g kg <sup>-1</sup>
GFDL	-2	-	0.15	0.90	-	-
IPCC AR4	< ±2	0.98	-	-	-	< 10%

### 2.2.1 Coupled Model Intercomparison Project (CMIP)

CMIP is an attempt to compare and contrast the global coupled ocean-atmosphere general circulation models used in support of research relied on by the 4<sup>th</sup> Assessment Report (AR4) of the Intergovernmental Panel on Climate Change (IPCC). The models used in CMIP are highly sophisticated; therefore their performance may be used as an upper bound on global model performance. Covey et al. (2003) indicate that the difference between a typical model simulation and a baseline set of observations is not much greater than the difference between different sets of observations. To the extent that different sets of observations (including model-based reanalyses) are equally reliable, this result implies that coupled GCM control runs are nearly as accurate as what the observational uncertainty allows them to be. Over most of the globe, the annual mean simulated surface temperature differs from observations by less than 2 °C, although larger differences are apparent in Polar Regions. These annual departures may be much smaller

than winter or summer seasonal errors reported by Lambert and Boer (2001). Zonally-averaged results show that all of the individual models in CMIP are successful in reproducing observed temperature structure, except in Polar Regions and over high terrain. The model mean temperature is generally too cold in the troposphere and polar stratosphere and too warm at lower latitudes in the stratosphere. For surface air temperature, all models achieve a correlation with observation greater than 0.93, for modeled sea level pressure the correlation with observation falls in the range 0.7-0.9; for modeled precipitation it falls in the range 0.4-0.7 (Covey et al., 2003). These results agree with the qualitative statement that models simulate temperature best, sea level pressure less well, and precipitation worst (e.g., Gates et al., 1996).

CMIP also provides insight into the abilities and shortcomings of global coupled models to predict precipitation. The study produces a relatively large inter-model standard deviation, showing that the models have difficulty in producing consistent precipitation simulations, which the authors explain with three reasons. First, this result should be expected because precipitation is a small scale process, secondly, there exist differences among the models in horizontal resolution and sub-grid scale parameterization schemes, and thirdly because precipitation is a difficult field to observe (Covey et al., 2003). Using Xie and Arkin (1997) precipitation observations for evaluation, the authors find that the models simulate approximately  $1 \text{ mm day}^{-1}$  too much precipitation in the mid-latitudes and too little in the tropics however the models correctly simulate the position of the annual mean Inter-Tropical Convergence Zone (ITCZ) slightly north of the Equator (Covey et al., 2003). The authors also report that the results for specific humidity display a systematic underestimate in the low latitude troposphere, although the departure of the model mean from ECMWF/ERA reanalysis is small ( $\sim 1 \text{ g kg}^{-1}$ ).

### **2.2.2 Atmospheric Model Intercomparison Project (AMIP)**

AMIP (Bader, 2004) is similar to CMIP, except that the models are the atmospheric component of the coupled system only. The study reports overall good performance for vertical temperature profile; besides an upper troposphere ( $\sim 200 \text{ hPa}$ ) summertime cold bias, throughout the troposphere the multi-model ensemble mean has differences of less than  $2 \text{ }^\circ\text{C}$  when

compared with the NCEP/NCAR Reanalysis. Annual mean surface temperature is also well simulated with correlation coefficients generally greater than 0.97 when compared with observations. Seasonal mean surface temperature is also discussed for winter (December, January, February (DJF)) and summer (June, July, August (JJA)) and exhibit slightly lower correlation coefficients with mean values of 0.95. Surface temperature prediction can be highly sensitive to topography, particularly in mountain areas and high plateaus where the mean model is more than 10 °C cooler than the reference data (Bader, 2004). Results for mean model specific humidity exhibit cross-section differences which suggest that the models are too dry in the tropical and subtropical lower troposphere, while elsewhere a comparison with ERA15 suggests that the mean model is too moist. Precipitation is discussed in depth and certain trends and conclusions are made about the ability of the GCMs to predict the location and amount of precipitation. Bader (2004) state that aside from uncertainties associated with the observations, the mean model overestimates the mid-latitude precipitation except in the Northern Hemisphere summer. In the tropics, the mean model compares well with the data in winter (DJF), but underpredicts summer (JJA) precipitation. The precipitation correlation coefficient of the mean model ranges between 0.7 and 0.9. Spatially, the authors show that the mean model overpredicts rainfall mid-latitudes of both the Northern and Southern Hemispheres, particularly in the 30°-40° latitude band. This is in stark contrast to the Tropics, in which the mean model underestimates precipitation tropical convergence zones. The authors suggest that the simulated ITCZ may not migrate with the seasons as much as is expected (Bader, 2004).

### **2.2.3 IPCC AR4**

The IPCC is a non-governmental body established by the World Meteorological Organization (WMO) and the United Nations Environment Programme (UNEP) to provide an objective source of information about climate change. The IPCC reports often reiterate the findings of AMIP and CMIP, and the portions of the report discussed here focus on Chapter 8, Climate Models and their Evaluation (Randall et al., 2007) and Chapter 11, Regional Climate

Projections (Christensen et al., 2007) of the IPCC AR4 to understand the current ability of GCMs to predict meteorological parameters on a global and regional scale. Randall et al. (2007) state that the mean model absolute error (outside Polar Regions and other data-poor regions) is less than 2 °C for surface temperature, which agrees with the findings of AMIP and CMIP. However, the authors also point out that individual models typically have larger errors, but in most cases still less than 3°C, except at high latitudes. Some of the larger errors in the mean model and individual models occur in regions of sharp elevation changes, which the authors explain as a result of inconsistencies between the smoothed model and actual topography. The report also states a tendency in the mean model for a slight, but general, cold bias. Correlation coefficient between the simulated and observed spatial patterns of annual mean temperature is typically about 0.98 °C for individual models. In the vertical, the multi-model mean absolute error in the zonal mean, annual mean air temperature is almost everywhere less than 2°C, with the exception of a high latitude cold bias near the tropopause. The IPCC also reports on the geographic distribution of rainfall in GCMs, with lower precipitation rates at higher latitudes, and higher precipitation rates at lower latitudes. There are local maxima at mid-latitudes, reflecting the tendency for GCMs to suppress precipitation in the subtropics and for storm systems to enhance precipitation at mid-latitudes. Randall et al. (2007) state that models capture these large-scale zonal mean precipitation differences, suggesting that they can adequately represent these features of atmospheric circulation, with rain-bearing systems being the largest source of inaccuracy. The IPCC also discusses the distribution of water vapor, with most models reproducing the overall trend of a decrease in humidity with both latitude and altitude. The multi-model mean bias in humidity, zonally and annually averaged, is less than 10% throughout most of the lower troposphere compared with reanalysis data.

Chapter 11 of the IPCC AR4, Regional Climate Projections (Christensen et al., 2007), provides insight into the current ability of GCMs to predict atmospheric states in various geographical regions around the world. The first region that the report discussed is Asia, in which the authors summarize basic features and known inaccuracies in models. The annual

average surface temperature range simulated over Asia is from  $-2.5^{\circ}\text{C}$  over the Tibetan Plateau to  $-1.4^{\circ}\text{C}$  over South Asia. For most of Asia, there is a  $6^{\circ}\text{C}$  to  $7^{\circ}\text{C}$  range in individual surface temperature model biases. The median bias in precipitation is less than 10% in Southeast Asia, South Asia, and Central Asia, however certain regions in Asia (e.g., Northern Asia and East Asia) exhibit larger values of +23%, and Tibetan Plateau exhibiting a very large value of +110%. Annual biases of rainfall in individual models are in the range of  $-50$  to  $+60\%$  across all regions except the Tibetan Plateau, where some models simulate annual precipitation 2.5 times that observed and even larger seasonal biases occur in winter and spring (Christensen et al., 2007). Christensen et al. (2007) state that the errors GCMs exhibit for the reproduction of accurate meteorology over Tibet is a difficulty simulating the effects of topography, as well as albedo feedbacks due to extensive snow cover. The next region mentioned in the report is Africa, over which most models reproduce temperature well, with the authors stating that the temperature biases are small enough to not affect the credibility of the model projections. However, precipitation is not as well predicted in southern Africa, with 90% of models in the IPCC overestimating precipitation in this region, by more than 20% on average (and in some cases by as much as 80%). The seasonal area mean temperature biases in northern Europe vary from  $-5^{\circ}\text{C}$  to  $6^{\circ}\text{C}$ , depending on specific location, model, and season. In the European summer, most models simulate too little precipitation, with better estimates found in southern Europe and the Mediterranean region. The IPCC also discussed the representation of both the Arctic and Antarctic regions in global models. When compared with the European Centre for Medium-Range Weather Forecasts 40-year (ERA40) Reanalysis, simulations over the Arctic are  $1^{\circ}\text{C}$  to  $2^{\circ}\text{C}$  colder than the reanalysis data, with larger biases over the high terrain areas of Alaska and northwest Canada. The annual bias pattern (positive over most parts of the Arctic) can be partly attributed to coarse topography and biased atmospheric storm tracks and sea ice cover. When simulations over the Antarctic are compared to National Centers for Environmental Prediction (NCEP) reanalysis, the mean bias is predominantly less than  $2^{\circ}\text{C}$  (Carril et al., 2005). North America is the next region the authors discussed, with ensemble-mean regional mean bias

ranging from  $-2.4\text{ }^{\circ}\text{C}$  to  $+0.4\text{ }^{\circ}\text{C}$  depending on region and season. Almost all of the models used in the IPCC overestimate precipitation for western and northern North America. The ensemble-mean regional mean precipitation bias varies from  $-16\%$  to  $+93\%$  depending on region and season. The ensemble-mean precipitation is excessive on the windward side of major mountain ranges, with overpredictions reaching  $1\text{ to }2\text{ mm day}^{-1}$  over high terrain in the western portion of the continent. Another study that investigated the prediction over a region of the Southern Plains ( $10^{\circ} \times 10^{\circ}$ ), used an ensemble of six Regional Climate Models (RCMs) in the North American Regional Climate Change Assessment Program (NARCCAP; Mearns et al., 2005) and had 76% of all monthly temperature biases within  $\pm 2\text{ }^{\circ}\text{C}$  and 82% of all monthly precipitation biases within  $\pm 50\%$ , for a single year. In the Central America and Amazon regions, most models have a cold bias of  $0\text{ }^{\circ}\text{C}$  to  $3\text{ }^{\circ}\text{C}$ , while performance is better in southern South America where average biases are close to zero. The mean simulation of South American temperatures shows a warm bias around  $30^{\circ}\text{S}$  and in parts of central South America, while over the rest of South America the biases tend to be predominantly negative. Annual precipitation bias over South America is in the range of  $-15\text{ to }25\%$ , with the largest biases occurring when precipitation is slight. For both the Amazon and southern South America, the ensemble annual mean precipitation is drier than observations, with about 60% of the models exhibiting a negative bias. The ensemble mean of temperatures over Australia is biased cold over land, with the coldest bias being larger than  $2^{\circ}\text{C}$ . Over northern Australia, the mean model error is 20% more precipitation than observed, however there is a large range of biases ( $-71\text{ to }+131\%$ ). The mean annual bias in southern Australian is  $-6\%$ , and the range of biases is smaller ( $-59\text{ to }+36\%$ ).

#### **2.2.4 Geophysical Fluid Dynamics Laboratory Model (GFDL)**

The GFDL Model is a sophisticated, coupled climate model that was included in the IPCC report. Temperature estimates from this model are compared with the NCEP–NCAR reanalysis. The model exhibits a cold tropospheric and warm stratospheric bias throughout the year, with typical seasonal mean temperature errors of 2 K for the troposphere and 4 K for the stratosphere. The largest model bias is a cold bias which occurs at the high latitudes of the

Southern Hemisphere from 100 to 500 hPa, which is common to many climate models (Anderson et al., 2004). The simulation of precipitation in GFDL is compared with the Climate Prediction Center (CPC) Merged Analysis of Precipitation (CMAP) (Xie and Arkin, 1997), and produces a high correlation coefficient (0.90). The geographic locations of the largest errors are underestimations of precipitation to the west of Maritime Continents, in the tropical and South Atlantic convergence zones, and in the eastern Pacific ITCZ (Anderson et al., 2004).

Precipitation overestimations occur over tropical Africa, the western Indian Ocean, and the northwest tropical Pacific Oceans. The GFDL simulates too much summertime precipitation in Siberia, Alaska, and northern Canada with the model producing double the CMAP precipitation. The positive bias in summertime high-latitude precipitation is also present in the annual mean and is common to many models. The global mean precipitation is  $0.15 \text{ mm day}^{-1}$  higher than the CMAP mean of  $2.68 \text{ mm day}^{-1}$ . The simulation of relative humidity in the model is compared to the Television and Infrared Observation Satellite (TIROS) Operational Vertical Sounder (TOVS; Soden and Bretherton 1993), and exhibits a moist bias in the upper troposphere (200–500 hPa). The moist bias from satellite observations is also present in both the ECMWF and NCEP–NCAR reanalyses, which indicate a moist bias in both relative and absolute humidity in the middle tropical troposphere. The model’s column water vapor, a measure primarily of lower tropospheric water vapor, is slightly low, partially reflecting the model’s cold bias.

### **2.2.5 Community Atmospheric Model version 3 (CAM3)**

The Community Atmospheric Model (CAM3) version 3 is the latest version of the climate model produced by NCAR. The simulation of precipitation in CAM3 is examined and compared with CMAP by Hurrell et al. (2006). The authors show that during winter (DJF), large rainfall rates associated with strong convection in both the South Pacific and South Atlantic convergence zones are reproduced by CAM3. During summer (JJA), rainfall rates are much smaller in both CAM3 and CMAP over these regions. CAM3 also agrees with CMAP estimates by reproducing another maximum in precipitation over middle latitudes during winter, associated with the passage of polar fronts. CAM3 captures many observed features of the global

precipitation distribution, however it shares many biases exhibited by other climate models. For instance, there is a tendency for the simulated tropical precipitation maxima associated with the ITCZ to remain in the Northern Hemisphere throughout the year. During winter, CAM3 produces higher estimates of precipitation over the western and eastern Pacific near the equator, over tropical Africa and the western Indian Ocean. During summer, CAM3 precipitation rates are overestimated over the western Indian Ocean and the Arabian Peninsula, but underestimated rainfall within the Pacific and Atlantic ITCZ.

### **2.3 Horizontal grid resolutions**

A fundamental problem in NWP is the compromise between computational cost and simulation improvements due to finer grid spacing. The mesoscale version of the WRF model is designed for resolutions of 1–10 km, whereas GWRF at its fine resolution of  $1^\circ \times 1^\circ$  has a resolution of approximately 1,000 km at the equator. The role of horizontal resolution and the measure of forecast improvement have been explored by a number of scientists for both meteorological (Mass et al., 2002; Weisman et al., 1997; Salvador et al., 1999) as well as chemical (Jimenez et al., 2005; Baklanov et al., 2002) forecasting. Mass et al. (2002) discusses the overall trend of an increase in computational power and a corresponding increase in horizontal grid resolution, using the National Meteorological Center barotropic model of the late 1950s having a horizontal grid spacing of 381 km and the 2002 NCEP Eta model having a resolution of 12 km as an example. The importance of grid size in mesoscale models, specifically with respect to the structure of convective systems, is discussed in Salvador et al. (1999) and Mass et al. (2002). Mass et al. (2002) references multiple other articles, in which this topic has been explored, with most models requiring a grid spacing of 4 km or less to replicate the observed structural evolution of a variety of mesoscale convective systems, with the most success during strongly-forced convection (e.g., fronts, drylines, or topography). The importance of accurate meteorological predictions to chemical prediction was investigated by Baklanov et al. (2002), with an emphasis on meteorology as a source of uncertainty in air pollution forecasting. This study also references a number of journal publications which state

that on an urban scale, the meteorological fields comprise a main source of uncertainty, which may be larger than the uncertainty in the chemical predictions. Jimenez et al. (2005) state the importance for a high horizontal grid resolution for chemical modeling and the advantages over large grid size simulations, which present a smoothed, homogenous field of chemical species. The optimum choice for horizontal grid resolutions is also investigated in climate models in Hack et al. (2006) which examine two different horizontal grid resolutions for the National Center for Atmospheric Research (NCAR) Community Climate System Model (CCSM). The two resolutions are a coarse T42 (~2.8°) and fine T85 (~1.4°). In this article, the authors state that the higher resolution simulation has a higher level accuracy because of a superior Arctic sea ice representation, as well as a superior land-use representation, which results in an improved simulation of air temperature and hydrology in some regions (Hack et al., 2006). The authors also state that there are some aspects of the simulation that degrade with the high-resolution atmosphere, such as a boreal winter warm bias at high latitudes and an overactive hydrological cycle at northern high latitudes year-round.

## **2.4 Sensitivity to Initial Conditions (IC) and Boundary Conditions (BC)**

### **2.4.1 Sensitivity on a Regional Scale**

Jankov et al. (2007) quantified the influence of various physical parameterizations and initial conditions inside the Advanced Research WRF (ARW) core on Quantitative Precipitation Forecasts (QPF). The study used a 1500 kilometer grid spacing over the central United States for 288 separate simulations with a variety of configurations: three different convective schemes, three different microphysics schemes, two different initialization methods, and two Planetary Boundary Layer (PBL) schemes (Jankov et al., 2007). This inter-comparison of configurations was tested for warm season mesoscale convective system (MCS) rainfall; from this study Jankov et al. concluded that due to the nature of warm season MCS development, convective parameterization and initialization are more important factors than microphysics in QPF bias (Jankov et al., 2007).

Druyan et al. (2007) determined the overall effect of various Initial Conditions (ICs) to Lateral Boundary Conditions (LBCs) in a Regional Climate Model (RCM). The authors quantify this impact by analyzing the outputs from a regional climate model (RCM) over West Africa, and compare the spatial distribution of precipitation to data from the Tropical Rainfall Measuring Mission (TRMM) and the NOAA Climate Prediction Center data for the African Famine Early Warning System (FEWS) (Druyan et al., 2007). The simulation is composed of five members, with five different initial conditions which are staggered by 36 hours from the first IC from May 9<sup>th</sup>, 2003 through May 15<sup>th</sup>, 2003. The RCM is driven by NCEP Reanalysis data from June through September of 2003. With regards to the influence of LBCs and ICs, the authors conclude that during this experiment the LBCs dominated the spatial distribution of precipitation, while the different ICs introduced nearly no perturbations into the overall pattern or smaller configurations of monsoon rain (Druyan et al., 2007).

Jones et al. (2007) explored the use of different Initial Conditions files and physics packages in mesoscale modeling to form Short-Range Ensemble Forecasts (SREFs). SREFs are popular because of their ability to combine a wide variety of initial states and physics schemes into a realistic ensemble forecast. This study utilized twelve different physics configurations and seven different initial conditions to test the ability of MM5 in short-range simulations over the Northeast U.S. on 12 kilometer grid spacing. The seven different initial conditions files were made from five National Center for Environmental Prediction (NCEP) Eta model runs, as well as the NCEP Global Forecast System (GFS). These larger domain simulations were then used as initialization files for the finer domain MM5 model (Jones et al., 2007). The seven IC files were then compared to seven random members of the physics schemes to gauge the influence of IC files to physics used in the model. This validation was completed for the warm season (5/2003 through 9/2003) and the cold season (10/2003 through 3/2004). The study shows that the various physics schemes outperformed the IC files in the cold season. However, when all of the members were compiled into one full ensemble, the authors point to inaccurate physics schemes as the most likely source of error in ensemble predictions (Jones et al., 2007).

Kjellstroem and Ruosteenoja (2007) examined the variability in future climate projections by using ten different RCMs to predict precipitation patterns over the Baltic Sea region. All 10 of the RCMs are driven with the same global climate model, the HadAM2H, and thus have the same LBCs. The ten RCMs are run for a control period of 1961-1990 and a future period of 2071-2100. After these ten control and ten future simulations are run, the authors utilize different emission scenarios, different BCs from other Atmospheric General Circulation Models (AGCMs), and the same LBCs but various ICs. Overall the study concludes that the present day runs indicate an increase in precipitation during the winter months, and that for future scenarios, the IC sea surface temperatures (SST) of the Baltic Sea have a large impact on the predicted precipitation.

#### **2.4.2 Sensitivity on a Global Scale**

Fennessey and Shukla (1998) investigated the impact of initial soil moisture on a coupled atmosphere-biosphere GCM, and examined the results for seasonal predictions. The authors complete a sensitivity study with two different configurations of observed initial atmospheric state and observed SST, with the only major difference being the initial soil moisture values. The authors pointed out the inherent error associated with soil moisture in a GCM due to a lack of global measurements of soil moisture and the variability of soil moisture within any grid box due to the heterogeneity of the land surface (Fennessey and Shukla, 1998). The study concludes that the influence of initial soil moisture is mainly localized and has the greatest impact on near-surface fields. Overall the study shows that using a realistic state of soil moisture is important when making accurate seasonal atmospheric predictions.

Kunkel et al. (2006) use 18 different coupled general circulation models (CGCMs) to complete 55 simulations with a variety of initial conditions, and evaluate their results on a regional scale. The purpose of their study is to reproduce the observed lack of warming over the central U.S. during the 20<sup>th</sup> century, as compared to the rest of the country. Only seven of the simulations recreated a negative temperature trend during the 20<sup>th</sup> century. The authors state that models with the same forcing, but different initial conditions exhibited a large variability.

Kunkel et al. (2006) concluded that the anomalous pattern over the region must have been due to internal variability produced by large scale models with different initial conditions, evaluated on a regional scale. Kunkel et al. (2006) also contributed the lack of correlation between model outputs and observations to external forcing from large scale oscillations.

**Table 2.3 Summary of studies investigating the role of IC/LBCs in GCMs.**

<b>Author</b>	<b>Date</b>	<b>Time Period</b>	<b>Domain</b>	<b>Subject</b>	<b># of ICs</b>
Druyan et al.	Oct-07	6/2003-9/2003	regional	Summer precipitation over West Africa	5
Han and Wang	Sep-07	1958-1999	global	East Asian Monsoon	4
Jankov et al.	Jun-07	2002 convective cases	regional	Convection over the Central U.S.	8
Kjellstroem and Ruossteenoja	May-07	2071-2100	regional	Precipitation over the Baltic Sea region	10
Jones et al.	Feb-07	5/2003-3/2004	regional	Northeastern U.S.	7
Kunkel et al.	2006	1901-1999	global	Cooling in the central United States	55
Fennessey and Shukla	1999	June - August 1988	global	Impact of global soil wetness on NWP	2

Han and Wang (2007) investigated the source of the variability of the East Asian Monsoon from various states of SST and sea-ice by using an AGCM. The model is initialized in four different ways and is forced with observed SST and sea ice distributions from 1958-1999; the model outputs are then compared to the ERA-40 dataset. The authors stated that there is a large discrepancy between the four integrations, and that only one of the simulations correctly reproduced changes observed over China. The authors concluded that the differences in SST and sea ice concentration during the last half century cannot be designated as sources for the inter-decadal variability associated with this monsoon (Han and Wang, 2007).

## 2.5 Radiation schemes

As shown in Table 2.3, the radiation configuration interacts with other physics schemes to calculate not only radiative variables within the model, but also influences potential temperature, water vapor mixing ratios, clouds, and precipitation. Radiation schemes calculate the ground heat budget by providing atmospheric heating based on downward longwave and shortwave radiation. The major processes included in a radiation parameterization are absorption, reflection, and scattering in both the atmosphere and at surfaces (Skamarock et al., 2008). Longwave radiation includes infrared or thermal radiation absorbed and emitted by gases and surfaces during the night. The only source of shortwave radiation in WRF is the sun, and therefore includes the visible and surrounding wavelengths that make up the solar spectrum. Within the atmosphere, the radiation responds to model-predicted cloud and water vapor distributions, as well as specified CO<sub>2</sub>, ozone, and (optionally) traces gas concentrations. All the radiation schemes in WRF currently are column (one-dimensional) schemes, so each column is treated independently. Model sensitivity studies using mesoscale WRF have examined the influence of changes in physical parameterizations to meteorological predictions (i.e., Jankov et al., 1997) and chemical predictions (i.e., Borge et al., 2008) however the examination of sensitivity on a global scale has not been conducted with WRF. This study may help elucidate the differences in sensitivity of physical configurations on a global scale.

**Table 2.4 WRF Radiation Physics Interactions. Adapted from Skamarock et al. (2008).**

<b>Atmospheric State Variable</b>	Potential Temperature	Input/output
	Water vapor	Input
	cloud	input
	precipitation	input
<b>Surface Flux</b>	Longwave up	input
	Longwave down	output
	Shortwave up	input
	Shortwave down	output

### **2.5.1 RRTM Longwave**

The Rapid Radiative Transfer Model (RRTM) was used in WRF's predecessor, MM5. The parameterization is based on the work of Mlawer et al. (1997). It is a spectral-band scheme, with 16 bands (as shown in Table 2.5) that uses the correlated-k method. The correlated k-method is a method for calculating radiative transfer in which k refers to the absorption coefficient which can describe the cumulative distribution of a radiation field within a spectral interval. The main advantage of the correlated-k method is its efficiency in iterative calculations (Goody et al., 1989). RRTM uses pre-set tables to accurately represent longwave processes due to water vapor, ozone, CO<sub>2</sub>, and trace gases (if present), as well as accounting for cloud optical depth.

### **2.5.2 CAM3 Longwave**

The CAM3 Longwave is a spectral-band scheme used in the NCAR Community Atmosphere Model (CAM 3.0) for climate simulations, thus the CAM modules are the only radiative parameterizations in the standard WRF framework designed for a global scale. CAM3

longwave scheme has two spectral bands, as shown in Table 2.5. It has the potential to handle several trace gases and interacts with resolved clouds and cloud fractions (Collins et al., 2004).

### **2.5.3 Dudhia Shortwave**

This scheme is based on Dudhia (1989) and is also taken from MM5. In the original study, it was designed for smaller scale calculations, such as a Cloud Resolving Model (CRM). It has a simple downward integration of solar flux, which accounts for clear-air scattering, water vapor absorption (Lacis and Hansen, 1974), and cloud albedo and absorption. It uses look-up tables for clouds from Stephens (1978) to reduce CPU cost. In WRF version 3.0, the scheme has an option to account for terrain slope and shadowing effects on the surface solar flux.

### **2.5.4 CAM Shortwave**

The CAM3 shortwave module is a 19 band spectral scheme used in the NCAR Community Atmosphere Model (CAM 3.0) for climate simulations. It has the ability to handle optical properties of several aerosol types and trace gases. It uses cloud fractions and overlap assumptions in unsaturated regions, and has a monthly zonal ozone climatology (Collins et al., 2004). The CAM radiation scheme is especially suited for regional climate simulations by having an ozone distribution that varies during the simulation according to monthly zonal-mean climatological data (Skamarock et al., 2008).

### **2.5.5 Goddard Shortwave**

The Goddard shortwave scheme is based on Chou and Suarez (1994). It has a total of 11 spectral bands and considers diffuse and direct solar radiation components in a two-stream approach that accounts for scattered and reflected components. Ozone is considered with several climatological profiles available.

**Table 2.5 Radiation parameterization options in WRFV3 (Skamarock et al., 2008).**

Scheme	Longwave/Shortwave	Spectral bands	absorbers
RRTM	Longwave	16	CO <sub>2</sub> , O <sub>3</sub> , clouds
GFDL LW	Longwave	14	CO <sub>2</sub> , O <sub>3</sub> , clouds
CAM3 LW	Longwave	2	CO <sub>2</sub> , O <sub>3</sub> , clouds
GFDL SW	Shortwave	12	CO <sub>2</sub> , O <sub>3</sub> , clouds
Dudhia (MM5) SW	Shortwave	1	clouds
Goddard	Shortwave	11	CO <sub>2</sub> , O <sub>3</sub> , clouds
CAM3 SW	Shortwave	19	CO <sub>2</sub> , O <sub>3</sub> , clouds

### 2.5.6 Radiation scheme sensitivity studies

There have been a number of studies which investigate the accuracy of radiation predictions in both Mesoscale (Zamora et al., 2005) and global simulations (Wild et al., 1995; Wild et al., 2001; Iacano et al., 2000; Anderson et al., 2004; Bader, 2004). A study conducted by Zamora et al. (2005) was a sensitivity study of radiation parameterization choice using two common mesoscale models: MM5 and the National Centers for Environmental Prediction (NCEP) Eta Model. The MM5 model uses a shortwave radiation scheme that is similar to the Dudhia scheme in WRFV3. Model results are compared to observations taken during the 2000 Texas Air Quality Experiment (TexAQS), the 2000 Central California Ozone Study (CCOS), and the New England Air Quality Study (NEAQS) 2002. The authors showed that the accuracy of model forecast irradiances are strongly dependent on the aerosol optical depth (AOD), with model errors up to 100 W m<sup>-2</sup> when the AOD exceeds 0.1. The authors estimated that the broadband solar fluxes from observations are accurate within  $\pm 10\text{--}15$  W m<sup>-2</sup>. The authors also stated that the results of Husar et al. (1997) suggests sophisticated radiative transfer parameterizations are needed in certain geographical regions to achieve accuracy better than 80–100 W m<sup>-2</sup>. Zamora et al. (2005) finally showed that a poorly-skilled forecast of radiation also results in a misrepresentation of surface temperature, with an 80 W m<sup>-2</sup> error in the clear-sky net irradiance resulting in a 1.5 K model error in forecasted skin temperature. This value suggests

that clear-sky solar irradiance errors can have a significant impact on numerical model performance. Wild et al (1995) and Wild et al (2001) validate radiative fluxes in general circulation models with surface based observations. The article estimates that the accuracy of the incoming shortwave measurements is within  $\pm 2\%$  of the correct value. Wild et al. (1995) estimate the differences between observations and GCM predictions of radiative fluxes greater than  $50 \text{ W m}^{-2}$  which corresponds to an error larger than 5%. This study shows that the majority of GCMs tend to overestimate global annual-mean incoming shortwave radiation at the surface due to an underestimation of atmospheric absorption, with a model-calculated global-mean surface shortwave absorption of  $165 \text{ W m}^{-2}$  accompanied by an overestimation of  $10\text{--}15 \text{ W m}^{-2}$ . The authors also compare the longwave component of the radiative fluxes in GCMs, with the conclusion that incoming longwave radiation at the surface is underestimated in ECHAM3 and other GCMs. This study shows that a common feature among GCMs is the correct simulation of the global mean surface net radiation with an average value of  $102 \text{ W m}^{-2}$ , resulting from an overestimation of shortwave flux and an underestimation of longwave flux. Seasonal and zonal analyses show that the largest overestimate in the incoming shortwave radiation of ECHAM3 is found at low latitudes year round and in the mid-latitude summer ( $\sim 45^\circ$ ), while at high latitudes and in mid-latitude winter the shortwave flux is underestimated. This latitudinal dependence of radiative flux prediction also corresponds to a latitudinal dependence of temperature prediction, with the excessive shortwave input at low latitudes resulting in an air temperature overestimation of  $1\text{--}2 \text{ }^\circ\text{C}$  over the continents, while at high latitudes the low shortwave input results in an underestimation of temperature. The model overestimation reaches up to  $40 \text{ W m}^{-2}$  for a segment near the equator, and a maximum underestimation of  $20 \text{ W m}^{-2}$  near  $60^\circ \text{ N}$  and  $50^\circ \text{ S}$ . Wild et al. (1995) explained this latitudinal dependence on cloud cover, in which the GCMs all substantially underestimated low latitude cloud amount in the annual mean, which is consistent with the overestimation of solar radiation; however the authors stated that inaccuracies in the parameterization of water vapor absorption may also be source of error in models. The authors also examined the longwave portion of the radiative fluxes simulated by GCMs. The longwave

radiation balance is between the surface and atmosphere is determined by two main components: upward longwave radiation, which is the thermal emission by the earth's surface, and downward longwave radiation, which is the atmospheric emission directed to the surface. The downward longwave radiation is a complex function of the vertical distribution of temperature and absorbers, and is very important to discussions about climate change because it is most affected by the presence of radiatively active gases. This study uses radiation measurements from the Global Energy Balance Archive (GEBA), which has a level of accuracy within  $\pm 5 \text{ W m}^{-2}$ . The article reports that at most sites the downward longwave radiation is largely underestimated, with the average model estimate error for a T106 ( $\sim 1^\circ \times 1^\circ$ ) being  $-14 \text{ W m}^{-2}$  or 5%, which corresponds to a mean observation of  $293 \text{ W m}^{-2}$  and a mean simulation of  $278 \text{ W m}^{-2}$  (Wild et al., 1995). The authors state that the major physical process that results in the underestimation is that the presence of low-level clouds substantially increases the atmospheric emission of longwave radiation directed toward the surface. For example, the ECHAM3 model tends to simulate too small fraction of low-level clouds, especially at low latitudes, leading to an underestimation of downward longwave radiation of  $10\text{-}15 \text{ W m}^{-2}$  in these areas.

Wild et al. (2001) update the 1995 study with a comparison of downward longwave fluxes in four of the most sophisticated coupled climate models in the world: ECHAM3, ECHAM4, HadAM2b, and HadAM3, however this time the authors use radiation measurements from the Baseline Surface Radiation Network (BSRN), which is also a dataset used to validate radiative fluxes within GWRP. The authors estimate the accuracy of downward longwave radiation from BSRN measurements is  $2\text{-}3 \text{ W m}^{-2}$ . The spread of the prediction of downward longwave radiation among the models is approximately  $40 \text{ W m}^{-2}$ . Overall, the GCMs calculated generally lower values, in the range of  $2$  to  $14 \text{ W m}^{-2}$ , than what the observations suggested. The authors again state that there is a latitudinal dependence for the accuracy of predicted downward longwave radiation, with the models overall doing better at low latitudes and fluxes with small absolute values, (e.g., cold, dry climates) are significantly underestimated, while the fluxes with higher absolute values (e.g., warm, humid climates) are closer to the observations.

The biases detected in this study are strongly dependent on the water vapor content, with a lack of thermal emission calculated under dry conditions and excessive emission under moist conditions. This suggests that it is primarily the dependence of downward longwave radiation on the water vapor content that is not adequately captured in the radiation schemes. It is likely that these problems are related to the formulation of the water vapor continuum, which to date still poses the largest source of uncertainty in longwave radiation modeling. This result is consistent with Iacono et al. (2000), who found a substantial increase in the downward longwave radiation at high latitudes when they included the RRTM radiation code, which uses the Clough-Kneizys-Davies (CKD) continuum model, in the NCAR Community Climate Model.

The study Anderson et al. (2004) uses the GFDL, a sophisticated climate model coupled with a land model to investigate the ability of GCMs to predict radiative fluxes when compared with observations. The study focuses on the comparison of long-term annual mean outgoing longwave radiation (OLR) and net shortwave absorbed (SWAbs) from AM2–LM2 to ERBE observations. Root-mean-square errors are about  $8 \text{ W m}^{-2}$  for OLR and  $13 \text{ W m}^{-2}$  for SWAbs. The authors stated the relationship of these radiative parameters to the formation of clouds and precipitation in the model, with error patterns for OLR and SWAbs resembling the patterns of the precipitation errors, suggesting that improvements in the simulation of precipitation would be accompanied by improvements in the radiation fields. For the shortwave radiation budget, the most prominent error is the overestimation of SWAbs in the coastal zones of the eastern subtropical oceans in which there is a severe deficit of coastal stratocumulus. The study then uses estimates from GEWEX and GISS for shortwave radiation absorbed at the surface, which is underestimated by  $5 \text{ W m}^{-2}$ . The authors explained that the deficiencies GCMs have with the simulation of clouds are responsible for the majority of the errors in OLR and Swabs.

## **2.6 Cloud microphysics schemes**

The testing and development of the microphysics routines in WRF is an important experiment for code development. Microphysics schemes are designed to consider the effects of precipitation, water vapor, and cloud processes which can be specifically resolved by the grid

cells in the domain (Skamarock et al., 2008). The WRF microphysics schemes include explicitly resolved water vapor, cloud, and precipitation processes. In the latest version of WRF-ARW, the microphysics scheme is carried out at the end of the time-step as a saturation adjustment process; this is because the condensation adjustment should be at the end of the time-step to guarantee that the final saturation balance is accurate for the updated temperature and moisture. As shown in Table 2.5, the various microphysics schemes have varying levels of complexity, with the most sophisticated having liquid, mixed-phase, and ice processes. Mixed-phase processes are those that result from the interaction of ice and water particles, such as riming, which produces graupel or hail. The WRF technical document for version 3.0 (Skamarock et al., 2008) advises using microphysics schemes for grid sizes less than 10 km, where updrafts may be resolved, mixed-phase schemes should be used, particularly in convective or icing situations. For coarser grids the added expense of these schemes is not worth it because riming is not likely to be well resolved (Skamarock et al., 2008).

**Table 2.6 Microphysics options in WRFV3, adapted from Skamarock et al., 2008.**

Scheme	Number of variables	Ice-Phase Processes	Mixed-Phase Processes
Kessler	3	N	N
Purdue-Lin	6	Y	Y
WSM3	3	Y	N
WSM5	5	Y	N
WSM6	6	Y	Y
Eta GCP	2	Y	Y
Thompson	7	Y	Y
Goddard	6	Y	Y
Morrison 2-Moment	10	Y	Y

### **2.6.1 WRF Single Moment 3-Class (WSM3)**

The WRF Single Moment 3-Class (WSM3) scheme predicts three categories of hydrometers, which are: vapor, cloud water/ice, and rain/snow, and is therefore a simple-ice scheme. WSM3 is a revised scheme by Hong et al. (2004) which includes ice sedimentation and other new ice-phase parameterizations. The new approach adapted by Hong et al. (2004) is a diagnostic relation based on ice mass content, rather than temperature, which is used for ice number concentration. The improved computational procedures of WSM3 are described in Hong and Lim (2006). The WRF Single Moment microphysics schemes (e.g., WSM3, WSM5, and WSM6) all share the fact that the freezing and melting processes are computed during the fall-term sub-steps to increase accuracy in the vertical heating profile of these processes. The order of the processes is also optimized to decrease the sensitivity of the scheme to the time step of the model. It follows Dudhia (1989) in assuming cloud water and rain for temperatures above freezing, and cloud ice and snow for temperatures below freezing. This scheme is computationally efficient for the inclusion of ice processes, but lacks super cooled water and gradual melting rates.

### **2.6.2 WRF Single Moment 6-class (WSM6)**

The six-class WRF Single Moment 6-class microphysics scheme (WSM6) extends the other, simpler WSM3 or WSM5 schemes to include graupel. Some of the graupel-related terms follow Lin et al. (1983), but its ice-phase behavior is much different due to the changes of Hong et al. (2004). A new method for representing mixed-phase particle fall speeds for the snow and graupel particles by assigning a single fall speed to both that is weighted by the mixing ratios, and applying that fall speed to both sedimentation and accretion processes is introduced (Dudhia et al., 2008). The behavior of the WSM3, WSM5, and WSM6 schemes differ little for coarser mesoscale grids, but they work much differently on cloud-resolving grids. Of the three WSM schemes, the WSM6 scheme is the most suitable for cloud-resolving grids, considering the efficiency and theoretical backgrounds (Hong and Lim, 2006).

### **2.6.3 Purdue-Lin**

Six classes of hydrometeors are included in the Purdue-Lin Microphysics scheme: water vapor, cloud water, rain, cloud ice, snow, and graupel. All parameterization production terms are based on Lin et al. (1983) and Rutledge and Hobbs (1984) with some modifications, including saturation adjustment following Tao et al. (1989) and ice sedimentation. This is a relatively sophisticated microphysics scheme in WRF, and it is most suitable for use in research studies. The scheme is taken from the Purdue cloud model, and the details can be found in Chen and Sun (2002).

### **2.6.4 Microphysics scheme sensitivity studies**

Depending on the version of WRF, the model exhibits a number of possible microphysics options. Recently a number of studies have been conducted using microphysics to gauge WRF performance. Isidora Jankov from Iowa State University produced two papers in 2007 dealing with various physical parameterization configurations inside the Advanced Research WRF (ARW) core, and their influence on Quantitative Precipitation Forecasts (QPF). The first study used a 1500 kilometer grid spacing for the central United States for two hundred and eighty eight separate simulations with a variety of configurations: three different convective schemes, three different microphysics schemes, two different initialization methods, and two Planetary Boundary Layer (PBL) schemes (Jankov et al., 2007a). This inter-comparison of configurations was tested for warm season mesoscale convective system (MCS) rainfall; from this study Jankov et al. conclude that due to the nature of warm season MCS development, convective parameterization and initialization are more important factors than microphysics in quantitative precipitation forecast bias (Jankov et al., 2007a). The second WRF configuration inter-comparison by Jankov et al. dealt with cold season quantitative precipitation forecasts in the western United States by using a smaller, three kilometer grid spacing with four different microphysics schemes, two different initialization methods, and two PBL schemes. This paper attempts to quantify the feedback between various microphysics and initialization techniques and

concludes that Quantitative Precipitation Forecasts may be improved by selecting the optimal configurations for each environment (Jankov et al. 2007b). Another study which used various WRF configurations to establish the feedback between physics schemes was conducted by Rao et al. (2007). The purpose of this study is to model three separate heavy rainfall events over the Bay of Bengal and India. The paper concludes that WRF has a superior combination of cumulus parameterization and microphysics which allow it to outperform the Eta model in all three scenarios (Rao et al., 2007).

The cumulus parameterization and microphysics schemes used in WRF are the result of several important papers in the field of modeling. As seen in Table 2.5 there are seven types of microphysics used in WRF, however only the WSM3, WSM6, and Purdue-Lin microphysics schemes are evaluated in this study. In 2004, Hong et al. published a paper detailing the need for a revised approach to hydrometeor modeling. The newer approach represented a step forward in the sophistication of Cloud Resolving Models (CRMs) by introducing several improvements that mainly deal with ice initiation and ice number concentration, as well as an accompanying case study which confirmed that microphysics and ice processes are important to all scales and thus needed in cloud, mesoscale, and general circulation models (Hong et al., 2004). Hong et al. followed up this paper in 2006 with a similar topic and suggestions for the formulation of a six class hydrometeor scheme to be utilized by WRF (Hong et al., 2006). In the 2006 study the authors use the same PBL scheme (Yongsei University) as well as the same cumulus parameterization (Kain-Fritsch) in conjunction with the WSM3 and WSM6 microphysics schemes, as used in this study, however at a much finer grid spacing (Hong et al., 2006). The paper concludes that more classes of hydrometeors would benefit the model because the specific ingredients in ice processes had a larger effect than the effect due to sedimentation velocity (Hong et al., 2006).

A number of studies have been conducted which investigate the role that microphysical treatment of hydrometeors plays in influencing forecast accuracy. The effect which microphysical treatment has on the QPF of precipitation in deep convection is explored in

Gilmore et al. (2004a), in which the comparison between a liquid-only and mixed phase microphysics treatment is compared. The study illustrates that the inclusion of ice in microphysics schemes is important when simulating mesoscale storms in the mid-latitudes. Gilmore et al. (2004b) revisited the topic of microphysics treatment in a second paper the same year, in which they showed that warm season precipitation forecasts are sensitive to microphysics treatment in WRF, as well as in the Regional Atmospheric Modeling System (RAMS) and Advanced Regional Prediction System (ARPS). Choice of microphysics parameterization is also important in winter storm forecasts as explored by Tremblay et al. (2001), in which the authors conduct a sensitivity study of the effect that three different microphysical treatments of varying complexity have on cold season QPF, with the more sophisticated cloud treatments producing better QPFs. The radiation budget, as well as QPF, may be affected by the choice of microphysical treatment, which is explored in Medaglia et al. (2005), in which the authors use a cloud resolving model (CRM) to show that precipitation, as well as cloud-radiation differences, exist for the same event when simulating mesoscale storms with different microphysics schemes.

## **2.7 Land Surface Modules (LSMs)**

The land-surface modules (LSMs) in WRF provide heat and moisture fluxes over land and sea-ice points by utilizing atmospheric information from other physical schemes within WRF. LSMs are provided internal information on grid points' state variables and land-surface properties and combine this with atmospheric information from the surface layer scheme, which in turn utilizes information from other physical schemes such as radiative forcing from the radiation scheme, and precipitation forcing from the microphysics and convective schemes. The heat and moisture fluxes provide a lower boundary condition for the vertical transport calculated in the PBL schemes.

**Table 2.7 LSM options in WRFV3, adapted from Skamarock et al., 2008.**

Scheme	Vegetation Processes	Soil Variables (Layers)	Snow Scheme
5-layer (Slab)	N	Temperature (5)	none
Noah	Y	Temperature, Water+Ice, Water (4)	1-layer, fractional
RUC	Y	Temperature, Ice, Water+Ice (6)	multi-layer
Pleim-Xiu	Y	Temperature, Moisture (2)	input only

As shown in Table 2.6, the land-surface models have various degrees of sophistication in dealing with heat and moisture fluxes in multiple layers of the soil and also may handle vegetation, root, and canopy effects, as well as surface snow-cover prediction. The land surface model provides no tendencies, but does update the land's state variables which include the ground (skin) temperature, soil temperature profile, soil moisture profile, snow cover, and possibly canopy properties. There is no horizontal interaction between neighboring points in the LSM, so it can be regarded as a one-dimensional column model for each WRF land grid-point, and many LSMs can be run in a stand-alone mode.

### 2.7.1 Noah LSM

The Noah LSM is the successor to the Ohio State University (OSU) LSM described by Chen and Dudhia (2001). The main improvements on the OSU model are that the Noah LSM predicts soil ice and fractional snow cover effects, has an improved urban treatment, and considers surface emissivity properties (Skamarock et al., 2008). The scheme was developed jointly by NCAR and NCEP. The Noah LSM is a more complex model than the Slab LSM and is a unified code for research and operational purposes, which is almost identical to the code used in the NCEP North American Mesoscale Model (NAM). It is a 4-layer soil temperature and moisture model with canopy moisture and snow cover prediction. The layer thicknesses are 10, 30, 60, and 100 cm (adding to 2 meters) from the top down. Noah LSM includes root zone, evapotranspiration, soil drainage, and runoff, taking into account vegetation categories, monthly

vegetation fraction, and soil texture. The scheme provides sensible and latent heat fluxes to the boundary-layer scheme.

### **2.7.2 Five Layer Thermal Diffusion (SLAB) LSM**

While the Noah LSM is more complex and based on the NAM, the five-layer thermal diffusion (or Slab) scheme is simple, and is based on the MM5 five layer soil temperature model. Soil moisture is also fixed with a land use- and season-dependent constant value, and there are no explicit vegetation effects. Individual layers are 1, 2, 4, 8, and 16 cm thick and below the bottom layer the temperature is fixed at a deep-layer average. The energy budget calculation includes radiation, sensible, and latent heat flux. It also allows for a snow-cover flag, but the snow cover is fixed in time.

### **2.7.3 LSM sensitivity studies**

A number of sensitivity studies have been conducted with WRF to investigate the possible modification of forecast accuracy by LSM choice. Tewari et al. (2004) conducted a sensitivity study of both the Slab and Noah models coupled with WRF and MM5, to investigate the role of the LSM choice in meteorological prediction. Overall the study concluded that the upgraded Noah LSM improves the simulations of temperature and water vapor mixing ratio at 2-meters for both the WRF and MM5 cases, as well as both of the summer and winter cases (Tewari et al., 2004). LSM not only affects near surface variables but studies have shown that the LSM choice affects the structure of convective precipitation. An example of one such study is Holt et al. (2006) in which the authors investigated the sensitivity of convective prediction to LSM choice (including Slab and Noah) to assess the impact of LSM on land-vegetative processes. Comparing model output to field observations, Holt et al. (2006) showed that the simulation with the Slab LSM has larger low-level temperature and moisture biases and root-mean-square errors, as well as larger errors with the location and timing for convection. The article explains these results by concluding that the physical parameterizations in the Slab model are insufficient to properly account for land-vegetative processes such as those occurring along

the dryline and frontal boundaries in this case and that a detailed surface parameterization is necessary for a realistic model forecast. LSM choice has an effect on the accuracy of meteorological prediction, which in turn may affect chemical predictions in an online coupled chemistry and meteorology model, as explored by Misenis et al. (2006) in which the authors conduct a sensitivity study of different LSMs (which include the Noah and Slab LSMs) in WRF/Chem and the resulting effect on meteorological variables and chemical predictions.

## 2.8 Cumulus parameterizations

Cumulus parameterizations in WRF are responsible for the sub-grid-scale effects of convective and shallow clouds, with the main objective being the representation of vertical fluxes due to unresolved updrafts and downdrafts outside of the clouds. They operate only on individual columns where the scheme is triggered and provide vertical heating and moistening profiles and some schemes additionally provide cloud and precipitation field tendencies in the column (Skamarock et al., 2008). The schemes all provide the convective component of surface rainfall. Cumulus parameterizations are theoretically only valid for coarser grid sizes, (e.g., greater than 10 km), where they are necessary to properly release latent heat on a realistic time scale in the convective columns. They have also been found to be helpful on the triggering of mesoscale convection (e.g., 5–10 km), however they generally should not be used when the model can resolve the convective eddies itself (e.g., less than 5 km grid), as recommended by Skamarock et al. (2008).

**Table 2.8 Cumulus parameterization options in WRFV3.0, adapted from Skamarock et al. (2008).**

Scheme	Cloud Detrainment	Type of scheme	Closure
Kain-Fritsch	Y	Mass flux	CAPE removal
Betts-Miller-Janjic	N	Adjustment	Sounding adjustment
Grell-Devenyi	Y	Mass flux	Various
Grell-3	Y	Mass flux	Various

### **2.8.1 Kain-Fritsch cumulus parameterization**

The current version of the Kain-Fritsch scheme (Kain , 2004) is based on previous a modified versions of the scheme (e.g., Kain and Fritsch (1990) and Kain and Fritsch (1993)), but has been modified based on testing within the Eta model. It utilizes a simple cloud model with moist updrafts and downdrafts, including the effects of detrainment, entrainment, and relatively simple microphysics. The updates that Kain-Fritsch made to the scheme involve a minimum entrainment rate which varies as a function of low-level convergence, a minimum convection depth for precipitating clouds that varies as a function of cloud-base temperature, and an improved downdraft parameterization with the mass flux specified as a fraction of updraft mass flux at cloud base.

### **2.8.2 Grell-Devenyi ensemble cumulus parameterization**

While the Kain-Fritsch cumulus parameterization is based on a trigger function for Convective Available Potential Energy (CAPE), CAPE values for a single updraft, Grell and Devenyi (2002) introduced an ensemble cumulus scheme in which multiple cumulus schemes and variants (typically 144) are run within each grid box and then the results are averaged to give the feedback to the model. The schemes are all mass-flux type schemes, but with differing updraft and downdraft entrainment and detrainment parameters, and precipitation efficiencies. These differences in static control are combined with differences in dynamic control, which is the method of determining cloud mass flux. The dynamic control closures are based on CAPE, low-level vertical velocity, or moisture convergence. Those based on CAPE either balance the rate of change of CAPE or relax the CAPE to a climatological value, or remove the CAPE in a convective time scale. The moisture convergence closure balances the cloud rainfall to the integrated vertical advection of moisture. Another control is the trigger, where the maximum cap strength that permits convection can be varied.

### 2.8.3 Cumulus parameterization sensitivity studies

The correct simulation of convection with cumulus parameterizations is a long standing challenge in Numerical Weather Prediction. Current cumulus parameterizations were developed for grid scales of 32 to 48 km (Arakawa, 2004). WRF targets a smaller grid scale, with scales between 1 and 10 km (Skamarock et al. 2005), however cumulus parameterizations typically work at a 12 km grid scale (Wang and Seaman, 1997). Studies about the comparison of cumulus parameterization schemes in the WRF model, and the resulting effect on forecast accuracy have been conducted. One such study (Gilliland and Rowe, 2007) investigated the sensitivity of warm season events in mesoscale WRF by comparing results from three different simulations using the Kain-Fritsch (KF), Betts-Miller-Janjic (BMJ), and Grell-Devenyi (GD) cumulus parameterizations. The authors chose summertime convection to determine the skill of these schemes in representing warm-season convective events, which have been shown (Wang and Seamen, 1997) to be represented less accurately than cold-season events because of the more accurate representation of large-scale forcing during cold-season events (Gilliland and Rowe, 2007). Also, during the warm season, prediction of convection and rainfall may vary due to the different timing and location of initial convection determined by the different cumulus parameterizations. The authors of this study then compared the results from the different simulations, in the context of the approach taken by the cumulus parameterization. Since the KF scheme is dependent on the amount of CAPE, it continues to trigger convection as long as there is CAPE present. Once the scheme is triggered, the KF scheme employs a cloud model to simulate the effects of clouds and their thermodynamic properties allowing heat and water vapor to be entrained into the updraft, which enhances the effectiveness of the updraft to produce precipitation. Overall the KF scheme is able to simulate isolated convection and the resulting precipitation better, due to its CAPE trigger approach. The GD case produced more wider/longer swath of precipitation, but is unable to simulate the isolated precipitation predicted by the KF scheme. In this study, the weakness of the GD scheme was in its early triggering of convection and development of a broad area of convection that is not representative of the actual isolated

nature of the convective cells. Overall, the authors conclude that the representation of summertime convection by WRF differed significantly depending on the choice of convective scheme, with the correct choice of cumulus parameterization depending on its ability to represent the synoptic and mesoscale forcing present in the environment (e.g., dry or moist) (Gilliland and Rowe, 2007).

## CHAPTER 3: SIMULATION DESIGN AND METHODOLOGY

### 3.1 Current-year initialization

GWRP is initialized using the WRF Preprocessing System version 3.0 (WPS3) which was released in April, 2008. This package is a system of programs designed to create input files for real data cases in WRF. The data used as input into WPS3 is from the National Center for Environmental Prediction (NCEP) Final Global Data Assimilation System (FNL) available from the WRF user's website. The NCEP FNL is used to initialize the Global Forecasting System (GFS) model and has a horizontal grid resolution of one degree and a temporal resolution of six hours. This dataset has a horizontal grid resolution of  $1^\circ$  latitude  $\times$   $1^\circ$  longitude and is available every six hours from 7/30/1999 to present. In this proposed thesis work, NCEP FNL data will be used to initialize GWRP in 2001.

### 3.2 Current-year simulation

#### 3.2.1 Baseline simulation

The baseline GWRP simulation will be conducted at a horizontal grid resolution of  $1^\circ \times 1^\circ$ . This simulation features a physics configuration that is designed for a long-term simulation over a global domain, as summarized in Table 3.1. The microphysics parameterization is the WRF Single Moment 3-class (WSM3) scheme, which is a simple-ice scheme with three categories of hydrometers (i.e., vapor, cloud water/ice, and rain/snow). The shortwave radiation option is the Goddard scheme which is a spectral band shortwave radiation scheme that accounts for diffuse and direct solar radiation components. The longwave radiation option is the Community Atmosphere Model (CAM) scheme which is adapted from the NCAR CAM 3.0, and is a spectral band scheme used for climate simulations. The PBL parameterization is the Yonsei University (YSU) scheme, which is an improved version of the Medium Range Forecast (MRF) model PBL scheme. The land-surface model (LSM) is the NOAH model which is the next generation of the Oregon State University LSM and is very similar to the LSM in the North American Mesoscale Model (NAM). The cumulus parameterization is the Kain-Fritsch which is

a modified version of the original scheme for use in an Eta model. It is a simple cloud model with moist updrafts and downdrafts and includes the effects of detrainment, entrainment, and simple microphysics.

### **3.2.2 Sensitivity simulations**

A number of sensitivity simulations will be conducted to evaluate the impacts of re-initialization time period, grid resolutions, and physics parameterizations based on the performance of these output variables. Table 4.1 summarizes the major physics configurations for the proposed sensitivity simulations. Additional simulations are being conducted at coarse ( $4^\circ$  latitude  $\times$   $5^\circ$  longitude) and fine ( $1^\circ$  latitude  $\times$   $1^\circ$  longitude) grid resolutions to examine the model sensitivity to horizontal grid resolution in GWRF for the year 2001. The modular nature of physics in the WRF system allows users to investigate the roles that various parameterizations of microphysics, cumulus formation, land surface models, and radiation have on simulation accuracy. The sensitivity of meteorological variables to various microphysics schemes at a grid resolution of  $1^\circ \times 1^\circ$  will be studied. These microphysics schemes include a simple-ice scheme, specifically the WRF Single Moment 3-class (WSM3) as well as two complex-ice microphysics schemes (i.e., the WRF Single Moment 6-class (WSM6) and the Purdue Lin (PL)). The major difference between the WSM3 and WSM6 schemes is the number of hydrometeor classes. WSM3 has three categories of hydrometers (i.e., vapor, cloud water/ice, and rain/snow). WSM6 and PL have six categories of hydrometers (i.e., vapor, rain, snow, cloud ice, graupel, and cloud water). PL has a combined ice and water saturation process, while WSM6 treats ice and water saturation separately. This part of the study will show how sensitive the model accuracy is to various treatments of ice. The influence of the cumulus parameterization on model performance is also evaluated by conducting a sensitivity simulation using the Grell-Devenyi ensemble scheme and comparing model results with those using the Kain-Fritsch scheme. The parameterization of land surface in the model may have a large effect on model performance; therefore a sensitivity test for Land Surface Models (LSMs) is conducted using the NOAH and Slab LSMs. The NOAH LSM is a complex Land Surface Model which was jointly developed by

NCEP and NCAR. The Slab model is a 5-layer thermal diffusion model based on the LSM in MM5. The Slab model does not account for snow or vegetation processes. Various longwave and shortwave radiation schemes may have an effect on model performance, thus three sets of radiation scheme combinations will be evaluated including Dudhia shortwave and Rapid Radiative Transfer Model (RRTM) long-wave schemes, the CAM shortwave and longwave radiation schemes, and CAM shortwave and RRTM longwave radiation schemes.

**Table 3.1 GWRf baseline and sensitivity simulations.**

Run Name	Resol-ution	Time Period	Micro-physics	Land-Surface Model	Cumulus Parameterization	Short-wave	Long-wave	PBL
Baseline	1°x1°	2001	WSM3	NOAH	Kain-Fritsch	Goddard	CAM	YSU
CMP1	1°x1°	DJF, JJA 2001	WSM6	NOAH	Kain-Fritsch	Goddard	CAM	YSU
CMP2	1°x1°	DJF, JJA 2001	Purdue Lin	NOAH	Kain-Fritsch	Goddard	CAM	YSU
LSM	1°x1°	JJA 2001	WSM3	Slab	Kain-Fritsch	Goddard	CAM	YSU
RAD1	1°x1°	JJA 2001	WSM3	NOAH	Kain-Fritsch	Dudhia	CAM	YSU
RAD2	1°x1°	JJA 2001	WSM3	NOAH	Kain-Fritsch	CAM	RRTM	YSU
RAD3	1°x1°	JJA 2001	WSM3	NOAH	Kain-Fritsch	CAM	CAM	YSU
CCP	1°x1°	JJA 2001	WSM3	NOAH	Grell-Devenyi	Goddard	CAM	YSU
low_res	4°x5°	2001	WSM3	NOAH	Kain-Fritsch	Goddard	CAM	YSU
Future	1°x1°	2050	WSM3	NOAH	Kain-Fritsch	Goddard	CAM	YSU

### 3.3 Future-year initialization and simulation

The ability of society to address the negative effects resulting from climate change is dependent on the models' ability to predict the global and regional impacts that are a consequence of a warming earth. GWRP presents a unique opportunity to researchers interested in this topic, and may be used in the near future by scientists to perform nested simulations of future climate scenarios. The ability of GWRP to accurately predict long term climate projections must therefore be evaluated. A GWRP one year future case will be completed for the year 2050 with the baseline physics configuration. Although there are some uncertainties in setting up the simulation such as uncertainties in future atmospheric, oceanic, and land use changes, the ability of GWRP to simulate future climates must be evaluated. GWRP will be initialized using atmospheric, land, and ocean/sea-ice output from the IPCC Special Report on Emission Scenario (SRES) B1 experiment for the year 2050. This dataset was chosen because of its good credentials as part of the IPCC 4<sup>th</sup> Assessment Report, and its availability of free, daily data for 2050 from the Earth Grid System (EGS) website (<https://esg.llnl.gov:8443/home/publicHomePage>). The IPCC model output information is available at [http://www-pcmdi.llnl.gov/ipcc/standard\\_output.html](http://www-pcmdi.llnl.gov/ipcc/standard_output.html). Initialization data for this future year GWRP case will be taken from the NCAR Community Climate System Model 3.0 (CCSM3) with hundred year simulation dataset ranges temporally from 2000-2100. The CCSM3 is a coupled atmosphere-ocean model at a spatial resolution of 257 x 129 grid points (1.4° latitude x 1.4° longitude). CCSM output is taken from the IPCC Special Report on Emission Scenarios (SRES) B1 550 ppm stabilization experiment, which is the low green house gas concentration scenario, in which carbon dioxide is set at 550 ppm. Besides carbon dioxide, there are other forcings which demarcate this scenario from others used by the IPCC such as ozone, sulfates, carbon aerosols, and natural aerosols (e.g., sea-salt and dust). After 2000, tropospheric monthly ozone profiles are the same as 2000 but are scaled by the ratio of the global mean radiative forcing between the month in question and the 2000 average. After 2000, stratospheric ozone is consistent with the Montreal Protocol. Sulfate emissions were produced

for each specific SRES and future SO<sub>x</sub> emissions were scaled versus the year 2000. Geographical distribution of carbon aerosols are scaled by future SO<sub>2</sub> amounts instead of keeping carbon aerosols constant after year 2000. The emissions of sea salt and dust are held constant at year 2000 values (Meehl et al., 2007). Each month of 2050 GWRP simulations were initialized using the corresponding monthly mean CCSM outputs. The CCSM outputs replace fields in a typical WPS output file for the beginning of each month. The three dimensional variables used to initialize GWRP from the atmospheric part of CCSM (CAM) are vertical profiles of temperature (T), relative humidity (RH), geopotential height (Z3), as well as the zonal (U) and meridional (V) components of wind speed, and surface pressure (PS) was used to vertically interpolate variables to the GWRP vertical structure. The CCSM sea-ice (ICEFRAC) is a two dimensional variable used to initialize GWRP in 2050. The three dimensional variables used to initialize GWRP in 2050 from the CCSM Community Land Model (CLM) are soil temperature and moisture. The first two layers of CLM soil temperature (TSOI) and soil moisture (H2OSOI) are interpolated into the first layer of GWRP soil temperature (0-10 cm) and the third through eighth layers are interpolated into the second GWRP layer (10-200 cm).

### **3.4 Surface Observational Networks**

GWRP output will be evaluated against a number of surface observational networks, remotely sensed satellite data, and gridded Reanalysis data which combines data from surface and satellite observations with model output to create a consistent, global dataset. The model evaluation focuses on major boundary layer meteorological variables including a combination of non-convective and convective weekly accumulated precipitation (RAINC+RAINNC), 2-meter temperature (T2) and specific humidity (Q2), and 10-meter wind velocities and their zonal (U10) and meridional (V10) components, as well as radiation variables such as downward shortwave flux (SWDOWN) and downward long-wave radiation at the surface (GLW). A summary of the datasets is shown in Table 3.2.

**Table 3.2 Summary of datasets used to evaluate GWRP.**

Database <sup>a</sup>	Variables <sup>b</sup>	Data Frequency	Number of sites
BSRN	SWD,LWD	Minutely	~28
NCDC	T2, Precipitation	Monthly	~200
NCEP/NCAR Reanalysis	T2, Q2, SWD, LWD, U10, V10	4-times daily	Gridded (2.5° × 2.5°)
GPCP	Precipitation	Monthly	Gridded (2.5° × 2.5°)

<sup>a</sup> BSRN, Baseline Surface Radiation network; NCDC, National Climactic Data Center; GPCP, Global Precipitation Climatology Project

<sup>b</sup> SWD, Downward Shortwave Flux; LWD, Downward longwave Flux, T2, Temperature at 2-meters; Q2, Water Vapor Mixing Ratio at 2-meters; U10, Zonal wind at 10-meters; V10, Meridional wind at 10-meters

### **3.4.1 Baseline Surface Radiation Network (BSRN)**

The BSRN is a surface based observation network for short and long wave surface radiation fluxes whose objective is to provide observations of the best possible quality as a tool for climate research (Ohmura et al., 1998). BSRN was established by the World Radiation Monitoring Center (WMRC) to provide a worldwide network of continuously measured radiative fluxes at the Earth's surface. Many of the stations began operation in 1992 and as of June 2008 there were 43 stations providing data to the BSRN archive, located at the Alfred Wegener Institute (AWI) in Bremerhaven, Germany. In 2004, the Joint Planning Staff (JPS) for the World Climate Research Programme (WCRP) endorsed BSRN as the global surface radiation network for the Global Climate Observing System (GCOS). The major objectives of the BSRN project are to: monitor the background shortwave and longwave radiative components with the best methods currently available, provide data for the calibration of satellite-based estimates of the surface radiative fluxes (i.e., Surface Radiation Budget (SRB) Project), and produce high quality observational data for the validation of the radiative fluxes produced by models. Observations used from this network are shortwave downward radiation (SWD measured by pyranometers and

longwave downward radiation (LWD) measured by pyrgeometers, both parameters are measured in  $W m^{-2}$ .

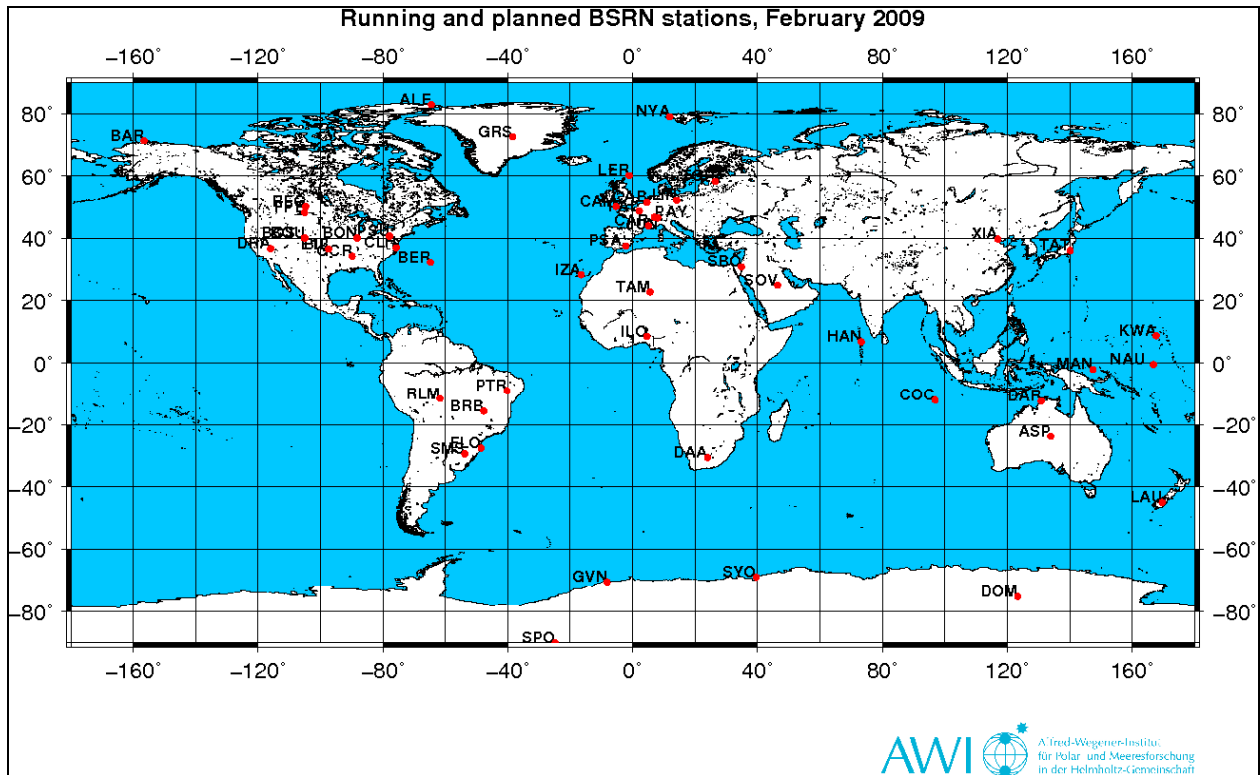


**Figure 3.1. Spatial distribution of BSRN sites as of February 2009.**

### 3.4.2 National Climactic Data Center (NCDC)

Meteorological parameters from NCDC are from the Global Climate Observing System (GSN) Surface Network, Monthly (GSNMON), with over 900 worldwide sites. This data is available free to download from the NCDC website. Fields available from this network are mean monthly temperature ( $^{\circ}C$ ) and total monthly precipitation (mm) for a site.

## **3.5 Remote Sensing**

### **3.5.1 Tropical Rainfall Measuring Mission (TRMM)**

The Tropical Rainfall Measuring Mission began in 1998 and is a satellite dedicated to measuring tropical and subtropical rainfall. Simpson et al. (1988) describe the original goals of the project as first a way to understand the hydrological cycle and second improve global circulation models and short-term climate models through the study of the variability and distribution of precipitation and latent-heat in the tropics. The satellite has a low altitude and low inclination so that it can monitor the tropics (35° N to 35° S) as often as possible. The satellite takes 91 minutes to complete one orbit around the Earth. Thus the TRMM satellite offers measurements for the entire range every 3 hours. This orbit allows for as much coverage of the tropics and extraction of rainfall data over the 24-hour day (16 orbits) as possible.

## **3.6 Reanalysis Datasets**

A Reanalysis is a way to combine, in an error weighted manner, surface based observations, satellite measured or derived quantities, and short-term forecasts to create an accurate, global dataset to validate General Circulation Models (GCMs) or other large scale models.

### **3.6.1 NCEP/NCAR Reanalysis**

The National Center for Environmental Prediction (NCEP) and the National Center for Atmospheric Research (NCAR) Reanalysis dataset is preeminent way to validate global simulations in the atmospheric modeling community. Members from NCEP/NCAR published a paper in 1996 to create a forty year record (1957-1996) of global atmospheric parameters for the climate change and modeling communities (Kalnay et al., 1996). Currently the project has been expanded to include the years 1948 – present and is plotted on a 2.5 × 2.5 degree latitude/longitude grid. The Reanalysis uses a combination of assimilated real data (remotely sensed and surface based) for each year and model regression to produce a global analyses of atmospheric fields.

### **3.6.2 Global Precipitation Climatology Project (GPCP)**

The Global Precipitation Climatology Project (GPCP) is a part of the Global Energy and Water Cycle Experiment (GEWEX) of the World Climate Research program (WCRP). Janowiak (1991) describes the GPCP as originally a program to create accurate global precipitation climatology from 1986-1995, based on monthly means on a  $2.5^{\circ} \times 2.5^{\circ}$  latitude-longitude grid. The project is a combination of satellite and surface-based rain gauges from over 6,000 stations and has currently produced precipitation estimates from 1979 to 2005 (Xie and Arkin, 1997). The version of GPCP used in this study is the 2.5-degree Version 2 which is comprised of 27 different precipitation products. The products are produced from an analysis designed by the Global precipitation Climatology Centre by merging precipitation estimates from microwave, infrared, and sounder data from international precipitation-related satellites, as well as from precipitation gauges.

### **3.7 Current-year simulation evaluation protocol**

The model evaluation focuses on major boundary layer meteorological variables including a combination of non-convective and convective weekly accumulated precipitation (RAIN+RAINNC), 2-meter temperature (T2) and specific humidity (Q2), and 10-meter wind velocities and their zonal (U10) and meridional (V10) components, as well as radiation variables such as downward shortwave flux (SWDOWN) and downward long-wave radiation at the surface (GLW). The overall performance of GWRP is evaluated in terms of spatial distribution, seasonal and temporal variations, and statistics such as the normalized mean bias and correlation coefficient over the global domain, the Northern and Southern Hemispheres, and the six populated continents. Also, the six circulations cells will be used as domains for model evaluation which include: the Northern and Southern Polar Cells, the Northern and Southern Ferrel Cells, and the Northern and Southern Hadley Cells. GWRP baseline and sensitivity simulations GWRP model output will be evaluated using observational datasets from a variety of sources including surface based observations, model reanalyzes, and remotely-sensed data to

evaluate the ability of GWRP to simulate atmospheric variables at the surface as well as aloft in 2001. The model reanalysis dataset used for GWRP evaluation is the NCEP/ NCAR Reanalysis. To evaluate GWRP precipitation output, the TRMM and the GPCP datasets will be used. Radiation output from GWRP will be evaluated against BSRN stations. Finally, meteorological data from surface-based networks that cover the entire globe such as the National Climactic Data Center (NCDC) monthly global surface data will be used.

### **3.7.1 Spatial Distribution**

A comparison of spatial trends across the domain between GWRP and observations and reanalysis datasets is completed for 2001 annual mean, as well as summer (JJA) and winter (December 2000, January and February 2001) is completed to expose geographic regions where the model is inaccurate. Annual, summer, and winter mean bias plots (simulated-observed) are created using a variety of NCAR Command Language (NCL) scripts. A comparison of color shading on the mean bias plots allows for an analysis of the model's ability to reproduce meteorological conditions. This evaluation allows a direct comparison between simulation and reference dataset to determine specific areas that show the highest sensitivity to physical parameterization. The comparison between observed and simulated values for the global domain allows for the determination of baseline simulation performance, as well as the sensitivity of regions to physical parameterization studies.

### **3.7.2 Temporal Variation**

Comparisons between summer (JJA) and winter (DJF) results for the global domain and sub-domains are completed for the major meteorological parameters. The temporal analysis of model accuracy compared with the reference dataset allows for an examination of the overall model performance throughout the simulation period, while identifying any seasonal contrasts in performance. The temporal evaluation is also designed to examine any differences in trends based on geographical location by comparing and contrasting temporal trends over the six populated continents. The temporal analysis is therefore designed to examine the diurnal and

seasonal trends of correlation between simulation and dataset. The examination of daily trends in meteorological variables is included to help identify the interactions among different parameters, and attribute model performance to specific physical parameterizations.

### 3.7.3 Performance Statistics Distribution

Observed and simulated values of T2, Q2, SWDOWN, GLW, and total precipitation, are compared through the calculation of statistical measures including normalized mean bias (NMB), normalized mean error (NME), mean bias (MB) and correlation coefficient (Corr) over the entire domain, sub-domains, and continental domains. The following formulas used to calculate these statistical metrics are taken from Yu et al. (2006):

$$NMB = \frac{\sum_{i=1}^N (M_i - O_i)}{\sum_{i=1}^N O_i} \bullet 100\%$$

$$NME = \frac{\sum_{i=1}^N |M_i - O_i|}{\sum_{i=1}^N O_i} \bullet 100\%$$

$$MB = \bar{M} - \bar{O}$$

$$Corr = \frac{\sum_{i=1}^N (M_i - \bar{M})(O_i - \bar{O})}{\left\{ \sum_{i=1}^N (M_i - \bar{M})^2 \sum_{i=1}^N (O_i - \bar{O})^2 \right\}^{1/2}}$$

Where  $O_i$  and  $M_i$  are the observed and simulated values at a specific time and location  $i$  in a given time period or spatial location or both up to  $N$  periods/locations. The mean values  $\overline{M}$ ,  $\overline{O}$  are the mean quantities of simulated and observed values. The statistical tool NMB provides if the model is overestimating or underestimating, as well as the degree of simulation inaccuracy. NMBs, however, do have a flaw when calculating a summation of individual components of opposite sign. This flaw is the combination of positive and negative biases, which causes the absolute magnitude of discrepancies to be underestimated. For this reason, NMEs are calculated because of its reliance on the absolute value of the simulation and observation at each point, which allows the overall degree of model discrepancy to be determined. MB is a commonly used metric to express the overall discrepancy between model and observations (Yu et al., 2006). Corr describes the strength of association between variables. This statistical evaluation technique is applied for annual and seasonal timescales for the selected meteorological parameters.

#### **3.7.4 Vertical Profile and Zonal Mean Distribution**

The previous evaluation protocols have been largely based on two-dimensional surface parameters, however in a global model whose top is 50 hPa, it is important to evaluate three-dimensional model performance in the vertical profile and zonal mean distribution. Vertical profile denotes a skew-T type diagram of vertical temperature distribution for NCEP/NCAR reanalysis and GWRF model output over each of the six populated continental domains. The zonal mean distribution may be described as a two-dimensional distribution of temperature based on latitude and height. A spatial overlay for zonal mean distribution will be completed to point out altitudinal temperature differences between the NCEP/NCAR reanalysis and GWRF model output.

#### **3.8 Future-year simulation evaluation protocol**

The ability of GWRF to predict meteorological parameters in 2050 will be evaluated against the CCSM3 model. Forcing for the GWRF atmosphere will be initialized daily for the year 2050

using the hundred year dataset. Hourly GWRP model output will then be processed to monthly means and compared with CCSM3 monthly mean data for 2050, as well as the baseline GWRP 2001 simulation. The evaluation protocol for this future case will be consistent with the retrospective application of GWRP. It will focus on major boundary layer variables such as temperature at 2 meters, specific humidity at 2 meters, the zonal and meridional components of winds at 10 meters, as well as downward shortwave radiation and downward long-wave radiation. The results from this future case will be evaluated in terms of spatial distribution, temporal variation, and statistics such as MB, NMB, and Corr over the global domain, the Northern and Southern Hemispheres, and the six populated continents.

CHAPTER 4: SENSITIVITY TO MODEL CONFIGURATIONS AND PHYSICAL OPTIONS

4.1 Baseline configuration evaluation

4.1.1 2001 Annual Mean Evaluation

4.1.1.1 2001 Temperature at 2-meter

The temperature at 2-meters above the surface in GWRf is compared with NCEP/NCAR Reanalysis for the annual mean of 2001. As shown in Figure 4.1, the majority of Mean Bias values fall within the  $\pm 10$  °C range, with the maximum mean bias value of 12.42 °C and a minimum mean bias value of -10.38 °C.

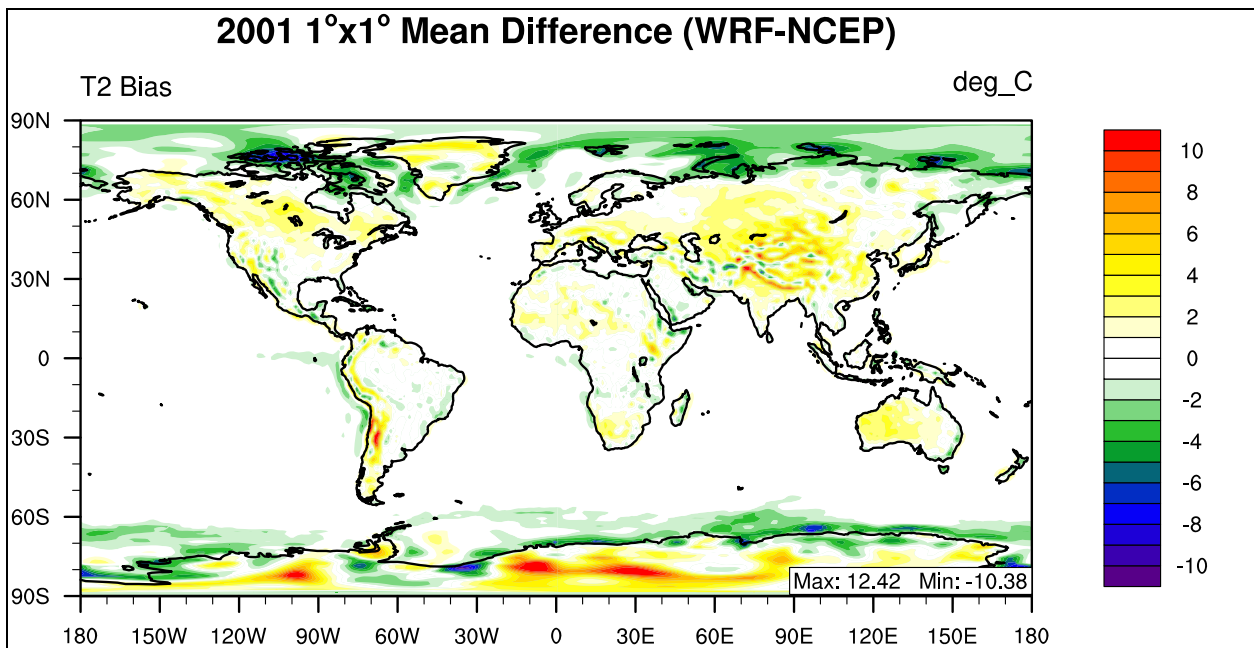


Figure 4.1 2001 Annual mean bias of temperature at 2-meters.

Model performance is best at the equator and worst at the poles as illustrated in Figure 4.1 and shown in Table 4.1, in which the Northern and Southern Hadley Cells have NMB values of less than 1%, while the rest of the circulation cells have NMB values over 1%. Globally, GWRf shows good statistical performance with a correlation value of 1.00 and an NMB value of less

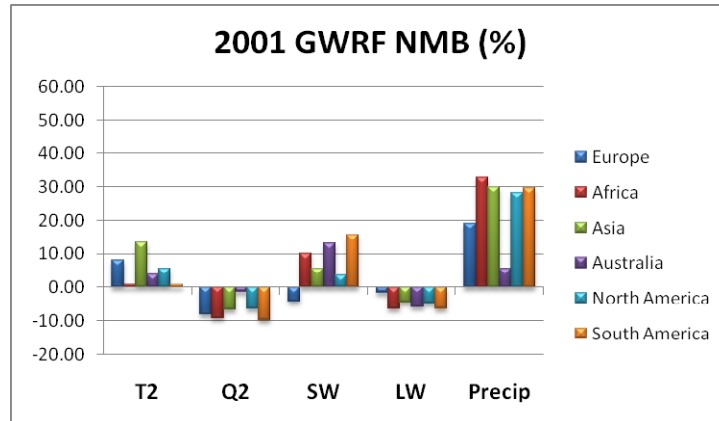
than 1% (-0.38%). Over the continents, the seasonal variation of GWRP T2 performance is shown in Figure 4.2, in which Europe has a large warm bias during winter and Asia and Australia have a warm bias during summer. This seasonal performance will be further investigated in sections 4.1.2 and 4.1.3.

**Table 4.1 Performance Statistics of GWRP 2001 Annual Mean temperature at 2-meter as compared with NCEP/NCAR Reanalysis.**

Name	MeanObs (°C)	MeanMod (°C)	Number	Corr	MB (°C)	RMSE	NMB%	NME%
Europe	6.67	7.22	1200	0.96	0.54	1.45	8.15	16.44
Africa	22.72	22.90	2925	0.92	0.18	1.20	0.81	3.79
Asia	8.98	10.17	5100	0.99	1.20	2.27	13.33	18.54
Australia	21.54	22.39	1200	0.97	0.85	1.43	3.96	4.82
N.A.	11.04	11.67	2400	0.99	0.62	1.43	5.63	9.77
S.A.	16.84	17.00	2450	0.98	0.16	1.67	0.95	5.74
N. Pole	-11.48	-12.72	10440	0.97	-1.24	2.29	-10.80	16.42
N. Ferrel	8.72	9.35	10800	0.98	0.63	1.68	7.25	12.87
N. Hadley	25.01	25.21	10800	0.96	0.20	0.96	0.80	2.22
S. Hadley	23.76	23.96	10800	0.96	0.21	0.99	0.87	2.38
S. Ferrel	9.92	9.66	10800	1.00	-0.27	0.70	-2.69	4.48
S. Polar	-25.26	-24.95	10440	0.99	0.32	3.14	1.25	9.41
N.H.	7.63	7.51	32040	1.00	-0.12	1.72	-1.62	15.45
S.H.	3.12	3.20	32040	1.00	0.08	1.93	2.66	35.73
Global	5.38	5.36	64080	1.00	-0.02	1.83	-0.38	21.34

An overview of statistical performance in terms of NMBs for the major boundary layer variables is shown graphically in Figure 4.2. For the continental domains, an overestimation of downward shortwave flux (except for Europe) is correlated with the overestimation of temperature at 2 meters. The anti-correlation between T2 and SWDOWN over Europe may be explained by examining the seasonal trend among these parameters. For summer, winter, and thus the annual mean, SWDOWN is underestimated, however during winter the simulated European temperature (-1.01 °C) is much too warm when compared with the observed value (-2.70 °C), which produces a very high winter NMB value of (62.59%) and contributes to the annual NMB value. During

winter the simulated Northern Ferrel temperature (0.13 °C) is too warm when compared with the observed value (-0.59 °C), which produces a very high winter NMB value of (121.83%) and contributes to the annual NMB value, explain the anti-correlation between T2 and SWDOWN. An underestimation of water vapor mixing ratio at 2 meters is correlated with an underestimation of downward longwave flux over all domains, which is physically consistent because downward longwave radiation is a function of the vertical distribution of atmospheric absorbers, of which a major constituent is water vapor. The overestimation of precipitation rate is evident in Figure 4.2, with large overestimations over all domains, indicating that precipitation rate is the worst of these variables simulated by GWRf. For the circulation cell domains, the correlation between an underestimation of water vapor mixing ratio at 2 meters and downward longwave flux is still present and the largest NMB values are still associated with daily precipitation rate. In the North Pole domain, the downward shortwave flux as well as the temperature at 2 meters is underestimated and this domain also shows the highest NMB values for precipitation rate.



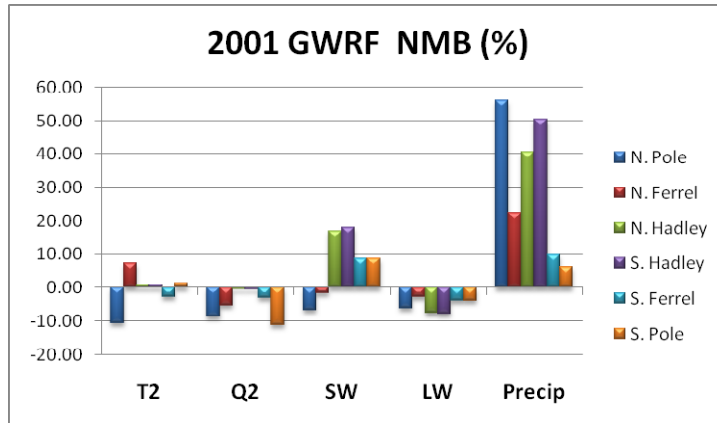


**Figure 4.2** 2001 Annual Mean normalized mean bias (%) of major meteorological variables for (a) the six continental domains and (b) the six circulation cell domains.

Figure 4.4 shows the annual zonal mean bias of temperatures simulated by GWRP versus those from NCEP/NCAR Reanalysis data. GWRP captures the vertical temperature distribution within  $\pm 2$  degrees up to approximately 300 hPa, with large overestimations near the surface over Antarctica. Zonally the model performs the best near the surface of the Northern mid-latitudes, with the model slightly underestimating temperatures over the Southern mid-latitudes. Overestimations exist in the lower troposphere over the ITCZ and polar domains. There is an underestimation of temperatures in the Southern Hadley Cell aloft between 400 hPa and 100 hPa. The most striking aspect of this image is the large underestimation of temperatures above the tropopause, with the contour following typical height of the tropopause, which is due to the absence of a prescribed ozone profile in this GWRP configuration, with heights of 8-10 km over Polar Regions, 10-12 km over the mid-latitudes and up to 16 km in the Tropics.

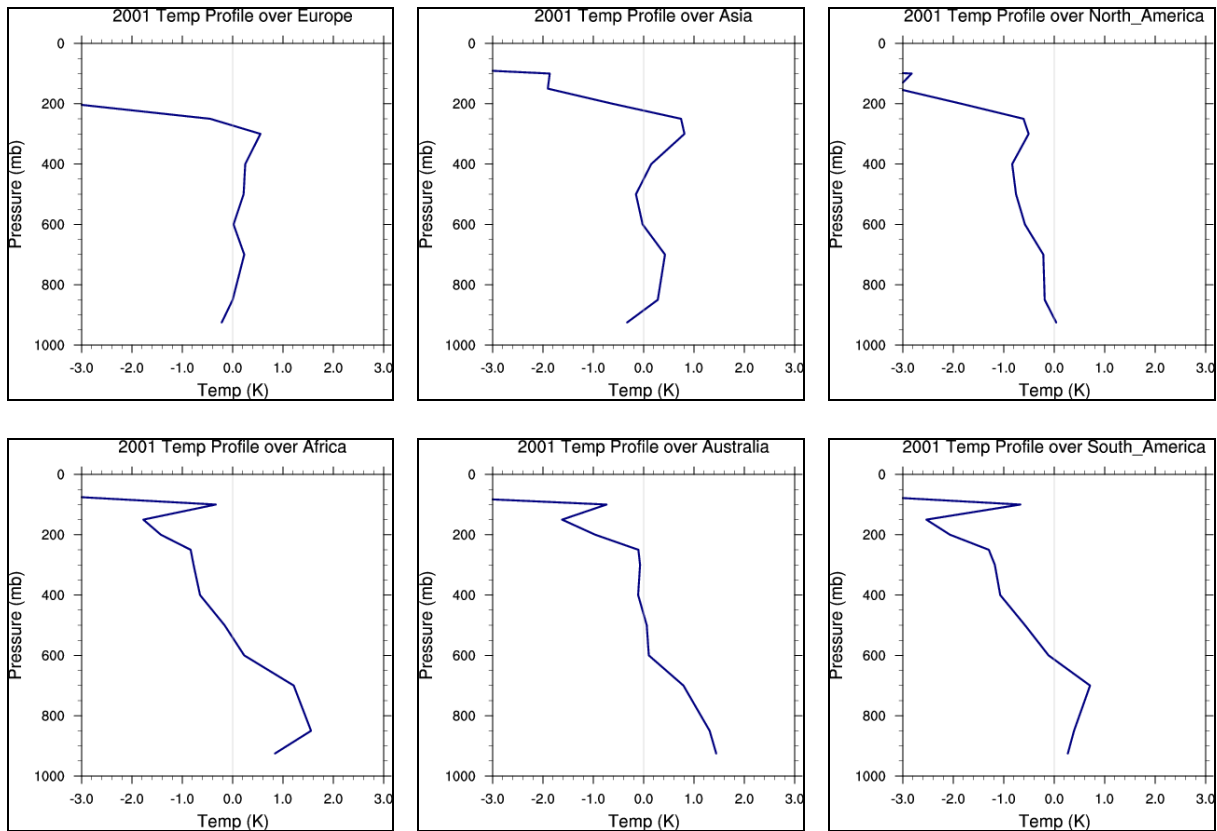


**Figure 4.3** Vertical profiles of annual mean temperature mean bias over the six populated continents.

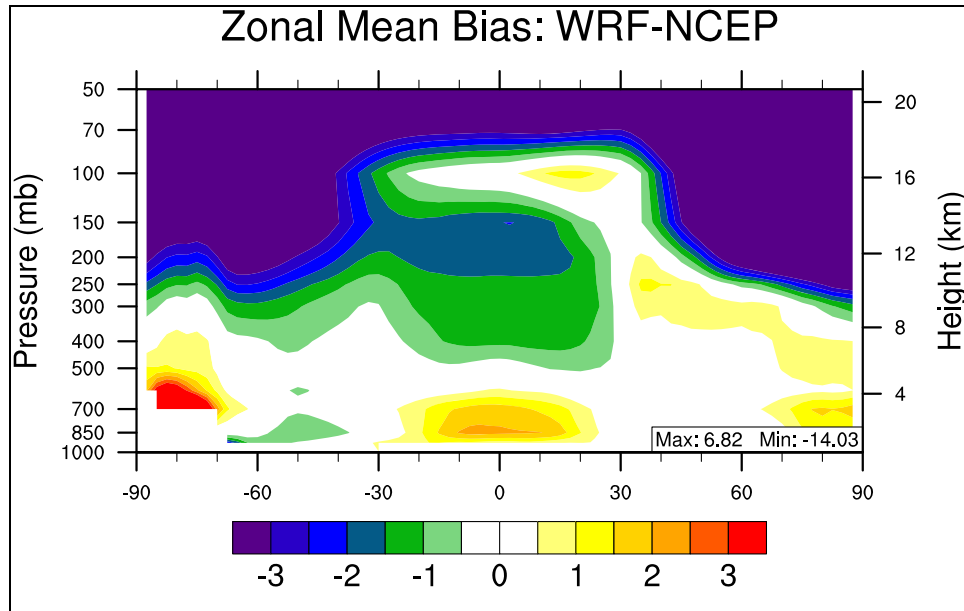


**Figure 4.4 2001 Annual mean zonal mean bias of temperature.**

#### **4.1.1.2 2001 Water Vapor Mixing ratio at 2-meter**

The global distribution of mean bias for water vapor mixing ratio at 2-meter is displayed in Figure 4.5 which shows an overall underestimation over the Tropics (30°N-30°S). Overall the majority of mean bias values are within the range of  $\pm 5 \text{ g kg}^{-1}$ , with a maximum mean bias of  $8.01 \text{ g kg}^{-1}$  and a minimum mean bias value of  $-7.43 \text{ g kg}^{-1}$ . The largest underestimations occur over humid regions (e.g., areas of India and sub-Saharan Africa), while the largest overestimations occur over shallow areas of water that are exposed to a large amount of insolation year round (e.g., Gulf of California, Persian Gulf, and Red Sea). The overall underestimation of Q2 is also reflected in Table 4.2 in which all circulation cells, as well as continental domains have a negative NMB value, with a global NMB value of -2.29%. Overall correlation values are high, with the circulation cells all having Corr values above 0.95, and all continental domains having Corr values above 0.93. Globally, the correlation coefficient value is 0.99.

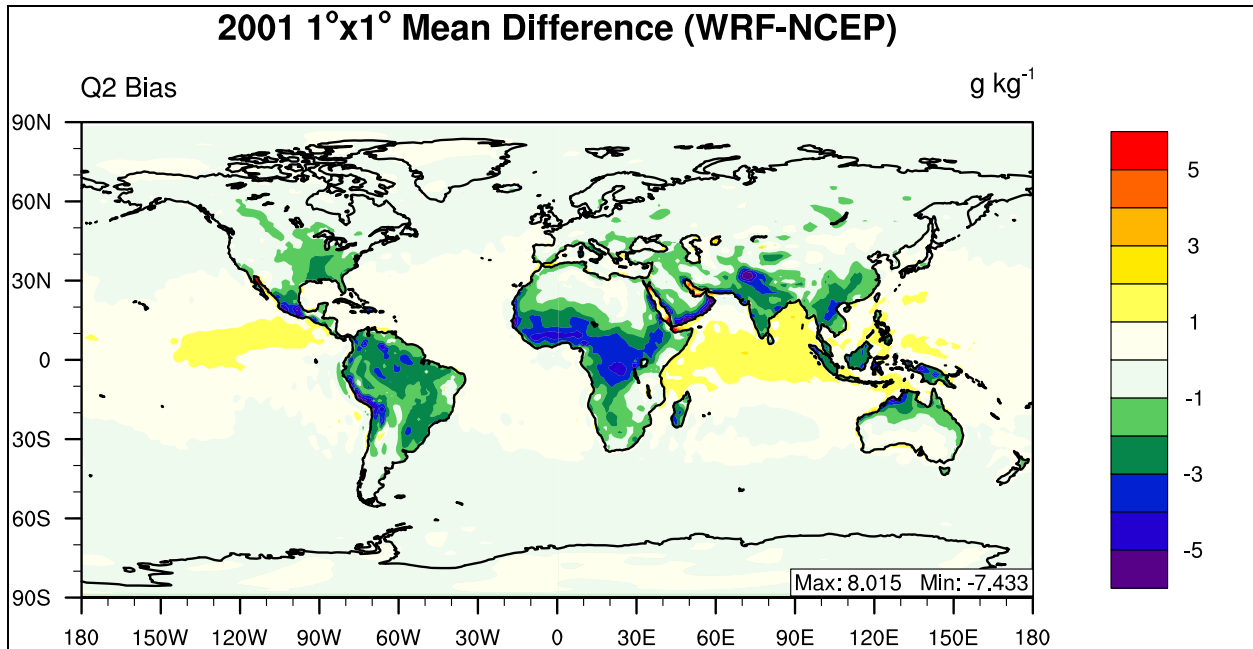


**Figure 4.5** 2001 annual mean bias of water vapor mixing ratio at 2-meter.

**Table 4.2** Performance Statistics of GWRF 2001 Annual Mean Water Vapor Mixing Ratio at 2-meter as compared with NCEP/NCAR Reanalysis.

Name	MeanObs ( $\text{g kg}^{-1}$ )	MeanMod ( $\text{g kg}^{-1}$ )	Number	Corr	MB ( $\text{g kg}^{-1}$ )	RMSE	NMB%	NME%
Europe	6.29	5.77	1200	0.94	-0.52	0.73	-8.27	9.72
Africa	11.11	10.07	2925	0.93	-1.04	1.92	-9.39	12.91
Asia	8.06	7.52	5100	0.98	-0.53	1.33	-6.63	11.74
Australia	10.56	10.41	1200	0.97	-0.16	1.16	-1.47	7.68
N.A.	8.62	8.06	2400	0.98	-0.55	1.06	-6.41	9.12
S.A.	11.75	10.61	2450	0.97	-1.14	1.64	-9.68	10.69
N. Pole	2.46	2.24	10440	0.99	-0.22	0.30	-8.76	9.65
N. Ferrel	7.03	6.64	10800	0.98	-0.38	0.75	-5.43	7.47
N. Hadley	15.43	15.36	10800	0.96	-0.07	1.49	-0.45	7.16
S. Hadley	15.33	15.24	10800	0.95	-0.09	1.16	-0.61	5.25
S. Ferrel	7.04	6.82	10800	0.99	-0.22	0.34	-3.06	3.70
S. Polar	1.29	1.15	10440	0.99	-0.14	0.23	-11.09	13.71
N.H.	8.37	8.15	32040	0.99	-0.22	0.98	-2.66	7.49
S.H.	7.96	7.81	32040	0.99	-0.15	0.71	-1.90	5.24
Global	8.17	7.98	64080	0.99	-0.19	0.86	-2.29	6.39

### 4.1.1.3 2001 Downward Shortwave Flux at Ground Surface

The pattern of downward shortwave flux mean bias is displayed graphically in Figure 4.6 in which the overall pattern is an overestimation in the Tropics (30°N-30°S), and a slight underestimation at higher latitudes. The majority of mean bias value fall within the range of  $\pm 100 \text{ W m}^{-2}$ , with a maximum mean bias of  $112.2 \text{ W m}^{-2}$  and a minimum mean bias value of  $-171.6 \text{ W m}^{-2}$ . Large underestimations of up to  $-100 \text{ W m}^{-2}$  are associated with the west coast of South America along the Peru Current, a large region of upwelling. The overall pattern of GWRP SWDOWN performance is reflected in Table 4.3 in which all of the circulation cell domains display a positive NMB value except for the high Northern latitudes, with a global NMB value of 8.91%. Correlation coefficient values are not as high as Q2 or T2, with the Southern Hadley Cell and Southern Pole Cell having Corr values of 0.32 and 0.31, respectively. Continental domains mainly in the Northern Hemisphere (Europe, Asia, and N.A.) have higher Corr values than those in the Southern Hemisphere (Africa, Australia, S.A.). Globally, the correlation coefficient value is 0.93.

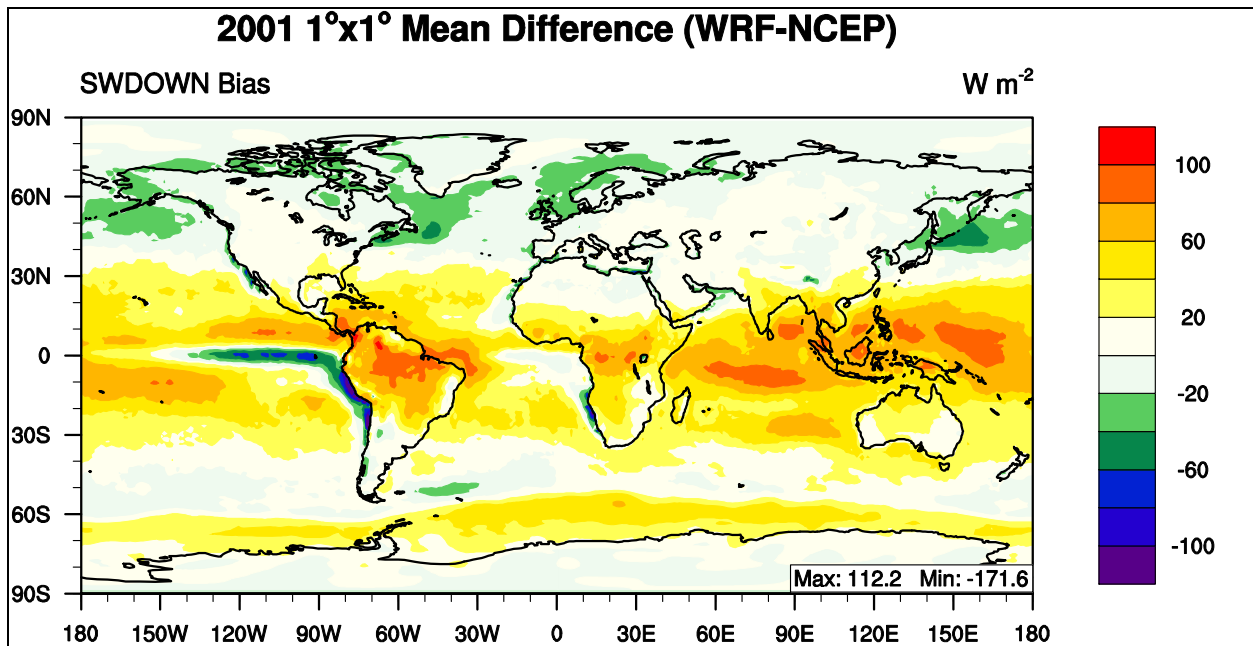


Figure 4.6 2001 annual mean bias of downward shortwave flux at the surface.

**Table 4.3 Performance Statistics of GWRP 2001 annual mean downward shortwave flux at the surface as compared with NCEP/NCAR Reanalysis.**

Name	MeanObs (W m <sup>-2</sup> )	MeanMod (W m <sup>-2</sup> )	Number	Corr	MB (W m <sup>-2</sup> )	RMSE	NMB%	NME%
Europe	167.36	160.24	1200	0.97	-7.12	13.98	-4.26	6.92
Africa	267.22	294.05	2925	0.63	26.83	37.35	10.04	11.26
Asia	214.97	227.24	5100	0.93	12.27	25.13	5.71	7.80
Australia	245.37	277.69	1200	0.89	32.32	35.04	13.17	13.18
N.A.	213.01	220.86	2400	0.93	7.85	18.71	3.68	6.76
S.A.	211.17	244.18	2450	0.80	33.01	48.28	15.63	18.06
N. Pole	131.12	122.15	10440	0.81	-8.97	12.20	-6.84	7.59
N. Ferrel	191.06	187.76	10800	0.96	-3.30	15.84	-1.73	6.49
N. Hadley	244.21	285.28	10800	0.55	41.07	48.61	16.82	17.63
S. Hadley	239.18	282.04	10800	0.32	42.86	50.83	17.92	19.41
S. Ferrel	164.36	178.63	10800	0.89	14.27	21.71	8.69	10.27
S. Polar	145.31	158.08	10440	0.31	12.77	20.70	8.79	10.25
N.H.	189.44	199.25	32040	0.95	9.81	30.49	5.18	11.58
S.H.	183.37	206.79	32040	0.92	23.42	34.20	12.77	14.29
Global	186.41	203.02	64080	0.93	16.62	32.40	8.91	12.91

#### 4.1.1.4 2001 Downward Longwave Flux at Ground Surface

The pattern of downward longwave flux mean bias is displayed graphically in Figure 4.7 in which the overall pattern is an underestimation with a global NMB value of -5.63% as shown in Table 4.4. All mean bias values fall within the range of  $\pm 100$  W m<sup>-2</sup>, with a maximum mean bias of 69.14 W m<sup>-2</sup> and a minimum mean bias value of -71.7 W m<sup>-2</sup>. The overall pattern of GWRP GLW performance is reflected in Table 4.4 in which all of the domains display a negative NMB value. This overall underestimation of GLW corresponds with the overall underestimation of Q2 as mentioned in section 4.1.1.2. Correlation values are higher than the associated SWDOWN values, with the continental domains and circulation cell domains all displaying a Corr coefficient value of greater than 0.89.

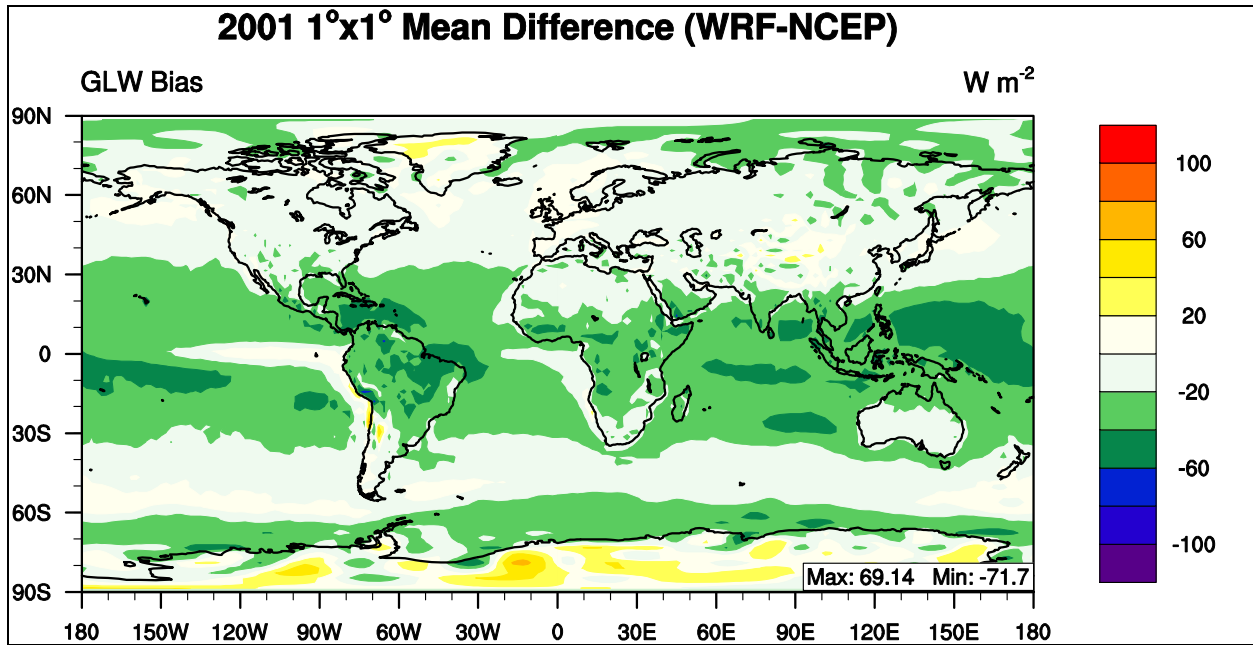


Figure 4.7 2001 annual mean bias of downward longwave flux at the surface.

Table 4.4 Performance Statistics of GWRf 2001 annual mean Downward Longwave Flux at the surface as compared with NCEP/NCAR Reanalysis.

Name	MeanObs (W m <sup>-2</sup> )	MeanMod (W m <sup>-2</sup> )	Number	Corr	MB (W m <sup>-2</sup> )	RMSE	NMB%	NME%
Europe	285.47	281.01	1200	0.91	-4.47	9.70	-1.56	2.84
Africa	359.41	336.60	2925	0.90	-22.81	25.98	-6.35	6.53
Asia	297.95	284.22	5100	0.98	-13.72	19.39	-4.61	5.36
Australia	356.96	335.45	1200	0.97	-21.51	23.91	-6.03	6.03
N.A.	309.70	294.90	2400	0.99	-14.79	17.73	-4.78	4.89
S.A.	348.76	326.52	2450	0.95	-22.25	28.89	-6.38	7.07
N. Pole	216.33	203.03	10440	0.94	-13.30	17.03	-6.15	6.84
N. Ferrel	298.66	290.56	10800	0.97	-8.10	12.50	-2.71	3.41
N. Hadley	391.16	361.84	10800	0.93	-29.32	31.68	-7.50	7.61
S. Hadley	388.87	358.63	10800	0.89	-30.24	32.53	-7.78	7.95
S. Ferrel	312.08	300.04	10800	0.95	-12.04	15.46	-3.86	4.15
S. Polar	155.84	149.70	10440	0.97	-6.14	23.85	-3.94	13.31
N.H.	303.01	286.06	32040	0.99	-16.95	22.03	-5.59	6.03
S.H.	287.05	270.80	32040	0.99	-16.25	24.95	-5.66	7.51
Global	295.03	278.43	64080	0.99	-16.60	23.54	-5.63	6.75

#### 4.1.1.5 2001 Zonal Wind Speed at 10-meter

The pattern of the mean bias zonal wind speed at 10-meters (U10) is displayed graphically in Figure 4.8 in which the overall pattern is a slight underestimation of the zonal component. Overall wind speed is the worst variable predicted by the model with a global NMB value of -452.13%. This corresponds to a global mean bias of  $0.5 \text{ m s}^{-1}$  and the very high NMB value is caused by a very low wind speed ( $-0.01 \text{ m s}^{-1}$ ) from the Reanalysis data. The majority of mean bias value fall within the range of  $\pm 5 \text{ m s}^{-1}$ , with a maximum mean bias of  $7.95 \text{ m s}^{-1}$  and a minimum mean bias value of  $-5.87 \text{ m s}^{-1}$ . The overall pattern of GWRP U10 performance is reflected in Table 4.5 in which the majority of domains display a negative NMB value. U10 displays the largest absolute NMB values of among all GWRP variables examined thus far, while Corr values are still relatively high with a global Corr value of 0.96.

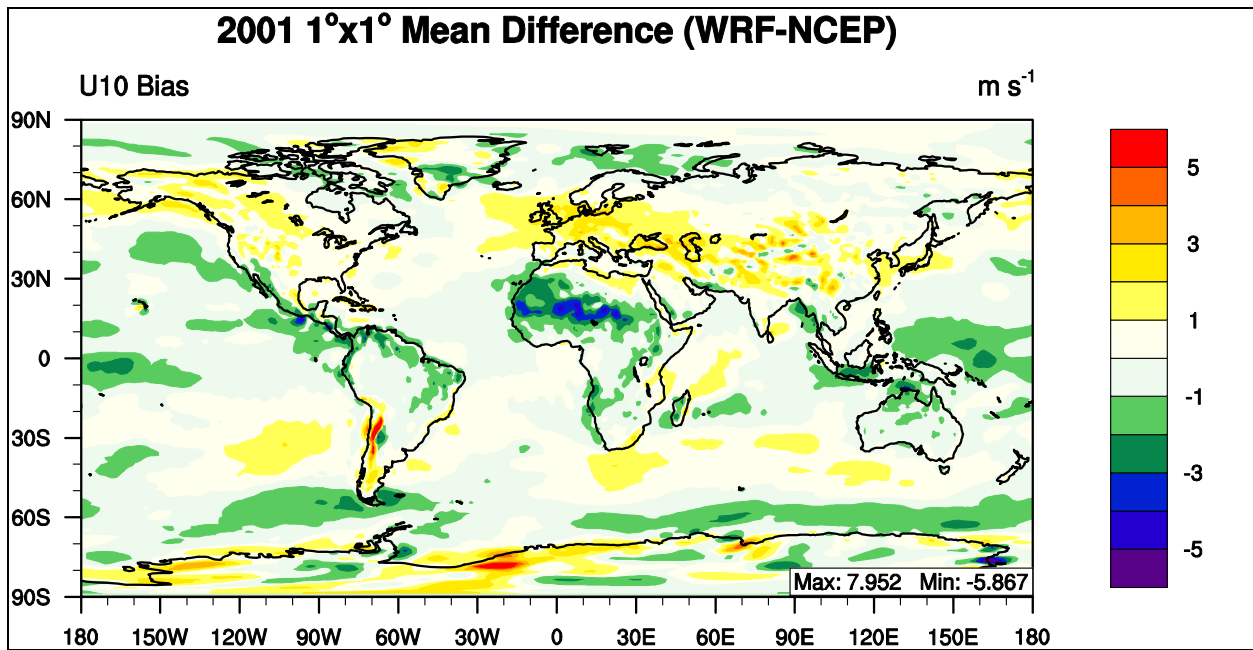


Figure 4.8 2001 annual mean bias of zonal wind at 10-meter.

**Table 4.5 Performance Statistics of GWRP 2001 annual mean zonal wind at 10-meter as compared with NCEP/NCAR Reanalysis.**

Name	MeanObs (m s <sup>-1</sup> )	MeanMod (m s <sup>-1</sup> )	Number	Corr	MB (m s <sup>-1</sup> )	RMSE	NMB%	NME%
Europe	0.68	1.73	1200	0.54	1.06	1.39	155.87	171.18
Africa	-0.63	-1.12	2925	0.80	-0.49	1.18	-79.02	140.06
Asia	0.31	0.71	5100	0.77	0.40	0.99	126.44	227.47
Australia	-0.77	-1.25	1200	0.97	-0.49	0.76	-63.64	80.01
N.A.	0.26	0.69	2400	0.92	0.43	0.84	163.50	269.44
S.A.	0.64	0.40	2450	0.94	-0.24	1.15	-37.54	134.70
N. Pole	0.09	0.02	10440	0.79	-0.07	0.71	-79.48	591.51
N. Ferrel	1.16	1.67	10800	0.77	0.51	1.03	43.73	70.85
N. Hadley	-2.09	-2.60	10800	0.95	-0.51	1.02	-24.23	37.21
S. Hadley	-2.99	-3.21	10800	0.93	-0.23	0.83	-7.69	21.13
S. Ferrel	4.35	4.31	10800	0.96	-0.05	0.88	-1.06	16.44
S. Polar	-0.62	-0.58	10440	0.95	0.04	1.23	6.18	155.69
N.H.	-0.28	-0.31	32040	0.93	-0.02	0.94	-8.22	253.39
S.H.	0.26	0.18	32040	0.97	-0.08	1.00	-30.90	294.64
Global	-0.01	-0.06	64080	0.96	-0.05	0.97	-452.13	6471.81

#### 4.1.1.6 2001 Meridional Wind Speed at 10-meter

The pattern of meridional wind speed at 10-meters (V10) mean bias is displayed graphically in Figure 4.9 and the spatial pattern appears to be similar to the zonal component with an overall slight underestimation. Meridional wind speed displays a global NMB value of -26.16%, which is significantly lower than the zonal component global domain average. This corresponds to a mean bias of  $-0.04 \text{ m s}^{-1}$  and the high NMB value is caused by a low wind speed ( $0.15 \text{ m s}^{-1}$ ) from the Reanalysis data. The majority of mean bias values fall within the range of  $\pm 5 \text{ m s}^{-1}$ , with a maximum mean bias of  $5.61 \text{ m s}^{-1}$  and a minimum mean bias value of  $-6.65 \text{ m s}^{-1}$ . The overall pattern of GWRP V10 performance is reflected in Table 4.6 in which the majority of domains display a negative NMB value. V10 also displays very large absolute NMB values and low Corr values for individual domains, but still displays a global Corr value of 0.90.

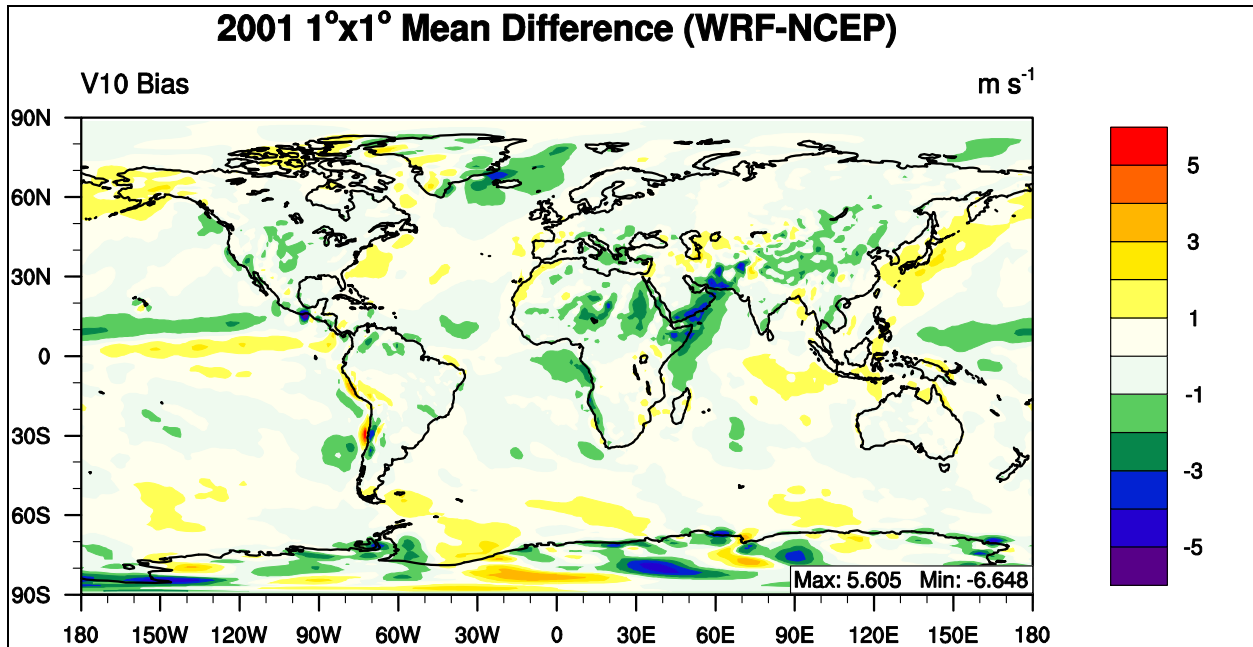


Figure 4.9 2001 annual mean bias of meridional wind at 10-meters.

Table 4.6 Performance Statistics of GWRP 2001 annual mean meridional wind at 10-meter as compared with NCEP/NCAR Reanalysis.

Name	MeanObs (m s <sup>-1</sup> )	MeanMod (m s <sup>-1</sup> )	Number	Corr	MB (m s <sup>-1</sup> )	RMSE	NMB%	NME%
Europe	0.27	0.10	1200	0.81	-0.17	0.51	-63.80	147.01
Africa	0.67	0.25	2925	0.93	-0.42	0.93	-63.07	106.48
Asia	0.11	-0.16	5100	0.62	-0.27	0.94	-248.13	656.70
Australia	1.04	1.17	1200	0.95	0.13	0.48	12.64	33.55
N.A.	-0.03	-0.15	2400	0.81	-0.12	0.65	-376.51	1667.78
S.A.	-0.74	-0.64	2450	0.81	0.11	0.80	14.18	76.80
N. Pole	-0.07	-0.13	10440	0.85	-0.06	0.68	-87.17	694.04
N. Ferrel	0.20	0.24	10800	0.78	0.04	0.76	17.88	300.58
N. Hadley	-0.61	-0.89	10800	0.87	-0.28	0.94	-45.80	117.85
S. Hadley	1.41	1.45	10800	0.94	0.04	0.65	2.51	34.53
S. Ferrel	-1.02	-0.83	10800	0.89	0.19	0.59	18.61	44.30
S. Polar	1.00	0.84	10440	0.90	-0.15	1.28	-15.36	97.51
N.H.	-0.16	-0.27	32040	0.85	-0.10	0.80	-63.37	374.94
S.H.	0.46	0.48	32040	0.93	0.03	0.89	5.72	138.93
Global	0.15	0.11	64080	0.90	-0.04	0.85	-26.16	423.01

#### 4.1.1.7 2001 Daily Precipitation Rate

The daily precipitation rate at the surface in GWRP is compared with the Global Precipitation Climatology Project (GPCP) for the annual mean of 2001. In Figure 4.10, the interval spacing is set to  $\pm 2$  mm day<sup>-1</sup> to show the spatial variability of GWRP precipitation. As shown in Figure 4.8, there are areas where GWRP overestimates precipitation rate in close proximity to areas where GWRP underestimates precipitation rate. The maximum mean bias is 11.55 mm day<sup>-1</sup> and a minimum mean bias value of -2.98 mm day<sup>-1</sup>, indicating a tendency of the model to overestimate rainfall rate. Overall spatial trend shows that performance is best at the mid-latitudes (Northern and Southern Ferrel Cells) and worst in the Tropics (Northern and Southern Hadley Cells) as illustrated in Figure 4.8 and shown in Table 4.7, in which the Northern and Southern Ferrel Cells have NMB values of less than 23%, while the Hadley cells have NMB values over 40%. Globally, GWRP shows good correlation (90%), but poor bias performance with an NMB value of greater than 30% (31.03%).

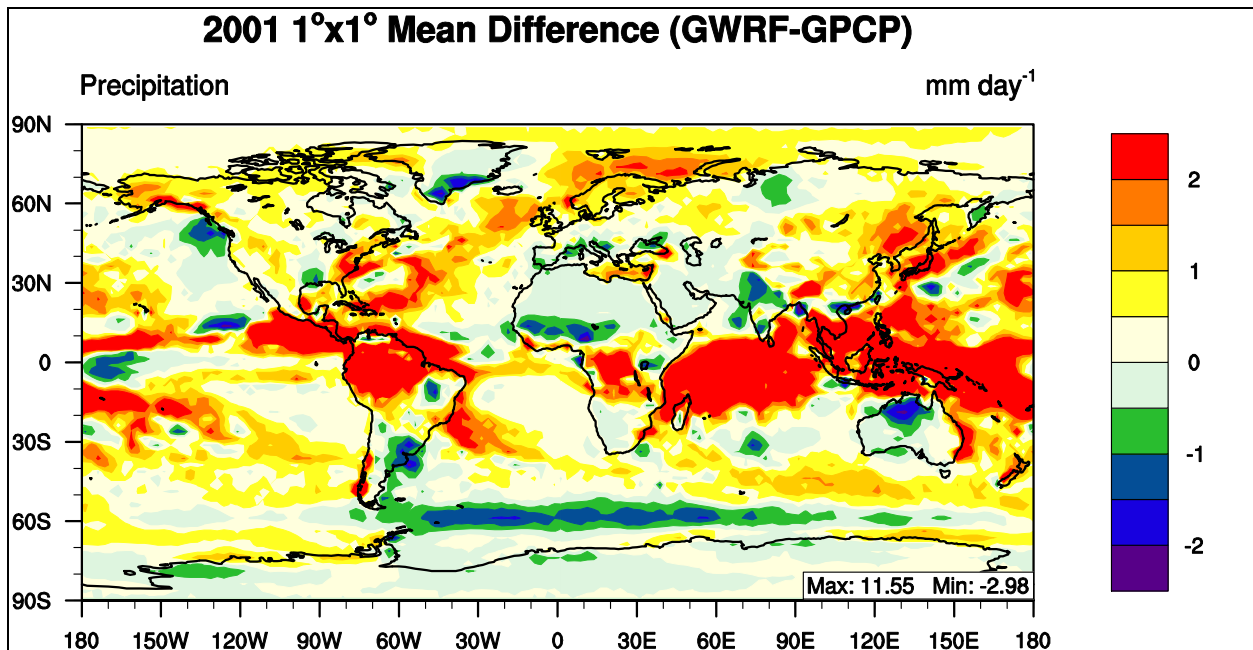


Figure 4.10 2001 annual mean bias of daily precipitation rate.

**Table 4.7 Performance Statistics of GWRP 2001 annual mean daily precipitation rate as compared with Global Precipitation Climatology Project.**

Name	MeanObs (mm d <sup>-1</sup> )	MeanMod (mm d <sup>-1</sup> )	Number	Corr	MB (mm d <sup>-1</sup> )	RMSE	NMB%	NME%
Europe	2.35	2.80	192	0.63	0.45	0.83	19.1	28.38
Africa	1.54	2.04	468	0.88	0.5	1.19	32.67	49.96
Asia	1.94	2.53	816	0.89	0.58	1.27	29.95	41.95
Australia	1.83	1.94	192	0.77	0.1	1.02	5.63	36.31
N.A.	2.1	2.69	384	0.85	0.59	0.96	28.23	33.23
S.A.	3.76	4.88	392	0.83	1.11	2.46	29.62	42.12
N. Pole	0.89	1.39	1728	0.81	0.5	0.71	56	64.26
N. Ferrel	2.41	2.96	1728	0.89	0.54	0.95	22.51	28.92
N. Hadley	3.08	4.33	1728	0.89	1.25	2.29	40.63	48.41
S. Hadley	2.73	4.11	1728	0.9	1.38	2.34	50.36	56.12
S. Ferrel	2.9	3.19	1728	0.66	0.29	0.8	9.9	21.43
S. Polar	0.91	0.97	1728	0.9	0.06	0.4	6.09	28.92
N.H.	2.13	2.89	5184	0.9	0.76	1.49	35.92	43.25
S.H.	2.18	2.76	5184	0.89	0.57	1.45	26.26	36.96
Global	2.15	2.82	10368	0.9	0.67	1.47	31.03	40.06

#### 4.1.2 2001 Evaluation of summer (JJA) Simulation

##### 4.1.2.1 Summer Temperature at 2-meter

The temperature at 2-meters above the surface in GWRP is compared with NCEP/NCAR Reanalysis for the summer of 2001 (June, July, and August 2001). As shown in Figure 4.11, the mean bias performance is slightly worse for the summer case as opposed to the annual mean. The majority of Mean Bias values fall within the  $\pm 10$  °C range, however there are larger exceptions with a maximum mean bias value of 17.50 °C and a minimum mean bias value of -15.77 °C. Model performance is exceptionally complicated over Antarctica with overestimations occurring over the land surface and underestimations occurring off shore over the Southern Ocean. Globally, GWRP shows good statistical performance with a correlation value of 99% and an NMB value of 2.70%. Over the continents, only Europe has a negative NMB value,

while T2 is overpredicted for the rest of the continental domains. Overall the Southern hemisphere has much worse statistical performance than the Northern Hemisphere, with NMB values of 26.57% and 0.84%, respectively.

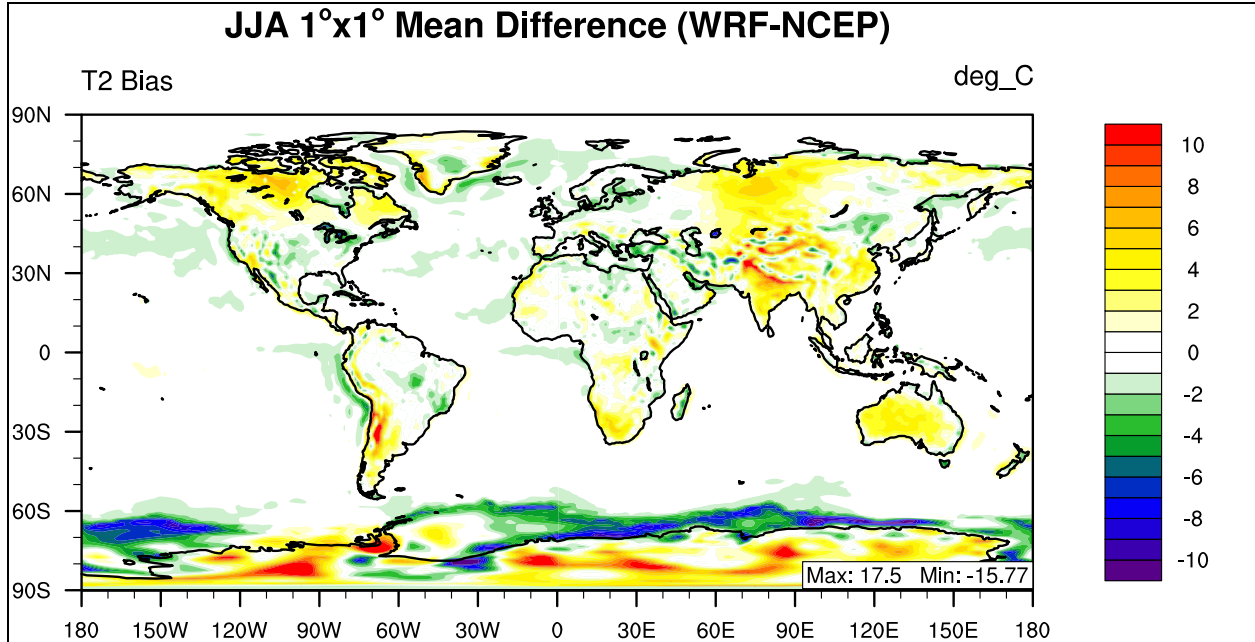


**Figure 4.11** 2001 summer mean bias of temperature at 2-meter compared with NCEP/NCAR Reanalysis.

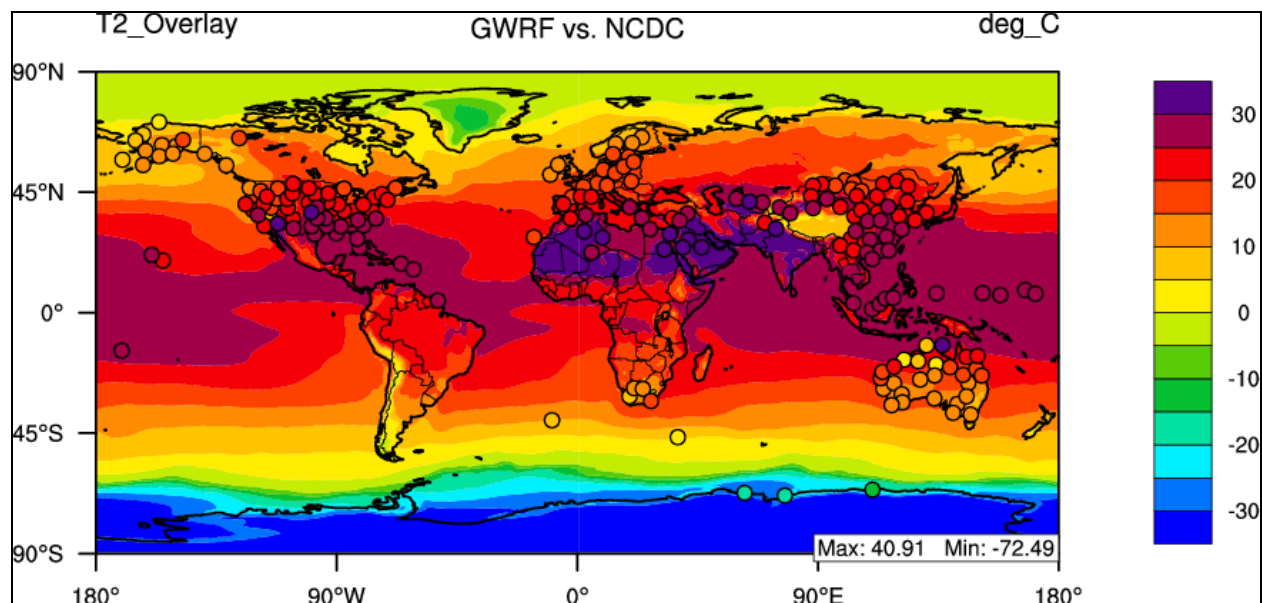
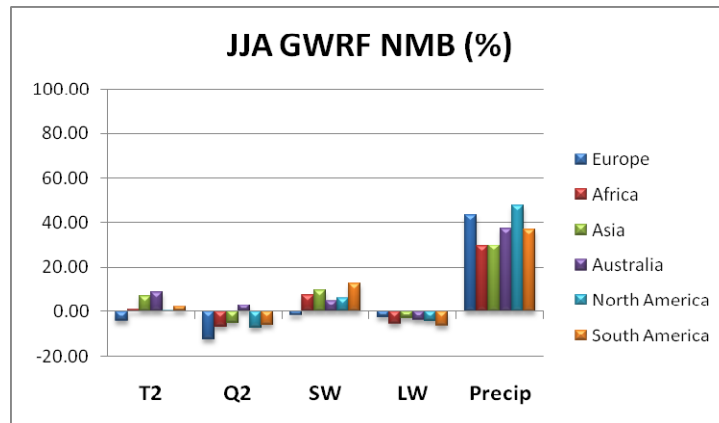


**Figure 4.12** 2001 summer mean bias of temperature at 2-meter compared with NCDC.

**Table 4.8** Performance Statistics of GWRf 2001 summer mean temperature at 2-meter compared with NCEP/NCAR Reanalysis and NCDC data.

Name	MeanObs (°C)	MeanMod (°C)	Number	Corr	MB (°C)	RMSE	NMB%	NME%
Europe	16.43	15.75	1200	0.96	-0.67	1.37	-4.10	6.67
Africa	23.83	24.05	2925	0.96	0.22	1.58	0.94	4.82
Asia	20.72	22.19	5100	0.94	1.47	2.95	7.12	10.62
Australia	17.02	18.49	1200	0.96	1.47	2.24	8.60	9.91
N.A.	20.51	20.54	2400	0.95	0.03	1.95	0.13	7.28
S.A.	14.76	15.06	2450	0.97	0.30	2.16	2.01	8.45
N. Pole	3.20	3.49	10439	0.96	0.29	1.80	9.14	38.12
N. Ferrel	17.65	17.67	10800	0.95	0.02	2.02	0.11	8.21
N. Hadley	26.64	26.74	10800	0.93	0.10	1.29	0.37	2.90
S. Hadley	22.26	22.68	10800	0.95	0.43	1.36	1.92	3.67
S. Ferrel	8.10	7.91	10800	0.99	-0.19	1.14	-2.35	7.62
S. Polar	-34.51	-33.93	10440	0.98	0.58	4.57	1.68	-10.45
N.H.	15.97	16.11	32039	0.99	0.13	1.73	0.84	7.18
S.H.	-1.01	-0.74	32040	0.99	0.27	2.81	26.57	-163.96
Global	7.48	7.68	64079	0.99	0.20	2.33	2.70	18.75
NCDC	20.77	20.27	199	0.88	-0.51	4.18	-2.43	12.24

When compared with NCDC data, the model exhibits an average lower correlation coefficient value than when it is compared to a gridded reanalysis dataset. The co-located NCDC and model values as shown in the last row of Table 4.8 are warmer than the comparison with reanalysis data because of the tendency of stations to be located in the Northern Hemisphere. When compared with real observations during the summer of 2001, GWRF exhibits a small MB value of (-0.51 °C). An overview of summer statistical performance for the major boundary layer variables when compared with NCEP/NCAR Reanalysis is shown graphically in Figure 4.13. The figure shows a similar pattern to the annual mean results, however in this case the NMB values are larger, specifically for precipitation rate. In the seasonal comparison, the inconsistency associated with Europe in the annual mean (as discussed in section 4.1.1.1) is absent. In the North Pole domain, the high NMB value for precipitation rate which was present in the annual comparison is even higher during the summer evaluation. The vertical profile of temperature performance is also evaluated. Figure 4.14 shows that GWRF captures vertical temperature distribution within  $\pm 2$  degrees up to approximately 300 hPa over the six continental domains, which is due to an absence of an ozone profile.



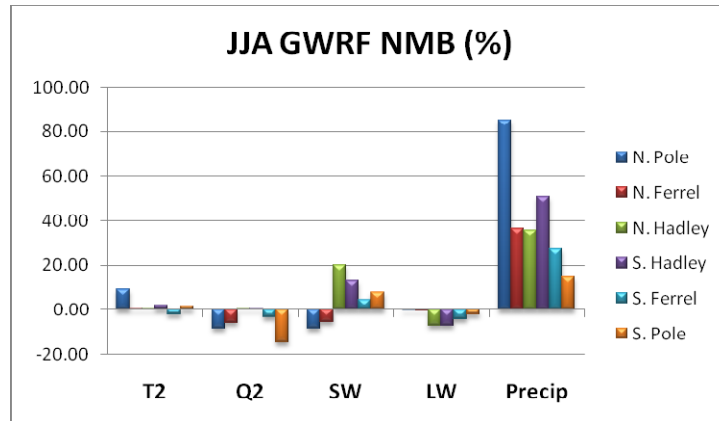


**Figure 4.13 2001 summer mean normalized mean bias (%) of major meteorological variables for (a) the six continental domains and (b) the six circulation cell domains.**

Figure 4.15 is the zonal mean bias of temperatures simulated by GWRP versus those from NCEP/NCAR Reanalysis data. Zonally the model performs worse than the annual mean with a higher maximum mean bias and lower minimum mean bias. The summer comparison of the vertical distribution of temperature exposes certain seasonal aspects which are not displayed in the annual evaluation. Overestimations exist in the lower troposphere over the ITCZ and polar domains. In the summer case, the model slightly underestimates temperatures throughout the Southern Ferrel Cell and the underestimation of temperatures between 400 hPa and 100 hPa now occupies both the Northern and Southern Hadley Cells. This image also shows the large underestimation of temperatures above the tropopause, however in this case the tropopause over Antarctica is anomalously high which is caused by the large overestimations of T2 in this region.

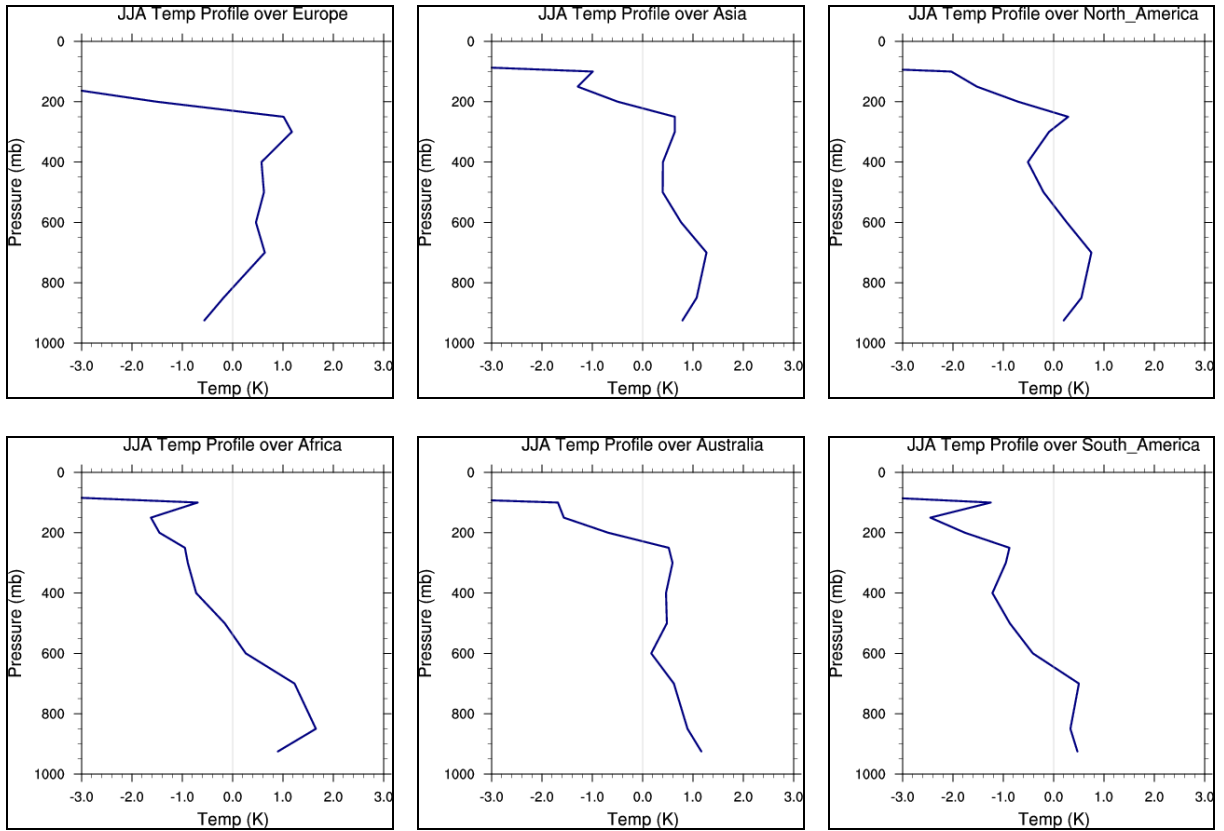


**Figure 4.14** Vertical profiles of summer mean temperature mean bias over the six populated continents.

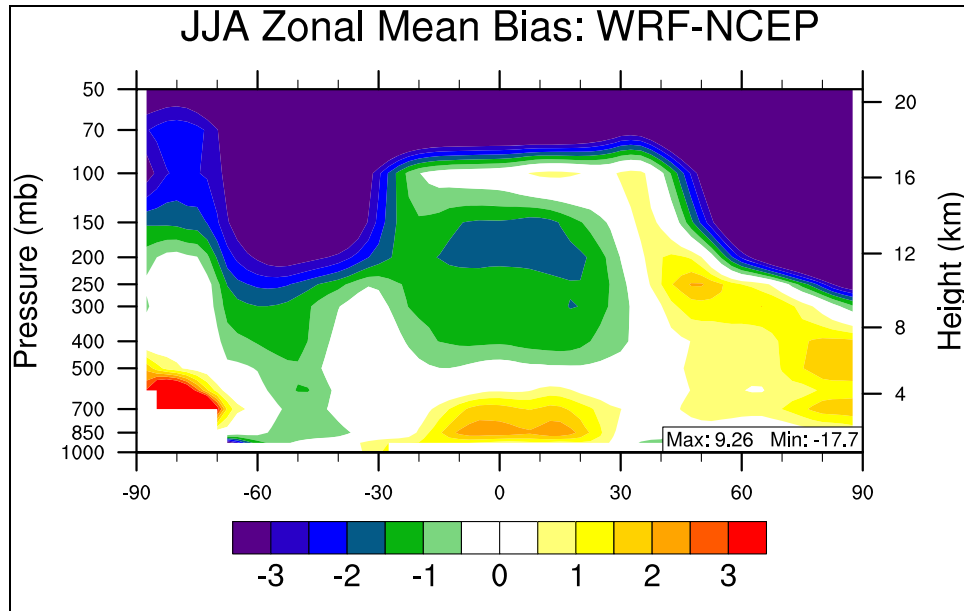


**Figure 4.15** 2001 summer mean zonal mean bias of temperature.

#### 4.1.2.2 Summer Water Vapor Mixing Ratio at 2-meter

The global distribution of summer mean bias for water vapor mixing ratio at 2-meter is displayed in Figure 4.16. When compared with the annual mean bias (shown in Figure 4.5), the underestimations over the Tropics are larger than the annual case, and the underestimation is also present in the Northern Hemisphere mid-latitudes. Overall the majority of mean bias values are within the range of  $\pm 5 \text{ g kg}^{-1}$ , however the biases are larger in this seasonal case as compared with the annual mean bias. The maximum mean bias is  $13.07 \text{ g kg}^{-1}$  and the minimum mean bias is  $-9.57 \text{ g kg}^{-1}$ . The overall underestimation of Q2 is also reflected in Table 4.9 in which the majority of all domains have a negative NMB value with the exception of the Tropics (Northern and Southern Hadley Cells) and Australia. The global summer mean NMB value is  $-2.39\%$ , which is similar to the annual value ( $-2.29\%$ ). Overall correlation coefficient values are similar to annual mean performance, with a global correlation coefficient value of 0.99.

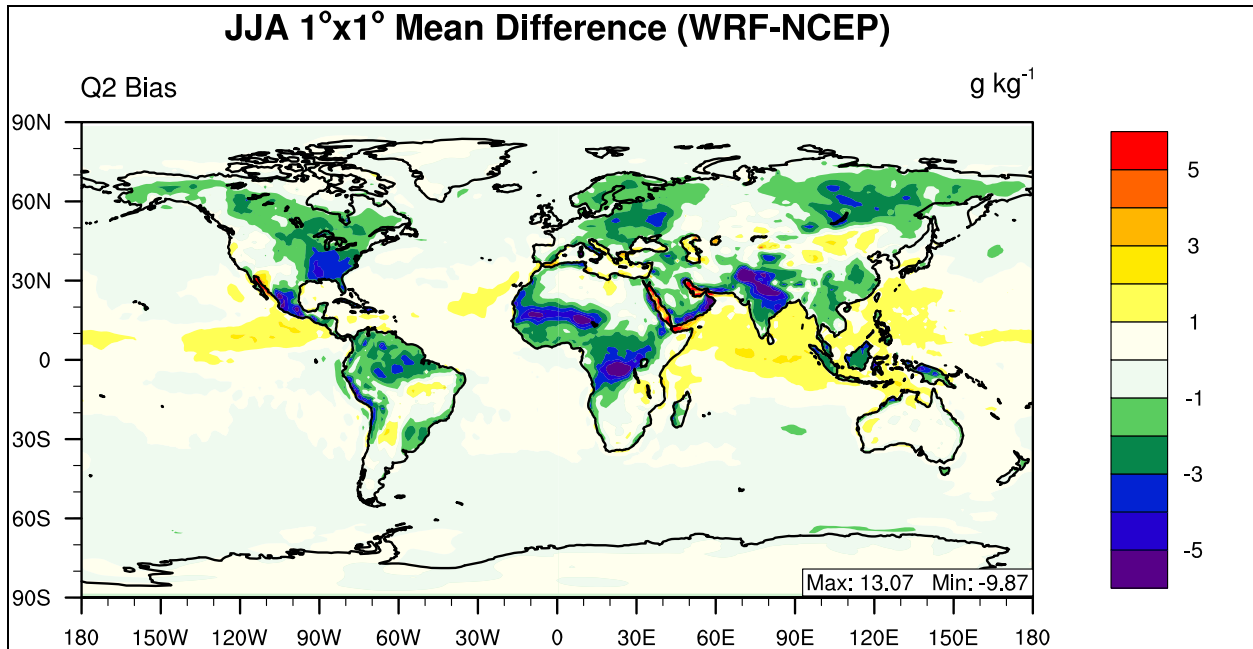


**Figure 4.16** 2001 summer mean bias of water vapor mixing ratio at 2-meter.

**Table 4.9** Performance Statistics of GWRF 2001 summer mean water vapor mixing ratio at 2-meter compared with NCEP/NCAR Reanalysis.

Name	MeanObs (g kg <sup>-1</sup> )	MeanMod (g kg <sup>-1</sup> )	Number	Corr	MB (g kg <sup>-1</sup> )	RMSE	NMB%	NME%
<b>Europe</b>	9.83	8.58	1200	0.85	-1.25	1.65	-12.70	14.45
<b>Africa</b>	10.88	10.16	2925	0.91	-0.72	2.00	-6.65	12.73
<b>Asia</b>	11.86	11.23	5100	0.95	-0.63	1.89	-5.29	12.12
<b>Australia</b>	8.53	8.78	1200	0.98	0.26	0.83	2.99	6.76
<b>N.A.</b>	12.34	11.43	2400	0.95	-0.91	1.78	-7.34	10.87
<b>S.A.</b>	10.02	9.40	2450	0.98	-0.62	1.29	-6.19	9.40
<b>N. Pole</b>	4.94	4.51	10440	0.97	-0.43	0.74	-8.63	9.74
<b>N. Ferrel</b>	10.18	9.57	10800	0.94	-0.61	1.31	-6.03	9.02
<b>N. Hadley</b>	16.78	16.84	10800	0.94	0.07	1.65	0.41	7.24
<b>S. Hadley</b>	13.91	13.93	10800	0.97	0.02	1.04	0.14	4.90
<b>S. Ferrel</b>	6.18	5.97	10800	0.99	-0.21	0.36	-3.44	4.67
<b>S. Pole</b>	0.74	0.63	10440	0.97	-0.11	0.28	-14.84	23.92
<b>N.H.</b>	10.70	10.37	32040	0.98	-0.32	1.29	-3.02	8.19
<b>S.H.</b>	7.01	6.91	32040	0.99	-0.10	0.66	-1.44	5.48
<b>Global</b>	8.85	8.64	64080	0.99	-0.21	1.03	-2.39	7.12

#### 4.1.2.3 Summer Downward Shortwave Flux at Ground Surface

The pattern of summer downward shortwave flux mean bias is displayed graphically in Figure 4.17, and reflects the annual pattern of an overestimation in the Tropics (30°N-30°S), however in the summer case the underestimation at high latitudes in the Northern hemisphere increases dramatically. The overestimation in the Tropics also increases, most noticeably over Southern Asia, while there are large areas of underestimation off the West coasts of Africa and South America in the Southern Hadley Cell. The majority of mean bias values still fall within the range of  $\pm 100 \text{ W m}^{-2}$ , but the maximum mean bias increases to  $130.5 \text{ W m}^{-2}$  and the minimum mean bias value decreases to  $-181.7 \text{ W m}^{-2}$ . This pattern of GWRP SWDOWN performance is reflected in Table 4.10 in which all of the circulation cell domains display a positive NMB value except for the high Northern latitudes (Northern Ferrel and Polar Cell) which display negative NMB values, with a global NMB value of 3.97%. Regions with poor correlation in the annual mean predictions are improved, with Corr value increasing from 0.32 to 0.67 in the Southern Hadley Cell and Corr value increasing from 0.32 to 1.00 in the Southern polar Cell. Continental domains mainly in the Southern Hemisphere (Europe, Asia, and N.A.) have higher Corr values than those in the Northern Hemisphere (Africa, Australia, and S.A.). Globally, the correlation coefficient value remains the same at 0.93.

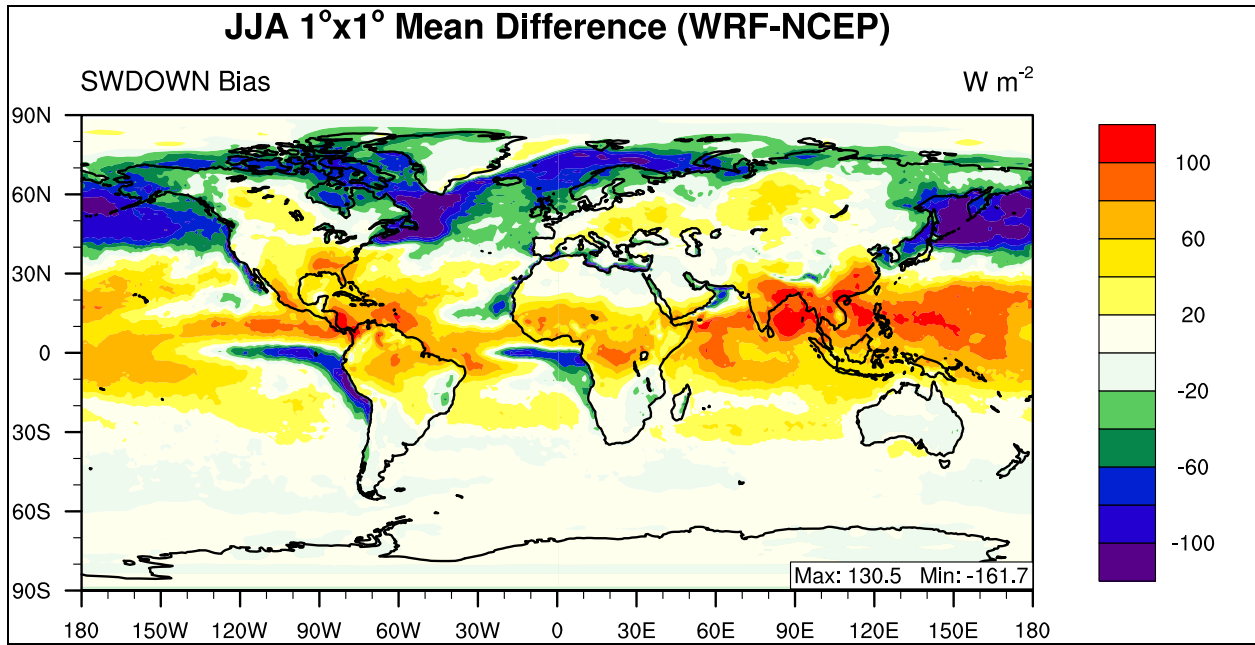


**Figure 4.17** 2001 summer mean bias of downward shortwave flux at the surface.

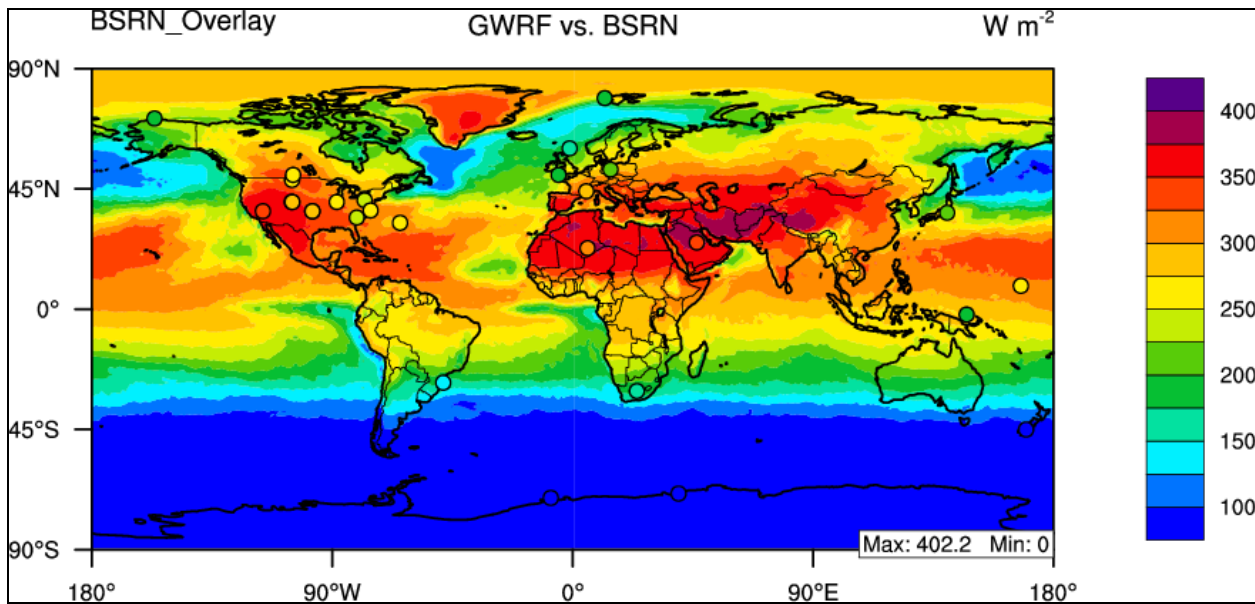


**Figure 4.18** 2001 summer mean bias of downward shortwave flux at the surface compared with BSRN.

**Table 4.10 Performance Statistics of GWRf 2001 summer mean downward shortwave flux at the surface compared with NCEP/NCAR Reanalysis and BSRN data.**

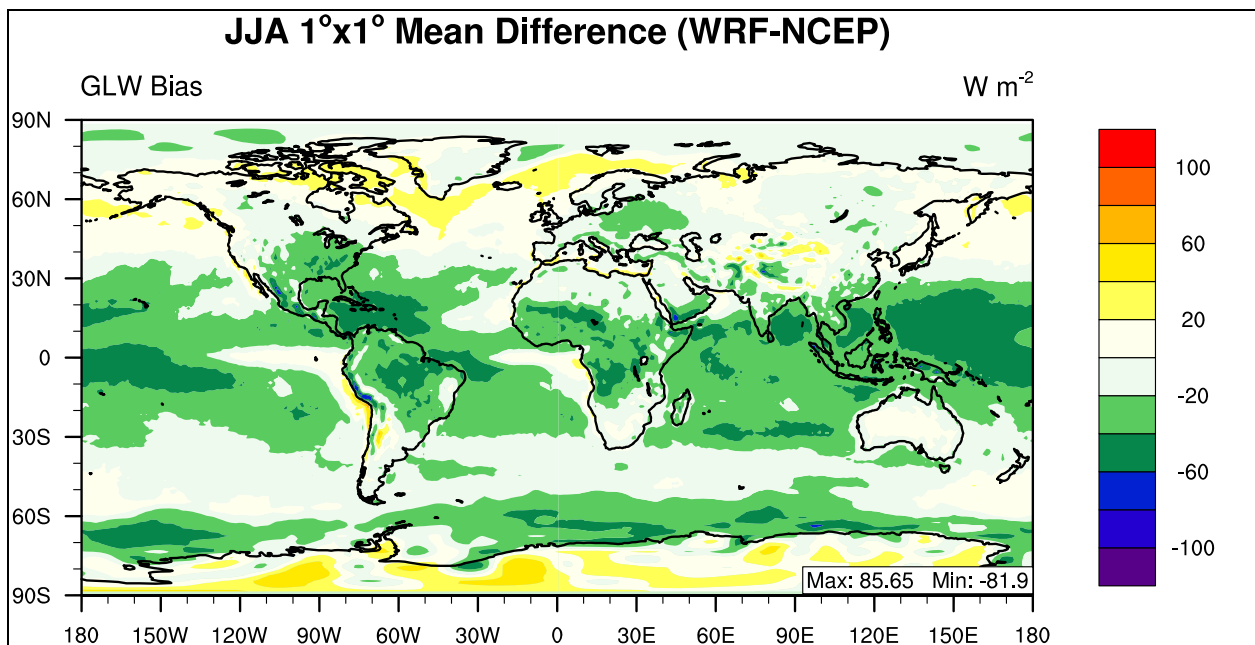
Name	MeanObs (W m <sup>-2</sup> )	MeanMod (W m <sup>-2</sup> )	Number	Corr	MB (W m <sup>-2</sup> )	RMSE	NMB%	NME%
Europe	276.03	271.01	1200	0.82	-5.02	35.83	-1.82	10.65
Africa	267.44	287.31	2925	0.85	19.86	41.90	7.43	12.00
Asia	282.36	309.50	5100	0.61	27.14	49.48	9.61	13.20
Australia	187.27	196.65	1200	0.93	9.38	19.19	5.01	7.30
N.A.	287.47	304.93	2400	0.55	17.45	42.85	6.07	12.54
S.A.	159.45	179.25	2450	0.95	19.80	37.48	12.42	16.27
N. Pole	278.24	254.78	10440	0.77	-23.47	38.58	-8.43	10.55
N. Ferrel	276.45	260.49	10800	0.86	-15.96	50.17	-5.77	13.74
N. Hadley	257.37	309.21	10800	0.55	51.85	63.58	20.14	22.14
S. Hadley	201.96	227.91	10800	0.67	25.95	40.76	12.85	16.68
S. Ferrel	79.47	83.10	10800	0.98	3.63	8.95	4.57	8.63
S. Polar	8.77	9.46	7920	1.00	0.68	1.40	7.80	8.70
N.H.	270.60	275.05	32040	0.56	4.45	51.92	1.64	15.36
S.H.	105.32	116.32	29520	0.98	11.00	25.25	10.45	14.28
Global	191.34	198.94	61560	0.93	7.59	41.34	3.97	15.08
BSRN	218.83	270.32	29	0.98	51.50	57.07	23.53	23.53

Figure 4.18 displays 2001 summer mean BSRN data overlaid with GWRf output. The statistical summary for this plot is located in the final row of Table 4.10 and shows a large overestimation by GWRf for insolation reaching the surface. This figure will be used as a reference when evaluating the seasonal sensitivity of GWRf incoming solar radiation to radiation configuration.

#### 4.1.2.4 Summer Downward Longwave Flux at Ground Surface

The pattern of summer downward longwave flux mean bias is displayed graphically in Figure 4.19 in which the overall pattern is an underestimation with a global NMB value of -4.14%, which is a slight improvement from the annual mean. All mean bias values fall within the range of  $\pm 100$  W m<sup>-2</sup>, with a larger maximum mean bias (85.65 W m<sup>-2</sup>) and a smaller minimum mean bias (-81.9 W m<sup>-2</sup>). The overall pattern of GWRf GLW performance is consistent with the annual mean, as shown in Table 4.11, in which all of the domains display a

negative NMB value. Correlation values are worse than the annual mean, with Europe having the lowest Corr value of the continental domains (0.57) and the Northern Hadley Cell having the worst performance of the circulation cell domains (0.73). Globally, the correlation value is 0.98. Figure 4.20 displays 2001 summer mean downward longwave BSRN data overlaid with GWRP output. The statistical summary for this plot is located in the final row of Table 4.11 and shows a large underestimation by GWRP for downward longwave flux reaching the surface, which is in agreement with Figure 4.19 and the rest of Table 4.11. This figure will be used as a reference when evaluating the seasonal sensitivity of downward longwave flux GWRP to radiation configuration.



**Figure 4.19** 2001 summer mean bias of downward longwave flux at the surface.

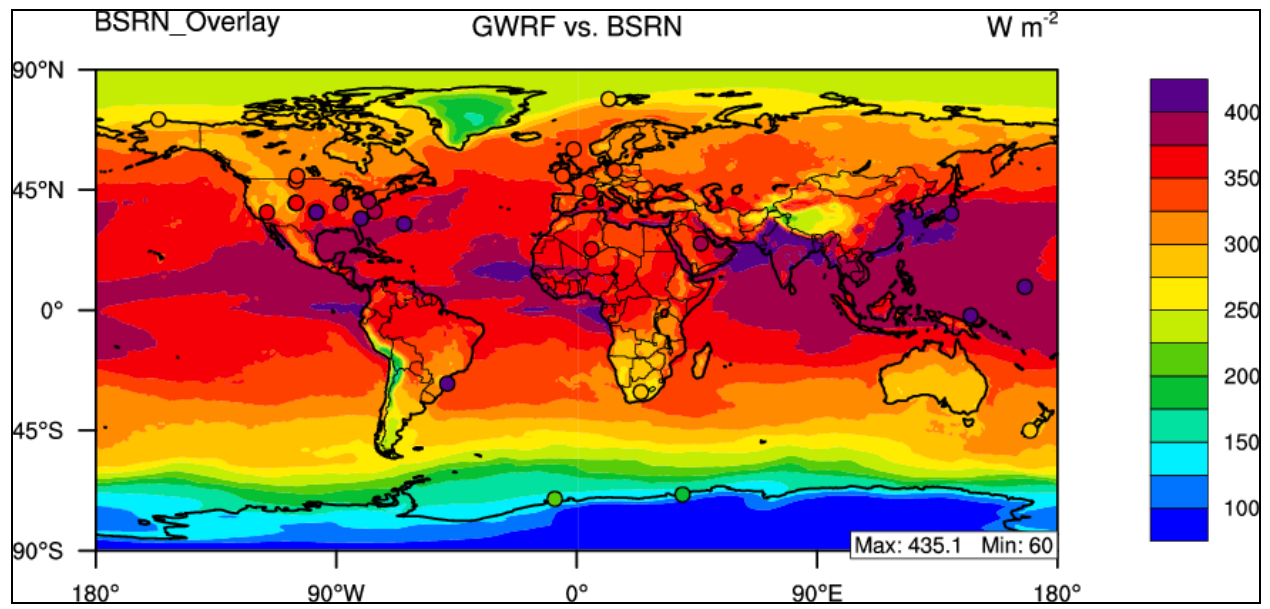


**Figure 4.20** 2001 summer mean bias of downward longwave flux at the surface compared with BSRN.

**Table 4.11 Performance Statistics of GWRf 2001 summer mean downward longwave flux at the surface compared with NCEP/NCAR Reanalysis and BSRN data.**

Name	MeanObs (W m <sup>-2</sup> )	MeanMod (W m <sup>-2</sup> )	Number	Corr	MB (W m <sup>-2</sup> )	RMSE	NMB%	NME%
Europe	333.15	324.01	1200	0.57	-9.14	17.42	-2.74	4.53
Africa	363.04	343.49	2925	0.83	-19.55	26.19	-5.38	6.16
Asia	355.61	344.70	5100	0.94	-10.91	20.66	-3.07	4.54
Australia	325.16	312.88	1200	0.96	-12.29	19.10	-3.78	4.61
N.A.	358.63	342.57	2400	0.91	-16.06	23.72	-4.48	5.53
S.A.	333.45	312.70	2450	0.95	-20.75	27.69	-6.22	7.14
N. Pole	272.40	271.26	10440	0.92	-1.14	13.74	-0.42	4.28
N. Ferrel	344.05	341.56	10800	0.85	-2.49	16.38	-0.72	3.91
N. Hadley	405.77	376.50	10800	0.73	-29.27	32.79	-7.21	7.45
S. Hadley	375.69	349.05	10800	0.90	-26.64	30.88	-7.09	7.56
S. Ferrel	299.44	286.65	10800	0.94	-12.79	17.00	-4.27	4.84
S. Polar	134.46	131.39	10440	0.96	-3.07	27.58	-2.29	17.78
N.H.	341.51	330.43	32040	0.95	-11.08	22.68	-3.24	5.42
S.H.	271.39	257.10	32040	0.99	-14.29	25.82	-5.27	8.20
Global	306.45	293.76	64080	0.98	-12.68	24.30	-4.14	6.65
BSRN	350.01	317.91	29	0.93	-32.10	39.63	-9.17	9.17

#### 4.1.2.5 Summer Zonal Wind Speed at 10-meters

The pattern of summer zonal wind speed at 10-meters (U10) mean bias is displayed graphically in Figure 4.21 in which the overall pattern appears to be a slight underestimation of the zonal component, however, over the Southern ocean there are large underestimations not present in the annual mean analysis. Overall wind speed is not well predicted by GWRf with a global NMB value of -387.21%, which is smaller than the bias present in the annual mean. This large, negative NMB value corresponds to a mean bias of  $-0.16 \text{ m s}^{-1}$  which is caused by a low observed wind speed ( $0.04 \text{ m s}^{-1}$ ) from the reanalysis data. The majority of mean bias values fall within the range of  $\pm 5 \text{ m s}^{-1}$ , however performance is less accurate than the annual mean with a maximum mean bias of  $10.66 \text{ m s}^{-1}$  and a minimum mean bias value of  $-6.83 \text{ W m}^{-2}$ . The overall pattern of GWRf U10 performance is reflected in Table 4.12 in which the majority of circulation

cell domains display a negative NMB value (with the exception of the Ferrel cell). U10 displays very large absolute NMB values but still has a global Corr value of 0.93, slightly lower than the annual mean.

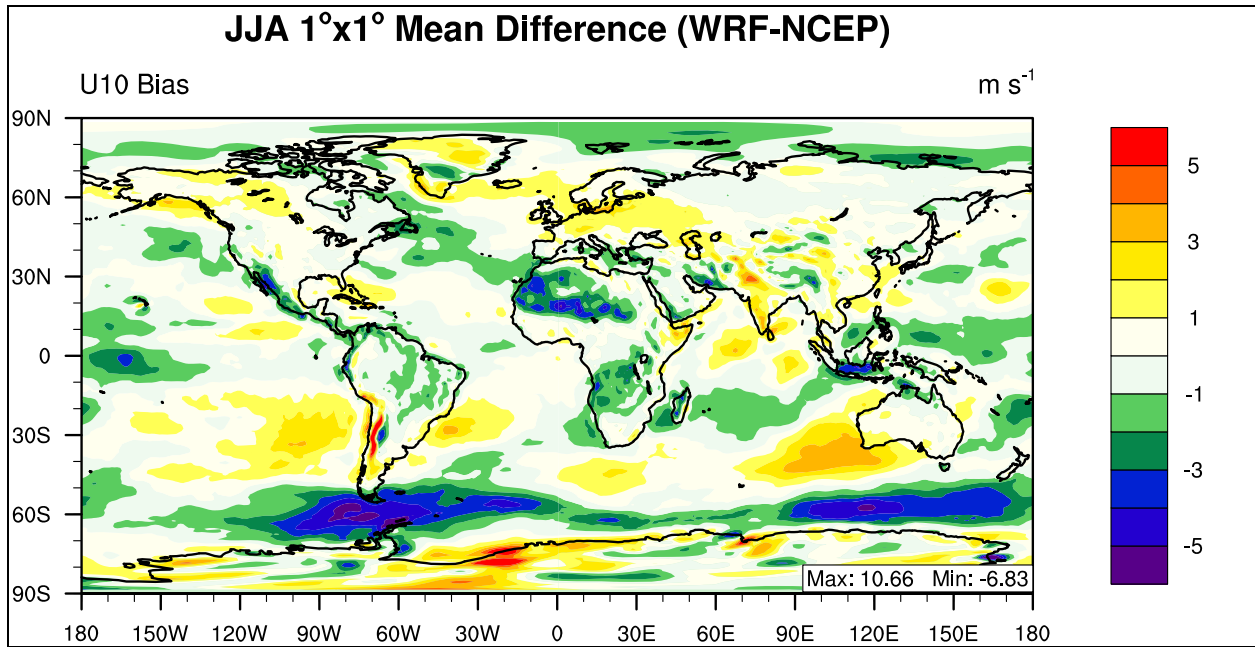


**Figure 4.21** 2001 summer mean bias of zonal wind at 10-meter.

**Table 4.12 Performance Statistics of GWRf 2001 summer mean Zonal Wind at 10-meter as compared with NCEP/NCAR Reanalysis.**

Name	MeanObs (m s <sup>-1</sup> )	MeanMod (m s <sup>-1</sup> )	Number	Corr	MB (m s <sup>-1</sup> )	RMSE	NMB%	NME%
Europe	0.55	1.48	1200	0.70	0.94	1.33	170.38	205.35
Africa	-0.34	-1.04	2925	0.85	-0.70	1.36	-206.46	-304.86
Asia	0.73	1.03	5100	0.89	0.30	1.07	40.27	108.62
Australia	-1.16	-0.47	1200	0.96	0.69	1.38	-59.79	-90.04
N.A.	0.11	0.15	2400	0.87	0.04	0.96	37.06	667.39
S.A.	0.83	0.30	2450	0.81	-0.52	1.94	-63.56	173.06
N. Pole	0.35	0.08	10440	0.48	-0.26	1.00	-75.94	234.88
N. Ferrel	0.65	0.66	10800	0.79	0.01	1.02	0.81	122.20
N. Hadley	-1.22	-1.40	10800	0.95	-0.18	1.23	-14.97	-77.66
S. Hadley	-3.42	-3.54	10800	0.90	-0.12	1.22	-3.59	-28.08
S. Ferrel	4.70	4.41	10800	0.76	-0.29	1.83	-6.19	29.47
S. Polar	-0.82	-0.94	10440	0.90	-0.11	1.90	-13.73	-178.69
N.H.	-0.08	-0.22	32040	0.92	-0.15	1.09	-185.01	-1083.90
S.H.	0.16	-0.01	32040	0.93	-0.18	1.68	-108.92	785.01
Global	0.04	-0.12	64080	0.93	-0.16	1.41	-387.21	2554.53

#### 4.1.2.6 Summer Meridional Wind Speed at 10-meters

The pattern of meridional wind speed at 10-meters (V10) mean bias is displayed graphically in Figure 4.22 and the spatial pattern appears to be similar to the zonal component with an overall slight underestimation. Meridional wind speed displays a global NMB value of -3.95%, which is significantly lower than the summer zonal component global domain average. This corresponds to a mean bias of -0.02 m s<sup>-1</sup>. The majority of mean bias values fall within the range of  $\pm 5$  m s<sup>-1</sup>, with a maximum mean bias of 5.82 m s<sup>-1</sup> and a minimum mean bias value of -6.84 m s<sup>-1</sup>, both of which increase in magnitude when compared with the annual mean. The overall pattern of GWRf V10 performance is reflected in Table 4.13 in which the majority of circulation cell and continental domains display a negative NMB value (with the exceptions of the Southern Hadley and Ferrel Cells). V10 also displays very large absolute NMB values but displays a global Corr value of 0.87.

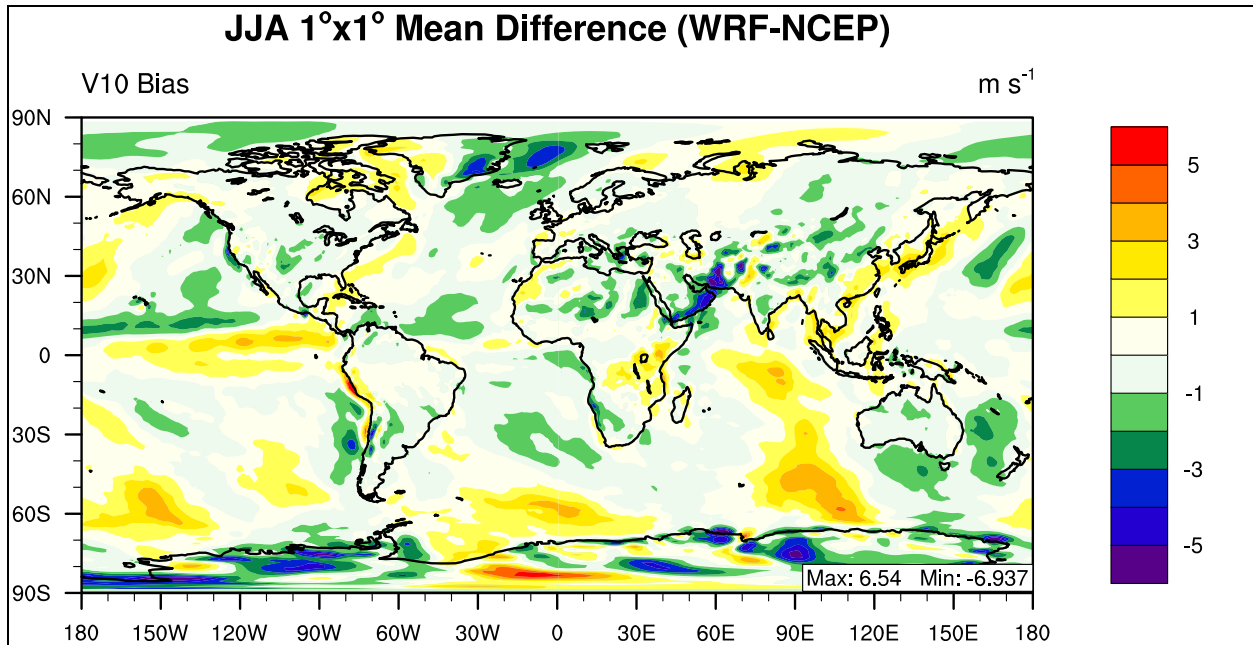


**Figure 4.22** 2001 summer mean bias of Meridional Wind at 10-meter.

**Table 4.13** Performance Statistics of GWRP 2001 summer mean Meridional Wind at 10-meter as compared with NCEP/NCAR Reanalysis.

Name	MeanObs (m s <sup>-1</sup> )	MeanMod (m s <sup>-1</sup> )	Number	Corr	MB (m s <sup>-1</sup> )	RMSE	NMB%	NME%
Europe	-0.08	-0.24	1200	0.85	-0.16	0.54	-199.14	-513.08
Africa	0.86	0.75	2925	0.93	-0.11	1.09	-12.94	98.56
Asia	0.50	0.27	5100	0.86	-0.23	1.23	-46.43	178.86
Australia	0.94	0.60	1200	0.95	-0.35	0.75	-36.69	66.06
N.A.	0.58	0.54	2400	0.87	-0.04	0.71	-7.33	99.27
S.A.	-0.44	-0.48	2450	0.81	-0.04	0.81	-9.50	-132.83
N. Pole	0.05	-0.11	10440	0.52	-0.16	0.99	-298.74	1488.10
N. Ferrel	0.19	0.09	10800	0.86	-0.09	0.97	-49.81	394.29
N. Hadley	0.42	0.38	10800	0.92	-0.03	1.18	-7.54	217.78
S. Hadley	1.99	2.11	10800	0.90	0.11	0.98	5.71	36.84
S. Ferrel	-1.06	-0.74	10800	0.68	0.32	1.24	29.91	-87.95
S. Polar	1.35	1.07	10440	0.87	-0.28	1.86	-20.50	108.48
N.H.	0.22	0.13	32040	0.87	-0.09	1.05	-42.41	367.67
S.H.	0.75	0.81	32040	0.87	0.06	1.40	7.30	137.66
Global	0.49	0.47	64080	0.87	-0.02	1.24	-3.95	189.73

#### 4.1.2.7 Summer Daily Precipitation Rate

The daily precipitation at the surface in GWRP is compared with the Global Precipitation Climatology Project (GPCP) for the summer of 2001 (JJA). Overall, the GWRP performance during summer appears to be overestimating daily precipitation rate and performing worse than the annual mean case. The maximum mean bias is higher ( $15.93 \text{ mm day}^{-1}$ ) and the minimum mean bias value is lower ( $-9.82 \text{ mm day}^{-1}$ ), indicating a tendency of the model to overestimate rainfall rate. Overall spatial trend shows that performance is the best in the Southern Hemisphere and worse in the Northern hemisphere as shown in Table 4.14. Globally, GWRP shows Corr values smaller than the annual mean (0.83), and worse bias performance with an NMB value of greater than 35% (38.64%). GWRP is compared with NCDC observations of monthly accumulated precipitation and it is shown that the spatial pattern is similar and the pattern of an overestimation of summer precipitation is consistent with the GPCP comparison.

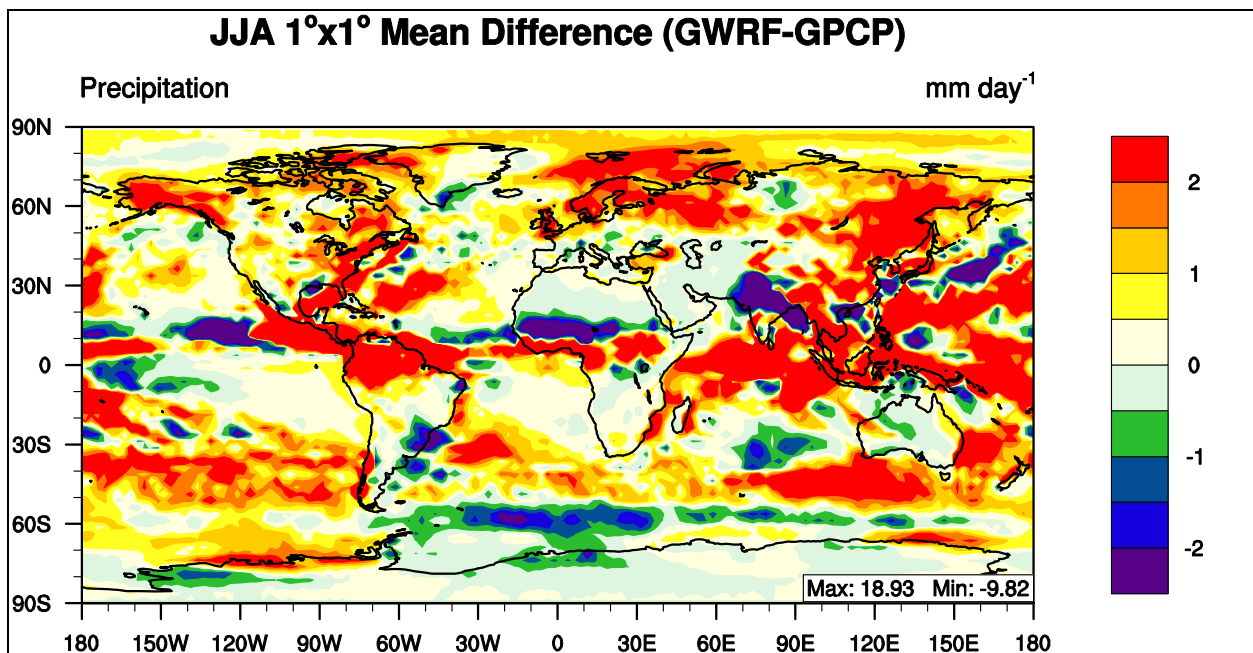
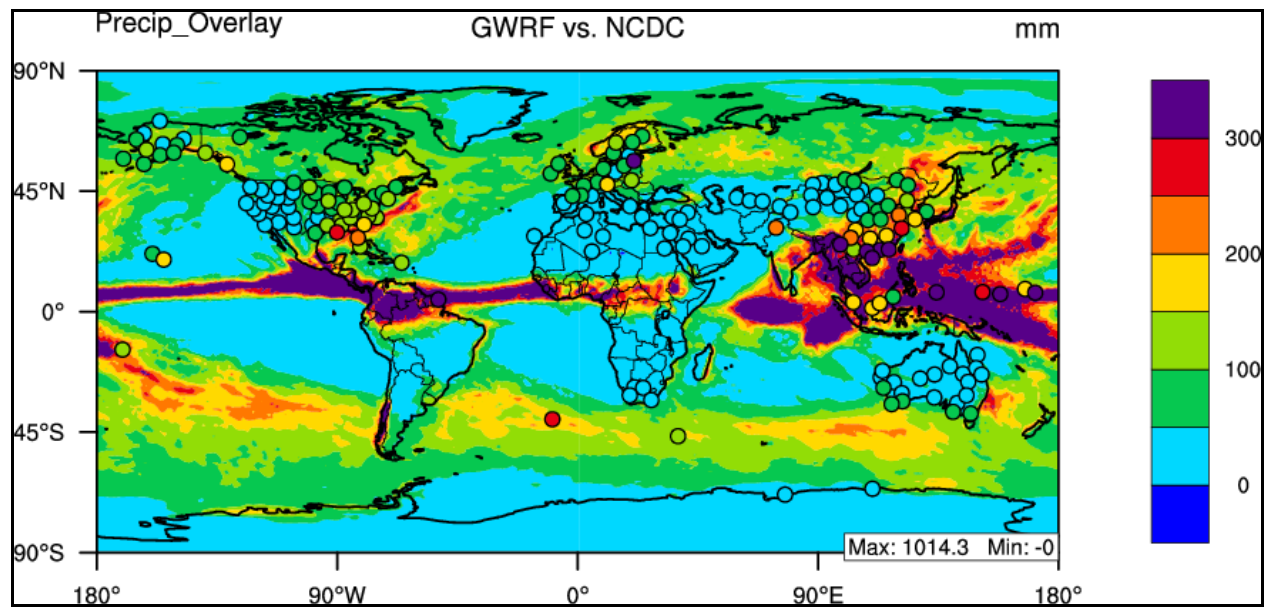


Figure 4.23 2001 summer mean bias of daily precipitation rate.



**Figure 4.24 2001 summer mean bias of monthly mean accumulated precipitation.**

**Table 4.14 Performance Statistics of GWRP 2001 summer mean daily rainfall rate for compared with GPCP (mm day<sup>-1</sup>) and NCDC (mm month<sup>-1</sup>).**

<b>Name</b>	<b>MeanObs (mm d<sup>-1</sup>)</b>	<b>MeanMod (mm d<sup>-1</sup>)</b>	<b>Number</b>	<b>Corr</b>	<b>MB (mm d<sup>-1</sup>)</b>	<b>RMSE</b>	<b>NMB%</b>	<b>NME%</b>
<b>Europe</b>	2.37	3.4	192	0.66	1.03	1.49	43.28	50.76
<b>Africa</b>	1.26	1.63	463	0.85	0.37	1.42	29.38	62.92
<b>Asia</b>	3.29	4.26	816	0.8	0.98	2.62	29.7	52.86
<b>Australia</b>	0.98	1.35	192	0.74	0.37	1	37.17	67.34
<b>N.A.</b>	2.49	3.68	384	0.71	1.19	1.8	47.6	55
<b>S.A.</b>	3.00	4.09	392	0.8	1.1	2.85	36.67	54.74
<b>N. Pole</b>	1.17	2.17	1728	0.64	1	1.28	85.17	89.48
<b>N. Ferrel</b>	2.30	3.14	1727	0.74	0.84	1.58	36.28	49.01
<b>N. Hadley</b>	4.04	5.48	1724	0.79	1.44	3.43	35.62	54.96
<b>S. Hadley</b>	1.79	2.69	1728	0.87	0.9	2.05	50.54	67.23
<b>S. Ferrel</b>	3.08	3.92	1728	0.5	0.84	1.56	27.3	39.51
<b>S. Polar</b>	0.97	1.11	1728	0.77	0.14	0.69	14.74	46.13
<b>N.H.</b>	2.5	3.6	5179	0.82	1.09	2.3	43.55	58.52
<b>S.H.</b>	1.94	2.57	5184	0.84	0.63	1.54	32.32	49.1
<b>Global</b>	2.22	3.08	10363	0.83	0.86	1.96	38.64	54.4
<b>NCDC</b>	93.20	116.77	172	0.67	23.57	88.50	25.29	58.48

### 4.1.3 Evaluation of 2001 winter (DJF) Simulation

#### 4.1.3.1 Winter Temperature at 2-meter

The temperature at 2-meters above the surface in GWRP is compared with NCEP/NCAR Reanalysis for the winter of 2001 (January, February, and December 2001). As shown in Figure 4.25, the mean bias performance is slightly worse for the winter case as opposed to the annual mean. The majority of mean bias values fall within the  $\pm 10$  °C range, however there are exceptions with a maximum mean bias value of 13.05 °C and a minimum mean bias value of -18.22 °C. Model performance is exceptionally complicated over the Polar Regions, with overestimations and underestimations in close proximity to each other over Antarctica and an overall underestimation over the arctic. Globally, GWRP shows good correlation values (0.99), but poor bias performance with an NMB value of -14.52%. This NMB value for the comparison with reanalysis data is similar to the comparison with NCDC data, which has a value of -17.21%, both of which are consistent showing an overall underprediction.

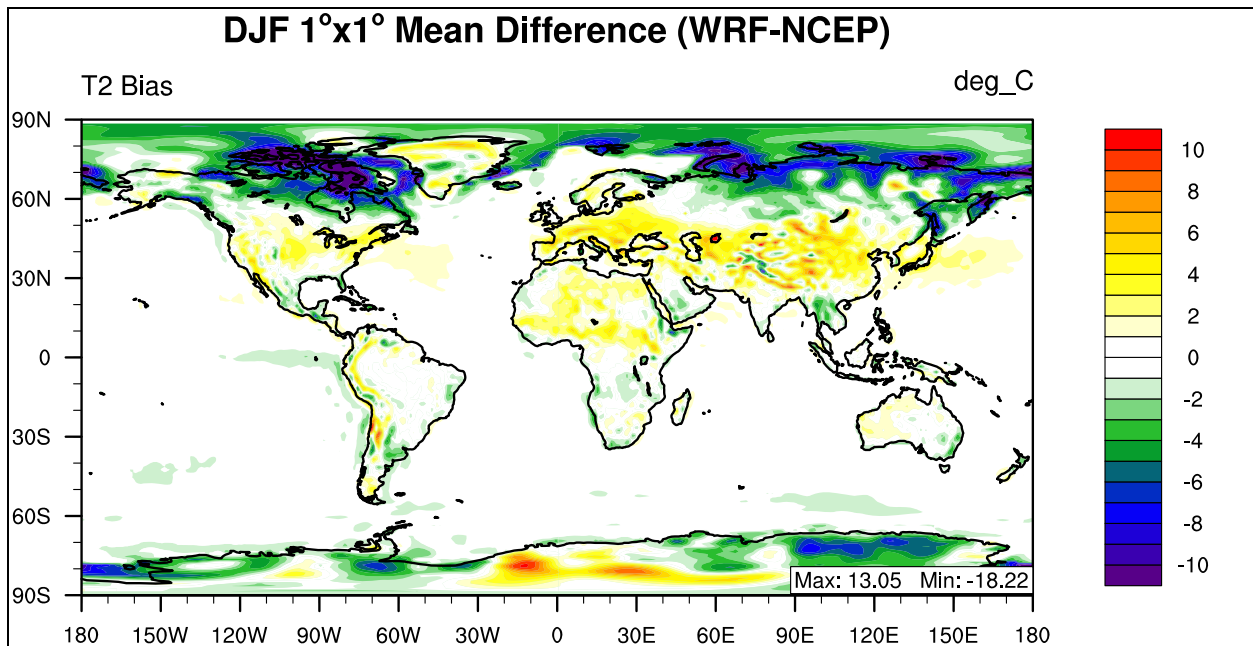
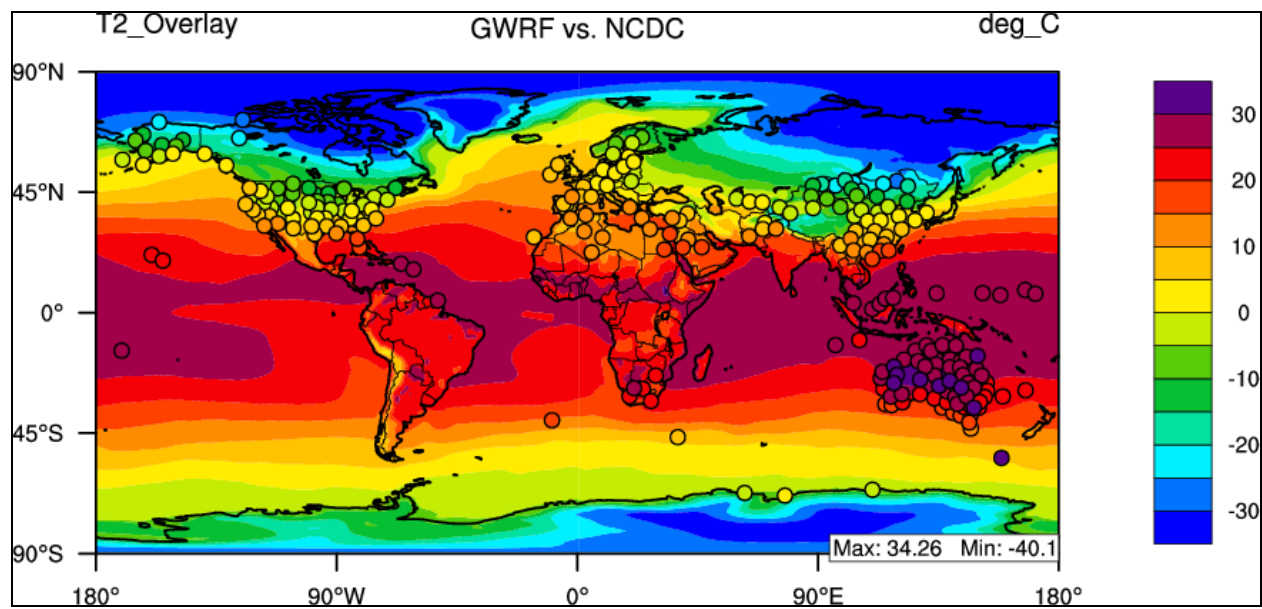


Figure 4.25 2001 winter mean bias of temperature at 2-meter.



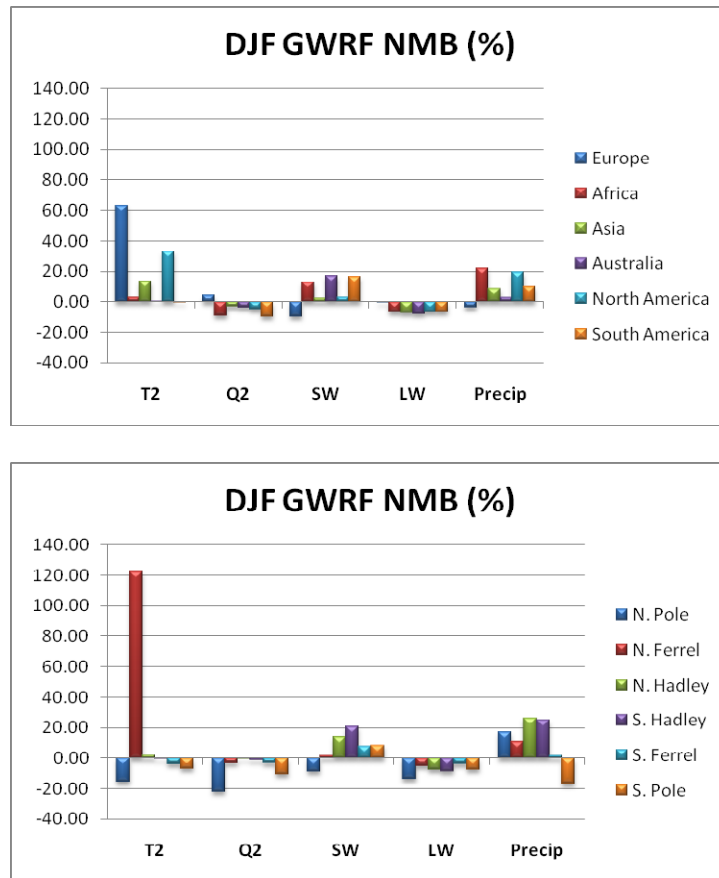
**Figure 4.26** 2001 winter mean bias of temperature at 2-meter compared with NCDC.

**Table 4.15 Performance Statistics of GWRf 2001 winter mean temperature at 2-meter as compared with NCEP/NCAR Reanalysis and NCDC data.**

Name	MeanObs (°C)	MeanMod (°C)	Number	Corr	MB (°C)	RMSE	NMB%	NME%
Europe	-2.70	-1.01	1200	0.94	1.69	2.87	62.59	85.50
Africa	20.32	20.89	2925	0.96	0.57	1.68	2.83	6.21
Asia	-3.50	-3.02	5100	0.99	0.48	3.01	13.59	65.19
Australia	25.96	26.08	1200	0.99	0.12	0.96	0.48	2.64
N.A.	1.00	1.32	2400	0.99	0.33	2.10	32.76	159.35
S.A.	18.67	18.62	2450	0.98	-0.05	1.54	-0.26	5.28
N. Pole	-23.27	-26.85	10440	0.95	-3.58	4.89	-15.37	17.02
N. Ferrel	-0.59	0.13	10800	0.98	0.72	2.41	121.83	286.57
N. Hadley	22.78	23.24	10800	0.97	0.46	1.26	2.00	3.73
S. Hadley	24.95	24.94	10800	0.96	-0.01	0.87	-0.03	2.04
S. Ferrel	11.88	11.40	10800	1.00	-0.47	0.72	-3.98	4.64
S. Polar	-12.29	-13.13	10440	0.98	-0.85	2.63	-6.89	15.16
N.H.	-0.10	-0.87	32040	0.99	-0.77	3.21	-738.14	2067.90
S.H.	8.41	7.97	32040	1.00	-0.44	1.64	-5.20	11.47
Global	4.15	3.55	64080	0.99	-0.60	2.55	-14.52	37.52
NCDC	11.62	9.62	243	0.55	-2.00	24.75	-17.21	36.23

An overview of statistical performance for the major boundary layer variables is shown graphically in Figure 4.27. Different from the annual and summer means, the largest NMB values are associated with temperature at 2-meters, and not daily precipitation rate, specifically for domains in the Northern mid-latitudes (e.g., Europe, N.A., Asia, and Northern Ferrel Cell). For the continental domains, the continents with large portions in the Northern Hemisphere (e.g., Europe, North America, and Asia) show a large overestimation of temperature at 2 meters. The largest overestimation of these domains occurs over Europe, with an NMB value of 62.59%, which actually corresponds to an MB of 1.69 °C. Over the circulation cell domains, the Northern Ferrel Cell is by far the largest with an NMB value of 121.83%, which corresponds to an MB value of 0.72. The winter case overall has lower NMBs for daily precipitation rate over both the continental and circulation cell domains, when compared with the annual and summer means. There is still a pattern of an underestimation of water vapor mixing ratio at 2 meters and an

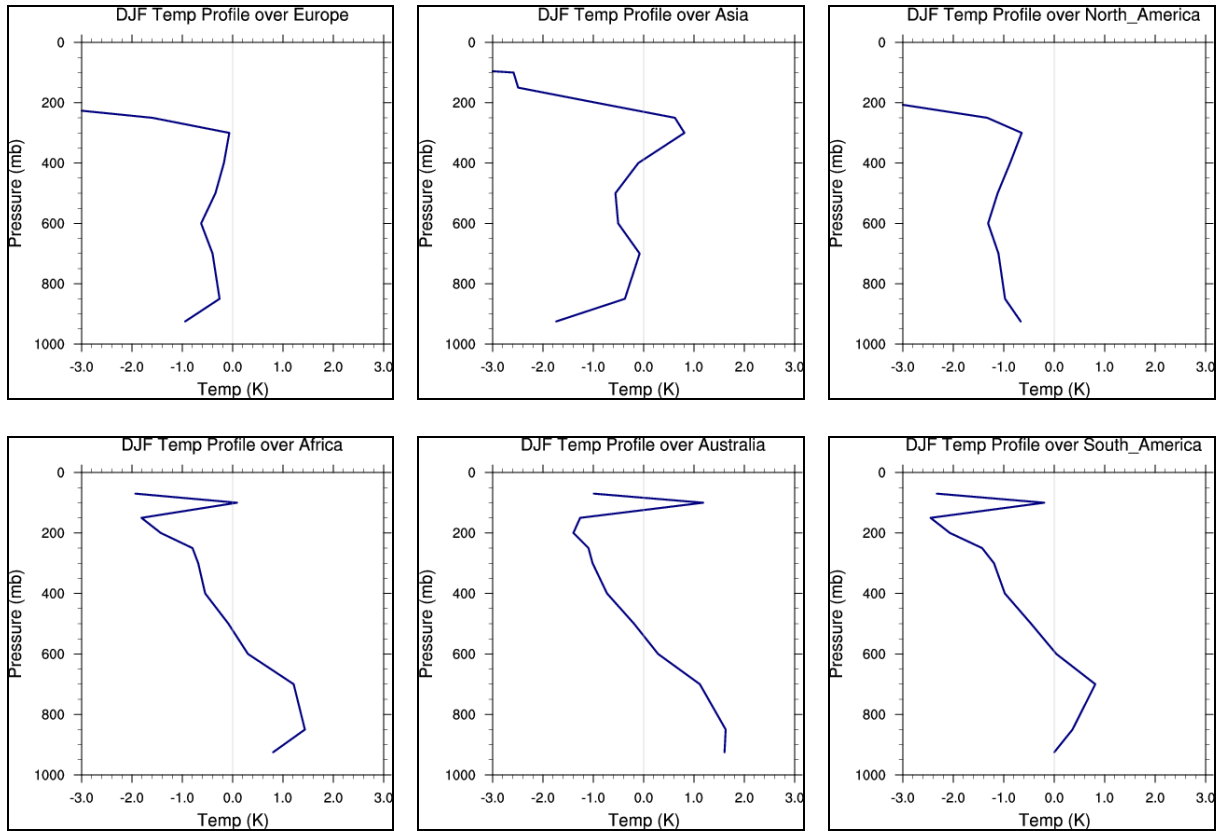
underestimation of downward longwave flux. The vertical profile of temperature performance is evaluated in Figure 4.28, which shows that GWRf captures vertical temperature distribution within  $\pm 2$  degrees up to approximately 300 hPa over the six continental domains.



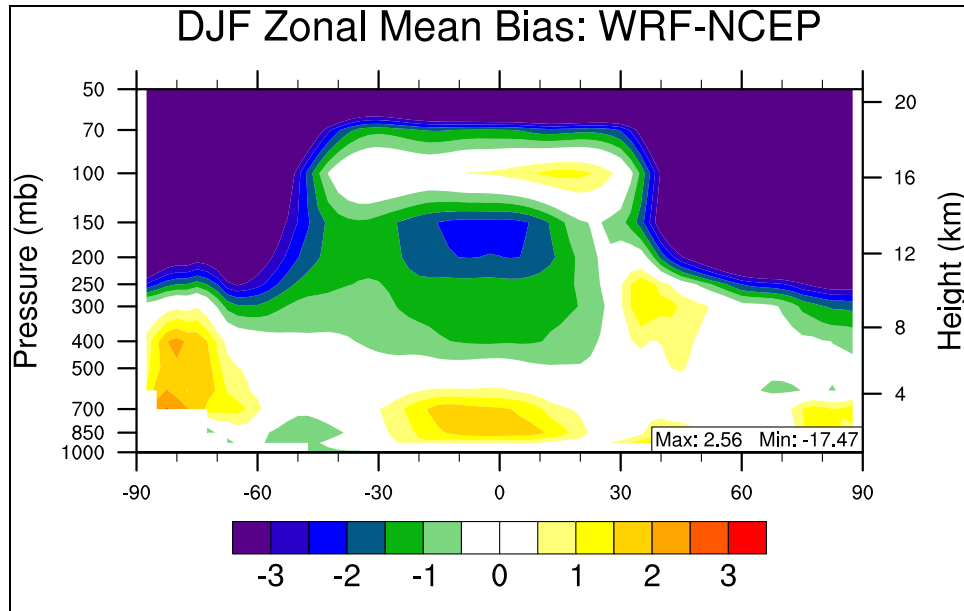
**Figure 4.27** 2001 winter mean normalized mean bias (%) of major meteorological variables for (a) the six continental domains and (b) the six circulation cell domains.

Figure 4.29 is the zonal mean bias of GWRf versus NCEP/NCAR Reanalysis data. GWRf captures the vertical temperature distribution within  $\pm 2$  degrees up to approximately 300 hPa, with smaller overestimations near the surface over Antarctica when compared with the annual and summer cases. Zonally the model performs the best near the surface of the Northern mid-latitudes, with the model slightly underestimating temperatures over the Southern mid-latitudes.

Slight overestimations exist in the lower troposphere over the ITCZ and polar domains. Aloft there is an underestimation of temperatures over the Tropics, with an emphasis on the Southern Hadley Cell, between 400 hPa and 100 hPa. The winter case also displays the large underestimation of temperatures above the tropopause.



**Figure 4.28** Vertical profiles of winter mean temperature mean bias over the six populated continents.



**Figure 4.29 2001 winter mean zonal mean bias of temperature.**

#### **4.1.3.2 Winter Water Vapor Mixing Ratio at 2-meter**

The global distribution of winter mean bias for water vapor mixing ratio at 2-meter is displayed in Figure 4.30. When compared with the annual spatial mean bias plot, the underestimations over the Tropics are larger than the annual case, and the areas of large underestimation shift to the Southern Hadley Cell and are co-located with areas that receive large amounts of convective precipitation during this season. Overall the majority of mean bias values are within the range of  $\pm 5 \text{ g kg}^{-1}$ , however, the performance during winter is better than the summer case with smaller maximum and minimum mean biases. The maximum mean bias is  $5.75 \text{ g kg}^{-1}$  and the minimum mean bias is  $-8.10 \text{ g kg}^{-1}$ . The overall underestimation of Q2 is also reflected in Table 4.16 in which all domains (except Europe and Northern Hadley Cell) have a negative NMB value. The global NMB value is similar to the annual case ( $-2.29\%$ ) and slightly better than the summer case, with a winter value of  $-2.22\%$ . Overall correlation coefficient values are similar to annual mean performance, with a global Corr value of 0.99.

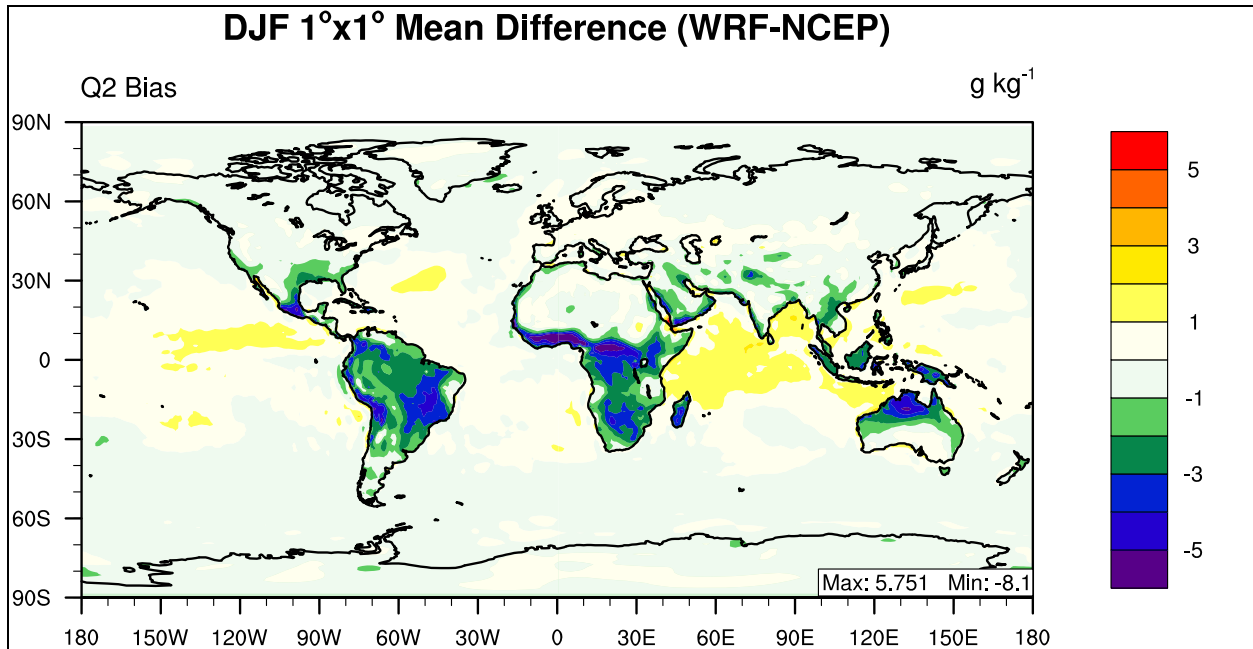


**Figure 4.30** 2001 winter mean bias of water vapor mixing ratio at 2-meter.

**Table 4.16** Performance Statistics of GWRF 2001 winter mean water vapor mixing ratio at 2-meter compared with NCEP/NCAR Reanalysis.

Name	MeanObs (g kg <sup>-1</sup> )	MeanMod (g kg <sup>-1</sup> )	Number	Corr	MB (g kg <sup>-1</sup> )	RMSE	NMB%	NME%
Europe	3.42	3.57	1200	0.95	0.15	0.43	4.49	9.63
Africa	10.86	9.87	2925	0.96	-0.99	1.91	-9.15	12.60
Asia	4.85	4.69	5100	0.99	-0.15	0.85	-3.18	11.44
Australia	13.03	12.53	1200	0.95	-0.51	1.68	-3.88	9.10
N.A.	5.51	5.24	2400	0.99	-0.27	0.79	-4.87	8.97
S.A.	13.10	11.77	2450	0.97	-1.33	1.91	-10.13	10.91
N. Pole	0.95	0.74	10440	0.98	-0.21	0.28	-22.07	23.71
N. Ferrel	4.40	4.25	10800	0.99	-0.15	0.51	-3.42	8.10
N. Hadley	13.86	13.87	10800	0.98	0.01	1.26	0.06	6.09
S. Hadley	16.57	16.36	10800	0.90	-0.21	1.37	-1.27	5.72
S. Ferrel	8.00	7.76	10800	0.99	-0.24	0.42	-3.01	3.94
S. Polar	2.15	1.92	10440	0.98	-0.23	0.36	-10.72	12.65
N.H.	6.46	6.35	32040	0.99	-0.12	0.81	-1.80	7.39
S.H.	8.98	8.76	32040	0.99	-0.23	0.86	-2.53	5.72
Global	7.72	7.55	64080	0.99	-0.17	0.83	-2.22	6.42

#### 4.1.3.3 Winter Downward Shortwave Flux at Ground Surface

The pattern of winter downward shortwave flux mean bias is displayed graphically in Figure 4.31, and reflects the annual pattern of an overestimation in the Tropics (30°N-30°S), however in the winter case there is a large underestimation off the Pacific Coast of South America and large overestimations over the Southern Oceans. The majority of mean bias values fall within the range of  $\pm 100 \text{ W m}^{-2}$ , the maximum mean bias is very similar to the summer case with a value of  $132.9 \text{ W m}^{-2}$ , while the minimum mean bias value largely decreases to  $-228.1 \text{ W m}^{-2}$ . The pattern of GWRP SWDOWN performance is reflected in Table 4.17 in which all of the circulation cell domains display a positive NMB value except for the high Northern latitudes (Northern Polar Cell and Europe) which display negative NMB values, with a global NMB value of 11.45%. Correlation values are improved from the annual mean, however, not as much as the summer case, with the Southern Hadley Cell increasing from 0.34 to 0.41 and the Southern Polar Cell Corr value increases from 0.32 to 0.88. Globally, the Corr value is improved to a value of 0.96.

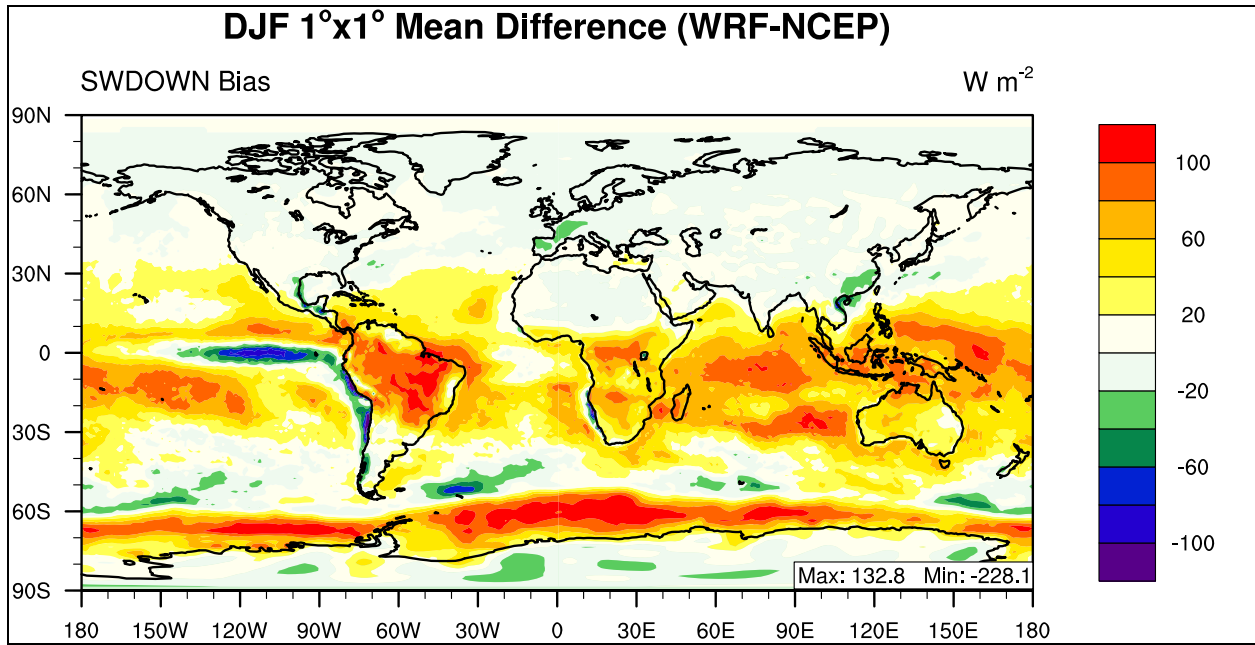


**Figure 4.31** 2001 winter mean bias of downward shortwave flux at the surface.

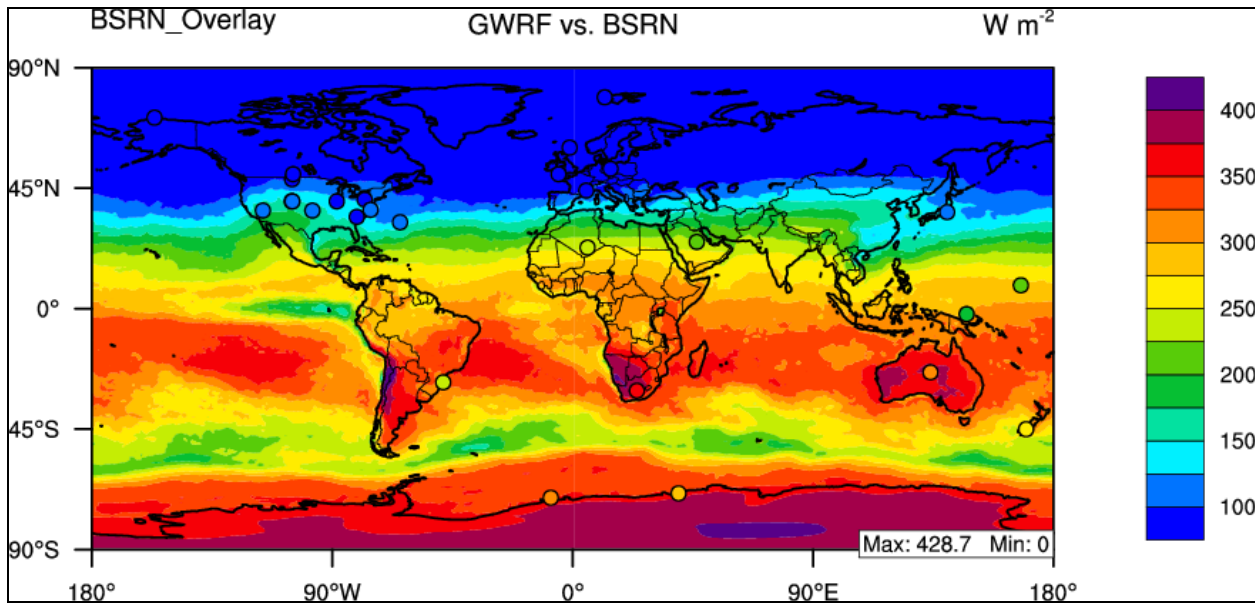


**Figure 4.32** 2001 winter mean bias of downward shortwave flux at the surface compared with BSRN.

A comparison with BSRN data reveals that GWRP overestimates SWDOWN over the Northern mid-latitudes, explaining the large overestimations of temperature in the Northern Ferrel cell. The mean BSRN values and the GWRP global mean both indicate an overall overestimation during winter of 2001 and display similar statistical performance.

**Table 4.17 Performance Statistics of GWRP 2001 winter mean downward shortwave flux at the surface as compared with NCEP/NCAR Reanalysis.**

Name	MeanObs (W m <sup>-2</sup> )	MeanMod (W m <sup>-2</sup> )	Number	Corr	MB (W m <sup>-2</sup> )	RMSE	NMB%	NME%
Europe	60.18	54.38	1200	0.98	-5.80	8.94	-9.64	10.49
Africa	258.91	292.25	2925	0.78	33.35	46.74	12.88	14.10
Asia	135.66	138.86	5100	0.98	3.20	15.88	2.36	6.50
Australia	297.89	349.05	1200	0.83	51.16	54.55	17.17	17.24
N.A.	126.88	130.86	2400	0.97	3.98	13.17	3.13	6.46
S.A.	261.50	305.07	2450	0.53	43.58	61.85	16.66	19.59
N. Pole	11.08	10.11	7907	1.00	-0.97	1.45	-8.76	9.84
N. Ferrel	100.30	101.89	10800	0.98	1.60	8.45	1.59	6.21
N. Hadley	218.24	248.20	10800	0.72	29.96	42.16	13.73	15.55
S. Hadley	270.01	326.31	10800	0.41	56.29	65.17	20.85	22.36
S. Ferrel	252.79	272.71	10800	0.67	19.92	37.29	7.88	11.12
S. Polar	333.05	361.01	10440	0.88	27.95	49.31	8.39	10.88
N.H.	119.56	130.85	29507	0.98	11.29	26.02	9.44	12.54
S.H.	284.75	319.55	32040	0.75	34.80	51.89	12.22	14.62
Global	205.55	229.08	61547	0.96	23.53	41.55	11.45	14.04
BSRN	143.08	181.61	28	0.98	38.53	46.42	26.92	27.08

#### 4.1.3.4 Winter Downward Longwave Flux at Ground Surface

The pattern of winter downward longwave flux mean bias is displayed graphically in Figure 4.33 in which the overall pattern is an underestimation with a global NMB value of -7.15%, which is a larger decrease from the annual mean than the summer case. All mean bias values fall within the range of  $\pm 100$  W m<sup>-2</sup>, with the maximum mean bias larger (95.98 W m<sup>-2</sup>) and a minimum mean bias (-84.14 W m<sup>-2</sup>) smaller than the annual mean. The overall pattern of GWRP GLW performance is consistent with the annual and summer means, as shown in Table

4.18, in which all of the domains display a negative NMB value. Overall Corr values are above 0.80, with the Southern Hadley Cell displaying the lowest value, which is consistent with the annual mean. Globally, the correlation value is 0.98. Figure 4.34 shows that when compared with BSRN observations; GWRf captures the spatial distribution of GLW well, with a trend for underestimation of GLW during winter. The BSRN mean and Global NCEP/NCAR Reanalysis comparisons are consistent, showing an overall underestimation and similar statistical performance.

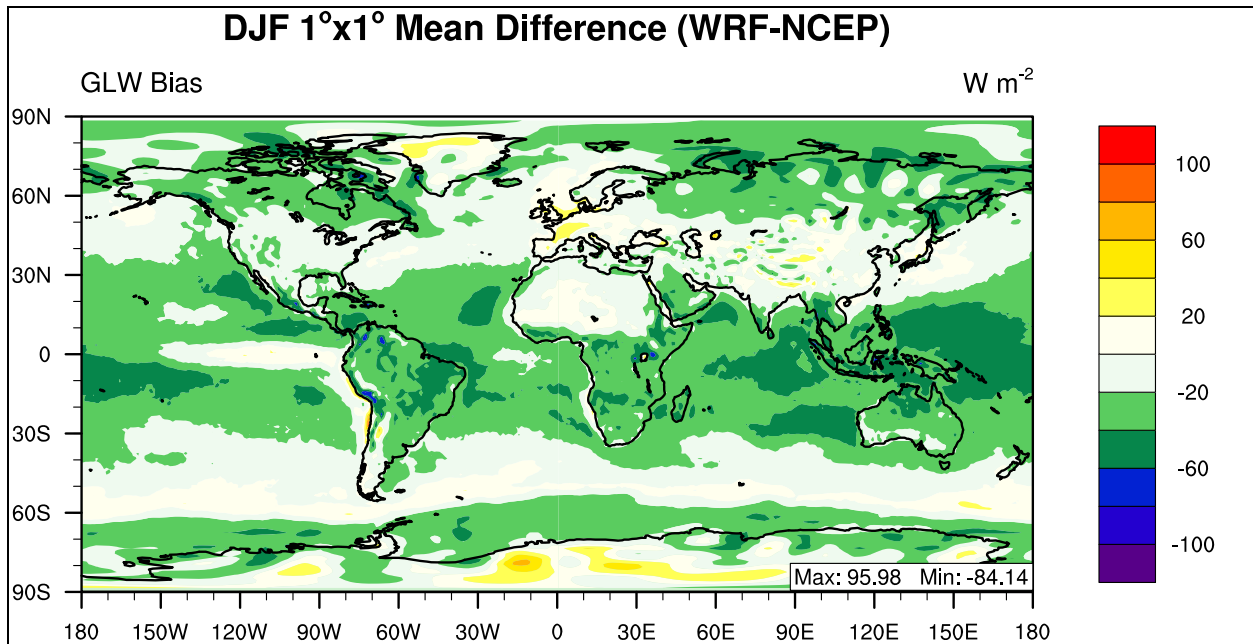


**Figure 4.33** 2001 winter mean bias of downward longwave flux at the surface.

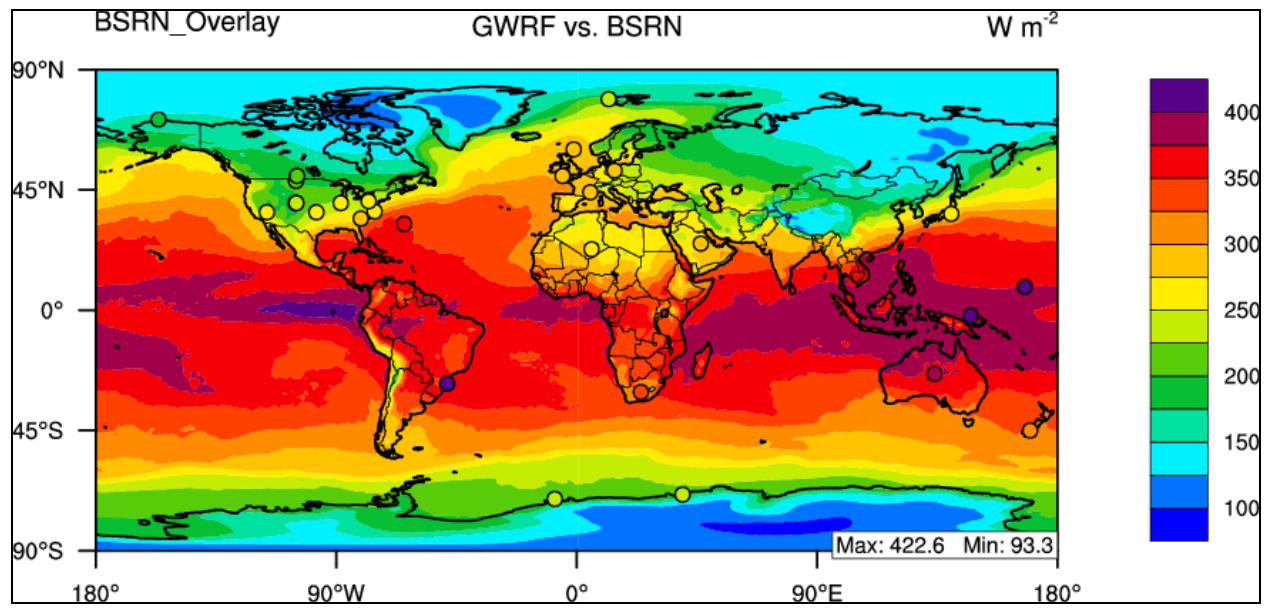


**Figure 4.34** 2001 winter mean bias of downward longwave flux at the surface as compared with BSRN.

**Table 4.18 Performance Statistics of GWRP 2001 winter mean downward longwave flux at the surface as compared with NCEP/NCAR Reanalysis and BSRN data.**

Name	MeanObs (W m <sup>-2</sup> )	MeanMod (W m <sup>-2</sup> )	Number	Corr	MB (W m <sup>-2</sup> )	RMSE	NMB%	NME%
Europe	242.95	241.81	1200	0.91	-1.14	14.62	-0.47	4.77
Africa	347.69	324.72	2925	0.96	-22.97	28.21	-6.61	7.00
Asia	244.26	226.80	5100	0.98	-17.46	24.42	-7.15	8.34
Australia	391.63	360.00	1200	0.95	-31.63	32.92	-8.08	8.08
N.A.	264.74	246.07	2400	0.99	-18.67	21.91	-7.05	7.17
S.A.	361.00	336.95	2450	0.92	-24.05	30.90	-6.66	7.46
N. Pole	176.36	152.89	10440	0.92	-23.47	27.28	-13.31	13.98
N. Ferrel	255.95	242.77	10800	0.97	-13.18	19.16	-5.15	6.27
N. Hadley	373.93	346.37	10800	0.95	-27.56	31.83	-7.37	7.64
S. Hadley	399.85	366.24	10800	0.80	-33.61	35.79	-8.40	8.59
S. Ferrel	325.11	313.71	10800	0.93	-11.40	17.14	-3.51	4.27
S. Polar	188.80	174.58	10440	0.96	-14.23	25.42	-7.54	11.79
N.H.	269.78	248.41	32040	0.99	-21.38	26.60	-7.92	8.55
S.H.	305.89	286.08	32040	0.98	-19.81	27.23	-6.48	7.69
Global	287.84	267.24	64080	0.98	-20.59	26.92	-7.15	8.09
BSRN	291.18	261.34	28	0.93	-30.04	39.59	-10.32	10.79

#### 4.1.3.5 Winter Zonal Wind Speed at 10-meter

The pattern of winter zonal wind speed at 10-meter (U10) mean bias is displayed graphically in Figure 4.35 in which the overall pattern appears to be a slight underestimation of the zonal component, however over the North Atlantic there are large overestimations not present in the annual mean analysis. Overall wind speed is not well predicted by GWRP with a global NMB value of -68.47%, which is smaller than the bias present in both the annual and summer mean. This large, negative NMB value corresponds to a mean bias of -0.04 m s<sup>-1</sup> and is caused by a very low wind speed (-0.06 m s<sup>-1</sup>) from the reanalysis dataset. The majority of mean bias values fall within the range of  $\pm 5$  m s<sup>-1</sup> and the performance is comparable to the annual mean with a maximum mean bias of 8.57 m s<sup>-1</sup> and a minimum mean bias value of -5.92 W m<sup>-2</sup>.

U10 displays very large absolute NMB values but still has a global Corr value of 0.94, slightly better than the summer mean.

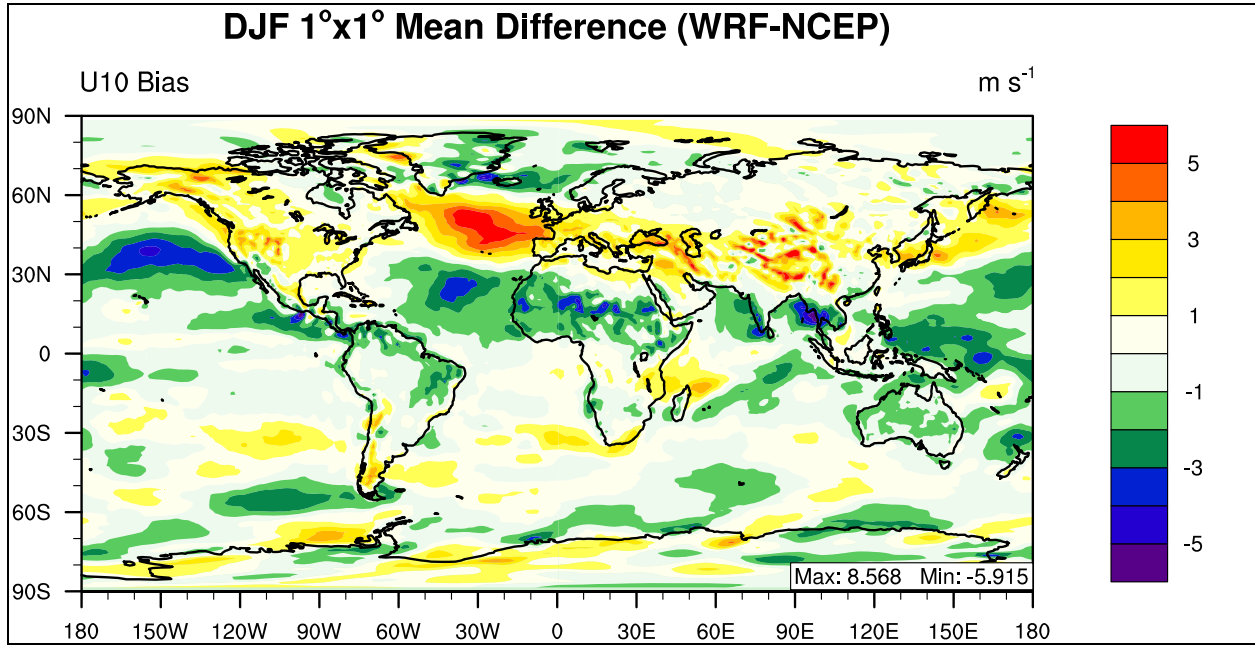


**Figure 4.35** 2001 winter mean bias of zonal wind at 10-meter.

**Table 4.19 Performance Statistics of GWRP winter mean zonal wind at 10-meter as compared with NCEP/NCAR Reanalysis.**

Name	MeanObs (m s <sup>-1</sup> )	MeanMod (m s <sup>-1</sup> )	Number	Corr	MB (m s <sup>-1</sup> )	RMSE	NMB%	NME%
Europe	0.68	1.36	1200	0.23	0.68	1.44	99.13	161.65
Africa	-0.71	-0.96	2925	0.82	-0.26	1.34	-36.32	147.68
Asia	-0.13	0.31	5100	0.88	0.45	1.63	336.87	844.55
Australia	-0.25	-1.04	1200	0.95	-0.79	1.01	-314.73	355.64
N.A.	0.69	1.31	2400	0.91	0.62	1.24	90.60	143.51
S.A.	0.59	0.36	2450	0.95	-0.23	1.17	-39.35	156.09
N. Pole	0.14	0.18	10440	0.77	0.04	1.03	26.52	529.57
N. Ferrel	1.75	2.64	10800	0.67	0.89	2.01	51.16	89.00
N. Hadley	-3.14	-4.05	10800	0.92	-0.91	1.51	-29.10	38.75
S. Hadley	-2.38	-2.67	10800	0.94	-0.29	1.00	-12.06	32.25
S. Ferrel	3.87	3.87	10800	0.96	-0.01	0.98	-0.14	19.98
S. Polar	-0.63	-0.60	10440	0.89	0.03	1.16	4.33	149.41
N.H.	-0.42	-0.41	32040	0.91	0.01	1.58	1.48	281.06
S.H.	0.30	0.21	32040	0.96	-0.09	1.05	-30.09	275.93
Global	-0.06	-0.10	64080	0.94	-0.04	1.34	-68.47	1642.83

#### 4.1.3.6 Winter Meridional Wind Speed at 10-meters

The pattern of winter meridional wind speed at 10-meters (V10) mean bias is displayed graphically in Figure 4.36 and the spatial pattern appears to be similar to the zonal component with an overall slight underestimation. Meridional wind speed displays a global NMB value of -31.31%, which is higher than both the summer and annual meridional means. This corresponds to a mean bias of -0.05 m s<sup>-1</sup>. The majority of mean bias values fall within the range of  $\pm 5$  m s<sup>-1</sup>, with a maximum mean bias of 5.19 m s<sup>-1</sup> and a minimum mean bias value of -8.96 m s<sup>-1</sup>, which is fairly close to the summer and annual means. The overall pattern of GWRP V10 performance is reflected in Table 4.20 in which the majority of domains display a negative NMB value, however this trend is not as clear as in the summer or annual cases. V10 also displays very large absolute NMB values and the low Corr values for individual domains, but still displays a global Corr value of 0.86.

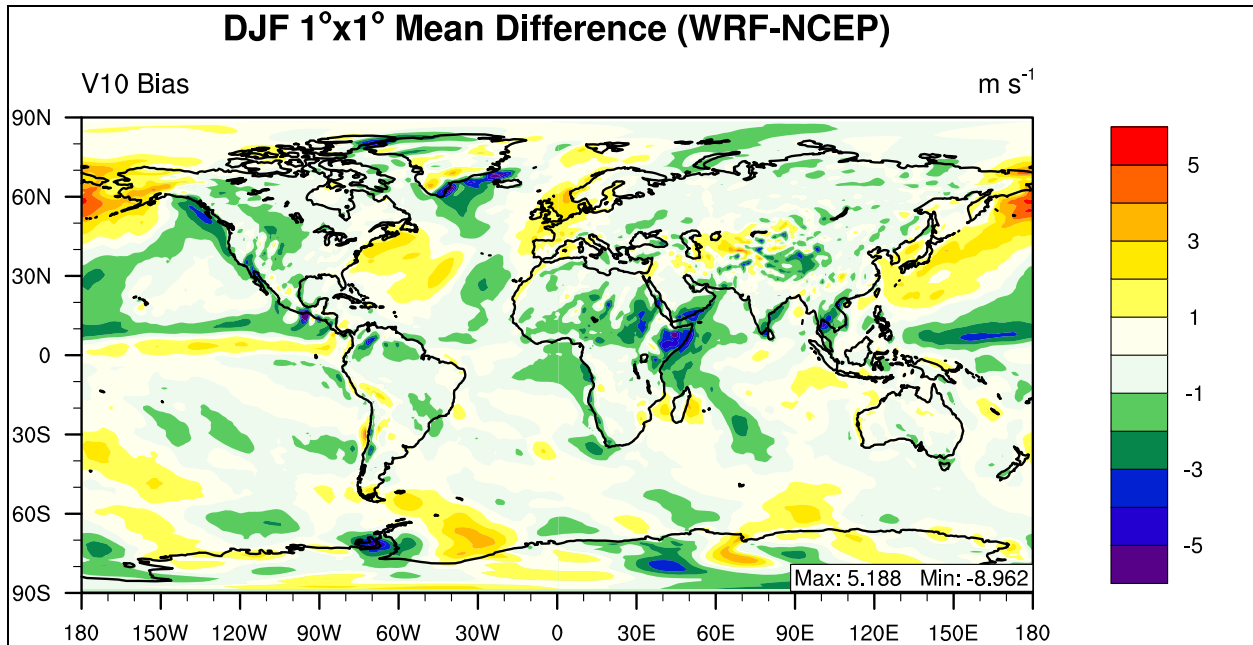


**Figure 4.36** 2001 winter mean bias of meridional wind at 10-meter.

**Table 4.20** Performance Statistics of GWRP 2001 winter mean meridional wind at 10-meter as compared with NCEP/NCAR Reanalysis.

Name	MeanObs (m s <sup>-1</sup> )	MeanMod (m s <sup>-1</sup> )	Number	Corr	MB (m s <sup>-1</sup> )	RMSE	NMB%	NME%
<b>Europe</b>	0.47	0.84	1200	0.74	0.37	1.10	77.66	176.41
<b>Africa</b>	0.36	-0.32	2925	0.92	-0.67	1.28	-189.11	270.23
<b>Asia</b>	-0.29	-0.59	5100	0.88	-0.30	1.09	-102.29	277.19
<b>Australia</b>	1.01	1.08	1200	0.95	0.07	0.62	7.11	47.51
<b>N.A.</b>	-0.38	-0.57	2400	0.74	-0.19	1.03	-50.64	207.36
<b>S.A.</b>	-1.06	-1.06	2450	0.82	0.00	1.02	0.00	73.86
<b>N. Pole</b>	0.05	0.09	10440	0.81	0.04	1.10	80.31	1655.17
<b>N. Ferrel</b>	0.31	0.46	10800	0.74	0.15	1.35	47.51	335.30
<b>N. Hadley</b>	-1.69	-2.22	10799	0.83	-0.53	1.30	-31.21	60.38
<b>S. Hadley</b>	0.76	0.67	10799	0.94	-0.09	0.81	-12.09	81.15
<b>S. Ferrel</b>	-0.90	-0.79	10800	0.88	0.11	0.80	11.72	67.34
<b>S. Polar</b>	0.50	0.52	10440	0.77	0.02	1.28	4.11	207.65
<b>N.H.</b>	-0.45	-0.57	32039	0.83	-0.12	1.26	-25.73	211.90
<b>S.H.</b>	0.12	0.13	32039	0.88	0.01	0.98	9.61	647.13
<b>Global</b>	-0.17	-0.22	64078	0.86	-0.05	1.13	-31.31	509.57

#### 4.1.3.7 Winter Daily Precipitation Rate

In Figure 4.37, GWRP during winter appears to be overestimating daily precipitation rate, with a complicated scenario in the Tropics. The maximum mean bias is higher (23.01 mm day<sup>-1</sup>) than the summer and annual cases, while the minimum mean bias value is lower (-9.82 mm day<sup>-1</sup>) than the annual case and comparable to the summer case, indicating a tendency of the model to overestimate rainfall rate during this season. Overall spatial trend agrees with the annual mean, in which performance is the best at the mid-latitudes (Northern and Southern Ferrel Cells) and the worst in the Tropics (Northern and Southern Hadley Cells) as illustrated in Figure 4.22 and shown in Table 4.21, in which the Northern and Southern Ferrel Cells have NMB values of less than 11%, while the Hadley cells have NMB values over 25%. To further evaluate GWRP precipitation performance, monthly mean accumulated precipitation is compared with NCDC observations in Figure 4.38, in which the distribution of precipitation aligns well with GWRP except for a few outliers.

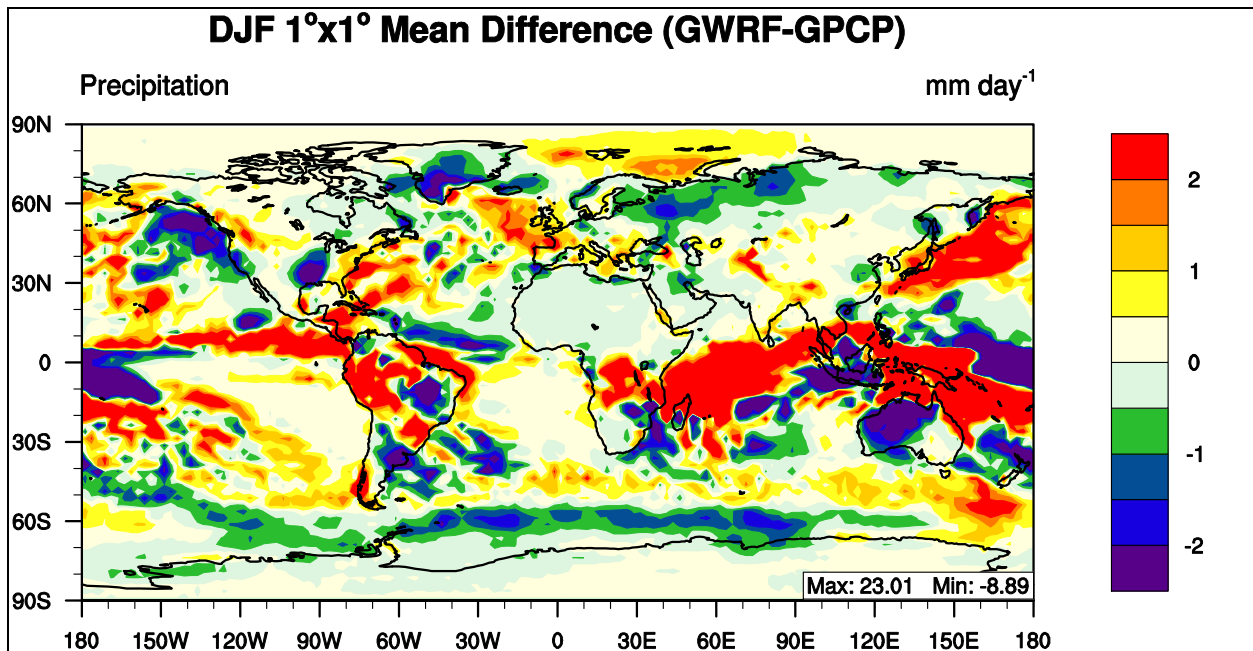
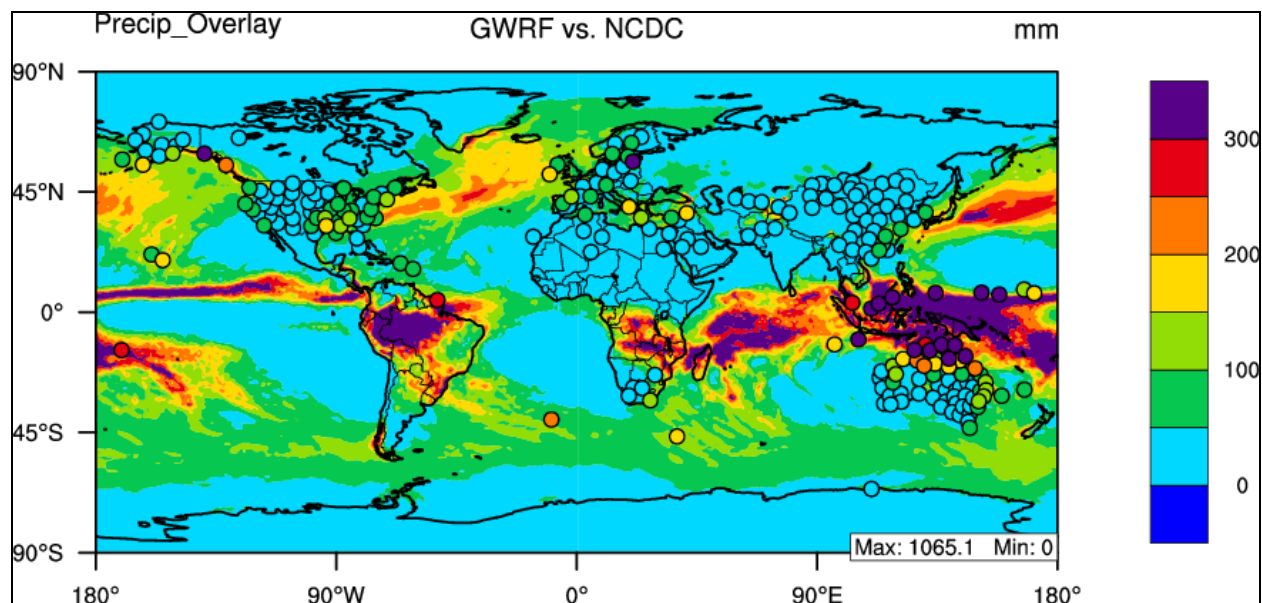


Figure 4.37 2001 winter mean bias of daily precipitation rate.



**Figure 4.38** 2001 winter mean bias of monthly mean accumulated precipitation.

**Table 4.21** Performance Statistics of GWRf 2001 winter mean daily precipitation rate as compared with GPCP ( $\text{mm day}^{-1}$ ) and NCDC ( $\text{mm month}^{-1}$ ).

Name	MeanObs	MeanMod	Number	Corr	MB	RMSE	NMB%	NME%
Europe	2.28	2.2	192	0.52	-0.08	0.76	-3.55	26.89
Africa	1.67	2.04	468	0.87	0.37	1.53	22.09	46.84
Asia	0.96	1.04	816	0.74	0.08	0.91	8.34	54.38
Australia	3.43	3.53	192	0.76	0.09	3.71	2.66	59.27
N.A.	1.55	1.84	384	0.76	0.3	1.11	19.18	45.52
S.A.	4.37	4.8	392	0.87	0.43	2.07	9.76	33.25
N. Pole	0.75	0.88	1724	0.79	0.13	0.66	16.78	63.23
N. Ferrel	2.63	2.92	1728	0.85	0.29	1.24	10.87	32.72
N. Hadley	2.09	2.63	1728	0.83	0.54	2.09	26.03	55.82
S. Hadley	3.7	4.63	1728	0.77	0.93	3.13	25.15	53.11
S. Ferrel	2.56	2.59	1728	0.58	0.04	1.03	1.49	30.36
S. Polar	0.77	0.65	1719	0.83	-0.13	0.45	-16.44	38.59
N.H.	1.83	2.15	5180	0.85	0.32	1.45	17.47	45.73
S.H.	2.34	2.63	5175	0.81	0.28	1.92	11.99	43.24
Global	2.09	2.39	10355	0.83	0.3	1.7	14.39	44.33
NCDC	82.83	78.56	223	0.71	-4.27	80.97	-5.15	55.36

## 4.2 Sensitivity to Horizontal Grid Resolution

### 4.2.1 2001 Simulations at a Horizontal Grid Resolution of $4^\circ \times 5^\circ$

#### 4.2.1.1 2001 Temperature at 2-meter

The temperature at 2-meter above the surface in GWRP is compared with NCEP/NCAR Reanalysis data for the annual mean of 2001. As shown in Figure 4.39, the majority of mean bias values fall within the  $\pm 10^\circ\text{C}$  range, with the maximum mean bias value of  $15.99^\circ\text{C}$  and a minimum mean bias value of  $-11.54^\circ\text{C}$ , both of these extremes are worse than the  $1^\circ \times 1^\circ$  annual case discussed in 4.1.1.1. Model performance is the best at the equator and worst at the poles as illustrated in Figure 4.39 and shown in Table 4.22, in which the Northern and Southern Hadley Cells have NMB values of less than 1%, which is also true in the annual  $1^\circ \times 1^\circ$  case. The difference here is that the South Pole cell also displays an NMB values less than 1% while the rest of the circulation cells have NMB values over 1%.

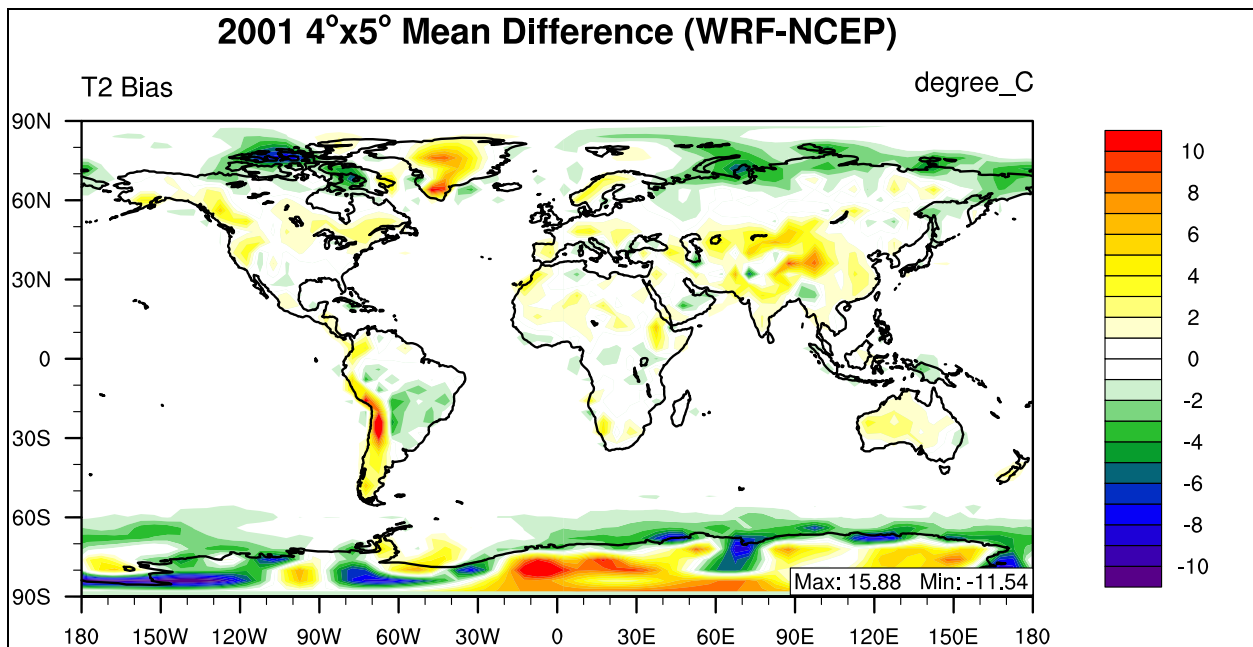


**Figure 4.39** 2001 mean bias of temperature at 2-meter.

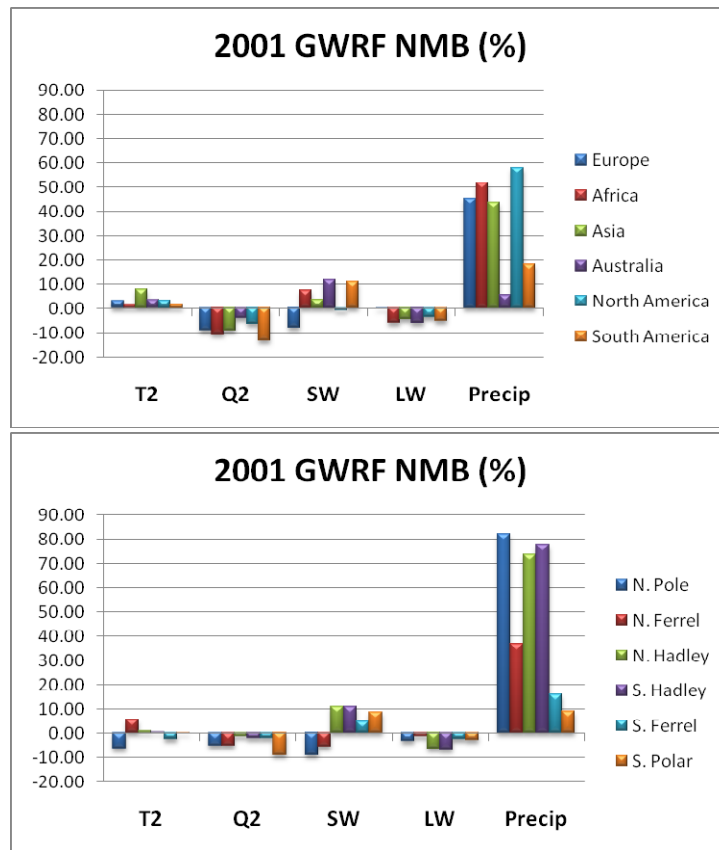
Globally, GWRP shows a slight decrease in Corr value (0.99) from the annual  $1^\circ \times 1^\circ$  case (1.0), but an improvement in NMB at  $4^\circ \times 5^\circ$ , with a value of less than 1% (0.07%). Over the continents, the seasonal variation of GWRP T2 performance is shown in Figure 4.39, in which Europe has a large warm bias during winter and Asia and Australia have a warm bias during summer. This seasonal performance will be further investigated in sections 4.2.2 and 4.2.3.

**Table 4.22 Performance Statistics of GWRP 2001 annual mean temperature at 2-meter as compared with NCEP/NCAR Reanalysis.**

Name	MeanObs (°C)	MeanMod (°C)	Number	Corr	MB (°C)	RMSE	NMB%	NME%
Europe	7.19	7.42	64	0.94	0.22	1.73	3.09	18.72
Africa	22.75	23.03	144	0.87	0.28	1.45	1.21	4.43
Asia	8.97	9.67	255	0.99	0.70	2.32	7.76	18.26
Australia	21.02	21.76	64	0.98	0.74	1.18	3.53	3.97
N.A.	10.90	11.26	132	0.99	0.37	1.29	3.40	8.49
S.A.	16.32	16.54	126	0.94	0.23	2.94	1.38	9.70
N. Pole	-10.93	-11.62	576	0.96	-0.68	2.15	-6.24	13.80
N. Ferrel	8.07	8.52	576	0.98	0.45	1.70	5.53	13.22
N. Hadley	25.07	25.27	576	0.94	0.20	1.02	0.81	2.43
S. Hadley	23.88	23.98	576	0.90	0.10	1.46	0.40	2.76
S. Ferrel	9.24	8.99	576	0.99	-0.24	0.84	-2.64	5.68
S. Polar	-24.34	-24.31	576	0.97	0.03	4.45	0.13	14.06
N.H.	7.75	7.74	1656	0.99	-0.01	1.70	-0.13	13.72
S.H.	3.07	3.07	1656	0.99	0.01	2.79	0.23	50.70
Global	4.96	4.96	3240	0.99	0.00	2.33	0.07	26.76

An overview of statistical performance for the major boundary layer variables is shown graphically in Figure 4.40. The figure shows a strong parallel with the  $1^\circ \times 1^\circ$  case with an overall correlation among associated variables, as well as the largest NMB values associated with daily precipitation rate. For the continental domains, an overestimation of downward shortwave flux (except for Europe) is correlated with the overestimation of temperature at 2 meters, while an underestimation of water vapor mixing ratio at 2 meters is correlated with an underestimation of downward longwave flux. For the circulation cell domains, the correlation

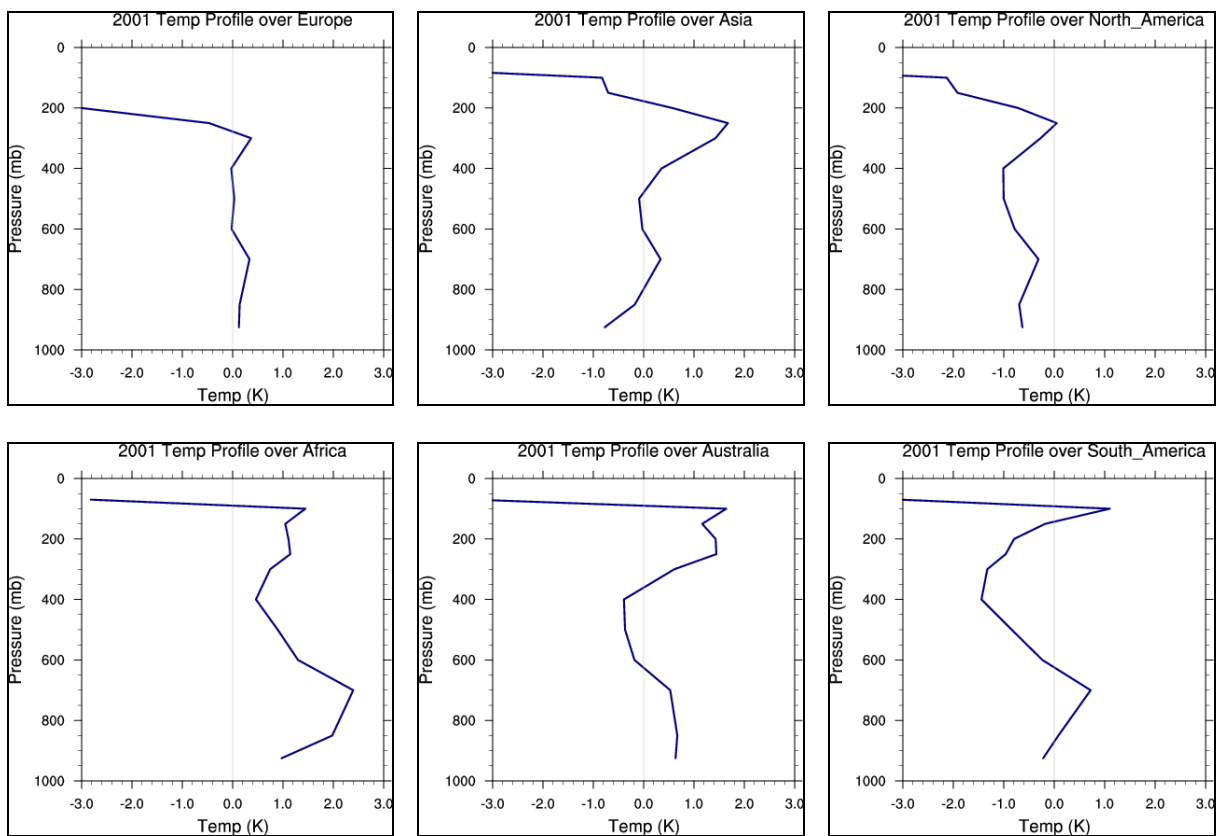
between an underestimation of water vapor mixing ratio at 2 meters and downward longwave flux is still present and the largest NMB values are still associated with daily precipitation rate. In the North Pole domain, the downward shortwave flux as well as the temperature at 2 meters is underestimated and this domain also shows the highest NMB values for precipitation rate. The vertical profile of temperature performance is also assessed. Figure 4.41 shows that GWRP captures vertical temperature distribution within  $\pm 2$  degrees up to approximately 300 hPa over the six continental domains.



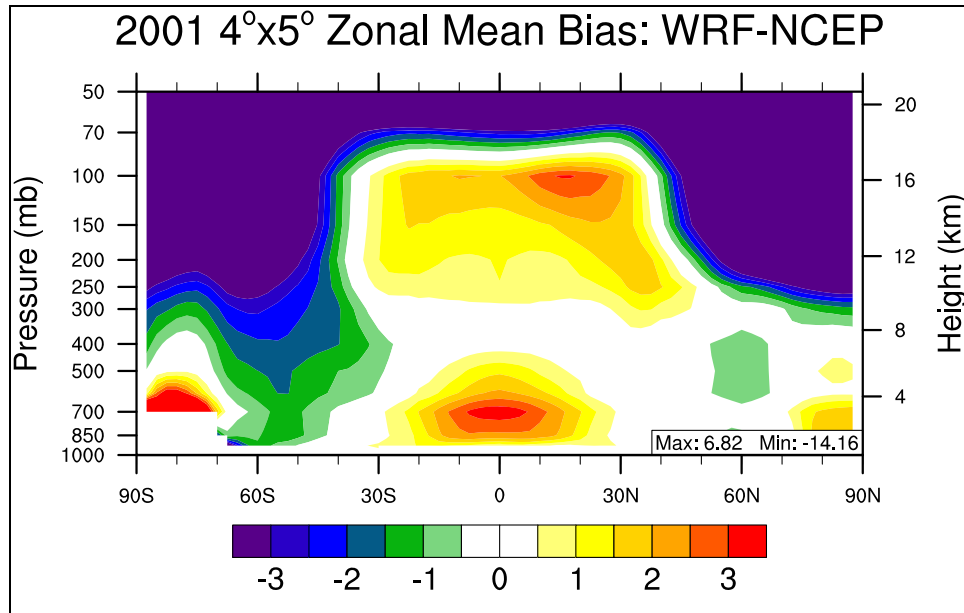
**Figure 4.40** 2001 annual mean normalized mean bias (%) of major meteorological variables for (a) the six continental domains and (b) the six circulation cell domains.

Figure 4.42 is the zonal mean bias of GWRP versus NCEP/NCAR Reanalysis data. This figure also shows that GWRP captures the vertical temperature distribution within  $\pm 2$  degrees up to

approximately 300 hPa. There exist a number of differences between Figure 4.42 and its corresponding Figure 4.4 for the  $1^\circ \times 1^\circ$  case. The two figures are similar because they both have large overestimations near the surface over Antarctica and large underestimation of temperatures above the tropopause. The two different resolutions create the vertical distribution of temperature over the Tropics differently, in which the coarse resolution case has larger overestimations near the surface of the equator as well as a strong overestimation aloft near 100 hPa. Also, the coarse resolution case does not underpredict temperatures in the Southern Hadley Cell between 400 hPa and 100 hPa, but the fine resolution case does.



**Figure 4.41 Vertical Profiles of Temperature Mean Bias over the six populated continents.**



**Figure 4.42 2001 Zonal Mean Bias of Temperature**

#### 4.2.1.2 2001 Water Vapor Mixing Ratio at 2-meter

The global distribution of mean bias for water vapor mixing ratio at 2-meter is displayed in Figure 4.43 which shows an overall underestimation over the Tropical land surfaces (30°N-30°S). Overall the majority of mean bias values are within the range of  $\pm 5 \text{ g kg}^{-1}$ , with a maximum mean bias of  $8.01 \text{ g kg}^{-1}$  and a minimum mean bias value of  $-7.43 \text{ g kg}^{-1}$ . The largest underestimations occur over India and sub-Saharan Africa. The overall underestimation of Q2 is also reflected in Table 4.23 in which all circulation cells, as well as continental domains, have a negative NMB value. The coarse resolution case displays a global NMB value of -2.67%, which is slightly worse than the annual global mean value for the fine resolution case. Overall correlation values are high, but worse than the fine resolution case, with the circulation cells all having Corr values above 0.91, and all continental domains having Corr values above 0.89. Globally, the Corr value is 0.99.

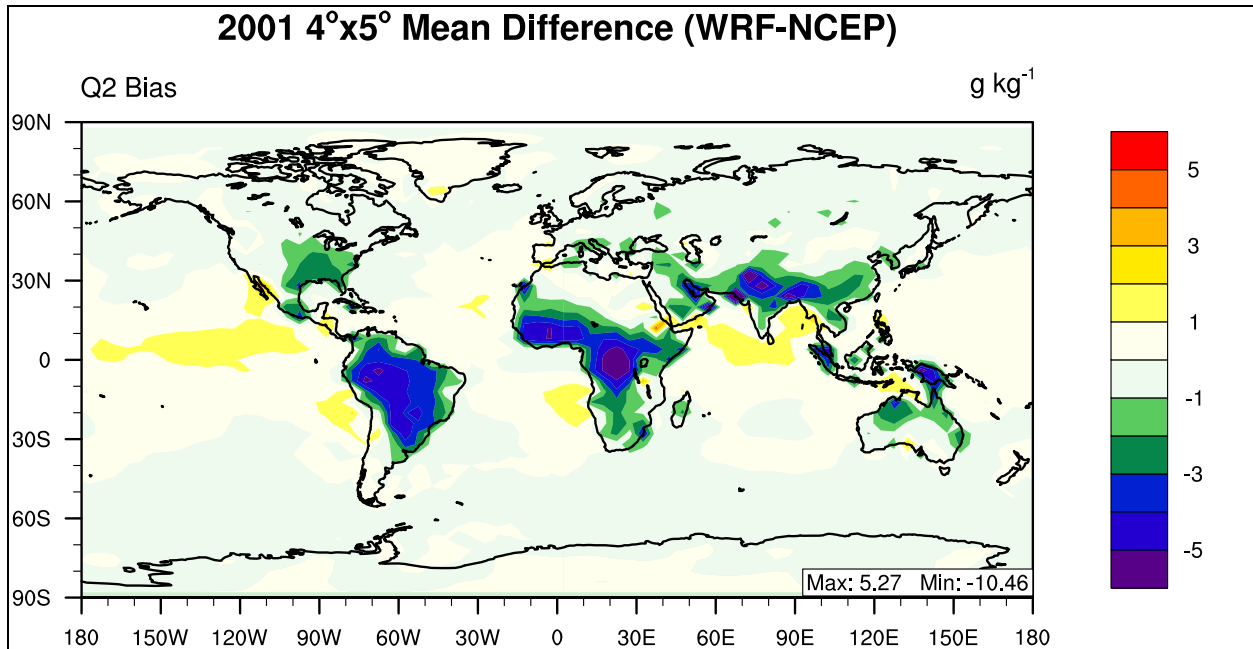


**Figure 4.43** 2001 mean bias of Water Vapor Mixing ratio at 2-meters.

**Table 4.23** Performance Statistics of GWRP 2001 annual mean temperature at 2-meter compared with NCEP/NCAR Reanalysis.

Name	MeanObs (g kg <sup>-1</sup> )	MeanMod (g kg <sup>-1</sup> )	Number	Corr	MB (g kg <sup>-1</sup> )	RMSE	NMB%	NME%
Europe	6.47	5.89	64	0.95	-0.58	0.77	-8.94	9.63
Africa	11.14	9.96	144	0.89	-1.17	2.30	-10.53	15.40
Asia	8.06	7.31	255	0.96	-0.75	1.74	-9.27	14.11
Australia	10.38	9.94	64	0.97	-0.44	1.35	-4.25	8.75
N.A.	8.73	8.16	132	0.97	-0.57	1.23	-6.50	9.55
S.A.	11.50	9.98	126	0.95	-1.52	2.38	-13.22	14.27
N. Pole	2.57	2.43	576	0.98	-0.14	0.30	-5.33	8.18
N. Ferrel	6.85	6.50	576	0.97	-0.36	0.81	-5.24	7.55
N. Hadley	15.59	15.37	576	0.94	-0.22	1.76	-1.43	7.56
S. Hadley	15.49	15.17	576	0.91	-0.32	1.58	-2.07	6.46
S. Ferrel	6.81	6.66	576	0.99	-0.15	0.38	-2.20	3.46
S. Polar	1.41	1.28	576	0.99	-0.13	0.25	-9.26	13.58
N.H.	8.51	8.27	1656	0.98	-0.24	1.15	-2.77	7.58
S.H.	8.09	7.89	1656	0.99	-0.20	0.97	-2.48	6.03
Global	8.09	7.87	3240	0.99	-0.22	1.04	-2.67	6.83

#### 4.2.1.3 2001 Downward Shortwave Flux

The pattern of downward shortwave flux mean bias is displayed graphically in Figure 4.44 in which the overall pattern is an overestimation in the Tropics (30°N-30°S), and a slight underestimation at higher latitudes, which is similar to the fine resolution case. In this coarse resolution case, all mean bias values fall within the range of  $\pm 100 \text{ W m}^{-2}$ , with a maximum mean bias of  $81.90 \text{ W m}^{-2}$  and a minimum mean bias value of  $-63.94 \text{ W m}^{-2}$ . The large underestimations associated with the west coast of South America that are present in the fine resolution case are not present in this coarse case. The overall pattern of GWRP SWDOWN performance is similar to the fine resolution case and shown in Table 4.24, in which all of the circulation cell domains display a positive NMB value except for the high Northern latitudes, with a global NMB value of 4.52%. Correlation values for sub-domains are not as high as Q2 or T2, with the Southern Hadley Cell and Southern Pole Cell having Corr value of 0.40 and 0.19, respectively. Continental domains mainly in the Northern Hemisphere (Europe, Asia, and N.A.) have higher Corr values than those in the Southern Hemisphere (Africa, Australia, and S.A.). Globally, the correlation value is the same as the fine resolution case (0.93).

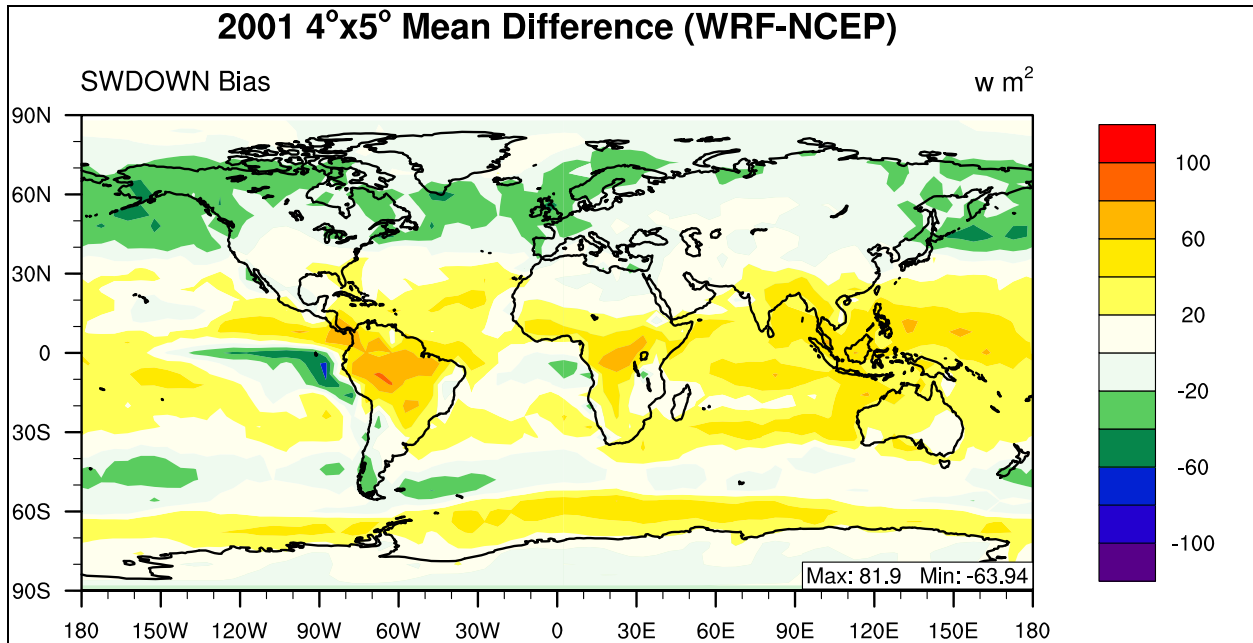


**Figure 4.44** 2001 annual mean bias of Downward Shortwave Flux at the surface.

**Table 4.24** Performance Statistics of GWRf 2001 annual mean Downward Shortwave Flux at the surface as compared with NCEP/NCAR Reanalysis.

Name	MeanObs (W m <sup>-2</sup> )	MeanMod (W m <sup>-2</sup> )	Number	Corr	MB (W m <sup>-2</sup> )	RMSE	NMB%	NME%
Europe	171.27	157.65	64	0.98	-13.62	17.17	-7.95	8.49
Africa	267.64	287.31	144	0.69	19.66	30.73	7.35	9.30
Asia	215.06	222.91	255	0.95	7.85	21.65	3.65	7.36
Australia	240.79	269.39	64	0.93	28.60	31.96	11.88	11.89
N.A.	211.89	209.90	132	0.95	-2.00	17.66	-0.94	7.19
S.A.	208.86	231.86	126	0.86	23.00	39.75	11.01	15.91
N. Pole	131.71	119.76	576	0.62	-11.95	16.39	-9.07	9.88
N. Ferrel	188.20	177.51	576	0.97	-10.69	19.65	-5.68	8.39
N. Hadley	244.22	271.17	576	0.70	26.95	34.13	11.03	12.10
S. Hadley	239.43	265.56	576	0.40	26.13	35.41	10.91	13.16
S. Ferrel	161.74	169.71	576	0.83	7.97	22.24	4.93	10.72
S. Polar	144.43	157.16	576	0.19	12.73	22.14	8.81	11.13
N.H.	189.90	192.25	1656	0.96	2.35	24.72	1.24	10.24
S.H.	184.33	199.47	1656	0.92	15.14	26.94	8.21	11.56
Global	185.88	194.29	3240	0.93	8.41	25.40	4.52	10.75

#### 4.2.1.4 2001 Downward Longwave Flux

The pattern of downward longwave flux mean bias is displayed graphically in Figure 4.45 in which the overall pattern is an underestimation with a global NMB value of -4.30% as shown in Table 4.25. All mean bias values fall within the range of  $\pm 100 \text{ W m}^{-2}$ , with a maximum mean bias of  $77.68 \text{ W m}^{-2}$  and a minimum mean bias value of  $-66.10 \text{ W m}^{-2}$ . The overall pattern of GWRf GLW performance is the same as the fine resolution case, which is reflected in Table 4.25 in which all of the domains display a negative NMB value. This overall underestimation of GLW corresponds with the overall underestimation of Q2 as mentioned in section 4.2.1.2. Correlation values are higher than the associated SWDOWN values, with the continental domains and circulation cell domains all displaying a Corr value of greater than 0.88.

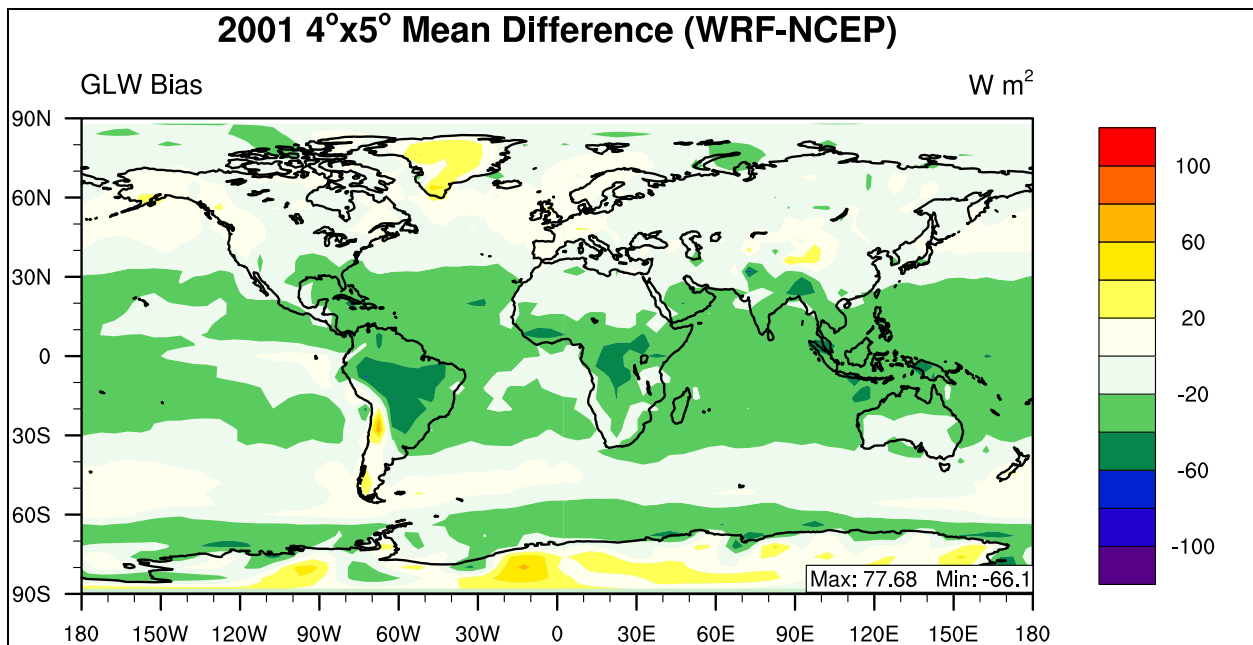


**Figure 4.45 2001 annual mean bias of Downward Longwave Flux at the surface.**

**Table 4.25 Performance Statistics of GWRP annual mean for 2001 of Downward Longwave Flux compared with NCEP/NCAR Reanalysis.**

Name	MeanObs (g kg <sup>-1</sup> )	MeanMod (g kg <sup>-1</sup> )	Number	Corr	MB (g kg <sup>-1</sup> )	RMSE	NMB%	NME%
Europe	287.49	286.67	64	0.88	-0.83	9.60	-0.29	2.72
Africa	359.78	338.35	144	0.88	-21.43	25.41	-5.96	6.12
Asia	297.91	284.13	255	0.98	-13.78	19.92	-4.63	5.45
Australia	355.05	333.43	64	0.97	-21.63	23.95	-6.09	6.09
N.A.	310.28	299.15	132	0.99	-11.13	16.25	-3.59	4.08
S.A.	345.78	327.36	126	0.93	-18.42	31.62	-5.33	7.80
N. Pole	218.73	211.19	576	0.93	-7.54	14.43	-3.45	5.60
N. Ferrel	295.93	291.45	576	0.96	-4.48	12.10	-1.51	3.15
N. Hadley	392.24	366.46	576	0.94	-25.78	27.76	-6.57	6.62
S. Hadley	389.94	364.28	576	0.88	-25.66	28.59	-6.58	6.82
S. Ferrel	308.72	300.80	576	0.93	-7.92	14.31	-2.56	3.70
S. Polar	160.13	155.38	576	0.96	-4.76	25.40	-2.97	13.75
N.H.	304.13	291.07	1656	0.99	-13.05	19.64	-4.29	5.31
S.H.	287.35	274.64	1656	0.99	-12.71	23.70	-4.42	7.00
Global	293.27	280.66	3240	0.99	-12.61	21.59	-4.30	6.12

#### 4.2.1.5 2001 Zonal Wind Speed

The pattern of zonal wind speed at 10-meters (U10) mean bias is displayed graphically in Figure 4.46 in which the overall pattern is similar to the fine resolution case with a slight underestimation of the zonal component. Overall wind speed is the worst variable predicted by the model with a global NMB value of -826.26%. This corresponds to a global mean bias of 0.15 m s<sup>-1</sup> and the very high NMB value is caused by a low observed wind speed (-0.02 m s<sup>-1</sup>). This mean bias is lower than the fine resolution case annual mean bias. The majority of mean bias values fall within the range of  $\pm 5$  m s<sup>-1</sup>, with a maximum mean bias of 5.27 m s<sup>-1</sup> and a minimum mean bias value of -8.14 W m<sup>-2</sup>. The overall pattern of GWRP U10 performance is reflected in Table 4.26 in which the majority of domains display a negative NMB value. U10 displays the largest absolute NMB values of any GWRP variable examined thus far, while Corr

values are still relatively high with a global Corr value of 0.93, lower than the fine resolution case.

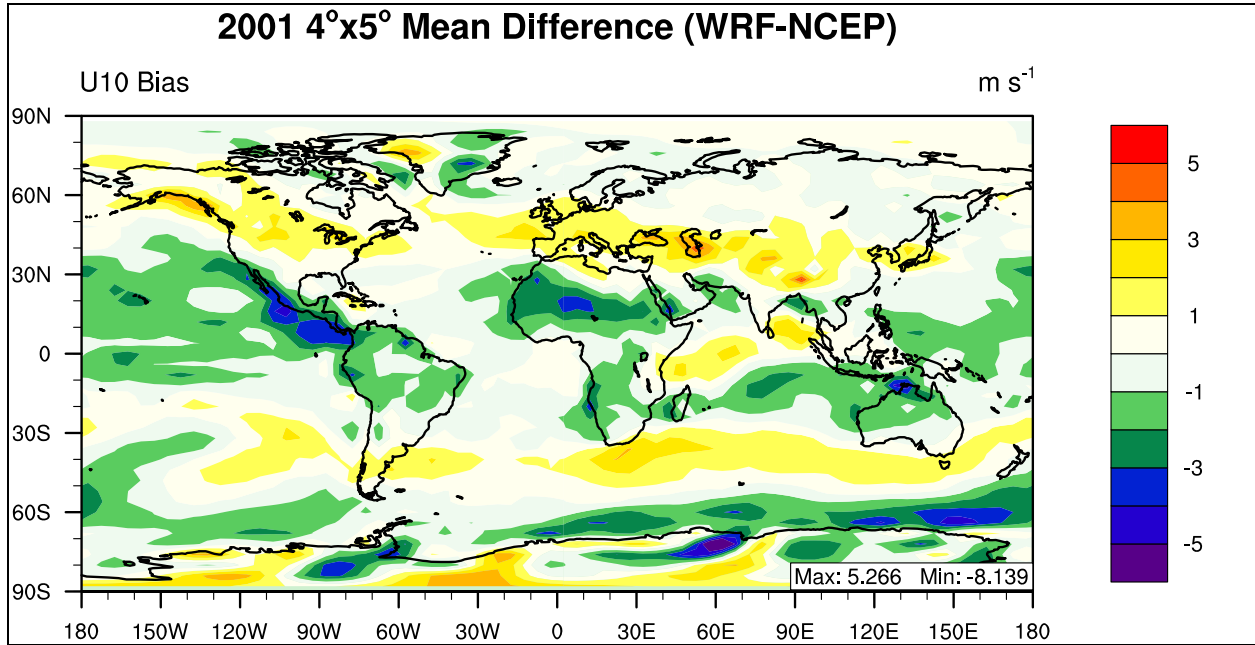


**Figure 4.46** 2001 annual mean bias of zonal wind at 10-meter.

**Table 4.26 Statistical Analysis of GWRf annual mean zonal wind at 10-meters for 2001 compared with NCEP/NCAR Reanalysis.**

Name	MeanObs (m s <sup>-1</sup> )	MeanMod (m s <sup>-1</sup> )	Number	Corr	MB (m s <sup>-1</sup> )	RMSE	NMB%	NME%
Europe	0.67	1.45	64	0.34	0.78	1.27	115.37	151.17
Africa	-0.65	-1.53	144	0.69	-0.88	1.52	-134.60	188.91
Asia	0.31	0.63	255	0.68	0.32	1.22	104.46	282.51
Australia	-0.46	-1.16	64	0.94	-0.70	1.51	-152.65	266.85
N.A.	0.14	0.50	132	0.84	0.36	1.31	251.41	727.88
S.A.	0.76	0.42	126	0.95	-0.34	1.19	-44.44	131.02
N. Pole	0.10	0.18	576	0.67	0.08	0.81	77.34	609.76
N. Ferrel	1.10	1.65	576	0.68	0.55	1.24	49.59	87.59
N. Hadley	-2.07	-2.95	576	0.92	-0.88	1.49	-42.57	58.94
S. Hadley	-2.89	-3.47	576	0.90	-0.58	1.17	-20.10	32.99
S. Ferrel	4.40	4.50	576	0.90	0.10	1.28	2.33	24.04
S. Polar	-0.24	-0.58	576	0.87	-0.34	1.98	-143.99	688.81
N.H.	-0.31	-0.41	1656	0.90	-0.10	1.22	-33.09	303.14
S.H.	0.21	0.00	1656	0.94	-0.21	1.50	-101.32	563.84
Global	-0.02	-0.17	3240	0.93	-0.15	1.37	-826.26	5851.79

#### 4.2.1.6 4° x 5° 2001 Meridional Wind Speed

The pattern of meridional wind speed at 10-meters (V10) mean bias is displayed graphically in Figure 4.47 and the spatial pattern appears to be similar to the zonal component with an overall slight underestimation. Meridional wind speed displays a global NMB value of -13.28%, which is significantly lower than the zonal component global domain average. This corresponds to a mean bias of -0.02 m s<sup>-1</sup> and the high NMB value is a function of the low observed wind speed (0.15 m s<sup>-1</sup>). The majority of mean bias values fall within the range of  $\pm 5$  m s<sup>-1</sup>, with a maximum mean bias of 4.34 m s<sup>-1</sup> and a minimum mean bias value of -5.14 m s<sup>-1</sup>. The overall pattern of GWRf V10 performance is reflected in Table 4.27 in which the majority of domains display a negative NMB value. V10 also displays very large absolute NMB values and low Corr values for individual domains, but still displays a global Corr value of 0.85, lower

than the fine resolution case. The large underestimation over the Southern Arabian Peninsula present in the fine resolution case is much more prominent in the coarse resolution case.

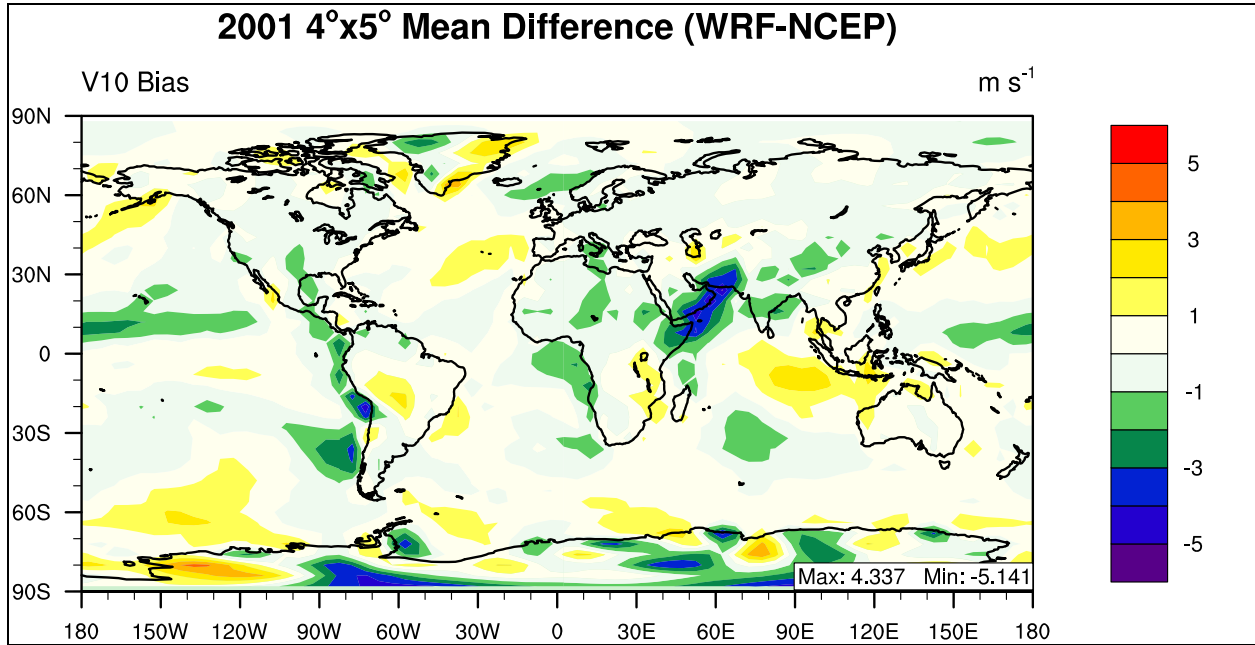


**Figure 4.47** 2001 annual mean bias of meridional wind at 10-meter.

**Table 4.27 Performance Statistics of GWRP 2001 annual mean meridional wind at 10-meters as compared with NCEP/NCAR Reanalysis.**

Name	MeanObs (m s <sup>-1</sup> )	MeanMod (m s <sup>-1</sup> )	Number	Corr	MB (m s <sup>-1</sup> )	RMSE	NMB%	NME%
Europe	0.21	-0.13	64	0.56	-0.34	0.67	-161.37	242.08
Africa	0.69	0.33	144	0.91	-0.36	1.01	-51.91	118.71
Asia	0.11	-0.33	255	0.41	-0.44	1.18	-401.53	716.34
Australia	0.95	1.42	64	0.91	0.47	0.78	49.74	59.13
N.A.	-0.10	-0.29	132	0.83	-0.19	0.63	-183.21	473.70
S.A.	-0.78	-0.59	126	0.69	0.18	0.97	23.52	88.28
N. Pole	-0.06	-0.02	576	0.76	0.04	0.74	62.71	832.31
N. Ferrel	0.18	0.25	576	0.78	0.07	0.77	36.19	329.08
N. Hadley	-0.53	-0.93	576	0.82	-0.40	1.07	-74.67	147.14
S. Hadley	1.37	1.58	576	0.86	0.21	0.95	15.29	52.64
S. Ferrel	-1.03	-0.87	576	0.78	0.16	0.78	15.66	58.75
S. Polar	0.84	0.76	576	0.82	-0.08	1.66	-10.06	155.02
N.H.	-0.14	-0.24	1656	0.80	-0.10	0.88	-73.44	456.31
S.H.	0.47	0.54	1656	0.86	0.07	1.20	14.79	187.92
Global	0.15	0.13	3240	0.85	-0.02	1.06	-13.28	507.30

#### 4.2.1.7 4° x 5° 2001 Daily Precipitation

The daily precipitation rate at the surface in GWRP is compared with the Global Precipitation Climatology Project (GPCP) for the annual mean of 2001. In Figure 4.48, the interval spacing is set to  $\pm 2$  mm day<sup>-1</sup> to show the spatial variability of GWRP precipitation. As shown in Figure 4.48, there are areas where GWRP overestimates precipitation rate in close proximity to areas where GWRP underestimates precipitation rate. Overall this coarse resolution case has larger overestimates of daily precipitation rate than the fine resolution case when Figures 4.10 and 4.48 are compared. The maximum mean bias is 19.86 mm day<sup>-1</sup> and a minimum mean bias value of -4.01 mm day<sup>-1</sup>, indicating a tendency of the model to overestimate rainfall rate. Both of these extreme mean bias values are worse than the fine resolution case. Overall spatial trend shows that performance is the best at the mid-latitudes (Northern and

Southern Ferrel Cells) and the worst in the Tropics (Northern and Southern Hadley Cells) as illustrated in Figure 4.48 and shown in Table 4.28, in which the Northern and Southern Ferrel Cells have NMB values of less than 37%, while the Hadley cells have NMB values over 73%. Polar cells both display very low observed daily precipitation rates; with the North Pole having a large overestimation of daily precipitation arte, and the South Pole has the best performance of any domain. Globally, the coarse GWRf simulation shows lower correlation (0.82) value and worse bias performance with an NMB value of almost 50% (49.37%).

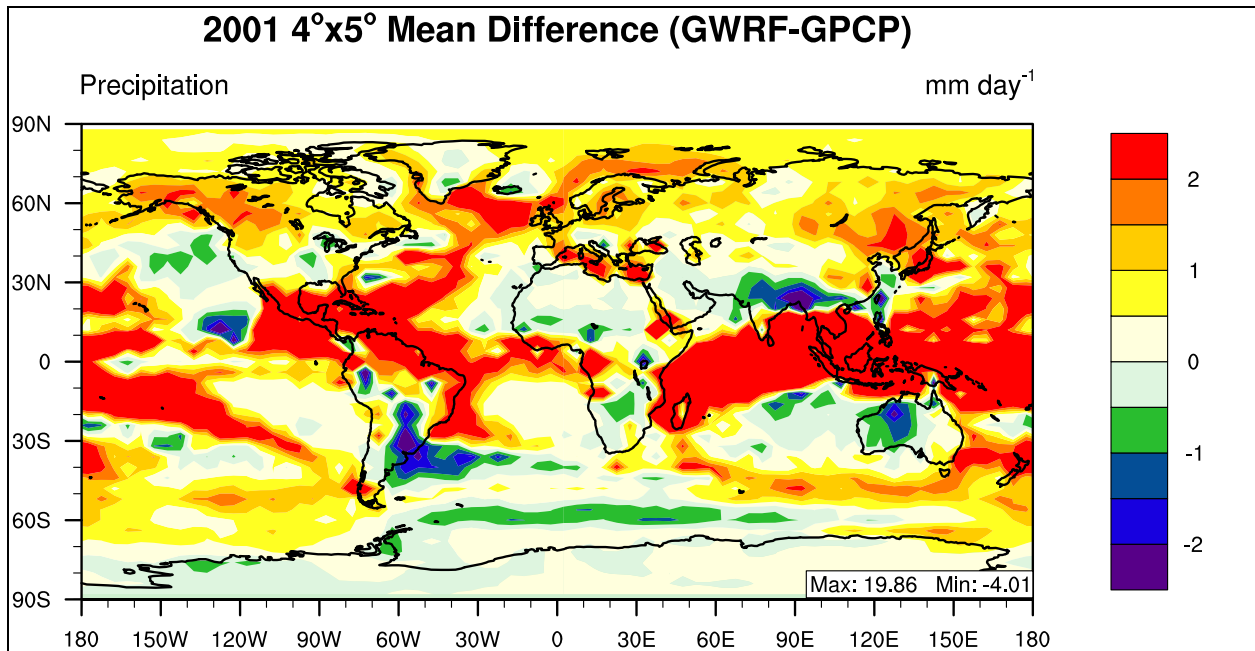


**Figure 4.48** 2001 annual mean bias of daily precipitation rate.

**Table 4.28 Performance Statistics of GWRf 2001 annual precipitation rate as compared with GPCP.**

Name	MeanObs (mm d <sup>-1</sup> )	MeanMod (mm d <sup>-1</sup> )	Number	Corr	MB (mm d <sup>-1</sup> )	RMSE	NMB%	NME%
Europe	2.32	3.36	64	0.27	1.05	1.39	45.21	48.11
Africa	1.55	2.35	144	0.61	0.80	2.40	51.82	71.26
Asia	1.94	2.79	255	0.75	0.85	2.17	43.71	64.09
Australia	1.84	1.94	64	0.75	0.10	1.15	5.37	43.72
N.A.	2.08	3.29	132	0.53	1.21	2.06	58.07	64.48
S.A.	3.74	4.42	126	0.63	0.68	2.16	18.13	41.38
N. Pole	0.97	1.77	576	0.86	0.80	0.98	82.33	84.48
N. Ferrel	2.40	3.27	576	0.84	0.88	1.31	36.56	42.19
N. Hadley	3.10	5.39	576	0.79	2.29	3.96	73.66	83.29
S. Hadley	2.80	4.96	576	0.82	2.16	3.92	77.36	87.73
S. Ferrel	2.89	3.35	576	0.48	0.46	1.05	15.86	28.23
S. Polar	1.06	1.15	576	0.92	0.10	0.42	9.04	28.23
N.H.	2.16	3.48	1656	0.83	1.32	2.51	61.36	68.69
S.H.	2.22	3.17	1656	0.82	0.95	2.40	42.87	54.88
Global	2.15	3.22	3240	0.82	1.06	2.29	49.37	59.32

#### 4.2.2 2001 4° × 5° Summer (JJA) simulation

##### 4.2.2.1 Summer Temperature at 2-meters

The temperature at 2-meters above the surface in GWRf is compared with NCEP/NCAR Reanalysis data for the summer of 2001 (June, July, and August 2001) at a coarse resolution of 4° latitude × 5° longitude. As shown in Figure 4.49, the mean bias performance is slightly worse for the summer case as opposed to the annual mean, but is similar to the summer fine resolution base case. In Figure 4.49, the majority of Mean Bias values fall within the ±10 °C range, however there are larger exceptions with a maximum mean bias value of 17.42 °C and a minimum mean bias value of -14.13 °C. Model performance is particularly worse than the annual case over Antarctica, with mainly overestimations occurring over the land surface and underestimations occurring off shore and over the Southern Ocean. Globally, GWRf shows

good statistical performance with a Corr value of 0.99 and an NMB value of 2.73%. This model performance is similar to the fine resolution summer case, except that both Europe and North America have negative NMB values, while T2 is overpredicted for the rest of the continental domains. Overall the Southern hemisphere has much worse statistical performance than the Northern Hemisphere, with NMB values of -19.10% and -1.06%, respectively.

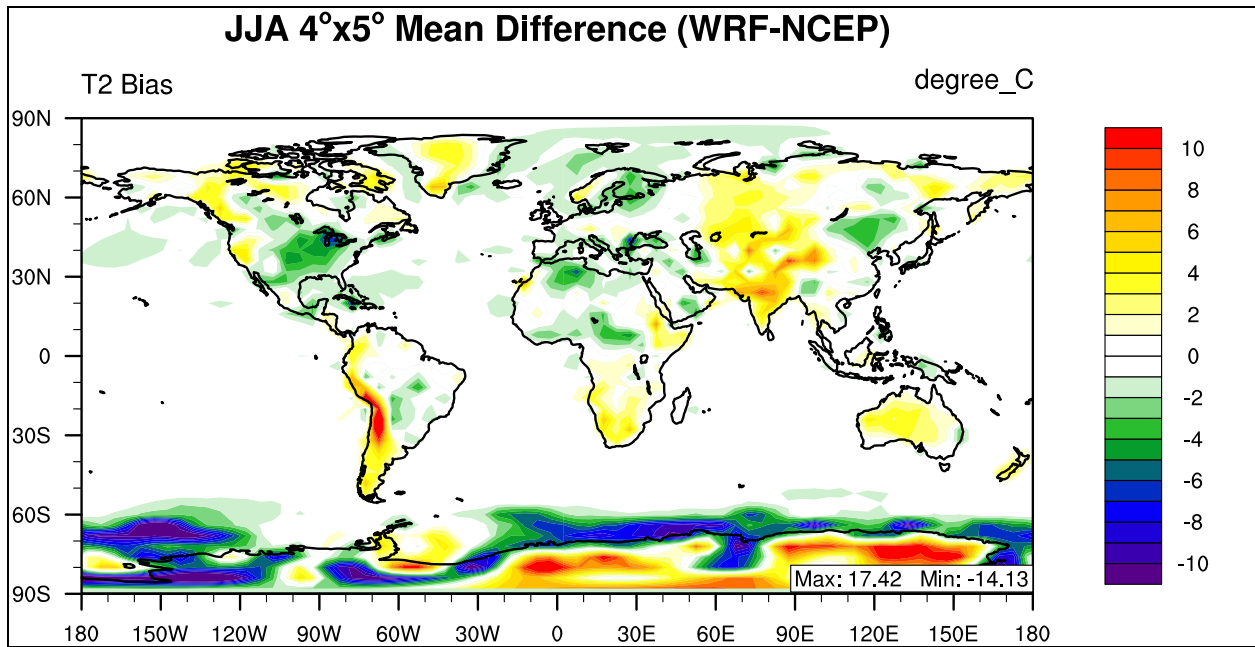


**Figure 4.49** 2001 annual mean bias of temperature at 2-meter.

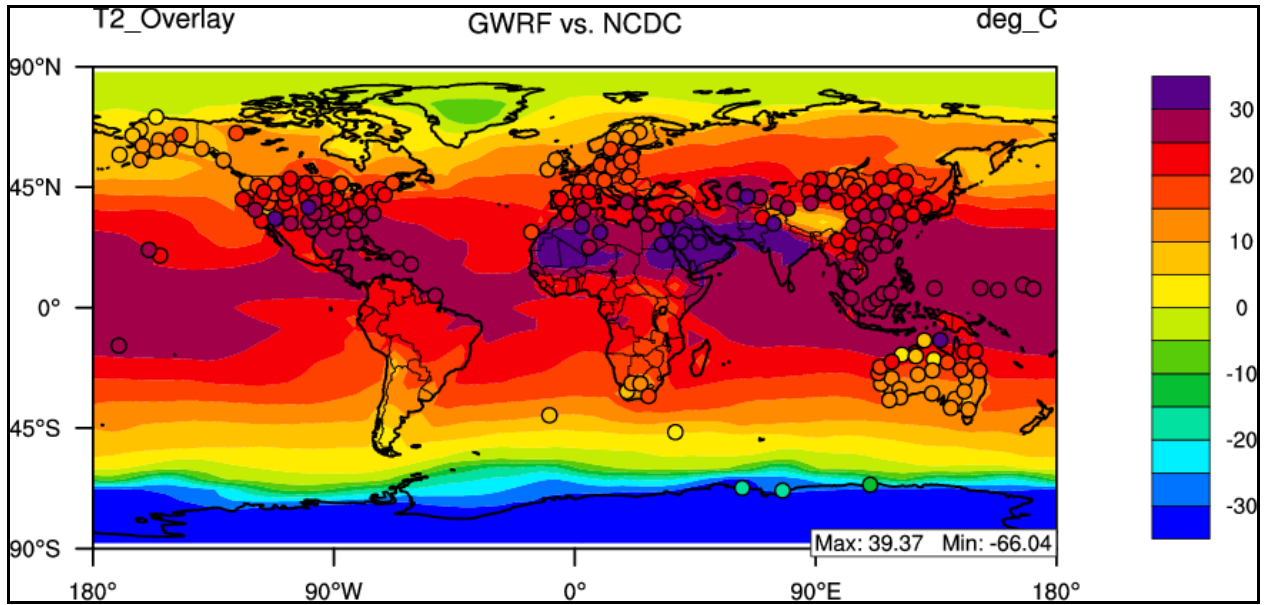
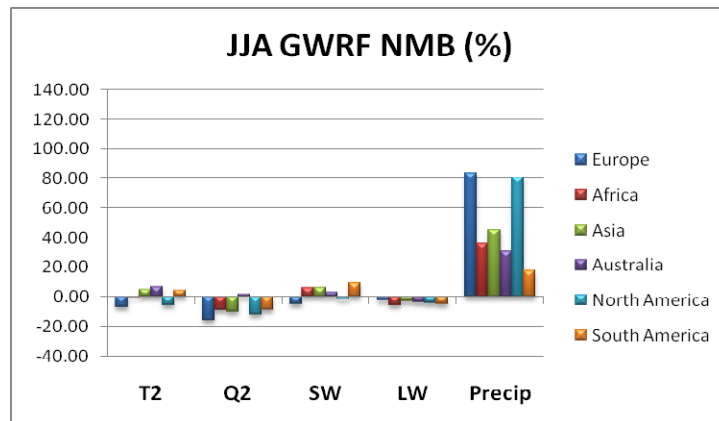


**Figure 4.50** 2001 annual mean bias of temperature at 2-meter as compared with NCDC.

**Table 4.29** Performance Statistics of GWRP 2001 summer temperature at 2-meter compared with NCEP/NCAR Reanalysis and NCDC observations.

Name	MeanObs (°C)	MeanMod (°C)	Number	Corr	MB (°C)	RMSE	NMB%	NME%
Europe	16.81	15.58	64	0.91	-1.23	2.29	-7.29	11.09
Africa	23.76	23.81	144	0.93	0.05	2.05	0.21	6.54
Asia	20.72	21.77	255	0.93	1.04	2.86	5.04	10.20
Australia	16.72	17.84	64	0.97	1.12	1.75	6.70	7.32
N.A.	20.19	19.00	132	0.96	-1.19	2.33	-5.88	9.06
S.A.	14.15	14.78	126	0.95	0.63	3.22	4.49	11.57
N. Pole	3.62	3.52	576	0.96	-0.10	1.63	-2.85	33.43
N. Ferrel	17.22	16.95	576	0.94	-0.27	2.13	-1.55	8.93
N. Hadley	26.56	26.45	576	0.89	-0.10	1.57	-0.39	3.52
S. Hadley	22.46	22.92	576	0.93	0.46	1.69	2.07	3.75
S. Ferrel	7.35	7.19	576	0.99	-0.16	1.19	-2.23	9.30
S. Polar	-33.24	-34.33	576	0.96	-1.10	5.87	-3.30	14.25
N.H.	16.00	15.83	1656	0.99	-0.17	1.79	-1.06	7.61
S.H.	-1.07	-1.28	1656	0.99	-0.20	3.64	-19.10	196.55
Global	7.07	6.87	3240	0.99	-0.19	2.90	-2.73	23.84
NCDC	20.77	19.12	199	0.84	-1.66	5.12	-7.99	17.02

Figure 4.50 overlays GWRf model output and NCDC observations, when this plot is combined with the statistical data in the last row of Table 4.29, the coarse resolution case has larger MB and NMB values, and lower Corr values, indicating the advantage of a fine resolution when evaluating model performance against a point observation. An overview of summer statistical performance for the major boundary layer variables is shown graphically in Figure 4.51. The figure shows an overall correlation among associated variables, as well as the largest NMB values associated with daily precipitation rate, similar to the annual mean results. For the continental domains, an overestimation of downward shortwave flux (except for Europe and North America) is correlated with the overestimation of temperature at 2 meters, while an underestimation of water vapor mixing ratio at 2 meters (except for Australia) is correlated with an underestimation of downward longwave flux. For the circulation cell domains, the correlation between an underestimation of water vapor mixing ratio at 2 meters and downward longwave flux is still present and the largest NMB values are still associated with daily precipitation rate. In the North Pole domain, the downward shortwave flux as well as the temperature at 2 meters is underestimated and this domain also shows the highest NMB values for precipitation rate, all of which are present in the fine resolution case. The vertical profile of temperature performance is also evaluated. Figure 4.52 shows that GWRf captures vertical temperature distribution within  $\pm 2$  degrees up to approximately 300 hPa over the six continental domains.



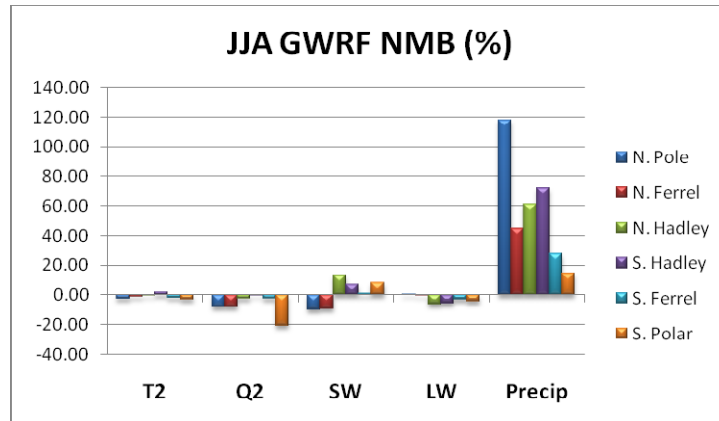


**Figure 4.51** 2001 summer mean normalized mean bias (%) of major meteorological variables for (a) the six continental domains and (b) the six circulation cell domains.

Figure 4.53 shows the zonal mean bias of GWRP versus NCEP/NCAR Reanalysis data. GWRP captures the vertical temperature distribution within  $\pm 2$  degrees up to approximately 300 hPa. The simulations at fine and coarse resolution in summer give similar extreme mean biases (see Figures 4.15 and 4.53); however there are a large number of differences in the vertical structure of temperature. The two different resolutions create the vertical distribution of temperature over the Tropics differently, in which the coarse resolution case has larger overestimations near the surface of the equator as well as stronger overestimations aloft between 300 and 100 hPa. Also, the coarse resolution case does not underpredict temperatures over the Tropics between 400 hPa and 100 hPa, but the fine resolution case does. In the summer case, the model strongly underestimates temperatures throughout the Southern Ferrel Cell. This image also shows the large underestimation of temperatures above the tropopause, however in this case the tropopause over Antarctica is anomalously high.

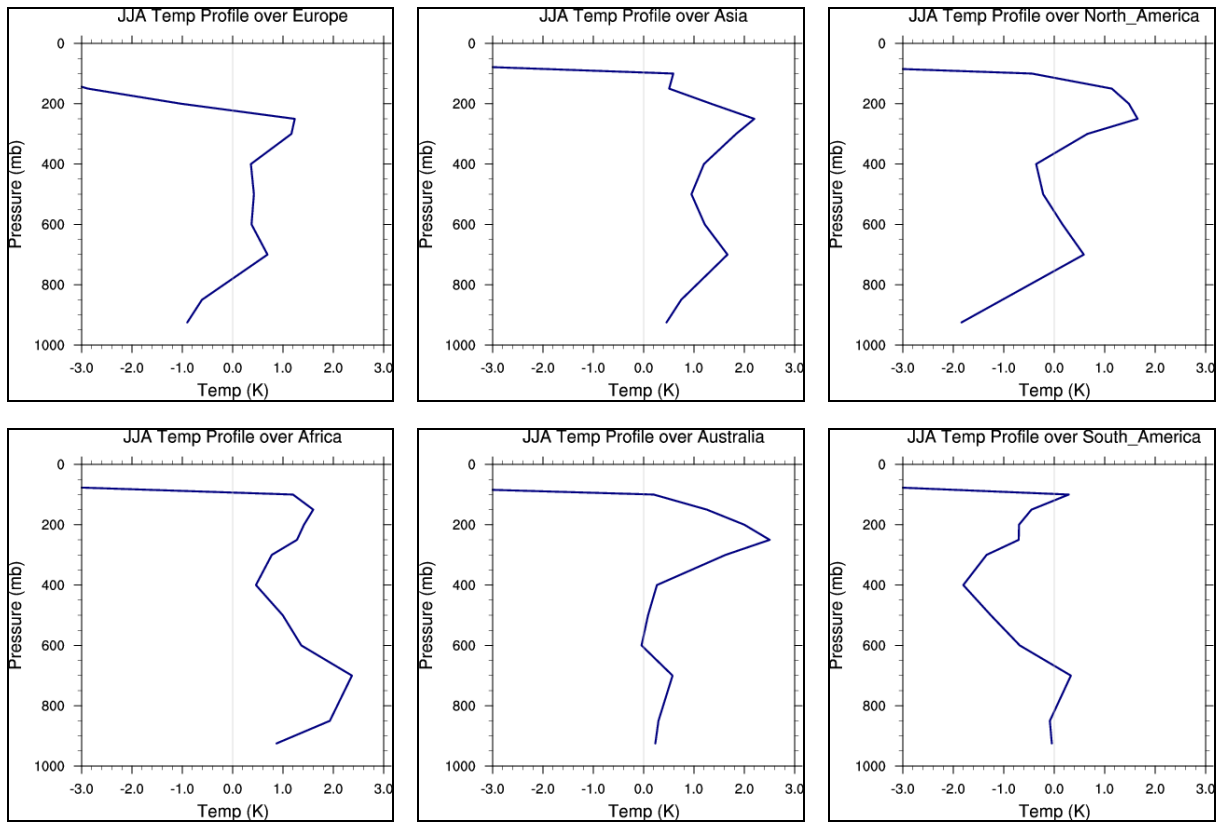


**Figure 4.52 Summer Vertical Profiles of Temperature Mean Bias over the six populated continents.**

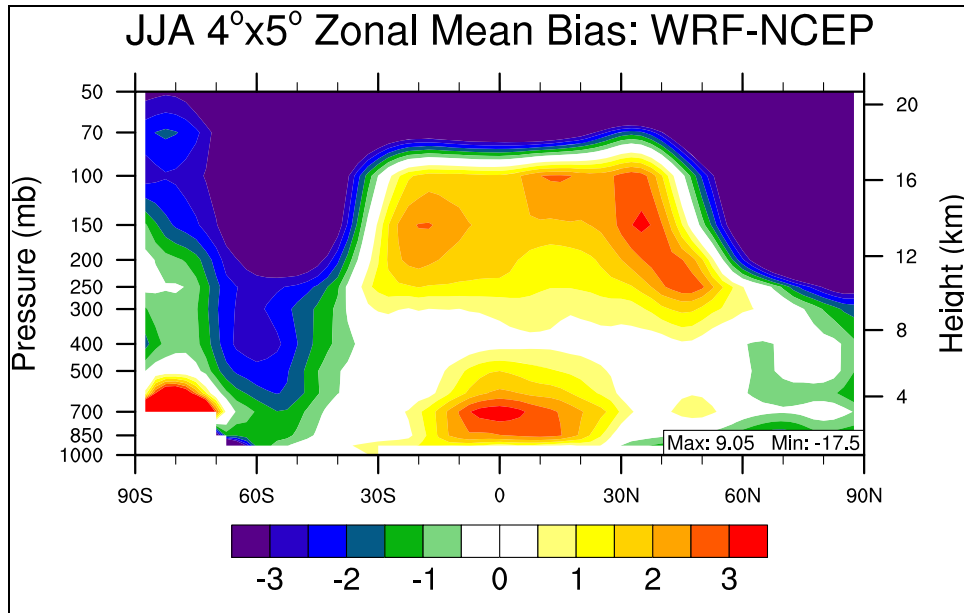


**Figure 4.53 Summer zonal mean bias of Temperature**

#### 4.2.2.2 Summer Water Vapor Mixing Ratio at 2-meters

The global distribution of summer mean bias for water vapor mixing ratio at 2-meter is displayed in Figure 4.54. When compared with the annual spatial mean bias plot, the underestimations over the Tropics are larger than the annual case, and the underestimation is also present in the Northern Hemisphere mid-latitudes. Overall the majority of mean bias values are within the range of  $\pm 5 \text{ g kg}^{-1}$ , however the biases are larger in this seasonal case as compared with the annual. The maximum mean bias is  $8.31 \text{ g kg}^{-1}$  and the minimum mean bias is  $-11.49 \text{ g kg}^{-1}$ . When compared with the summer fine resolution case, the coarse resolution summer case has larger areas of underestimation over land surfaces. The overall underestimation of Q2 is also reflected in Table 4.30 in which the majority of all domains have a negative NMB value with the exception of the Southern Hadley Cell and Australia. The global NMB value is worse than the annual case ( $-2.67\%$ ), with a summer value of  $-3.67\%$ . Overall correlation values are similar to annual mean performance, with a global Corr value of 0.98.

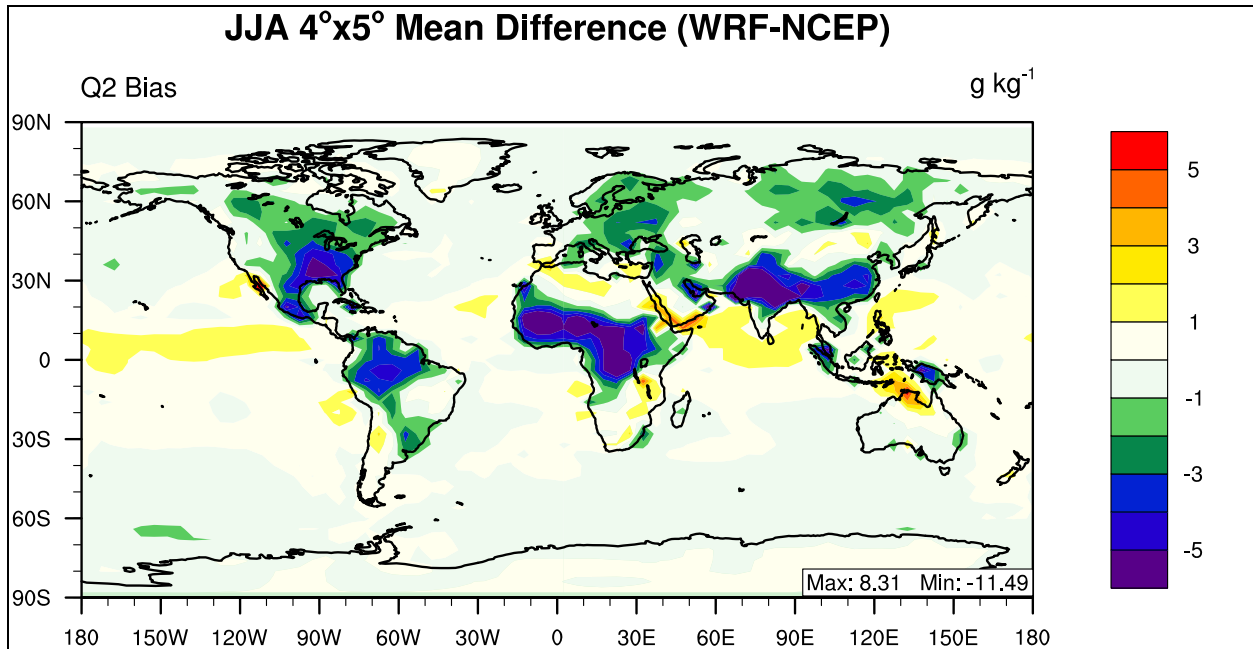


**Figure 4.54** 2001 summer mean bias of Water Vapor Mixing Ratio at 2-meter.

**Table 4.30** Performance Statistics of GWRP 2001 summer Water Vapor Mixing Ratio at 2-meter compared with NCEP/NCAR Reanalysis.

Name	MeanObs (g kg <sup>-1</sup> )	MeanMod (g kg <sup>-1</sup> )	Number	Corr	MB (g kg <sup>-1</sup> )	RMSE	NMB%	NME%
Europe	10.00	8.44	64	0.90	-1.56	1.80	-15.57	15.69
Africa	10.86	9.90	144	0.82	-0.97	2.68	-8.89	17.66
Asia	11.85	10.65	255	0.92	-1.20	2.58	-10.13	15.49
Australia	8.41	8.55	64	0.96	0.14	1.26	1.66	9.08
N.A.	12.32	10.84	132	0.93	-1.48	2.32	-12.01	13.95
S.A.	9.80	8.95	126	0.97	-0.84	1.70	-8.60	11.18
N. Pole	5.10	4.67	576	0.96	-0.43	0.77	-8.41	10.22
N. Ferrel	10.03	9.19	576	0.92	-0.83	1.57	-8.32	10.45
N. Hadley	16.82	16.43	576	0.88	-0.39	2.24	-2.32	8.51
S. Hadley	14.13	14.13	576	0.95	0.00	1.29	0.01	5.58
S. Ferrel	5.97	5.81	576	0.99	-0.16	0.40	-2.71	4.53
S. Polar	0.87	0.69	576	0.97	-0.18	0.32	-20.82	23.75
N.H.	10.77	10.24	1656	0.97	-0.53	1.65	-4.96	9.30
S.H.	7.16	7.06	1656	0.99	-0.11	0.82	-1.48	5.97
Global	8.78	8.45	3240	0.98	-0.32	1.29	-3.67	8.03

#### 4.2.2.3 4° x 5° Summer Downward Shortwave Flux

The pattern of summer downward shortwave flux mean bias is displayed graphically in Figure 4.55, and reflects the annual pattern of an overestimation in the Tropics (30°N-30°S), however in the summer case the underestimation at high latitudes in the Northern hemisphere increases dramatically. The overestimation in the Tropics also increases, most noticeably over Southern Asia. The areas of underestimation off the West coast of Africa and South America in the Southern Hadley Cell, which are present in the fine resolution summer case, are not as prominent in this coarse resolution case. The majority of mean bias values still fall within the range of  $\pm 100 \text{ W m}^{-2}$ , but the maximum mean bias has increased to  $123.8 \text{ W m}^{-2}$  and the minimum mean bias value has decreased to  $-141.4 \text{ W m}^{-2}$ . This pattern of GWRP SWDOWN performance is reflected in Table 4.31 in which all of the circulation cell domains display a positive NMB value except for the high Northern latitudes (Northern Ferrel and North Polar Cell) which display negative NMB values, with a global NMB value of -0.20%. Regions with a poor correlation in the annual mean are improved, with the Corr value increasing from 0.40 to 0.70 in the Southern Hadley Cell and the Corr value increases from 0.19 to 0.99 in the Southern polar Cell. Continental domains mainly in the Southern Hemisphere (Africa, Australia, S.A.) have higher Corr values than those in the Northern Hemisphere (Europe, Asia, and N.A.). Globally, the Corr value remains comparable at 0.94. Performance statistics for the coarse resolution case compared with BSRN data shows that SWDOWN is not as sensitive to horizontal grid resolution as temperature when the fine and coarse resolution cases produce similar statistics.

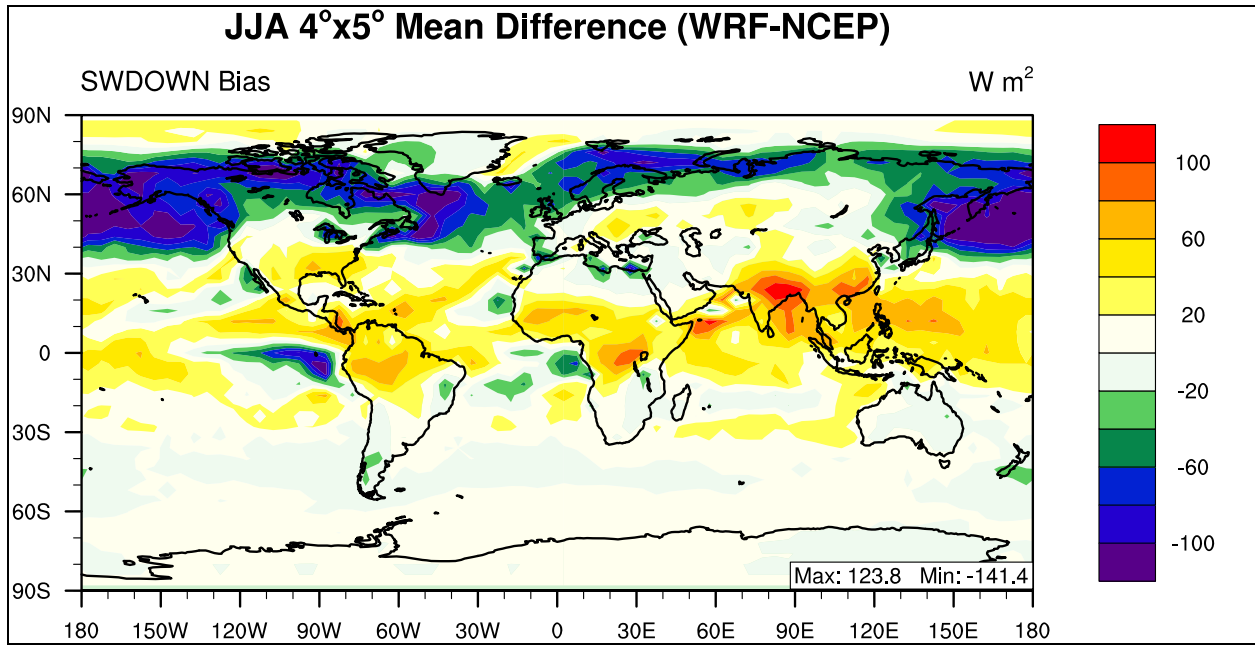


**Figure 4.55 2001 summer mean bias of Downward Shortwave Flux at 2-meter.**

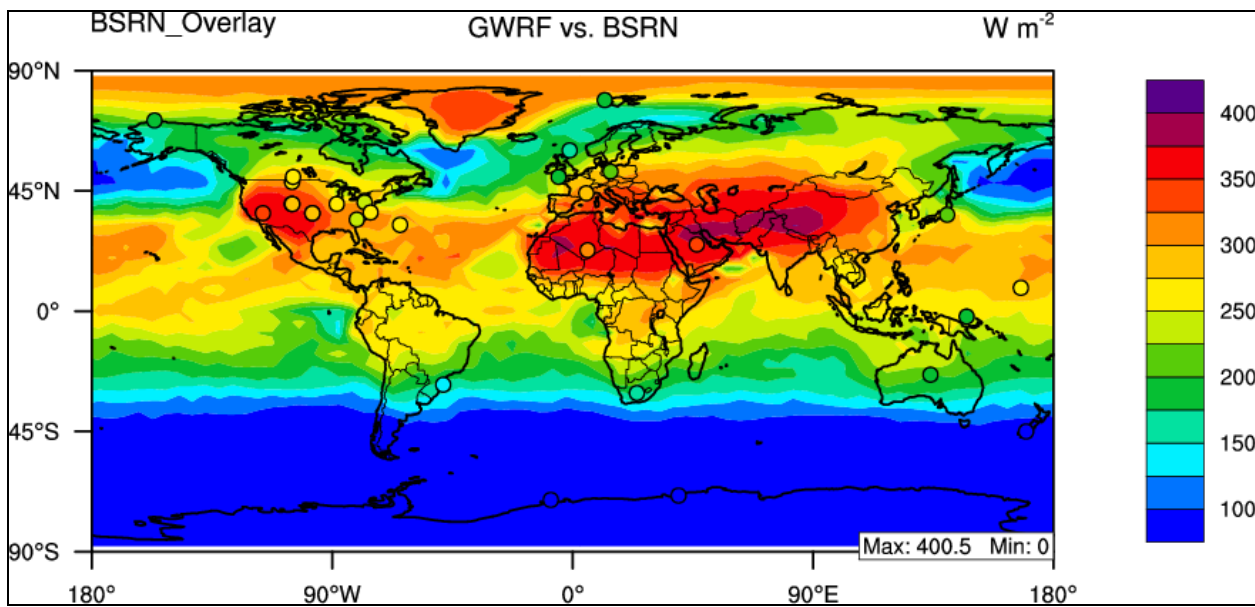


**Figure 4.56 2001 summer mean bias of Downward Shortwave Flux at 2-meter as compared to BSRN.**

**Table 4.31 Performance Statistics of GWRP 2001 summer Downward Shortwave Flux as compared with NCEP/NCAR Reanalysis and BSRN.**

Name	MeanObs (W m <sup>-2</sup> )	MeanMod (W m <sup>-2</sup> )	Number	Corr	MB (W m <sup>-2</sup> )	RMSE	NMB%	NME%
Europe	279.70	266.04	64	0.83	-13.66	38.60	-4.88	11.17
Africa	266.21	282.58	144	0.87	16.37	37.37	6.15	11.04
Asia	282.27	300.58	255	0.69	18.31	44.11	6.49	12.03
Australia	181.53	186.81	64	0.95	5.28	16.68	2.91	7.01
N.A.	285.82	281.07	132	0.62	-4.75	42.06	-1.66	12.07
S.A.	155.90	170.83	126	0.97	14.93	29.89	9.58	14.00
N. Pole	276.87	249.02	576	0.76	-27.85	49.80	-10.06	14.12
N. Ferrel	275.10	248.12	576	0.87	-26.98	55.38	-9.81	15.43
N. Hadley	255.88	289.39	576	0.69	33.51	45.93	13.10	15.36
S. Hadley	204.13	218.17	576	0.70	14.04	30.98	6.88	11.89
S. Ferrel	75.99	76.77	576	0.97	0.78	8.56	1.02	8.64
S. Polar	10.50	11.32	432	0.99	0.83	1.85	7.87	10.44
N.H.	270.04	264.97	1656	0.63	-5.07	49.66	-1.88	14.65
S.H.	108.39	114.14	1512	0.98	5.75	19.85	5.30	10.97
Global	191.94	191.55	3096	0.94	-0.39	38.20	-0.20	13.53
BSRN	218.83	264.83	29	0.97	46.00	54.10	21.03	21.02

#### 4.2.2.4 Summer Downward Longwave Flux

The pattern of summer downward longwave flux mean bias is displayed graphically in Figure 4.57 in which the overall pattern is an underestimation with a global NMB value of -3.54%, which is an improvement from the annual mean performance. All mean bias values fall within the range of  $\pm 100$  W m<sup>-2</sup>, with a larger maximum mean bias (8.51 W m<sup>-2</sup>) and a smaller minimum mean bias (-68.62 W m<sup>-2</sup>). The overall pattern of GWRP GLW performance is consistent with the annual mean, as shown in Table 4.32 in which all of the domains display a negative NMB value, with the exception of a slight overestimation over the North Pole. Correlation values are lower than the annual mean, with Europe having the lowest Corr value of the continental domains (0.62) and the Northern Hadley Cell having the worst performance of the circulation cell domains (0.79). Globally, the Corr value is 0.98. Similar to SWDOWN, GLW displays little sensitivity to horizontal grid resolution when compared to the BSRN

network, in which the fine and coarse resolution simulations produce very similar performance statistics.

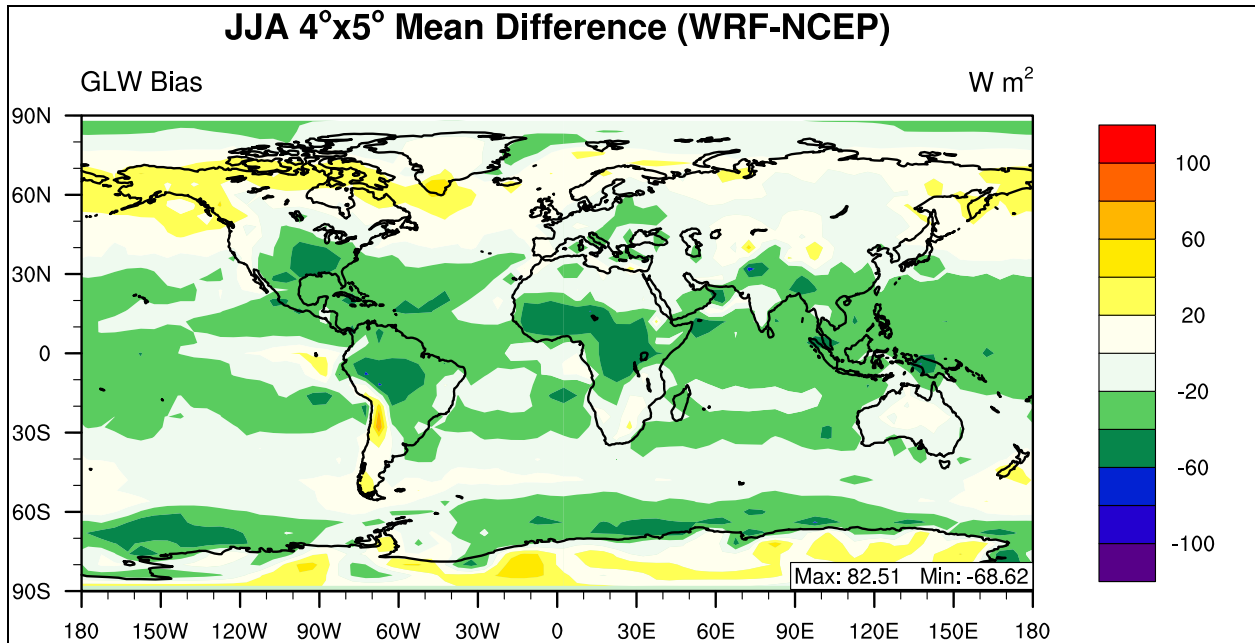


**Figure 4.57** 2001 summer mean bias of Downward Longwave Flux at 2-meter.

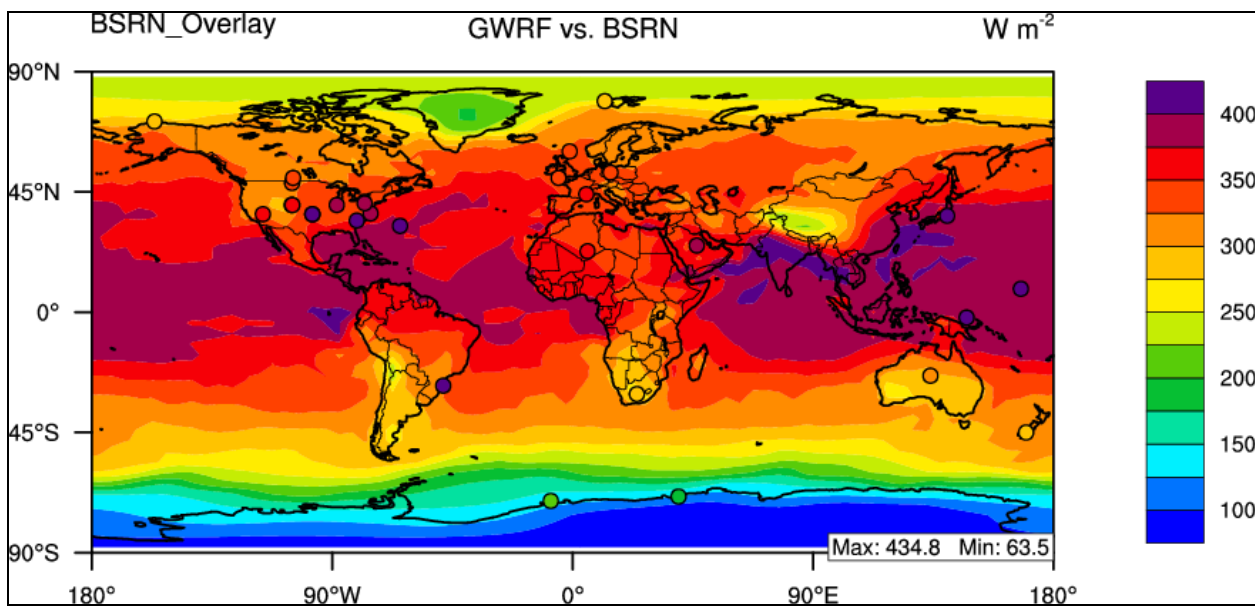


**Figure 4.58** 2001 summer mean bias of Downward Longwave Flux at 2-meters for as compared to BSRN.

**Table 4.32 Performance Statistics of GWRf 2001 summer Downward Longwave Flux compared with NCEP/NCAR Reanalysis and BSRN.**

Name	MeanObs (W m <sup>-2</sup> )	MeanMod (W m <sup>-2</sup> )	Number	Corr	MB (W m <sup>-2</sup> )	RMSE	NMB%	NME%
Europe	334.47	326.09	64	0.62	-8.38	16.70	-2.51	4.32
Africa	363.02	341.12	144	0.76	-21.90	29.80	-6.03	6.78
Asia	355.73	344.20	255	0.94	-11.53	21.31	-3.24	4.57
Australia	324.54	312.40	64	0.95	-12.15	17.48	-3.74	4.25
N.A.	358.03	343.02	132	0.89	-15.01	25.91	-4.19	6.00
S.A.	330.12	314.05	126	0.93	-16.07	30.16	-4.87	7.71
N. Pole	274.73	275.79	576	0.89	1.05	18.22	0.38	5.77
N. Ferrel	341.95	340.90	576	0.80	-1.05	18.47	-0.31	4.35
N. Hadley	405.74	379.01	576	0.79	-26.73	29.88	-6.59	6.76
S. Hadley	377.41	355.30	576	0.91	-22.10	27.01	-5.86	6.40
S. Ferrel	296.11	286.12	576	0.93	-9.99	16.09	-3.37	4.50
S. Polar	139.38	133.44	576	0.95	-5.94	27.87	-4.26	17.43
N.H.	341.98	332.16	1656	0.94	-9.81	22.97	-2.87	5.71
S.H.	271.88	259.54	1656	0.99	-12.34	24.24	-4.54	7.55
Global	304.77	293.98	3240	0.98	-10.79	23.48	-3.54	6.52
BSRN	350.01	316.06	29	0.89	-33.95	44.34	-9.70	10.50

#### 4.2.2.5 Summer Zonal Wind Speed

The pattern of summer zonal wind speed at 10-meters (U10) mean bias is displayed graphically in Figure 4.58 in which the overall pattern appears to be a slight underestimation of the zonal component, however over the Southern ocean there are large underestimations not present in the annual mean analysis. Overall wind speed is not well predicted by GWRf with a global NMB value of -377.97%, which is smaller than the bias present in the annual mean. This large, negative NMB value corresponds to a global mean bias of  $-0.14 \text{ m s}^{-1}$  which is a function of the low observed wind speed ( $0.04 \text{ m s}^{-1}$ ). The majority of mean bias values fall within the range of  $\pm 5 \text{ m s}^{-1}$ , however the performance is worse than the annual mean with a maximum mean bias of  $5.25 \text{ m s}^{-1}$  and a minimum mean bias value of  $-10.79 \text{ W m}^{-2}$ . The overall pattern of GWRf U10 performance is reflected in Table 4.33 in which the majority of circulation cell domains display a negative NMB value (with the exception of the North Pole and Southern

Ferrel cells). U10 displays very large absolute NMB values but still has a global Corr value of 0.91, slightly lower than the annual mean.

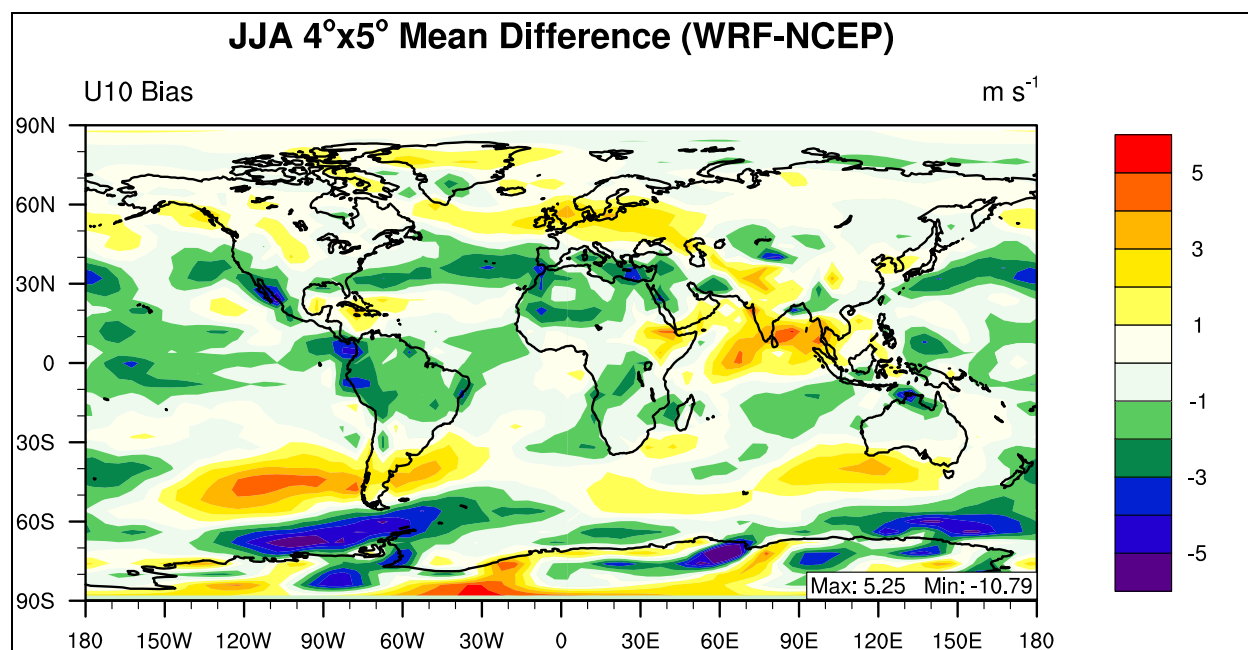


**Figure 4.58** 2001 summer mean bias of zonal wind at 10-meter.

**Table 4.33 Statistical Analysis of GWRf summer mean zonal wind at 10-meters for 2001 compared with NCEP/NCAR Reanalysis.**

Name	MeanObs (m s <sup>-1</sup> )	MeanMod (m s <sup>-1</sup> )	Number	Corr	MB (m s <sup>-1</sup> )	RMSE	NMB%	NME%
Europe	0.53	1.54	64	0.57	1.01	1.71	189.04	261.71
Africa	-0.37	-1.04	144	0.78	-0.67	1.49	-182.11	320.57
Asia	0.73	1.11	255	0.87	0.37	1.45	51.08	142.73
Australia	-0.76	-0.68	64	0.97	0.09	1.61	11.16	153.05
N.A.	-0.04	-0.24	132	0.75	-0.20	1.39	-515.32	2626.20
S.A.	0.97	0.42	126	0.84	-0.55	2.08	-56.79	183.19
N. Pole	0.35	0.49	576	0.63	0.14	0.81	40.02	182.10
N. Ferrel	0.63	0.53	576	0.71	-0.10	1.47	-15.91	183.27
N. Hadley	-1.27	-1.61	576	0.93	-0.34	1.63	-27.09	101.07
S. Hadley	-3.30	-3.87	576	0.92	-0.57	1.23	-17.25	28.65
S. Ferrel	4.70	4.98	576	0.76	0.29	1.91	6.11	32.71
S. Polar	-0.46	-0.84	576	0.82	-0.38	2.52	-82.81	438.88
N.H.	-0.12	-0.25	1656	0.90	-0.13	1.36	-116.97	900.04
S.H.	0.12	-0.04	1656	0.92	-0.16	1.94	-136.22	1285.88
Global	0.04	-0.10	3240	0.91	-0.14	1.68	-377.97	3460.50

#### 4.2.2.6 4° x 5° 2001 Meridional Wind Speed

The pattern of meridional wind speed at 10-meters (V10) mean bias is displayed graphically in Figure 4.59 and the spatial pattern appears to be similar to the zonal component with an overall slight underestimation. Meridional wind speed displays a global NMB value of -7.94%, which is significantly better than the summer zonal component global domain average, but is worse than the fine resolution case. This corresponds to a mean bias of -0.04 m s<sup>-1</sup>. The majority of mean bias values fall within the range of  $\pm 5$  m s<sup>-1</sup>, with a maximum mean bias of 5.82 m s<sup>-1</sup> and a minimum mean bias value of -6.84 m s<sup>-1</sup>, both of which increase in magnitude when compared with the annual mean. The overall pattern of GWRf V10 performance is reflected in Table 4.36 in which the majority of circulation cell domains display a negative NMB value (with the exceptions of the Southern Hadley and Ferrel Cells). V10 also displays very large absolute NMB values but displays a global Corr value of 0.84.

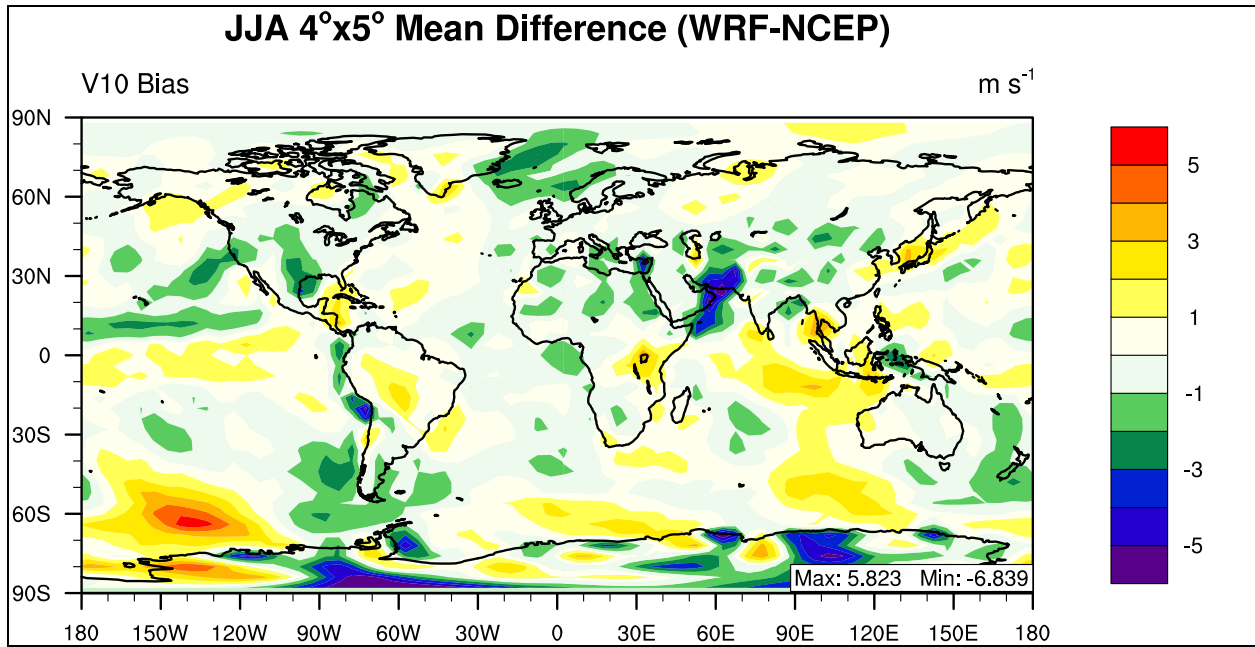


**Figure 4.59** 2001 summer mean bias of meridional wind at 10-meter.

**Table 4.34 Performance Statistics of GWRf 2001 summer mean meridional wind at 10-meter as with NCEP/NCAR Reanalysis.**

Name	MeanObs (m s <sup>-1</sup> )	MeanMod (m s <sup>-1</sup> )	Number	Corr	MB (m s <sup>-1</sup> )	RMSE	NMB%	NME%
<b>Europe</b>	-0.17	-0.68	64	0.74	-0.51	0.85	-299.52	382.81
<b>Africa</b>	0.89	0.71	144	0.93	-0.18	1.10	-19.97	93.76
<b>Asia</b>	0.51	0.13	255	0.77	-0.38	1.46	-74.17	203.59
<b>Australia</b>	0.77	1.05	64	0.89	0.28	0.91	36.02	86.92
<b>N.A.</b>	0.48	0.21	132	0.70	-0.27	1.02	-55.83	162.67
<b>S.A.</b>	-0.44	-0.43	126	0.54	0.01	1.22	1.44	217.55
<b>N. Pole</b>	0.07	0.05	576	0.58	-0.02	0.80	-23.35	914.61
<b>N. Ferrel</b>	0.18	0.03	576	0.86	-0.15	1.00	-82.56	415.31
<b>N. Hadley</b>	0.50	0.38	576	0.89	-0.12	1.26	-23.56	187.30
<b>S. Hadley</b>	1.99	2.28	576	0.86	0.29	1.12	14.68	43.72
<b>S. Ferrel</b>	-1.06	-0.89	576	0.61	0.16	1.24	15.24	90.61
<b>S. Polar</b>	1.18	0.98	576	0.78	-0.21	2.31	-17.38	153.66
<b>N.H.</b>	0.25	0.15	1656	0.86	-0.10	1.04	-41.49	304.35
<b>S.H.</b>	0.78	0.83	1656	0.83	0.05	1.64	6.15	154.35
<b>Global</b>	0.49	0.45	3240	0.84	-0.04	1.38	-7.94	202.45

#### 4.2.2.7 4° x 5° summer Daily Precipitation

The daily precipitation at the surface in GWRf is compared with the Global Precipitation Climatology Project (GPCP) for the summer of 2001 (June, July, and August 2001). Overall, the GWRf performance during summer appears to be largely overestimating daily precipitation rate and performing worse than the annual mean case as shown in Figure 4.60. The maximum mean bias is higher (28.35 mm day<sup>-1</sup>) and the minimum mean bias value is lower (-9.12 mm day<sup>-1</sup>), indicating a tendency of the model to overestimate rainfall rate. Overall spatial trend shows that performance is better in the Southern Hemisphere than the Northern hemisphere as shown in Table 4.35. Globally, GWRf shows Corr values smaller than the annual mean (0.74), and worse bias performance with an NMB value of greater than 50% (52.66%). As with the annual case, the low resolution simulation produces larger error values for precipitation rate than the high

resolution case. This is also true for the comparison with NCDC data for monthly mean accumulated precipitation, in which the low resolution case produces higher MB and NMB values and lower Corr values.

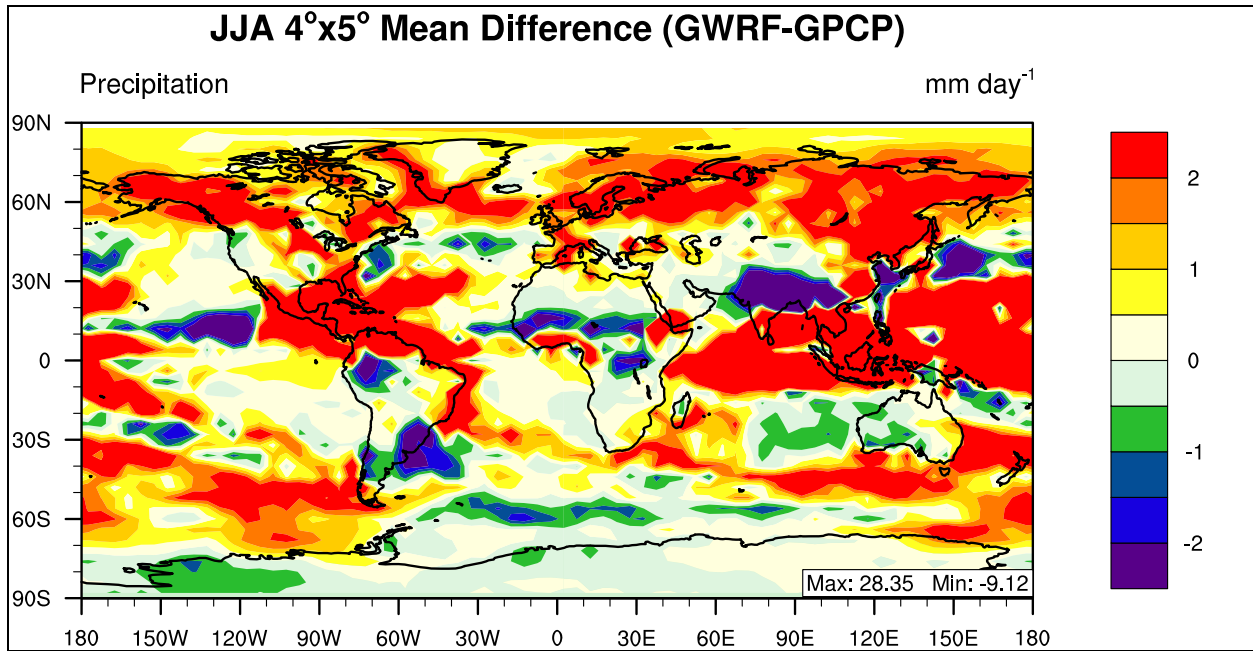


**Figure 4.60** 2001 summer mean bias of daily precipitation rate.

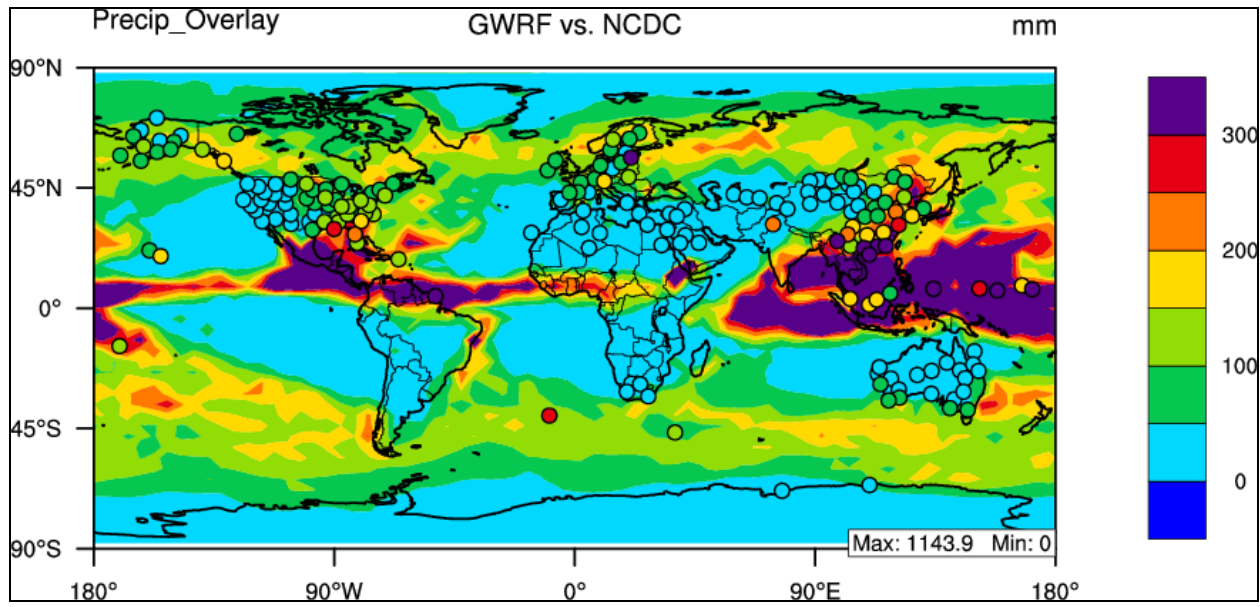


**Figure 4.61** 2001 summer mean bias of monthly accumulated precipitation as compared to NCDC.

**Table 4.35** Performance Statistics of GWRf summer precipitation for 2001 compared with GPCP (mm day<sup>-1</sup>) and NCDC (mm month<sup>-1</sup>).

Name	MeanObs	MeanMod	Number	Corr	MB	RMSE	NMB%	NME%
Europe	2.24	4.12	64	0.48	1.88	2.38	83.90	85.79
Africa	1.26	1.71	144	0.59	0.45	3.05	35.79	85.64
Asia	3.28	4.76	255	0.69	1.49	3.97	45.28	78.75
Australia	1.07	1.39	64	0.73	0.33	1.17	30.61	74.39
N.A.	2.50	4.52	132	0.50	2.02	3.49	80.78	94.00
S.A.	2.99	3.51	126	0.67	0.53	2.75	17.74	55.68
N. Pole	1.25	2.72	576	0.76	1.47	1.81	117.86	118.26
N. Ferrel	2.30	3.32	576	0.60	1.02	1.95	44.44	63.53
N. Hadley	3.95	6.35	576	0.68	2.40	4.96	60.75	84.40
S. Hadley	1.87	3.22	576	0.77	1.35	3.29	71.83	94.92
S. Ferrel	3.06	3.90	576	0.31	0.84	1.66	27.54	42.17
S. Polar	1.12	1.27	576	0.84	0.16	0.72	14.18	41.97
N.H.	2.51	4.11	1656	0.73	1.60	3.27	63.99	83.10
S.H.	1.97	2.78	1656	0.75	0.81	2.20	40.84	60.52
Global	2.22	3.39	3240	0.74	1.17	2.72	52.66	72.09
NCDC	93.20	125.88	172	0.64	32.68	101.87	35.07	70.98

### 4.2.3 4° × 5° Winter Simulation

#### 4.2.3.1 Winter Temperature at 2-meters

The temperature at 2-meter above the surface in GWRP is compared with NCEP/NCAR Reanalysis for the winter of 2001 (DJF). As shown in Figure 4.43, the mean bias performance is slightly worse for the winter case as opposed to the annual mean. In Figure 4.43, the majority of Mean Bias values fall within the  $\pm 10$  °C range, however there are exceptions with a maximum mean bias value of 15.22 °C and a minimum mean bias value of -16.75 °C. This coarse resolution horizontal grid spacing produces larger errors than the fine resolution winter case. Model performance is exceptionally complex over the Polar Regions, with overestimations and underestimations in close proximity to each other over Antarctica and an overall underestimation over the Arctic. Globally, GWRP shows good Corr values (0.99), but poor bias performance with an NMB value of -8.87%.

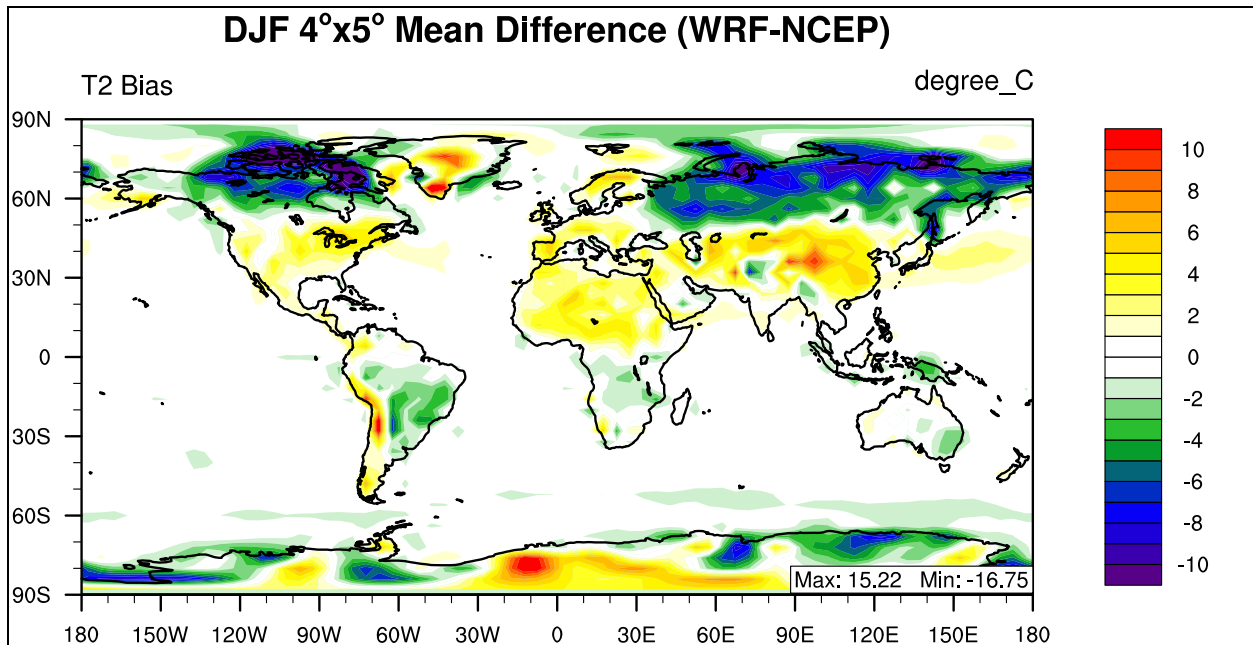
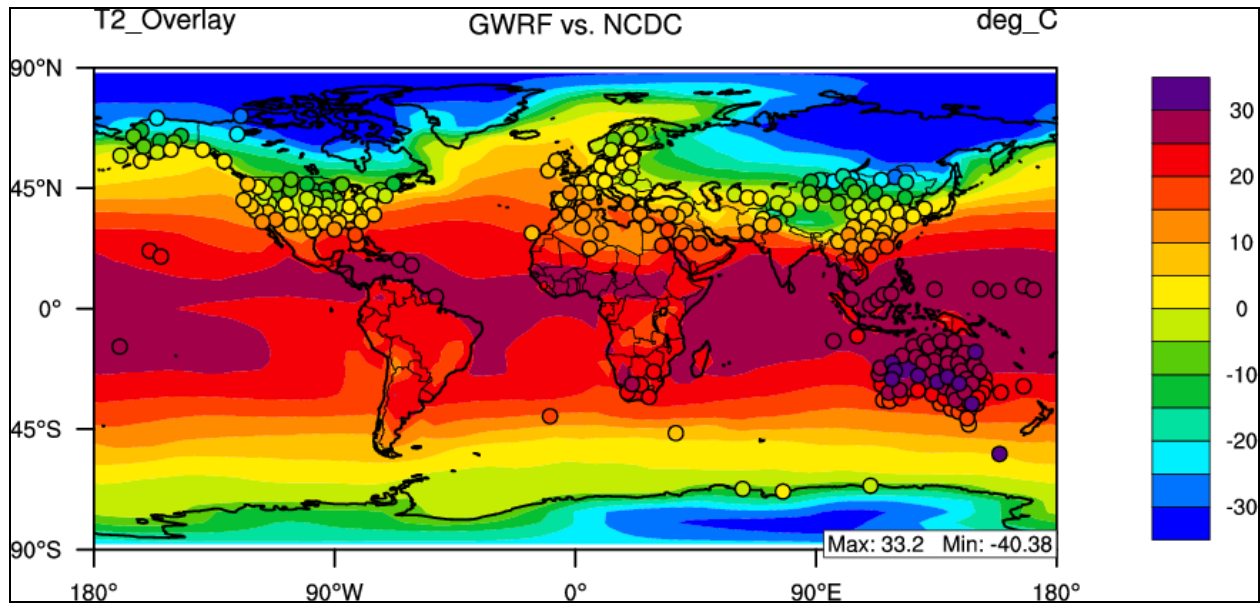


Figure 4.62 2001 winter mean bias of temperature at 2-meter.

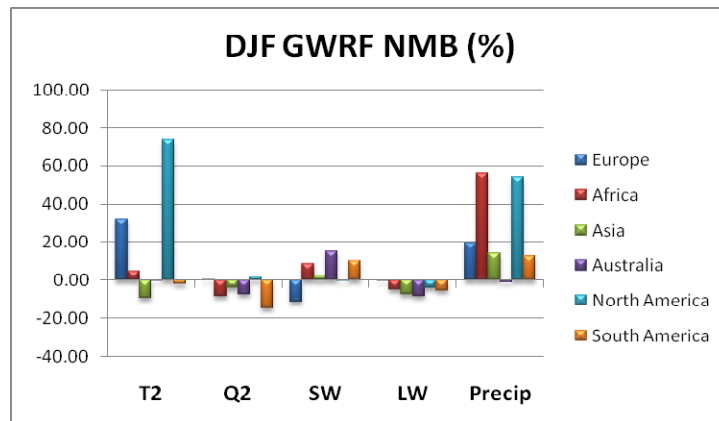


**Figure 4.63** 2001 winter mean bias of temperature at 2-meter as compared with NCDC.

**Table 4.36** Performance Statistics of GWRf 2001 winter temperature at 2-meter compared with NCEP/NCAR Reanalysis and NCDC.

Name	MeanObs (°C)	MeanMod (°C)	Number	Corr	MB (°C)	RMSE	NMB%	NME%
Europe	-2.07	-1.42	64	0.92	0.66	2.85	31.63	103.30
Africa	20.46	21.42	144	0.92	0.96	2.39	4.69	9.26
Asia	-3.51	-3.84	255	0.98	-0.33	4.30	-9.40	99.09
Australia	25.24	25.20	64	0.98	-0.04	1.10	-0.14	3.13
N.A.	0.96	1.67	132	0.99	0.71	2.44	73.79	195.03
S.A.	18.17	17.82	126	0.93	-0.34	2.77	-1.90	9.75
N. Pole	-22.71	-25.19	576	0.94	-2.48	4.65	-10.92	15.27
N. Ferrel	-1.44	-1.05	576	0.98	0.39	3.00	26.89	152.05
N. Hadley	22.99	23.61	576	0.96	0.62	1.49	2.70	4.15
S. Hadley	25.00	24.68	576	0.89	-0.32	1.45	-1.28	3.07
S. Ferrel	11.21	10.75	576	1.00	-0.47	0.86	-4.15	5.65
S. Polar	-11.87	-11.91	575	0.96	-0.05	3.43	-0.38	21.22
N.H.	0.15	-0.27	1656	0.99	-0.42	3.28	-285.37	1458.18
S.H.	8.40	8.15	1655	0.99	-0.25	2.25	-3.00	15.78
Global	3.80	3.46	3239	0.99	-0.34	2.84	-8.87	46.51
NCDC	11.62	9.32	243	0.54	-2.30	80.97	-19.77	42.29

An overview of statistical performance for the major boundary layer variables is shown graphically in Figure 4.64. Different from the annual and summer means, the largest NMB values are associated with temperature at 2-meter, and not daily precipitation rate. For the continental domains, the largest overestimation occurs over North America, with an NMB value of 73.79%, which actually corresponds to an MB of 0.71 °C. Over the circulation cell domains, the Northern Ferrel Cell is the largest with an NMB value of 26.89%, which corresponds to a MB value of 0.39. The northern Ferrel Cell also displays a large NMB value for winter of the fine resolution simulation. Unlike the high resolution case, the winter case has comparable NMBs for daily precipitation rate over both the continental and circulation cell domains, when compared to the annual and summer means. There is still a pattern of an underestimation of water vapor mixing ratio at 2 meters and an underestimation of downward longwave flux. The vertical profile of temperature performance is also assessed. Figure 4.65 shows that GWRP captures vertical temperature distribution within  $\pm 2$  degrees up to approximately 300 hPa over the six continental domains.



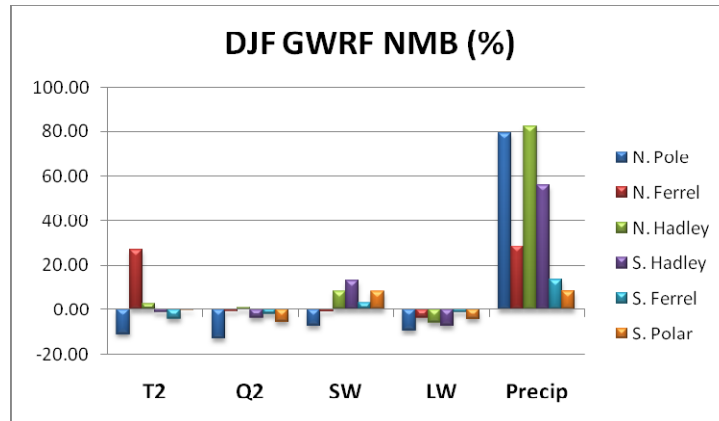


**Figure 4.64** 2001 winter mean normalized mean bias (%) of major meteorological variables for (a) the six continental domains and (b) the six circulation cell domains.

Figure 4.66 is the zonal mean bias of GWRP versus NCEP/NCAR Reanalysis data. This figure also shows that GWRP captures the vertical temperature distribution within  $\pm 2$  degrees up to approximately 300 hPa. The winter coarse resolution case shares a similar structure with the summer and annual coarse resolution cases, in which it shows large overestimations near the surface of the equator and large underestimations above the tropopause. Also, the coarse resolution case does not underpredict temperatures over the Tropics between 400 hPa and 100 hPa like the fine resolution case does. When compared with the summer case, during winter the model does not underestimate temperatures throughout the Southern Ferrel Cell as badly. The winter season does not overestimate temperatures aloft between 300 and 100 hPa as badly as the summer case.

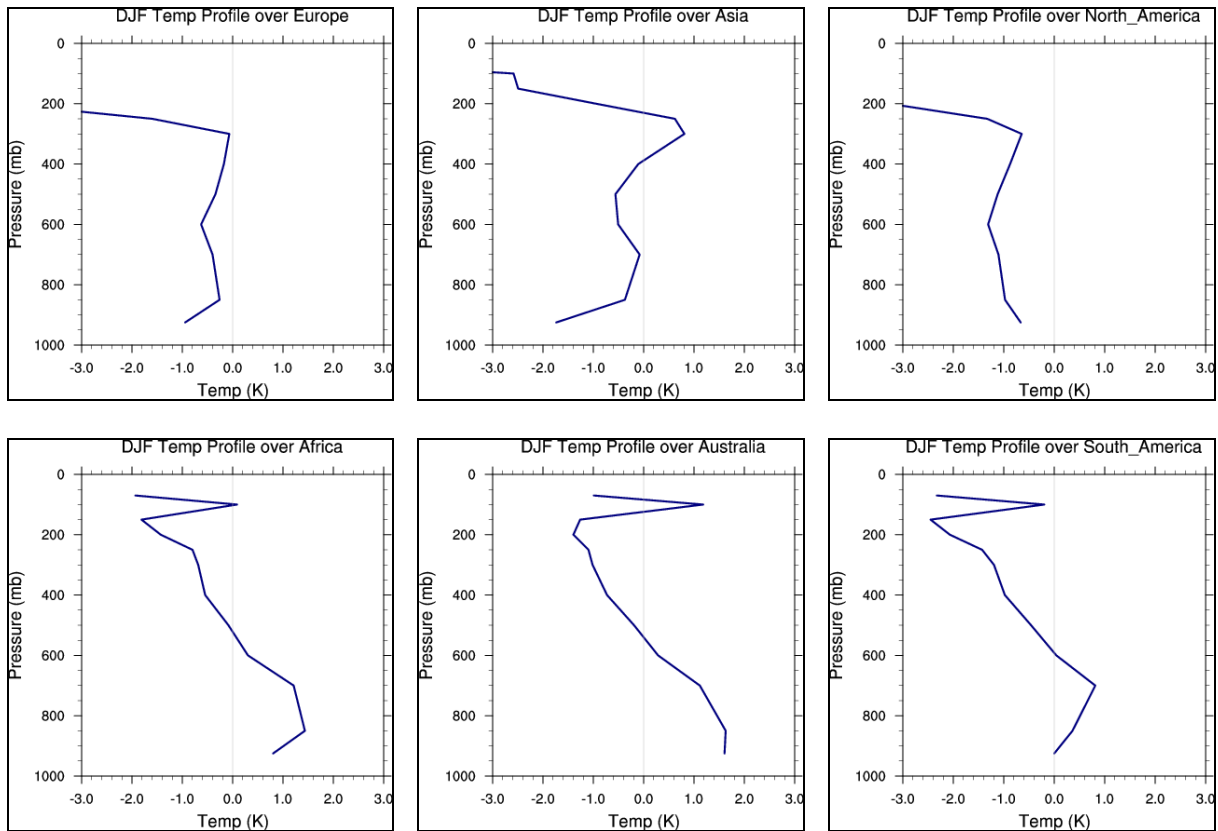


**Figure 4.65 Winter Vertical Profiles of Temperature Mean Bias over the six populated continents.**

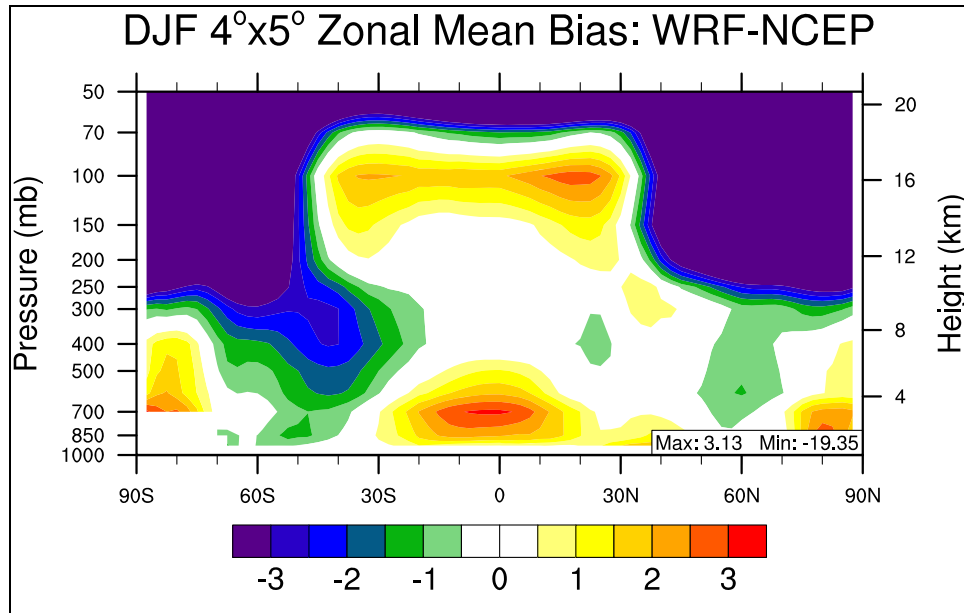


**Figure 4.66 Winter zonal mean bias of Temperature.**

#### 4.2.3.2 Winter Water Vapor Mixing Ratio at 2-meter

The global distribution of winter mean bias for water vapor mixing ratio at 2-meter is displayed in Figure 4.67. When compared with the annual spatial mean bias plot, the underestimations over the Tropics are larger than the annual case, and the areas of large underestimation have shifted to the Southern Hadley Cell and are co-located with areas that receive large amounts of convective precipitation during this season. Overall the majority of mean bias values are within the range of  $\pm 5 \text{ g kg}^{-1}$ , with a maximum mean bias of  $6.82 \text{ g kg}^{-1}$  and the minimum mean bias is  $-8.86 \text{ g kg}^{-1}$ . The shift from Northern to Southern Hemisphere of the underestimation of Q2 is also reflected in Table 4.37 in which Europe, North America, and the Northern Hadley Cell have negative NMB values, while all other sub-domains have positive NMB values. The global NMB value is better than both the annual and summer cases with a winter value of -2.08%. Overall the Corr values are similar to annual mean performance, with a global Corr value of 0.99.

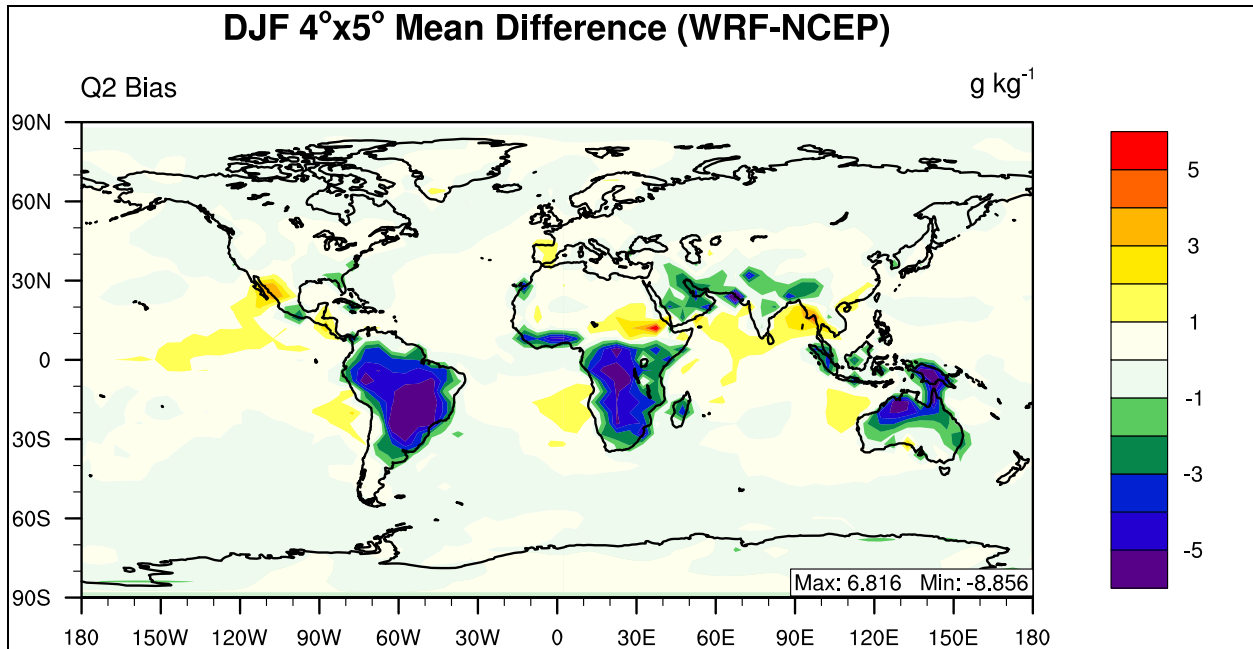


**Figure 4.67** 2001 winter mean bias of Water Vapor Mixing Ratio at 2-meter.

**Table 4.37** Performance Statistics of GWRP 2001 winter mean of Water Vapor Mixing Ratio at 2-meter as compared with NCEP/NCAR Reanalysis.

Name	MeanObs (g kg <sup>-1</sup> )	MeanMod (g kg <sup>-1</sup> )	Number	Corr	MB (g kg <sup>-1</sup> )	RMSE	NMB%	NME%
Europe	3.59	3.61	64	0.94	0.02	0.52	0.50	11.35
Africa	10.92	10.02	144	0.91	-0.91	2.48	-8.30	16.60
Asia	4.85	4.67	255	0.98	-0.19	1.29	-3.89	16.14
Australia	12.78	11.81	64	0.92	-0.98	2.18	-7.63	11.33
N.A.	5.73	5.81	132	0.98	0.08	0.92	1.43	9.36
S.A.	12.83	10.90	126	0.91	-1.93	3.03	-15.07	16.23
N. Pole	1.01	0.88	576	0.97	-0.13	0.29	-12.97	21.45
N. Ferrel	4.24	4.20	576	0.99	-0.04	0.52	-0.92	8.91
N. Hadley	14.13	14.22	576	0.96	0.09	1.45	0.65	6.67
S. Hadley	16.66	16.04	576	0.79	-0.62	2.02	-3.72	7.43
S. Ferrel	7.74	7.58	576	0.99	-0.17	0.52	-2.19	3.87
S. Polar	2.23	2.10	576	0.97	-0.12	0.37	-5.52	11.84
N.H.	6.65	6.63	1656	0.99	-0.02	0.92	-0.30	7.82
S.H.	9.09	8.77	1656	0.98	-0.31	1.25	-3.43	6.82
Global	7.65	7.49	3240	0.99	-0.16	1.08	-2.08	7.31

#### 4.2.3.3 Winter Downward Shortwave Flux

The pattern of winter downward shortwave flux mean bias is displayed graphically in Figure 4.68, and reflects the annual pattern of an overestimation in the Tropics (30°N-30°S), however, in the winter case there are large overestimations over the Southern Ocean. The large underestimation off of the Pacific Coast of South America that is well defined in the fine grid resolution case is not as prominent in this case. The majority of mean bias value fall within the range of  $\pm 100 \text{ W m}^{-2}$ , the maximum mean bias is very similar to the summer case with a value of  $127.1 \text{ W m}^{-2}$ , while the minimum mean bias value is better than the summer case, with a value of  $-103.7 \text{ W m}^{-2}$ . The pattern of GWRP SWDOWN performance is reflected in Table 4.38 in which all of the domains display a positive NMB value except for the high Northern latitudes (circulation cells: Northern Polar Cell and Northern Ferrel Cell, continents: Europe and North America) which display negative NMB values, with a global NMB value of 6.90%. Correlation values are improved from the annual mean, but not as improved as in the summer mean, with the Southern Hadley Cell increasing from 40% to 54% and the Southern Polar Cell Corr value increases from 19% to 80%. Globally, the correlation value is improved with a value of 0.96. Both the Global mean as compared with Reanalysis data and the BSRN mean comparison indicates an overestimation of SWDOWN during winter of 2001 and also demonstrates Corr values greater than 0.96.

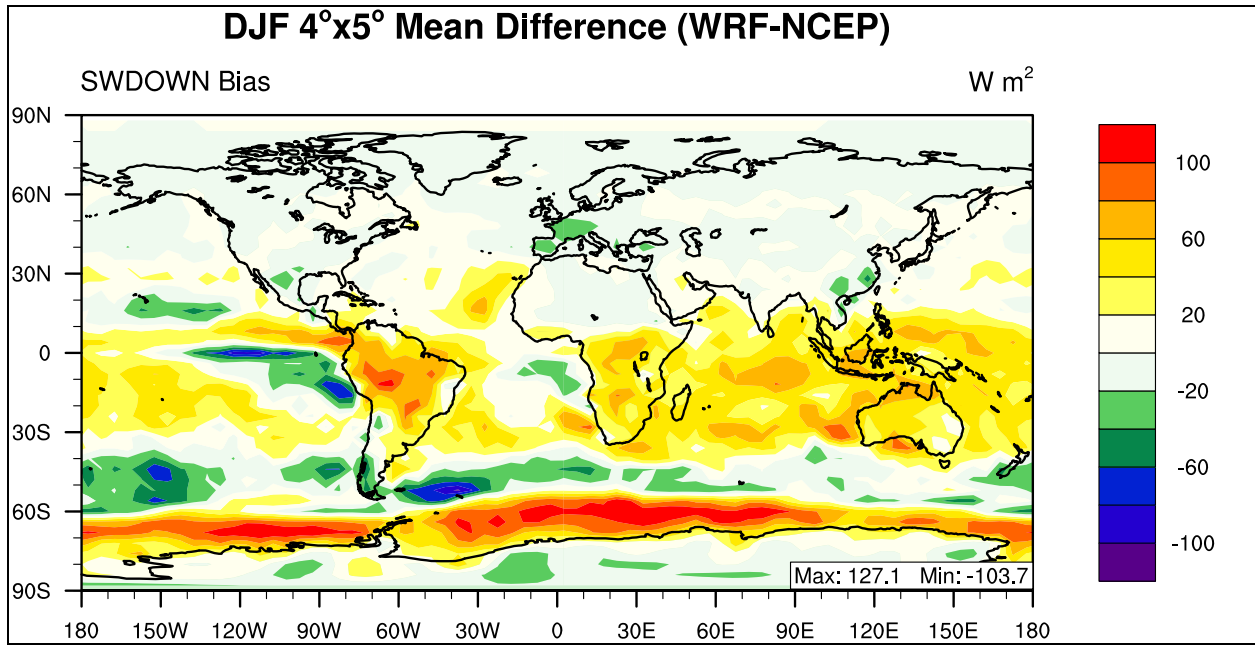


**Figure 4.68** 2001 winter mean bias of Downward Shortwave Flux at 2-meter.

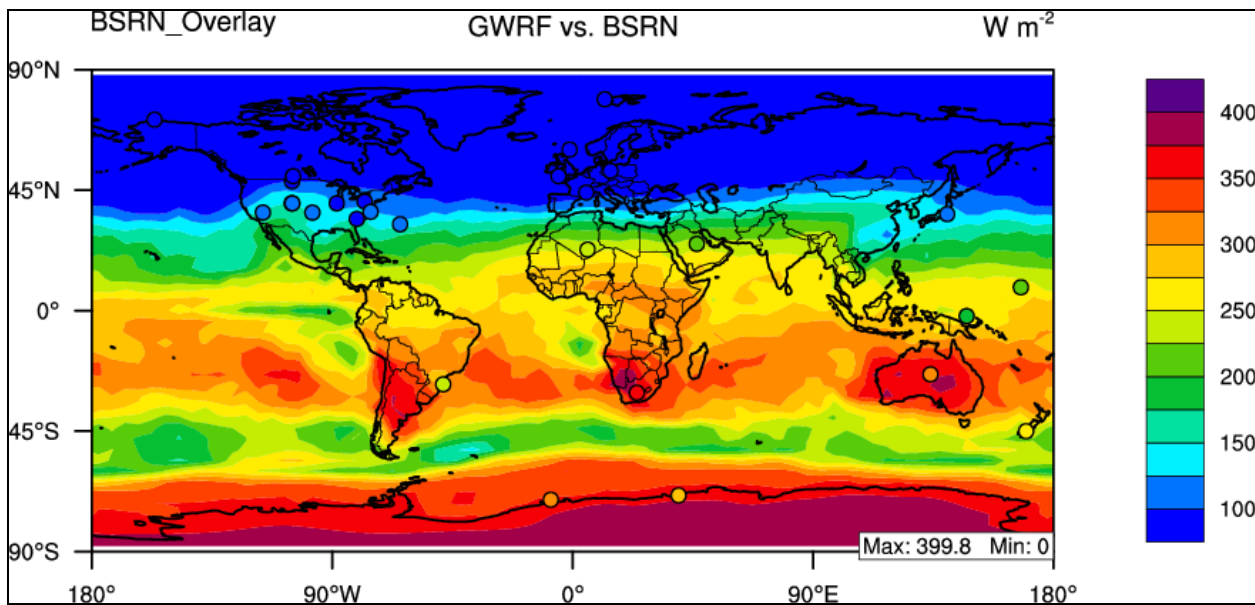


**Figure 4.69** 2001 winter mean bias of Downward Shortwave Flux at 2-meter as compared with BSRN.

**Table 4.38 Performance Statistics of GWRP 2001 winter mean for Downward Shortwave Flux compared with NCEP/NCAR Reanalysis and BSRN.**

Name	MeanObs (W m <sup>-2</sup> )	MeanMod (W m <sup>-2</sup> )	Number	Corr	MB (W m <sup>-2</sup> )	RMSE	NMB%	NME%
Europe	64.29	56.88	64	0.98	-7.41	11.90	-11.53	12.09
Africa	260.83	283.08	144	0.79	22.25	37.16	8.53	10.98
Asia	135.71	138.58	255	0.99	2.88	14.63	2.12	6.65
Australia	295.23	340.36	64	0.79	45.13	49.82	15.29	15.42
N.A.	126.55	126.16	132	0.98	-0.39	9.76	-0.31	5.42
S.A.	260.81	286.80	126	0.61	25.98	51.06	9.96	16.86
N. Pole	13.39	12.43	432	1.00	-0.95	1.59	-7.12	8.59
N. Ferrel	96.13	95.04	576	0.98	-1.09	9.29	-1.14	7.04
N. Hadley	219.90	237.88	576	0.74	17.98	32.89	8.18	11.68
S. Hadley	268.10	302.22	576	0.54	34.13	46.58	12.73	15.51
S. Ferrel	251.26	259.62	576	0.57	8.36	42.23	3.33	13.04
S. Polar	328.93	355.66	576	0.80	26.73	52.59	8.13	12.07
N.H.	122.46	128.67	1512	0.98	6.21	21.10	5.07	10.29
S.H.	285.08	307.12	1656	0.76	22.04	45.88	7.73	12.96
Global	206.68	220.93	3096	0.96	14.26	35.87	6.90	12.04
BSRN	143.08	173.31	28	0.98	30.23	39.25	21.13	22.75

#### 4.2.3.4 Winter Downward Longwave Flux

The pattern of winter downward longwave flux mean bias is displayed graphically in Figure 4.70 in which the overall pattern is an underestimation with a global NMB value of -5.15%, which is worse than the annual or summer means. All mean bias values fall within the range of  $\pm 100$  W m<sup>-2</sup>, with a smaller maximum mean bias (69.45 W m<sup>-2</sup>) and a comparable minimum mean bias (-66.67 W m<sup>-2</sup>) with the annual mean. The overall pattern of GWRP GLW performance is consistent with the annual and summer means, as shown in Table 4.39, in which all of the domains display a negative NMB value. Overall Corr values are above 0.70, with the Southern Hadley Cell displaying the lowest value (0.73), which is consistent with the annual mean. Globally, the correlation value is 0.98. In this case, GLW during winter 2001 is

underestimated when the model is evaluated using NCEP/NCAR Reanalysis and BSRN data and displays high (>0.90) Corr values.

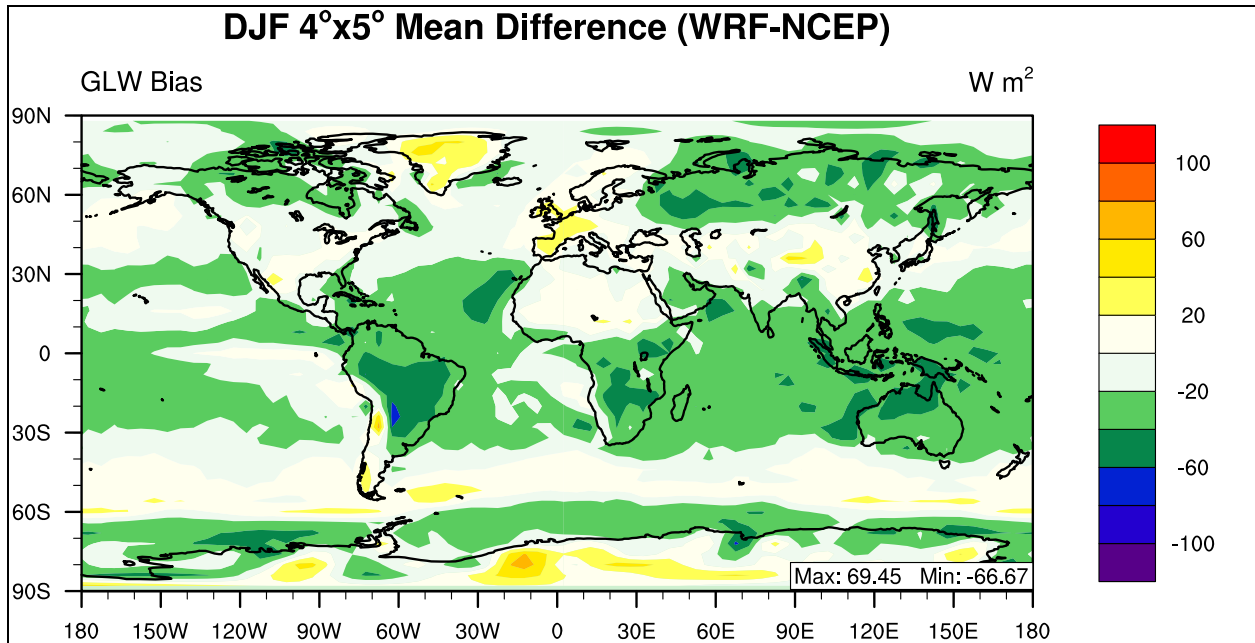


**Figure 4.70** 2001 winter mean bias of Downward Longwave Flux at 2-meter.

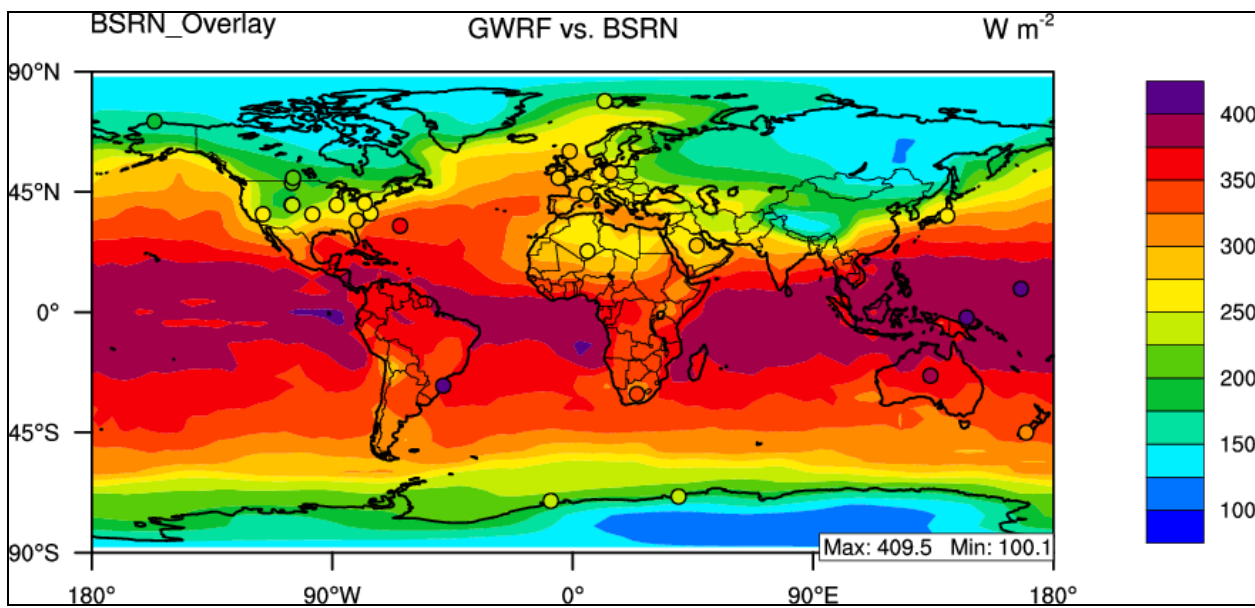


**Figure 4.71** 2001 winter mean bias of Downward Longwave Flux at 2-meter as compared to BSRN.

**Table 4.39 Performance Statistics of GWRP 2001 winter mean for Downward Longwave Flux as compared with NCEP/NCAR Reanalysis and BSRN.**

Name	MeanObs (W m <sup>-2</sup> )	MeanMod (W m <sup>-2</sup> )	Number	Corr	MB (W m <sup>-2</sup> )	RMSE	NMB%	NME%
Europe	245.41	245.09	64	0.87	-0.32	17.22	-0.13	5.45
Africa	348.41	331.18	144	0.92	-17.23	27.05	-4.95	6.39
Asia	244.15	225.64	255	0.97	-18.51	27.75	-7.58	9.52
Australia	388.32	355.84	64	0.94	-32.48	34.75	-8.36	8.37
N.A.	266.15	254.87	132	0.98	-11.28	17.37	-4.24	5.50
S.A.	358.22	338.14	126	0.89	-20.08	33.96	-5.60	8.19
N. Pole	178.48	161.93	576	0.89	-16.56	23.75	-9.28	11.55
N. Ferrel	252.82	243.47	576	0.96	-9.35	19.48	-3.70	5.96
N. Hadley	376.16	354.40	576	0.94	-21.76	27.08	-5.78	6.45
S. Hadley	400.26	371.77	576	0.73	-28.49	32.05	-7.12	7.40
S. Ferrel	321.71	317.11	576	0.88	-4.61	17.01	-1.43	4.22
S. Polar	191.76	183.11	576	0.93	-8.65	27.74	-4.51	12.48
N.H.	271.62	255.89	1656	0.98	-15.74	23.55	-5.79	7.33
S.H.	305.95	291.74	1656	0.98	-14.21	26.48	-4.64	7.34
Global	286.15	271.41	3240	0.98	-14.74	24.93	-5.15	7.35
BSRN	291.18	267.82	28	0.91	-23.37	36.63	-8.02	9.51

#### 4.2.3.5 Winter Zonal Wind Speed

The pattern of winter zonal wind speed at 10-meters (U10) mean bias is displayed graphically in Figure 4.72 in which the overall pattern appears to be a slight underestimation of the zonal component, however there are large overestimations over the North Atlantic and large underestimations of zonal wind speed over the Northern Pacific, which are not present in the annual mean analysis. Overall wind speed is not well predicted by GWRP with a global NMB value of -332.73%, which is smaller than the bias present in both the annual and summer mean. This large, negative NMB value corresponds to a mean bias of  $-0.23 \text{ m s}^{-1}$  and is caused by a low wind speed ( $-0.07 \text{ m s}^{-1}$ ) from the Reanalysis data. The majority of mean bias values fall within the range of  $\pm 5 \text{ m s}^{-1}$  and the performance is worse than the annual mean with a maximum mean bias of  $9.34 \text{ m s}^{-1}$  and a minimum mean bias value of  $-7.09 \text{ W m}^{-2}$ . U10 displays very large

absolute NMB values but still has a global Corr value of 0.88, slightly worse than the summer mean.

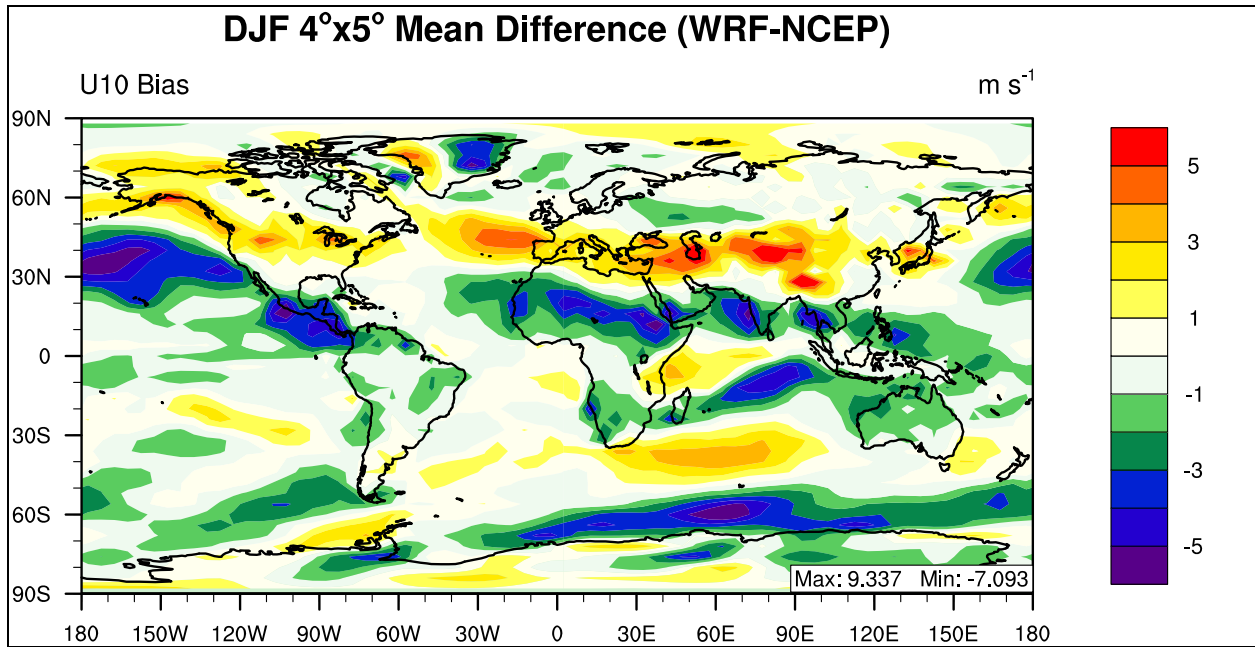


**Figure 4.72** 2001 winter mean bias of zonal wind at 10-meter.

**Table 4.40 Statistical Analysis of GWRP winter mean zonal wind at 10-meters for 2001 compared with NCEP/NCAR Reanalysis.**

Name	MeanObs (m s <sup>-1</sup> )	MeanMod (m s <sup>-1</sup> )	Number	Corr	MB (m s <sup>-1</sup> )	RMSE	NMB%	NME%
Europe	0.67	1.21	64	0.22	0.54	1.60	80.96	174.75
Africa	-0.74	-1.67	144	0.69	-0.93	2.25	-125.29	243.50
Asia	-0.14	0.27	255	0.79	0.41	2.34	301.16	1215.39
Australia	-0.04	-1.19	64	0.90	-1.15	1.46	-3269.03	3538.66
N.A.	0.52	1.07	132	0.89	0.55	1.69	105.21	245.48
S.A.	0.64	0.23	126	0.95	-0.41	1.16	-63.86	145.69
N. Pole	0.12	0.40	576	0.59	0.28	1.30	221.20	748.30
N. Ferrel	1.64	2.39	576	0.48	0.75	2.38	45.50	111.72
N. Hadley	-3.05	-4.26	576	0.85	-1.21	2.03	-39.52	50.96
S. Hadley	-2.35	-2.86	576	0.88	-0.51	1.40	-21.74	46.46
S. Ferrel	3.86	3.54	576	0.86	-0.33	1.73	-8.45	33.85
S. Polar	-0.31	-0.83	576	0.75	-0.52	1.91	-167.97	485.16
N.H.	-0.45	-0.53	1656	0.84	-0.08	1.97	-18.43	326.64
S.H.	0.24	-0.14	1656	0.92	-0.38	1.63	-159.85	523.95
Global	-0.07	-0.30	3240	0.88	-0.23	1.82	-332.73	1985.28

#### 4.2.3.6 Winter Meridional Wind Speed

The pattern of winter meridional wind speed at 10-meters (V10) mean bias is displayed graphically in Figure 4.51 and the spatial pattern appears to be similar to the zonal component with an overall slight underestimation. Meridional wind speed displays a global NMB value of 18.66%, which is higher than both the summer and annual meridional means, which both presented negative NMBs. This corresponds to a mean bias of 0.03 m s<sup>-1</sup>. The majority of mean bias values fall within the range of  $\pm 5$  m s<sup>-1</sup>, with a maximum mean bias of 7.04 m s<sup>-1</sup> and a minimum mean bias value of -5.68 m s<sup>-1</sup>, which exhibits a tendency to overestimate meridional wind speeds when compared with the summer and annual means. The overall pattern of GWRP V10 performance is reflected in Table 4.41 in which the majority of domains display a positive NMB value, which is different from the summer or annual cases. V10 also displays very large

absolute NMB values and the low Corr values for individual domains, but still displays a global Corr value of 78%.

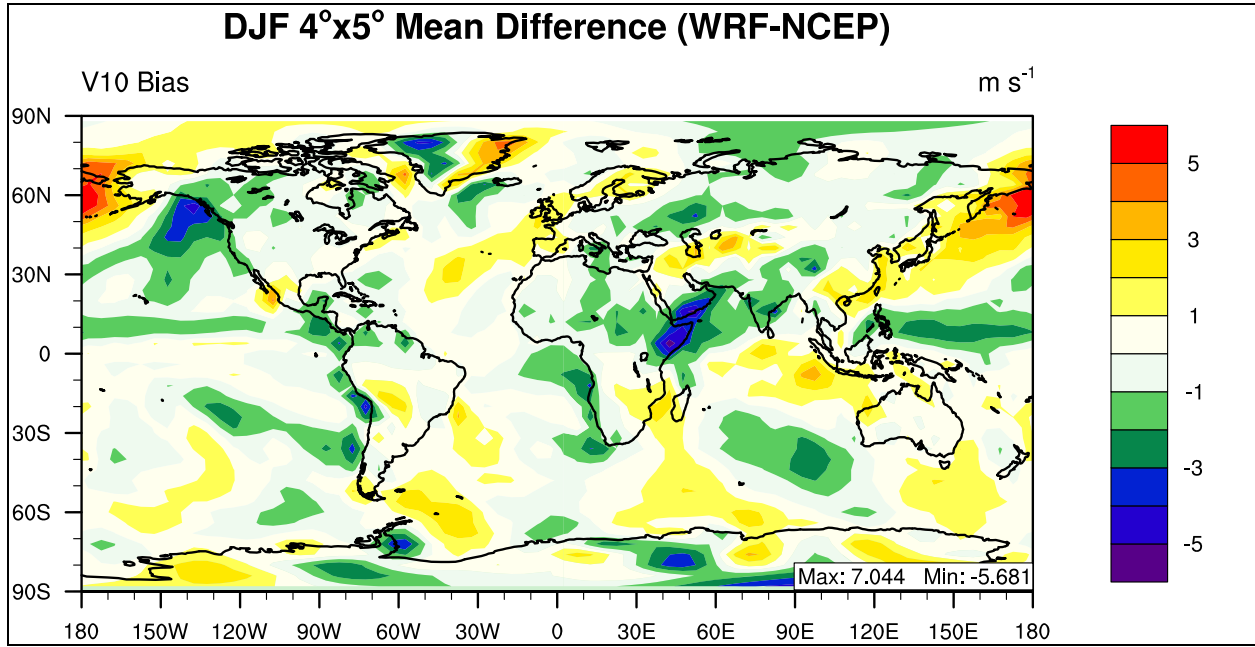


**Figure 4.73** 2001 winter mean bias of meridional wind at 10-meter.

**Table 4.41 Performance Statistics of GWRP 2001 winter mean meridional wind at 10-meter as compared with NCEP/NCAR Reanalysis.**

Name	MeanObs (m s <sup>-1</sup> )	MeanMod (m s <sup>-1</sup> )	Number	Corr	MB (m s <sup>-1</sup> )	RMSE	NMB%	NME%
Europe	0.42	0.53	64	0.56	0.11	1.11	25.29	218.66
Africa	0.36	-0.13	144	0.86	-0.48	1.42	-134.95	310.62
Asia	-0.29	-0.68	255	0.79	-0.39	1.46	-132.83	395.08
Australia	0.99	1.44	64	0.92	0.44	0.90	44.52	70.18
N.A.	-0.47	-0.67	132	0.80	-0.20	0.91	-43.67	144.88
S.A.	-1.09	-0.72	126	0.70	0.38	1.24	34.66	85.06
N. Pole	0.04	0.21	576	0.61	0.17	1.49	465.22	3008.55
N. Ferrel	0.28	0.42	576	0.60	0.14	1.62	50.45	431.96
N. Hadley	-1.61	-2.11	575	0.80	-0.50	1.35	-30.87	64.80
S. Hadley	0.70	0.83	575	0.88	0.14	1.07	19.43	116.15
S. Ferrel	-0.89	-0.67	576	0.75	0.22	1.10	24.41	101.09
S. Polar	0.40	0.51	576	0.71	0.10	1.42	26.23	281.82
N.H.	-0.44	-0.51	1655	0.74	-0.07	1.47	-16.73	253.12
S.H.	0.11	0.25	1655	0.82	0.13	1.20	120.64	842.42
Global	-0.16	-0.13	3239	0.78	0.03	1.35	18.66	641.77

#### 4.2.3.7 Winter Daily Precipitation

In Figure 4.74, the interval spacing is set to  $\pm 2$  mm day<sup>-1</sup> to show the spatial variability of GWRP precipitation rate performance. Overall, the GWRP performance during winter appears to be overestimating daily precipitation rate, with a complicated scenario in the Tropics. The maximum (21.82 mm day<sup>-1</sup>) and minimum (-7.08 mm day<sup>-1</sup>) mean bias values are better than the summer case but worse than the annual case. The overall spatial trend agrees with the annual mean, in which performance is best at the mid-latitudes (Northern and Southern Ferrel Cells) and worst in the Tropics (Northern and Southern Hadley Cells) as illustrated in Figure 4.74 and shown in Table 4.42, in which the Northern and Southern Ferrel Cells have NMB values of less than 29%, while the Hadley cells have NMB values over 50%. In this winter case, daily precipitation rate is highly overestimated over the North Pole domain.

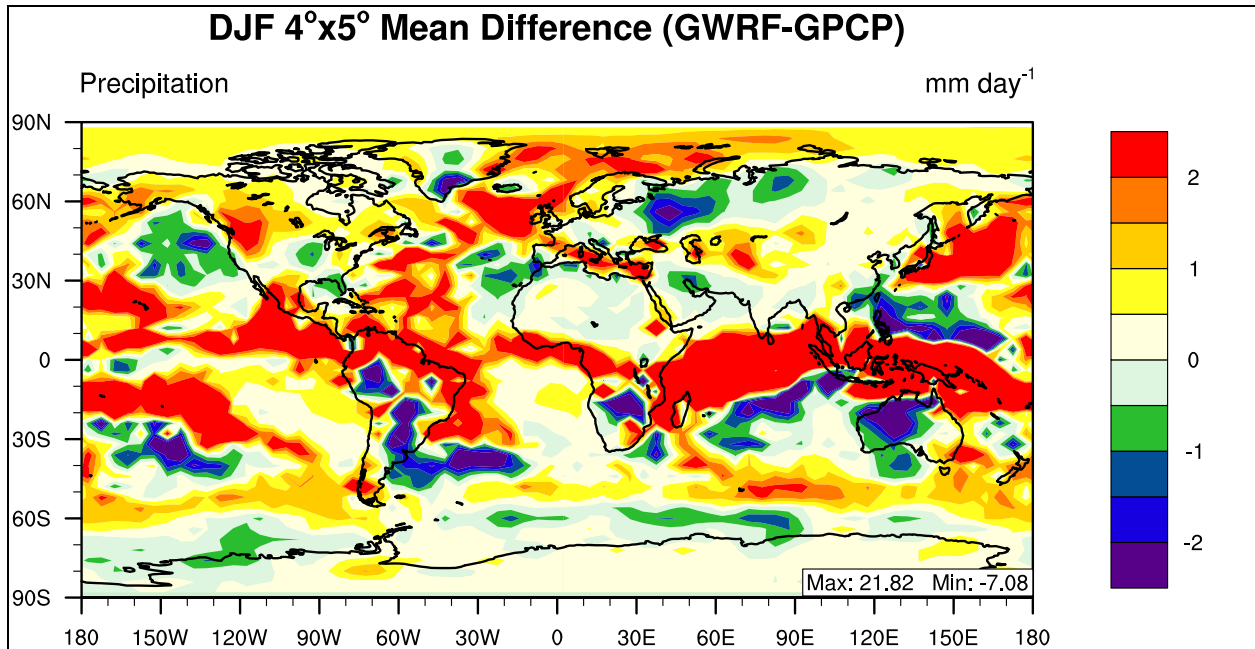


**Figure 4.74** 2001 winter mean bias of daily precipitation rate.

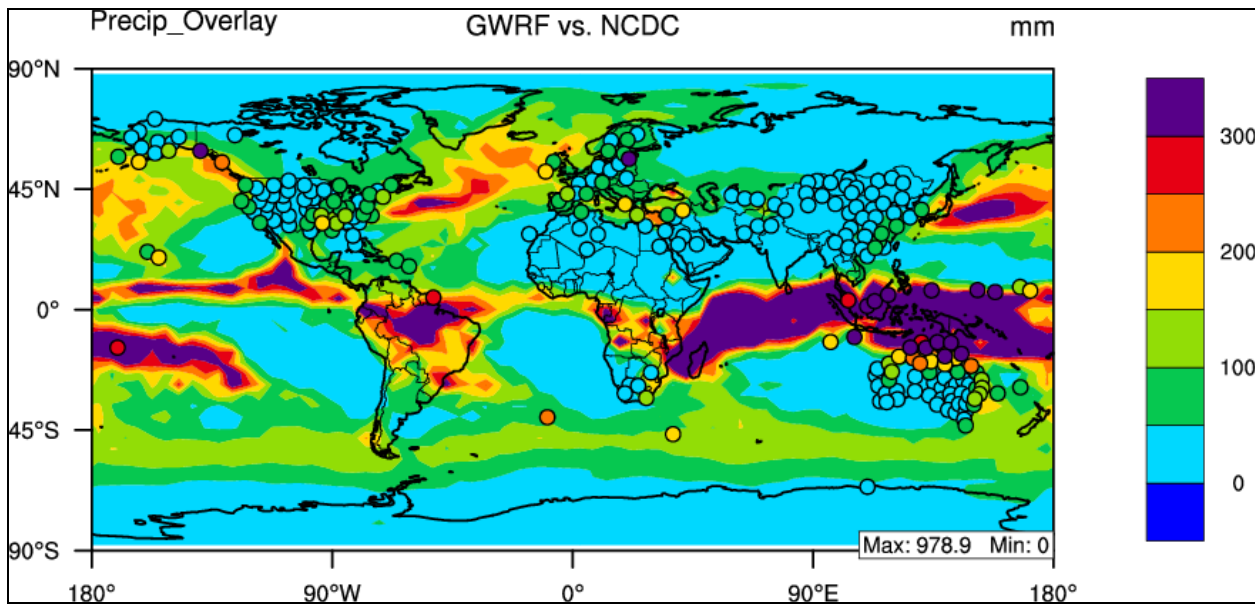


**Figure 4.75** 2001 winter mean bias of monthly precipitation rate as compared to NCDC.

**Table 4.42 Performance Statistics for GWRP 2001 winter precipitation compared with GPCP (mm day<sup>-1</sup>) and NCDC (mm month<sup>-1</sup>).**

<b>Name</b>	<b>MeanObs</b>	<b>MeanMod</b>	<b>Number</b>	<b>Corr</b>	<b>MB</b>	<b>RMSE</b>	<b>NMB%</b>	<b>NME%</b>
<b>Europe</b>	2.32	2.77	64	0.44	0.45	1.35	19.43	41.52
<b>Africa</b>	1.67	2.61	144	0.76	0.94	2.57	56.25	86.59
<b>Asia</b>	0.96	1.10	255	0.56	0.13	1.00	13.87	67.36
<b>Australia</b>	3.32	3.27	64	0.81	-0.04	2.47	-1.34	50.84
<b>N.A.</b>	1.51	2.32	132	0.60	0.82	1.54	54.12	67.19
<b>S.A.</b>	4.33	4.88	126	0.77	0.55	2.19	12.65	38.64
<b>N. Pole</b>	0.83	1.49	576	0.74	0.66	1.07	79.20	101.33
<b>N. Ferrel</b>	2.59	3.32	576	0.79	0.73	1.70	28.38	45.59
<b>N. Hadley</b>	2.21	4.02	576	0.78	1.81	3.87	82.15	100.56
<b>S. Hadley</b>	3.72	5.78	576	0.73	2.07	4.45	55.59	75.98
<b>S. Ferrel</b>	2.55	2.88	576	0.47	0.34	1.15	13.22	35.09
<b>S. Polar</b>	0.89	0.96	576	0.88	0.07	0.42	8.32	35.09
<b>N.H.</b>	1.87	2.96	1656	0.78	1.08	2.55	57.79	76.20
<b>S.H.</b>	2.38	3.24	1656	0.79	0.86	2.72	36.30	57.78
<b>Global</b>	2.08	2.98	3240	0.78	0.89	2.45	42.83	63.59
<b>NCDC</b>	82.83	88.99	223	0.74	6.16	79.05	7.45	57.31

### **4.3 Sensitivity to radiation schemes**

#### **4.3.1 Summer (JJA) RAD1 mean evaluation**

##### **4.3.1.1 Summer Temperature at 2-meter**

The temperature at 2-meters above the surface for GWRf sensitivity simulation RAD1 is compared with NCEP/NCAR Reanalysis for the summer of 2001 (June, July, and August 2001). This sensitivity simulation replaces the Goddard shortwave scheme from the baseline simulation with the Dudhia shortwave scheme. When Figure 4.76 is compared with Figure 4.11, there are large differences between the two figures, specifically that the RAD1 simulation produces larger areas of underestimation of temperature over land surfaces. The model performance is still complicated over Antarctica with overestimations occurring over the land surface and underestimations occurring off shore over the Southern Ocean. Globally, GWRf shows good statistical performance with a correlation value of 0.99, but an NMB value of -15.64% which is very different from the baseline value (2.70%), indicating a tendency for RAD1 to underestimate T2 when compared to the baseline simulation. This is reflected in Table 4.43 when all of the continental and circulation cell domains have negative NMB values and is consistent with the NCDC evaluation.

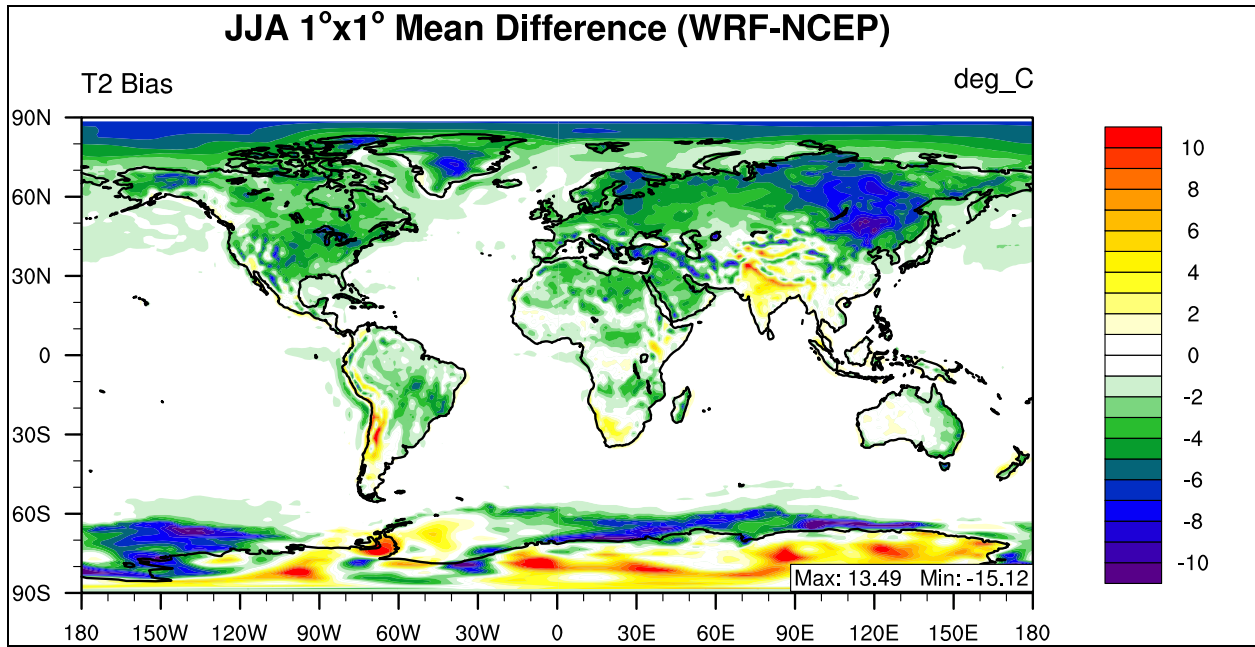


**Figure 4.76** 2001 summer mean bias of temperature at 2-meter.

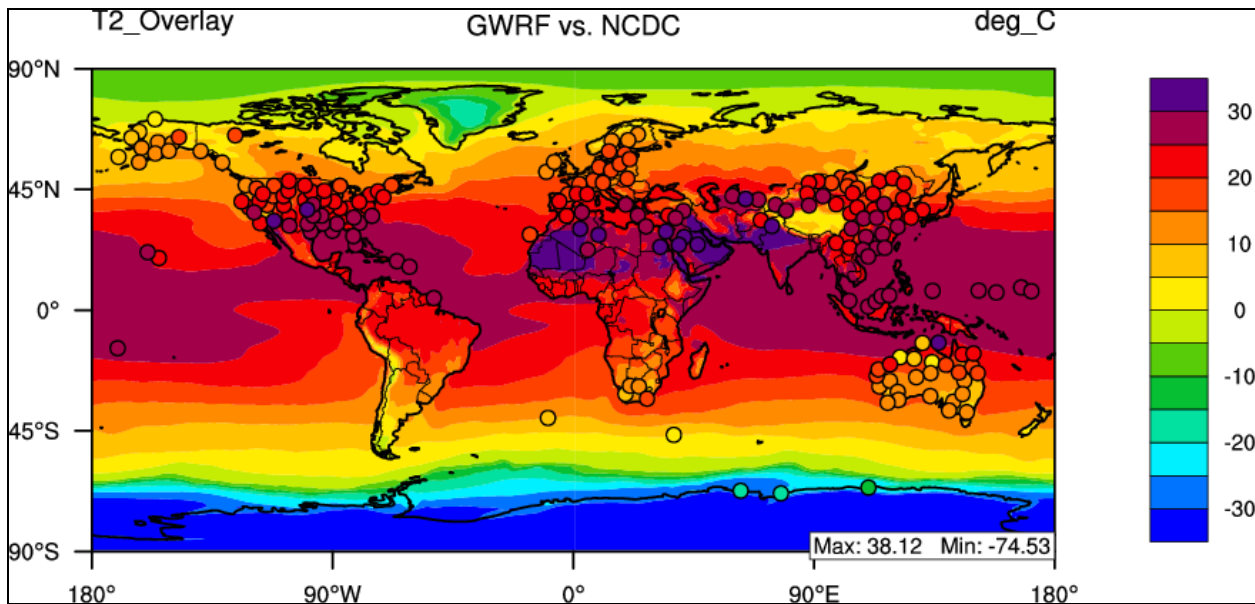


**Figure 4.77** 2001 summer mean bias of temperature at 2-meter as compared to NCDC.

**Table 4.43 Performance Statistics of GWRf 2001 summer mean temperature at 2-meter summer compared with NCEP/NCAR Reanalysis and NCDC.**

Name	MeanObs (°C)	MeanMod (°C)	Number	Corr	MB (°C)	RMSE	NMB%	NME%
Europe	16.43	13.05	1200	0.92	-3.37	3.79	-20.52	20.68
Africa	23.83	22.57	2925	0.95	-1.26	2.17	-5.30	7.11
Asia	20.72	18.28	5100	0.94	-2.44	4.05	-11.76	15.50
Australia	17.02	16.63	1200	0.98	-0.40	1.28	-2.32	5.16
N.A.	20.51	18.04	2400	0.97	-2.48	3.05	-12.08	12.72
S.A.	14.76	14.04	2450	0.97	-0.72	2.31	-4.87	10.85
N. Pole	3.20	-0.76	10439	0.95	-3.96	4.35	-123.65	124.14
N. Ferrel	17.65	15.48	10800	0.94	-2.17	3.06	-12.30	13.42
N. Hadley	26.64	26.20	10800	0.91	-0.44	1.40	-1.64	3.23
S. Hadley	22.26	22.16	10800	0.96	-0.09	1.32	-0.42	3.55
S. Ferrel	8.10	7.73	10800	0.99	-0.37	1.04	-4.54	7.47
S. Polar	-34.51	-34.56	10440	0.98	-0.05	4.73	-0.14	11.00
N.H.	15.97	13.80	32039	0.99	-2.17	3.16	-13.57	14.91
S.H.	-1.01	-1.18	32040	0.99	-0.17	2.87	-16.99	168.82
Global	7.48	6.31	64079	0.99	-1.17	3.02	-15.64	27.34
NCDC	20.78	17.78	199	0.86	-3.00	5.33	-14.43	20.15

An overview of RAD1 summer statistical performance for the major boundary layer variables is shown graphically in Figure 4.78. This Figure contrasts with Figure 4.13 (summer base case) by, with the exception of daily precipitation rate, all major boundary layer variables being underestimated over the majority of all continental and circulation cell sub-domains. Overall, daily precipitation rate is still overestimated, which is similar to the base case. Large error values for the North Polar domain persist for all major boundary layer variables except downward longwave flux. The vertical profile of temperature performance is explored in Figure 4.79 which is the zonal mean bias of GWRf versus NCEP/NCAR Reanalysis data. This figure also shows that GWRf generally captures the vertical temperature distribution within  $\pm 2$  degrees up to approximately 300 hPa, however in the RAD1 simulation large underestimations exist over the North Pole, which is consistent with Figure 4.78. The RAD1 simulation does share many

similarities with the base case summer zonal mean bias (Figure 4.13), with large overestimations near the surface over Antarctica and the equator, underestimations of temperatures throughout the Southern Ferrel Cell and the underestimation of temperatures between 400 hPa and 100 hPa over the Tropics

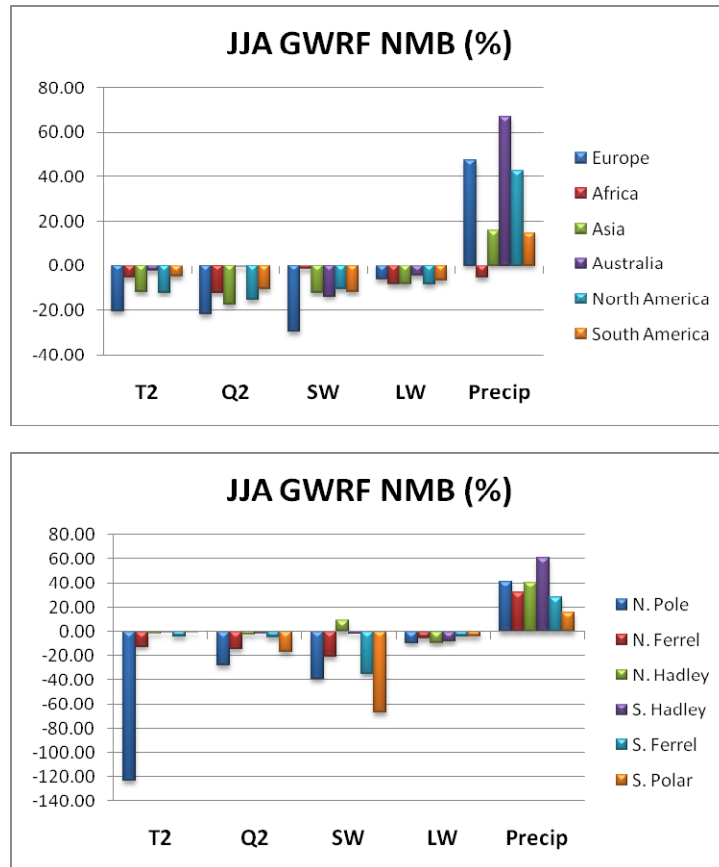


**Figure 4.78** 2001 summer mean normalized mean bias (%) of major meteorological variables for (a) the six continental domains and (b) the six circulation cell domains.

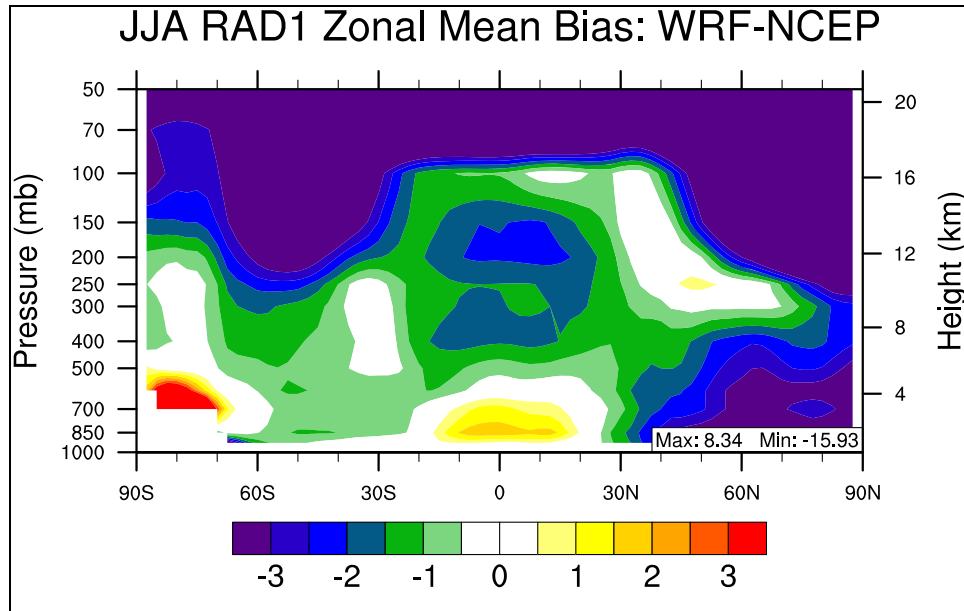


**Figure 4.79 2001 summer zonal mean bias of Temperature**

#### 4.3.1.2 Summer Water Vapor Mixing ratio at 2-meter

The global distribution of RAD1 summer mean bias for water vapor mixing ratio at 2-meters is displayed in Figure 4.80. When compared with the base simulation spatial mean bias plot, the areas of underestimation over land surfaces are similar; however the magnitude of underestimation in RAD1 is larger. Also, in RAD1 Q2 over the North Pole is largely underestimated, which is not as defined in the base case. The overall underestimation of Q2 is also reflected in Table 4.44 in which all domains have a negative NMB value, which is a clearer signal of underestimation than the base case. Performance over the North Pole is much worse than the corresponding baseline case, with RAD1 displaying a -21.78% NMB for this domain, which is worse than the baseline value (-8.63%). The global RAD1 NMB value is -7.45% which is worse than the base case whose summer value is -2.39%. Overall Corr values are similar to baseline performance, with a global Corr value of 0.98.

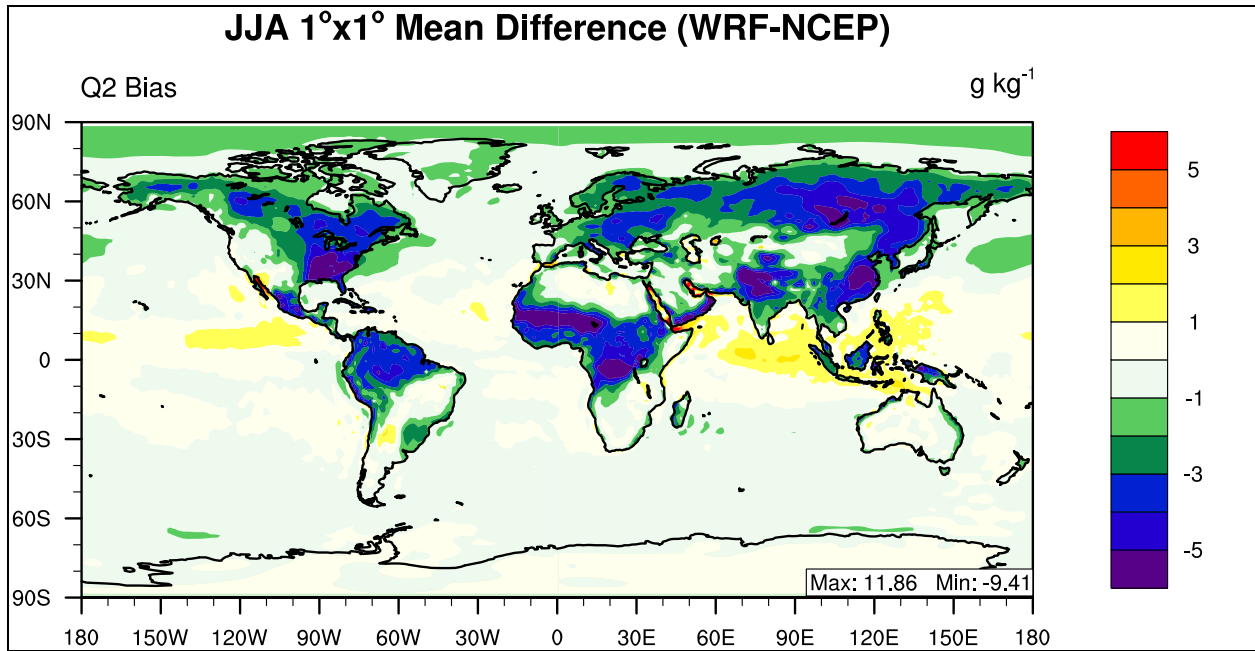


**Figure 4.80** 2001 summer mean bias of water vapor mixing ratio at 2-meter.

**Table 4.44 Performance Statistics of GWRP summer mean water vapor mixing ratio at 2-meter as compared with NCEP/NCAR Reanalysis.**

Name	MeanObs (g kg-1)	MeanMod (g kg-1)	Number	Corr	MB (g kg-1)	RMSE	NMB%	NME%
Europe	9.83	7.69	1200	0.81	-2.14	2.42	-21.78	22.17
Africa	10.88	9.55	2925	0.87	-1.33	2.56	-12.27	15.93
Asia	11.86	9.76	5100	0.94	-2.10	2.95	-17.72	20.89
Australia	8.53	8.47	1200	0.98	-0.06	0.85	-0.75	6.71
N.A.	12.34	10.43	2400	0.93	-1.90	2.63	-15.44	17.14
S.A.	10.02	8.98	2450	0.97	-1.04	1.76	-10.36	12.04
N. Pole	4.94	3.57	10440	0.91	-1.37	1.64	-27.68	27.68
N. Ferrel	10.18	8.65	10800	0.90	-1.53	2.17	-15.05	15.84
N. Hadley	16.78	16.37	10800	0.92	-0.40	1.94	-2.39	7.59
S. Hadley	13.91	13.67	10800	0.96	-0.24	1.20	-1.72	4.94
S. Ferrel	6.18	5.89	10800	0.99	-0.29	0.41	-4.73	5.37
S. Polar	0.74	0.61	10440	0.97	-0.13	0.29	-17.59	25.26
N.H.	10.70	9.60	32040	0.97	-1.10	1.93	-10.26	13.26
S.H.	7.01	6.79	32040	0.99	-0.22	0.75	-3.16	5.76
Global	8.85	8.19	64080	0.98	-0.66	1.46	-7.45	10.29

#### 4.3.1.3 Summer Downward Shortwave Flux at Ground Surface

The pattern of summer downward shortwave flux mean bias is displayed graphically in Figure 4.81, and reflects the annual pattern of an overestimation in the Tropics (30°N-30°S), with large underestimations at high latitudes in the Northern hemisphere. There are also large areas of underestimation off the West coasts of Africa and South America in the Southern Hadley Cell, which are present in the baseline simulation. The RAD1 spatial plot displays much worse performance for this time period than the baseline simulation. The pattern of GWRP SWDOWN underestimation is reflected in Table 4.45 in which all of the domains display a negative NMB value except for the Northern Hadley Cell. The RAD1 simulation has a global NMB value of -16.59%. Overall the RAD1 simulation also displays worse correlation values than the baseline simulation, with values of 0.88 and 0.93 respectively when compared with NCEP/NCAR Reanalysis. When compared with NCDC, RAD1 performs much better than BASE with MB values of 51.50 W m<sup>-2</sup> and 8.16 W m<sup>-2</sup> respectively.

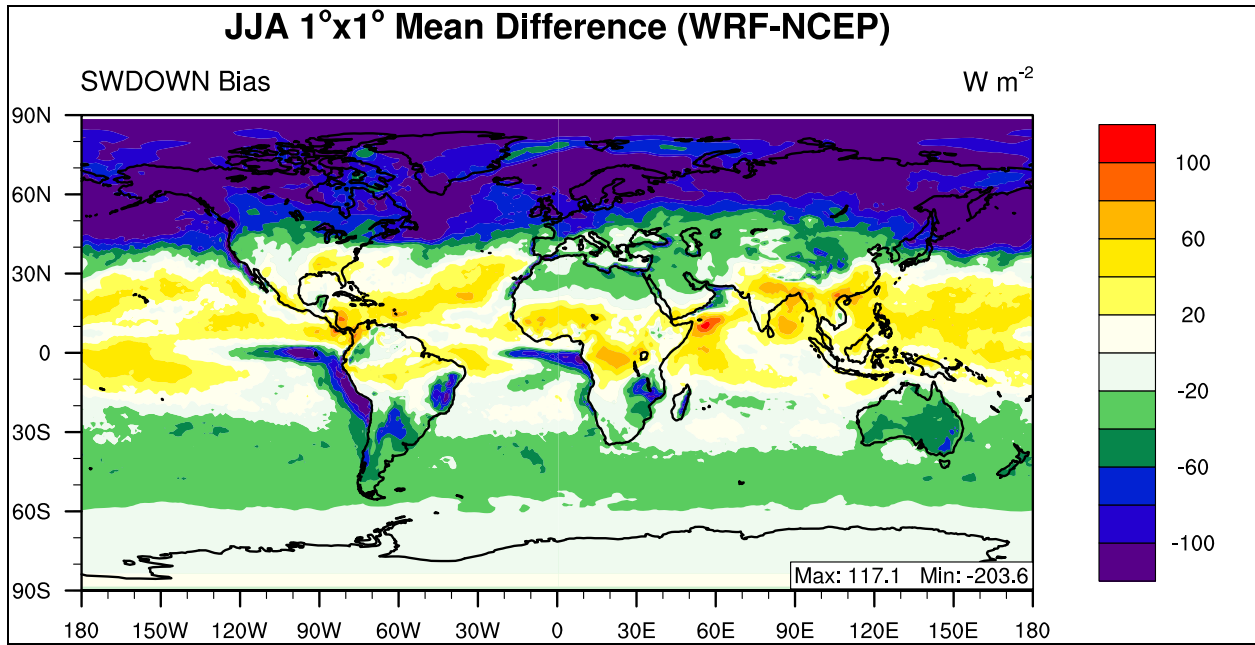


**Figure 4.81** 2001 summer mean bias of downward shortwave flux at the surface.

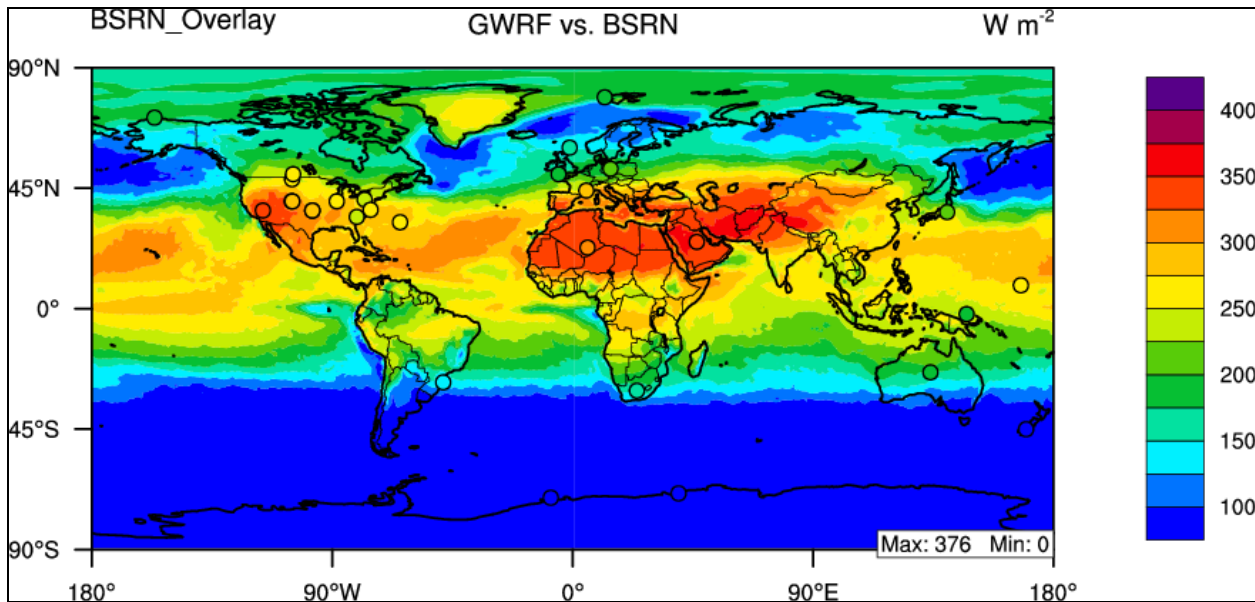


**Figure 4.82** 2001 summer mean bias of downward shortwave flux at the surface as compared with BSRN.

**Table 4.45 Performance Statistics of GWRf 2001 summer mean downward shortwave flux at the surface as compared with NCEP/NCAR Reanalysis and BSRN.**

Name	MeanObs (W m <sup>-2</sup> )	MeanMod (W m <sup>-2</sup> )	Number	Corr	MB (W m <sup>-2</sup> )	RMSE	NMB%	NME%
Europe	276.03	193.33	1200	0.89	-82.70	92.27	-29.96	29.99
Africa	267.44	263.17	2925	0.87	-4.28	34.22	-1.60	10.22
Asia	282.36	248.32	5100	0.56	-34.04	67.98	-12.06	20.00
Australia	187.27	161.24	1200	0.90	-26.03	34.22	-13.90	16.24
N.A.	287.47	257.32	2400	0.50	-30.16	53.27	-10.49	14.69
S.A.	159.45	141.03	2450	0.94	-18.43	36.33	-11.56	18.70
N. Pole	278.24	167.46	10440	0.76	-110.79	112.64	-39.82	39.82
N. Ferrel	276.45	217.16	10800	0.87	-59.28	74.00	-21.45	22.59
N. Hadley	257.37	279.46	10800	0.76	22.10	35.02	8.59	11.59
S. Hadley	201.96	197.48	10800	0.72	-4.49	31.69	-2.22	11.82
S. Ferrel	79.47	51.69	10800	0.97	-27.78	29.17	-34.96	35.06
S. Polar	8.77	2.85	7920	0.97	-5.93	8.05	-67.56	67.56
N.H.	270.60	221.97	32040	0.42	-48.63	79.96	-17.97	24.84
S.H.	105.32	91.92	29520	0.97	-13.39	26.38	-12.72	19.48
Global	191.34	159.61	61560	0.88	-31.74	60.51	-16.59	23.42
BSRN	218.83	226.99	29	0.98	8.16	21.08	3.73	8.19

#### 4.3.1.4 Summer Downward Longwave Flux at Ground Surface

The pattern of summer downward longwave flux mean bias is displayed graphically in Figure 4.83 in which the overall pattern is an underestimation with a global NMB value of -7.15%, which is worse than the baseline simulation. Figure 4.83 also displays this larger underestimation than the baseline simulation, with larger areas of mean biases less than -60 W m<sup>-2</sup>. The overall pattern of GWRf GLW performance is consistent with the baseline simulation, as shown in Table 4.46, in which all of the domains display a negative NMB value. Globally, the correlation values for the RAD1 and baseline simulations are both 0.98. The evaluation of GLW with BSRN data also shows an overall underestimation by GWRf, but high (>0.93) Corr values.

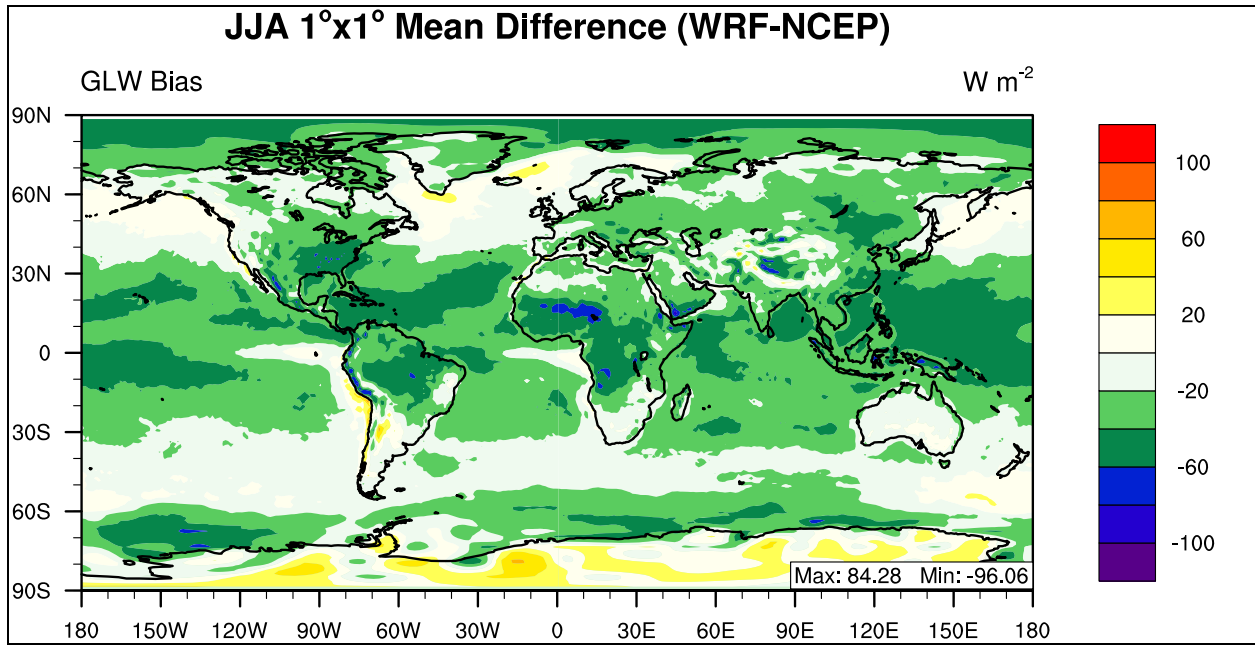


**Figure 4.83** 2001 summer mean bias of downward longwave flux at the surface.

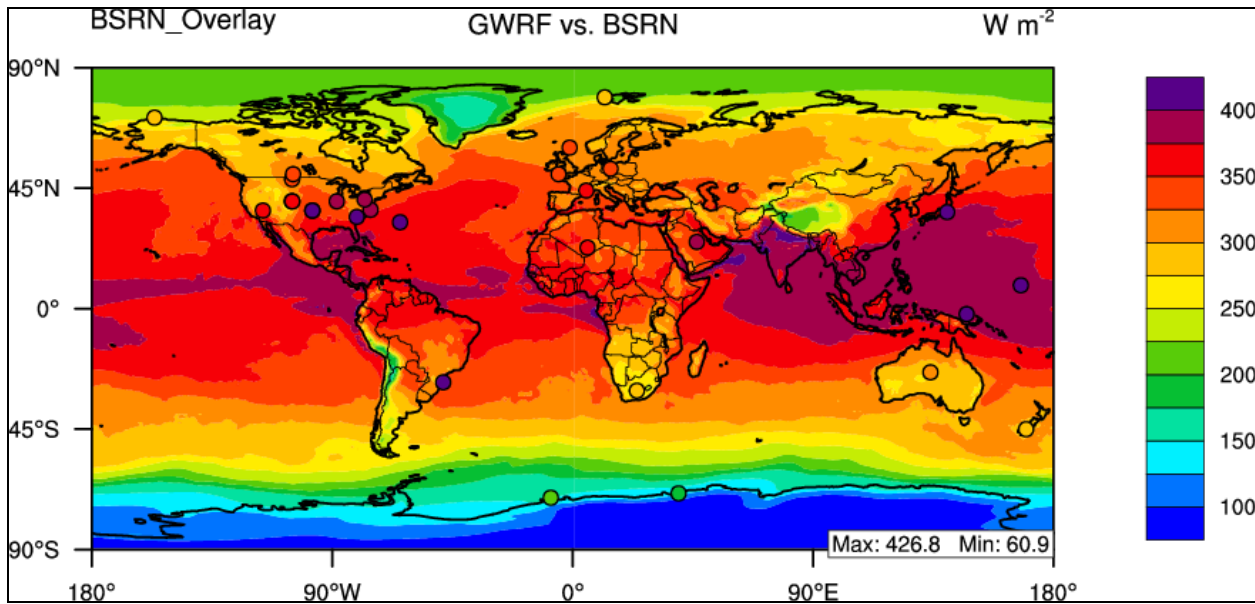


**Figure 4.84** 2001 summer mean bias of downward longwave flux at the surface as compared with BSRN.

**Table 4.46 Performance Statistics of GWRf 2001 summer mean downward longwave flux at the surface as compared with NCEP/NCAR Reanalysis and BSRN.**

Name	MeanObs (W m <sup>-2</sup> )	MeanMod (W m <sup>-2</sup> )	Number	Corr	MB (W m <sup>-2</sup> )	RMSE	NMB%	NME%
Europe	333.15	312.77	1200	0.72	-20.38	23.81	-6.12	6.23
Africa	363.04	333.31	2925	0.83	-29.73	34.37	-8.19	8.41
Asia	355.61	326.55	5100	0.96	-29.06	32.31	-8.17	8.36
Australia	325.16	310.25	1200	0.97	-14.91	19.65	-4.59	4.83
N.A.	358.63	328.47	2400	0.95	-30.16	32.99	-8.41	8.52
S.A.	333.45	311.30	2450	0.94	-22.16	30.30	-6.64	7.74
N. Pole	272.40	245.66	10440	0.92	-26.74	30.83	-9.82	10.18
N. Ferrel	344.05	325.56	10800	0.84	-18.49	24.98	-5.37	6.08
N. Hadley	405.77	368.29	10800	0.85	-37.48	39.12	-9.24	9.29
S. Hadley	375.69	346.07	10800	0.91	-29.62	33.10	-7.88	8.14
S. Ferrel	299.44	285.92	10800	0.93	-13.53	17.52	-4.52	5.01
S. Polar	134.46	129.18	10440	0.96	-5.28	27.81	-3.93	17.91
N.H.	341.51	313.93	32040	0.96	-27.58	32.18	-8.08	8.43
S.H.	271.39	255.12	32040	0.99	-16.26	26.92	-5.99	8.55
Global	306.45	284.53	64080	0.98	-21.92	29.67	-7.15	8.49
BSRN	350.01	306.27	29	0.93	-43.74	49.36	-12.50	12.50

#### 4.3.1.5 Summer Daily Precipitation Rate

The daily precipitation at the surface in GWRf is compared with the Global Precipitation Climatology Project (GPCP) for the summer of 2001 (June, July, and August 2001). In Figure 4.85, the interval spacing is set to  $\pm 2$  mm day<sup>-1</sup> to show the spatial variability of GWRf precipitation rate performance. Overall, the GWRf RAD1 performance during summer appears to be overestimating daily precipitation rate and performing similar to the baseline simulation, due to the large similarities between Figure 4.85 and Figure 4.15. Maximum and minimum mean bias values are very similar between the RAD1 and BASE simulations, indicating that the choice of radiation parameterization does not largely influence daily precipitation rate. Globally, RAD1 shows a slightly lower Corr value of 0.79 as compared to the 0.83 in the BASE case, while NMB values are comparable between RAD1 and BASE with values of 37.15% and

38.64% respectively. The evaluation against NCDC average monthly precipitation shows a large improvement from the BASE NCDC evaluation, with MB values of 5.70 and 23.57 mm month<sup>-1</sup>.

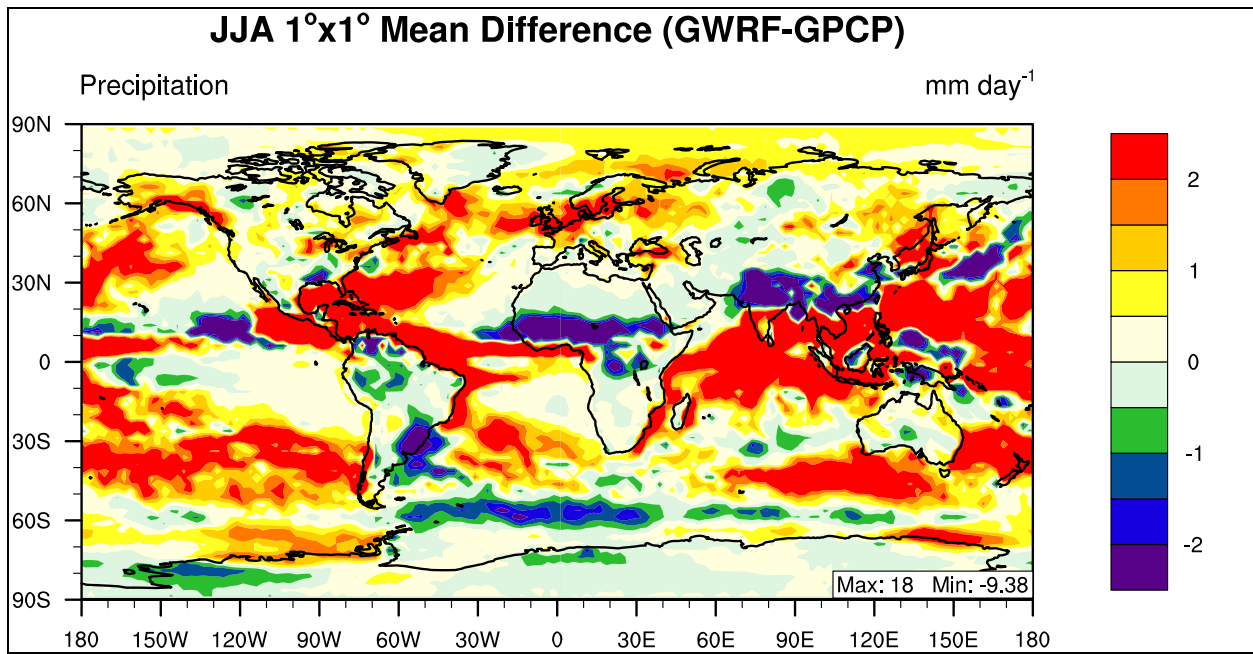


**Figure 4.85** 2001 summer mean bias of daily precipitation rate.

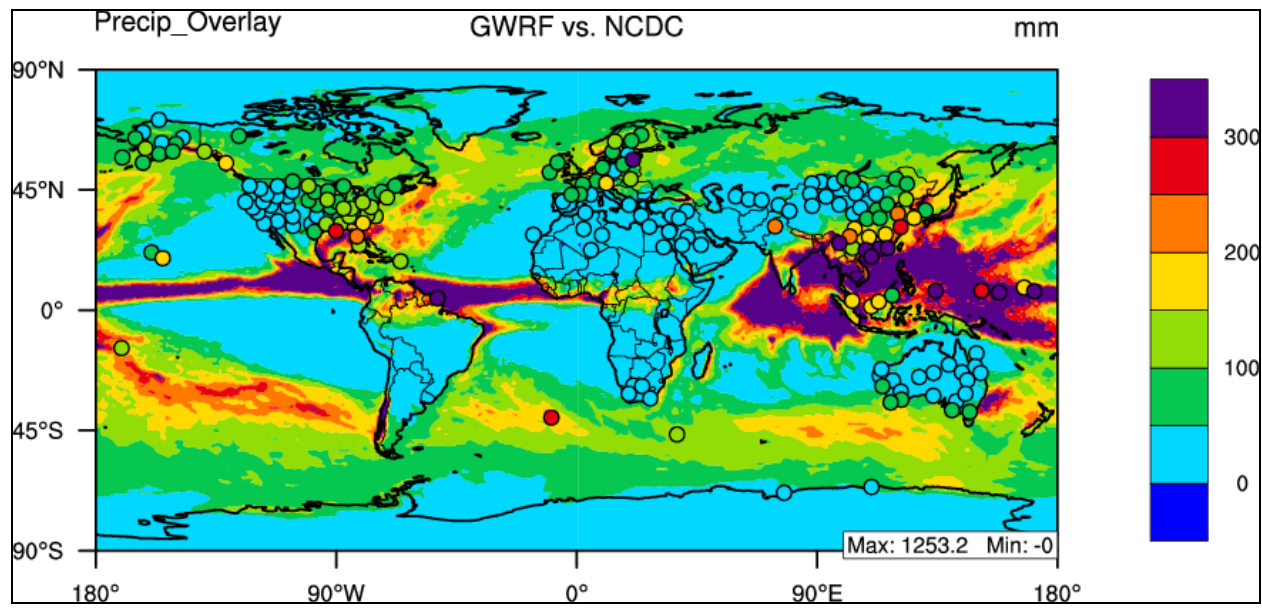


**Figure 4.86** 2001 summer mean bias of monthly precipitation rate as compared to NCDC.

**Table 4.47 Performance Statistics of GWRf 2001 summer precipitation rate for as compared with GPCP (mm day<sup>-1</sup>) and NCDC (mm month<sup>-1</sup>).**

Name	MeanObs	MeanMod	Number	Corr	MB	RMSE	NMB%	NME%
Europe	2.37	3.50	192	0.41	1.13	1.69	47.57	54.49
Africa	1.26	1.19	463	0.68	-0.07	1.59	-5.39	69.62
Asia	3.29	3.81	816	0.81	0.53	2.60	16.10	43.09
Australia	0.98	1.64	192	0.77	0.66	1.16	66.95	81.65
N.A.	2.49	3.56	384	0.60	1.07	2.07	42.92	52.97
S.A.	3.00	3.44	392	0.60	0.44	3.20	14.68	52.65
N. Pole	1.17	1.65	1728	0.77	0.48	0.73	41.04	48.59
N. Ferrel	2.30	3.05	1727	0.72	0.74	1.54	32.29	46.56
N. Hadley	4.04	5.67	1724	0.72	1.63	3.93	40.26	64.58
S. Hadley	1.79	2.86	1728	0.82	1.08	2.32	60.47	75.92
S. Ferrel	3.08	3.95	1728	0.44	0.87	1.74	28.39	42.73
S. Polar	0.97	1.12	1728	0.80	0.15	0.68	15.96	44.90
N.H.	2.50	3.45	5179	0.78	0.95	2.47	37.94	56.56
S.H.	1.94	2.65	5184	0.80	0.70	1.72	36.15	53.25
Global	2.22	3.05	10363	0.79	0.83	2.13	37.15	55.11
NCDC	93.20	98.90	172	0.70	5.70	77.26	6.12	49.58

### 4.3.2 Summer (JJA) RAD2 mean evaluation

#### 4.3.2.1 Summer Temperature at 2-meter

The temperature at 2-meters above the surface for GWRf sensitivity simulation RAD2 is compared with NCEP/NCAR Reanalysis for the summer of 2001 (JJA). This sensitivity simulation replaces the Goddard shortwave scheme from the baseline simulation with the CAM shortwave scheme as well as replacing the CAM longwave module with the RRTM longwave module. When Figure 4.87 is compared with Figure 4.11 (summer baseline), the two figures appear very similar, except for a distinct pattern of overestimation over land surfaces in Figure 4.87. This is shown in Table 4.48 and Figure 4.89, in which all continental domains have a positive NMB value. Globally, GWRf shows good statistical performance with a Corr value of 0.99 (same as baseline simulation), and a NMB value of 8.01% which is different from the

baseline value (2.70%). The comparison with NCDC data during this time is consistent with the NCEP/NCAR Reanalysis evaluation in which T2 is overestimated by RAD2, with a mean NCDC MB of 0.82.

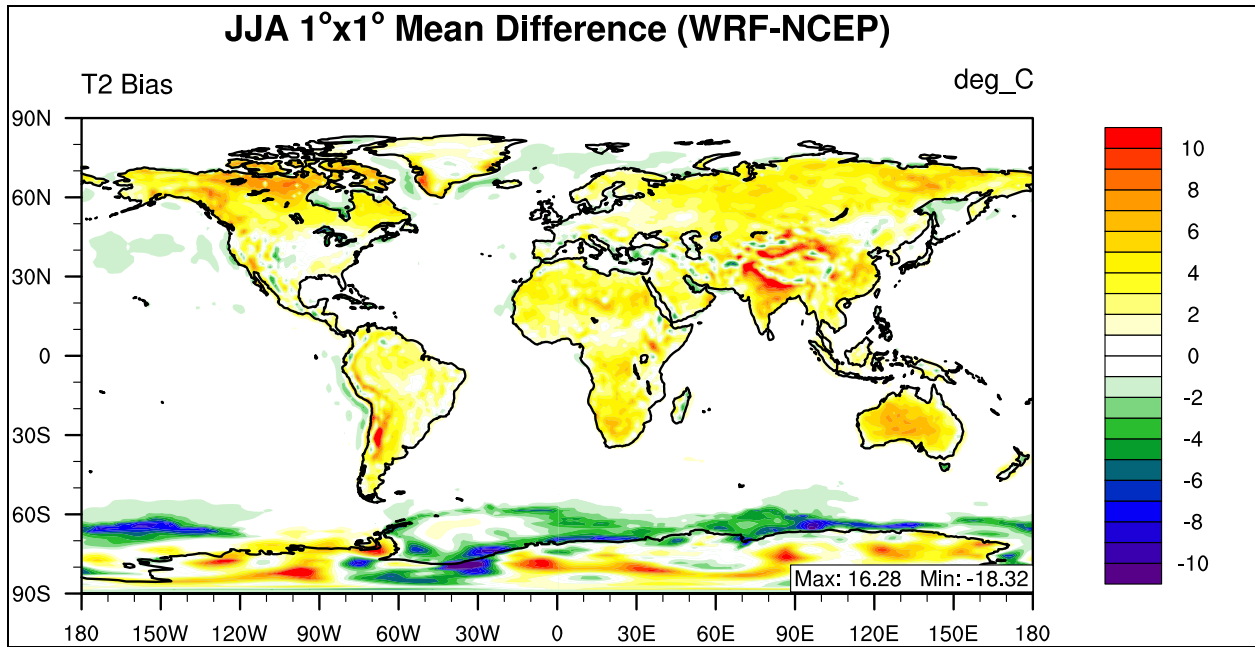


**Figure 4.87** 2001 summer mean bias of temperature at 2-meter.

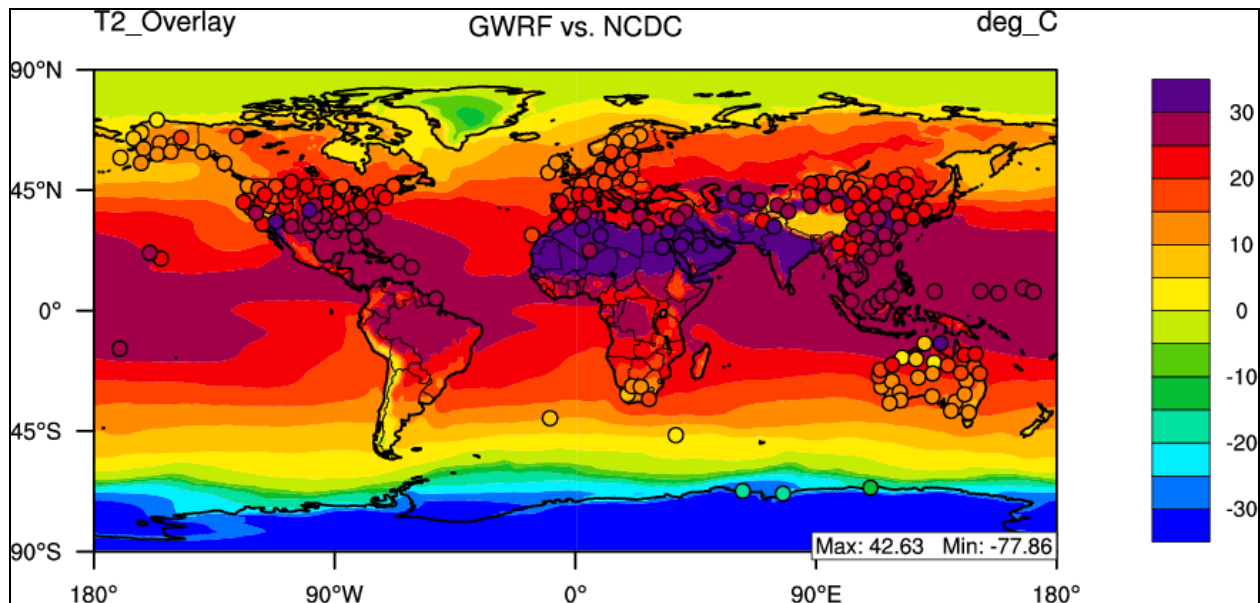
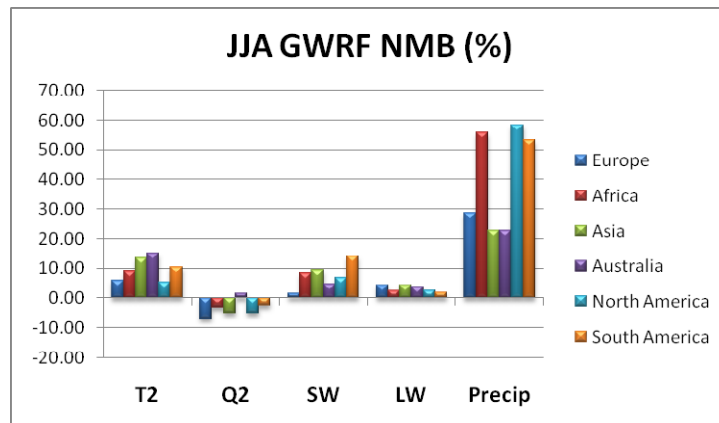


**Figure 4.88** 2001 summer mean bias of temperature at 2-meter as compared with NCDC.

**Table 4.48** Performance Statistics of GWRf 2001 summer mean temperature at 2-meter as compared with NCEP/NCAR Reanalysis and NCDC.

Name	MeanObs (°C)	MeanMod (°C)	Number	Corr	MB (°C)	RMSE	NMB%	NME%
Europe	16.43	17.40	1200	0.93	0.97	1.88	5.90	9.39
Africa	23.83	25.98	2925	0.94	2.15	2.91	9.01	9.76
Asia	20.72	23.51	5100	0.94	2.79	3.87	13.48	15.02
Australia	17.02	19.58	1200	0.90	2.56	3.59	15.03	15.51
N.A.	20.51	21.61	2400	0.93	1.09	2.48	5.32	9.03
S.A.	14.76	16.29	2450	0.97	1.53	2.74	10.35	12.80
N. Pole	3.20	4.22	10439	0.95	1.02	2.61	31.85	53.56
N. Ferrel	17.65	18.58	10800	0.93	0.93	2.56	5.29	10.13
N. Hadley	26.64	27.40	10800	0.88	0.76	1.97	2.87	4.26
S. Hadley	22.26	23.14	10800	0.92	0.89	1.88	3.98	4.64
S. Ferrel	8.10	8.02	10800	0.99	-0.08	1.16	-0.97	8.03
S. Polar	-34.51	-34.44	10440	0.98	0.07	3.85	0.19	8.64
N.H.	15.97	16.87	32039	0.98	0.90	2.39	5.66	9.67
S.H.	-1.01	-0.72	32040	1.00	0.29	2.54	29.07	152.20
Global	7.48	8.08	64079	0.99	0.60	2.47	8.01	20.61
NCDC	20.78	21.60	199	0.87	0.82	4.36	3.95	12.01

An overview of RAD2 summer statistical performance for the major boundary layer variables is shown graphically in Figure 4.89. The similarities between BASE and RAD2 are also shown in the similarities between Figures 4.13 (baseline) and 4.89. The RAD2 simulation exhibits many of the same characteristics of the BASE case mainly: a large overestimation of daily precipitation rate, an underestimation of Q2 and GLW, and an overestimation of T2 and SWDOWN. In the North Pole domain, the temperature at 2 meters is overestimated and this domain also shows the highest NMB values for precipitation rate, which is the same as the BASE case. The vertical profile of temperature performance is plotted in Figure 4.90 which is the zonal mean bias of GWRf versus NCEP/NCAR Reanalysis data. This figure also shows that GWRf generally captures the vertical temperature distribution within  $\pm 2$  degrees up to approximately 300 hPa. Figure 4.90 is also very similar to the corresponding Figure 4.15 for the summer BASE case, displaying large overestimations near the surface over Antarctica and the equator and underestimations of temperatures throughout the Southern Ferrel Cell. RAD2 differs from the BASE case by predicting a much lower tropopause over the Tropics and also does not reproduce the small overestimations aloft over the Northern latitudes.



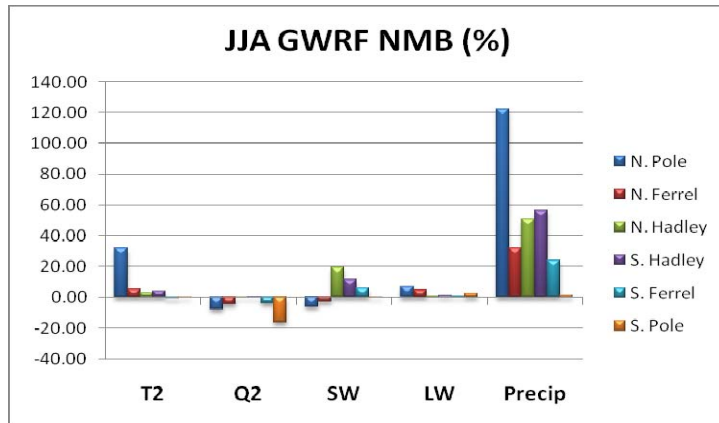


**Figure 4.89** 2001 summer mean normalized mean bias (%) of major meteorological variables for (a) the six continental domains and (b) the six circulation cell domains.

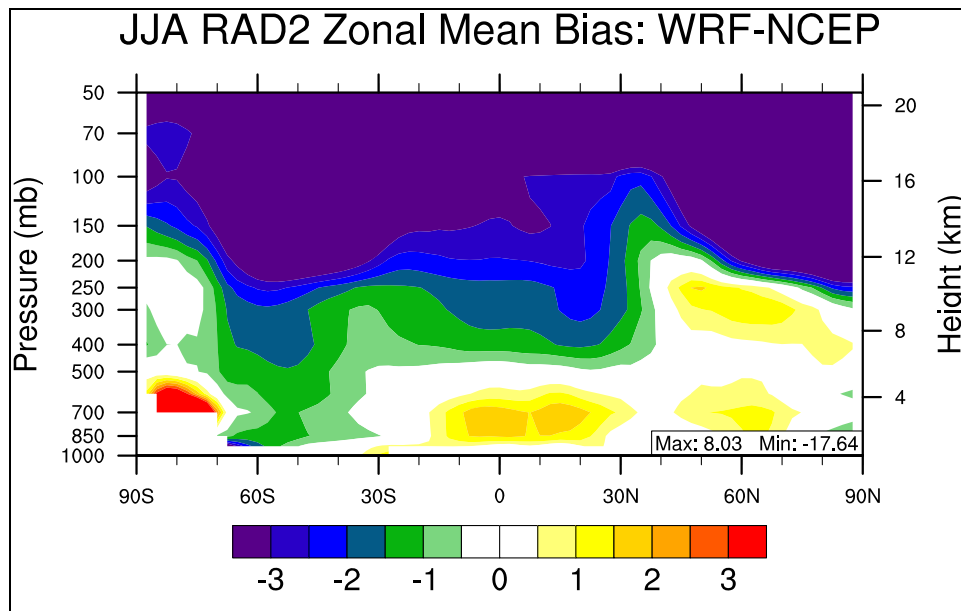


**Figure 4.90** 2001 summer zonal mean bias of Temperature.

#### 4.3.2.2 Summer Water Vapor Mixing ratio at 2-meter

The global distribution of RAD2 summer mean bias for water vapor mixing ratio at 2-meters is displayed in Figure 4.91. When compared with the base simulation spatial mean bias plot, the areas and magnitude of underestimation over land surfaces are very similar, reinforcing

the similarities between the RAD2 and BASE simulations. The overall underestimation of Q2 and is also reflected in Table 4.49 in which all domains have a negative NMB value (except Australia). This Figure differs from the baseline simulation because the Northern and Southern Hadley Cells are also underpredicted which is not true in the BASE case. The global RAD2 NMB value is -2.52% which is almost identical to the baseline case whose summer value is -2.39%. Overall Corr values are the same as baseline performance, with a global Corr value of 0.99.

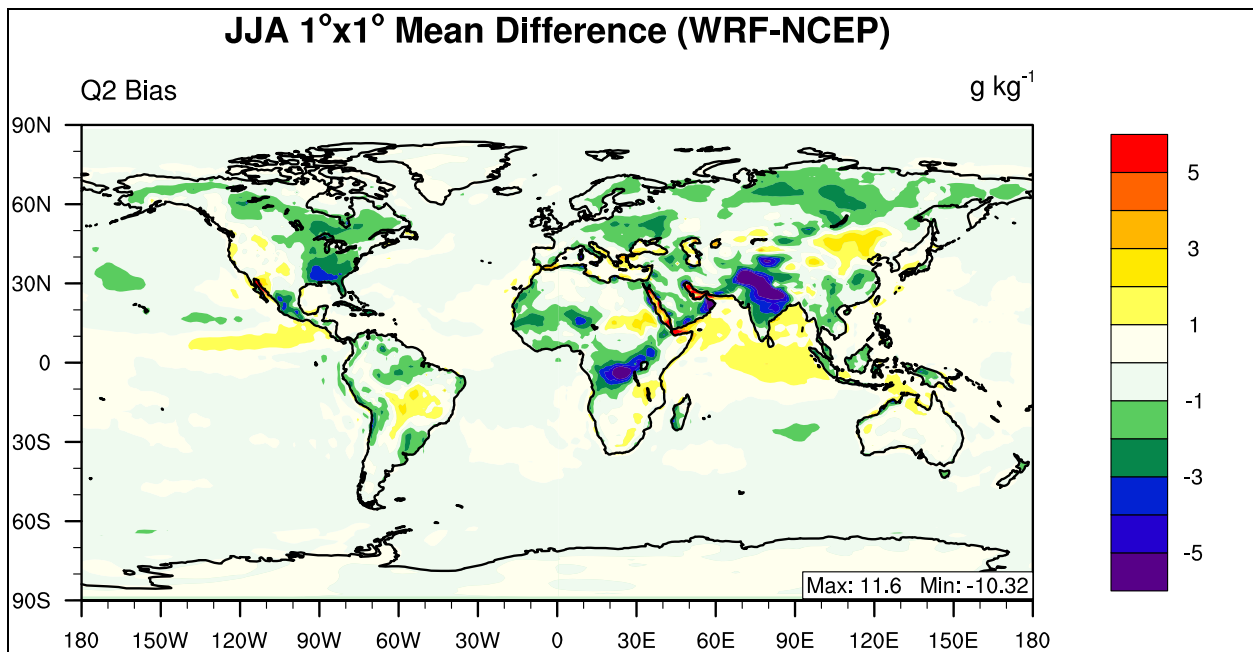


**Figure 4.91** 2001 summer mean bias of water vapor mixing ratio at 2-meter.

**Table 4.49 Performance Statistics of GWRf summer mean water vapor mixing ratio at 2-meter as compared with NCEP/NCAR Reanalysis.**

<b>Name</b>	<b>MeanObs</b>	<b>MeanMod</b>	<b>Number</b>	<b>Corr</b>	<b>MB</b>	<b>RMSE</b>	<b>NMB%</b>	<b>NME%</b>
<b>Europe</b>	9.83	9.16	1200	0.89	-0.67	1.13	-6.82	9.17
<b>Africa</b>	10.88	10.53	2925	0.94	-0.35	1.58	-3.23	9.58
<b>Asia</b>	11.86	11.25	5100	0.95	-0.61	1.86	-5.11	11.35
<b>Australia</b>	8.53	8.66	1200	0.99	0.13	0.74	1.56	6.06
<b>N.A.</b>	12.34	11.71	2400	0.96	-0.63	1.39	-5.07	8.14
<b>S.A.</b>	10.02	9.76	2450	0.99	-0.25	0.90	-2.53	6.78
<b>N. Pole</b>	4.94	4.57	10440	0.97	-0.37	0.64	-7.57	8.71
<b>N. Ferrel</b>	10.18	9.73	10800	0.95	-0.45	1.17	-4.40	7.98
<b>N. Hadley</b>	16.78	16.70	10800	0.96	-0.07	1.27	-0.42	4.86
<b>S. Hadley</b>	13.91	13.81	10800	0.98	-0.09	0.84	-0.67	4.03
<b>S. Ferrel</b>	6.18	5.95	10800	0.99	-0.23	0.35	-3.79	4.58
<b>S. Polar</b>	0.74	0.62	10440	0.98	-0.12	0.25	-16.11	21.35
<b>N.H.</b>	10.70	10.40	32040	0.99	-0.30	1.07	-2.77	6.44
<b>S.H.</b>	7.01	6.86	32040	1.00	-0.15	0.55	-2.12	4.78
<b>Global</b>	8.85	8.63	64080	0.99	-0.22	0.85	-2.52	5.78

#### **4.3.2.3 Summer Downward Shortwave Flux at Ground Surface**

The pattern of RAD2 summer downward shortwave flux mean bias agrees well with the BASE simulation and is displayed graphically in Figure 4.92. It reflects the baseline pattern of an overestimation in the Tropics (30°N-30°S), with large underestimations at high latitudes in the Northern hemisphere. The areas of underestimation off the West coasts of Africa and South America in the Southern Hadley Cell which are present in the baseline simulation are not present in RAD2. The agreement between RAD2 and BASE for GWRf SWDOWN is reflected in Table 4.50 in which the only RAD2 domains that display negative NMB values (e.g., North Pole and Ferrel Cells) are the only BASE domains which display negative NMB values; however RAD2 eliminates the underprediction over Europe. The rest of the domains in both cases display positive NMBs, indicating an overprediction of SWDOWN. The RAD2 simulation has a global NMB value of 4.88%, which is less than the BASE simulation NMB of 3.97%. Overall the

RAD2 simulation also displays slightly improved correlation values than the baseline simulation, with values of 0.95 and 0.93 respectively.

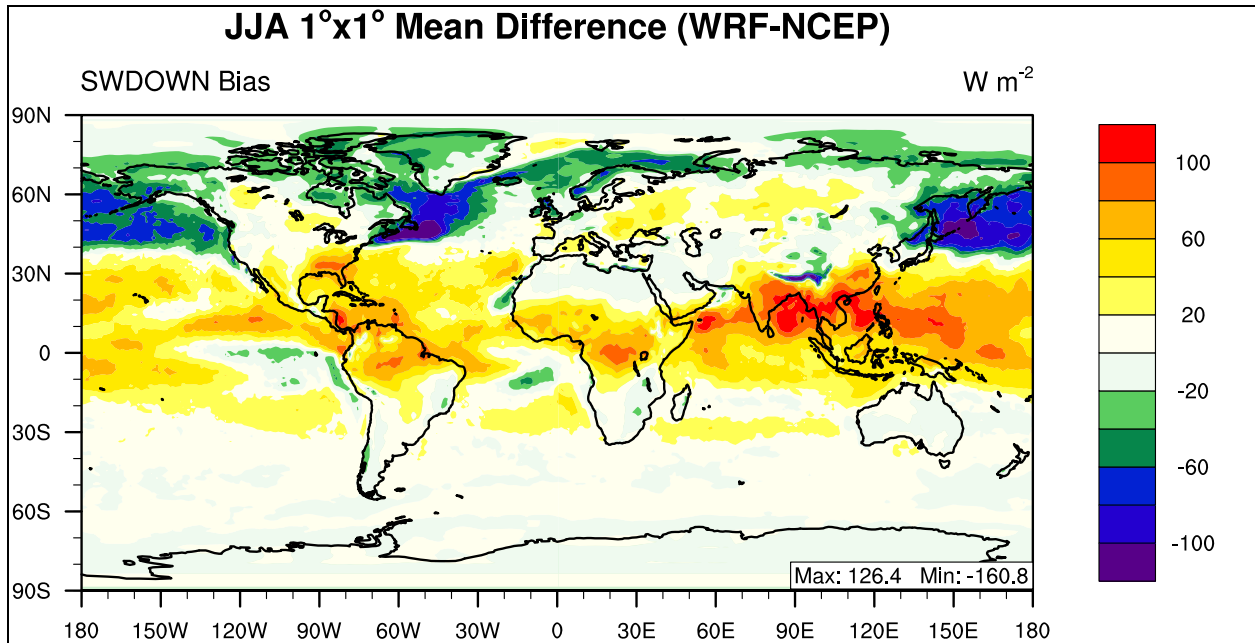


**Figure 4.92** 2001 summer mean bias of downward shortwave flux at the surface.

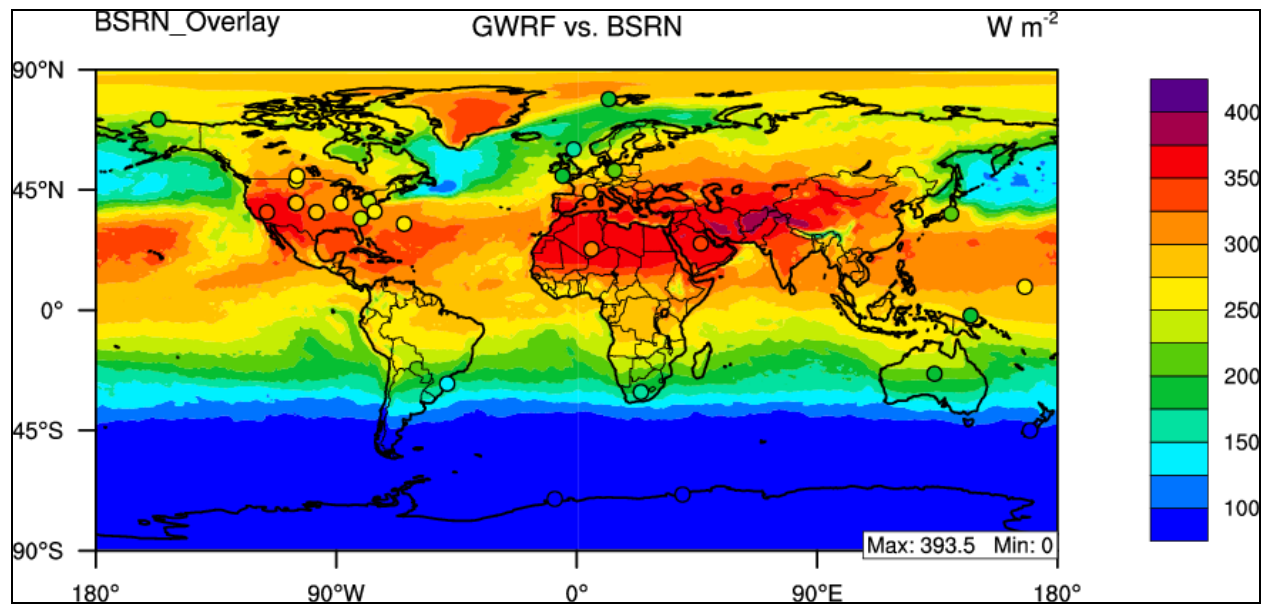


**Figure 4.93** 2001 summer mean bias of downward shortwave flux at the surface as compared to BSRN.

The evaluation with BSRN data shows very similar statistical performance to the BASE case in which SWDOWN is overestimated which is consistent with the NCEP/NCAR Reanalysis evaluation. The BSRN BASE and RAD2 evaluations display very similar MB values (51.50 and 49.85  $\text{W m}^{-2}$ , respectively) and Corr values (0.98 and 0.97, respectively) indicating good agreement between the Goddard and CAM shortwave schemes for this period.

**Table 4.50 Performance Statistics of GWRf 2001 summer mean downward shortwave flux at the surface as compared with NCEP/NCAR Reanalysis and BSRN.**

<b>Name</b>	<b>MeanObs</b>	<b>MeanMod</b>	<b>Number</b>	<b>Corr</b>	<b>MB</b>	<b>RMSE</b>	<b>NMB%</b>	<b>NME%</b>
<b>Europe</b>	276.03	279.97	1200	0.84	3.95	26.29	1.43	7.79
<b>Africa</b>	267.44	290.42	2925	0.90	22.98	36.38	8.59	10.34
<b>Asia</b>	282.36	308.63	5100	0.61	26.28	47.93	9.31	12.24
<b>Australia</b>	187.27	196.16	1200	0.94	8.90	17.64	4.75	6.26
<b>N.A.</b>	287.47	307.20	2400	0.54	19.72	37.38	6.86	10.49
<b>S.A.</b>	159.45	181.76	2450	0.96	22.31	35.33	13.99	15.52
<b>N. Pole</b>	278.24	260.74	10440	0.80	-17.50	26.57	-6.29	7.72
<b>N. Ferrel</b>	276.45	268.74	10800	0.86	-7.71	40.60	-2.79	11.11
<b>N. Hadley</b>	257.37	307.33	10800	0.69	49.97	58.20	19.42	20.33
<b>S. Hadley</b>	201.96	225.14	10800	0.79	23.18	33.09	11.48	13.07
<b>S. Ferrel</b>	79.47	84.17	10800	0.99	4.70	8.05	5.91	7.63
<b>S. Polar</b>	8.77	8.80	7920	0.99	0.03	0.94	0.30	6.30
<b>N.H.</b>	270.60	279.14	32040	0.59	8.54	43.90	3.16	12.93
<b>S.H.</b>	105.32	115.52	29520	0.99	10.21	20.60	9.69	11.42
<b>Global</b>	191.34	200.68	61560	0.95	9.34	34.74	4.88	12.53
<b>BSRN</b>	218.83	268.67	29	0.97	49.85	54.95	22.78	22.78

#### **4.3.2.4 Summer Downward Longwave Flux at ground surface**

The pattern of summer downward longwave flux mean bias is displayed graphically in Figure 4.94 in which the overall pattern is an overestimation with a global NMB value of 2.60%, which is slightly worse than the baseline simulation. Figure 4.94 displays a very different spatial pattern than the BASE case. The overall pattern of GWRf GLW performance is opposite than the baseline simulation, as shown in Table 4.51, in which all of the domains display a positive NMB value. Globally, the correlation value for RAD2 is slightly higher (0.99) than the baseline simulation (0.98). BASE and RAD2 longwave evaluation against BSRN displays a large improvement with MB values of -32.10 and -7.72 W m<sup>-2</sup> indicating that the RRTM longwave module is more accurate in this case than the CAM longwave module.

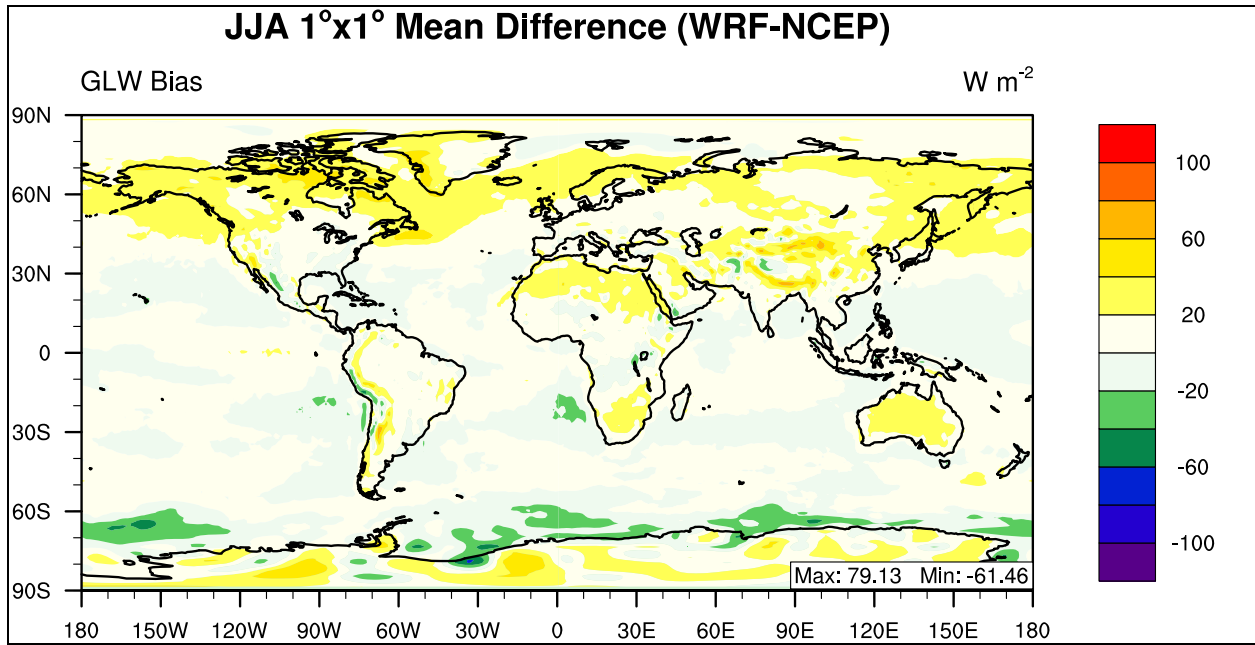


**Figure 4.94** 2001 summer mean bias of downward longwave flux at the surface.

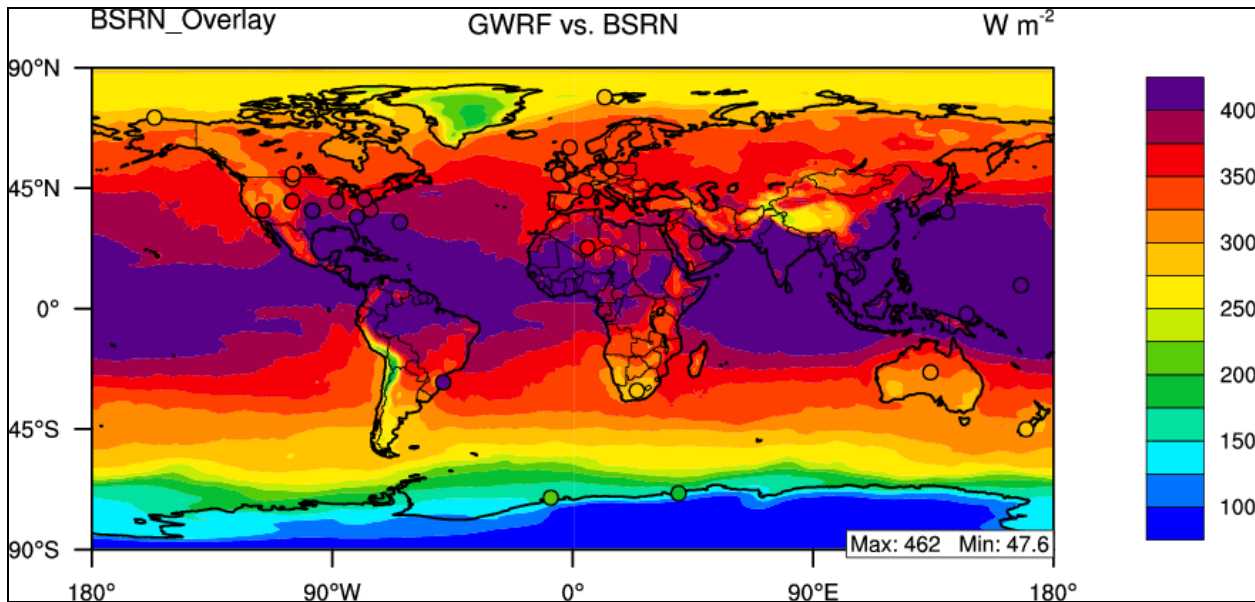


**Figure 4.95** 2001 summer mean bias of downward longwave flux at the surface as compared with BSRN.

**Table 4.51 Performance Statistics of GWRf 2001 summer mean downward longwave flux at the surface as compared with NCEP/NCAR Reanalysis and BSRN.**

<b>Name</b>	<b>MeanObs</b>	<b>MeanMod</b>	<b>Number</b>	<b>Corr</b>	<b>MB</b>	<b>RMSE</b>	<b>NMB%</b>	<b>NME%</b>
<b>Europe</b>	333.15	347.62	1200	0.86	14.48	17.55	4.35	4.44
<b>Africa</b>	363.04	372.23	2925	0.88	9.20	17.21	2.53	3.87
<b>Asia</b>	355.61	370.90	5100	0.96	15.29	20.80	4.30	4.84
<b>Australia</b>	325.16	337.71	1200	0.95	12.54	18.28	3.86	4.62
<b>N.A.</b>	358.63	367.99	2400	0.96	9.36	16.02	2.61	3.39
<b>S.A.</b>	333.45	339.28	2450	0.98	5.83	13.87	1.75	3.07
<b>N. Pole</b>	272.40	290.77	10440	0.93	18.37	22.00	6.74	6.89
<b>N. Ferrel</b>	344.05	360.35	10800	0.92	16.30	20.34	4.74	5.01
<b>N. Hadley</b>	405.77	409.53	10800	0.87	3.76	11.28	0.93	1.92
<b>S. Hadley</b>	375.69	379.40	10800	0.95	3.71	11.75	0.99	2.37
<b>S. Ferrel</b>	299.44	301.85	10800	0.97	2.41	8.07	0.80	1.99
<b>S. Polar</b>	134.46	137.96	10440	0.97	3.50	21.17	2.60	13.02
<b>N.H.</b>	341.51	354.26	32040	0.98	12.75	18.44	3.73	4.26
<b>S.H.</b>	271.39	274.59	32040	0.99	3.20	14.65	1.18	3.95
<b>Global</b>	306.45	314.42	64080	0.99	7.98	16.65	2.60	4.12
<b>BSRN</b>	350.01	342.29	29	0.93	-7.72	25.11	-2.21	4.64

#### **4.3.2.5 Summer Daily Precipitation Rate**

The daily precipitation at the surface in GWRf is compared with the Global Precipitation Climatology Project (GPCP) for the summer of 2001 (JJA). Overall, the GWRf RAD2 performance during summer appears to be overestimating daily precipitation rate and performing similar to the baseline simulation, due to the large similarities between Figure 4.96 and Figure 4.23 (summer baseline). Maximum and minimum mean bias values are more extreme for RAD2 (25.57 and -13.55, respectively) than the BASE simulation (18.93 and -9.82, respectively). Globally, RAD2 shows a slightly lower Corr value of 0.74 as compared to the 0.83 in the BASE case, while NMB values are slightly better than BASE with values of 44.62% and 38.64% respectively. BSRN observations show that RAD2 overestimates monthly precipitation rate more than the BASE simulation with MB values of 32.16 and 23.57 mm month<sup>-1</sup>.

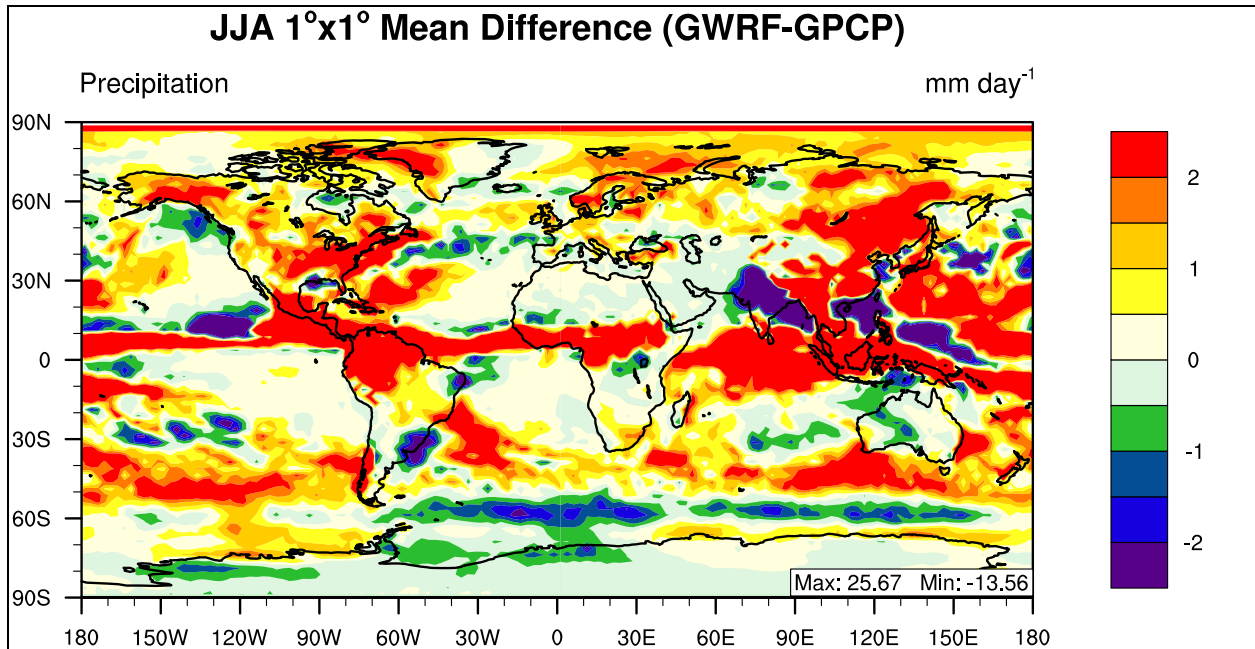


**Figure 4.96** 2001 summer mean bias of daily precipitation rate.

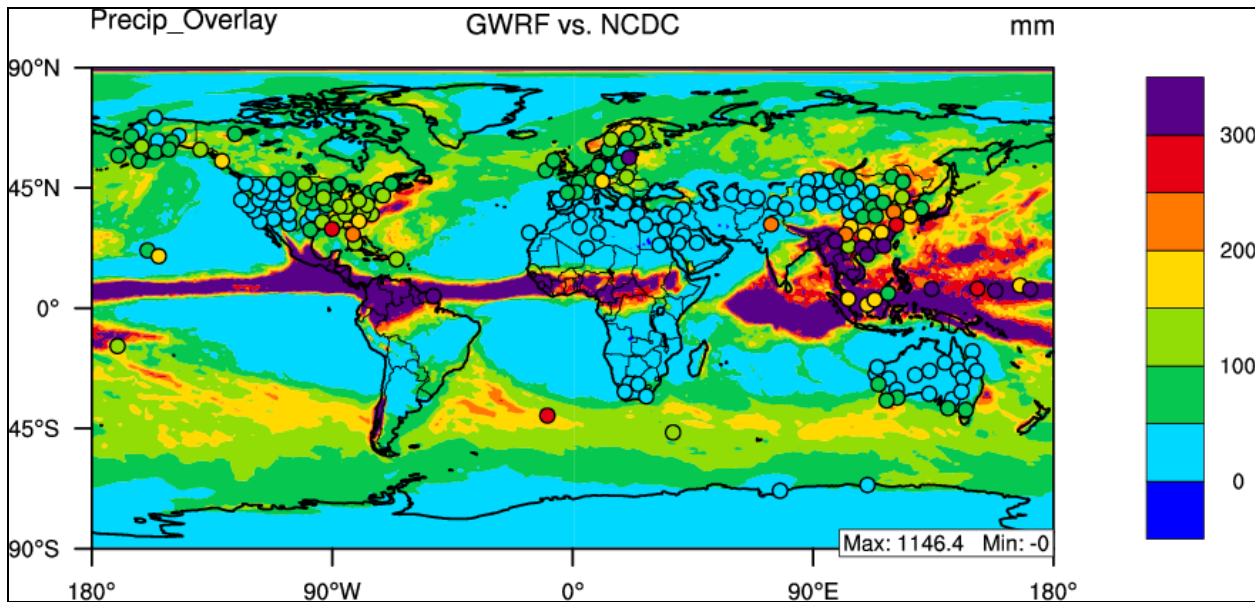


**Figure 4.97** 2001 summer mean bias of monthly precipitation rate as compared with NCDC.

**Table 4.52 Performance Statistics of GWRP 2001 summer mean precipitation rate for as compared with GPCP (mm day<sup>-1</sup>) and NCDC (mm day<sup>-1</sup>).**

Name	MeanObs	MeanMod	Number	Corr	MB	RMSE	NMB%	NME%
Europe	2.37	3.05	192	0.68	0.68	1.22	28.55	39.94
Africa	1.26	1.96	463	0.92	0.70	1.82	55.71	70.57
Asia	3.29	4.03	815	0.67	0.74	3.16	22.59	60.26
Australia	0.98	1.21	192	0.75	0.22	1.12	22.69	72.38
N.A.	2.49	3.94	384	0.70	1.45	2.17	58.14	65.76
S.A.	3.00	4.59	392	0.79	1.60	3.68	53.31	70.11
N. Pole	1.17	2.60	1728	0.06	1.43	2.53	122.00	128.39
N. Ferrel	2.30	3.04	1727	0.72	0.74	1.63	32.02	49.45
N. Hadley	4.05	6.09	1723	0.71	2.05	4.63	50.54	73.55
S. Hadley	1.79	2.79	1728	0.82	1.00	2.69	56.22	74.02
S. Ferrel	3.08	3.81	1728	0.41	0.73	1.54	23.75	38.48
S. Polar	0.97	0.98	1728	0.81	0.01	0.56	1.31	41.69
N.H.	2.51	3.91	5178	0.71	1.40	3.19	56.01	74.71
S.H.	1.94	2.53	5184	0.80	0.58	1.82	29.96	49.89
Global	2.22	3.22	10362	0.74	0.99	2.59	44.62	63.86
NCDC	93.20	125.36	172	0.60	32.16	110.75	34.51	70.19

### 4.3.3 Summer (JJA) RAD3 mean evaluation

#### 4.3.3.1 Summer Temperature at 2-meter

The temperature at 2-meters above the surface for GWRP sensitivity simulation RAD3 is compared with NCEP/NCAR Reanalysis for the summer of 2001. This sensitivity simulation replaces the Goddard shortwave scheme from the baseline simulation with the CAM shortwave scheme. When Figure 4.98 is compared with Figure 4.11, the two figures appear very similar. The model performance is still complicated over Antarctica with overestimations occurring over the land surface and underestimations occurring off shore over the Southern Ocean. Globally, GWRP shows good statistical performance with a correlation value of 0.99 (same as baseline simulation), and an NMB value of 0.14% which is different from the baseline value (2.70%). The strong similarities of temperature performance is shown in the comparison between Tables 4.8 and 4.53 when the continental and circulation cell domains have similar model predictions in

both the RAD3 and BASE case. Evaluation against NCDC data is also very similar between RAD3 and BASE, with very similar MB values (-0.57 and -0.51, respectively) and the same Corr values (0.88).

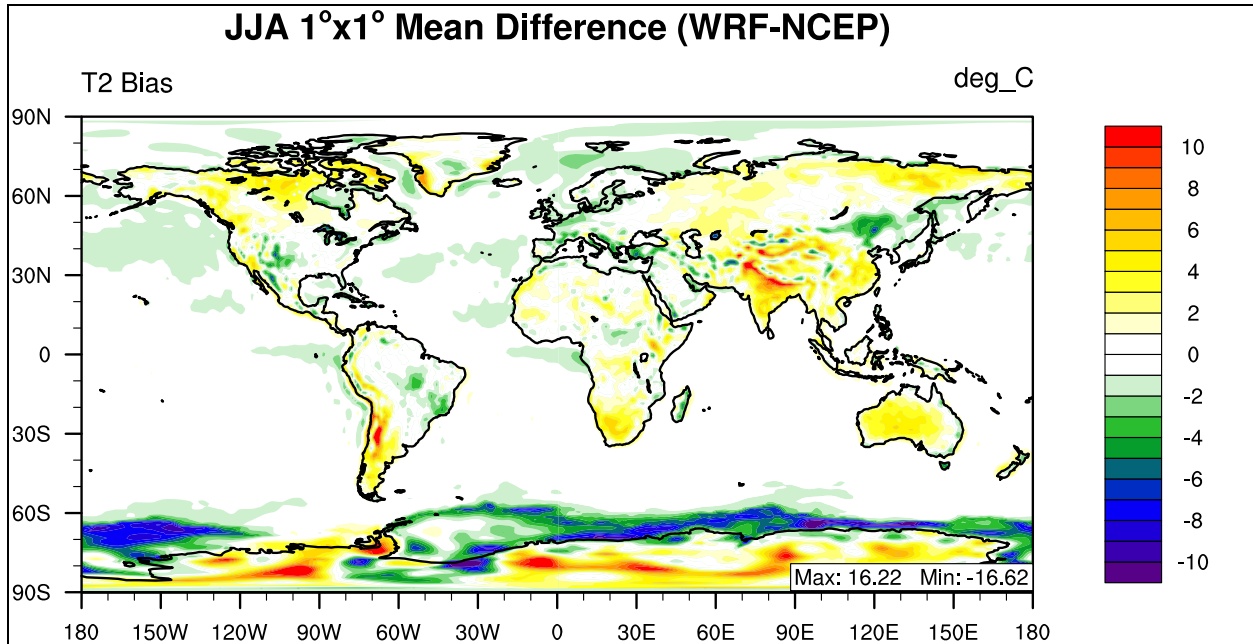


**Figure 4.98** 2001 summer mean bias of temperature at 2-meter.

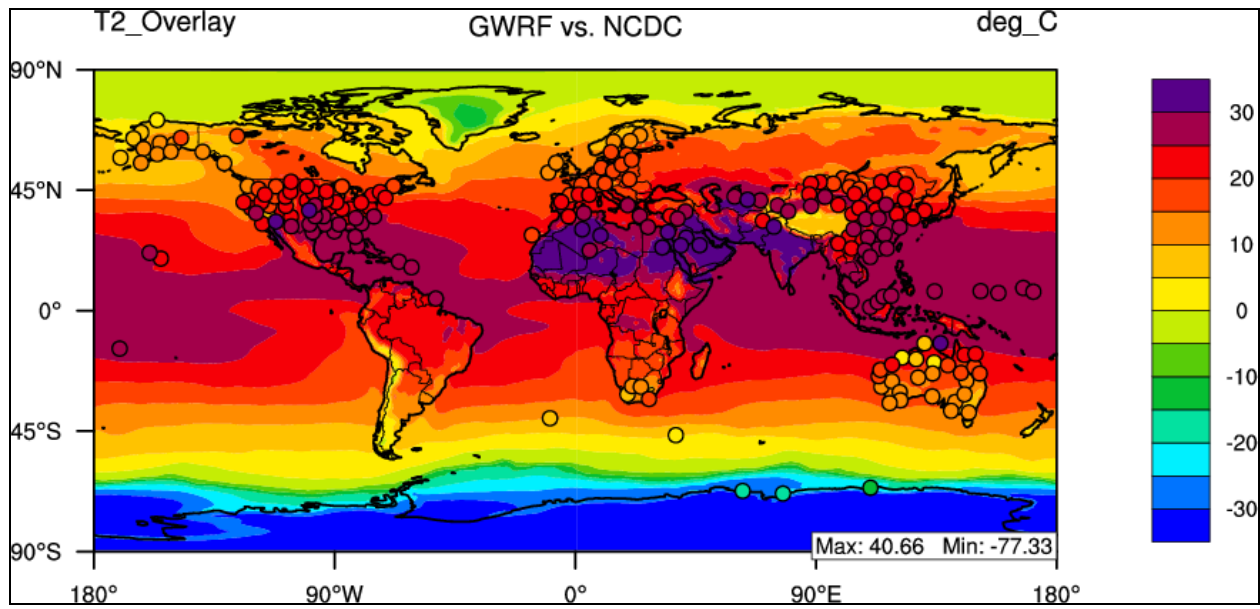
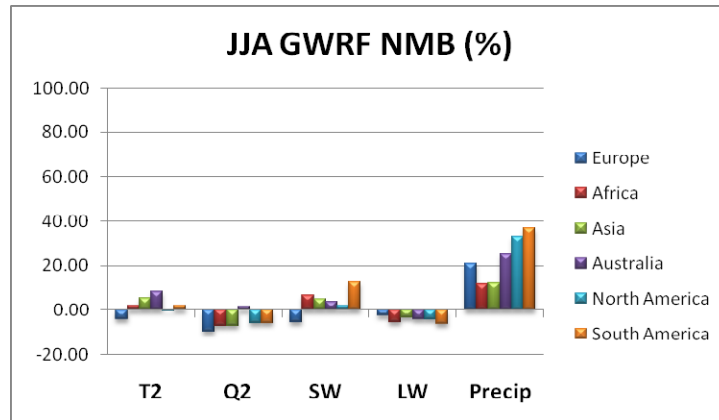


**Figure 4.99** 2001 summer temperature at 2-meter compared with NCDC.

**Table 4.53** Performance Statistics of GWRP 2001 summer mean temperature at 2-meter as compared with NCEP/NCAR Reanalysis and NCDC.

Name	MeanObs	MeanMod	Number	Corr	MB	RMSE	NMB%	NME%
<b>Europe</b>	16.43	15.75	1200	0.96	-0.68	1.42	-4.11	6.80
<b>Africa</b>	23.83	24.32	2925	0.96	0.49	1.65	2.07	5.04
<b>Asia</b>	20.72	21.85	5100	0.95	1.13	2.62	5.48	9.14
<b>Australia</b>	17.02	18.42	1200	0.96	1.40	2.18	8.21	9.50
<b>N.A.</b>	20.51	20.36	2400	0.96	-0.15	1.70	-0.73	6.10
<b>S.A.</b>	14.76	15.09	2450	0.97	0.33	2.20	2.24	8.77
<b>N. Pole</b>	3.20	3.23	10439	0.96	0.03	1.71	1.09	40.57
<b>N. Ferrel</b>	17.65	17.44	10800	0.96	-0.21	1.86	-1.18	7.69
<b>N. Hadley</b>	26.64	26.79	10800	0.92	0.16	1.36	0.58	3.07
<b>S. Hadley</b>	22.26	22.69	10800	0.96	0.43	1.35	1.94	3.64
<b>S. Ferrel</b>	8.10	7.91	10800	0.99	-0.19	1.20	-2.40	8.19
<b>S. Pole</b>	-34.51	-34.67	10440	0.98	-0.16	4.49	0.47	-10.36
<b>N.H.</b>	15.97	15.96	32039	0.99	-0.01	1.65	-0.04	7.24
<b>S.H.</b>	-1.01	-0.98	32040	0.99	0.03	2.77	-2.73	-164.29
<b>Global</b>	7.48	7.49	64079	0.99	0.01	2.28	0.14	18.84
<b>NCDC</b>	20.78	20.21	199	0.88	-0.57	4.18	-2.73	12.26

An overview of RAD3 summer statistical performance for the major boundary layer variables is shown graphically in Figure 4.100. The similarities between BASE and RAD3 are also shown in the similarities between Figures 4.13 and 4.100. The RAD3 simulation exhibits many of the same characteristics of the BASE case e.g., a large overestimation of daily precipitation rate, an underestimation of Q2 and GLW, and an overestimation of T2 and SWDOWN. In the North Pole domain, the downward shortwave flux as well as the temperature at 2 meters is underestimated and this domain also shows the highest NMB values for precipitation rate, which is the same as the BASE case. The vertical profile of temperature performance is explored in Figure 4.101 which is the zonal mean bias of GWRP versus NCEP/NCAR Reanalysis data. This figure also shows that GWRP generally captures the vertical temperature distribution within  $\pm 2$  degrees up to approximately 300 hPa. Figure 4.101 is also very similar to the corresponding Figure 4.15 for the summer BASE case, displaying large overestimations near the surface over Antarctica and the equator, underestimations of temperatures throughout the Southern Ferrel Cell and the underestimation of temperatures between 400 hPa and 100 hPa over the Tropics. RAD3 does not predict the large area of underestimation aloft over the Tropics as strongly as the BASE case, and also does not reproduce the small overestimations aloft over the Northern latitudes outside of the Tropics.



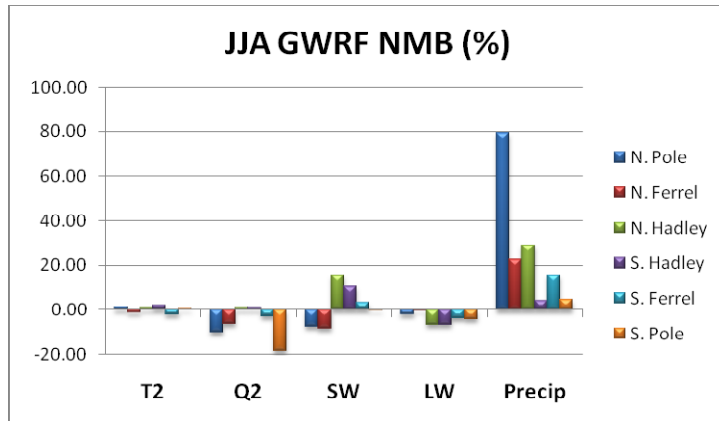


**Figure 4.100** 2001 summer mean normalized mean bias (%) of major meteorological variables for (a) the six continental domains and (b) the six circulation cell domains.

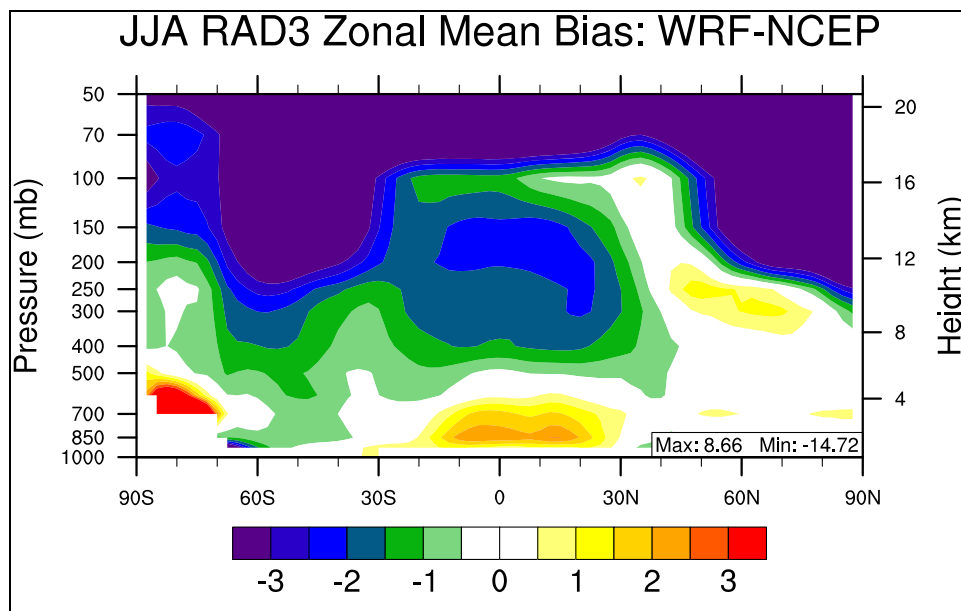


**Figure 4.101** 2001 summer zonal mean bias of Temperature.

#### 4.3.3.2 Summer Water Vapor Mixing ratio at 2-meter

The global distribution of RAD3 summer mean bias for water vapor mixing ratio at 2-meters is displayed in Figure 4.102. When compared with the base simulation spatial mean bias plot, the areas and magnitude of underestimation over land surfaces are very similar, reinforcing the similarities between the RAD3 and BASE simulations. The overall underestimation of Q2

and similarity to the BASE case is also reflected in Table 4.54 in which the domains that have a positive NMB value (e.g., Australia, Northern and Southern Hadley Cells) are the same domains as in the BASE simulation, while the rest of the domains display a negative NMB value. The global RAD3 NMB value is -2.39% which is almost identical to the baseline case whose summer value is -2.39%. Overall correlation values are the same as baseline performance, with a global Corr value of 0.99.

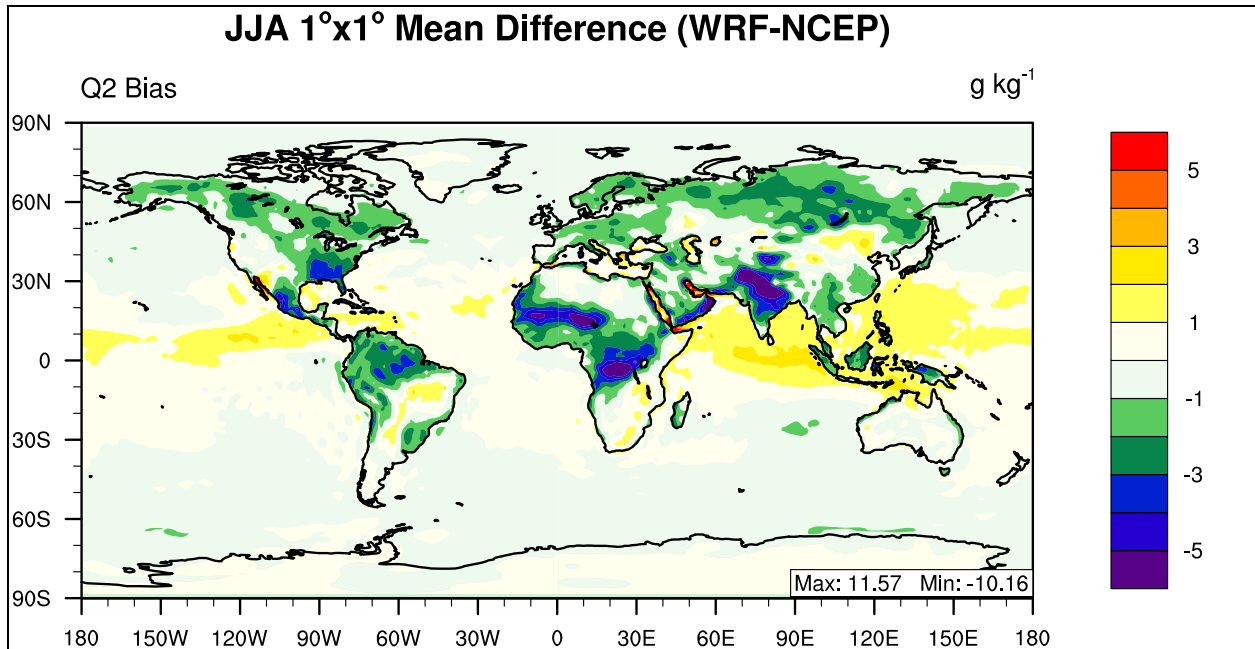


**Figure 4.102 2001 summer mean bias of water vapor mixing ratio at 2-meter.**

**Table 4.54 Performance Statistics of GWRf summer mean water vapor mixing ratio at 2-meter compared with NCEP/NCAR Reanalysis.**

<b>Name</b>	<b>MeanObs</b>	<b>MeanMod</b>	<b>Number</b>	<b>Corr</b>	<b>MB</b>	<b>RMSE</b>	<b>NMB%</b>	<b>NME%</b>
<b>Europe</b>	9.83	8.85	1200	0.91	-0.98	1.32	-9.96	11.80
<b>Africa</b>	10.88	10.09	2925	0.91	-0.79	2.02	-7.28	12.86
<b>Asia</b>	11.86	11.02	5100	0.95	-0.84	2.04	-7.06	13.46
<b>Australia</b>	8.53	8.67	1200	0.98	0.14	0.85	1.67	6.75
<b>N.A.</b>	12.34	11.60	2400	0.96	-0.74	1.59	-6.00	10.15
<b>S.A.</b>	10.02	9.43	2450	0.98	-0.59	1.30	-5.84	9.37
<b>N. Pole</b>	4.94	4.43	10440	0.97	-0.51	0.80	-10.31	11.10
<b>N. Ferrel</b>	10.18	9.53	10800	0.95	-0.65	1.26	-6.40	8.97
<b>N. Hadley</b>	16.78	16.89	10800	0.94	0.12	1.69	0.71	7.65
<b>S. Hadley</b>	13.91	14.00	10800	0.97	0.09	1.06	0.66	5.18
<b>S. Ferrel</b>	6.18	5.99	10800	0.99	-0.19	0.34	-3.06	4.39
<b>S. Polar</b>	0.74	0.60	10440	0.97	-0.14	0.29	-18.44	25.05
<b>N.H.</b>	10.70	10.35	32040	0.98	-0.35	1.31	-3.23	8.59
<b>S.H.</b>	7.01	6.93	32040	0.99	-0.08	0.67	-1.10	5.63
<b>Global</b>	8.85	8.64	64080	0.99	-0.21	1.04	-2.39	7.41

#### **4.3.3.3 Summer Downward Shortwave Flux at ground surface**

The pattern of RAD3 summer downward shortwave flux mean bias agrees well with the BASE simulation and is displayed graphically in Figure 4.103. It reflects the annual pattern of an overestimation in the Tropics (30°N-30°S), with large underestimations at high latitudes in the Northern hemisphere. There are also large areas of underestimation off the West coasts of Africa and South America in the Southern Hadley Cell, which are present in the baseline simulation. From a comparison between Figures 4.17 and 4.103, RAD3 creates smaller areas of underestimation and overestimation and also has less extreme maximum and minimum mean bias values. The agreement between RAD3 and BASE for GWRf SWDOWN is reflected in Table 4.55 in which the only RAD3 domains that display negative NMB values (e.g., Northern Pole Cell, Northern Ferrel Cell, and Europe) are the only BASE domains which display negative NMB values. The rest of the domains in both cases display positive NMBs. The RAD3

simulation has a global NMB value of 1.76%, which is less than the BASE simulation NMB of 3.97%. Overall the RAD3 simulation also displays slightly improved correlation values than the baseline simulation, with values of 0.95 and 0.93 respectively. The BSRN evaluation shows a slight improvement in SWDOWN between BASE and RAD3, with both exhibiting Corr value of 0.98 and respective NMBs of 51.50 and 43.09  $W m^{-2}$ . The very similar statistical performance between BASE and RAD3 indicate consistent performance between the Goddard and CAM shortwave schemes.

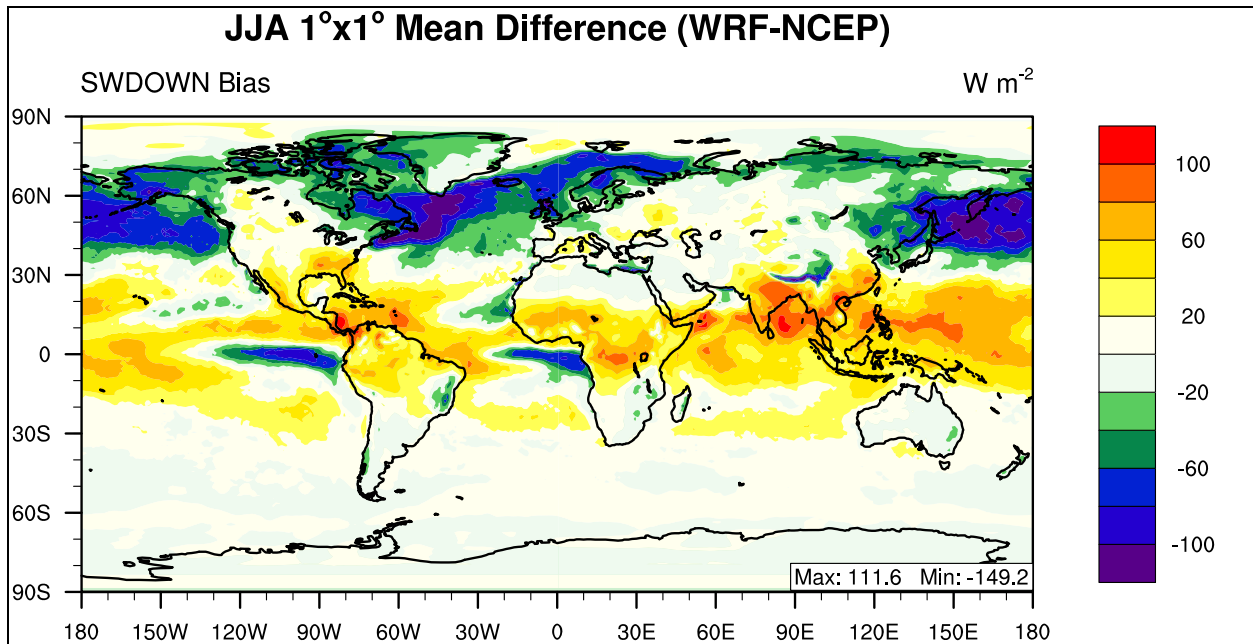


**Figure 4.103** 2001 summer mean bias of downward shortwave flux at the surface.

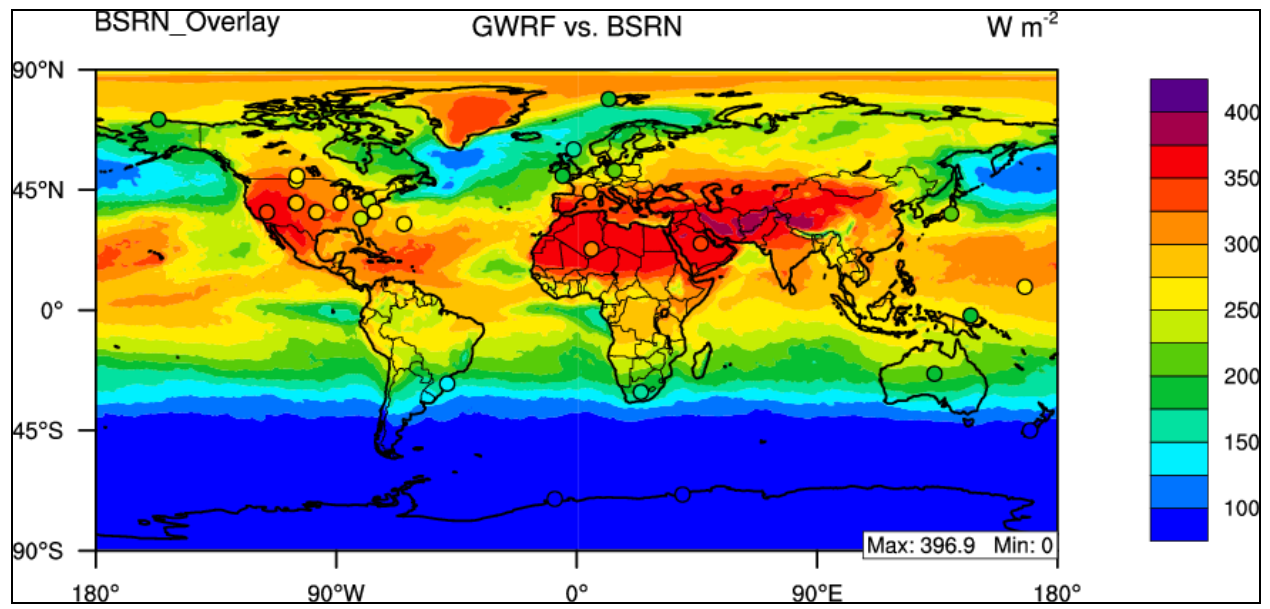


**Figure 4.104** 2001 summer mean bias of downward shortwave flux at the surface as compared with BSRN.

**Table 4.55 Performance Statistics of GWRf 2001 summer mean downward shortwave flux at the surface compared with NCEP/NCAR Reanalysis and BSRN.**

<b>Name</b>	<b>MeanObs</b>	<b>MeanMod</b>	<b>Number</b>	<b>Corr</b>	<b>MB</b>	<b>RMSE</b>	<b>NMB%</b>	<b>NME%</b>
<b>Europe</b>	276.03	260.97	1200	0.86	-15.06	33.96	-5.46	9.83
<b>Africa</b>	267.44	285.50	2925	0.88	18.06	37.16	6.75	10.65
<b>Asia</b>	282.36	296.30	5100	0.65	13.95	42.44	4.94	11.21
<b>Australia</b>	187.27	194.50	1200	0.94	7.23	17.08	3.86	6.29
<b>N.A.</b>	287.47	293.71	2400	0.63	6.24	37.18	2.17	10.34
<b>S.A.</b>	159.45	174.31	2450	0.97	14.86	29.11	9.32	13.05
<b>N. Pole</b>	278.24	257.28	10440	0.78	-20.96	34.44	-7.53	9.50
<b>N. Ferrel</b>	276.45	252.96	10800	0.89	-23.49	46.97	-8.50	12.81
<b>N. Hadley</b>	257.37	296.85	10800	0.63	39.48	51.82	15.34	17.61
<b>S. Hadley</b>	201.96	222.93	10800	0.73	20.97	33.90	10.38	13.56
<b>S. Ferrel</b>	79.47	82.00	10800	0.98	2.53	7.68	3.19	7.59
<b>S. Polar</b>	8.77	8.77	7920	0.99	0.00	0.94	-0.03	6.37
<b>N.H.</b>	270.60	269.16	32040	0.62	-1.44	45.12	-0.53	13.24
<b>S.H.</b>	105.32	113.91	29520	0.98	8.60	21.03	8.16	11.75
<b>Global</b>	191.34	194.71	61560	0.95	3.37	35.66	1.76	12.85
<b>BSRN</b>	218.83	261.92	29	0.98	43.09	48.51	19.69	19.69

#### **4.3.3.4 Summer Downward Longwave Flux at Ground Surface**

The pattern of summer downward longwave flux mean bias is displayed graphically in Figure 4.105 in which the overall pattern is an underestimation with a global NMB value of -4.27%, which is slightly worse than the baseline simulation. Figure 4.105 displays a very similar spatial pattern to the BASE case. The overall pattern of GWRf GLW performance is consistent with the baseline simulation, as shown in Table 4.56, in which all of the domains display a negative NMB value. Globally, the correlation values for RAD1 and baseline simulations are both 0.98. The underestimation of GLW is also present in the BSRN evaluation in which RAD3 exhibits a mean NMB value of -9.29%. RAD3 and BASE are very consistent in statistical performance for the BSRN evaluation because they both utilize the CAM longwave module, with MB values of -32.53 and -32.10 W m<sup>-2</sup>.

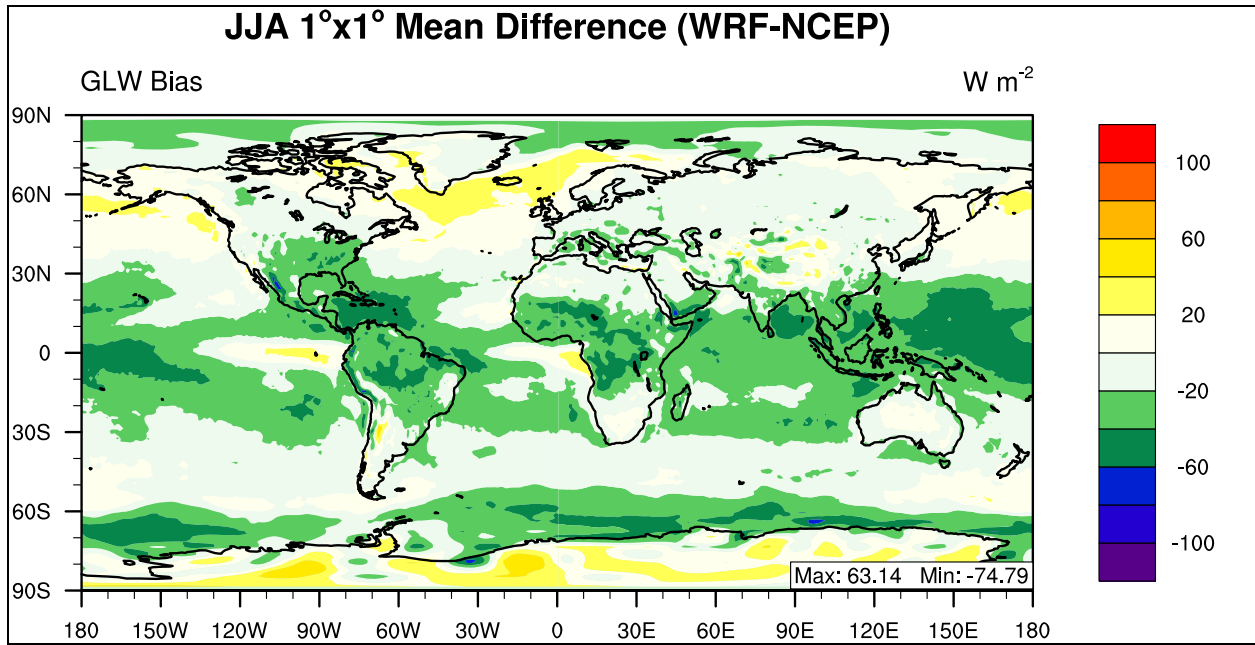


**Figure 4.105** 2001 summer mean bias of downward longwave flux at the surface.

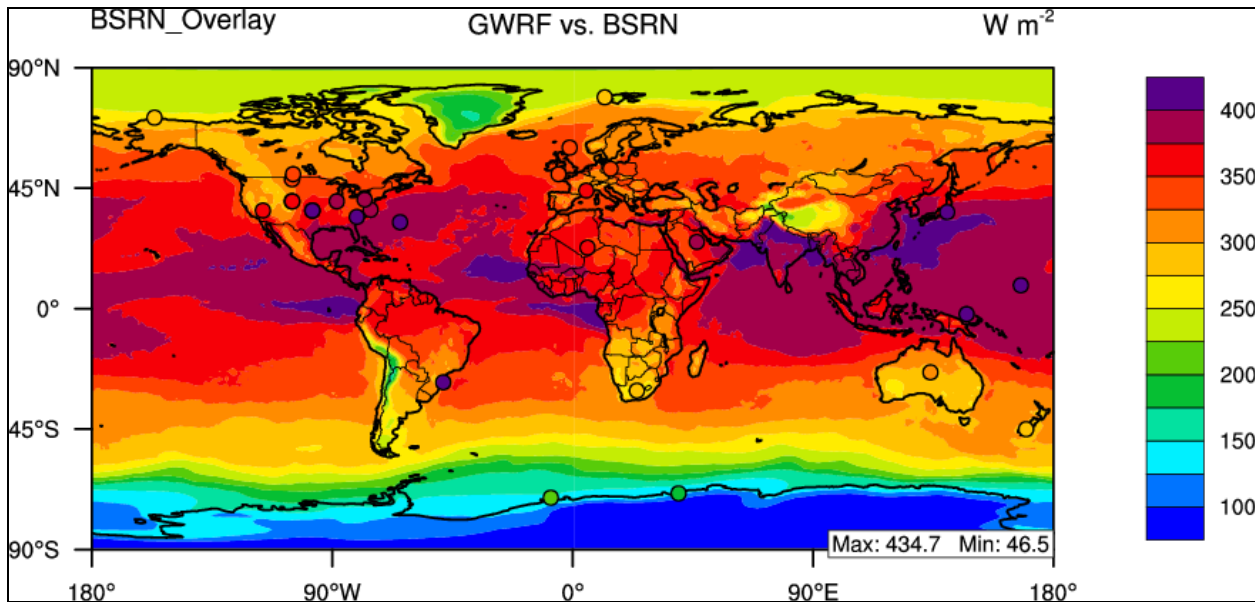


**Figure 4.106** 2001 summer mean bias of downward longwave flux at the surface as compared with BSRN.

**Table 4.56 Performance Statistics of GWRf 2001 summer mean downward longwave flux at the surface as compared with NCEP/NCAR Reanalysis and BSRN.**

<b>Name</b>	<b>MeanObs</b>	<b>MeanMod</b>	<b>Number</b>	<b>Corr</b>	<b>MB</b>	<b>RMSE</b>	<b>NMB%</b>	<b>NME%</b>
<b>Europe</b>	333.15	324.38	1200	0.72	-8.77	15.20	-2.63	4.01
<b>Africa</b>	363.04	342.52	2925	0.83	-20.51	26.80	-5.65	6.31
<b>Asia</b>	355.61	342.64	5100	0.95	-12.97	20.18	-3.65	4.53
<b>Australia</b>	325.16	311.54	1200	0.97	-13.63	18.89	-4.19	4.57
<b>N.A.</b>	358.63	343.01	2400	0.93	-15.63	22.11	-4.36	5.18
<b>S.A.</b>	333.45	312.99	2450	0.97	-20.46	26.67	-6.14	6.81
<b>N. Pole</b>	272.40	266.80	10440	0.91	-5.60	16.09	-2.06	5.04
<b>N. Ferrel</b>	344.05	341.87	10800	0.87	-2.18	15.45	-0.63	3.77
<b>N. Hadley</b>	405.77	378.73	10800	0.72	-27.04	31.00	-6.66	6.91
<b>S. Hadley</b>	375.69	350.26	10800	0.92	-25.43	29.06	-6.77	7.10
<b>S. Ferrel</b>	299.44	287.74	10800	0.94	-11.71	16.12	-3.91	4.51
<b>S. Polar</b>	134.46	128.41	10440	0.95	-6.05	27.93	-4.50	17.88
<b>N.H.</b>	341.51	329.83	32040	0.95	-11.67	22.11	-3.42	5.36
<b>S.H.</b>	271.39	256.90	32040	0.99	-14.49	25.03	-5.34	7.87
<b>Global</b>	306.45	293.36	64080	0.98	-13.08	23.61	-4.27	6.47
<b>BSRN</b>	350.01	317.48	29	0.92	-32.53	40.56	-9.29	9.33

#### **4.3.3.5 Summer Daily Precipitation Rate**

The daily precipitation at the surface in GWRf is compared with the Global Precipitation Climatology Project (GPCP) for the summer of 2001. Overall, the GWRf RAD3 performance during summer appears to be overestimating daily precipitation rate and performing similar to the baseline simulation, due to the large similarities between Figure 4.107 and Figure 4.23. Maximum and minimum mean bias values are very similar between the RAD1 and BASE simulations, indicating that the choice of radiation parameterization does not largely influence daily precipitation rate. Globally, RAD3 shows the same value as RAD1 which is a slightly lower Corr value of 0.79 as compared to the 0.83 in the BASE case, while NMB values are slightly better than BASE with values of 29.12% and 38.64% respectively. Comparison with NCDC data also shows a tendency of GWRf to overestimate precipitation; however the overestimation is not as strong as the BASE simulation with NMBs of 12.36% and 25.29%.

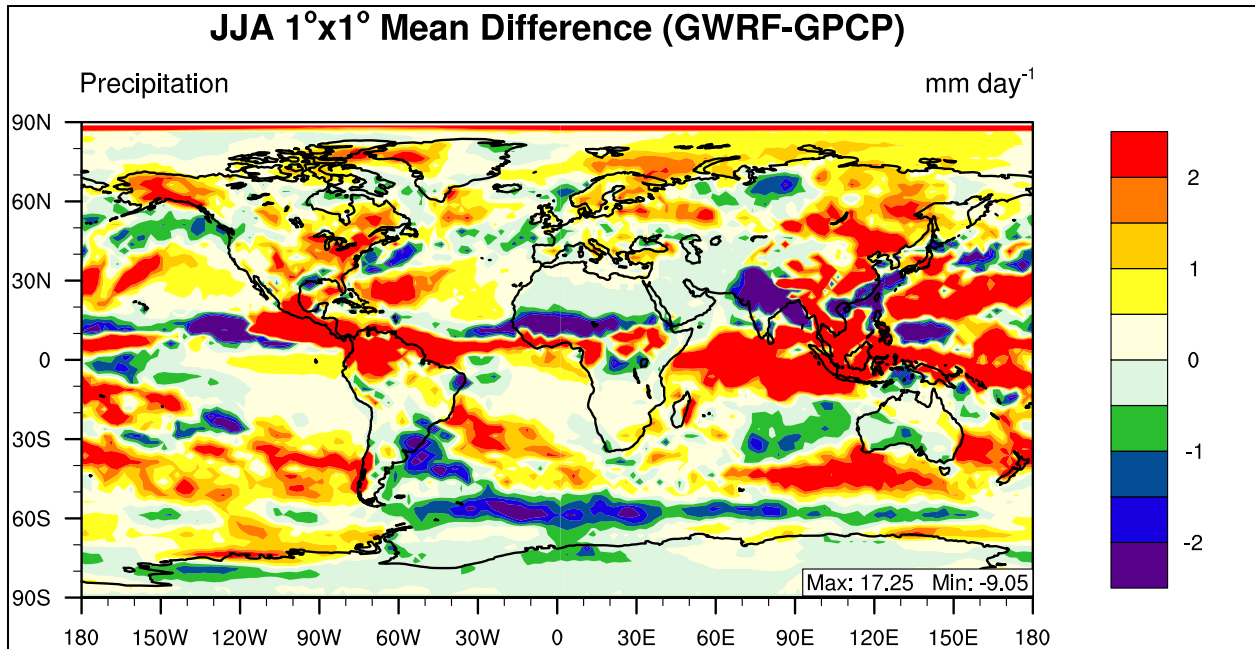


**Figure 4.107** 2001 summer mean bias of daily precipitation rate.

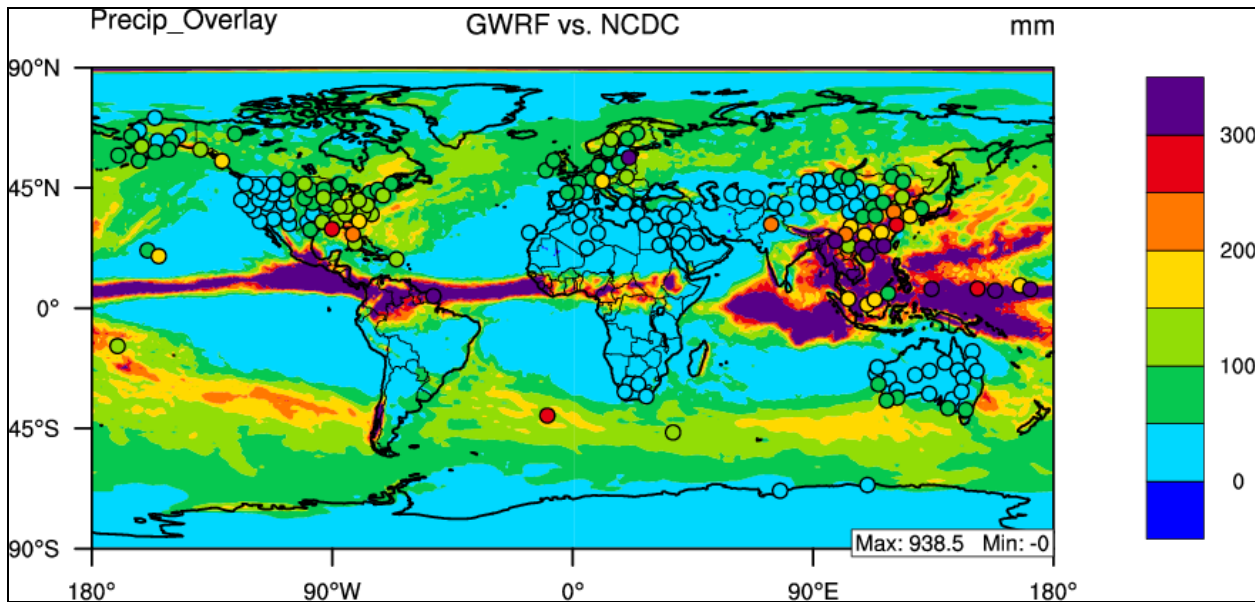


**Figure 4.108** 2001 summer monthly precipitation rate as compared to NCDC.

**Table 4.57 Performance Statistics of GWRP 2001 summer mean precipitation rate as compared with GPCP (mm day<sup>-1</sup>) and NCDC (mm month<sup>-1</sup>).**

<b>Name</b>	<b>MeanObs</b>	<b>MeanMod</b>	<b>Number</b>	<b>Corr</b>	<b>MB</b>	<b>RMSE</b>	<b>NMB%</b>	<b>NME%</b>
<b>Europe</b>	2.37	2.86	192	0.65	0.49	1.00	20.73	33.91
<b>Africa</b>	1.26	1.41	463	0.84	0.15	1.34	11.80	57.59
<b>Asia</b>	3.29	3.69	814	0.77	0.40	2.48	12.00	47.02
<b>Australia</b>	0.98	1.23	192	0.73	0.25	0.98	25.17	63.30
<b>N.A.</b>	2.49	3.32	384	0.69	0.83	1.49	33.19	45.86
<b>S.A.</b>	3.00	3.67	392	0.78	0.67	2.52	22.53	48.95
<b>N. Pole</b>	1.17	2.10	1728	0.13	0.93	1.89	79.08	92.06
<b>N. Ferrel</b>	2.30	2.82	1727	0.74	0.52	1.35	22.40	40.63
<b>N. Hadley</b>	4.05	5.21	1722	0.77	1.16	3.31	28.69	53.62
<b>S. Hadley</b>	1.79	2.54	1728	0.86	0.76	2.00	42.56	63.15
<b>S. Ferrel</b>	3.08	3.56	1728	0.46	0.48	1.38	15.60	34.69
<b>S. Polar</b>	0.97	1.01	1728	0.81	0.05	0.59	4.68	41.67
<b>N.H.</b>	2.51	3.37	5177	0.77	0.87	2.34	34.62	55.63
<b>S.H.</b>	1.94	2.37	5184	0.82	0.43	1.44	22.04	44.56
<b>Global</b>	2.22	2.87	10361	0.79	0.65	1.94	29.12	50.79
<b>NCDC</b>	93.20	104.72	172	0.72	11.52	78.91	12.36	49.61

#### **4.3.3.6 Intercomparison of radiation configuration**

Tables 4.58 and 4.59 compare the spread of downward longwave flux predictions by the various radiation configurations presented in this chapter. In both Tables 4.58 and 4.59, the RAD1 radiation configuration predicts the lowest amount of GLW, while RAD2 predicts the largest amount. Among the circulation cell domains, the North Pole has the largest average standard deviation among the modules, indicating a high sensitivity to radiation parameterization for this domain. Among the continental domains, domains with large land masses in the Northern Hemisphere (e.g., Europe, North America, and Asia) have an overall larger standard deviation among the radiation modules for GLW prediction. An analysis of the NMB values of these radiation configurations shows that the RAD2 configuration predicts the most accurate GLW for summer 2001.

**Table 4.58 Intercomparison of GWRf GLW over circulation cell domains for summer 2001 compared with NCEP/NCAR Reanalysis.**

<b>Domain</b>	<b>BASE MeanMod</b>	<b>RAD1 MeanMod</b>	<b>RAD2 MeanMod</b>	<b>RAD3 MeanMod</b>	<b>Stdev</b>
<b>N. Pole</b>	271.26	245.66	290.77	266.80	18.51
<b>N. Ferrel</b>	341.56	325.56	360.35	341.87	14.22
<b>N. Hadley</b>	376.50	368.29	409.53	378.73	18.08
<b>S. Hadley</b>	349.05	346.07	379.40	350.26	15.57
<b>S. Ferrel</b>	286.65	285.92	301.85	287.74	7.58
<b>S. Polar</b>	131.39	129.18	137.96	128.41	4.34
<b>Average</b>	<b>292.74</b>	<b>283.45</b>	<b>313.31</b>	<b>292.30</b>	<b>13.05</b>

**Table 4.59 Intercomparison of GWRf GLW over continental domains for summer 2001 compared with NCEP/NCAR Reanalysis.**

<b>Domain</b>	<b>BASE MeanMod</b>	<b>RAD1 MeanMod</b>	<b>RAD2 MeanMod</b>	<b>RAD3 MeanMod</b>	<b>Stdev</b>
<b>Europe</b>	324.01	312.77	347.62	324.38	14.64
<b>Africa</b>	343.49	333.31	372.23	342.52	16.86
<b>Asia</b>	344.70	326.55	370.90	342.64	18.36
<b>Australia</b>	312.88	310.25	337.71	311.54	13.12
<b>N.A.</b>	342.57	328.47	367.99	343.01	16.44
<b>S.A.</b>	312.70	311.30	339.28	312.99	13.50
<b>Average</b>	<b>330.06</b>	<b>320.44</b>	<b>355.96</b>	<b>329.51</b>	<b>15.49</b>

Tables 4.60 and 4.61 compare the spread of downward shortwave flux predictions by the various radiation configurations presented in this chapter. In both Tables 4.60 and 4.61, the RAD1 radiation configuration predicts the lowest amount of SWDOWN, while RAD2 predicts the largest amount. Among the circulation cell domains, the North Pole has the largest average standard deviation among the modules, indicating a high sensitivity to radiation parameterization for this domain. Among the continental domains, domains with large land masses in the Northern Hemisphere (e.g., Europe, North America, and Asia) have an overall larger standard

deviation among the radiation modules for SWDOWN prediction. An analysis of the NMB values of these radiation configurations shows that the RAD3 configuration predicts the most accurate SWDOWN for summer 2001.

**Table 4.60 Intercomparison of GWRf SWDOWN over circulation cell domains for summer 2001 compared with NCEP/NCAR Reanalysis.**

<b>Domain</b>	<b>BASE MeanMod</b>	<b>RAD1 MeanMod</b>	<b>RAD2 MeanMod</b>	<b>RAD3 MeanMod</b>	<b>Stdev</b>
<b>N. Pole</b>	254.78	167.46	260.74	257.28	45.14
<b>N. Ferrel</b>	260.49	217.16	268.74	252.96	22.72
<b>N. Hadley</b>	309.21	279.46	307.33	296.85	13.63
<b>S. Hadley</b>	227.91	197.48	225.14	222.93	14.07
<b>S. Ferrel</b>	83.10	51.69	84.17	82.00	15.73
<b>S. Polar</b>	9.46	2.85	8.80	8.77	3.10
<b>Average</b>	<b>190.82</b>	<b>152.68</b>	<b>192.49</b>	<b>186.80</b>	<b>19.06</b>

**Table 4.61 Intercomparison of GWRf SWDOWN over continental domains for summer 2001 compared with NCEP/NCAR Reanalysis.**

<b>Domain</b>	<b>BASE MeanMod</b>	<b>RAD1 MeanMod</b>	<b>RAD2 MeanMod</b>	<b>RAD3 MeanMod</b>	<b>Stdev</b>
<b>Europe</b>	271.01	193.33	279.97	260.97	39.43
<b>Africa</b>	287.31	263.17	290.42	285.50	12.46
<b>Asia</b>	309.50	248.32	308.63	296.30	28.88
<b>Australia</b>	196.65	161.24	196.16	194.50	17.29
<b>N.A.</b>	304.93	257.32	307.20	293.71	23.08
<b>S.A.</b>	179.25	141.03	181.76	174.31	18.96
<b>Average</b>	<b>258.11</b>	<b>210.73</b>	<b>260.69</b>	<b>250.88</b>	<b>23.29</b>

#### **4.4 Sensitivity to cloud microphysics schemes**

##### **4.4.1 WRF Single Moment 6-Class Summer (JJA) mean evaluation**

###### **4.4.1.1 Summer Temperature at 2-meter**

The temperature at 2-meters above the surface for GWRf sensitivity simulation CMP1 is compared with NCEP/NCAR Reanalysis for the summer of 2001. This sensitivity simulation replaces the WRF Single Moment 3-Class (WSM3) from the baseline simulation with the WRF Single Moment 6-Class (WSM6) microphysics scheme. When Figure 4.109 is compared with Figure 4.11, the two figures appear very similar. The largest difference between the two Figures is that the CMP1 simulation creates large areas of underestimation, over ocean surfaces in the Northern high and mid-latitudes. Globally, GWRf shows good statistical performance with a Corr value of 0.99 (same as baseline simulation), and an NMB value of -0.38% which is of different sign and smaller in magnitude than the baseline value (2.70%). The large areas of underestimation in CMP1 are shown in the comparison between Tables 4.8 and 4.62 when CMP1 produces large, negative NMB values over the North Pole (-15.25%), while the BASE case predicted a large, positive NMB value 9.14%. CMP1 also underpredicts temperature over the Northern Ferrel and Hadley Cells, which contribute to the Northern Hemispheric NMB value of -2.32%, which is of opposite sign than the BASE case. The evaluation of GWRf T2 with NCDC data performs very similarly for CMP1 and BASE simulations with the same Corr value (0.88) and similar NMBs (-3.91% and -2.43%, respectively), indicating an overall weak sensitivity of T2 to microphysics choice for point observations.

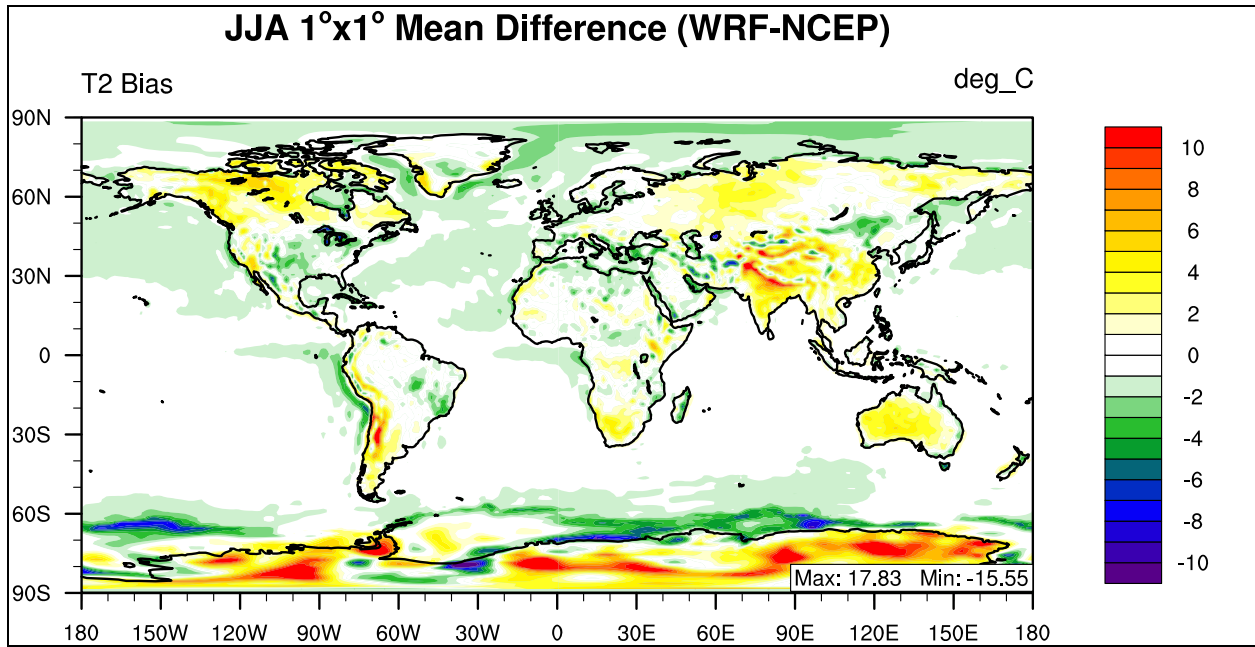


**Figure 4.109 2001 summer mean bias of temperature at 2-meter.**

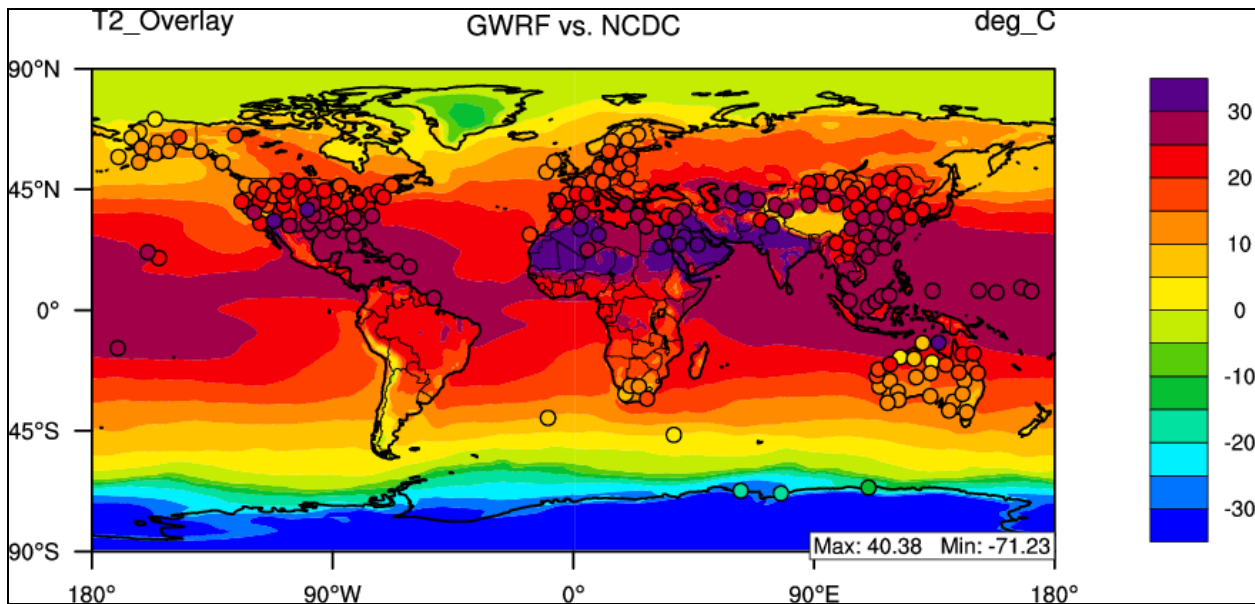


**Figure 4.110 2001 summer temperature at 2-meter as compared with NCDC.**

**Table 4.62 Performance Statistics of GWRf 2001 summer mean temperature at 2-meter as compared with NCEP/NCAR Reanalysis and NCDC.**

<b>Name</b>	<b>MeanObs</b>	<b>MeanMod</b>	<b>Number</b>	<b>Corr</b>	<b>MB</b>	<b>RMSE</b>	<b>NMB%</b>	<b>NME%</b>
<b>Europe</b>	16.43	15.98	1200	0.95	-0.44	1.39	-2.68	6.74
<b>Africa</b>	23.83	23.66	2925	0.96	-0.17	1.54	-0.70	4.87
<b>Asia</b>	20.72	21.73	5100	0.95	1.02	2.64	4.90	9.35
<b>Australia</b>	17.02	18.08	1200	0.95	1.06	2.06	6.21	9.04
<b>N.A.</b>	20.51	20.22	2400	0.95	-0.29	2.02	-1.44	7.93
<b>S.A.</b>	14.76	14.91	2450	0.98	0.15	2.09	1.03	8.58
<b>N. Pole</b>	3.20	2.71	10439	0.97	-0.49	1.91	-15.25	51.13
<b>N. Ferrel</b>	17.65	17.31	10800	0.95	-0.34	2.05	-1.94	9.07
<b>N. Hadley</b>	26.64	26.35	10800	0.92	-0.29	1.36	-1.08	3.51
<b>S. Hadley</b>	22.26	22.26	10800	0.96	0.01	1.28	0.04	3.15
<b>S. Ferrel</b>	8.10	7.55	10800	0.99	-0.55	1.10	-6.83	9.88
<b>S. Polar</b>	-34.51	-32.98	10440	0.98	1.53	4.67	4.43	10.53
<b>N.H.</b>	15.97	15.60	32039	0.99	-0.37	1.79	-2.32	8.69
<b>S.H.</b>	-1.01	-0.70	32040	1.00	0.31	2.84	31.05	167.09
<b>Global</b>	7.48	7.45	64079	0.99	-0.03	2.38	-0.38	20.58
<b>NCDC</b>	20.78	19.96	199	0.88	-0.81	4.21	-3.91	12.63

An overview of CMP1 summer statistical performance for the major boundary layer variables is shown graphically in Figure 4.111. The similarities between BASE and CMP1 are also shown in the similarities between Figures 4.13 and 4.111. The CMP1 simulation, as in the BASE case, exhibits a large overestimation of daily precipitation rate across all domains. In the North Pole domain, downward shortwave flux as well as the temperature at 2 meters is underestimated and this domain also shows very large NMB values for precipitation rate, which is the same as the BASE case. The vertical profile of temperature performance is explored in Figure 4.112 which is the zonal mean bias of GWRf versus NCEP/NCAR Reanalysis data. This figure also shows that GWRf generally captures the vertical temperature distribution within  $\pm 2$  degrees up to approximately 300 hPa. Figure 4.112 is also very similar to the corresponding Figure 4.15 for the summer BASE case, displaying large overestimations near the surface over Antarctica and the equator, underestimations of temperatures throughout the Southern Ferrel Cell and the

underestimation of temperatures between 400 hPa and 100 hPa over the Tropics. CMP1 does not predict the large area of underestimation aloft over the Tropics as strongly as the BASE case.

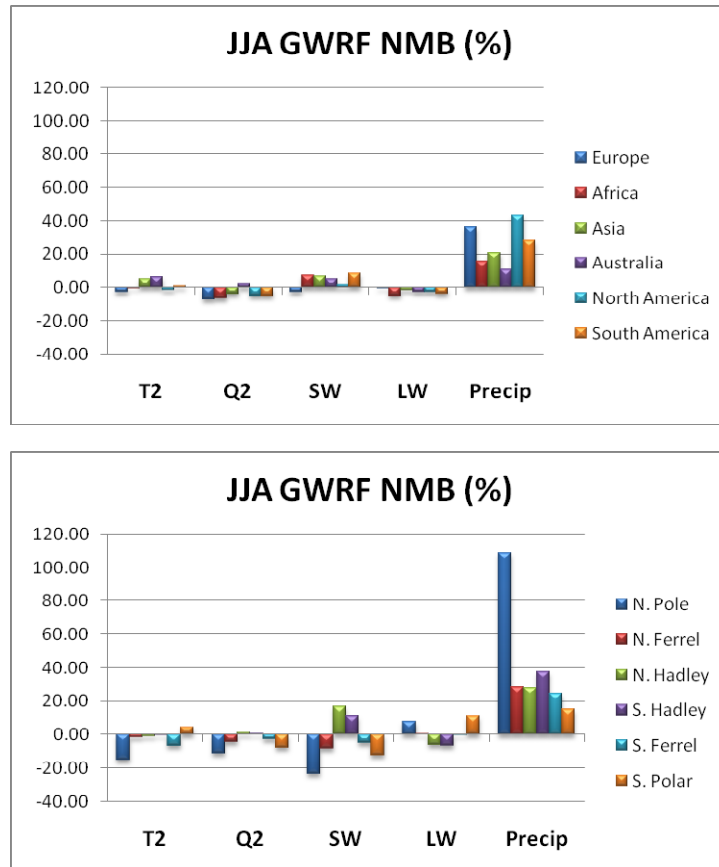


**Figure 4.111** 2001 summer mean normalized mean bias (%) of major meteorological variables for (a) the six continental domains and (b) the six circulation cell domains.

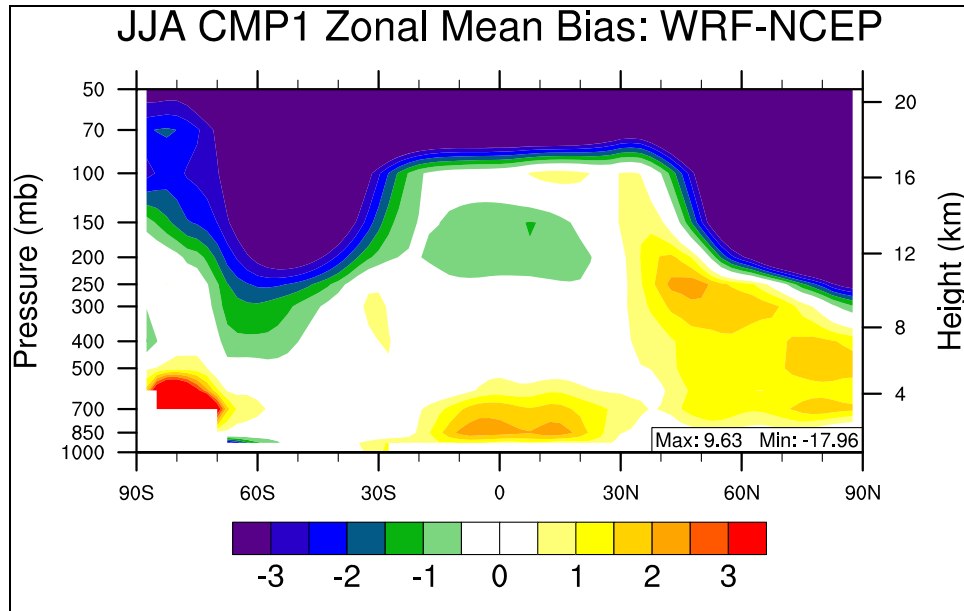


**Figure 4.112 2001 summer zonal mean bias of Temperature**

#### 4.4.1.2 Summer Water Vapor Mixing ratio at 2-meter

The global distribution of CMP1 summer mean bias for water vapor mixing ratio at 2-meters is displayed in Figure 4.113. When compared with the baseline simulation spatial mean bias plot, the areas and magnitude of underestimation over land surfaces are very similar, reinforcing the similarities between the CMP1 and BASE simulations. The overall underestimation of Q2 and similarity to the BASE case is also reflected in Table 4.63 in which the domains that have a positive NMB value (e.g., Australia, Northern and Southern Hadley Cells) are the same domains as in the BASE simulation, while the rest of the domains display a negative NMB value. The global CMP1 NMB value is -1.74% which is slightly improved from the baseline case whose summer value is -2.39%. Overall Corr values are the same as baseline performance, with a global Corr value of 0.99.

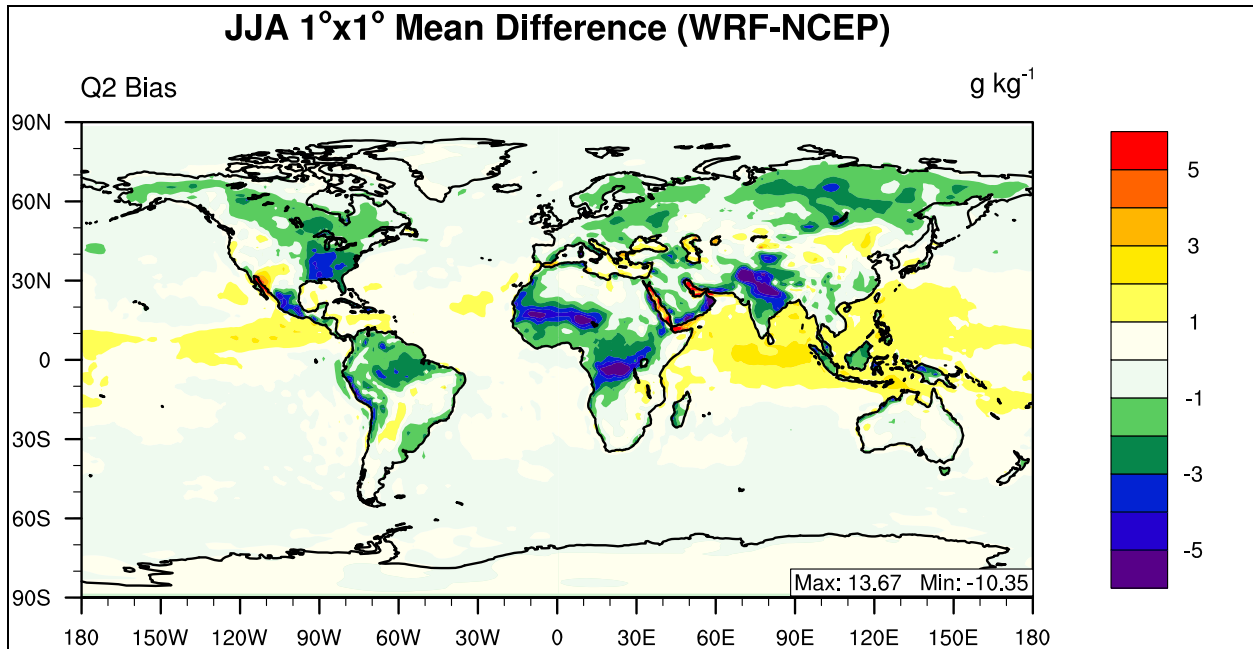


**Figure 4.113** 2001 summer mean bias of water vapor mixing ratio at 2-meter.

**Table 4.63** Performance Statistics of GWRF 2001 summer mean water vapor mixing ratio at 2-meter summer 2001 compared with NCEP/NCAR Reanalysis.

Name	MeanObs	MeanMod	Number	Corr	MB	RMSE	NMB%	NME%
Europe	9.83	9.09	1200	0.89	-0.74	1.19	-7.49	9.93
Africa	10.88	10.17	2925	0.92	-0.72	1.92	-6.59	12.00
Asia	11.86	11.37	5100	0.96	-0.49	1.83	-4.14	11.85
Australia	8.53	8.70	1200	0.98	0.17	0.90	2.03	7.25
N.A.	12.34	11.69	2400	0.95	-0.65	1.68	-5.28	10.39
S.A.	10.02	9.48	2450	0.98	-0.53	1.18	-5.33	8.49
N. Pole	4.94	4.40	10440	0.96	-0.54	0.78	-10.98	11.75
N. Ferrel	10.18	9.71	10800	0.95	-0.47	1.20	-4.58	8.15
N. Hadley	16.78	17.00	10800	0.95	0.23	1.63	1.35	7.32
S. Hadley	13.91	14.00	10800	0.97	0.09	1.05	0.66	5.10
S. Ferrel	6.18	6.00	10800	0.99	-0.18	0.33	-2.95	4.11
S. Polar	0.74	0.68	10440	0.98	-0.06	0.22	-8.15	19.79
N.H.	10.70	10.44	32040	0.98	-0.26	1.26	-2.41	8.25
S.H.	7.01	6.96	32040	0.99	-0.05	0.65	-0.72	5.31
Global	8.85	8.70	64080	0.99	-0.15	1.00	-1.74	7.09

#### **4.4.1.3 Summer Downward Shortwave Flux at Ground Surface**

The pattern of CMP1 summer downward shortwave flux mean bias agrees well with the BASE simulation and is displayed graphically in Figure 4.114. It reflects the baseline pattern of an overestimation in the Tropics (30°N-30°S), with large underestimations at high latitudes in the Northern hemisphere. There are also large areas of underestimation off the West coasts of Africa and South America in the Southern Hadley Cell, which are present in the baseline simulation. From a comparison between Figures 4.17 and 4.114, CMP1 creates large areas of underestimation over the North Pole, with a NMB value (-23.37%) much worse than the corresponding baseline value (-8.43%), which most likely is a result of the complex treatment of ice in the WSM6 microphysics scheme. The CMP1 simulation has a global NMB value of -2.28%, which is less than the BASE simulation NMB of 3.97%. Overall the CMP1 simulation displays slightly worse correlation values than the baseline simulation, with values of 0.91 and 0.93 respectively. Evaluation with BSRN data shows that in CMP1, WSM6 reduces the large overestimations present in the BASE case, thus providing a more accurate SWDOWN estimate than BASE with NMBs of 18.58% and 23.53%, respectively.

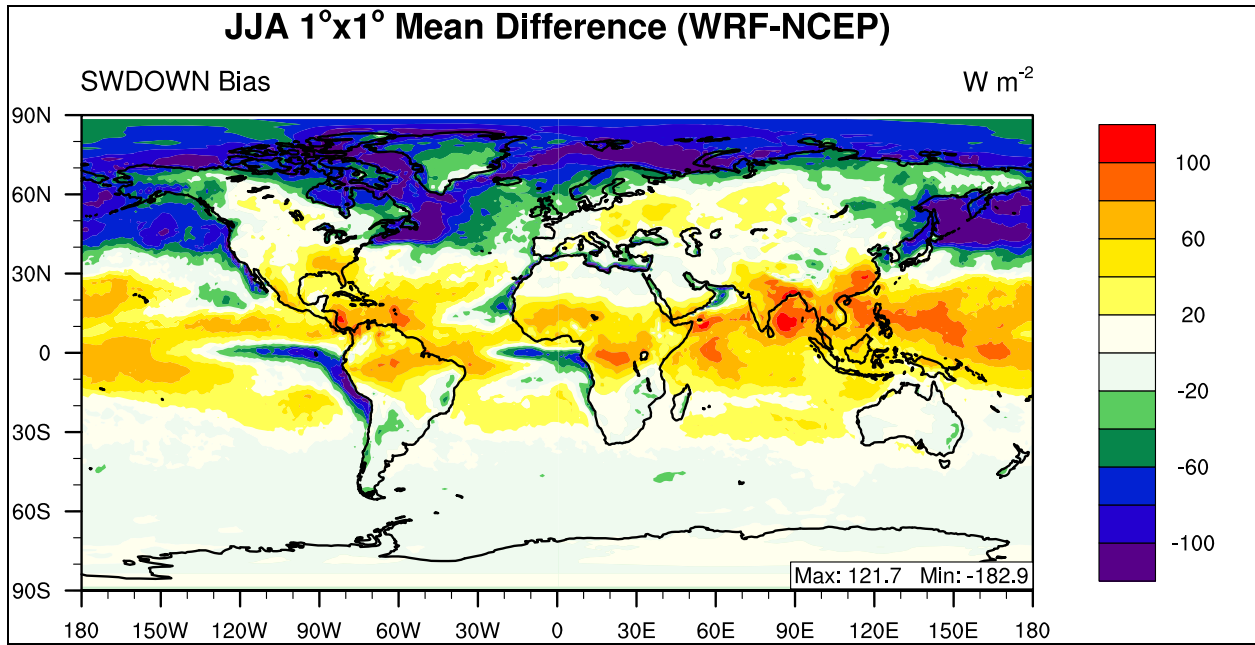


**Figure 4.114 2001 summer mean bias of downward shortwave flux at the surface.**

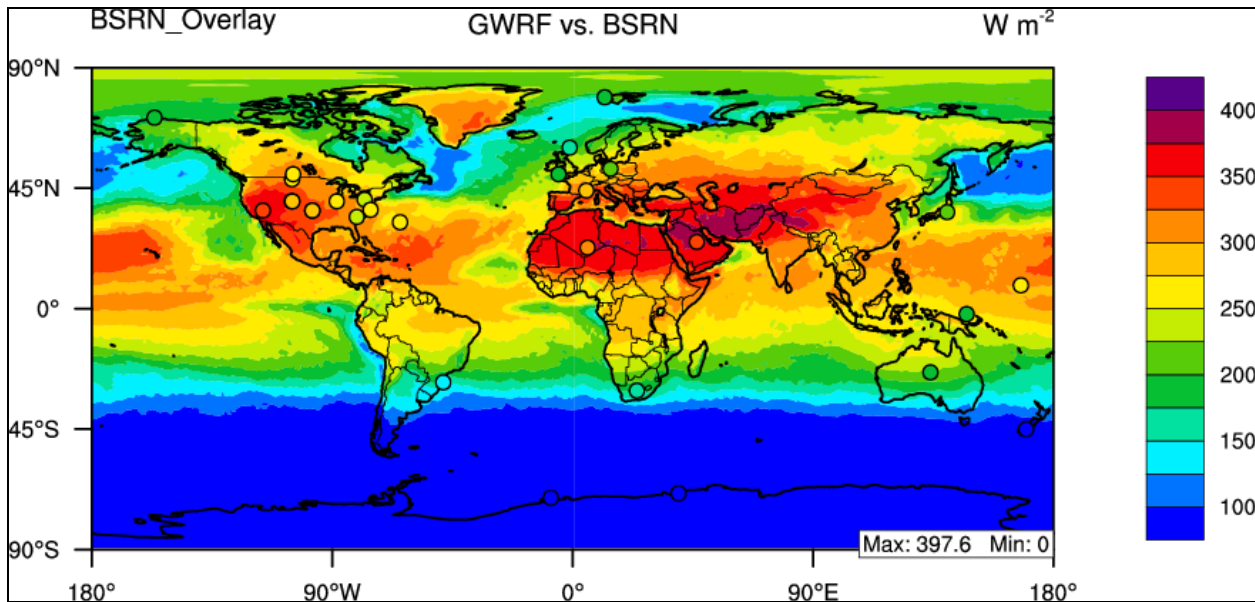


**Figure 4.115 2001 summer mean bias of downward shortwave flux at the surface as compared with NCDC.**

**Table 4.64 Performance Statistics of GWRf 2001 summer mean downward shortwave flux at the surface as compared with NCEP/NCAR Reanalysis and BSRN.**

Name	MeanObs (W m <sup>-2</sup> )	MeanMod (W m <sup>-2</sup> )	Number	Corr	MB (W m <sup>-2</sup> )	RMSE	NMB%	NME%
Europe	276.03	268.46	1200	0.78	-7.57	35.00	-2.74	10.54
Africa	267.44	286.48	2925	0.87	19.03	39.16	7.12	11.14
Asia	282.36	300.74	5100	0.66	18.38	43.60	6.51	11.59
Australia	187.27	196.34	1200	0.95	9.07	17.71	4.84	6.69
N.A.	287.47	292.13	2400	0.59	4.65	38.95	1.62	10.59
S.A.	159.45	172.44	2450	0.95	12.98	35.29	8.14	16.07
N. Pole	278.24	213.21	10440	0.61	-65.03	71.83	-23.37	23.65
N. Ferrel	276.45	253.63	10800	0.87	-22.82	49.97	-8.25	13.46
N. Hadley	257.37	299.87	10800	0.64	42.50	54.18	16.51	18.71
S. Hadley	201.96	224.95	10800	0.69	22.98	37.91	11.38	15.18
S. Ferrel	79.47	75.56	10800	0.98	-3.91	9.46	-4.92	9.74
S. Polar	8.77	7.70	7920	0.99	-1.07	1.92	-12.24	13.45
N.H.	270.60	256.04	32040	0.48	-14.56	59.27	-5.38	18.55
S.H.	105.32	112.01	29520	0.98	6.69	23.66	6.35	13.64
Global	191.34	186.97	61560	0.91	-4.37	45.79	-2.28	17.26
BSRN	218.83	259.31	29	0.98	40.48	46.18	18.50	18.70

**4.4.1.4 Summer Downward Longwave Flux at ground surface**

The pattern of summer downward longwave flux mean bias is displayed graphically in Figure 4.116 in which the overall pattern is an underestimation over the Tropics and an overestimation over the high latitudes, with a global NMB value of -0.79%, which is better than the baseline simulation. The consistency with the baseline simulation is shown in Table 4.65, in which all of the continental domains display a negative NMB value. However the departure from the baseline simulation is evident with the North and South Pole domains producing large, positive NMB value of 7.92% and 10.90%, respectively. These values are much different than the corresponding baseline NMB values which are -0.42% for the North Pole and -2.29 for the South Pole. Globally, the correlation value for the CMP1 and baseline simulations is 0.98. The comparison with BSRN data shows that both WSM3 and WSM6 underestimate GLW, however

WSM6 does produce a more accurate estimate than WSM3 with MB values of -24.32 and -32.10  $W m^{-2}$ .

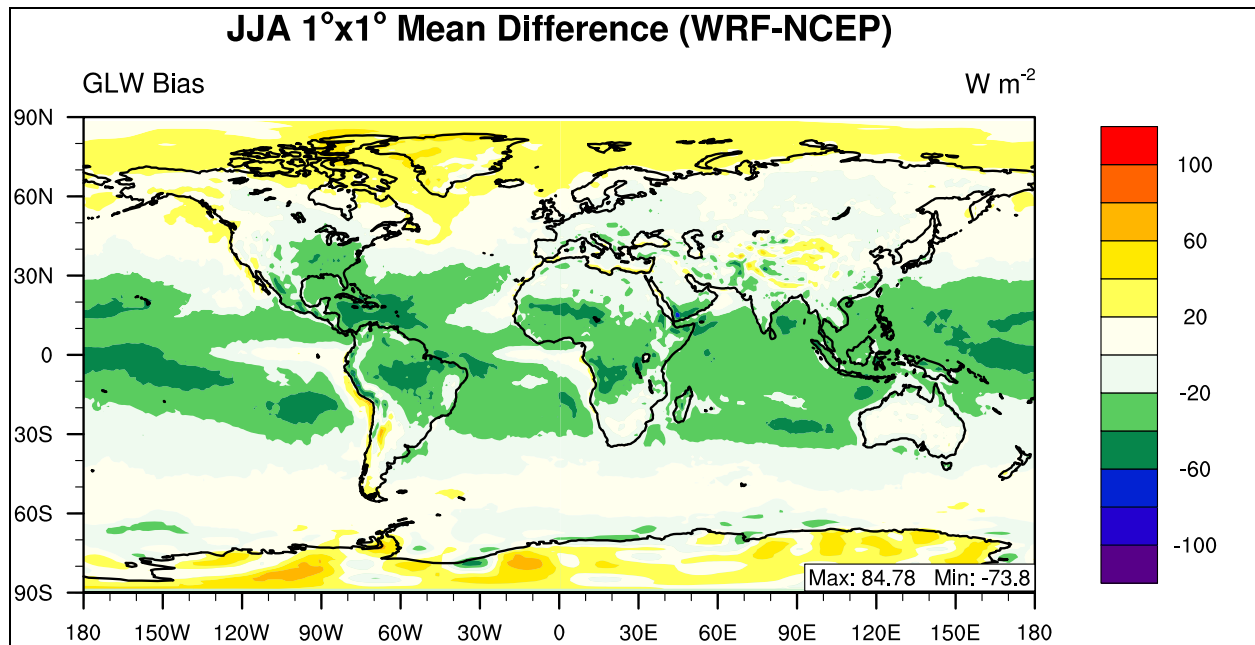


**Figure 4.116** 2001 summer mean bias of downward longwave flux at the surface.

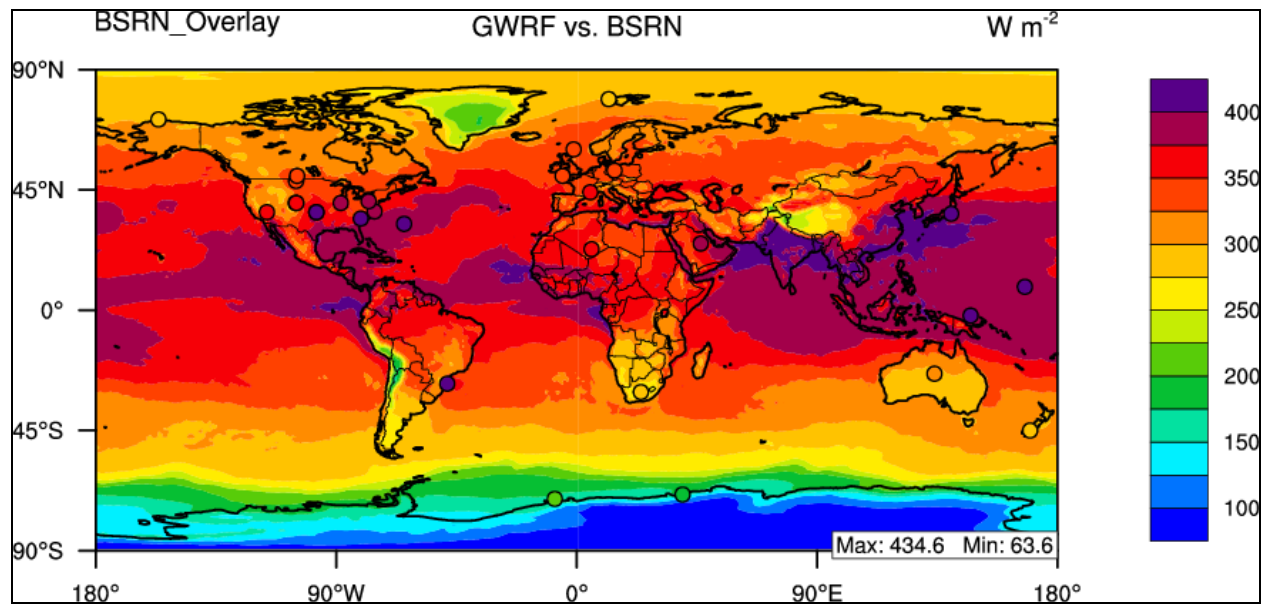


**Figure 4.117** 2001 summer mean bias of downward longwave flux at the surface as compared to BSRN.

**Table 4.65 Performance Statistics of GWRf 2001 summer mean downward longwave flux at the surface as compared with NCEP/NCAR Reanalysis and BSRN.**

<b>Name</b>	<b>MeanObs</b>	<b>MeanMod</b>	<b>Number</b>	<b>Corr</b>	<b>MB</b>	<b>RMSE</b>	<b>NMB%</b>	<b>NME%</b>
<b>Europe</b>	333.15	330.68	1200	0.67	-2.46	13.39	-0.74	3.35
<b>Africa</b>	363.04	344.06	2925	0.85	-18.97	25.16	-5.23	5.92
<b>Asia</b>	355.61	349.31	5100	0.95	-6.29	17.65	-1.77	3.69
<b>Australia</b>	325.16	315.36	1200	0.97	-9.80	16.23	-3.01	3.77
<b>N.A.</b>	358.63	347.90	2400	0.92	-10.73	20.39	-2.99	4.68
<b>S.A.</b>	333.45	320.64	2450	0.94	-12.81	25.91	-3.84	6.60
<b>N. Pole</b>	272.40	293.98	10440	0.92	21.58	24.43	7.92	8.16
<b>N. Ferrel</b>	344.05	345.17	10800	0.88	1.12	14.42	0.33	3.36
<b>N. Hadley</b>	405.77	380.33	10800	0.76	-25.44	29.02	-6.27	6.52
<b>S. Hadley</b>	375.69	350.93	10800	0.91	-24.76	29.07	-6.59	7.02
<b>S. Ferrel</b>	299.44	299.11	10800	0.94	-0.34	11.47	-0.11	3.18
<b>S. Polar</b>	134.46	149.12	10440	0.96	14.66	25.72	10.90	15.32
<b>N.H.</b>	341.51	340.34	32040	0.96	-1.16	23.42	-0.34	5.87
<b>S.H.</b>	271.39	267.70	32040	0.99	-3.68	23.34	-1.36	6.93
<b>Global</b>	306.45	304.02	64080	0.98	-2.42	23.38	-0.79	6.34
<b>BSRN</b>	350.01	325.69	29	0.93	-24.32	32.81	-6.95	7.28

**4.4.1.5 Summer Daily Precipitation Rate**

The daily precipitation at the surface in GWRf is compared with the Global Precipitation Climatology Project (GPCP) for the summer of 2001. Overall, the GWRf CMP1 performance during summer appears to be overestimating daily precipitation rate and performing similar to the baseline simulation, due to the large similarities between Figure 4.118 and Figure 4.23. Maximum and minimum mean bias values are very similar between the CMP1 and BASE simulations, indicating that the choice of microphysics parameterization does not largely influence daily precipitation rate. Globally, CMP1 shows a slightly lower Corr value of 0.80 as compared to the 0.83 in the BASE case, while NMB values are slightly better than BASE with values of 34.77% and 38.64% respectively. Evaluation of GWRf with monthly mean NCDC precipitation data is consistent with the finding that WSM6 gives a slightly improved estimate of precipitation, reducing the overestimation present in the BASE simulation. CMP1 has an NCDC mean NMB value of 19.83%, while BASE has an NCDC mean NMB value of 25.29%

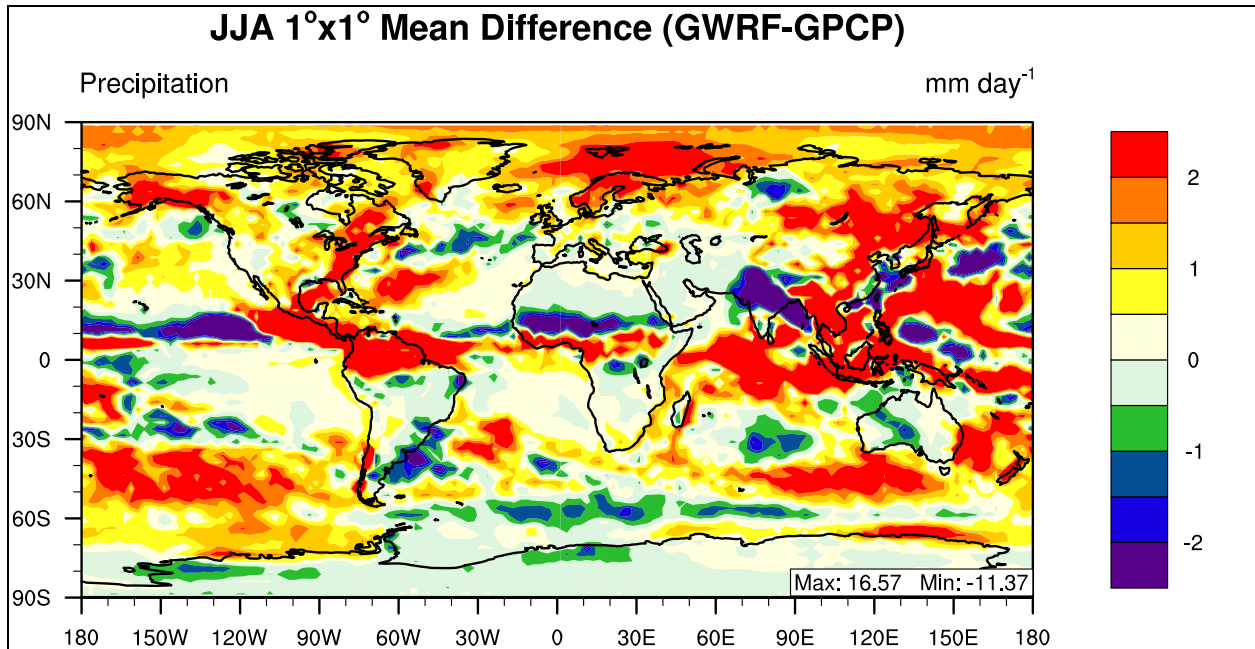


**Figure 4.118** 2001 summer mean bias of daily precipitation rate.

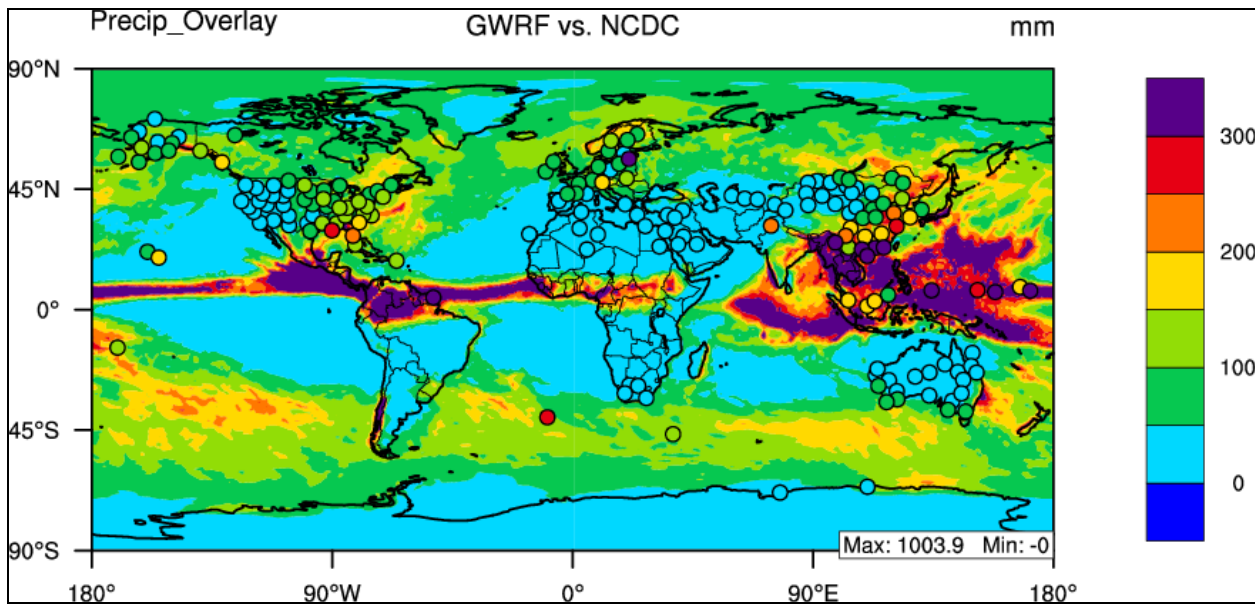


**Figure 4.119** 2001 summer mean bias of monthly precipitation rate as compared to NCDC.

**Table 4.66 Performance Statistics of GWRf mean daily rainfall rate for summer 2001 compared with GPCP (mm day<sup>-1</sup>) and NCDC (mm month<sup>-1</sup>).**

<b>Name</b>	<b>MeanObs</b>	<b>MeanMod</b>	<b>Number</b>	<b>Corr</b>	<b>MB</b>	<b>RMSE</b>	<b>NMB%</b>	<b>NME%</b>
<b>Europe</b>	2.37	3.23	192	0.66	0.86	1.31	36.11	43.58
<b>Africa</b>	1.26	1.45	463	0.87	0.20	1.20	15.52	55.01
<b>Asia</b>	3.29	3.96	816	0.78	0.68	2.51	20.61	49.71
<b>Australia</b>	0.98	1.09	192	0.78	0.11	0.83	10.67	59.60
<b>N.A.</b>	2.49	3.57	384	0.73	1.08	1.70	43.23	49.93
<b>S.A.</b>	3.00	3.84	392	0.81	0.84	2.67	28.04	52.60
<b>N. Pole</b>	1.17	2.44	1728	0.55	1.27	1.49	108.41	112.16
<b>N. Ferrel</b>	2.30	2.96	1727	0.71	0.66	1.49	28.57	46.00
<b>N. Hadley</b>	4.04	5.18	1724	0.76	1.14	3.36	28.14	53.09
<b>S. Hadley</b>	1.79	2.45	1728	0.85	0.67	1.84	37.46	58.47
<b>S. Ferrel</b>	3.08	3.84	1728	0.45	0.76	1.50	24.72	37.33
<b>S. Polar</b>	0.97	1.11	1728	0.84	0.15	0.68	15.05	45.30
<b>N.H.</b>	2.50	3.53	5179	0.78	1.02	2.29	40.79	60.13
<b>S.H.</b>	1.94	2.47	5184	0.83	0.53	1.43	27.01	45.13
<b>Global</b>	2.22	3.00	10363	0.80	0.77	1.91	34.77	53.57
<b>NCDC</b>	93.20	111.67	172	0.66	18.48	89.37	19.83	56.85

#### **4.4.2 Purdue-Lin Summer (JJA) mean evaluation**

##### **4.4.2.1 Summer Temperature at 2-meter**

The temperature at 2-meters above the surface for GWRf sensitivity simulation CMP2 is compared with NCEP/NCAR Reanalysis for the summer of 2001. This sensitivity simulation replaces the WRF Single Moment 3-Class (WSM3) from the baseline simulation with the Purdue-Lin microphysics scheme. The largest difference between Figures 4.11 and 4.120 is that the CMP2 simulation creates large areas of overestimation over Antarctica and Greenland, indicating that may not be suitable for use in the Polar Regions. Over the continents the model recreates the general pattern of the baseline simulation except for smaller errors over oceanic surfaces and larger errors over Northern Africa and the Middle East. Globally, CMP2 shows worse statistical performance than the baseline simulation with a Corr value of 0.96 (baseline

simulation is 0.99), and a NMB value of 57.30% which is much larger than the baseline value (2.70%). This global value is dominated by the huge overestimations over the Polar Regions, with a CMP2 value of 41.03% for the North Pole and 66.99% for the South Pole, as shown in Table 4.67. The large overestimation of temperatures over the Antarctic and Greenland are also present when comparing Figures 4.121 and 4.12 in which the minimum GWRP T2 values is -72.49 °C in the baseline simulation and only -27.52 °C in CMP2. The errors over the poles are not reflected in the mean NCDC analysis because of a lack of stations in Greenland and only 3 out of the 199 stations being in Antarctica.

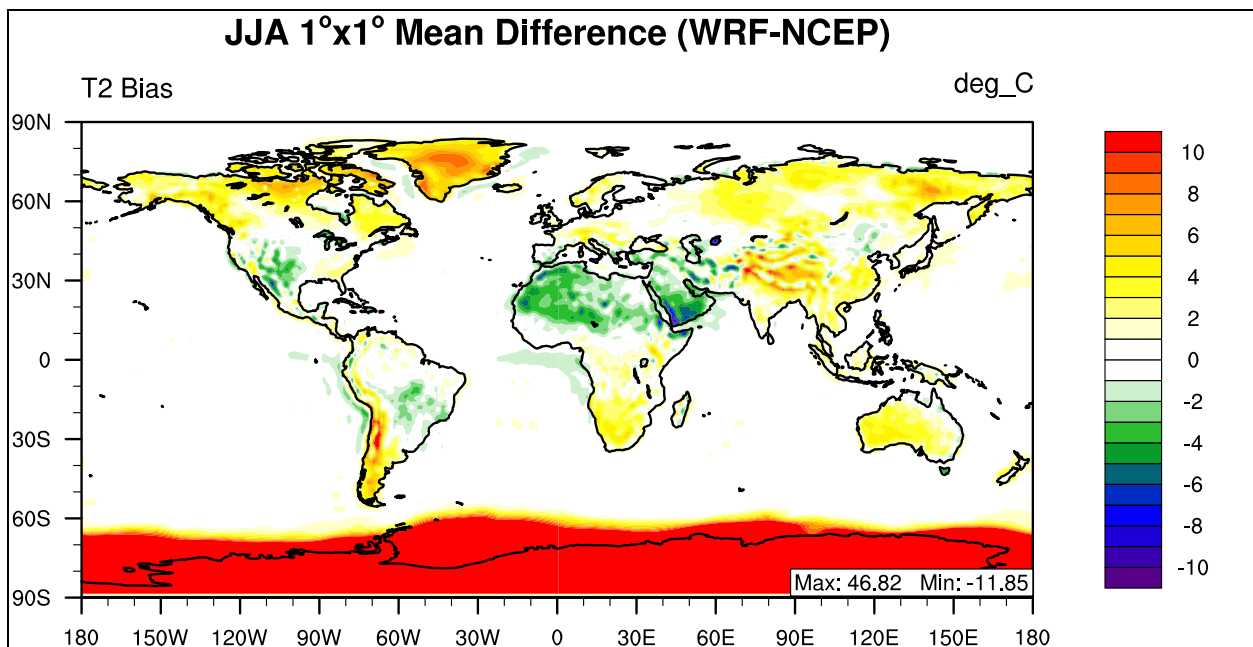


**Figure 4.120 2001 summer mean bias of temperature at 2-meter.**

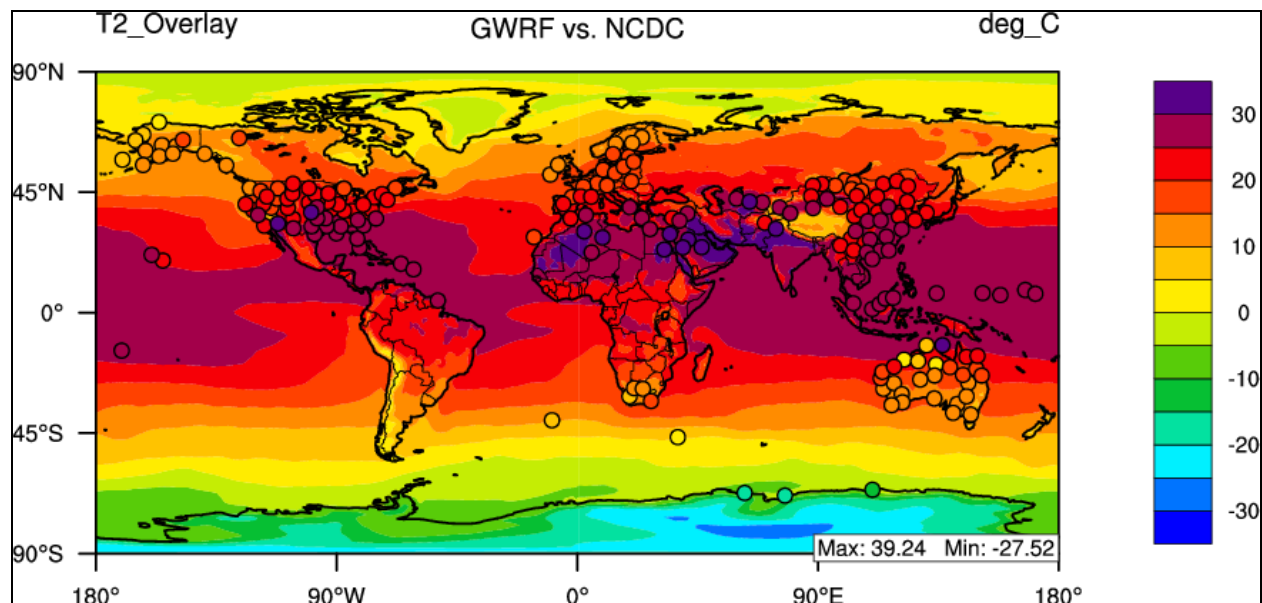
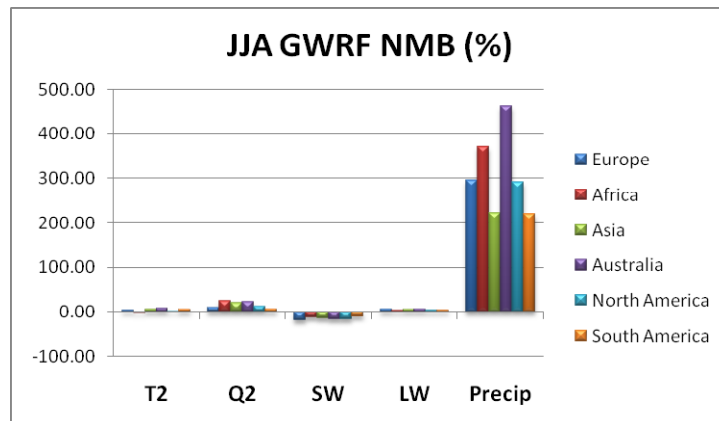


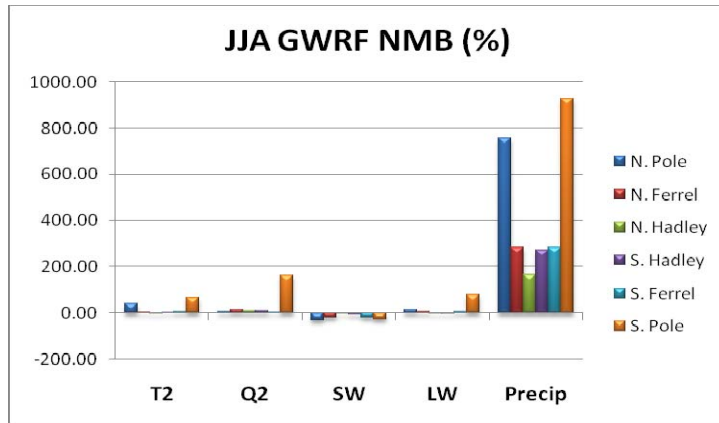
Figure 4.121 2001 summer temperature at 2-meter as compared with NCDC.

Table 4.67 Performance Statistics of GWRf summer mean temperature at 2-meter as compared with NCEP/NCAR Reanalysis and NCDC.

Name	MeanObs	MeanMod	Number	Corr	MB	RMSE	NMB%	NME%
Europe	16.43	17.15	1200	0.96	0.72	1.44	4.40	6.43
Africa	23.83	23.56	2925	0.94	-0.27	2.11	-1.15	6.89
Asia	20.72	21.97	5100	0.95	1.25	2.69	6.04	9.95
Australia	17.02	18.37	1200	0.97	1.35	2.05	7.91	8.98
N.A.	20.51	20.93	2400	0.96	0.42	1.79	2.03	6.37
S.A.	14.76	15.54	2450	0.97	0.78	2.38	5.26	9.99
N. Pole	3.20	4.51	10438	0.93	1.31	2.50	41.03	49.55
N. Ferrel	17.65	18.37	10800	0.96	0.72	1.90	4.10	7.23
N. Hadley	26.64	26.64	10800	0.89	0.00	1.46	0.01	3.39
S. Hadley	22.26	22.81	10800	0.96	0.55	1.34	2.47	3.89
S. Ferrel	8.10	8.64	10800	0.98	0.54	1.25	6.63	7.76
S. Pole	-34.51	-11.39	10440	0.96	23.12	25.94	66.99	66.99
N.H.	15.97	16.64	32038	0.99	0.67	2.00	4.21	7.83
S.H.	-1.01	6.89	32040	0.97	7.90	14.85	780.98	794.55
Global	7.48	11.77	64078	0.96	4.29	10.59	57.30	62.08
NCDC	20.78	20.74	199	0.86	-0.03	4.24	-0.17	11.49

An overview of CMP2 summer statistical performance for the major boundary layer variables is shown graphically in Figure 4.122. The CMP2 simulation, as in the BASE case, exhibits the largest overestimation of any of the GWRf simulations of daily precipitation rate across all domains; however these NMB values are much larger than any other GWRf configuration explored in this study. The largest overestimations are in the Polar Regions, furthering the observation that the advanced mixed-phase and ice treatments within the Purdue-Lin scheme are not appropriate for the Polar Regions in GWRf. The vertical profile of temperature performance is explored in Figure 4.123 which is the zonal mean bias of GWRf versus NCEP/NCAR Reanalysis data. This figure shows the worst model and observation agreement of any of the model simulations. In CMP2, GWRf is too cold above the tropopause and almost exclusively too warm in the middle and lower troposphere.





**Figure 4.122** 2001 summer mean normalized mean bias (%) of major meteorological variables for (a) the six continental domains and (b) the six circulation cell domains.

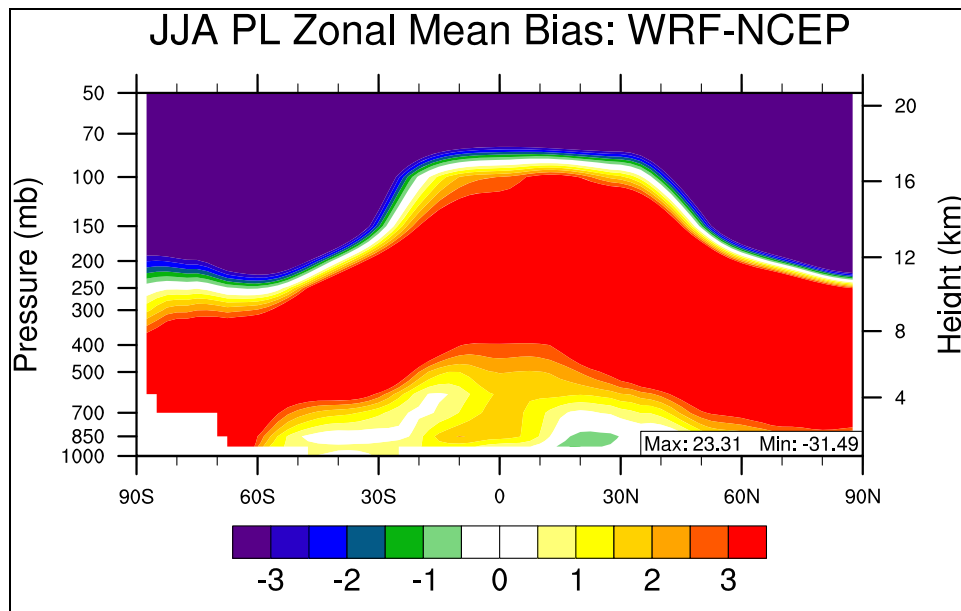


**Figure 4.123** 2001 summer zonal mean bias of Temperature

#### 4.4.2.2 Summer Water Vapor Mixing ratio at 2-meter

The global distribution of CMP2 summer mean bias for water vapor mixing ratio at 2-meters is displayed in Figure 4.124. When compared with the baseline simulation spatial mean bias plot, the overall pattern for CMP2 is an overestimation of Q2, with a global NMB value of

11.96%, which is much different than the overall underestimation exhibited by the BASE case. The overall overestimation of Q2 is also reflected in Table 4.68 in which all domains have a positive NMB value, which is much different than the BASE case. The largest overestimation is over the South Pole with a NMB value of 162.92%. Large overestimations exist over arid regions such as North Africa, the Arabian Peninsula, and the interior of Australia. Large overestimations also exist over oceanic surfaces, a trend not present in the baseline simulation. Overall Corr values are slightly worse than baseline performance, with a global Corr value of 0.98.

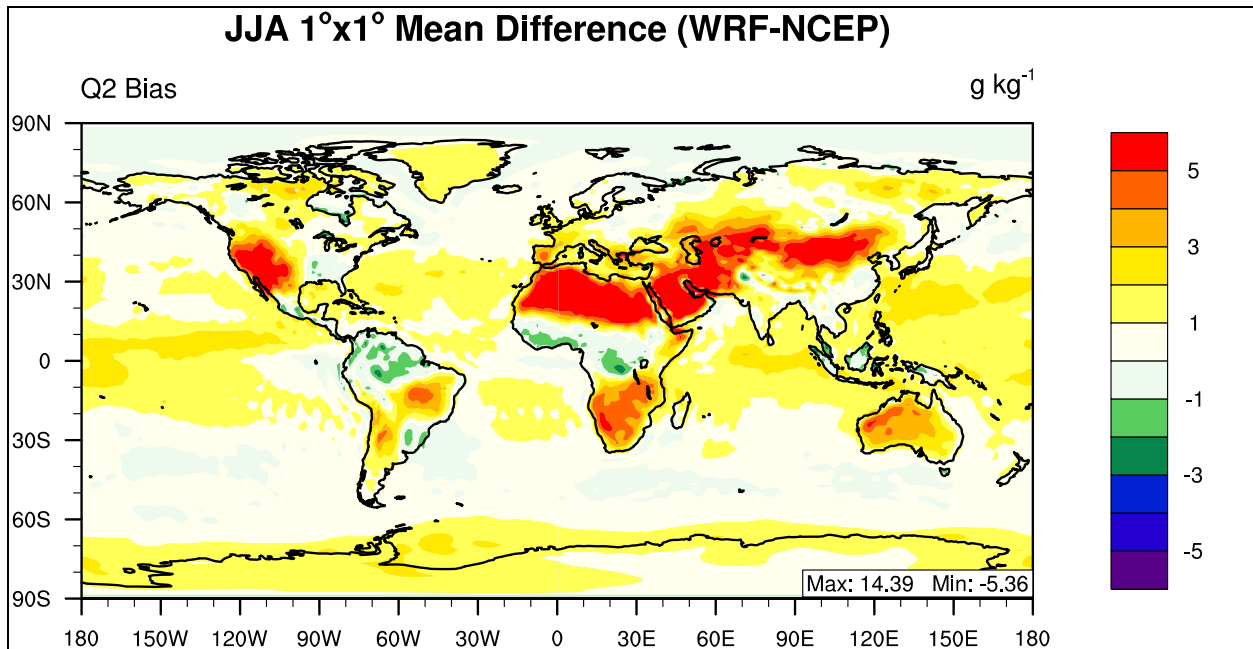


**Figure 4.124 2001 summer mean bias of water vapor mixing ratio at 2-meter.**

**Table 4.68 Performance Statistics of GWRP 2001 summer mean water vapor mixing ratio at 2-meter as compared with NCEP/NCAR Reanalysis.**

<b>Name</b>	<b>MeanObs</b>	<b>MeanMod</b>	<b>Number</b>	<b>Corr</b>	<b>MB</b>	<b>RMSE</b>	<b>NMB%</b>	<b>NME%</b>
<b>Europe</b>	9.83	10.72	1200	0.92	0.89	1.32	9.06	9.76
<b>Africa</b>	10.88	13.53	2925	0.84	2.64	3.70	24.27	26.40
<b>Asia</b>	11.86	14.18	5100	0.93	2.32	3.09	19.53	20.10
<b>Australia</b>	8.53	10.50	1200	0.95	1.97	2.38	23.08	23.38
<b>N.A.</b>	12.34	13.92	2400	0.91	1.59	2.42	12.88	14.29
<b>S.A.</b>	10.02	10.66	2450	0.96	0.64	1.51	6.38	10.90
<b>N. Pole</b>	4.94	5.29	10440	0.95	0.35	0.83	7.04	11.01
<b>N. Ferrel</b>	10.18	11.77	10800	0.87	1.59	2.36	15.63	16.26
<b>N. Hadley</b>	16.78	18.45	10800	0.90	1.68	2.43	9.99	10.85
<b>S. Hadley</b>	13.91	15.17	10800	0.96	1.27	1.70	9.10	9.92
<b>S. Ferrel</b>	6.18	6.44	10800	0.98	0.25	0.53	4.11	5.00
<b>S. Polar</b>	0.74	1.94	10440	0.86	1.20	1.30	162.92	162.93
<b>N.H.</b>	10.70	11.91	32040	0.96	1.21	2.03	11.36	12.61
<b>S.H.</b>	7.01	7.91	32040	0.99	0.90	1.27	12.88	13.70
<b>Global</b>	8.85	9.91	64080	0.98	1.06	1.69	11.96	13.04

#### **4.4.2.3 Summer Downward Shortwave Flux at ground surface**

The pattern of CMP2 summer downward shortwave flux mean bias depicts an overall pattern of underestimation when compared with the BASE simulation and is displayed graphically in Figure 4.125. It differs from the baseline pattern with only slight overestimations in the Tropics, and very large underestimations at high latitudes in the Northern hemisphere, with every domain (except the slightly positive Northern Hadley cell) having a negative NMB value as shown in Table 4.69. There are also large areas of underestimation off the West coasts of Africa and South America in the Southern Hadley Cell, which are worse than in the baseline simulation. From a comparison between Figures 4.17 and 4.125, CMP2 creates large areas of underestimation over the North Pole, with a NMB value (-32.02%) much worse than the corresponding baseline value (-8.43%), which most likely is a result of the complex treatment of ice in the WSM6 microphysics scheme. The CMP2 simulation has a global NMB value of -

15.55%, which is much less than the BASE simulation NMB of 3.97%. Overall the CMP2 simulation displays slightly worse correlation values than the baseline simulation, with values of 0.92 and 0.93 respectively. BSRN data is consistent with the NCEP/NCAR reanalysis in which the CMP2 produces an overall underestimation of SWDOWN, which is the only simulation in which this occurs. A comparison of BSRN evaluation between the BASE and CMP2 simulations yields very different statistical performance with NMBs of and 23.53% and -3.75%.

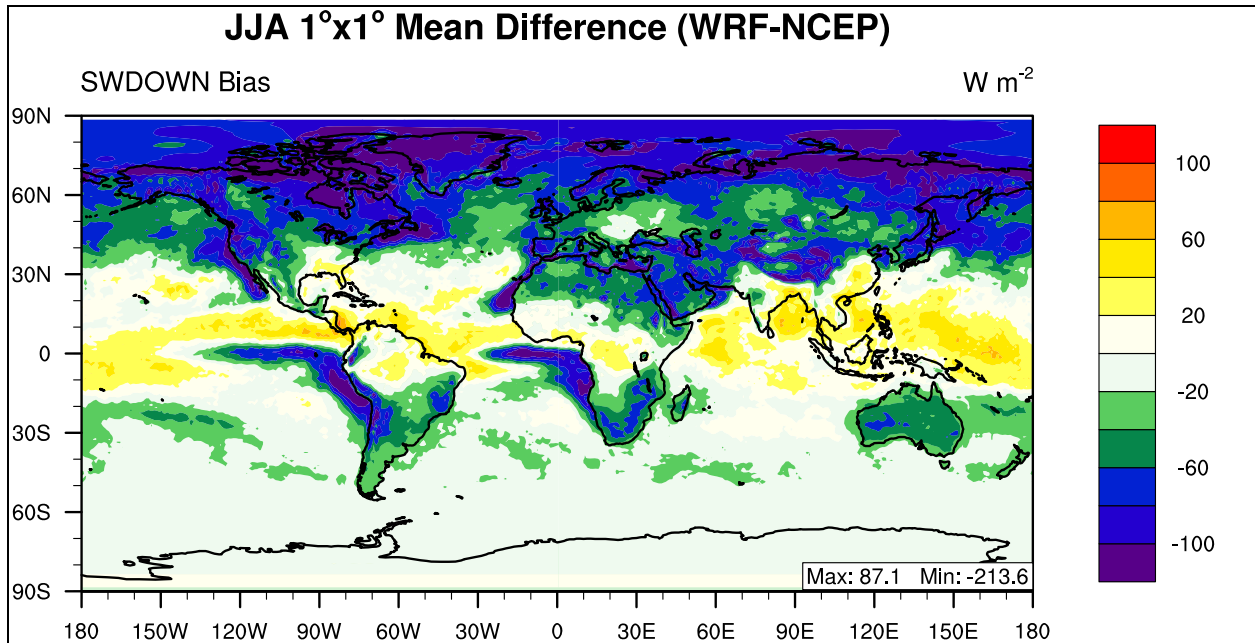


**Figure 4.125** 2001 summer mean bias of downward shortwave flux at the surface.

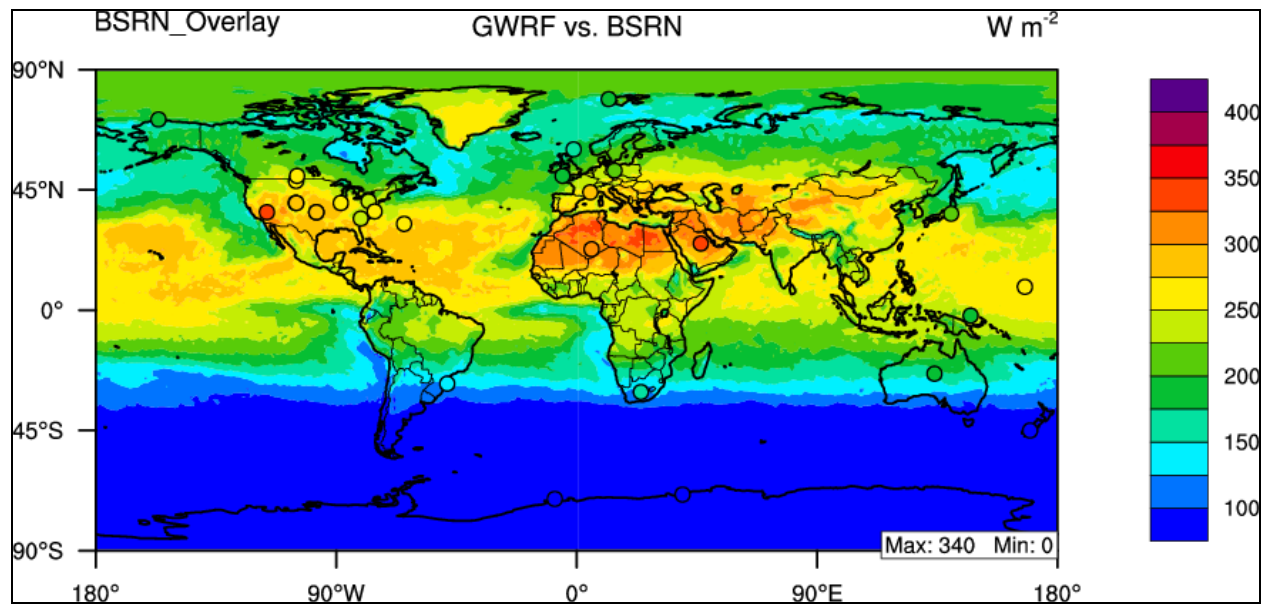


**Figure 4.126** 2001 summer mean bias of downward shortwave flux at the surface as compared to BSRN.

**Table 4.69 Performance Statistics of GWRP 2001 summer mean downward shortwave flux at the surface as compared with NCEP/NCAR Reanalysis and BSRN.**

<b>Name</b>	<b>MeanObs</b>	<b>MeanMod</b>	<b>Number</b>	<b>Corr</b>	<b>MB</b>	<b>RMSE</b>	<b>NMB%</b>	<b>NME%</b>
<b>Europe</b>	276.03	222.99	1200	0.81	-53.04	58.66	-19.22	19.22
<b>Africa</b>	267.44	232.56	2925	0.85	-34.88	49.67	-13.04	15.14
<b>Asia</b>	282.36	240.59	5100	0.54	-41.77	60.65	-14.79	19.14
<b>Australia</b>	187.27	155.66	1200	0.89	-31.61	37.93	-16.88	18.06
<b>N.A.</b>	287.47	240.28	2400	0.41	-47.19	61.82	-16.42	17.85
<b>S.A.</b>	159.45	140.98	2450	0.92	-18.47	35.78	-11.59	18.12
<b>N. Pole</b>	278.24	189.16	10440	0.72	-89.09	91.25	-32.02	32.02
<b>N. Ferrel</b>	276.45	221.85	10800	0.82	-54.60	61.60	-19.75	20.06
<b>N. Hadley</b>	257.37	259.46	10800	0.52	2.09	36.12	0.81	10.92
<b>S. Hadley</b>	201.96	188.45	10800	0.63	-13.52	35.17	-6.69	13.21
<b>S. Ferrel</b>	79.47	63.84	10800	0.97	-15.63	17.66	-19.67	19.73
<b>S. Polar</b>	8.77	6.35	7920	0.99	-2.42	3.21	-27.64	27.64
<b>N.H.</b>	270.60	223.87	32040	0.39	-46.73	66.57	-17.27	21.13
<b>S.H.</b>	105.32	94.00	29520	0.97	-11.31	23.86	-10.74	15.33
<b>Global</b>	191.34	161.60	61560	0.92	-29.75	50.79	-15.55	19.60
<b>BSRN</b>	218.83	210.63	29	0.96	-8.20	24.55	-3.75	8.85

#### **4.4.2.4 Summer Downward Longwave Flux at ground surface**

The pattern of summer downward longwave flux mean bias is displayed graphically in Figure 4.127 in which the overall pattern is a slight underestimation over the Tropics and an overestimation over the high latitudes, with a global NMB value of 9.64%, much larger than the baseline simulation (-4.14%). Similar to Figure 4.120 for T2, there are huge overestimations over the Polar Regions, with NMB values of 14.71% and 77.75% for the North and South poles, respectively. These values are much larger than their corresponding baseline simulation values with NMB values of -0.42% and -2.29% for the North and South Poles, respectively. Globally, the Corr value for the CMP2 simulation (0.97) is slightly less than the baseline simulations (0.98). BSRN evaluation reveals that CMP2 is the only simulation which overestimates GLW, while the rest of the simulations largely underestimate this field, indicating the large

overestimation of clouds when using the Purdue-Lin scheme on a global scale. CMP2 produces a much larger NMB value (2.35%) than the corresponding baseline simulation value (-9.17%).

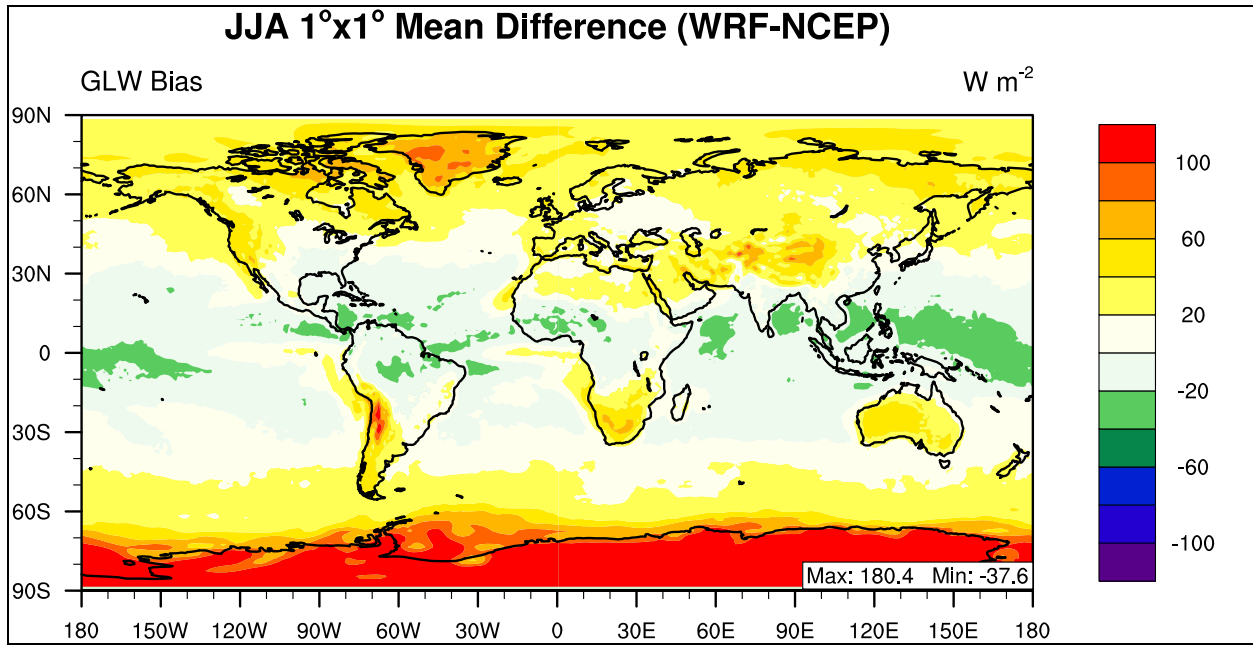


**Figure 4.127** 2001 summer mean bias of downward longwave flux at the surface.

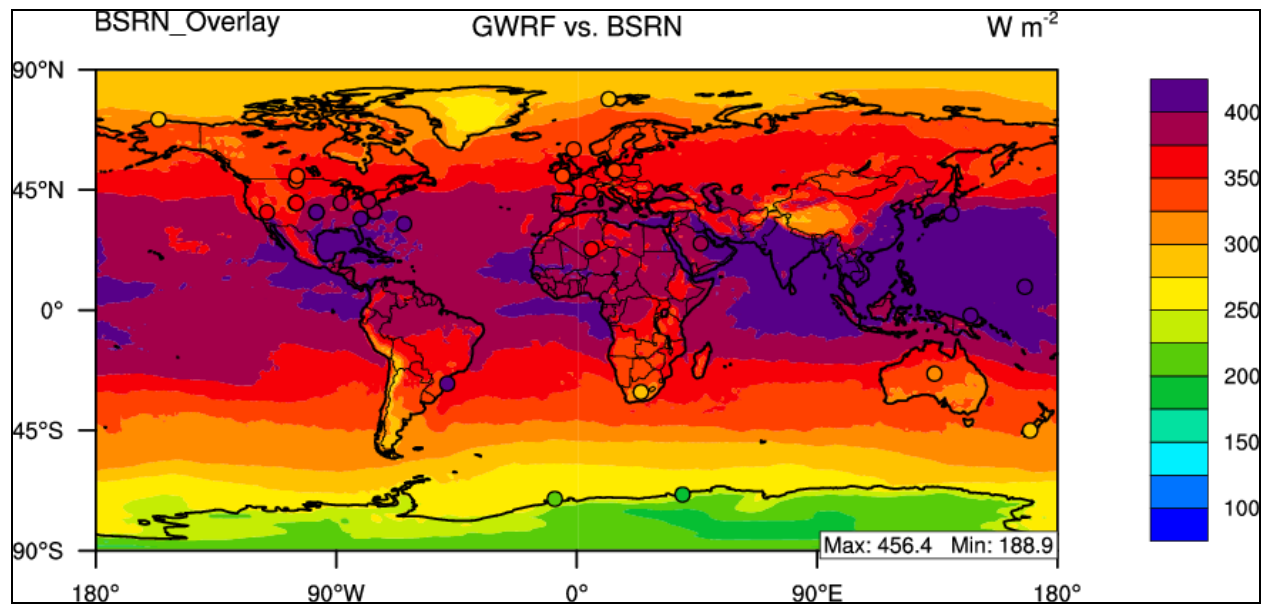


**Figure 4.128** 2001 summer downward longwave flux at the surface as compared with BSRN.

**Table 4.70 Performance Statistics of GWRf 2001 summer mean downward longwave flux at the surface as compared with NCEP/NCAR Reanalysis and BSRN.**

<b>Name</b>	<b>MeanObs</b>	<b>MeanMod</b>	<b>Number</b>	<b>Corr</b>	<b>MB</b>	<b>RMSE</b>	<b>NMB%</b>	<b>NME%</b>
<b>Europe</b>	333.15	355.32	1200	0.86	22.17	24.11	6.66	6.66
<b>Africa</b>	363.04	375.46	2925	0.75	12.42	24.02	3.42	5.41
<b>Asia</b>	355.61	375.98	5100	0.93	20.37	30.31	5.73	7.38
<b>Australia</b>	325.16	347.30	1200	0.94	22.14	29.84	6.81	7.80
<b>N.A.</b>	358.63	373.91	2400	0.93	15.27	24.68	4.26	5.72
<b>S.A.</b>	333.45	347.17	2450	0.95	13.72	29.69	4.11	7.07
<b>N. Pole</b>	272.40	312.47	10440	0.91	40.07	41.72	14.71	14.71
<b>N. Ferrel</b>	344.05	366.98	10800	0.90	22.94	27.09	6.67	6.86
<b>N. Hadley</b>	405.77	398.77	10800	0.70	-6.99	17.05	-1.72	3.66
<b>S. Hadley</b>	375.69	375.94	10800	0.90	0.25	19.18	0.07	3.76
<b>S. Ferrel</b>	299.44	318.79	10800	0.96	19.35	22.44	6.46	6.56
<b>S. Polar</b>	134.46	239.01	10440	0.96	104.55	113.03	77.75	77.75
<b>N.H.</b>	341.51	359.94	32040	0.97	18.43	30.21	5.40	7.62
<b>S.H.</b>	271.39	312.06	32040	0.98	40.67	66.76	14.99	16.75
<b>Global</b>	306.45	336.00	64080	0.97	29.55	51.81	9.64	11.66
<b>BSRN</b>	350.01	358.23	29	0.92	8.22	28.07	2.35	5.74

#### 4.4.2.5 Summer Daily Precipitation Rate

The daily precipitation at the surface in GWRf is compared with the Global Precipitation Climatology Project (GPCP) for the summer of 2001. Overall, the GWRf CMP2 performance during summer appears to be greatly overestimating daily precipitation rate. Figure 4.129 is highly saturated, indicating that the majority of the global domain is overestimated by at least 2 mm day<sup>-1</sup>. The minimum mean bias value is very similar between the CMP1 and BASE simulations with respective values of -10.25 and -9.82, however the CMP2 simulation has a much larger maximum mean bias with respective values of 49.78 and 15.93, indicating that the Purdue-Lin microphysics parameterization overestimates precipitation of almost 50 mm day<sup>-1</sup>. Globally, CMP2 shows a much lower Corr value of 0.60 as compared to the 0.83 in the BASE case, while NMB values are much worse than BASE with values of 334.31% and 38.64% respectively. The overestimation of precipitation by CMP2 during this period is consistent with

the NCDC evaluation shown in Figure 4.130. Statistically, CMP2 is the worst simulation for precipitation evaluation with NCDC with a mean NMB value of 205.48%, as compared to the more reasonable 25.29% in the baseline simulation.

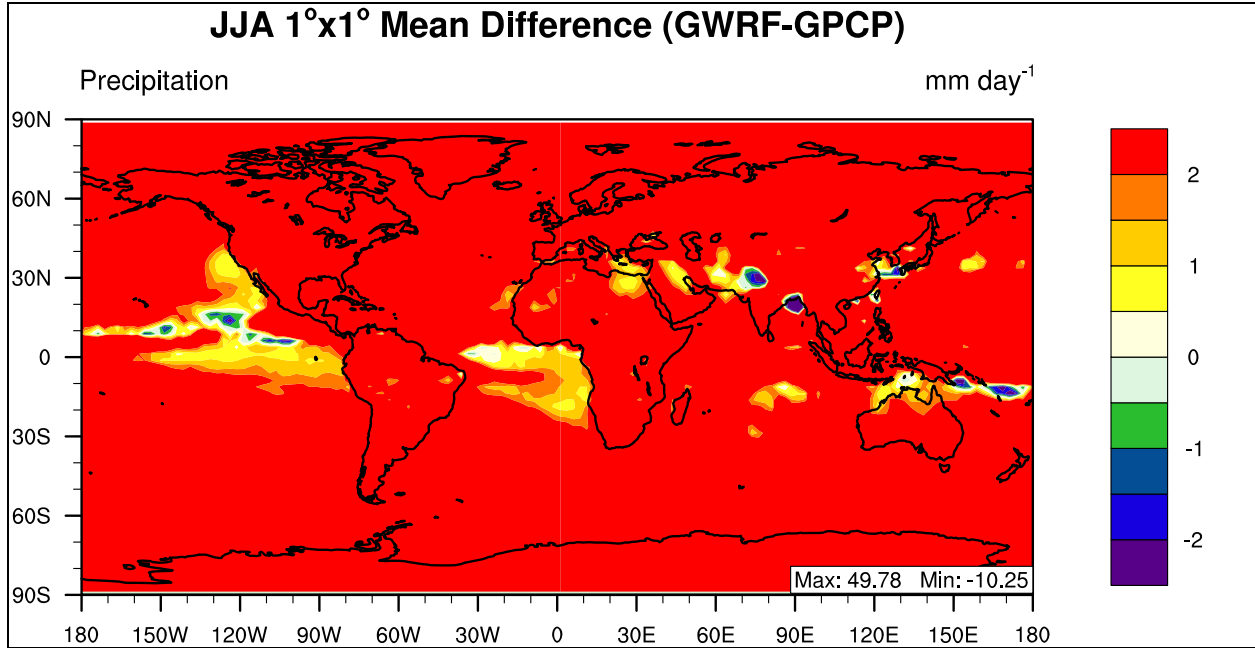


**Figure 4.129** 2001 summer mean bias of daily precipitation rate.

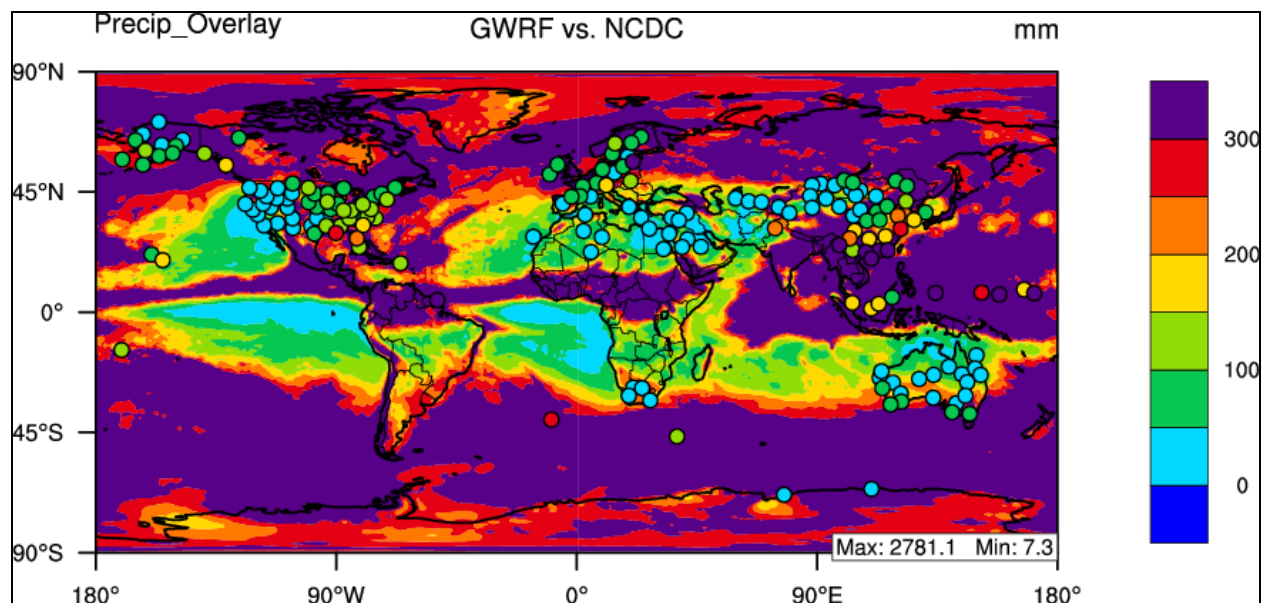


**Figure 4.130 2001 summer mean bias of daily precipitation rate.**

**Table 4.71 Performance Statistics of GWRP 2001 summer mean precipitation rate for summer 2001 compared with GPCP (mm day<sup>-1</sup>) and NCDC (mm month<sup>-1</sup>).**

Name	MeanObs	MeanMod	Number	Corr	MB	RMSE	NMB%	NME%
Europe	2.37	9.37	192	0.58	7.00	7.49	295.57	295.57
Africa	1.26	5.92	463	0.68	4.66	6.42	370.33	370.62
Asia	3.29	10.57	816	0.63	7.28	8.43	221.69	226.09
Australia	0.98	5.53	192	0.83	4.54	5.35	461.41	461.41
N.A.	2.49	9.74	384	0.57	7.25	7.76	291.02	291.02
S.A.	3.00	9.61	392	0.72	6.62	7.28	221.00	221.00
N. Pole	1.17	10.04	1728	0.48	8.87	8.95	757.66	757.66
N. Ferrel	2.30	8.83	1727	0.54	6.53	7.10	283.42	284.21
N. Hadley	4.04	10.74	1724	0.65	6.69	8.50	165.52	167.81
S. Hadley	1.79	6.64	1728	0.78	4.85	6.10	271.80	273.52
S. Ferrel	3.08	11.78	1728	0.51	8.70	8.92	282.49	282.49
S. Polar	0.97	9.94	1728	0.42	8.97	9.07	926.37	926.37
N.H.	2.50	9.87	5179	0.59	7.36	8.22	294.02	295.49
S.H.	1.94	9.45	5184	0.63	7.51	8.14	386.16	386.68
Global	2.22	9.66	10363	0.60	7.44	8.18	334.31	335.37
NCDC	91.20	284.69	172	0.60	191.50	219.92	205.48	213.91

## **4.5 Sensitivity to Land Surface Modules (LSMs)**

### **4.5.1 Summer Temperature at 2-meter**

This sensitivity simulation replaces the NOAH LSM from the baseline simulation with the SLAB LSM. When Figure 4.131 is compared with Figure 4.11, there are areas of the globe that the choice of LSM has a large impact on T2. Over land surfaces in the Polar Regions, the choice of LSM has a large impact on T2 prediction as shown by the large underprediction of T2 over Greenland and the Antarctic land surface, neither of which is present in the BASE case. The choice of LSM also has an impact on the prediction over Polar ocean surfaces, with the LSM case creating slight overpredictions in the Arctic Ocean and large overpredictions in the Southern Ocean, both of which differ from the BASE case. The differences between LSM and Base simulations are not restricted to the Polar Regions. There are also large discrepancies over areas largely covered by desert such as the Arabian Peninsula, North Africa, and the interior of Australia. In all three of these regions, the LSM simulation produces lower T2 values than the baseline simulation. Globally, GWRP shows good statistical performance with a correlation value of 0.99, but an NMB value of 0.07% which is much smaller than the baseline value (2.70%).

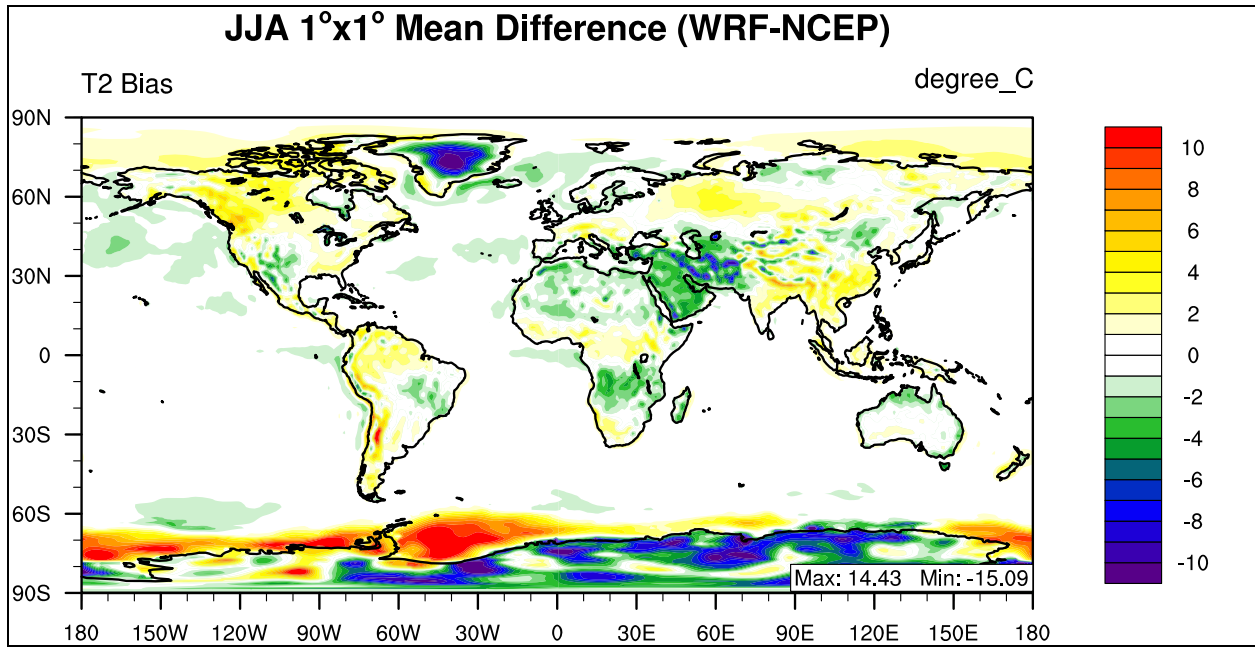


**Figure 4.131 2001 summer mean bias of temperature at 2-meter.**

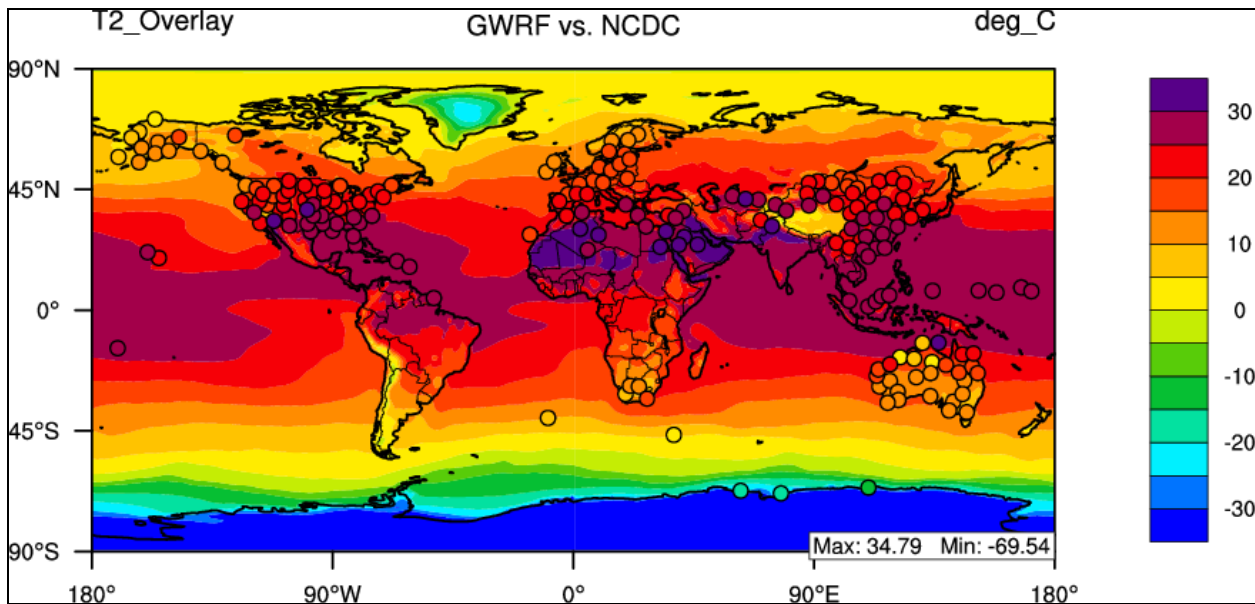


**Figure 4.132 2001 summer temperature at 2-meter as compared with NCDC.**

**Table 4.72 Performance Statistics of GWRf 2001 summer mean temperature at 2-meter as compared with NCEP/NCAR Reanalysis and NCDC.**

<b>Name</b>	<b>MeanObs</b>	<b>MeanMod</b>	<b>Number</b>	<b>Corr</b>	<b>MB</b>	<b>RMSE</b>	<b>NMB%</b>	<b>NME%</b>
<b>Europe</b>	16.43	16.34	1200	0.96	-0.08	1.32	-0.50	6.23
<b>Africa</b>	23.83	23.21	2925	0.95	-0.63	1.83	-2.62	6.01
<b>Asia</b>	20.72	20.88	5100	0.95	0.16	2.38	0.79	8.62
<b>Australia</b>	17.02	16.83	1200	0.98	-0.19	1.04	-1.12	4.36
<b>N.A.</b>	20.51	20.88	2400	0.96	0.37	1.82	1.79	6.72
<b>S.A.</b>	14.76	15.38	2450	0.98	0.62	1.96	4.19	8.48
<b>N. Pole</b>	3.20	3.79	10439	0.94	0.59	2.08	18.55	48.19
<b>N. Ferrel</b>	17.65	17.44	10800	0.95	-0.21	1.86	-1.18	7.82
<b>N. Hadley</b>	26.64	26.55	10800	0.91	-0.08	1.35	-0.31	3.20
<b>S. Hadley</b>	22.26	22.40	10800	0.97	0.14	1.14	0.65	3.14
<b>S. Ferrel</b>	8.10	8.02	10800	0.99	-0.08	0.77	-0.96	5.89
<b>S. Polar</b>	-34.51	-34.83	10440	0.97	-0.33	5.47	-0.95	12.88
<b>N.H.</b>	15.97	16.07	32039	0.99	0.10	1.79	0.60	7.86
<b>S.H.</b>	-1.01	-1.10	32040	0.99	-0.08	3.23	-8.32	182.39
<b>Global</b>	7.48	7.48	64079	0.99	0.01	2.61	0.07	20.72
<b>NCDC</b>	20.78	19.84	199	0.89	-0.94	4.04	-4.50	11.77

An overview of LSM statistical performance for the major boundary layer variables is shown graphically in Figure 4.133. The main difference between Figure 4.133 and Figure 4.13 (base case) are the large overestimations of Q2 in the LSM sensitivity study, which is discussed further in the following section (4.5.2). Overall, daily precipitation rate is still overestimated, which is similar to the base case. Large error values for the North Pole domain T2 and daily precipitation rate domain persist. The vertical profile of temperature performance is explored in Figure 4.134 which is the zonal mean bias of GWRf versus NCEP/NCAR Reanalysis data. This figure also shows that GWRf generally captures the vertical temperature distribution within  $\pm 2$  degrees up to approximately 300 hPa. The LSM simulation does share many similarities with the base case summer zonal mean bias (Figure 4.15), with large overestimations near the surface over Antarctica and the equator and underestimations of temperatures throughout the Southern Ferrel Cell. The two images do depict areas of disagreement, namely the LSM produces larger

underestimation of temperatures between 400 hPa and 100 hPa over the Tropics but does not produce the slight overestimations aloft over the Northern latitudes that is present in BASE.

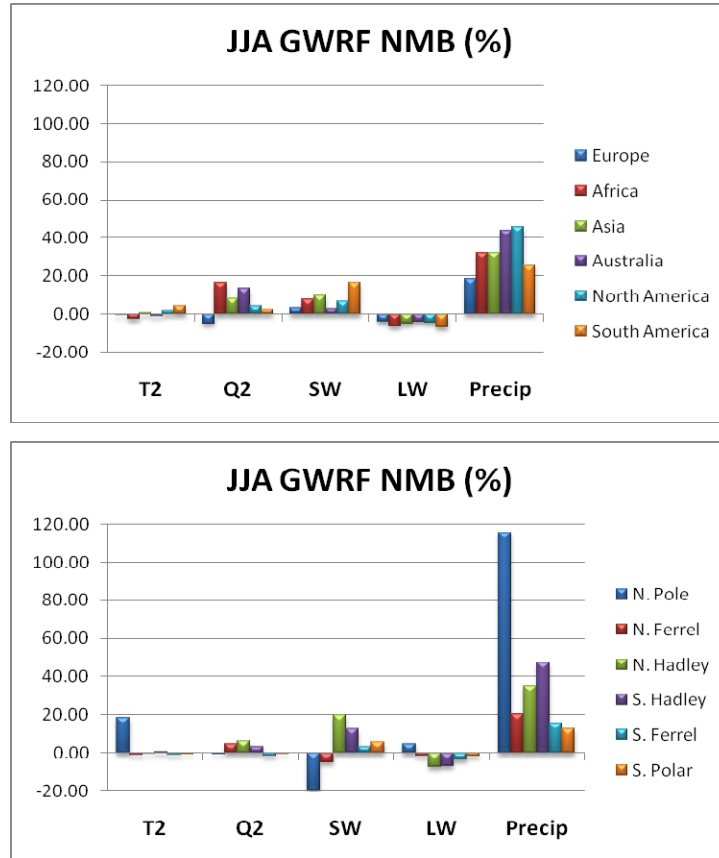


**Figure 4.133** 2001 summer mean normalized mean bias (%) of major meteorological variables for (a) the six continental domains and (b) the six circulation cell domains.

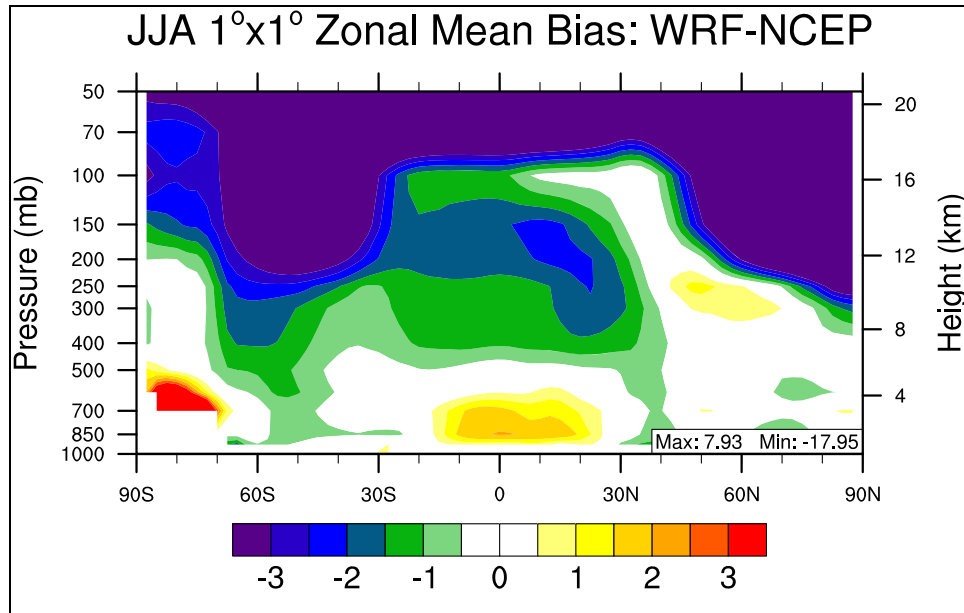


**Figure 4.134 2001 summer zonal mean bias of Temperature.**

#### **4.5.2 Summer Water Vapor Mixing ratio at 2-meter**

The global distribution of LSM summer mean bias for water vapor mixing ratio at 2-meters is displayed in Figure 4.135. Large differences exist between Figure 4.135 and Figure 4.16. The SLAB LSM creates large overestimation of Q2 over desert regions such as North Africa, the Arabian Peninsula, Western North America, and the interior of Australia. Also, the large underestimations present in BASE are much smaller in the LSM case. Overall, the SLAB LSM improves estimations over ocean surfaces. The differences between LSM and BASE for Q2 are also reflected in Table 4.73. Tropical domains (e.g., Northern and Southern Hadley Cells) which were slightly overpredicted in the BASE case show much larger overestimations in the LSM case. Also, in the baseline simulation all sub-domains displayed an underestimation of Q2, while LSM shows underestimation only in the domains: Europe, North Pole, Southern Ferrel and South Pole Cell, while the rest of the domains in LSM display an overprediction. The global LSM NMB value is 3.52% which is different than the base case whose summer value is -2.39%. Overall Corr values are similar to baseline performance, with a global Corr value of 0.98.

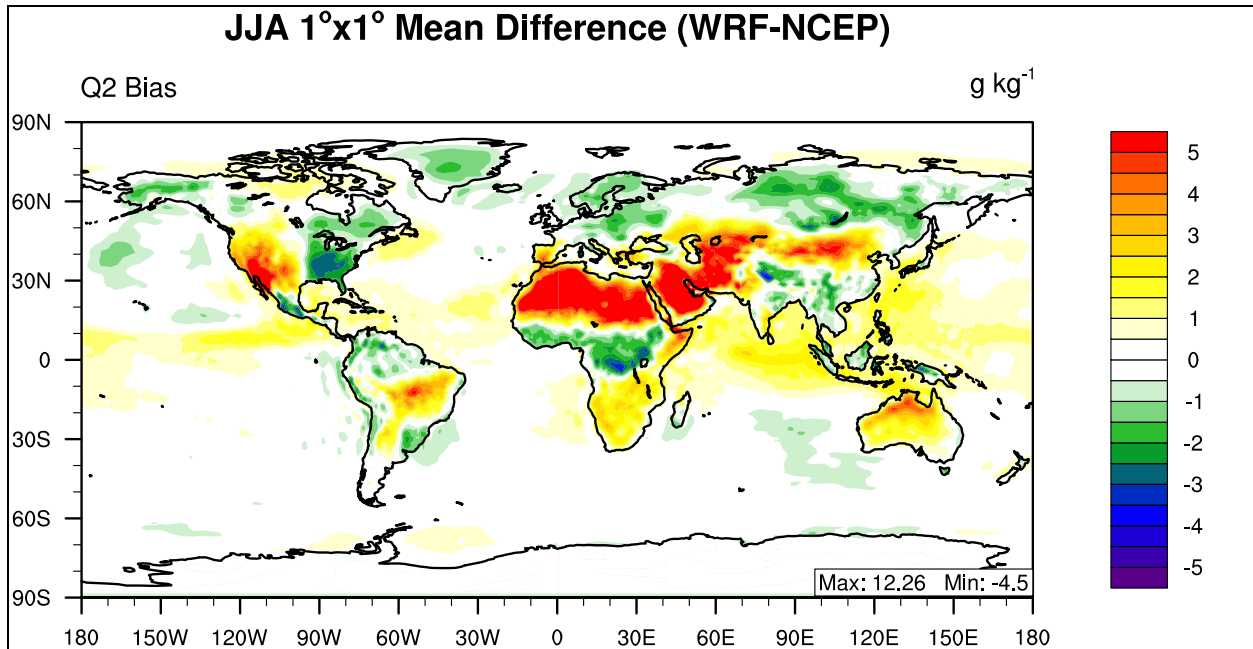


**Figure 4.135** 2001 mean bias of water vapor mixing ratio at 2-meter.

**Table 4.73** Performance Statistics of GWRF 2001 summer mean water vapor mixing ratio at 2-meter as compared with NCEP/NCAR Reanalysis.

Name	MeanObs	MeanMod	Number	Corr	MB	RMSE	NMB%	NME%
Europe	9.83	9.32	1200	0.91	-0.51	1.05	-5.20	9.04
Africa	10.88	12.67	2925	0.81	1.79	3.17	16.41	21.87
Asia	11.86	12.80	5100	0.92	0.94	2.38	7.91	14.80
Australia	8.53	9.68	1200	0.95	1.15	1.72	13.54	15.39
N.A.	12.34	12.84	2400	0.90	0.51	2.06	4.12	11.41
S.A.	10.02	10.25	2450	0.97	0.23	1.24	2.28	8.31
N. Pole	4.94	4.90	10440	0.95	-0.04	0.62	-0.90	9.31
N. Ferrel	10.18	10.65	10800	0.86	0.47	1.81	4.64	11.30
N. Hadley	16.78	17.84	10800	0.89	1.06	2.13	6.32	8.47
S. Hadley	13.91	14.37	10800	0.97	0.46	1.10	3.34	5.32
S. Ferrel	6.18	6.09	10800	0.99	-0.10	0.32	-1.56	3.73
S. Polar	0.74	0.73	10440	0.97	-0.01	0.23	-0.80	19.99
N.H.	10.70	11.20	32040	0.96	0.50	1.66	4.69	9.51
S.H.	7.01	7.13	32040	0.99	0.12	0.68	1.74	5.35
Global	8.85	9.17	64080	0.98	0.31	1.27	3.52	7.86

### 4.5.3 Summer Downward Shortwave Flux at Ground Surface

The pattern of summer downward shortwave flux mean bias is displayed graphically in Figure 4.136, and reflects the annual pattern of an overestimation in the Tropics (30°N-30°S), with large underestimations at high latitudes in the Northern hemisphere. There are also large areas of underestimation off the West coasts of Africa and South America in the Southern Hadley Cell, which are present in the baseline simulation. The LSM spatial plot displays much larger areas of underestimation over the extreme Northern latitudes than the baseline simulation. The pattern of GWRP SWDOWN underestimation in the high northern latitudes is reflected in Table 4.74 in which the same circulation cell domains as the BASE case have negative NMBs (e.g., Northern Pole and Northern Hadley Cells), except that the LSM NMB value over the North Pole (-19.67%) is over twice that of the baseline simulation (-8.43%). The LSM simulation has a global NMB value of 1.12%, which is smaller than the corresponding baseline value (3.97%). Overall the LSM simulation displays slightly worse Corr values than the baseline simulation, with values of 0.91 and 0.93, respectively. This is consistent with the BSRN evaluation in which the SLAB LSM gives a slightly lower Corr value than the BASE case with values of 0.97 and 0.98, respectively. NMB values for the BSRN evaluation are also very similar with the baseline simulation producing values of 23.53% and the LSM simulation producing a value of 24.40%, indicating a weak sensitivity of SWDOWN to LSM module.

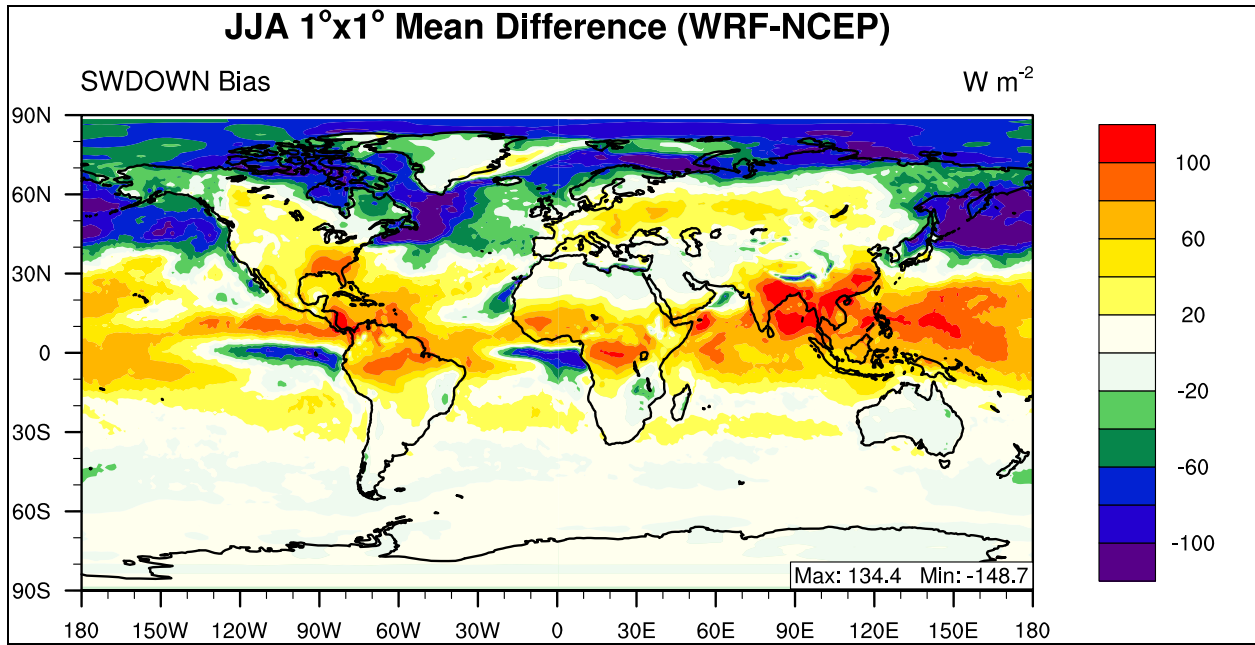


**Figure 4.136 2001 summer mean bias of downward shortwave flux at the surface.**

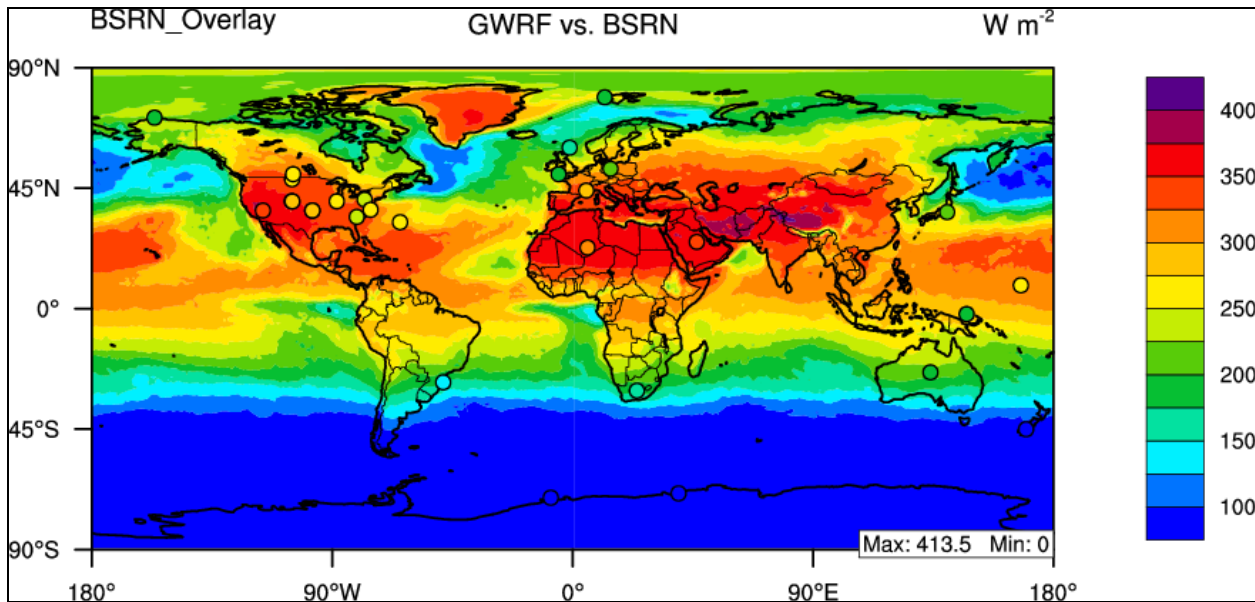


**Figure 4.137 2001 summer mean bias of downward shortwave flux at the surface as compared to BSRN.**

**Table 4.74 Performance Statistics of GWRf 2001 summer mean downward shortwave flux at the surface as compared with NCEP/NCAR Reanalysis.**

<b>Name</b>	<b>MeanObs</b>	<b>MeanMod</b>	<b>Number</b>	<b>Corr</b>	<b>MB</b>	<b>RMSE</b>	<b>NMB%</b>	<b>NME%</b>
<b>Europe</b>	276.03	284.33	1200	0.81	8.30	36.82	3.01	11.31
<b>Africa</b>	267.44	288.34	2925	0.84	20.89	42.19	7.81	11.91
<b>Asia</b>	282.36	310.09	5100	0.60	27.73	51.17	9.82	13.82
<b>Australia</b>	187.27	192.82	1200	0.93	5.55	17.11	2.97	6.52
<b>N.A.</b>	287.47	306.53	2400	0.58	19.05	43.78	6.63	12.92
<b>S.A.</b>	159.45	185.76	2450	0.96	26.30	40.42	16.50	17.96
<b>N. Pole</b>	278.24	223.51	10440	0.62	-54.73	63.35	-19.67	20.40
<b>N. Ferrel</b>	276.45	262.74	10800	0.86	-13.71	51.31	-4.96	14.36
<b>N. Hadley</b>	257.37	308.39	10800	0.53	51.02	63.26	19.82	21.77
<b>S. Hadley</b>	201.96	226.77	10800	0.71	24.80	38.55	12.28	15.22
<b>S. Ferrel</b>	79.47	82.10	10800	0.98	2.63	8.72	3.31	8.61
<b>S. Polar</b>	8.77	9.28	7920	0.99	0.51	1.29	5.79	7.96
<b>N.H.</b>	270.60	265.35	32040	0.47	-5.26	59.53	-1.94	18.76
<b>S.H.</b>	105.32	115.49	29520	0.98	10.17	23.92	9.66	13.23
<b>Global</b>	191.34	193.49	61560	0.91	2.14	46.03	1.12	17.30
<b>BSRN</b>	218.83	272.21	29	0.97	53.38	60.70	24.40	24.40

#### **4.5.4 Summer Downward Longwave Flux at Ground Surface**

The pattern of summer downward longwave flux mean bias is displayed graphically in Figure 4.138 in which the overall pattern is an underestimation with a global NMB value of -3.45%, which is a slight improvement from the annual mean. Figure 4.138 displays a very similar spatial pattern to the BASE case. The overall pattern of GWRf GLW performance is consistent with the baseline simulation, as shown in Table 4.75, in which all of the domains display a negative NMB value, with the exception of the North Pole which displays a strong overestimation with a NMB of 4.61%. Globally, the correlation value for the LSM and baseline simulations is 0.98. The BSRN evaluation also reveals similar Corr values with a baseline value of 0.93 and an LSM simulation value of 0.92, as well as very similar NMB values of -9.17% and -9.57%, indicating weak sensitivity of GLW to LSM module.

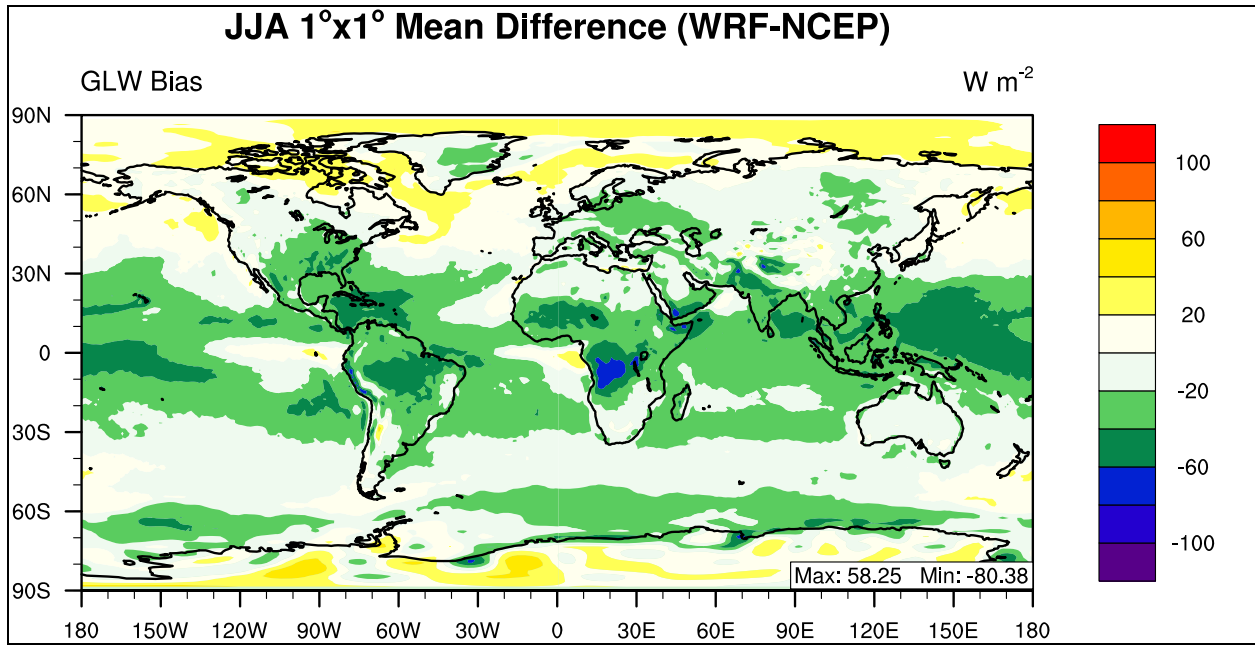


**Figure 4.138** 2001 summer mean bias of downward longwave flux at the surface.

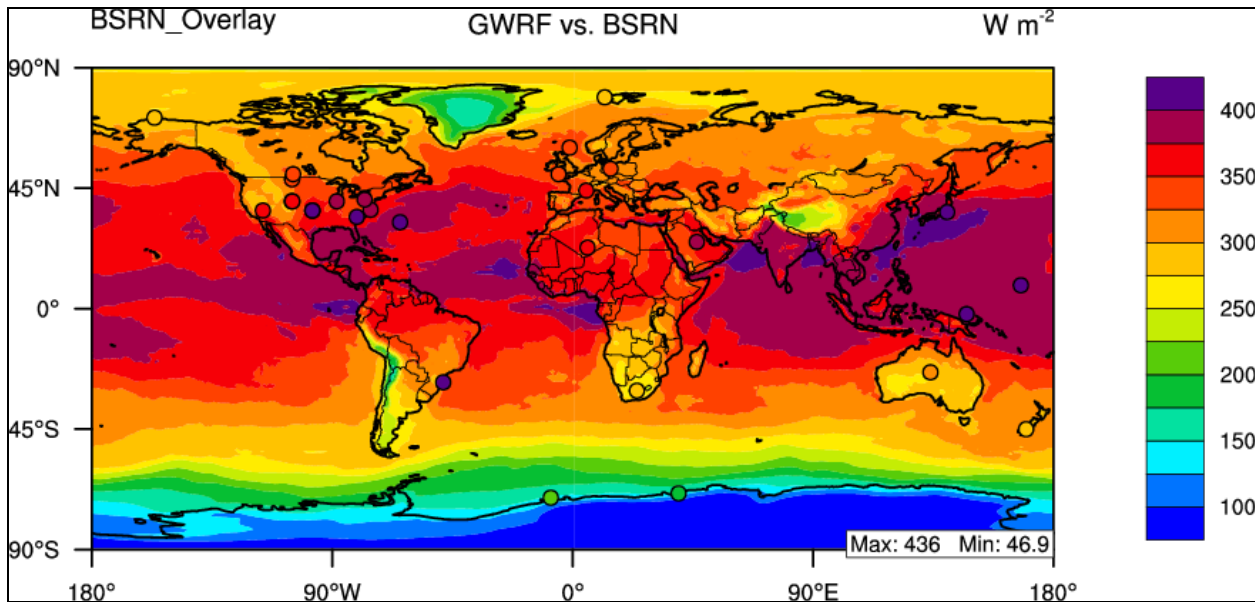


**Figure 4.139** 2001 summer mean bias of downward longwave flux at the surface as compared to BSRN.

**Table 4.75 Performance Statistics of GWRP 2001 summer mean downward longwave flux at the surface as compared with NCEP/NCAR Reanalysis.**

<b>Name</b>	<b>MeanObs</b>	<b>MeanMod</b>	<b>Number</b>	<b>Corr</b>	<b>MB</b>	<b>RMSE</b>	<b>NMB%</b>	<b>NME%</b>
<b>Europe</b>	333.15	319.87	1200	0.63	-13.27	19.17	-3.98	5.11
<b>Africa</b>	363.04	338.35	2925	0.82	-24.69	30.56	-6.80	7.24
<b>Asia</b>	355.61	337.61	5100	0.96	-18.00	23.50	-5.06	5.55
<b>Australia</b>	325.16	310.96	1200	0.98	-14.20	17.51	-4.37	4.48
<b>N.A.</b>	358.63	341.30	2400	0.93	-17.33	23.97	-4.83	5.55
<b>S.A.</b>	333.45	310.32	2450	0.97	-23.13	28.78	-6.94	7.49
<b>N. Pole</b>	272.40	284.97	10440	0.86	12.57	19.30	4.61	6.27
<b>N. Ferrel</b>	344.05	338.75	10800	0.86	-5.30	17.23	-1.54	4.19
<b>N. Hadley</b>	405.77	375.98	10800	0.77	-29.79	32.78	-7.34	7.50
<b>S. Hadley</b>	375.69	348.97	10800	0.92	-26.72	29.95	-7.11	7.29
<b>S. Ferrel</b>	299.44	288.60	10800	0.93	-10.84	15.60	-3.62	4.42
<b>S. Polar</b>	134.46	132.08	10440	0.96	-2.39	23.02	-1.77	14.44
<b>N.H.</b>	341.51	333.78	32040	0.95	-7.73	24.16	-2.26	6.06
<b>S.H.</b>	271.39	257.95	32040	0.99	-13.44	23.60	-4.95	7.38
<b>Global</b>	306.45	295.86	64080	0.98	-10.59	23.88	-3.45	6.64
<b>BSRN</b>	350.01	316.50	29	0.92	-33.51	40.97	-9.57	9.73

#### **4.5.5 Summer Daily Precipitation Rate**

The daily precipitation at the surface in GWRP is compared with the Global Precipitation Climatology Project (GPCP) for the summer of 2001. Overall, GWRP LSM performance during summer is overestimating daily precipitation rate and performing similar to the baseline simulation, due to the large similarities between Figure 4.140 and Figure 4.23. Maximum (24.52) and minimum (-11.98) mean bias values are more extreme for the LSM simulation as compared with the BASE simulations, with values of 15.93 and -9.82. This large difference indicates that the choice of LSM does have an effect on daily precipitation rate. Globally, LSM shows a lower Corr value of 0.73 as compared to the 0.83 in the BASE case, while NMB values are slightly better than BASE with values of 35.08% and 38.64% respectively. NCDC evaluation also shows an overestimation of precipitation by GWRP which is consistent with the

NCEP/NCAR Reanalysis. The LSM simulation reduces the overestimation present in the BASE case, creating a prediction closer to the NCDC observations. The NCDC LSM NMB value is 7.02%, which is better than the baseline NMB value of 25.29%.

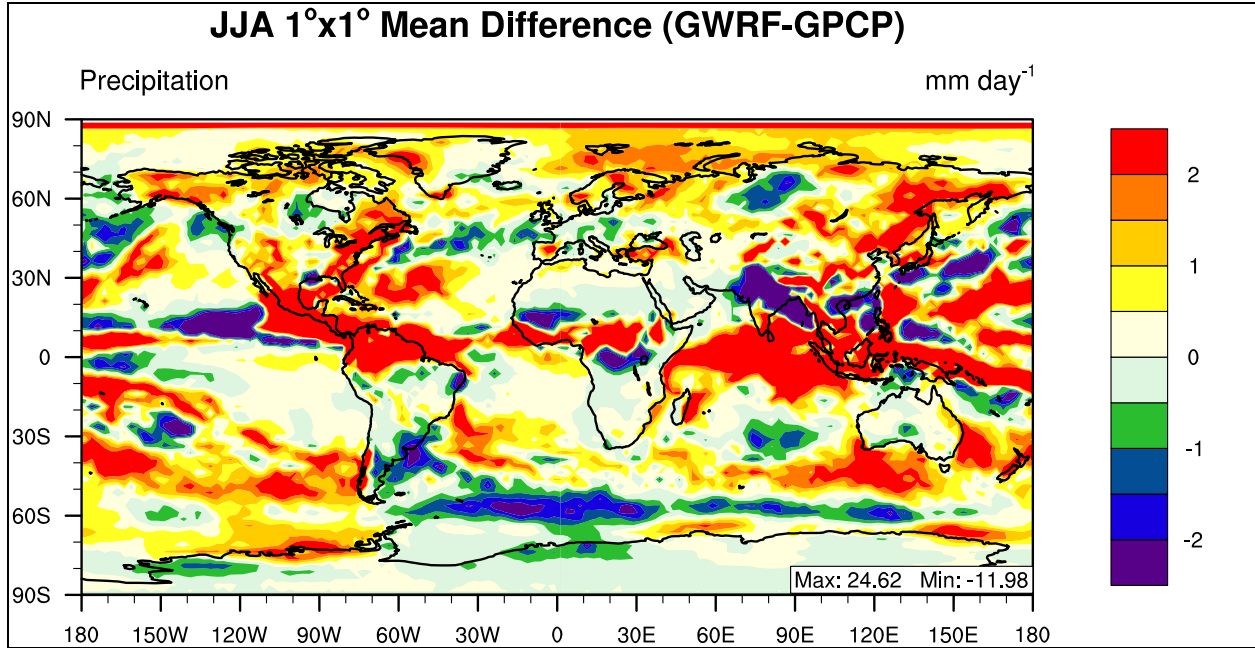


**Figure 4.140** 2001 summer mean bias of daily precipitation rate.

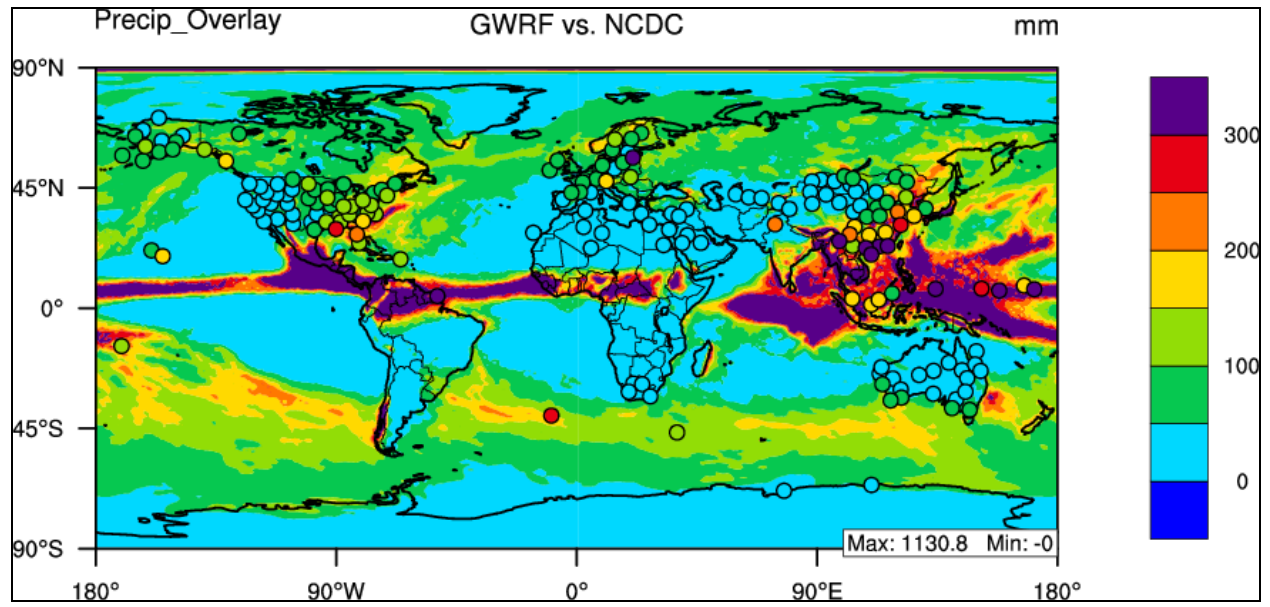


**Figure 4.141** 2001 summer monthly precipitation rate.

**Table 4.76 Performance Statistics of GWRP 2001 summer mean precipitation rate as compared with GPCP (mm day<sup>-1</sup>) and NCDC (mm month<sup>-1</sup>).**

<b>Name</b>	<b>MeanObs</b>	<b>MeanMod</b>	<b>Number</b>	<b>Corr</b>	<b>MB</b>	<b>RMSE</b>	<b>NMB%</b>	<b>NME%</b>
<b>Europe</b>	2.37	2.80	192	0.63	0.43	1.01	18.25	32.35
<b>Africa</b>	1.26	1.66	463	0.88	0.40	1.61	32.16	64.64
<b>Asia</b>	3.29	3.66	815	0.71	0.37	2.64	11.39	48.68
<b>Australia</b>	0.98	1.41	192	0.78	0.43	1.00	43.67	66.26
<b>N.A.</b>	2.49	3.63	384	0.65	1.14	1.97	45.67	57.27
<b>S.A.</b>	3.00	3.75	392	0.82	0.76	2.70	25.28	51.21
<b>N. Pole</b>	1.17	2.52	1728	0.05	1.35	2.52	115.29	123.19
<b>N. Ferrel</b>	2.30	2.77	1727	0.69	0.47	1.42	20.20	43.73
<b>N. Hadley</b>	4.05	5.47	1723	0.70	1.42	4.00	35.08	60.38
<b>S. Hadley</b>	1.79	2.63	1728	0.84	0.84	2.41	47.31	68.04
<b>S. Ferrel</b>	3.08	3.56	1728	0.44	0.48	1.38	15.69	34.97
<b>S. Polar</b>	0.97	1.09	1728	0.77	0.12	0.67	12.51	45.75
<b>N.H.</b>	2.51	3.58	5178	0.69	1.08	2.85	43.03	65.07
<b>S.H.</b>	1.94	2.43	5184	0.80	0.48	1.65	24.84	46.88
<b>Global</b>	2.22	3.00	10362	0.73	0.78	2.33	35.08	57.12
<b>NCDC</b>	93.20	99.74	172	0.67	6.54	81.80	7.02	49.14

## **4.6 Sensitivity to cumulus parameterizations**

### **4.6.1 Summer Temperature at 2-meter**

This sensitivity simulation replaces the Kain-Fritsch cumulus parameterization with the Grell-Devenyi ensemble cumulus parameterization. When Figure 4.142 is compared with Figure 4.11 the two plots agree overall, however there are areas of the globe that the choice of LSM has a large impact on T2. The choice of cumulus parameterization has an impact on the prediction over ocean surfaces, with the CCP case creating underpredictions over the majority of ocean surfaces, which are stronger than the BASE case. The differences between LSM and Base simulations are not restricted to ocean surfaces because there is also an underprediction present over Europe which is not shown in Figure 4.11. Europe displays a NMB value (-9.86%) that is more than twice as low as the baseline simulation (-4.10%). Another major difference between

CCP and BASE is that CCP creates strong underestimations for all of the circulation cell domains, while BASE has only one (Southern Ferrel Cell) domain with an underprediction. Globally, GWRP shows good statistical performance with a Corr value of 0.99, but an NMB value of -9.92% which is much worse than the baseline value (2.70%), indicating a sensitivity of T2 to cumulus parameterizations. This underestimation by CCP is also present in the NCDC evaluation of T2 in which the CCP NMB is -6.58%, this value is also worse than the NCDC BASE NMB value of -2.43%.

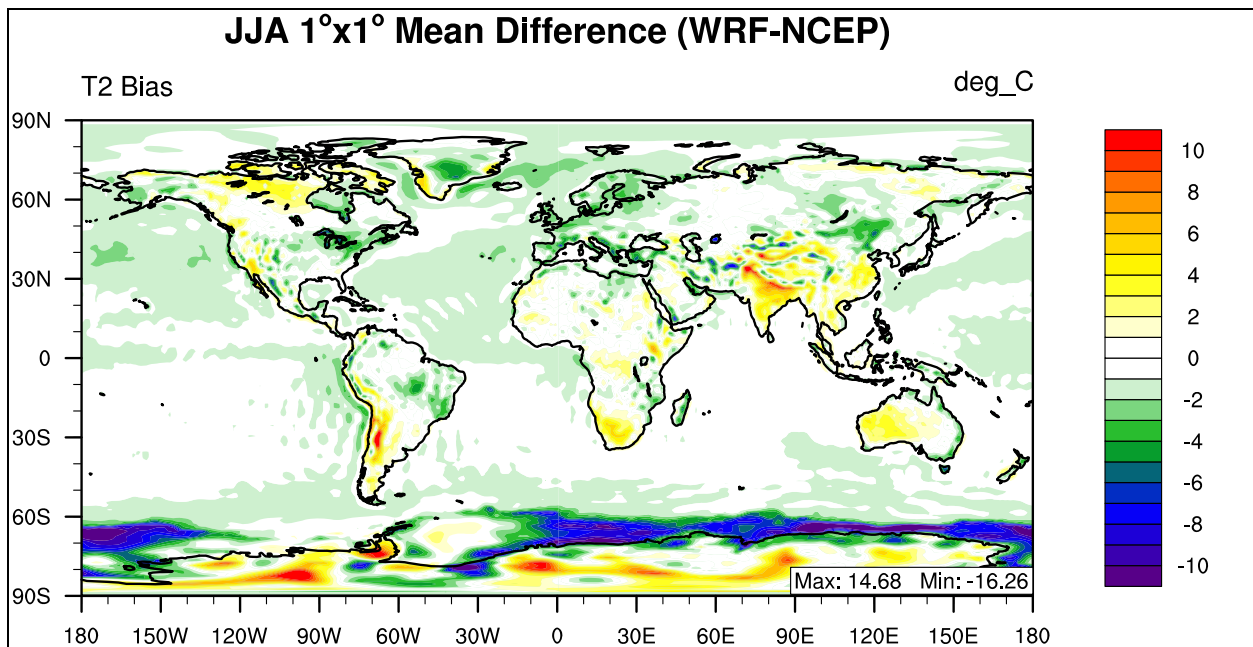


**Figure 4.142 2001 summer mean bias of temperature at 2-meter.**

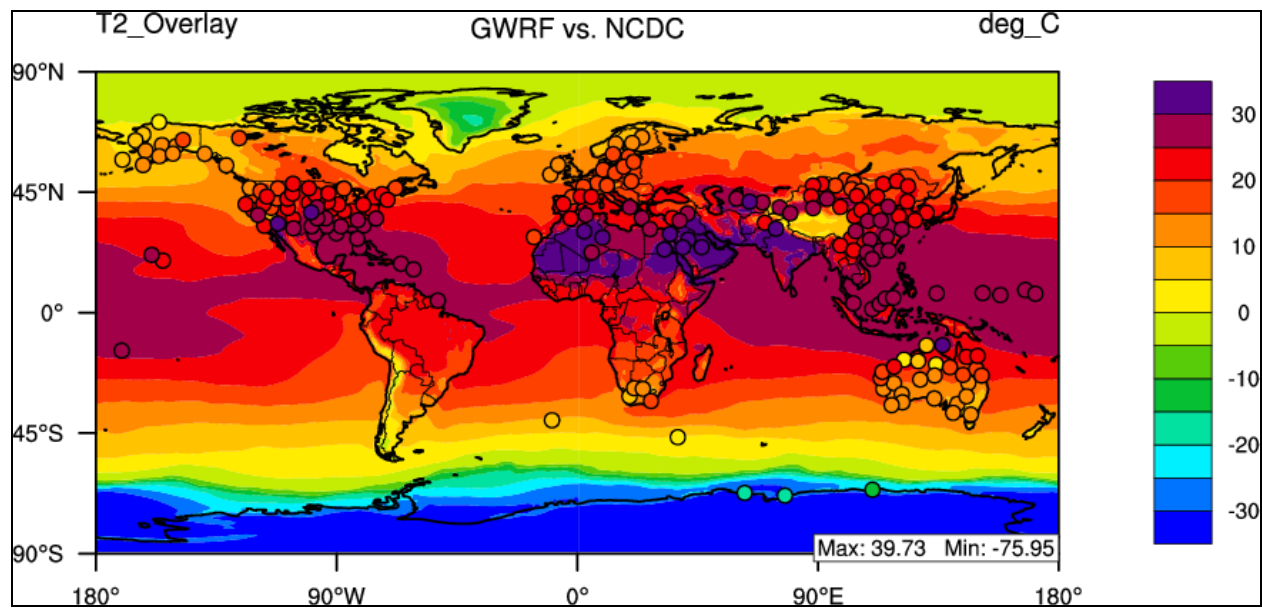


**Figure 4.143** 2001 summer temperature at 2-meter as compared to NCDC.

**Table 4.77 Performance Statistics of GWRf 2001 summer mean temperature at 2-meter as compared with NCEP/NCAR Reanalysis and NCDC.**

<b>Name</b>	<b>MeanObs</b>	<b>MeanMod</b>	<b>Number</b>	<b>Corr</b>	<b>MB</b>	<b>RMSE</b>	<b>NMB%</b>	<b>NME%</b>
<b>Europe</b>	16.43	14.85	1200	0.97	-1.57	1.94	-9.58	10.19
<b>Africa</b>	23.83	23.78	2925	0.96	-0.05	1.53	-0.22	4.85
<b>Asia</b>	20.72	20.67	5100	0.96	-0.04	2.25	-0.21	7.59
<b>Australia</b>	17.02	17.40	1200	0.96	0.37	1.57	2.18	7.04
<b>N.A.</b>	20.51	19.75	2400	0.97	-0.76	1.78	-3.73	6.71
<b>S.A.</b>	14.76	14.52	2450	0.98	-0.24	2.02	-1.64	9.34
<b>N. Pole</b>	3.20	2.49	10439	0.97	-0.71	1.52	-22.15	39.44
<b>N. Ferrel</b>	17.65	16.79	10800	0.97	-0.86	1.85	-4.87	8.17
<b>N. Hadley</b>	26.64	26.15	10800	0.92	-0.49	1.41	-1.84	4.15
<b>S. Hadley</b>	22.26	21.86	10800	0.96	-0.40	1.27	-1.79	4.04
<b>S. Ferrel</b>	8.10	7.28	10800	0.99	-0.82	1.27	-10.14	12.33
<b>S. Pole</b>	-34.51	-35.69	10440	0.98	-1.18	4.72	-3.43	10.49
<b>N.H.</b>	15.97	15.28	32039	0.99	-0.69	1.61	-4.29	7.95
<b>S.H.</b>	-1.01	-1.81	32040	0.99	-0.80	2.89	-78.85	179.96
<b>Global</b>	7.48	6.74	64079	0.99	-0.74	2.34	-9.92	20.65
<b>NCDC</b>	20.78	19.41	199	0.88	-1.37	4.42	-6.58	14.05

An overview of CCP statistical performance for the major boundary layer variables is shown graphically in Figure 4.144. The main difference between Figure 4.144 and Figure 4.13 (base case) are the large underestimations of Q2 over continental domains in the CCP sensitivity study, which is discussed further in the following section (4.6.2). CCP also provides the first instance of an underestimation of daily precipitation rate for any of the model simulations over the domains Australia and South America. There are also large underestimations of downward shortwave flux, which was not present in the BASE case. Large error values for the North Pole domain T2 and daily precipitation rate domain are consistent with the baseline simulation; however T2 is underestimated in this sensitivity simulation. The vertical profile of temperature performance is explored in Figure 4.145 which is the zonal mean bias of GWRf versus NCEP/NCAR Reanalysis data. The differences between Figure 4.145 and Figure 4.15 show that the vertical distribution of temperature s highly sensitive to the choice of cumulus

parameterization. This figure shows that GWRf generally captures the vertical temperature distribution within  $\pm 2$  degrees up to approximately 300 hPa. The CCP simulation does share many similarities with the base case summer zonal mean bias (Figure 4.15), with large overestimations near the surface over Antarctica and the equator and underestimations of temperatures throughout the Southern Ferrel Cell. The two images do depict areas of disagreement, namely the CCP produces stronger underestimation of temperatures between 400 hPa and 200 hPa over the Tropics and actually produces slight underestimations aloft over the Northern latitudes, while BASE generally overestimates temperatures in this layer. Also, CCP predicts overestimations of temperature at the top of the troposphere over the Tropics around 100 hPa.

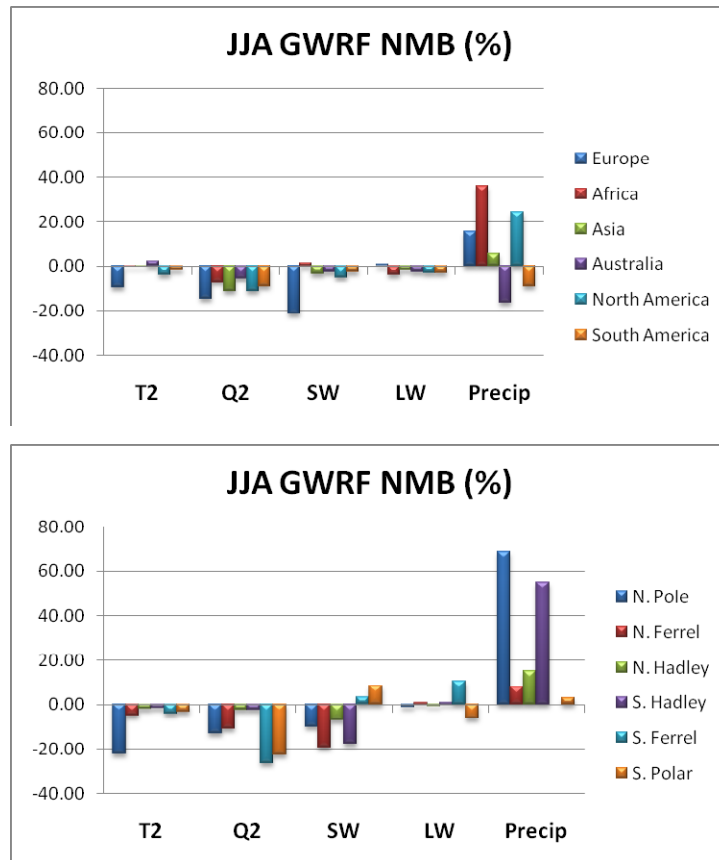


**Figure 4.144** 2001 summer mean normalized mean bias (%) of major meteorological variables for (a) the six continental domains and (b) the six circulation cell domains.

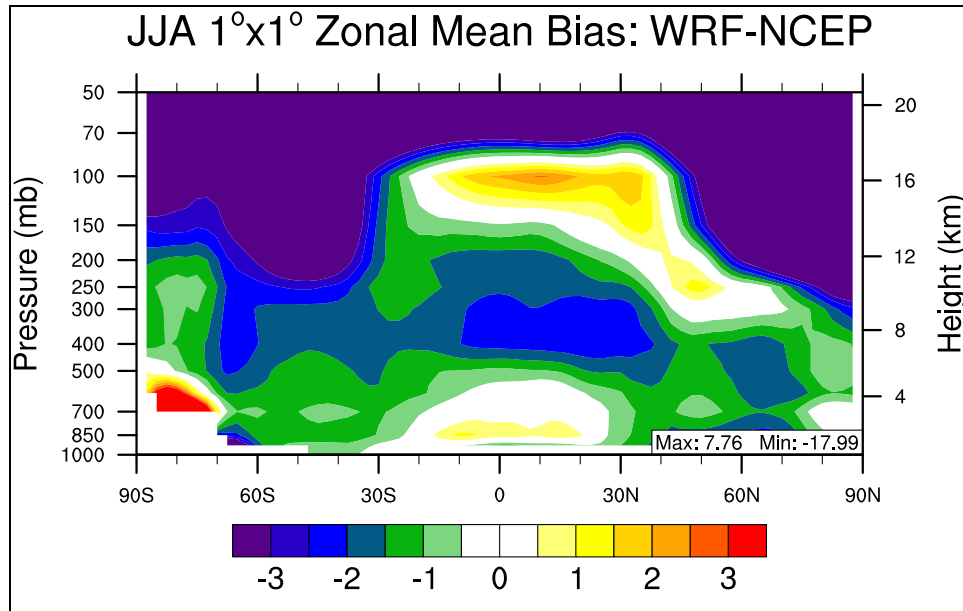


**Figure 4.145** Summer zonal mean bias of Temperature

#### 4.6.2 Summer Water Vapor Mixing ratio at 2-meter

The global distribution of CCP summer mean bias for water vapor mixing ratio at 2-meters is displayed in Figure 4.146. Overall Figures 4.146 and 4.16 are very similar, indicating a weak sensitivity of Q2 to cumulus parameterization choice. The strong underestimation of Q2 by the Grell-Devenyi cumulus parameterization is reflected in Table 4.78 in which all domains have a negative NMB value. Table 4.78 also shows that CCP performs worse than the BASE case when all corresponding domains have worse performance in CCP than BASE. The strongest underestimations of Q2 exist in the Polar Regions, with the North Pole and South Pole (-12.99% and -22.45%, respectively) displaying much lower NMBs than their corresponding BASE values (-8.63% and -14.84%, respectively). The global CCP NMB value is -5.49% which

is worse than the baseline case whose summer value is -2.39%. Overall correlation values are the same as baseline performance, with a global Corr value of 0.99.

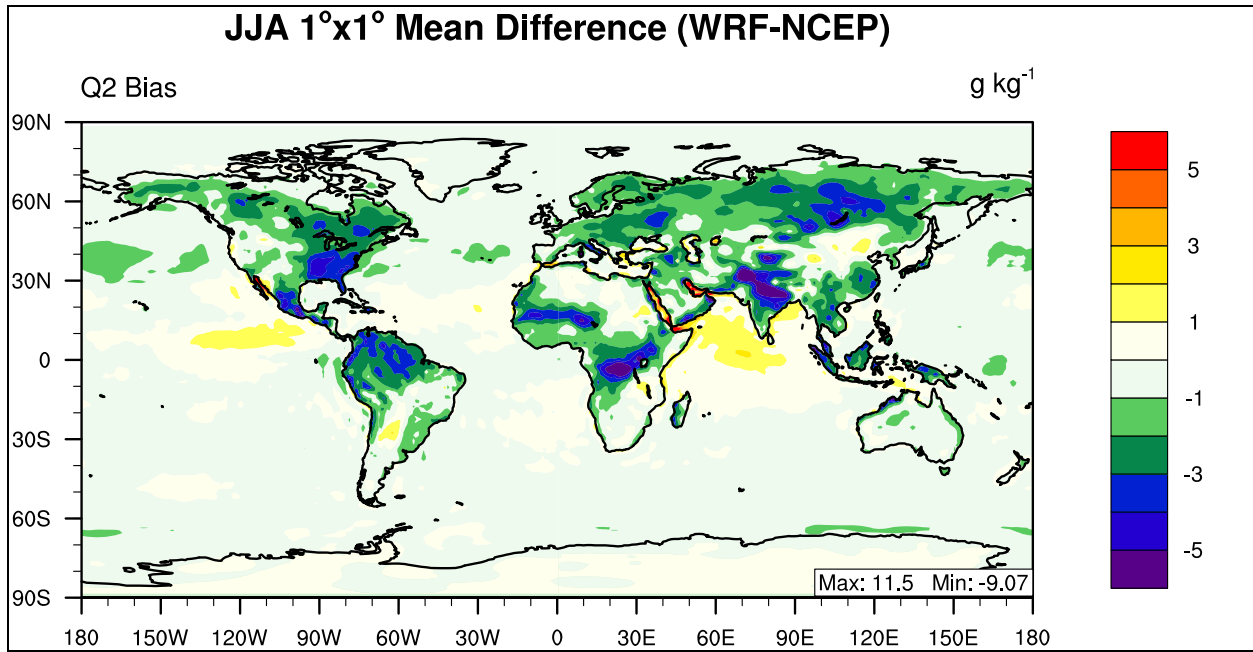


**Figure 4.146 2001 summer mean bias of water vapor mixing ratio at 2-meter.**

**Table 4.78 Performance Statistics of GWRP 2001 summer mean water vapor mixing ratio at 2-meter as compared with NCEP/NCAR Reanalysis.**

<b>Name</b>	<b>MeanObs</b>	<b>MeanMod</b>	<b>Number</b>	<b>Corr</b>	<b>MB</b>	<b>RMSE</b>	<b>NMB%</b>	<b>NME%</b>
<b>Europe</b>	9.83	8.39	1200	0.85	-1.44	1.76	-14.61	15.76
<b>Africa</b>	10.88	10.12	2925	0.93	-0.77	1.82	-7.05	11.32
<b>Asia</b>	11.86	10.52	5100	0.96	-1.34	2.18	-11.26	14.76
<b>Australia</b>	8.53	8.07	1200	0.98	-0.46	0.91	-5.40	7.40
<b>N.A.</b>	12.34	10.92	2400	0.95	-1.41	1.99	-11.45	12.83
<b>S.A.</b>	10.02	9.10	2450	0.98	-0.91	1.45	-9.13	10.24
<b>N. Pole</b>	4.94	4.30	10440	0.96	-0.64	0.97	-12.99	13.21
<b>N. Ferrel</b>	10.18	9.09	10800	0.94	-1.09	1.58	-10.70	11.92
<b>N. Hadley</b>	16.78	16.38	10800	0.94	-0.39	1.48	-2.33	5.60
<b>S. Hadley</b>	13.91	13.55	10800	0.97	-0.36	1.00	-2.60	4.46
<b>S. Ferrel</b>	6.18	5.92	10800	0.99	-0.26	0.36	-4.22	4.57
<b>S. Polar</b>	0.74	0.57	10440	0.96	-0.17	0.33	-22.45	27.30
<b>N.H.</b>	10.70	9.99	32040	0.98	-0.71	1.37	-6.62	8.77
<b>S.H.</b>	7.01	6.75	32040	1.00	-0.26	0.65	-3.76	5.28
<b>Global</b>	8.85	8.37	64080	0.99	-0.49	1.07	-5.49	7.39

### 4.6.3 Summer Downward Shortwave Flux at Ground Surface

The pattern of summer downward shortwave flux mean bias is displayed graphically in Figure 4.147, and strongly differs from the baseline simulation pattern of an overestimation in the Tropics (30°N-30°S) and with large underestimations at high latitudes in the Northern Hemisphere. The CCP pattern is one of strong underestimation over all ocean surfaces outside of the Polar Regions, which exhibit a slight overestimation of SWDOWN. Land surfaces appear very similar to the baseline simulation. The pattern of overall GWRP SWDOWN underestimation is reflected in Table 4.79 in which all circulation cell domains, with the exception of the South Pole, have negative NMBs. The CCP simulation has a global NMB value of -14.16%, which is much worse than the corresponding baseline value (3.97%), indicating the overall underestimation of SWDOWN. Overall the CCP simulation displays slightly worse Corr values than the baseline simulation, with values of 0.91 and 0.93, respectively. BSRN evaluation

for both the baseline simulation and CCP show an overall overestimation of SWDOWN by GWRP most likely due to the fact that all BSRN sites are located over a land surface. For the BSRN evaluation, CCP creates a more accurate overall estimate of SWDOWN than BASE, with NMB values of 11.68% and 23.53%, respectively.

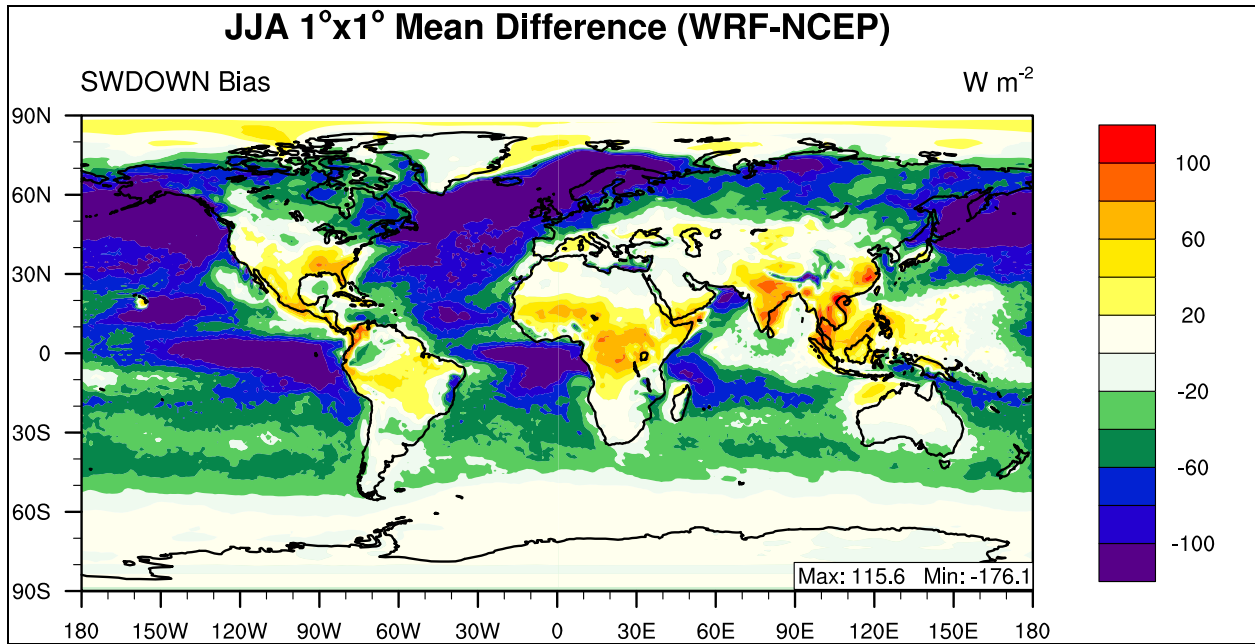


**Figure 4.147 2001 summer mean bias of downward shortwave flux at the surface.**

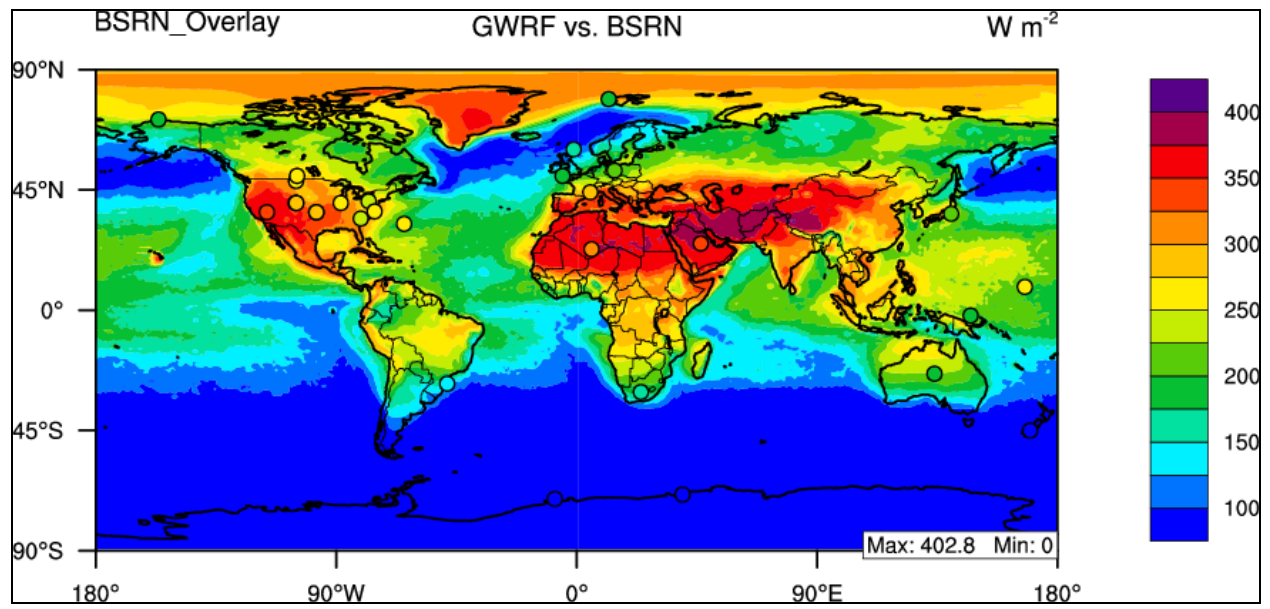


**Figure 4.148** 2001 summer mean bias of downward shortwave flux at the surface as compared to BSRN.

**Table 4.79 Performance Statistics for GWRP 2001 summer mean downward shortwave flux at the surface as compared with NCEP/NCAR Reanalysis and BSRN.**

<b>Name</b>	<b>MeanObs</b>	<b>MeanMod</b>	<b>Number</b>	<b>Corr</b>	<b>MB</b>	<b>RMSE</b>	<b>NMB%</b>	<b>NME%</b>
<b>Europe</b>	276.03	216.96	1200	0.89	-59.07	80.29	-21.40	23.83
<b>Africa</b>	267.44	271.28	2925	0.85	3.84	44.84	1.43	12.90
<b>Asia</b>	282.36	272.89	5100	0.74	-9.47	48.01	-3.35	14.05
<b>Australia</b>	187.27	182.57	1200	0.95	-4.70	21.75	-2.51	9.02
<b>N.A.</b>	287.47	273.45	2400	0.67	-14.02	43.26	-4.88	12.57
<b>S.A.</b>	159.45	155.86	2450	0.95	-3.60	26.92	-2.26	13.54
<b>N. Pole</b>	278.24	250.03	10440	0.79	-28.22	55.84	-10.14	15.03
<b>N. Ferrel</b>	276.45	223.31	10800	0.92	-53.14	75.20	-19.22	22.36
<b>N. Hadley</b>	257.37	239.44	10800	0.57	-17.93	58.11	-6.97	18.55
<b>S. Hadley</b>	201.96	166.46	10800	0.59	-35.51	55.26	-17.58	22.51
<b>S. Ferrel</b>	79.47	58.37	10800	0.86	-21.10	27.27	-26.55	29.06
<b>S. Polar</b>	8.77	9.53	7920	1.00	0.76	1.45	8.62	9.43
<b>N.H.</b>	270.60	237.45	32040	0.74	-33.15	63.73	-12.25	18.68
<b>S.H.</b>	105.32	84.81	29520	0.93	-20.51	37.28	-19.47	24.03
<b>Global</b>	191.34	164.26	61560	0.91	-27.09	52.73	-14.16	20.09
<b>BSRN</b>	218.83	244.39	29	0.93	25.57	47.45	11.68	18.82

#### **4.6.4 Summer Downward Longwave Flux at Ground Surface**

The pattern of summer downward longwave flux mean bias is displayed graphically in Figure 4.149. This CCP pattern has many elements in common with the baseline simulation, such as an overestimation over Antarctica, an underestimation over the Southern Ocean, and an overall overestimation over continental land surfaces. The major difference between Figure 4.149 and 4.19 is that CCP creates large areas of overestimation over ocean surfaces, while the baseline simulation created areas of underestimation. This is evident in Table 4.80 in which the Northern Hemisphere is underestimated, while the Southern Hemisphere is overestimated. Also, CCP has a stronger underestimation of GLW over the North Pole (-1.41%), as compared to the baseline value (-0.42%). Overall, CCP performs better than BASE for GLW, with a global NMB value of 0.09%, which is an improvement from baseline value (-4.14%). Globally, the Corr value for the CCP and baseline simulations is 0.98. Evaluation with BSRN also shows that

although CCP still underestimates GLW, it creates larger estimates of GLW than the baseline simulation. BSRN NMB values are -7.67% for CCP, as compared to -9.17% for BASE. The underestimation of SWDOWN over ocean surfaces and the overestimation of GLW indicates the presence of clouds affecting the radiation budget within this sensitivity simulation.

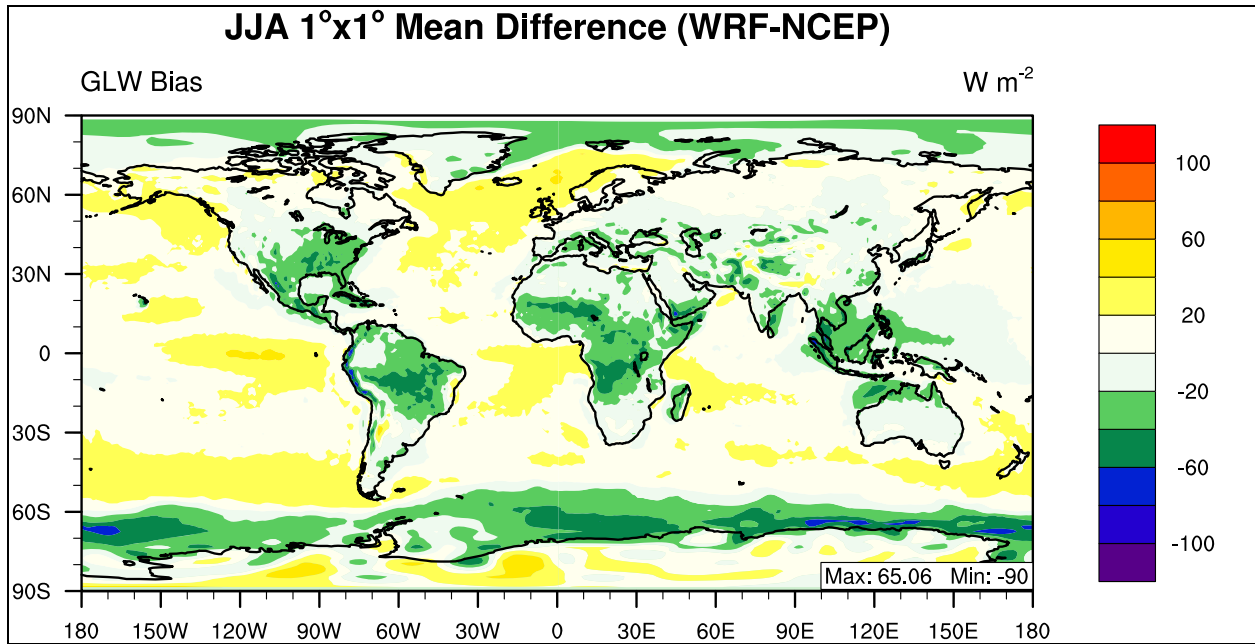


**Figure 4.149** 2001 summer mean bias of downward longwave flux at the surface.

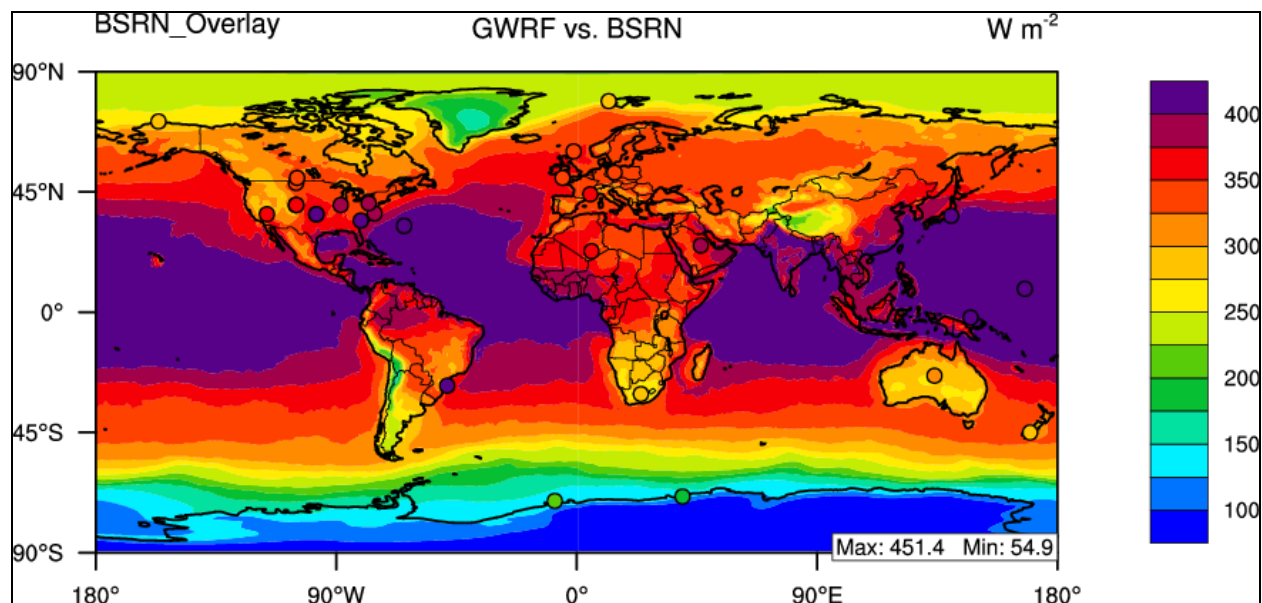


**Figure 4.150** 2001 summer mean bias of downward longwave flux at the surface.

**Table 4.80** Performance Statistics of GWRP 2001 summer mean downward longwave flux at the surface as compared with NCEP/NCAR Reanalysis and BSRN.

Name	MeanObs	MeanMod	Number	Corr	MB	RMSE	NMB%	NME%
Europe	333.15	335.54	1200	0.16	2.39	18.86	0.72	4.58
Africa	363.04	349.85	2925	0.81	-13.19	24.18	-3.63	5.56
Asia	355.61	349.19	5100	0.95	-6.42	16.44	-1.81	3.51
Australia	325.16	317.22	1200	0.92	-7.94	17.04	-2.44	4.22
N.A.	358.63	347.93	2400	0.91	-10.71	19.41	-2.98	4.21
S.A.	333.45	323.41	2450	0.93	-10.04	23.57	-3.01	5.86
N. Pole	272.40	268.57	10440	0.93	-3.83	18.46	-1.41	5.97
N. Ferrel	344.05	347.60	10800	0.86	3.55	17.75	1.03	4.38
N. Hadley	405.77	402.23	10800	0.73	-3.54	19.90	-0.87	4.00
S. Hadley	375.69	379.58	10800	0.89	3.89	20.35	1.04	4.54
S. Ferrel	299.44	309.22	10800	0.93	9.78	19.94	3.27	5.91
S. Polar	134.46	125.86	10440	0.95	-8.60	28.96	-6.40	18.21
N.H.	341.51	340.26	32040	0.96	-1.25	18.73	-0.36	4.64
S.H.	271.39	273.19	32040	0.98	1.81	23.38	0.67	7.26
Global	306.45	306.73	64080	0.98	0.28	21.18	0.09	5.80
BSRN	350.01	323.15	29	0.92	-26.86	38.18	-7.67	8.76

#### **4.6.5 Summer Daily Precipitation Rate**

The daily precipitation at the surface in GWRP is compared with the Global Precipitation Climatology Project (GPCP) for the summer of 2001. Overall, GWRP CCP performance during summer is overestimating daily precipitation rate and creating different rainfall rates spatially than the baseline simulation (Figure 4.23). Maximum (22.01) and minimum (-14.49) mean bias values are more extreme for the CCP simulation as compared with the BASE simulations, with values of 15.93 and -9.82. This large difference indicates that the choice of cumulus parameterization has a large effect on the location and magnitude of daily precipitation rate. In CCP there exists a large area of an overestimation of precipitation rate over the North Pole domain, which is shown in Table 4.81 where CCP has a large NMB value of 68.94%. Globally, CCP shows a slightly lower Corr value of 0.73 as compared to the 0.83 in the BASE case, while NMB values are better than BASE with values of 22.10% and 38.64% respectively. Evaluation with NCDC data shows an even larger improvement in GWRP for CCP as compared to BASE, with NMB values of 0.71% and 25.29%, respectively. When Figure 4.24 (baseline summer) and Figure 4.152 are compared, the large overestimations of monthly mean precipitation over the East Indies and Southeast Asia present in the BASE case are largely reduced.

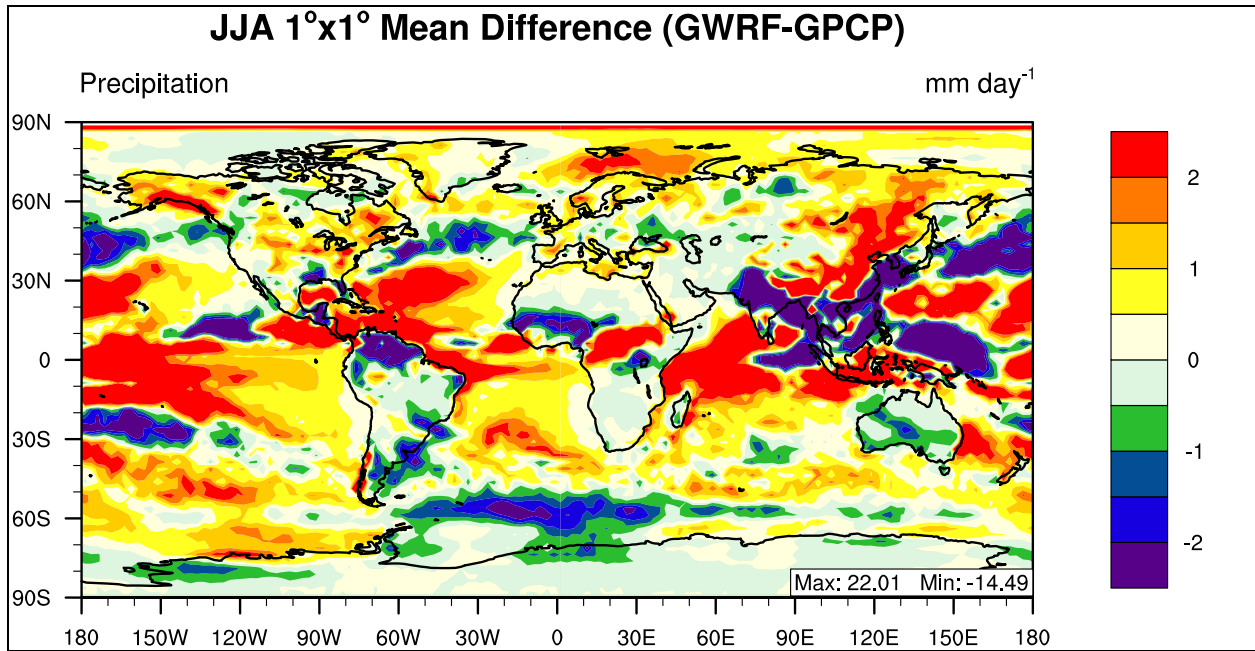


**Figure 4.151 2001 summer mean bias of daily precipitation rate.**

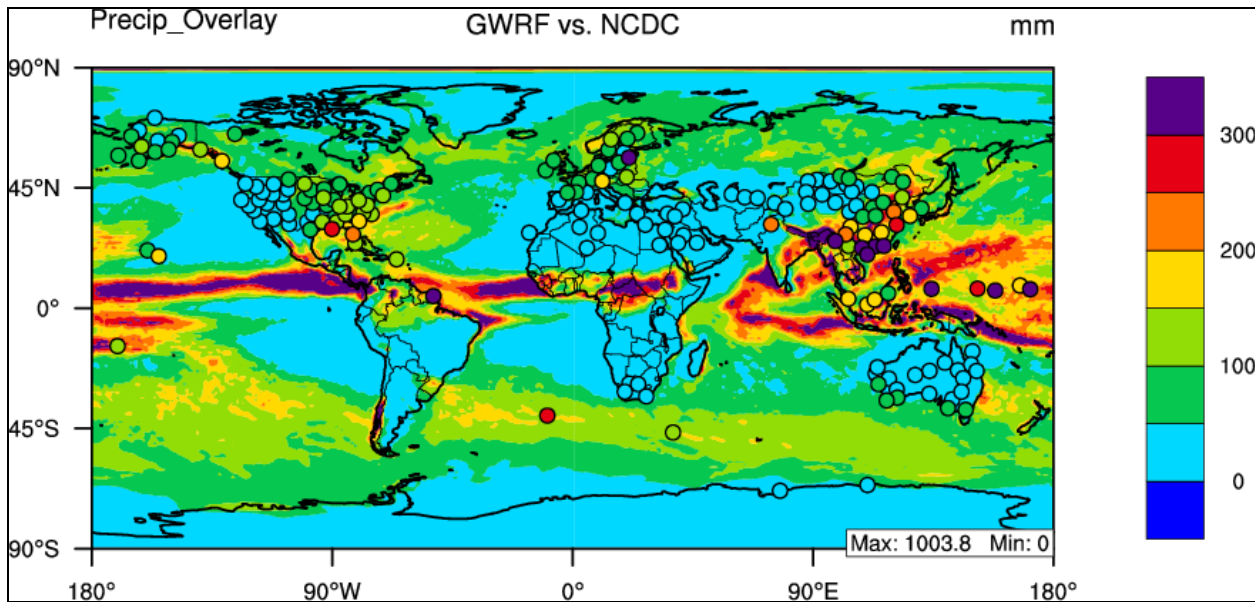


**Figure 4.152 2001 summer mean bias of daily precipitation rate.**

**Table 4.81 Statistical Analysis of GWRf mean daily rainfall rate for summer 2001 compared with GPCP.**

<b>Name</b>	<b>MeanObs</b>	<b>MeanMod</b>	<b>Number</b>	<b>Corr</b>	<b>MB</b>	<b>RMSE</b>	<b>NMB%</b>	<b>NME%</b>
<b>Europe</b>	2.37	2.74	192	0.69	0.37	0.87	15.63	28.76
<b>Africa</b>	1.26	1.71	463	0.85	0.46	1.53	36.17	68.81
<b>Asia</b>	3.29	3.47	816	0.67	0.18	2.82	5.46	51.34
<b>Australia</b>	0.98	0.82	192	0.71	-0.16	0.73	-16.52	57.80
<b>N.A.</b>	2.49	3.10	384	0.71	0.61	1.27	24.49	39.59
<b>S.A.</b>	3.00	2.72	392	0.75	-0.28	1.61	-9.32	34.66
<b>N. Pole</b>	1.17	1.98	1728	0.31	0.81	1.46	68.94	78.08
<b>N. Ferrel</b>	2.30	2.49	1727	0.57	0.18	1.48	7.94	44.30
<b>N. Hadley</b>	4.04	4.66	1724	0.70	0.61	2.94	15.16	52.43
<b>S. Hadley</b>	1.79	2.77	1728	0.72	0.98	2.12	55.16	82.01
<b>S. Ferrel</b>	3.08	3.41	1728	0.52	0.33	1.10	10.76	28.33
<b>S. Polar</b>	0.97	1.00	1728	0.81	0.03	0.59	3.12	41.34
<b>N.H.</b>	2.50	3.04	5179	0.72	0.53	2.08	21.34	53.94
<b>S.H.</b>	1.94	2.39	5184	0.76	0.45	1.42	23.08	46.92
<b>Global</b>	2.22	2.72	10363	0.73	0.49	1.78	22.10	50.87
<b>NCDC</b>	93.20	93.86	172	0.54	0.66	96.05	0.71	54.95

## CHAPTER 5: FUTURE-YEAR SIMULATION RESULTS

### 5.1 2050 GWRF/CCSM Results

Future climate change in 2050 is examined in this chapter by comparing model outputs from 2001 and 2050 by initializing GWRF with CCSM model output. In sections 5.2 and 5.3, the seasonal variation is discussed for winter (January) and summer (July), respectively. A limitation of this evaluation when compared with the IPCC results are that the IPCC uses a decade to decade mean comparison, while in this study GWRF was initialized with decade average CCSM variables, but compared with the GWRF 2001 baseline simulation. It should be noted that among the three IPCC Special Report on Emission Scenarios (SRES: B1, A1B, and A2) there is little variance among the scenarios when it comes to warming. The 10<sup>th</sup> chapter of the IPCC AR4 states that among the coupled models used the warming averaged for the beginning of the 21<sup>st</sup> century (2011 to 2030) when compared to the late 20<sup>th</sup> century (1980 to 1999) is between +0.64°C and +0.69°C, with a range of only 0.05°C (IPCC 10). However by midcentury (2046–2065), the choice of scenario becomes more important to globally averaged surface warming, with a larger spread among B1, A1B and A2 with values of +1.3°C, +1.8°C and +1.7°C, respectively. The spread becomes even larger toward the end of the 21<sup>st</sup> century (2090 to 2099), in which the multi-model mean surface warming relative to the late 20<sup>th</sup> century (1980 to 1999) for B1 is +1.8°C (1.1°C to 2.9°C). The IPCC B1 scenario multi-model ensemble mean increases by 1.29 K during the mid-21<sup>st</sup> century (2045-2065) relative to the late 20<sup>th</sup> century (1980-1999) (Meehl et al., 2007). Geographically, all scenarios project similar patterns (with varying degree of magnitude) of warming which show greatest temperature increases over land and at high northern latitudes, and less warming over the southern oceans and North Atlantic. Precipitation patterns are also expected to change, as reported by the IPCC which indicates that precipitation generally increases in areas of regional tropical precipitation maxima (over the tropical Pacific in particular) with general decreases in the subtropics, and increases at high latitudes. This is attributed to a general intensification of the global hydrological cycle in which globally averaged mean water vapor, evaporation and precipitation are projected to

increase. In all scenarios daily precipitation rate ( $\text{mm day}^{-1}$ ) increased, with the IPCC B1 scenario multi-model ensemble mean increasing by  $0.06 \text{ mm day}^{-1}$  during the mid-21<sup>st</sup> century (2045-2065) relative to the late 20<sup>th</sup> century (1980-1999) (Meehl et al., 2007). Possible limitations of the GWRf simulation are temporal variability, no increase in  $\text{CO}_2$  concentration (550 ppm), future ozone concentrations, and the effect of aerosols.

### **5.1.1 2050 January Temperature at 2-meter**

Temperature at 2-meter simulated by GWRf in 2050 as compared with 2001 indicates an overall warming trend with localized regions of cooling over North America and the Southern Ferrel Cell, as shown in Figure and Table 5.1. Warming is the most pronounced over the North Polar Region, where the warming trend is over  $4^\circ \text{C}$ . Overall the climactic variability between GWRf 2001 and 2050 simulations is larger than the differences between GWRf model and NCEP/NCAR Reanalysis data, and indicates a warming trend. The large global mean warming of near surface temperatures present in the IPCC B1 scenario (1.29 K), is replicated by the GWRf simulation (1.32 K). The 2050 simulation shows a global trend of warming, with only the high southern latitudes exhibiting cooling. The largest areas of warming are the high northern latitudes, as shown in Table 5.1.

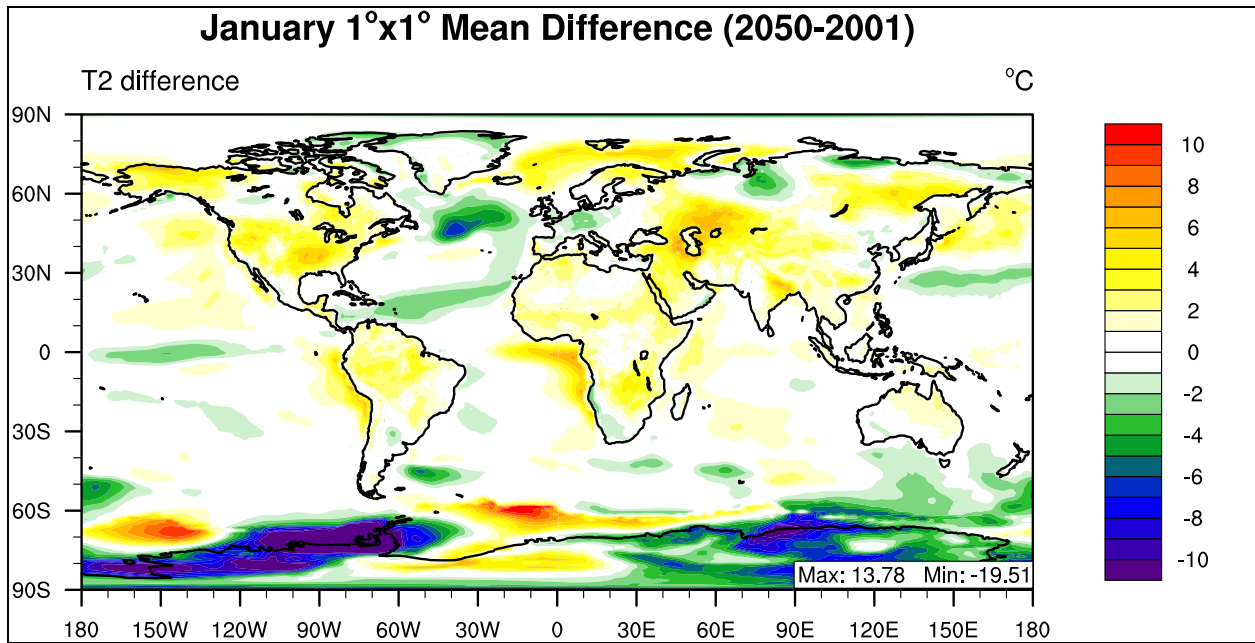


**Figure 5.1** Spatial distribution of January mean temperatures at 2-m simulated by GWRP 2001 and 2050 simulations.

**Table 5.1 Performance Statistics of GWRP 2001 and 2050 January Mean temperature at 2-meter.**

<b>Domain</b>	<b>2001 (°C)</b>	<b>2050 (°C)</b>	<b>Absolute Difference (°C)</b>	<b>Percent Difference (%)</b>
<b>Europe</b>	-0.86	-0.74	0.12	13.66
<b>Africa</b>	20.70	22.19	1.49	7.20
<b>Asia</b>	-4.75	-2.62	2.13	44.78
<b>Australia</b>	27.01	26.97	-0.03	-0.12
<b>N.A.</b>	0.40	-0.69	-1.10	-272.82
<b>S.A.</b>	18.67	19.84	1.17	6.27
<b>N. Pole</b>	-28.21	-23.90	4.31	15.27
<b>N. Ferrel</b>	-0.60	0.15	0.75	124.82
<b>N. Hadley</b>	22.84	23.40	0.56	2.45
<b>S. Hadley</b>	25.01	26.22	1.21	4.82
<b>S. Ferrel</b>	11.59	11.55	-0.04	-0.34
<b>S. Polar</b>	-13.37	-12.24	1.13	8.46
<b>N.H.</b>	-1.99	-0.12	1.87	94.02
<b>S.H.</b>	7.74	8.51	0.77	9.89
<b>Global</b>	2.88	4.20	1.32	45.89

### **5.1.2 2050 January Water Vapor Mixing Ratio at 2-meter**

Water Vapor Mixing Ratio at 2-meter in 2050 are larger than those values in 2001, as shown in Figure 5.2, with the largest increases over the Tropics. Globally, 2050 has a slight increase in Q2 ( $0.52 \text{ g kg}^{-1}$ ), which corresponds to increased surface temperatures and thus increased evaporation. Increases in water vapor are consistent with the trend indicated in the IPCC AR4 in which there is a general intensification of the global hydrological cycle in which globally averaged mean water vapor, evaporation and precipitation are projected to increase (Meehl et al., 2007).

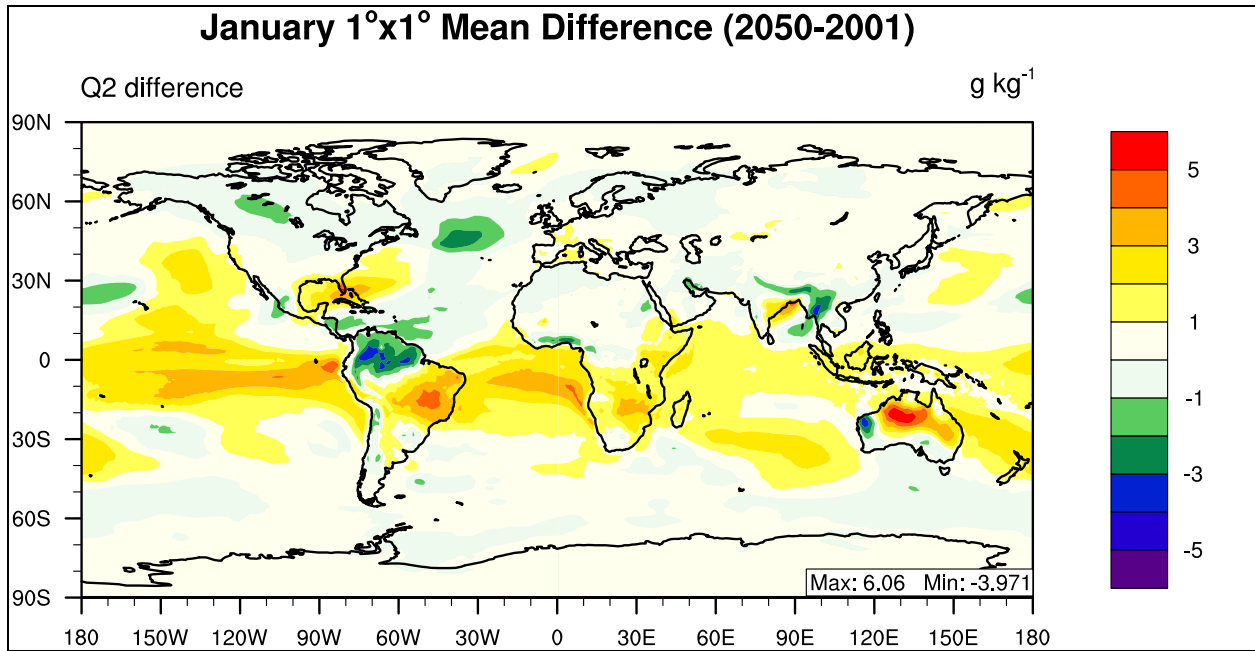


**Figure 5.2** Spatial distribution of January mean water vapor mixing ratio at 2-m simulated by GWRf 2001 and 2050 simulations.

**Table 5.2 Performance Statistics of GWRP 2001 and 2050 January Mean water vapor mixing ratio at 2-meter.**

<b>Domain</b>	<b>2001 (g kg<sup>-1</sup>)</b>	<b>2050 (g kg<sup>-1</sup>)</b>	<b>Absolute Difference (g kg<sup>-1</sup>)</b>	<b>Percent Difference (%)</b>
<b>Europe</b>	3.59	3.76	0.16	4.57
<b>Africa</b>	9.61	10.66	1.05	10.97
<b>Asia</b>	4.46	4.65	0.19	4.17
<b>Australia</b>	12.95	14.10	1.16	8.93
<b>N.A.</b>	4.78	5.17	0.39	8.08
<b>S.A.</b>	11.81	12.28	0.46	3.93
<b>N. Pole</b>	0.64	0.76	0.12	18.36
<b>N. Ferrel</b>	4.11	4.36	0.25	6.18
<b>N. Hadley</b>	13.53	14.11	0.57	4.21
<b>S. Hadley</b>	16.38	18.02	1.64	10.04
<b>S. Ferrel</b>	7.83	8.18	0.35	4.48
<b>S. Polar</b>	1.86	2.04	0.18	9.69
<b>N.H.</b>	6.10	6.41	0.31	5.15
<b>S.H.</b>	8.69	9.42	0.73	8.35
<b>Global</b>	7.39	7.91	0.52	7.03

### **5.1.3 2050 January Downward Shortwave Flux at the Surface**

Downward shortwave radiation at the surface in 2050 is slightly less than that in 2001, specifically over the oceans, which potentially indicates a larger amount of clouds over the ocean to block out the solar radiation. The global decrease in downward shortwave flux in this future climate scenario is relatively small, with an absolute difference value of 4.31 W m<sup>-2</sup>, indicating a relatively constant amount of solar radiation and a modifying effect by future clouds. Although it seems counter intuitive for solar radiation to slightly decrease and surface temperatures to slightly increase, the temperatures slightly increase because of an increase in GLW, which prevents the ability of the Earth to cool itself at night.

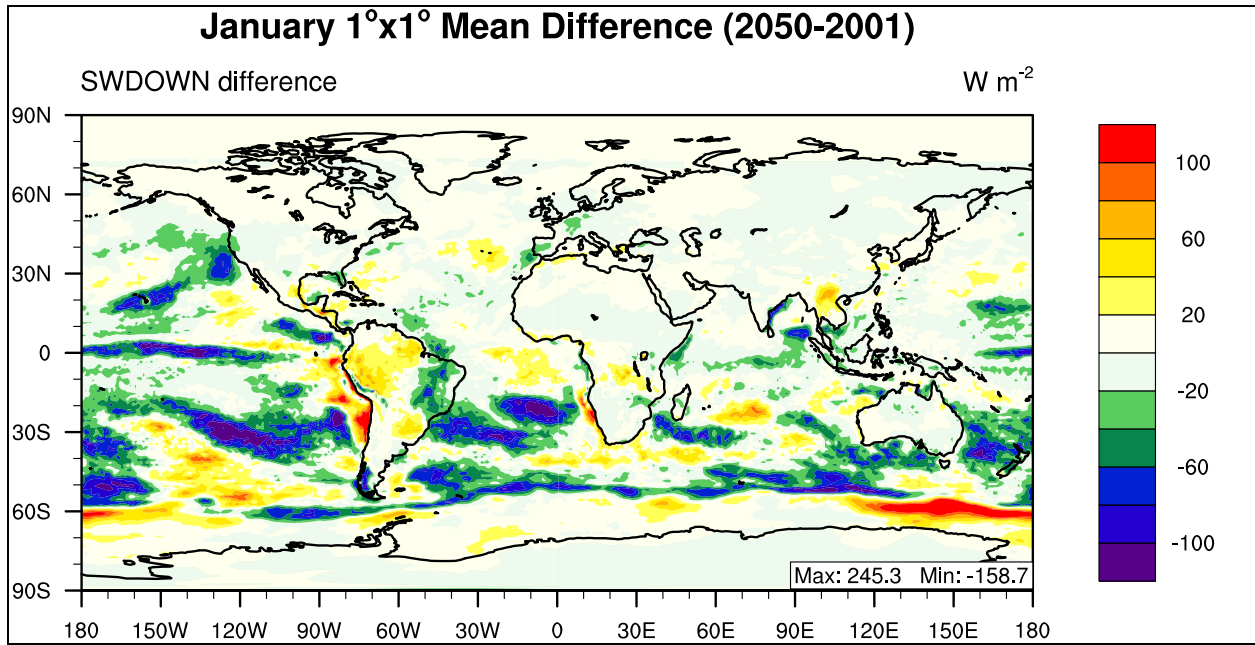


**Figure 5.3** Spatial distribution of January mean downward shortwave flux at the surface simulated by GWRf 2001 and 2050 simulations.

**Table 5.3 Performance Statistics of GWRP 2001 and 2050 January Mean downward shortwave flux at the surface.**

<b>Domain</b>	<b>2001 (W m<sup>-2</sup>)</b>	<b>2050 (W m<sup>-2</sup>)</b>	<b>Absolute Difference (W m<sup>-2</sup>)</b>	<b>Percent Difference (%)</b>
<b>Europe</b>	46.05	43.60	-2.45	-5.33
<b>Africa</b>	293.27	292.91	-0.36	-0.12
<b>Asia</b>	129.11	129.80	0.69	0.53
<b>Australia</b>	350.44	341.78	-8.65	-2.47
<b>N.A.</b>	123.89	125.93	2.05	1.65
<b>S.A.</b>	312.77	309.97	-2.80	-0.90
<b>N. Pole</b>	8.20	8.35	0.15	1.87
<b>N. Ferrel</b>	92.74	91.96	-0.78	-0.85
<b>N. Hadley</b>	243.69	239.46	-4.23	-1.74
<b>S. Hadley</b>	330.29	320.83	-9.46	-2.86
<b>S. Ferrel</b>	287.85	274.62	-13.23	-4.60
<b>S. Polar</b>	392.51	396.83	4.31	1.10
<b>N.H.</b>	140.79	138.74	-2.05	-1.46
<b>S.H.</b>	336.88	330.76	-6.12	-1.82
<b>Global</b>	249.45	245.15	-4.31	-1.73

#### **5.1.4 2050 January Downward Longwave Flux at the Surface**

The overall decrease of SWDOWN over ocean regions shown in Figure 5.3 corresponds to an overall increase of downward longwave radiation in Figure 5.4, further justifying the important role clouds play in future climate scenarios. The increase in evaporation due to higher temperatures, and the increase in water vapor mixing ratio near the surface results in a decrease in the ability of longwave radiation to escape out to space, and an overall increase of GLW in 2050. This is shown spatially in Figure 5.4, and numerically in Table 5.4, in which the global domain has an absolute difference value of 8.99 W m<sup>-2</sup>. The global increase of the longwave radiation component corresponds to the slight increase in global temperatures in 2050.

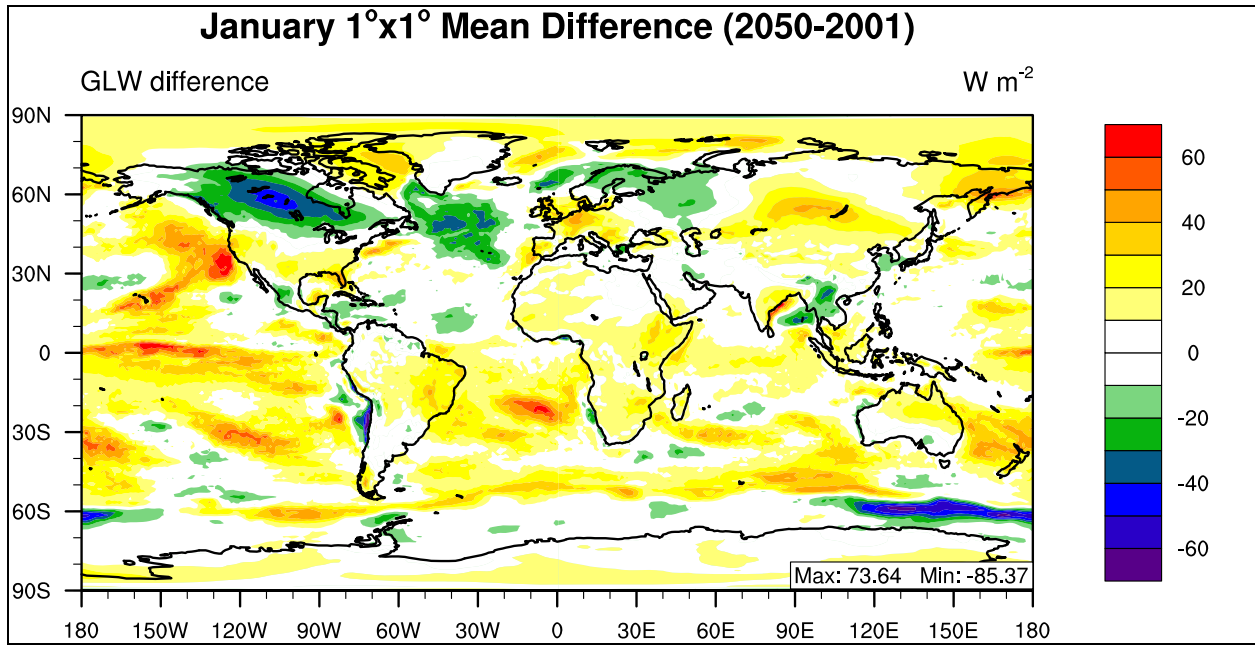


**Figure 5.4** Spatial distribution of January mean downward longwave flux at the surface simulated by GWRP 2001 and 2050 simulations.

**Table 5.4 Performance Statistics of GWRf 2001 and 2050 January Mean downward longwave flux at the surface.**

<b>Domain</b>	<b>2001 (W m<sup>-2</sup>)</b>	<b>2050 (W m<sup>-2</sup>)</b>	<b>Absolute Difference (W m<sup>-2</sup>)</b>	<b>Percent Difference (%)</b>
<b>Europe</b>	239.57	242.93	3.36	1.40
<b>Africa</b>	319.85	330.91	11.06	3.46
<b>Asia</b>	219.61	226.55	6.94	3.16
<b>Australia</b>	364.42	373.17	8.76	2.40
<b>N.A.</b>	238.70	236.73	-1.97	-0.82
<b>S.A.</b>	335.82	345.43	9.61	2.86
<b>N. Pole</b>	145.63	155.34	9.70	6.66
<b>N. Ferrel</b>	237.78	243.49	5.71	2.40
<b>N. Hadley</b>	341.22	348.89	7.67	2.25
<b>S. Hadley</b>	364.22	379.86	15.64	4.29
<b>S. Ferrel</b>	311.17	322.84	11.66	3.75
<b>S. Polar</b>	170.51	174.07	3.57	2.09
<b>N.H.</b>	241.54	249.24	7.70	3.19
<b>S.H.</b>	281.97	292.26	10.29	3.65
<b>Global</b>	261.76	270.75	8.99	3.44

### 5.1.5 2050 January Daily Rainfall Rate

When GWRf January 2050 and 2001 precipitation rates are compared, the future case has an increase in daily precipitation of 0.73 mm day<sup>-1</sup> on a global scale, which is much larger than the value reported by the IPCC AR4 (0.06 mm day<sup>-1</sup>). The increase in temperature and water vapor mixing ratio at 2-meter in the January simulation both result in a larger amount of clouds and precipitation, as shown in Figure 5.5. Due to increased cloud cover, there is a decrease in downward shortwave flux and an increase in downward longwave flux. This pattern is reflected on the global scale and the majority of smaller domains; however the seasonal and spatial consistency of this overall pattern must be examined in the following section. The ability of GWRf to accurately reproduce precipitation in the Polar Regions does not inspire confidence based on the analysis in the previous chapter (e.g., Figure 4.10 and Table 4.7).

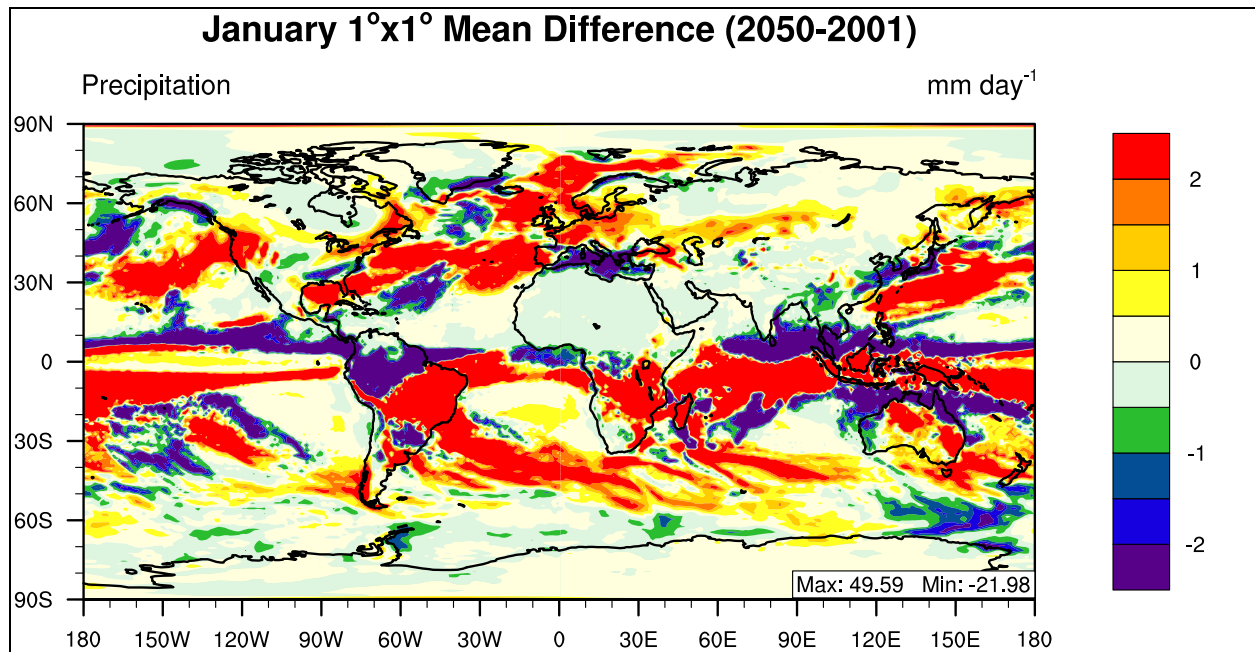


**Figure 5.4** Spatial distribution of January mean downward longwave flux at the surface simulated by GWRP 2001 and 2050 simulations.

**Table 5.5 Performance Statistics of GWRP 2001 and 2050 January Mean daily precipitation rate.**

<b>Domain</b>	<b>2001 (mm d<sup>-1</sup>)</b>	<b>2050 (mm d<sup>-1</sup>)</b>	<b>Absolute Difference (mm d<sup>-1</sup>)</b>	<b>Percent Difference (%)</b>
<b>Europe</b>	1.33	2.30	0.96	72.34
<b>Africa</b>	1.82	3.07	1.24	67.99
<b>Asia</b>	0.71	0.78	0.07	9.35
<b>Australia</b>	2.79	2.24	-0.54	-19.51
<b>N.A.</b>	1.07	1.96	0.90	84.31
<b>S.A.</b>	3.34	5.12	1.78	53.13
<b>N. Pole</b>	0.56	0.85	0.29	51.72
<b>N. Ferrel</b>	1.97	2.75	0.78	39.83
<b>N. Hadley</b>	2.01	1.67	-0.35	-17.18
<b>S. Hadley</b>	3.25	6.05	2.79	85.86
<b>S. Ferrel</b>	1.75	2.51	0.76	43.64
<b>S. Polar</b>	0.43	0.44	0.01	1.82
<b>N.H.</b>	1.50	1.76	0.26	16.99
<b>S.H.</b>	1.81	3.00	1.19	65.61
<b>Global</b>	1.66	2.38	0.73	43.83

## **5.2 2050 July Results**

### **5.2.1 2050 July Temperature at 2-meter**

The differences in T2 between the summer of 2050 and the summer of 2001 are displayed in Figure 5.6. Large areas of warming occur over the North Pole region, with a large area of cooling over Canada. The global average absolute difference value is -0.13 °C, an average which is dominated by the large negative difference in the South Pole domain as shown in Table 5.6. Due to the large cooling in the South Pole and to a lesser extent in the Southern Ferrel Cell domain, the Southern Hemisphere experiences a larger cooling during its winter.

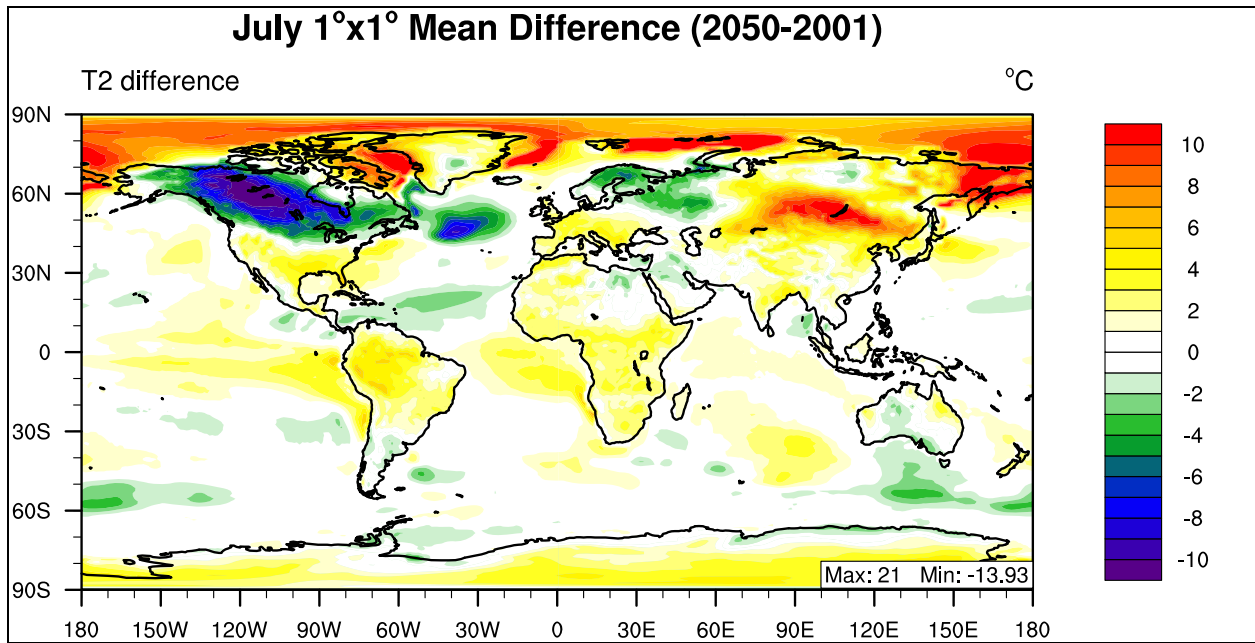


**Figure 5.6** Spatial distribution of July mean temperature at 2-meter simulated by GWRP 2001 and 2050 simulations.

**Table 5.6 Performance Statistics of GWRP 2001 and 2050 July mean temperature at 2-meter.**

<b>Domain</b>	<b>2001 (°C)</b>	<b>2050 (°C)</b>	<b>Absolute Difference (°C)</b>	<b>Percent Difference (%)</b>
<b>Europe</b>	17.27	17.78	0.51	2.95
<b>Africa</b>	23.95	25.59	1.64	6.84
<b>Asia</b>	22.76	24.26	1.50	6.61
<b>Australia</b>	17.77	18.06	0.28	1.60
<b>N.A.</b>	21.31	22.82	1.51	7.09
<b>S.A.</b>	14.56	15.40	0.83	5.73
<b>N. Pole</b>	4.25	4.68	0.42	9.98
<b>N. Ferrel</b>	18.35	19.40	1.04	5.69
<b>N. Hadley</b>	26.81	27.34	0.53	1.97
<b>S. Hadley</b>	22.41	23.07	0.67	2.98
<b>S. Ferrel</b>	7.64	7.36	-0.28	-3.71
<b>S. Polar</b>	-35.47	-38.63	-3.17	-8.93
<b>N.H.</b>	16.47	17.14	0.67	4.04
<b>S.H.</b>	-1.81	-2.73	-0.93	-51.35
<b>Global</b>	7.33	7.20	-0.13	-1.78

### **5.2.2 2050 July Water Vapor Mixing Ratio at 2-meter**

In the global domain, there is slight increase during July in the water vapor mixing ratio at 2-meter from 2001 to 2050, however the increase during the summer comparison is less than the winter comparison. During summer, the Hadley cells both exhibit the largest increase in water vapor mixing ratio (Table 5.7), indicating larger evaporation rates in these domains, and corresponding to increased T2 as shown in Table 5.6. The large decrease in T2 over the Southern Ocean in 2050 in Figure 5.6 is also shown to affect evaporation rates, in which Q2 decreases in this domain in the future case. While this change exists, overall the largest spatial variability during summer is in the Northern Hemisphere.

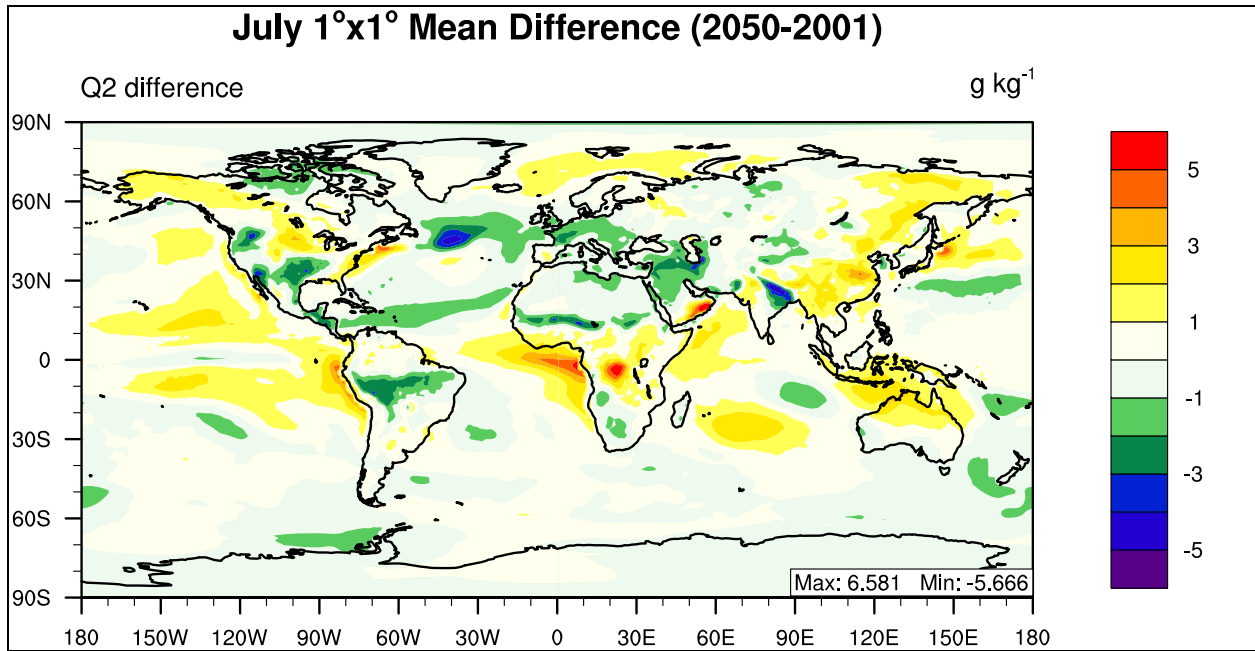


**Figure 5.7** Spatial distribution of July mean water vapor mixing ratio at 2-meter simulated by GWRf 2001 and 2050 simulations.

**Table 5.7 Performance Statistics of GWRP 2001 and 2050 July mean water vapor mixing ratio at 2-meter.**

<b>Domain</b>	<b>2001 (g kg<sup>-1</sup>)</b>	<b>2050 (g kg<sup>-1</sup>)</b>	<b>Absolute Difference (g kg<sup>-1</sup>)</b>	<b>Percent Difference (%)</b>
<b>Europe</b>	9.40	9.23	-0.17	-1.76
<b>Africa</b>	10.12	10.48	0.37	3.62
<b>Asia</b>	11.71	12.07	0.36	3.07
<b>Australia</b>	8.13	8.94	0.81	9.94
<b>N.A.</b>	11.83	12.03	0.20	1.70
<b>S.A.</b>	9.19	9.14	-0.04	-0.49
<b>N. Pole</b>	4.78	4.93	0.15	3.21
<b>N. Ferrel</b>	9.98	10.08	0.10	0.99
<b>N. Hadley</b>	16.95	17.33	0.38	2.22
<b>S. Hadley</b>	13.64	14.20	0.56	4.13
<b>S. Ferrel</b>	5.90	5.87	-0.02	-0.42
<b>S. Polar</b>	0.58	0.47	-0.10	-17.65
<b>N.H.</b>	10.57	10.78	0.21	1.98
<b>S.H.</b>	6.70	6.85	0.15	2.17
<b>Global</b>	8.64	8.82	0.18	2.06

### 5.2.3 2050 July Downward Shortwave Flux at the Surface

The summer comparison of downward shortwave flux at the surface shows an overall pattern of decreasing SWDOWN over Northern Hemispheric oceans, and an increase of SWDOWN over Northern Hemispheric land surfaces (Figure 5.8). Overall, the change is small when the percentage difference is examined. When compared with the winter evaluation, the summer evaluation of SWDOWN yields a larger decrease of solar radiation for the Northern Hemisphere (6.79 and 2.05 W m<sup>-2</sup>, respectively), a smaller decrease of solar radiation for the Southern Hemisphere (1.65 and 6.12 W m<sup>-2</sup>) but a comparable decrease for the global mean (4.50 and 4.31 W m<sup>-2</sup>), as shown in Table 5.8.

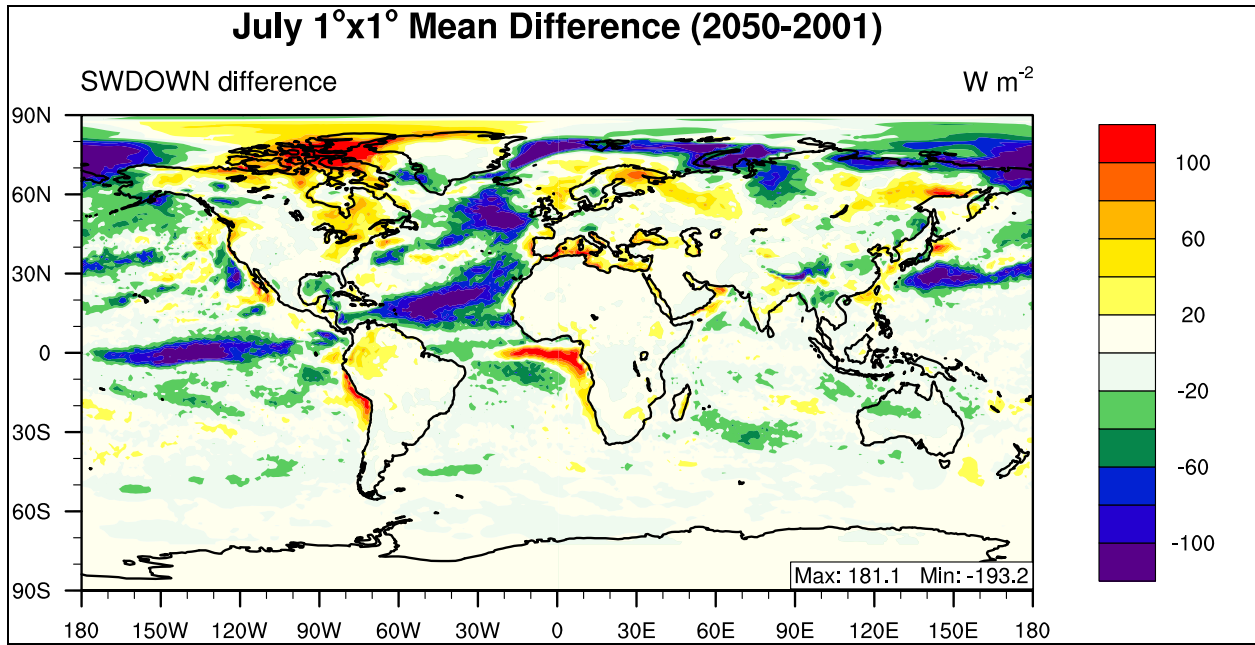


**Figure 5.8** Spatial distribution of July mean downward shortwave flux at the surface simulated by GWRf 2001 and 2050 simulations.

**Table 5.8 Performance Statistics of GWRP 2001 and 2050 July mean downward shortwave flux at the surface.**

<b>Domain</b>	<b>2001 (W m<sup>-2</sup>)</b>	<b>2050 (W m<sup>-2</sup>)</b>	<b>Absolute Difference (W m<sup>-2</sup>)</b>	<b>Percent Difference (%)</b>
<b>Europe</b>	283.85	301.52	17.67	6.22
<b>Africa</b>	285.13	293.91	8.78	3.08
<b>Asia</b>	316.12	317.48	1.36	0.43
<b>Australia</b>	191.26	183.19	-8.07	-4.22
<b>N.A.</b>	313.19	323.60	10.41	3.32
<b>S.A.</b>	171.26	177.09	5.83	3.40
<b>N. Pole</b>	261.00	254.09	-6.91	-2.65
<b>N. Ferrel</b>	266.02	262.67	-3.35	-1.26
<b>N. Hadley</b>	309.62	299.51	-10.11	-3.26
<b>S. Hadley</b>	220.68	217.02	-3.66	-1.66
<b>S. Ferrel</b>	72.30	71.90	-0.39	-0.54
<b>S. Polar</b>	6.95	7.19	0.25	3.55
<b>N.H.</b>	278.88	272.09	-6.79	-2.43
<b>S.H.</b>	123.23	121.59	-1.65	-1.34
<b>Global</b>	209.70	205.20	-4.50	-2.15

#### **5.2.4 2050 July Downward Longwave Flux at the Surface**

Similar to SWDOWN, GLW exhibit a relatively small change during the first half of the 21<sup>st</sup> century during July. The South Pole domain is dominated by the largest decrease in 2050 from 2001 of any sub-domain (13.76 W m<sup>-2</sup>), which influences the Southern hemisphere domain to also indicate a decrease. The July global mean has a positive increase in GLW value, but it is smaller than the January comparison, indicating an overall increase in GLW in 2050 as compared with 2001.

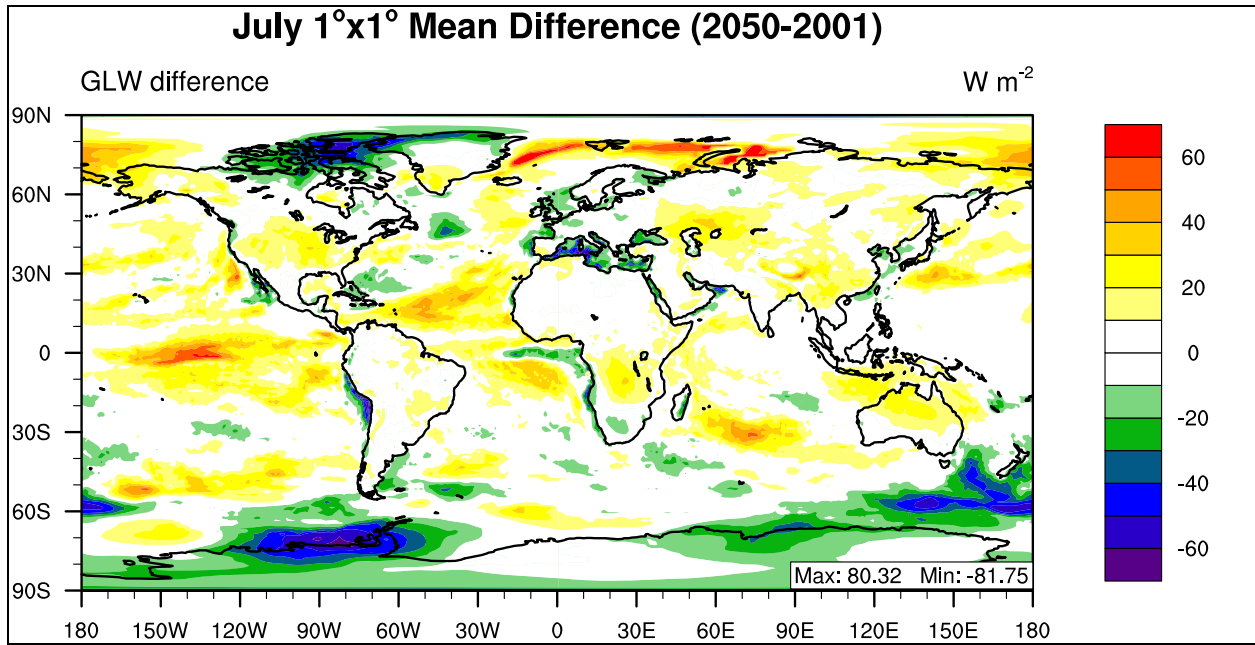


**Figure 5.9** Spatial distribution of July mean downward longwave flux at the surface simulated by GWRf 2001 and 2050 simulations.

**Table 5.9 Performance Statistics of GWRP 2001 and 2050 July mean downward longwave flux at the surface.**

<b>Domain</b>	<b>2001 (W m<sup>-2</sup>)</b>	<b>2050 (W m<sup>-2</sup>)</b>	<b>Absolute Difference (W m<sup>-2</sup>)</b>	<b>Percent Difference (%)</b>
<b>Europe</b>	332.61	327.17	-5.44	-1.64
<b>Africa</b>	343.00	346.51	3.51	1.02
<b>Asia</b>	349.01	355.93	6.92	1.98
<b>Australia</b>	305.31	315.01	9.70	3.18
<b>N.A.</b>	346.98	351.34	4.37	1.26
<b>S.A.</b>	310.74	312.48	1.74	0.56
<b>N. Pole</b>	280.90	285.48	4.58	1.63
<b>N. Ferrel</b>	346.55	352.11	5.56	1.61
<b>N. Hadley</b>	377.44	385.15	7.70	2.04
<b>S. Hadley</b>	346.84	354.64	7.80	2.25
<b>S. Ferrel</b>	286.83	285.65	-1.18	-0.41
<b>S. Polar</b>	127.50	113.73	-13.76	-10.79
<b>N.H.</b>	334.96	340.91	5.95	1.78
<b>S.H.</b>	253.72	251.34	-2.38	-0.94
<b>Global</b>	294.34	296.13	1.79	0.61

### 5.2.5 2050 July Daily Rainfall Rate

Globally, GWRP predicts a decrease in July 2050 precipitation rate relative to 2001, as compared to the large increase in January 2050. The spatial patterns of difference plots of the winter and summer comparisons (Figures 5.5 and 5.10, respectively) are very different, with the summer comparison exhibiting larger decreases. The maximum decrease of summer 2050 and 2001 comparison is  $-33.92 \text{ mm day}^{-1}$ , compared to the maximum decrease of annual 2050 and 2001 comparison  $-21.98 \text{ mm day}^{-1}$ . The IPCC AR4 also comments on this and states that the overall intensity of future precipitation events is projected to increase, but that during summer there is a tendency of drying for mid-continental regions which would result in larger precipitation differences in the summer of 2050 (Meehl et al., 2007).

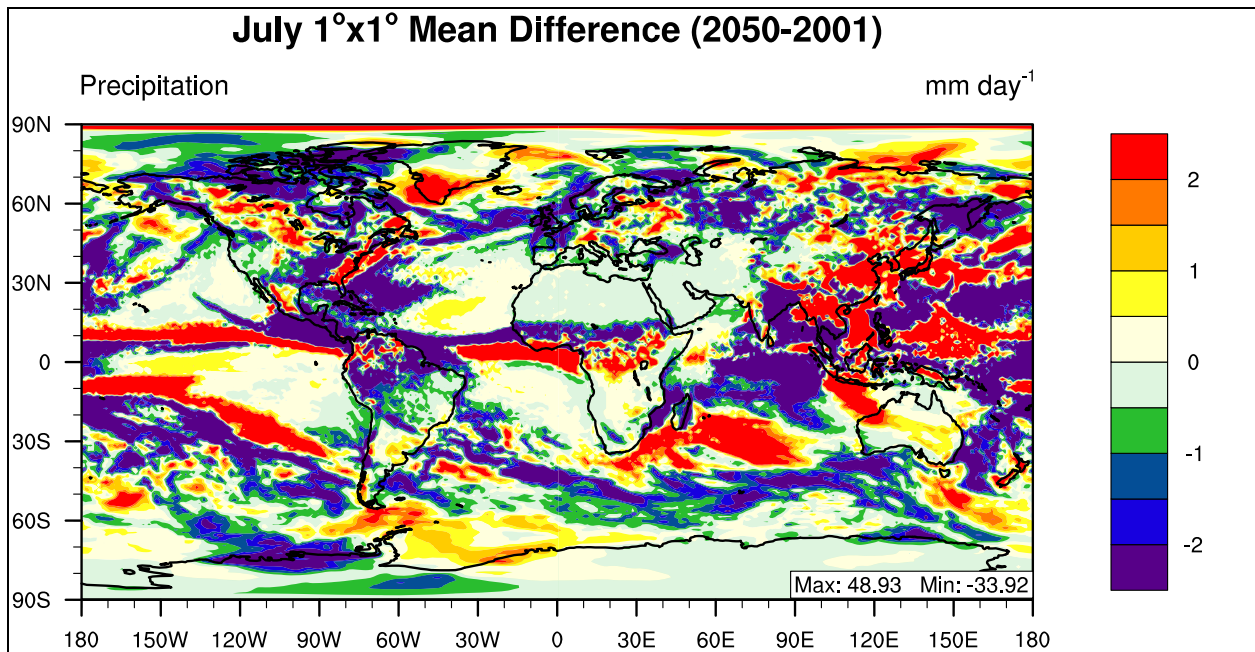


**Figure 5.10** Spatial distribution of July mean daily precipitation rate by GWRP 2001 and 2050 simulations.

**Table 5.10 Performance Statistics of GWRf 2001 and 2050 July mean daily precipitation rate.**

<b>Domain</b>	<b>2001 (mm d<sup>-1</sup>)</b>	<b>2050 (mm d<sup>-1</sup>)</b>	<b>Absolute Difference (mm d<sup>-1</sup>)</b>	<b>Percent Difference (%)</b>
<b>Europe</b>	3.37	2.80	-0.57	-16.80
<b>Africa</b>	1.84	1.86	0.03	1.54
<b>Asia</b>	4.72	4.66	-0.06	-1.24
<b>Australia</b>	0.97	1.41	0.44	45.69
<b>N.A.</b>	3.80	2.96	-0.84	-22.01
<b>S.A.</b>	4.08	3.07	-1.00	-24.56
<b>N. Pole</b>	2.28	2.79	0.52	22.70
<b>N. Ferrel</b>	3.14	2.88	-0.26	-8.35
<b>N. Hadley</b>	5.85	5.37	-0.48	-8.28
<b>S. Hadley</b>	2.65	2.21	-0.44	-16.55
<b>S. Ferrel</b>	3.98	3.59	-0.39	-9.80
<b>S. Polar</b>	1.10	0.89	-0.21	-19.02
<b>N.H.</b>	3.73	3.66	-0.07	-1.92
<b>S.H.</b>	2.58	2.23	-0.35	-13.43
<b>Global</b>	3.15	2.94	-0.21	-6.65

### **5.3 2050 Summary**

Future climate change in 2050 is examined in this chapter by comparing model outputs from 2001 and 2050 by initializing GWRf with decade averages of CCSM model output fields. GWRf replicate the large near surface warming as shown in the IPCC AR4 (1.29 K) during January (1.32 K), but predicts a slight cooling during July (0.13 K) of the mid-21<sup>st</sup> century relative to the late 20<sup>th</sup> century. Geographically, annual and seasonal GWRf-CCSM comparisons consistently show the largest T2 differences at high latitudes, which is consistent with the IPCC report. The general intensification of the global hydrological cycle, with increasing values of globally averaged mean water vapor, evaporation and precipitation as reported by the IPCC is also present in the GWRf simulations. The value projected by the IPCC B1 scenario multi-model ensemble mean (0.06 mm day<sup>-1</sup>) during the mid-21<sup>st</sup> century relative to

the late 20<sup>th</sup> century is much smaller than the January (+0.41 mm day<sup>-1</sup>) GWRP value, while the July GWRP simulation predicts an overall decrease in precipitation (-0.21 mm day<sup>-1</sup>).

## CHAPTER 6: SUMMARY AND RECOMMENDATIONS

### 6.0 Summary and Recommendations

The Weather Research and Forecasting (WRF) model was originally developed by NCAR as a model for both atmospheric research and operational forecasting, and currently has potential for climate research with the release of GWRF in WRFV3.0. The specific objectives of this thesis research were: to quantify the accuracy of the GWRF model for a baseline configuration for the year 2001, conduct a number of sensitivity simulations to physical parameterizations which produce the highest level of accuracy, and assess the capability of GWRF to predict future-year climate compared with CCSM. The evaluation of sensitivity of meteorological predictions to physics configuration represents a novel study of the WRF model because although numerous studies have examined sensitivity of WRF on a mesoscale, this is the first study known to the author of an examination on the global scale. The evaluation featured within this thesis is a first step toward the forecasting of future climate and air quality by GWRF which will lead to other studies regarding unanswered, but important scientific questions in climate science regarding the global transport of air pollutants and the impact of emissions on global air quality and thus radiative forcing.

The baseline GWRF simulation was conducted at a horizontal grid resolution of  $1^\circ \times 1^\circ$ , for the year 2001 with a baseline physical configuration designed for a long-term simulation over a global domain as defined in Table 3.1 (Chapter 3: Simulation Design and Methodology). A number of sensitivity simulations were conducted to evaluate the impacts of grid resolution, as well as different parameterizations of microphysics, cumulus formation, land surface models, and radiation, the details of which are also summarized in Table 3.1 (Chapter 3: Simulation Design and Methodology). The baseline physics configuration is also utilized for a GWRF one year future case (2050), initialized with input data from the coupled atmosphere-ocean CCSM simulations of the IPCC Special Report on Emission Scenario (SRES) B1 experiment. The baseline GWRF simulation was evaluated for annual, summer, and winter means of 2001 with

data from observational networks (e.g., NCDC and BSRN) and gridded Reanalysis data (e.g., NNR and GPCP) with a focus on major boundary layer meteorological variables. The sensitivity of GWRP to horizontal grid resolution was evaluated for the annual, summer, and winter means of 2001, while the sensitivity to physical configuration simulations were evaluated for the summer of 2001 with a focus on the same major boundary layer meteorological variables as the baseline simulation. The future year simulation was compared with the baseline simulation of 2001 major boundary layer meteorological variables to establish potential future climate changes under this emission scenario. The overall performance of GWRP baseline, sensitivity, and future simulations were evaluated in terms of spatial distribution, seasonal and temporal variations, and statistics, such as the normalized mean bias and correlation coefficient for boundary layer variables. Figures and statistics were created over the global domain, the Northern and Southern Hemispheres, the six populated continents, as well as the six circulations cells. The evaluation of the three-dimensional atmosphere also requires an evaluation of temperatures aloft, which is accomplished by the vertical profile of temperature bias over the six populated continents and the zonal mean bias for the global domain.

## **6.1 Summary of Baseline Simulation Results**

The BASE simulation is evaluated using for annual and seasonal (summer and winter) means, against a combination of gridded climate Reanalyses and observational data. These results are then put into context and compared with the results of the literature survey in Chapter 2. When the annual, global domain average is compared with NNR data, the BASE configuration provides the most accurate (lowest MB and NMB, high Corr value) estimate of T2 which is the best predicted field and U10 is the field predicted with the lowest level of accuracy. Globally, GWRP predicts the surface variables T2 and Q2 with the highest level of accuracy with NMB values of -0.38% and -2.29%, respectively. GWRP predicts the radiation variables SWDOWN and GLW with the second highest level of accuracy with NMB values of 8.91% and -5.63%. Wind speeds are consistently predicted with the lowest accuracy with NMB values for

U10 and V10 of -452.13% and -26.16%, respectively. Except for wind speeds, daily precipitation rate is predicted with the least amount of accuracy, in which it is largely overpredicted with an annual, global NMB value of 31.03%. GWRf model performance shows a large sensitivity to seasonality, indicating the importance of examining model performance in time intervals of less than one year. T2 shows a large sensitivity to season, with winter global NMB values (-14.52%) larger in magnitude than annual (-0.38%) or summer (2.7%) values, the large bias values during winter are associated with errors in the high Northern Latitudes. Model performance of GWRf shows little sensitivity of Q2 and GLW to seasonality, with similar negative NMB values for all three time periods for both variables, indicating an overall underestimation for both variables. GWRf exhibits overestimations of SWDOWN for all three means, but it also shows a large sensitivity to seasonality, with the winter mean having larger overpredictions (11.45%) than the annual (8.91%) or summer means (3.97%). Overall U10 is the least accurate of the variables simulated by GWRf and is consistently underpredicted, with the winter NMB (-68.47%) value being the least underpredicted when compared with the annual (-452.13%) and summer (-387.21%) NMBs. V10 is predicted with a higher level of accuracy than U10 and is also underpredicted for the global mean of all three time periods, with a distinct advantage during summer (NMB of -3.95%). Precipitation is overpredicted during the annual, summer, and winter means with NMB values of 31.03%, 38.64%, and 14.39% respectively indicating best performance during winter.

To put the results of the annual baseline simulation in context, the results are compared with results from the literature survey performed in Chapter 2. Globally T2 performs much better than expectations outlined in Table 2.2 with a MB of -0.02 and Corr value of 1.00, which is better than the  $\pm 2$  °C, and highest Corr value (IPCC AR4: 0.98). All sub-domain means fall within  $\pm 2$  °C, and Africa is the only sub-domain that reports a Corr value lower than the lowest value (CMIP: 0.93) in Table 2.2. Table 2.2 sets the requirements for model specific humidity bias as (CMIP) 1 g kg<sup>-1</sup> or (IPCC AR4) <10% error. GWRf performs at the upper level of this performance standard on the global scale, with a MB value of -0.19 g kg<sup>-1</sup> and a NMB value -

2.29% NMB. The majority of sub-domain averages also perform within this standard of  $1 \text{ g kg}^{-1}$  MB with the exceptions of South America ( $1.14 \text{ g kg}^{-1}$ ) and Africa ( $-1.04 \text{ g kg}^{-1}$ ) which slightly exceed the limit. The South Pole is the only domain average with values slightly larger than the <10% standard set by IPCC AR4, with a value of -11.09%. The expectation set by CMIP for model precipitation performance is that the models will have a MB value of  $1 \text{ mm day}^{-1}$  and a Corr value between 0.4 and 0.7, while a more stringent standard is set for the GFDL model with a MB value of  $0.15 \text{ mm day}^{-1}$  and a Corr value of 0.9, compared with these, GWRP performs better than the CMIP standard and worse than the GFDL standard. GWRP on a global scale compared with GPCP data has a MB value of  $0.67 \text{ mm day}^{-1}$  and a Corr value of 0.90. The only sub-domain averages which perform within the GFDL standard of MB are Australia ( $0.10 \text{ mm day}^{-1}$ ) and the South Pole ( $0.06 \text{ mm day}^{-1}$ ). All domains meet the MB CMIP standard with the exceptions of South America ( $1.11 \text{ mm day}^{-1}$ ), and the Northern ( $1.25 \text{ mm day}^{-1}$ ) and Southern ( $1.38 \text{ mm day}^{-1}$ ) Hadley Cells. All domains also meet or exceed the Corr standard from CMIP. Based upon this analysis, GWRP performs at the upper limit of standards for general circulation models. A potential source of uncertainty in this evaluation is an error which was introduced to WRFV3.0 for the Kain-Fritsch cumulus parameterization scheme which may cause long lasting cloud in rare areas, as noted on the WRF model user's site.

The literature survey conducted in Chapter 2 also provides some model standards for radiative prediction in GCMs. Wild et al., 1995 comment that there is a tendency common to all GCMs which overestimate downward shortwave flux by an average of  $10\text{-}15 \text{ W m}^{-2}$ . The GCMs also show a latitudinal dependence on performance, with overpredictions present over the low latitudes reaching up to  $40 \text{ W m}^{-2}$  and underestimations over the high latitudes reaching up to  $20 \text{ W m}^{-2}$  due to an underestimation of cloud cover in the annual mean. Annual 2001 GWRP compares well with these numbers and trends, exhibiting the largest MB values of SWDOWN over the Northern ( $41.07 \text{ W m}^{-2}$ ) and Southern ( $42.86 \text{ W m}^{-2}$ ) Hadley Cells, and the largest underestimations over the North Pole which has a MB value of  $-8.97 \text{ W m}^{-2}$ . Wild et al. (1995) also point out a tendency of GCMs to underestimate downward longwave flux due to an

underestimation of low-level clouds by an average of 10-15  $\text{W m}^{-2}$  which corresponds to a mean observation of 293  $\text{W m}^{-2}$  and a mean simulation of 278  $\text{W m}^{-2}$ . GWRP also underestimates GLW in the baseline simulation with a global MB value of -16.60  $\text{W m}^{-2}$ , which corresponds to a mean observation of 295.03  $\text{W m}^{-2}$  and a mean simulation of 278.43  $\text{W m}^{-2}$ . Overall GWRP results are consistent with the previous study.

## **6.2 Summary of Sensitivity Simulations**

### **6.2.1 Sensitivity to Horizontal Grid Resolution**

The fine (BASE) and coarse (low\_res) horizontal grid resolution simulations are compared for annual and seasonal (summer and winter) means. When the annual, global domain average is compared with NNR data, the BASE configuration provides the most accurate (lowest MB and NMB, high Corr value) estimate of daily precipitation rate, zonal wind speed (U10), and Q2, while low\_res provides the most accurate estimates of T2, SWDOWN, GLW, and meridional wind speed (V10). This indicates that a fine grid resolution may not be necessary for the accurate prediction of radiation parameters SWDOWN and GLW. The fine resolution simulation presents the largest improvement in daily precipitation rate, as well as zonal wind speed. The potential for improved accuracy with coarser grid resolution may be an artifact of the regridding process described in the methodology section in which the finer resolution is always regridded to the coarser resolution to avoid loss of data. This process may result in enhanced accuracy of the 4° × 5° resolution simulation, therefore it is important to compare the seasonal results to point observations (e.g., NCDC, BSRN) to expose the true sensitivity of results to resolution.

When the summer, global domain average is compared with NNR data, the BASE configuration provides the most accurate (lowest MB and NMB, high Corr value) estimate of T2, Q2, U10, and daily precipitation rate, while low\_res provides the most accurate estimates of SWDOWN, GLW, and meridional wind speed (V10). Similar to the annual case, the coarse resolution produces a higher level of accuracy for radiation fields, while the fine resolution

simulation presents the largest improvement in daily precipitation rate. The evaluation of the fine and coarse grid resolutions with observational data requires no regridding technique, and thus provides a more accurate investigation of the sensitivity to grid resolution. When the summer, global domain average of T2 and accumulated precipitation are compared with corresponding NCDC observation locations, the BASE provides a distinctly better estimate than the low\_res case, with an approximately 5% improvement in NMB for T2 and ~10% improvement for accumulated precipitation. The GWRf model output compared with corresponding BSRN observations reveals that low\_res provides a more accurate estimate of SWDOWN, while BASE is slightly (<1%) more accurate at estimating GLW. When compared with the summer baseline simulation and other sensitivity simulations, low\_res produces the least accurate estimates for both T2 and accumulated precipitation on a global scale when compared with NCDC and BSRN observations.

When the winter, global domain average is compared with NNR data, the BASE configuration provides the most accurate (lowest MB and NMB, high Corr value) estimate of U10, and daily precipitation rate, while low\_res provides the most accurate estimates of T2, Q2, SWDOWN, GLW, and meridional wind speed (V10). Similar to the annual and summer means, the coarse resolution produces a higher level of accuracy for radiation fields, while the fine resolution simulation presents the largest improvement in daily precipitation rate. The evaluation of the fine and coarse grid resolutions with observational data requires no regridding technique, and thus provides a more accurate investigation of the sensitivity to grid resolution. When the winter, global domain average of T2 and accumulated precipitation are compared with corresponding NCDC observation locations, the BASE provides a distinctly better estimate than the low\_res case. The GWRf model output compared with corresponding BSRN observations reveals that low\_res provides a more accurate estimate of SWDOWN and GLW. The fine resolution case during winter shows a distinct advantage in the prediction of precipitation, with an improvement on the global scale of greater than 25% (28.44%) NMB when compared with GPCP data. The overall improvement in precipitation prediction by using a finer horizontal grid

resolution during the annual, summer, and winter means is consistent with the literature review conducted in Chapter 2, in which a finer resolution is required to recreate the structure of precipitation systems.

### **6.2.2 Sensitivity to Microphysics**

In the sensitivity to microphysics configuration, there are essentially two sensitivity studies, one sensitivity study between WSM3 (BASE simulation) and WSM6 (CMP1 simulation), as well as one sensitivity study between WSM3 and Purdue-Lin (CMP2 simulation). In addition to the sensitivity of microphysical parameterization, there is also a need to identify which configuration produces the overall best results for the five meteorological fields in question (e.g., T2, Q2, SWDOWN, GLW, and Precipitation). When compared with reanalysis data (e.g., NNR and GPCP), the WSM6 (CMP2 simulation) performs better (lower MB and NMB, high Corr value) than WSM3 and Purdue-Lin for all five of the variables. Overall when compared with the baseline simulation and other sensitivity simulations, WSM6 produces the most accurate estimate for Q2 in the global domain. The improved accuracy of CMP1 over BASE and PL simulations for these variables is also consistent with the comparison of the sub-domains, in which the majority of sub-domains (circulation cell and continental domains) exhibit a lower MB value for CMP1 than BASE or CMP2. A potential source for the errors associated with the Purdue-Lin scheme is a bug introduced to the microphysics scheme in WRFV3.0 code which can cause an overprediction of cloud ice and graupel and may also cause an overprediction of surface rainfall, which is definitely the case here. The improved accuracy of precipitation, as well as radiative variables, with a more sophisticated microphysics option (WSM6) is consistent with results from the literature review conducted in Chapter 2.

### **6.2.3 Sensitivity to Radiation Configuration**

In the sensitivity to radiation configuration study there are essentially three sensitivity simulations, two sensitivities to shortwave option, and an additional sensitivity to longwave option. In addition to the sensitivity of radiation parameters, there is also a need to identify

which configuration produces the overall best results for the five meteorological fields in question (e.g., T2, Q2, SWDOWN, GLW, and Precipitation). When compared with reanalysis data (e.g., NNR and GPCP), the RAD3 configuration performs best (lowest MB and NMB, high Corr value) for four out of the five variables, with GLW best simulated by RAD2. The first sensitivity to shortwave option is a comparison between BASE and RAD3 which evaluates the Goddard and CAM shortwave options; the second shortwave sensitivity simulation is between BASE and RAD1, which evaluates the Goddard and Dudhia shortwave options. The third sensitivity simulation, and only one for longwave, is RAD2 and RAD3, which compares the RRTM and CAM longwave options.

The first sensitivity to shortwave option on a global scale evaluation with NNR shows that although BASE and RAD3 produce the lowest MB (and thus NMB) values of the four configurations, RAD3 performs best, indicating an advantage for the CAM over the Goddard shortwave scheme at this resolution. The second sensitivity to shortwave option on a global scale evaluation with NNR for BASE and RAD1 shows that BASE performs much better than RAD1, indicating an advantage for the Goddard over the Dudhia shortwave scheme at this resolution. RAD1 is also the only configuration that offers a large underestimate when compared with the NNR dataset, indicating a tendency of the Dudhia scheme to underestimate SWDOWN. The first two sensitivity tests of shortwave option rank the following shortwave parameterizations in the following rank of decreasing accuracy: CAM, Goddard, and Dudhia. The fine horizontal grid resolution that the model is being investigated at makes the CAM option the most logical because it is normally employed in simulation of large scale and long time periods, while the Goddard scheme is normally employed at the mesoscale, and the Dudhia scheme was originally developed for CRMs. The first sensitivity to longwave option on a global scale evaluation with NNR for RAD2 and RAD3 shows that RAD2 produces the only overestimation out of the four configurations, while the other three produce large underestimations. RAD2 performs much better than RAD3, indicating an advantage for the RRTM over the CAM longwave scheme at this resolution. As indicated in the literature review

about radiation sensitivity studies in Chapter 2, the RRTM produces larger values of GLW than other schemes because of an improved water vapor continuum, because water vapor is the major driver of GLW.

#### **6.2.4 Sensitivity to Land Surface Module**

The NOAH (BASE simulation) and SLAB (LSM simulation) Land Surface Modules (LSMs) are compared for overall accuracy, with the potentially most affected variables being the near-surface parameters T2 and Q2. When the global domain average is compared with reanalysis data (e.g., NNR and GPCP), the BASE configuration provides the most accurate (lowest MB and NMB, high Corr value) estimate of Q2, while LSM provides the most accurate estimates of T2, SWDOWN, GLW, and daily precipitation rate. LSM produces the only reliable overestimation of Q2 of any of the simulations (CMP2 also produces an overestimation which may be associated with a code error, see microphysics section for details). Model output of T2 and accumulated precipitation are compared with corresponding NCDC observation locations. The BASE provides the lowest MB value for T2, while LSM produces a large improvement in accumulated precipitation with a NMB value of 7.02%, compared with the BASE value of 25.29%. The GWRP model output compared with corresponding BSRN observations reveals that BASE provides slightly better estimates of both SWDOWN and GLW than LSM. When compared with the baseline simulation and other sensitivity simulations, LSM produces one of the most accurate estimates for both T2 and SWDOWN on a global scale when compared with NNR. The improved accuracy of LSM over the BASE simulation when compared with NNR for T2, SWDOWN, GLW, and daily precipitation rate is also consistent with the comparison of the sub-domains, in which the majority of sub-domains (circulation cell and continental domains) exhibit a lower MB value for these variables in LSM than BASE. The literature survey conducted in Chapter 2 for sensitivity to LSM were all based on regional models, while this study test the sensitivity on a global scale. NOAH produces a better estimate of Q2, which is consistent with the literature. On this global scale, the SLAB LSM does present small advantages when compared with NOAH.

### 6.2.5 Sensitivity to Cumulus Parameterization

The Kain-Fritsch (BASE simulation) and Grell-Devenyi (CCP simulation) cumulus parameterizations are compared for overall accuracy, with the potentially most affected variable being precipitation, as well as the two components of the radiation budget examined (GLW and SWDOWN) due to the effects of clouds on these parameters. When the global domain average is compared with reanalysis data (e.g., NNR and GPCP), the BASE configuration provides the most accurate (lowest MB and NMB, high Corr value) estimates of T2, Q2, and SWDOWN, while CCP provides the most accurate estimates of GLW and a more accurate daily precipitation rate estimate with a NMB value of 22.1% compared to the BASE value of 38.64%. Model output of T2 and accumulated precipitation are compared with corresponding NCDC observation locations, the BASE provides the lowest MB value for T2, while CCP provides a highly accurate estimate of accumulated precipitation with a NMB value of 0.71%, compared with the BASE value of 25.29%. The GWRf model output compared with corresponding BSRN observations reveals that CCP produces better estimates of both SWDOWN and GLW than BASE. When compared with the baseline simulation and other sensitivity simulations, CCP produces the most accurate estimate of both daily rate and monthly accumulated precipitation, as well as the best estimate of GLW for the global domain. The improved accuracy of CCP over the BASE simulation for these variables is also consistent with the comparison of the sub-domains, in which the majority of sub-domains (circulation cell and continental domains) exhibit a lower MB value for GLW and daily precipitation rate in CCP than BASE. The Grell-Devenyi scheme presents a distinct advantage over BASE for simulated precipitation. Overall BASE (Kain-Fritsch) creates large overestimations, while CCP (Grell-Devenyi scheme) overestimates precipitation to a lesser extent, creating a more accurate estimate. The large grid scale and CAPE trigger approach of Kain-Fritsch is the most likely reason for the large overpredictions, while The Grell-Devenyi ensemble cumulus scheme produces more reasonable value when compared with GPCP.

## **6.2 Summary of Future year (2050) Results**

Future climate change in 2050 is examined in this chapter by comparing model outputs from 2001 and 2050 by initializing GWRP with decade averages of CCSM model output fields. GWRP replicate the large near surface warming as shown in the IPCC AR4 (1.29 K) during January (1.32 K), but predicts a slight cooling during July (0.13 K) of the mid-21<sup>st</sup> century relative to the late 20<sup>th</sup> century. Geographically, annual and seasonal GWRP-CCSM comparisons consistently show the largest T2 differences at high latitudes, which is consistent with the IPCC report. The general intensification of the global hydrological cycle, with increasing values of globally averaged mean water vapor, evaporation and precipitation as reported by the IPCC is also present in the January GWRP simulations. In both the January and July simulations, downward shortwave flux slightly decreases and downward longwave flux increases in 2050, relative to the respective months in 2001. The value precipitation increase projected by the IPCC B1 scenario multi-model ensemble mean (0.06 mm day<sup>-1</sup>) during the mid-21<sup>st</sup> century relative to the late 20<sup>th</sup> century is much smaller than the January (+0.41 mm day<sup>-1</sup>) GWRP value, while the July GWRP simulation predicts an overall decrease in precipitation (-0.21 mm day<sup>-1</sup>). Geographically, annual and seasonal GWRP-CCSM comparisons consistently show the largest T2 differences at high latitudes, which is consistent with the IPCC report.

## **6.3 Recommendations**

Based on the analysis and evaluation presented in this study, the ideal baseline simulation for regional WRF and GWRP are different. Due to differences in spatial scales and the importance of processes on these scales, the baseline configuration must be altered to more accurately predict meteorological fields when evaluated with a variety of observational and gridded climate datasets. The results from a baseline simulation of 2001 show that GWRP is able to reproduce meteorological fields with comparable or improved accuracy to the majority of current, mature GCMs. As for the sensitivity to grid resolution, the fine resolution simulation was able to produce point observations with a higher level of accuracy than the coarse resolution simulation. The baseline simulation employed the baseline GWRP simulation features WSM3

microphysics, Goddard shortwave, CAM longwave, NOAA Land Surface Module, and the Kain-Fritsch cumulus parameterization at a horizontal grid resolution of  $1^\circ \times 1^\circ$ . Based on the results from this study, the new configuration should be WSM6 microphysics, CAM shortwave, RRTM longwave, SLAB Land Surface Module, and the Grell-Devenyi cumulus parameterization. This configuration may be influenced by the interaction among the physics schemes which may represent a new source of uncertainty and could produce larger errors. This new configuration is designed to optimize the accuracy of a fine resolution ( $1^\circ \times 1^\circ$ ), global, annual simulation. To use GWRP for future simulations, a more sophisticated interface between CCSM output and GWRP input may be developed, and should use ten year averages of fields from CCSM. Although GWRP still exhibits some instability in run-time, the model is mature for future studies for a variety of applications. Future studies using this as a source for optimum physical configuration should make sure that the goals of future studies are aligned with this one, as the best configuration for the simulation of processes may depend on the specific goals of the study.

## References

- Anderson, J. L., et al. (2004), The new GFDL global atmosphere and land model AM2/LM2: Evaluation with prescribed SST simulations, *J. Clim.*, 17, 4641–4673.
- Arakawa, A., and V.R. Lamb (1977), Computational Design of the basic dynamical processes of the UCLA General Circulation Model, in *General Circulation Models of the Atmosphere*, edited by J. Chang, pp. 173-265, Academic Press, San Francisco.
- Arakawa, A., 2004: The cumulus parameterization problem: Past, present, and future. *J. Climate*, 17, 2493-2525.
- Bader, D., Ed., 2004: *An Appraisal of Coupled Climate Model Simulations*. Lawrence Livermore National Laboratory, 36-73.
- Baklanov, A., A. Rasmussen, B. Fay, E. Berge, and S. Finardi (2002), Potential and shortcomings of numerical weather prediction models in providing meteorological data for urban air pollution forecasting, *Water, Air, and Soil Pollution: Focus 2*, 43-60
- Borge, R., Alexandrov, V., del Vas J. J., Lumbreras, J., Rodriguez, E. (2008), A comprehensive sensitivity analysis of the WRF model for air quality applications over the Iberian Peninsula, *Atmospheric Environment*, 42 (37), 8560-8574.
- Charney, J.G., R. Fjortoft and J. von Neumann, (1950), Numerical integration of the barotropic vorticity equation, *Tellus*, 2, 237-254.
- Chen, S. -H. and J. Dudhia, (2000), Annual Report: WRF Physics. [Available online at <http://www.mmm.ucar.edu/wrf/users/docs/wrf-doc-physics.pdf>.]
- Chen, S.-H., and W.-Y. Sun, 2002: A one-dimensional time dependent cloud model. *J. Meteor. Soc. Japan*, 80, 99–118.
- Chou M.-D., and M. J. Suarez (1994), An efficient thermal infrared radiation parameterization for use in general circulation models. NASA Tech. Memo. 104606, 3, 85.
- Christensen, J.H., B. Hewitson, A. Busuioc, A. Chen, X. Gao, I. Held, R. Jones, R.K. Kolli, W.-T. Kwon, R. Laprise, V. Magaña Rueda, L. Mearns, C.G. Menéndez, J. Räisänen, A. Rinke, A. Sarr and P. Whetton, 2007: Regional Climate Projections. In: *Climate Change 2007: The Physical Science Basis. Contribution of Working Group I to the Fourth Assessment Report of the Intergovernmental Panel on Climate Change* [Solomon, S., D.

- Qin, M. Manning, Z. Chen, M. Marquis, K.B. Averyt, M. Tignor and H.L. Miller (eds.)]. Cambridge University Press, Cambridge, United Kingdom and New York, NY, USA.
- Covey, C., K. M. AchutaRao, U. Cubasch, P. Jones, S. J. Lambert, M. E. Mann, T. J. Phillips, and K. E. Taylor, (2003), An Overview of Results from the Coupled Model Intercomparison Project (CMIP), *Global and Planetary Change*, **37**, 103-133.
- Collins, W.D. et al., (2004): Description of the NCAR Community Atmosphere Model (CAM 3.0), NCAR Technical Note, NCAR/TN-464+STR, 226.
- D. Randall (Ed.) (2000), *General Circulation Model Development*, International Geophysics Series, 70, pp. 67-87, Academic Press, San Diego, Calif.
- Druyan, L. M., M. Fulakeza, and P. Lonergan, (2007), Spatial variability of regional model simulated June-September mean precipitation over West Africa, *Geophys. Res. Lett.*, **34**(18).
- Dudhia, J. (1989), Numerical study of convection observed during the winter monsoon experiment using a mesoscale two-dimensional model, *J. Atmos. Sci.*, **46**, 3077–3107.
- Dudhia, J., S.-Y. Hong, and K.-S. Lim, (2008), A new method for representing mixed-phase particle fall speeds in bulk microphysics parameterizations. *J. Met. Soc. Japan*, in press.
- Fennessy M. J., and J. Shukla (1999), Impact of Initial Soil Wetness on Seasonal Atmospheric Prediction, *J. Clim.* **12**(11), 3167-3180.
- Gates, W. L., and Coauthors, 1996: Climate models - Evaluation. *Climate Change 1995: The Science of Climate Change*, J. T. Houghton et al., Eds., Cambridge University Press, 229-284.
- Gilliland, E. K., C.M. Rowe (2007), A comparison of cumulus parameterization schemes in the WRF model. Proceedings of the 87th Annual AMS Meeting. [np].
- Gilmore, M.S., J.M. Straka, and E.N. Rasmussen (2004a), Precipitation and evolution sensitivity in simulated deep convective storms: Comparison between liquid-only and simple ice and liquid phase microphysics, *Monthly Weather Review*, **132**, 1897-1916.
- Gilmore, M.S., J.M. Straka, and E.N. Rasmussen (2004b), Precipitation uncertainty due to variations in precipitation particle parameters within a simple microphysics scheme, *Monthly Weather Review*, **132**, 2610-2627.

- Goody, R., R. West, L. Chen, and D. Crisp (1989), The Correlated-k Method for Radiation Calculations in Nonhomogeneous Atmospheres, *Journal of Quantitative Spectroscopy and Radiative Transfer*, 42(6), 539-550.
- Grell, G. A., and D. Devenyi, 2002: A generalized approach to parameterizing convection combining ensemble and data assimilation techniques. *Geophys. Res. Lett.*, **29**, 1693-1696.
- Hack, J. J., J. M. Caron, G. Danabasoglu, K. W. Oleson, C. Bitz, and J. E. Truesdale, (2006), CCSM–CAM3 Climate Simulation Sensitivity to Changes in Horizontal Resolution, *Journal of Climate*, 19(11), 2267–2289.
- Han, J., and H. Wang (2007), Interdecadal Variability of the East Asian Summer Monsoon in an AGCM, *Adv. Atmos. Sci.* 24(5), 808-818.
- Hansen, J. (1984) Climate sensitivity: analysis of feedback mechanisms. *American Geophysical Union* 29, 130-163.
- Hansen, James E. (1992), Potential Climate Impact of Mount Pinatubo Eruption, *Geophysical Research Letters* 19: 142-58.
- Holland, G., (2006), The WRF Modeling System: A Successful Community Activity, National Center for Atmospheric Research, Boulder, Colorado, 6/20/2006. [Available online at [http://www.ametsoc.org/boardpages/cwce/docs/2006/WRF\\_Overview.pdf](http://www.ametsoc.org/boardpages/cwce/docs/2006/WRF_Overview.pdf)].
- Holt, T.R., D. Niyogi, F. Chen, K. Manning, M.A. LeMone, and A. Qureshi (2006), Effect of Land-Atmosphere Interactions on the IHOP 24-25 May 2002 Convection Case, *Monthly Weather Review*, 134(1), 113-133.
- Hong, S, -Y, H. -M. H. Juang and Q. Zhao (1998), Implementation of Prognostic Cloud Scheme for a Regional Spectral Model, *Monthly Weather Review*, 126, 2621-2639.
- Hong, S. -Y., J. Dudhia, S.H. Chuen (2004), A Revised Approach to Ice Microphysical Processes for the Bulk Parameterization of Clouds and Precipitation, *Monthly Weather Review*, 132, 103-120.
- Hong, S. -Y. and J. O. Lim (2006), The WRF single moment 6-class microphysics scheme (WSM6), *Journal of the Korean Meteorology Society*, 42, 129-151.
- Hurrell, J. W., J. J. Hack, A. S. Phillips, J. Caron, and J. Yin, 2006: The dynamical simulation of the Community Atmosphere Model version 3 (CAM3). *J. Climate*, **19**, 2162–2183.

- Iacono M. J., E. J. Mlawer, S. A. Clough, and J. J. Morcrette, 2000: Impact of an improved longwave radiation model, RRTM, on the energy budget and thermodynamic properties of the NCAR community climate model, CCM3. *J. Geophys. Res.*, **105**, 14 873–14 890.
- Jankov, I., W. A. Gallus, M. Segal, and S. E. Koch (2007a), Influence of Initial Conditions on the WRF-ARW Model QPF Response to Physical Parameterization Changes, *Weather and Forecasting*, *22*, 501-519.
- Jankov, I., P. J. Schultz, C.J. Anderson, and S.E. Koch (2007b), The Impact of Different Physical Parameterizations and Their Interactions on Cold Season QPF in the American Basin, *Journal of Hydrometeorology*, *8*, 1141-1151.
- Janowiak, J. E. (1991), The Reliance on Operational Weather Satellites for the Production of a Global Precipitation Climatology, *Global and Planetary Change*, *4*(1-3), 93-98.
- Jimenez, P., O. Jorba, R. Parra, and J.M. Baldasano (2005), Influence of high-model grid resolution on photochemical modelling in very complex terrains, *International Journal of Environment and Pollution*, *24*, 180-200.
- Jones, M.S., B.A. Colle, and J.S. Tongue (2007) Evaluation of a Mesoscale Short-Range Ensemble Forecast System over the Northeast United States, *Weather and Forecasting*, *22*(1), 36-55.
- Kain, J. S., 2004: The Kain-Fritsch convective parameterization: An update. *J. Appl. Meteor.*, **43**, 170-181.
- Kain, J. S., and J. M. Fritsch, 1990: A one dimensional entraining/detraining plume model and its application in convective parameterization. *J. Atmos. Sci.*, **47**, 2784-2802.
- Kain, J. S., and J. M. Fritsch, 1993: Convective parameterization for mesoscale models: The Kain-Fritsch scheme. *The Representation of Cumulus Convection in Numerical Models*, *Meteor. Monogr.*, No. 24, Amer. Meteor. Soc. 165-170.
- Kalnay, E. et al. (1996), The NCEP/NCAR 40-Year Reanalysis Project, *Bulletin of the American Meteorological Society*, *77*(3), 437-471.
- Kjellstroem, E., and K. Ruosteenoja, (2007), Present-day and future precipitation in the Baltic Sea region as simulated in a suite of regional climate models, *Clim. Change*, *81*(1), 281-291.

- Kunkel, K. E., X. Liang, J. Zhu, and Y. Lin, (2006), Can GCMs Simulate the Twentieth – Century ‘Warming Hole’ in the Central United States, *J. Clim.*, 19(17):4137-4153.
- Lambert, S. J., and G. J. Boer, 2001: CMIP: Evaluation and intercomparison of coupled climate models. *Climate Dynamics*, **17**, 83-106.
- Lacis, A. A., and J. E. Hansen (1974), A parameterization for the absorption of solar radiation in the earth’s atmosphere. *J. Atmos. Sci.*, 31, 118–133.
- Lin, Y.-L., R. D. Farley, and H. D. Orville, 1983: Bulk parameterization of the snow field in a cloud model. *J. Climate Appl. Meteor.*, 22, 1065–1092.
- Manabe, S. and K. Bryan (1969), Climate Calculations with a Combined Ocean-Atmosphere Model. *Journal of the Atmospheric Sciences*, 26, 786-789.
- Manabe, S. (1970), The dependence of atmospheric temperature on the concentration of carbon dioxide, in “Global Effects of Environmental Pollution” edited by S.F. Singer, pp. 25-29. D. Reidel, Dallas, TX.
- Manabe, S. (1971), Estimates of future change of climate due to the increase of carbon dioxide, in “Man’s Impact on the Climate” edited by W.H. Matthews, W.W. Kellogg, and G.D. Robinson, pp. 250-264, MIT Press, Cambridge, MA.
- Manabe, S., and R.T. Wetherald (1975), The Effects of Doubling the CO<sub>2</sub> Concentration on the climate of a General Circulation Model, *Journal of the Atmospheric Sciences* 32, 3-15.
- Mass, C.F., D. Ovens, K. Westrick, and B.A. Cole, (2002), Does increasing horizontal resolution produce more skillful forecasts?, *Bulletin of the American Meteorological Society*, 407-430.
- Medaglia, C.M., C. Adamo, F. Baordo, S. Dietrich, S. Di Michele, V. Kotroni, K. Lagouvardos, A. Mugnai, S. Pinori, E.A. Smith, and G.J. Tripoli (2005), Comparing microphysical/dynamical outputs by different cloud resolving models: Impact on passive microwave precipitation retrieval from satellite, *Advances in Geosciences*, 2, 195-199.
- Meehl, G.A., T.F. Stocker, W.D. Collins, P. Friedlingstein, A.T. Gaye, J.M. Gregory, A. Kitoh, R. Knutti, J.M. Murphy, A. Noda, S.C.B. Raper, I.G. Watterson, A.J. Weaver and Z.-C. Zhao, 2007: Global Climate Projections. In: *Climate Change 2007: The Physical Science Basis. Contribution of Working Group I to the Fourth Assessment Report of the Intergovernmental Panel on Climate Change* [Solomon, S., D. Qin, M. Manning, Z.

- Chen, M. Marquis, K.B. Averyt, M. Tignor and H.L. Miller (eds.)]. Cambridge University Press, Cambridge, United Kingdom and New York, NY, USA.
- Misenis, C., X. Hu, S. Krishnan, Y. Zhang, and J. D. Fast (2006), Sensitivity of WRF/Chem Predictions to Meteorological Schemes, AMS Conference on the Applications of Air Pollution Meteorology [AMS Conf. Appl. Air Pollut.]. Vol. 14, [np].
- Mlawer, E. J., S. J. Taubman, P. D. Brown, M. J. Iacono, and S. A. Clough (1997), Radiative transfer for inhomogeneous atmosphere: RRTM, a validated correlated-k model for the longwave, *J. Geophys. Res.*, 102 (D14), 16663–16682.
- Ohmura, A. et al. (1998), “Baseline Surface Radiation Network (BSRN/WCRP): New Precision Radiometry for Climate,” *Bulletin of the American Meteorological Society*, 79(10), 2115-2136.
- Phillips, N. A. (1956), The general circulation of the atmosphere: A numerical experiment. *Quarterly Journal of Royal Meteorological Society*, 82, 123-164.
- Platzman, G.W. (1979), The ENIAC Computations of 1950-gateway to numerical weather prediction. *Bulletin of the American Meteorological Society*, 60, 302–312.
- Randall, D.A., R.A. Wood, S. Bony, R. Colman, T. Fichefet, J. Fyfe, V. Kattsov, A. Pitman, J. Shukla, J. Srinivasan, R.J. Stouffer, A. Sumi and K.E. Taylor, (2007), Climate Models and Their Evaluation, in *Climate Change 2007: The Physical Science Basis. Contribution of Working Group I to the Fourth Assessment Report of the Intergovernmental Panel on Climate Change*, edited by Solomon, S., D. Qin, M. Manning, Z. Chen, M. Marquis, K.B. Averyt, M. Tignor and H.L. Miller, Cambridge University Press, Cambridge, United Kingdom and New York, NY, USA.
- Rao, Y. V. R., H. R. Hatwar, A.K. Salah, and Y. Sudhakar (2007), An Experiment Using the High Resolution Eta and WRF Models to Forecast Heavy Precipitation over India, *Pure and Applied Geophysics* 164, 1593-1615.
- Richardson, M. I., A. D. Toigo, and C. E. Newman (2005), Non-conformal projection, global, and planetary versions of WRF, presented at the 6<sup>th</sup> WRF/15<sup>th</sup> MM5 User’s Workshop. Boulder, Colorado, June 27-30, 2005.
- Richardson, M. I., A. D. Toigo, and C. E. Newman (2007), PlanetWRF: A general purpose, local to global numerical model for planetary atmosphere and climate dynamics, *J. Geophys. Res.*, 112, E09001.

- Rutledge, S. A., and P. V. Hobbs, (1984), The mesoscale and microscale structure and organization of clouds and precipitation in midlatitude cyclones. XII: A diagnostic modeling study of precipitation development in narrow cloud-frontal rainbands. *Journal of Atmospheric Science*, 20, 2949–2972.
- Salvador, R., J. Calbo, M.M. Millan (1999), Horizontal grid size selection and its influence on mesoscale model simulations, *Journal of Applied Meteorology*, 38, 1311-1329.
- Skamarock, W.C. (2008), Global WRF Development, Presented at the 8th WRF User’s Workshop, National Center for Atmospheric Research, Boulder, Colorado, USA, June 23 - 27, 2008. [Available online at <http://www.mmm.ucar.edu/wrf/users/workshops/WS2008/presentations/1-2.pdf>].
- Skamarock W. C., J. B. Klemp, J. Dudhia, D. O. Gill, D. M. Barker, W. Wang, and J. G. Powers (2007), A Description of the Advanced Research WRF Version 2, NCAR technical note, pp 51-56. National Center for Atmospheric Research, Boulder, Colorado, USA. [Available online at [http://www.mmm.ucar.edu/wrf/users/docs/arw\\_v2.pdf](http://www.mmm.ucar.edu/wrf/users/docs/arw_v2.pdf)].
- Skamarock W. C., J. B. Klemp, J. Dudhia, D. O. Gill, D. M. Barker, M. G. Duda, X.-Y. Huang, W. Wang, and J. G. Powers, (2008), A Description of the Advanced Research WRF Version 3, NCAR technical note, National Center for Atmospheric Research, Boulder, Colorado, USA. [Available online at [http://www.mmm.ucar.edu/wrf/users/docs/arw\\_v3.pdf](http://www.mmm.ucar.edu/wrf/users/docs/arw_v3.pdf)].
- Smagorinsky, J. (1958), On the numerical integration of the primitive equations of motion for baroclinic flow in a closed region. *Monthly Weather Review*, 86, 457-466.
- Smagorinsky, J., S. Manabe, and J. L. Holloway, (1965), Numerical Results from a nine-level general circulation model of the atmosphere. *Monthly Weather Review*, 93, 727-768.
- Simpson, J., Adler, R. F., North, G. R., (1988), “A Proposed Tropical Rainfall Measuring Mission (TRMM) Satellite,” *Bulletin of the American Meteorological Society*, 69(3), 278-295.
- Stephens, G. L., 1978: Radiation profiles in extended water clouds. Part II: Parameterization schemes, *J. Atmos. Sci.*, 35, 2123–2132.
- Tao, W.-K., J. Simpson, and M. McCumber 1989: An ice-water saturation adjustment, *Mon. Wea. Rev.*, 117, 231–235.

- Tewari, M., F. Chen, W. Wang, J. Dudhia, M. A. LeMone, K. Mitchell, M. Ek, J. Wegiel, and R. H. Cuenca (2004), Numerical Experiments with MM5 and WRF using the upgraded unified Noah Land Surface Model, Presented at the 5th WRF/14th MM5 Users' Workshop, Boulder Colorado, National Center for Atmospheric Research, June 22-25, 2004. Available at [<http://www.mmm.ucar.edu/mm5/workshop/ws04/Session1/Tewari.Mukul.pdf>]
- Tremblay, A., A. Glazer, and L. Garand (2001), Comparison of three cloud schemes in winter storm forecasts, *Monthly Weather Review*, **129**, 2923-2938.
- Weisman, M. L., J. B. Klemp, and R. Rotunno, (1988), Structure and evolution of numerically simulated squall lines. *J. Atmos. Sci.*, **45**, 1990–2013.
- Skamarock, W. C., M. L. Weisman, and J. B. Klemp, (1994), Three-dimensional evolution of simulated long-lived squall lines. *J. Atmos. Sci.*, **51**, 2563–2584.
- Tao, W.-K., J. Simpson, and M. McCumber, (1989), An ice-water saturation adjustment, *Mon. Wea. Rev.*, **117**, 231–235.
- Wang, W., and N. L. Seaman, 1997: A comparison study of convective parameterization schemes in a mesoscale model. *Mon. Wea. Rev.*, **125**, 252-278.
- Weisman, M.L., W.C. Skamarock, and J.B. Klemp (1997), The resolution dependence of explicitly modeled convective systems, *Monthly Weather Review*, **125**, 527-548.
- Wen, X (2007), An overview of Climate Modeling, presented at Advanced Air Quality, NCSU, Raleigh, N.C., 11 November.
- Wild, M., A. Ohmura, H. Gilgen, J.J. Morcrette, A. Slingo (2001) Evaluation of Downward Longwave Radiation in General Circulation Models, *Journal of Climate*, **14**(15), 3227-3239.
- Wild, M., A. Ohmura, H. Gilgen, E. Roeckner, (1995) Validation of General Circulation Model Radiative Fluxes Using Surface Observations, *Journal of Climate*, **8**(5), 1309-1324.
- Xie, P., and P. Arkin, 1997: Global precipitation: a 17-year monthly analysis based on gauge observations, satellite estimates, and numerical model outputs. *Bull. Amer. Meteor. Soc.*, **78**, 2539-2558.
- Yu, S., B. Eder, R. Dennis, S.-H. Chu, and S.E. Schwartz (2006), New unbiased symmetric metrics for evaluation of air quality models, *Atmospheric Science Letters*, **7**(1), 26-34.

Zamora, R.J., E.G. Dutton, M. Trainer, S.A. McKeen, J.M. Wilczak, and Y.T. Hou, 2005: The Accuracy of Solar Irradiance Calculations Used in Mesoscale Numerical Weather Prediction. *Mon. Wea. Rev.*, **133**, 783–792.

